THE EFFECTS OF WAVE ACTION ON LONG SEA OUTFALLS

Thesis submitted in accordance with the requirements of the University of Liverpool for the degree of Doctor of Philosophy

by

Richard Brian Mort, B.Eng.

September 1989

To my family for all

their support over the

past few years.

DECLARATION

I declare that no portion of the work referred to in this thesis has been submitted in support of any application for another degree or qualification of this or any other university or other institution of Learning.

R.B. Mort

Abstract

This thesis deals with both theoretical and experimental modelling studies to investigate the influence that wave action exerts on the hydraulic performance of sea outfalls. This particular research stems from the United Kingdom's dependency upon the use of the marine environment for the treatment and disposal of sewage, with the consequential concern of ensuring that sea outfalls operate satisfactorily, thereby, offering an adequate degree of environmental protection. Clear evidence exists that sewage outfalls do suffer from saline intrusion sometimes exacerbated by wave action, particularly if the outfall is in shallow water, seriously inhibiting their performance.

Experimental work was undertaken with a newly-designed sea outfall model which was positioned in one of the Civil Engineering department's wave flumes. Experiments were performed to determine how velocities within outfall risers are affected by the action of waves over the manifold system during varying rates of controlled discharge. Velocities within the risers were measured using an ultrasonic probe.

A series of experiments were also undertaken to investigate the hydraulic effects of saline wedges in open ended pipes in order to establish validation data for the main research programme, and for the development of one of the two mathematical models used in the studies.

The mathematical models for analysing wave action on outfalls and for determining lengths of saline wedges in open ended pipes, were written on the University's main frame computer. Both models are readily

transferable to the IBMPC or other comparable systems so long as a Fortran compiler is available. Major restructuring though will be involved as the graphical plotting routines will not be compatible. The results produced by the calibrated models compared favourably with those produced during the experimental programmes.

One of a number of important conclusions drawn from this research is that wave action will enhance the circulation of seawater within an outfall manifold system should the risers already be under intrusive conditions. The condition of saline intrusion is clearly caused when the rate of effluent discharge is less than the designed flow for the outfall system. Moreover it was discovered that wave action causes both high and low instantaneous velocities which could well increase the volume of marine sediment being forced into the system.

The final part of the programme examines the effect of attaching diffuser caps to the risers. The evidence here is that diffuser caps reduce the inhibiting effect of wave action, simultaneously producing increases in friction which facilitates the purging of seawater from the outfall when the rate of discharge is lower than that of the design parameter.

ACKNOWLEDGEMENTS

I would like to thank my Supervisor Dr. R. Burrows for his constant help during this study and his thorough review of the original drafts. I would also like to thank Dr. K.H.M. Ali for additional information and help during this study period, and to Mr. R.G. Tickell for the use of the Keelavite Flume in which the experiments were performed.

My sincere thanks are due to the Marine Technology Directorate of the Science and Engineering Research Council for funding the research on which this thesis is based.

I am extremely grateful to Mr. T. Sharpe, and his fellow technicians who helped in the construction of the experimental apparatus; to Mr. J. Wilkinson who helped in the production of the data collection software; to Mrs. D. Eccles and Miss E. Black for their careful preparation of the typescript and to Mrs. B. Cotgreave for her diligent work on the diagrams.

Finally I would like to say a special word of thanks to my parents who have supported me through this and all my other academic endeavours.

Notation

Unless otherwise stated in individual sections the following notation is used throughout the thesis.

A	-	Area
a	-	Speed of pressure pulse wave in pipe
B	-	Perimeter
C_d	-	Coefficient of discharge
D	-	Pipe diameter
d	-	Depth of water
E	-	Youngs modulus of elasticity
F	-	Force (also occasionally used to denote Froude number)
F_R	-	Froude number
f	-	Friction factor in pipes
f_i	-	Interfacial friction factor
g	-	Acceleration due to gravity
g'	-	Reduced gravitational acceleration
H	-	Total Head
H_w	-	Wave height
h	-	Difference in hydraulic head
h_{if}	-	Head loss due to friction
L	-	Length of outfall pipe
L_o	-	Saline wedge length inside pipe
N_R	-	Reynolds number
P	-	Pressure
Q	-	Flow rate in pipes
q_{So}	-	Flow rate in riser pipes

T - Waveperiod

t - Time

t' - Thickness of pipe wall

U - Vertical velocity in drop shaft

V - Velocity

V_r - Pipe velocity

V_Δ - Densimetric velocity

V_L - Volume

W - Width of interface between liquids of different density

Z - Height of pipe above datum

α, β - Angles of salt/fresh water interface

θ - Longitudinal slope of pipe

ϵ - $\dfrac{\rho_2 - \rho_1}{\rho^2}$

λ - Wave length

γ - Weight of fluid

ρ - Density of fluid

τ - Shear stress acting on fluid

μ - Viscosity

ν - Kinematic viscosity

$\overline{V}$ = mean velocity

V_f = flow rate/local cross sectional area

$\emptyset$ = pipe diameter

Unless otherwise stated all units are expressed in S.I.

CONTENTS

CHAPTER 1

INTRODUCTION

The trading pre-eminence of Britain grew because of its strong links with and ready access to the sea. Small coastal and river mouth settlements swelled into large communities in response to increases in maritime commerce and other related interests. In turn, these communities developed into major connurbations whose industrial and commercial interests became diverse.

Human activity creates waste; in the past this was municipal only. Since the unprecedented industrial development during the nineteenth century industrial waste has also had to be dealt with. Almost all coastal towns in Britain discharge sewage to the sea as an economical method of disposal. It is done either without treatment or with screening and maceration (or disintegration) only. Many of the outfalls through which domestic sewage and trade wastes are discharged were constructed in the nineteenth century, and are still in use today. A great many of them discharge sewage at a point not much further out than low water mark under ordinary spring tides. At some of these places, where the current regime is favourable or the outfall is remote from accessible beaches, there are no visible signs of sewage pollution and no smell or other indication of the presence of sewage in any frequented locality. At other places signs of sewage detectable to the eye or nose occur near or on beaches occasionally. In winter and very wet weather, this may cause little or no concern, but in summer if pollution of the beaches occurs then most people find it highly objectionable. At a few places such objectionable conditions occur quite frequently and there may be accumulations of sewage solids both offshore and on the beach. Situations of this kind are a source of concern to the public who are becoming increasingly aware that many beaches and foreshores in the United Kingdom are an affront to the standards a civilised society should demand of its environment.

This need to alleviate pollution along shorelines, together with improving water quality because of the growing popularity of water contact sports, has seen the adoption of the European Economic Community (EEC) standards for bathing waters; involving over 300 beaches around the coast of Britain.

To implement the EEC standards will require a great deal of economic funding,(most of which will have to come from central government)and this is bringing to general awareness that the economy of Britain can be influenced by its environment. The economy is now so complex, and the environment so finely balanced, that a clear regime of sensible environmental regulation and control is vital to avoid a process of environmental degeneration which would bring in its wake serious economic consequences. Indeed, it can be argued that in the United Kingdom the degeneration process has already begun, too frequently manifesting itself through infrastructure dereliction arising from failure to respond to the need to agree, plan and implement asset replacement programmes.

The absence of such programmes has, among other things, sometimes led to the collapse of major sewers and water mains serving large connurbations, and bringing disruption to the city centres concerned. Other instances point to the neglect of known malfunctioning sea outfalls causing gross pollution of foreshores, beaches and water courses, all of which are now recognised as being high amenity areas. So it is vital to preserve and improve the quality of life and to recognise that as the economy grows money should be made available for improvements to the environment.

A major consequence of the EEC bathing water directives is that new marine outfalls are being constructed further out to sea, to discharge into greater depths of water. Increases in distance between shoreline and outfall discharge location demands greater capital investment, as well as higher design and construction skills. It is to be expected that intense interest is now being given to producing efficient and trouble-free outfall pipes and diffusers with a view to minimising maintenance expenditure and enhancing cost-benefits.

As outfalls become longer and start discharging into greater depths of water it becomes essential to determine the behaviour of the marine discharge in terms of dilution and dispersion. These are governed by a variety of physical factors such as sea temperature and salinity, tidal and ocean currents, winds and waves. Yet only in recent times have we begun to look closely at the effect of these physical factors within the outfall conduit and its manifold.

For many years it has been known that the performance of some long sea outfalls fell short of design expectations, although the underlying reasons for this were never fully investigated and, in consequence, not understood. Often it was assumed that the problems were, in the main, related to faulty diffusers; however, now that more intensive investigations are being carried out on the determination of hydraulic characteristics of outfalls during their operation, it has been observed that both saline intrusion and marine life cause a variety of problems such as blocked risers and diffusers[42] and corrosion causing the breaking away of risers from the manifold[24]. Both problems result in very different effluent dilution and dispersion values when compared with those for which the outfall was designed. Whilst the foregoing difficulties are sometimes construction related, the problem of blocked risers is more probably caused by poor design leading to an inhibited outfall system.

The aim of this thesis is to investigate the effects wave action and saline intrusion have on a sea outfall and to shed light on some of the problems they may cause. The main area of laboratory investigation centres on the effect that wave action has on a submerged marine outfall diffuser system, whilst a series of complementary experiments were also undertaken to examine in detail how saline wedges might develop during a cycle of steady flow within an open ended outfall pipe. Both investigations were implemented using experimental and mathematical modelling thus providing, through the numerical model, a basis for the analysis of prototype outfalls.

An important feature within the experimental programme was the design and assembly of a scaled model outfall whose physical characteristics are described in Chapter 4. This was placed inside a wave flume capable of generating both random and sinusoidal wave forms. Data collection apparatus, comprising pressure transducers, velocity meters and wave gauges, were connected to a computerised data collection system and the results stored on tapes. A second outfall model was used for measuring saline wedge lengths and profiles forming in a horizontal pipe. Results from this latter experiment were obtained manually.

Mathematical models were also developed to run parallel with the experimental models so that results from both could be compared. Analysis was undertaken in several stages with the eventual aim that a single mathematical model could be used to describe the behaviour of a multiport diffuser system for future design purposes.

The thesis therefore is divided into eight sections, with this, the introduction being section 1. Section 2 is a literature survey in which a brief outline is given of the present 'state of the art' on both two layer flow and outfall behaviour. The next section, section 3, deals with the theoretical modelling, including the derivation of equations and their development into equational mathematical models - which in turn are outlined in appendix D. Three mathematical models were developed, one to perform an analysis of saline wedges in pipes and two to investigate outfall behaviour, the first looked at single port outfalls whilst the second looked at multiport diffuser systems.

Sections 4 and 5 deal with the design of the experimental apparatus and the experimental procedures respectively. Appendices A and B also form an integral part of section 4.

Sections 6, 7 and appendix E cover the results obtained, both experimentally and theoretically, for saline wedge analysis and multiport diffuser analysis. Section 8 presents the conclusions deduced the work carried out and recommends further work which could be undertaken to extend the understanding of outfall behaviour.

CHAPTER 2

LITERATURE REVIEW

2.1 Saline Wedges and Two Density Flow

A great deal of work has been undertaken by various researchers in an attempt to analyse stratified flow phenomena and its consequential effects; much of the research has been carried out on fresh and salt water stratification caused by changes in water temperature (thermal stratification). A major proportion of these investigations has been restricted to either open-channel or estuarial flow situations, with very little research having been directed towards the stratification of flows in conduits.

One of the earliest papers to cover this subject is that by Schijf and Schonfeld(50) which describes a survey of the theoretical investigations carried out in Holland to examine the motion of salt and fresh water in estuaries and canal locks. Within their paper the authors look at the long wave phenomena at the interface of two sharply separated liquids and the effect of critical flow at the end of the wedge. They also consider the stability of the interface and finally they look at how the mixing process in a brackish water region can be clarified. The authors also list the basic equations for motion and continuity in open channel flow situations for salt wedge analysis which are cited by various researchers in subsequent papers.

Harleman[26] and Keulegan[34] have both written chapters, for specialist texts, dealing with the effects of saline intrusion in open channel flow situations; that by Harleman is principally theoretical and looks into the effects of turbulent and laminar flow situations on the saline wedge and how internal wave action develops. The chapter written by Keulegan deals primarily with experimental data collected during both field and laboratory tests to examine the lengths and profiles of saline wedges in open channels and estuaries. A paper written by Partheniades, Dermissis and Mehta[45] also deals with experimental data collected over a period of time and produced in graphical form to enable practising engineers to determine the approximate length of potential saline wedges developing within estuaries. The importance of this is that if an estuary is dredged then it is possible to determine the extent to which sea water intrusion will change.

Turning to work carried out solely in connection with open channels, as opposed to estuaries, a paper by Smith and Elsayed[52] focuses attention on gradually varied flows in a two layer system where significant energy losses arise due to boundary and/or interfacial friction. In their paper the authors consider channels of arbitrary geometry and derive relationships for energy gradients and surface slopes of the upper and lower layers in terms of shear stresses at the solid boundaries, as well as at the interface. One result of their work has been the production of a suite of computer programs to solve a range of problems involving gradually varied two-layer stratified flow. The authors then compare the predictions obtained with published laboratory and field data, such as that produced by Keulegan[34]. Of particular note, however, is their discussion relating to the calculation of interfacial friction factors. These define the levels of interfacial shear stress between the layers of salt and fresh water. The shear stress equations contained in this paper were produced by various researchers using field data and are outlined below: (all equations are shown in Smith and Elsayed[52])

(i) From Ippen and Harleman for lower layer flowing

$$f_i = 11.3/N_{R_2} \tag{2.1}$$

where $N_{R_2} = \frac{V_2}{\nu_2} \left(\frac{A_2}{B_2 + W}\right)$

and
f_i = interfacial friction factor
N_R = Reynold s number
V_2 = velocity
ν = kinematic viscosity
A = area of flowing layer
B = wetted perimeter
W = width of interface
and subscript '2' indicates lower layer.

(ii) From Bata for one layer flowing

$$f_i = \frac{384}{N_R} \frac{(3 + N)}{(3 + 4N)} \tag{2.2}$$

where $N = \left(\frac{a_1}{a}\right) . \left(\frac{\mu}{\mu_1}\right)$

and subscript '1' denotes stagnant layer, and μ is the dynamic viscosity.

(iii) From Bata for one layer flowing

$$\frac{(384 - f_i N_R)^{3/2}}{4 f_i N_R - 384} = \frac{31.2}{(N_R M)^{1/2}} \tag{2.3}$$

where M = hydraulic radius.

(iv) From Keulegan for one layer flowing

$$f_i = K/N_{R_x}^{1/2} \tag{2.4}$$

where $N_{R_x} = \frac{Vx}{\nu}$

(v) From Dick and Marselak for lower layer flowing

$$f_i = 0.316/N_{R_2}^{0.25} \tag{2.5}$$

where $N_{R_2} = \frac{4 V_2}{\nu_2} (\frac{A_2}{B_2 + W})$

Smith and Elsayed then determined which of the above five equations to use by determining the value of the ratio

$$\frac{\text{Richardson number}}{\text{Reynolds number}}$$

The foregoing suggests that interfacial shear stress is strongly dependent upon boundary conditions, and that interfacial shear stress values for flows within pipes could be markedly different to those calculated for open channel situations.

A paper prepared by Holley and Waddell[29] dealt with stratified flow in a series of regulating culverts constructed at specific locations through a railway causeway which effectively splits the Great Salt Lake, Utah, USA, into two separate lakes. The culverts are designed to keep the levels of water and salt concentration at specified tolerances within each section of the lake. Perhaps the most interesting feature of this work was that it dealt with both the experimental and theoretical analysis of stratified flows in an enclosed conduit, rather than in open channels or estuaries. The theoretical work was undertaken using open channel equations as the culvert was rarely flowing in a full condition.

A paper by Abraham, Karelse and van Os[1] elaborates on the reasons why subcritical stratified flows may be treated as two layer flows without mixing; they also give a summary of experimental data used to determine interfacial shear. Here the authors find that the values of K_i, where

$$K_i = \frac{f_i}{8}$$

decreases with increasing Reynold s numbers, but tending to a constant value for larger Reynold s numbers. Again all of the results arise from research carried out for open channel flow situations.

The words detailed above were those which had been utilized in the present study of two density flows. In addition, a paper by Hino, Hung and Nakamura[28], on entrainment and friction at the interface of a salt wedge, proved useful whilst investigating interfacial friction.

One interesting feature relating to saline wedges is the way Dutch engineers have employed the inhibiting effect of stratified flow to their advantage, enabling sea locks to be operated to permit seagoing vessels to move from existing inland fresh water lakes out to sea, whilst preventing sea water contamination. This operation is carried out in a number of ways which are illustrated in a paper by Van der Kuur(54).

Research into the consequences and motion of stratified flow within pipes is relatively limited, when compared with that work already carried out to analyse similar problems in open channels; moreover, current knowledge of the problem is meagre, and has only been acquired in recent years. One of the earliest papers on the subject, produced by Ellison and Turner(22), investigates the behaviour of a layer of dense salt solution on the floor of a sloping rectangular pipe in which there is turbulent flow. Another early paper was written by Sharp and Wang(51) and this presents the results of a series of experiments to determine how an arrested saline wedge was formed within a modelled sea outfall pipe. To facilitate experimental work they inverted the outfall system so that salt water was passed through the pipe and into a large body of fresh water, leaving a fresh water wedge to form along the soffit of the pipe as shown in Figure 2.1.

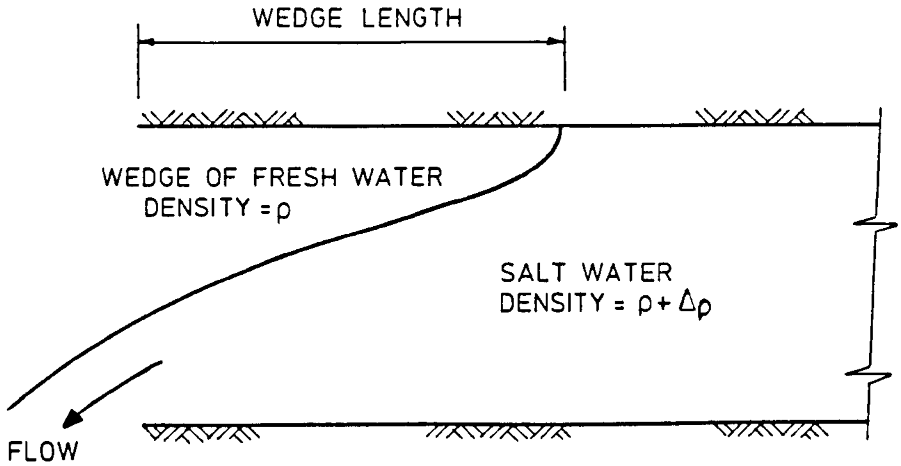

Sketch of inverted outfall showing position of wedge

Figure 2.1

Sharp and Wang then compared their experimental results of both wedge length and profile with open channel theoretical and experimental results which had previously been determined by other authors, including Keulegan[34], Polk and Benedict[46]. No additional theoretical work dealing with the problems of saline wedges in pipeflow was undertaken by Sharp and Wang, but the concept of running salt water, as opposed to fresh water, through the outfall pipe was a procedure adopted for all initial experiments on a new outfall model facility constructed at Liverpool University and reported upon in this thesis.

In 1981 the Water Research Centre (WRc) recognised the existence of potentially serious problems arising from the intrusion of sea water in outfall pipes. A short report dealing with the problem of saline wedge formation was produced by Munro[41] in which a number of suggestions are made as to how the problem of wedge formation can be alleviated. At the time of issue of the WRc report there was still no in depth experimental work being carried out to assess what was actually happening within the outfall structure, consequently the recommendations made by WRc are based primarily on predictions of what may occur within the outfall pipe.

During the last few years, however, more research has been undertaken to determine the effects and causes of saline wedges in both open ended outfall pipes and outfalls comprising risers and diffusers at their discharge end. To date the main thrust of research activity within the United Kingdom has been carried out at the University of Dundee under the direction of Dr. J. Charlton and latterly by Dr. P. Davies. At Dundee they have carried out experiments both in the field, using prototype outfalls, and in the laboratory to observe the formation and effect of saline wedges in pipelines having either open ended discharge arrangements or with diffuser systems (Figure 2.2).

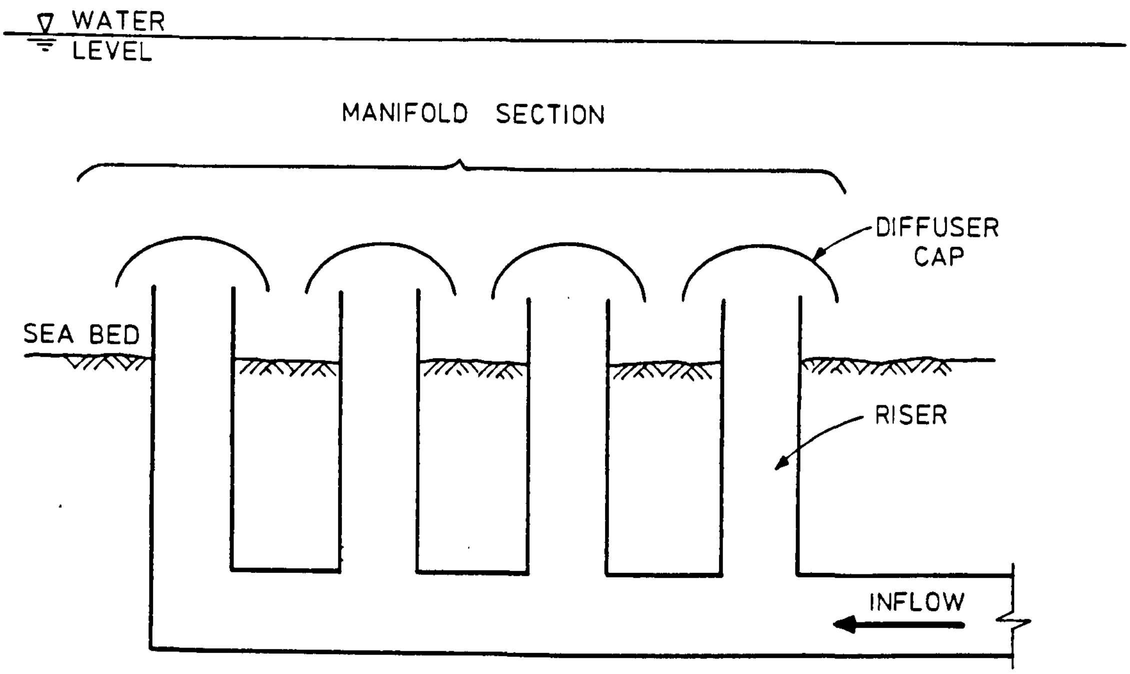

Schematic Sketch of Outfall with Riser/diffuser system

Figure 2.2

The work carried out at Dundee has been published extensively and covers a number of issues relating to saline intrusion. Two early papers published by Charlton look at saline intrusion into multi-port sea outfalls(13), together with the hydraulic modelling of the effects of saline intrusion into sea outfalls(14). Dealing firstly with the paper on hydraulic modelling, it is noted that Charlton initially divides the various outfalls into four main groups which are:

(i) Sea bed outfall pipes with the diffuser section being entirely above the sea bed,

(ii) Shallowly buried outfall pipes with the diffuser section consisting of a number of short riser pipes,

(iii) Tunnelled outfalls where the diffuser section consists of a number of shafts connecting the soffit of the tunnel to sea bed diffuser heads and

(iv) Tunnelled outfalls were the diffuser section consists of a number of staggered shafts (connections made on alternate sides of the main outfall pipe) joining the invert of the tunnel to sea bed diffuser heads.

The paper then looks at various criteria for designing diffuser systems and proceeds to describe the experimental model, a scaled model of the Aberdeen sea outfall, which was at that time under construction. Charlton discusses the model requirements and scaling, before finally giving informative observations on the operation of the model. His observations show that downward intrusive seawater flow will occur in the seawater filled risers if the discharging fresh water velocity is not great enough to purge the system; moreover, the greater the riser length the greater the required flow. If the risers are connected to the invert of the outfall then the interface between fresh and salt water tends to be horizontal and whilst some risers will eventually be purged as more fresh water enters the system, other risers will still permit an inflow of sea water. Finally, the intrusion of sea water will attenuate as the rate of fresh water discharge increases.

In the paper on the subject of saline intrusion into multi-port outfalls[13] Charlton describes the intrusive process in greater detail and promotes the concept of the action of events taking the form of a hysteresis loop (see Figure 2.4) which is described later in this chapter.

Charlton[15] also defines the scale of saline intrusion within an outfall as being either 'primary' or 'secondary'. Primary intrusion is the term given to a salt wedge which is contained within a diffuser cap and can be readily cleared by a small increase in flow rate. This form of intrusion is unlikely to cause serious hydraulic problems within the outfall system. Secondary intrusion occurs when the salt water wedge passes through the diffuser piece and down the riser into the main outfall pipe. This will possibly cause a wedge to form in the main pipe so causing changes in the hydraulic characteristics of the system and requiring a large increase in flow rate to remove it. Secondary intrusion frequently occurs during outfall shutdown periods. In a satisfactory outfall design it is assumed that initial peak flow rates, upon first commissioning, are such that the system will be purged of all saline water. In conclusion, Charlton states that because of the general configuration of outfalls all will be susceptible to saline intrusion but, depending on their design and construction, some will be less prone than others. Whilst investigating the consequences of sea water intrusion Charlton also observed that little harm will come to the outfall system if the intrusive process is cyclic and the outfall is purged of salt water during operation. Should this not be the case then problems, such as sediment deposition, are likely to occur.

At this stage only those papers giving descriptive preliminary studies undertaken by Charlton had been studied. The way forward was to examine other documented experimental work that had been undertaken in this field. Early research by Charlton[12] to establish both profiles and lengths of saline wedges developing in open ended pipes, similar in scope to the work of Sharp and Wang[51] involved simulating a submerged marine outfall arrangement, conveying fresh water along the pipe discharging into a tank of salt water. From the results of the experiments on an open ended pipe they produced a formula based on early work by Keulegan[34]. Keulegans work was undertaken in open channels, and by converting the terms from an open channel system to a pipe flow system, the length of a saline wedge within a submerged open ended pipe could be estimated empirically. The formula is given as:

$$\frac{L_0}{D} = K \left[\frac{2\,V_r}{V_\Delta} \right]^{-3.4} \left[\frac{V_\Delta\, D}{\nu} \right]^{-0.76} \tag{2.6}$$

where L_0 = saline wedge length

D = pipe diameter

V_r = free stream velocity in full pipe

ν = kinematic viscosity

V_Δ = densimetric velocity and is given by

$$V_\Delta = [g\, D\, (\frac{\rho_1 - \rho_2}{\rho_1})]^{1/2}]$$

g = acceleration due to gravity

and ρ_1, ρ_2 = density of salt and fresh water respectively.

Charlton et al[12] give the value of K as being approximately 12000 so that the theoretical and experimental results are comparable.

This work has recently been superceeded in a paper produced by Davies et al[21], in which the formula given in (2.6) has been refined to give:

$$\frac{Lo}{D} = K \left[\frac{2V_r}{V_\Delta}\right]^{-7.93} \left[\frac{V_\Delta D}{\nu}\right]^{b} \tag{2.7}$$

where $b = 0.56 \left[\frac{2Vr}{V_\Delta}\right]^{0.89}$; and

$$K = 0.054 \left[\frac{2Vr}{V_\Delta}\right]^{-3.69} \mathrm{Ln} \left[\frac{2Vr}{V_\Delta}\right]$$

From a rigorous investigation of the theoretical and experimental results produced by Charlton, Davies et al, and by comparing the results obtained from the equation with experimental results acquired herein it was found that the expression for K, given above had been wrongly derived. Consequently, the equation in its published form is subject to large errors. Once the revised expression for k has been introduced, see Section 6.4, the results obtained from the equation (2.7), compare favourably with the experimental results.

Another equally interesting point arising from the report by Charlton et al[12] is the boundary condition at the discharge section of the pipe. They found that if the Densimetric Froude number of a particular discharge was calculated using the mean (pipe full) velocity and the depth of flow at the exit, then the densimetric Froude number remained at a constant value of unity. They do mention that the measurement of the depth and mean velocity depends upon observations of the interface discharge profile and the establishment of where a realistic depth value should be measured. Further experimental work has recently been accomplished on this subject by Porter[47].

Focusing attention on the more complicated modelling of multiport sea outfalls, work at Dundee concentrated on the configurations illustrated in Figure 2.2 as opposed to a pipe with a series of ports along one side only (Figure 2.3).

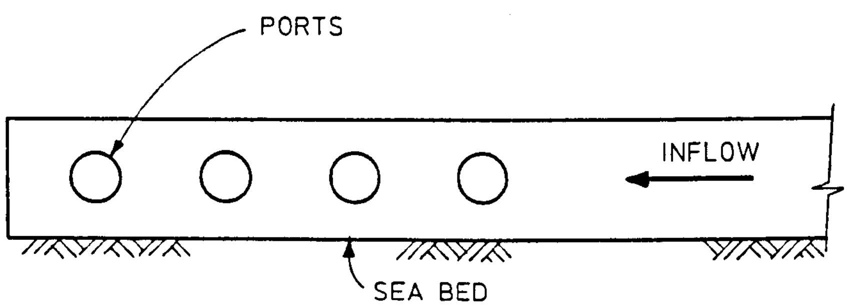

Sketch of an outfall with ports along its axis

Figure 2.3

Comprehensive experimental modelling was undertaken at Dundee, all of which served to demonstrate that if an outfall is not continuously discharging at its design flow rate, then sea water will penetrate the system unless mechanical means are installed to prevent this. In a paper by Charlton, Davies and Bethune[17], they discuss some of the results obtained from their experimental model. Here they discuss the problems of primary and secondary intrusion, and how to overcome this during the purging process. During a simulated outfall purging process they examined how the driving head changed as each riser was purged (see Figure 2.5) and compared the purging performance of soffit and invert connected risers. In this case it was found that an invert connected multi-riser system purged more efficiently than a soffit connected arrangement.

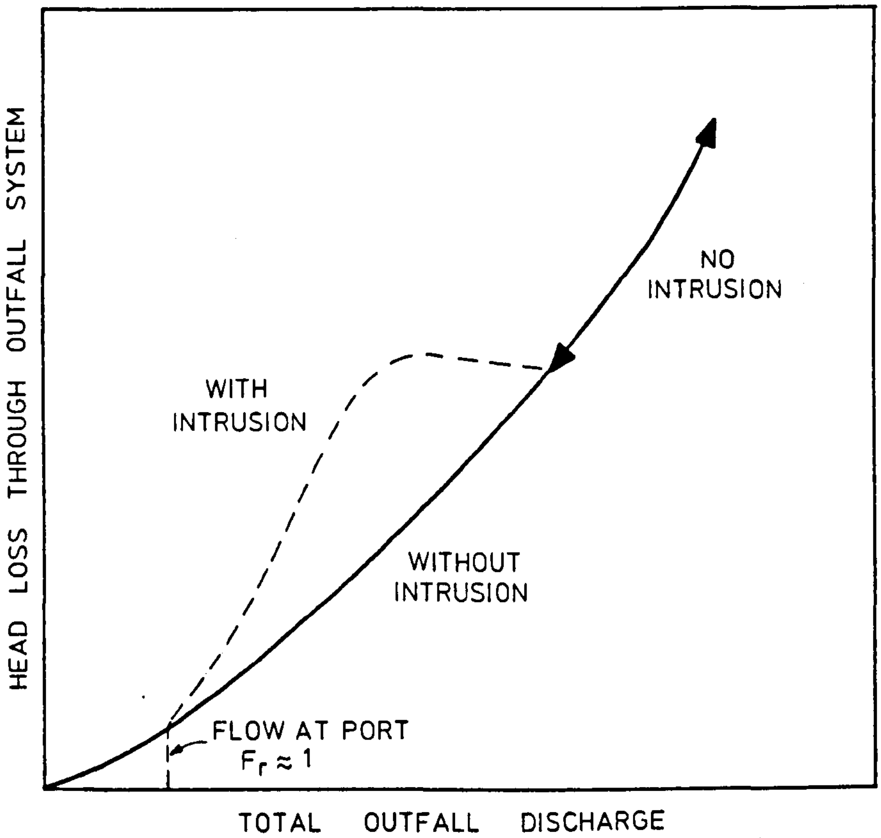

Diagram showing the effect of seawater intrusion on the head loss in a complete outfall system. (From Charlton[15]).

<u>Figure 2.4</u>

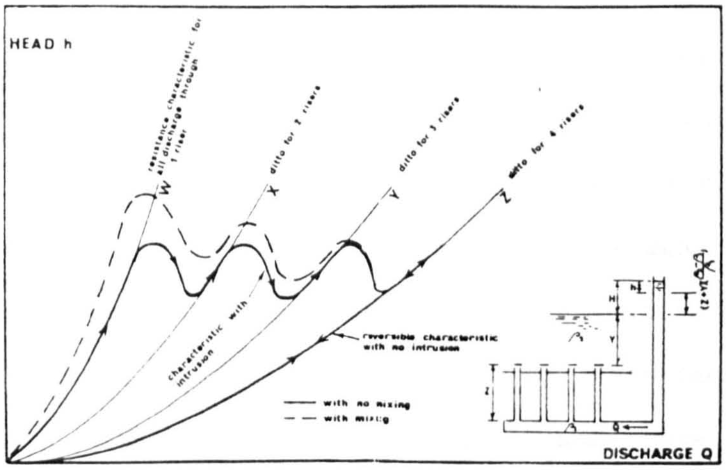

The head/discharge characteristic for a four riser outfall with and without saline intrusion. (From Charlton[15]).

Figure 2.5

Mention should be made of the fact that both Munro[41] and Charlton observed that saline intrusion often causes severe operational difficulties, principally because tunnelled outfalls are invariably constructed with slack backfalls to facilitate drainage during construction and to enable the system to be emptied for inspection and maintenance purposes; consequently, sea water can, if allowed, gravitate along the pipeline towards the headworks dropshaft.

Another important area of work carried out by Charlton et al was the monitoring of discharges from prototype outfalls[19]. In this paper the authors give a brief outline on how the work was implemented using remote sensing. It is known that other studies of prototype outfalls are currently being carried out by WRc, the results of which have not yet been published.

Significantly, Charlton's research has led to the possibility of development of pressure charts which can be used as a guide, to the operators of sea outfalls, of outfall performance, indicating the likely number of risers discharging and the various stages of purging. Moreover, the experiments assisted with the determination of the most efficient location of risers on an outfall in order to facilitate the purging process. Charlton has also examined some novel ideas for preventing intrusion into multiport diffuser systems[15], and these include the installation of venturi constrictions[16] either immediately upstream of the diffuser manifold or within the diffuser head, and the use of Taylor-Dunlop valves positioned at the outlet of each riser, (see Figures 2.6 and 2.7 respectively).

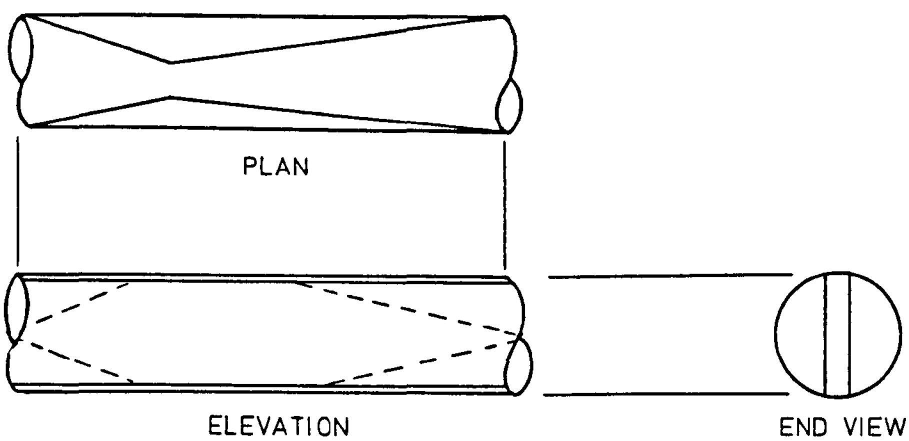

Venturi intrusion control

Figure 2.6

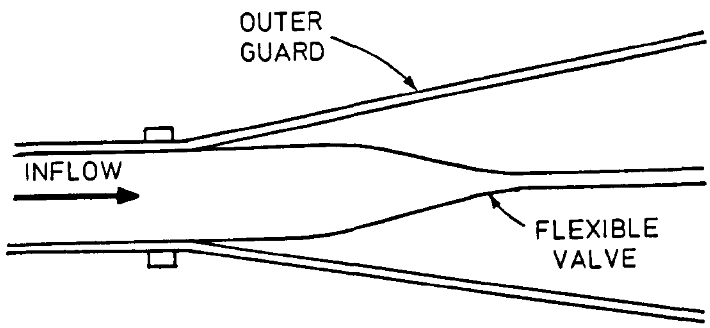

Anti intrusion flexible duck bill valve

Figure 2.7

At the present time little information about the operational performance of these innovations has been made known, although a venturi has been incorporated into an outfall built at Aberdeen; it is also known that other outfall designs include the provision of a venturi. Taylor-Dunlop valves have been used successfully on the Weymouth outfall which is operated by Wessex Water Authority[49]. There are, however, disadvantages to the use of these devices, one of which is the increased head required to overcome the additional constriction incurred by the devices. A major shortcoming of the valve can arise when used on a pumped system as the rubber membrane, which is an integral part of the valve, often suffers 'blow back' under the development of negative pumping pressures in the pipeline, thus inhibiting flow from the outfall.

Research into the effects of saline wedges on diffuser manifolds has been carried out in Australia by Wilkinson[58, 59, 60]. Initially studies were undertaken to examine the effect of seawater circulation within outfall manifolds and, in so doing, he produced both theoretical and experimental results for his work[58, 60]. All the results obtained by Wilkinson are restricted to a two riser system. In his first paper[58] Wilkinson discusses the various problems and effects of saline intrusion and intrusive conditions and then moves on to discuss circulation blocking (the drawing of seawater down landward risers), which he says occurs after a shut-down of sewage flow into the outfall tunnel or the premature commencement of sewage discharge following a shut-down. Wilkinson then produces a theoretical analysis to determine the sewage flow required to purge a blocked riser and discovered that his agreement between theoretical and experimental results was close. He concludes, however, that unlike saline wedge blocking of an outfall tunnel, circulation blocking cannot be prevented by modification of the manifold system but that it can be avoided by ensuring that all transient motion has ceased before the system is restarted. In his second paper[60] Wilkinson arrives at the following theoretical equation to determine the flow of seawater circulating around the manifold system, the equation is based on Fig. 2.8 and is given as:-

$$\frac{Q_s}{Q_c} = \{[1 + 2r + (4 - F_c^2)\frac{r^2}{2}]\ (1 + r)^{-1/2}\}^{-1/2} \qquad (2.8)$$

thus indicating that the ratio of circulating sea water to sewage flow (r) is determined by the ratio of sewage discharge (Q_s) to the critical purging discharge (Q_c) and the critical outfall Froude number (F_c).

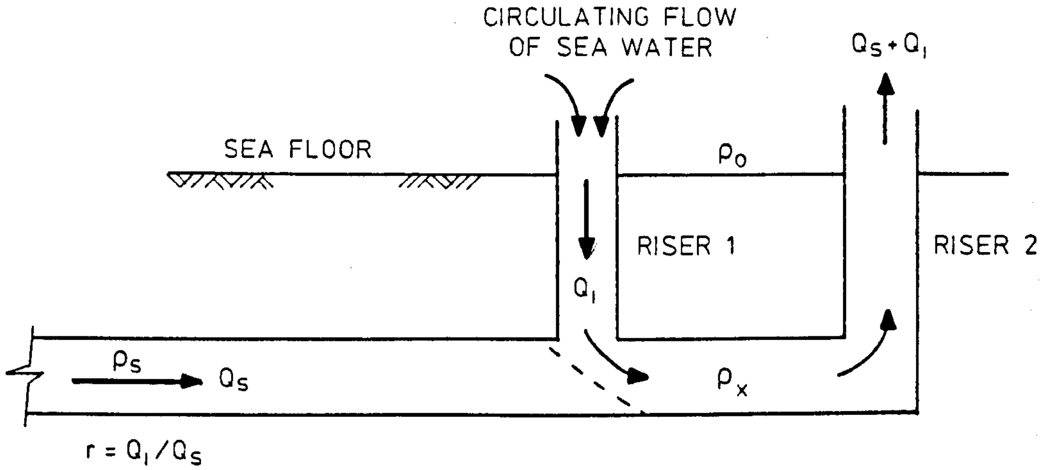

Sketch of circulation blocked outfall

Figure 2.8

Wilkinson produces experimental data using his model outfall and demonstrates that the experimental results agree closely with the theoretical results obtained from equation (2.8). After examining the circulatory effects within the manifold system, Wilkinson then progressed with further work relating to the purging of saline wedges from outfalls having manifolds attached at the downstream end.

In his paper on purging flows[59] he deduces an equation, using Fig. 2.9, to determine the critical flow required for purging a riser once the upstream risers had been purged. The equation is given as:

$$Q_c = \sqrt{2}\ [2\ S_m + (1 + \frac{fh}{d})(\frac{D}{d})^4 + k_c - 1]^{-1/2}\ [A\ (g'h)^{1/2}] \qquad (2.9)$$

where Q_c = critical discharge

S_m = dimensionless momentum factor

f, k_c – respective friction factors of riser pipe and bend

h – height of riser from outfall tunnel centreline

D – diameter of outfall tunnel

d – diameter of riser

A – area of riser

and g' is the reduced gravitational acceleration, caused by the change in density and is given by

$$g' = \left[\frac{\rho_1 - \rho_2}{\rho_2}\right] g$$

which is slightly different to that defined by other researchers.

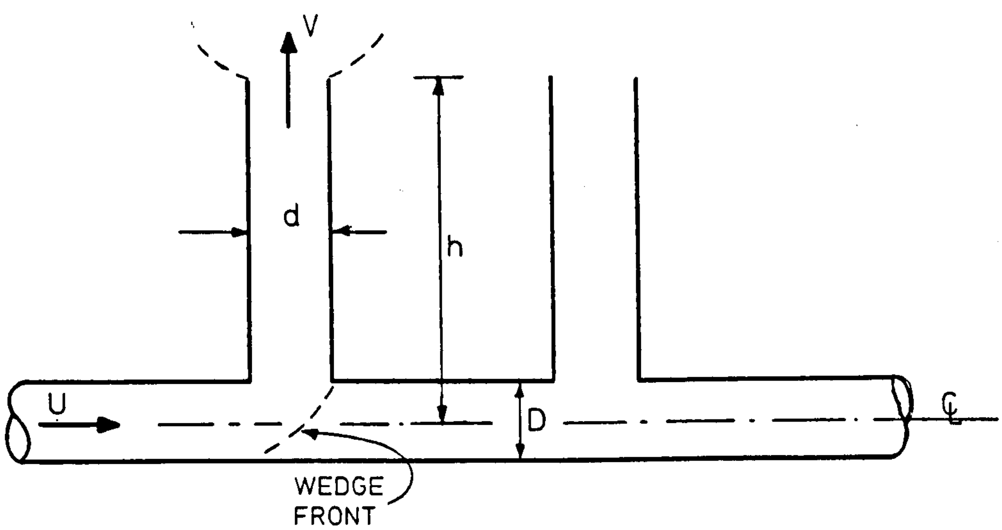

Schematic diagram of critical flow condition for calculation of equation 2.9.

Figure 2.9

Again Wilkinson carried out experimental modelling to compare with the results obtained from the theoretical analysis and again good agreement was achieved.

Leaving aside for a moment the problems of outfall behaviour, and moving along to deal with the physical modelling of outfalls, it should be noted that great care is necessary when building an outfall model to ensure that it truly represents a prototype outfall. The problem originates from the choice of scaling parameters, i.e. whether to size the outfall using densimetric Froude numbers, which would cater for the possibility of stratification occurring within the outfall, but would not accurately model shear stresses within the system, or use Reynolds numbers which would take into account shear stresses but not stratification. In a discussion document(18) written by Charlton et al, they appear to be sceptical about whether the results obtained by Wilkinson could be used to predict what was happening in a prototype outfall, since they believe that his model was too small. The outfall model used by Wilkinson has a tunnel diameter of 25mm, whereas the model used by Charlton et al incorporates tunnel diameters of between 88mm and 120mm. This criticism is refuted by Wilkinson(18) and, to prove his point, refers work carried out by Keulegan(33) on the effect of viscosity on shear instabilities and how this can be used with the densimetric Froude number to establish appropriate scales for model studies.

It can be concluded from the foregoing discussion that very little numerical modelling has been undertaken to analyse the profile of flow stratification within enclosed outfall pipes, both with and without a diffuser section when compared to the large amount of work which has been successfully completed on open channel flow conditions. However, this situation is steadily changing and research has recently been undertaken in France by Viollet[56] dealing with the numerical modelling of two density currents. The reason for Viollet's work however was to examine thermal stratification in pipes caused when hot water passes along the pipe after it has left the cooling system of a fast breeder reactor. This method of numerical modelling could be used as a possible extension to the work performed herein.

2.2 Outfall Hydraulics and the Behaviour of Manifolds under Wave Action

2.2.1. The hydraulics of flow manifolds.

Before the consequences of wave action upon an outfall can be investigated, it is essential that the hydraulics of the outfall and its manifold are examined and understood. Several papers were looked at to investigate possible methods of modelling outfall behaviour. The first is a publication by Acrivos, Babcock and Pigford[2] describing the one dimensional fluid mechanics calculation method, together with pertinant experimental data, relating to manifolds of the simplest type in which the main pipe has a constant cross-section terminating in a closed end, and provided with equally spaced uniformly-sized side tubes attached to the main pipe at right angles. Experimental and theoretical models for both blowing and sucking manifolds were studied, and a series of graphs were produced from which it should be possible to determine what was happening within the manifold system.

The second paper by Ramamurthy and Satish[48] looks at the internal hydraulics of diffusers with uniform lateral momentum distribution. Again they use a main pipe of constant cross-section, but then assume the manifold to be large, subsequently using the equations for a porous manifold system. After having carried out both theoretical and experimental investigations on this system, they found that the two sets of results agreed fairly well.

2.2.2 <u>The effects on outfall headworks of wave action in receiving waters.</u> (Unsteady flow analysis)

The first reference on this subject is that prepared by F.M. Henderson[27]. This report outlines a desk study in which the equations of motion and continuity are applied to an outfall to yield the storage volume required in the head works to accommodate the fluctuations in flow rate as a wave passes over the outfall's manifold. The equation of motion is given as:-

$$h - \frac{H_w}{2} \sin \frac{2\pi t}{T} = \left[\frac{fL}{D} + \frac{A_0{}^2}{A_2{}^2}\right] \frac{V^2}{2g} + \frac{L}{g}\frac{dV}{dt} \qquad (2.10)$$

and the equation of continuity as:-

$$Q_0 = A_1 \frac{dh}{dt} + A_0 V \qquad (2.11)$$

where h = difference in levels between water in the upstream tank and sea water level

H_w = wave height

T = wave period

f = Darcy friction factor

L - outfall length

D - outfall diameter

A_0, A_1, A_2 - areas of outfall pipe, upstream tank and discharge port area respectively

Q_0 - inflow into upstream tank

and V - velocity of flow in pipe.

The equation Henderson derives for the additional storage (s) is,

$$s = \frac{A_0 \ gH_w \ T^2}{8\pi L} \tag{2.12}$$

In obtaining the above results, two simplifying assumptions have been made as follows:- (i) the change of water level in the upstream tank is negligibly small, and (ii) the change in resistance plus velocity head term on the right hand side of equation 2.10 is negligibly small. These two assumption reduce equation 2.10 to:-

$$\frac{H_w}{2} \sin \frac{2\pi t}{T} = - \frac{L}{g} \frac{dV}{dt} \tag{2.13}$$

From which Henderson derives equation (2.12). He then offers reasons for the two assumptions, for the first he states that it is desirable to keep the change in water level small and consequently the objective of his design study is to find out whether, and under what conditions, these variations can be kept small. He then states that the second assumption is plausible in view of the considerable length of the outfall being studied, and hence the large inertia of the water-column contained within it. The conclusion reached is that the additional storage required within the system as a wave passes over the manifold is negligible, but this would only be the case for long outfall pipes and will not necessarily apply to short outfalls[5]. This simplified approach by Henderson provides no indication of possible problems that might arise within the outfall caused by wave induced oscillation and circulation within the manifold structure, and this is a matter that is examined in detail herein.

2.2.3 The effects of wave action on the internal flows in multi riser outfalls.

Larsen[35] has reported a numerical study of the problem which he addresses to the case of small diameter plastic pipe outfalls constructed in shallow water off the coast of Denmark. Larsen's theoretical analysis uses the method of characteristics to solve the equation of motion and continuity. For his time simulation he models a random wave field acting over the outfall by a JONSWAP (Joint North Sea Wave Project) spectrum.

Prototype outfalls in Denmark have riser heights of between 1 and 2 metres which are small when compared to the overall outfall length which may vary between 500 and 2000 metres. For his analysis Larsen used an outfall consisting of "off pipe" diffuser ports (i.e. no risers Fig. (2.10) as opposed to Fig. (2.2)) and a tunnel in which the cross sectional area varied (Fig. 2.10).

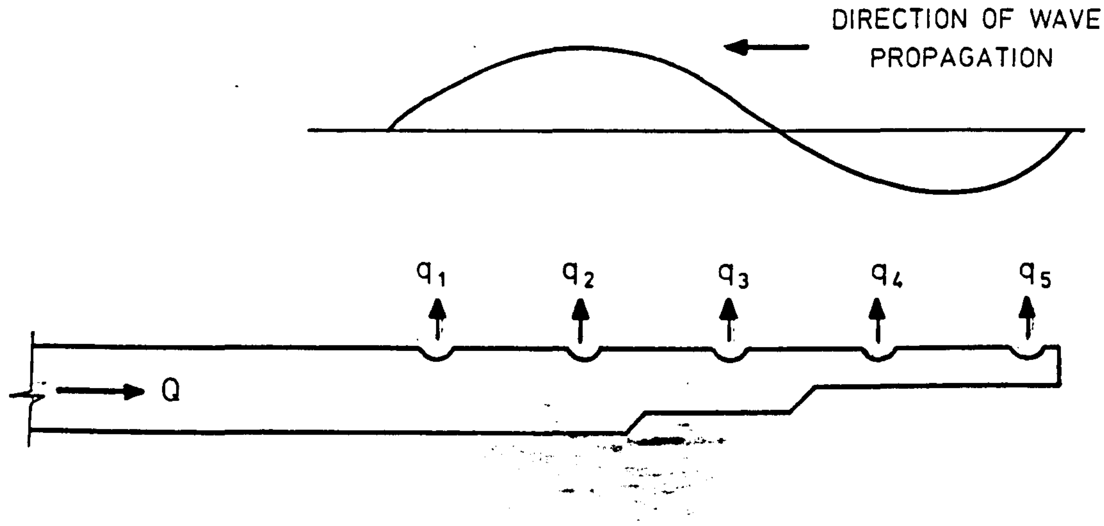

Instantaneous flow in diffuser under wave action

Figure 2.10

He found that under certain wave conditions, a reversal of flow will take place within at least one of the diffuser ports of the outfall system signifying saline intrusion, even though all would be discharging in the absence of waves.

Another problem which is cited by Larsen is the effect of resonance within the outfall pipe; from the numerical model it is shown that the damping of standing waves is very small and the pressure fluctuations are large. This phenomenon could be further investigated experimentally in the new model facility at Liverpool University developed as part of this study but has not been pursued as part of the present work.

Apart from the references given above, there is very little documentation of the possible effects of wave action on outfall manifolds. It is understood, however, that a confidential report by Palmer[44] also addresses this topic.

2.3 Other Aspects of Outfall Design

The design of outfalls has now become a very complex procedure and is reflected by the large number of papers dealing with the subject, particularly in relation to dispersion and dilution of effluent. Several papers have examined this subject in a variety of ways, for instance, a publication by Vigliani et al[55] investigates the dilution of a domestic sewage source discharged to sea, under various conditions of the dispersion plume. In this case dilution was determined by measurement of the salinity and concentration of silicates within the plume, together with the physical properties (velocity, temperature and dimensions) and was compared with the values obtained using available theoretical formulae and graphs. The theoretical formulae and diagrams used in this publication are the Cederwall formula, the Cooley and Harris formula, the Rawn, Bowerman and Brooks diagram and the Fischer and Brooks diagram. These have also been used in many other technical publications.

Another report by Isaacson et al[30], looks at plume dilution for diffusers with multiport risers. Each riser was evenly spaced containing two to eight ports, and the plume dilutions were measured in a two dimensional hydraulic model. Experimental results from this model were compared with a mathematical model developed previously by one of the authors.

The two aforementioned papers are laboratory investigations into plume dilutions, but a third paper by Bennett[9] looks at the plume dilution from an outfall already in use, in this case the Hastings long sea outfall operated by Southern Water Authority. To measure the diffusion Rhodamine WT dye was injected within the riser and the resulting dye-sewage concentrations were measured at the mouth of the port and at the sea surface. Tidal stream, salinity, temperature and depth measurements were also taken during the study. The information obtained by Bennett[9] was correlated and the results compared with the theories of the Water Research Centre and the Hydraulics Research Station. It was found that the results from the Hastings outfall fell between the two theoretical curves produced by the two aforementioned research institutes.

In a paper on staged multiport diffusers Almquist and Stolzenbach[7] investigate the efficiency of this type of diffuser arrangement on mixing between effluent and the receiving body of water. A schematic diagram of a staged diffuser configuration is shown in (Fig.2.11) along with two other typical diffuser sections.

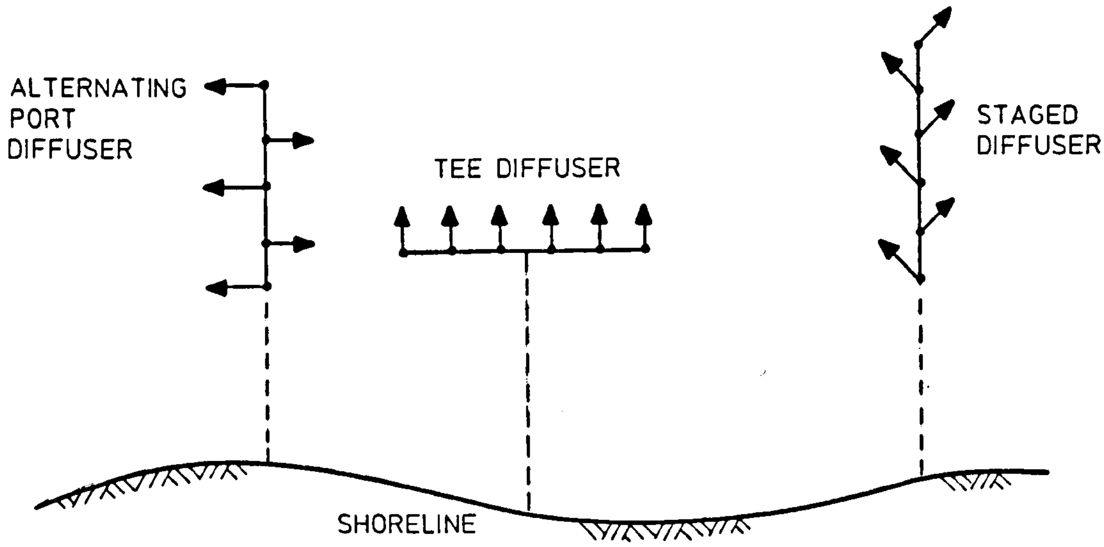

Typical diffuser configuration

Figure 2.11

Elsayed[23] also considers a staged multiport diffuser but he investigates the effects of the fluid buoyancy on the mixing characteristics from such a diffuser. This paper is another dealing with the effects of thermal rather than density stratification.

Earlier in this chapter, reference was made to the design of valves to prevent the intrusion of sea water into an outfall during periods of low or zero flow through the system[15]. Other references have also been noted regarding the development of valves[25]. During the design stages of the new San Francisco outfall it was decided to include valves on the riser heads because of the large differences in discharge requirements between summer and winter conditions. During summer the expected flows were approximately between 50 and 150 mgd

(180 and 570 mld) but during winter, peak flows exceeded 1500 mgd (5700 mld). The type of valve being investigated in this case was a "poppet" type, i.e. a type of valve which would open when pressures in the pipe become greater than the extended pressure of the seawater. Once the valve opened the effluent passed through a multiport diffuser and into the receiving water.

Another paper by Larsen[36] deals with the dispersion of sewage plumes discharged into the coastal zone. Larsen's paper describes a numerical model based on the Monte Carlo (or random walk) principle. The model traces the 3-dimensional path of every particle and the stochastic element of the movement is controlled by random numbers. The model can simulate the unsteady case of dilution from a sea outfall were both wind induced and tidal currents are taken into consideration.

The mathematical modelling of diffusion and dispersion of effluent discharged from sea outfalls is now becoming more widely used for determining the siting and length of any new marine discharges. For example, extensive simulation using a mathematical model coupled with information from field studies, has determined the length and positioning of the new outfall at Cowes on the Isle of Wight[38].

One of the major reasons for the development and use of computer models is the stricter requirements being imposed on outfall designers to achieve higher levels of diffusion and dispersion of sewage leaving the outfall and discharging into the receiving water. One of several new codes of practice published on outfall design is the European Community directives which were introduced to restore and improve the quality of bathing beaches around the coasts of Europe. In response to this document, the Water Research centre began a series of studies and experiments into the operation of sewage outfalls.

Previously WRc had undertaken work on various aspects of outfall design, such as initial dilution[3] from sewage outfalls to achieve efficient dispersion, in addition to comparing the effects of different discharge velocities[40]. The report on initial dilution[3] summarised available data on jet dilution in still water so that it could be applied to engineering design; it also indicated how jet dilution is affected when the body of receiving water is moving relative to the outfall; it also discusses the relevance of initial dilution to water quality criteria together with the determination of outfall length. The second WRc paper[40] deals with a topic which is probably the most disputed in outfall design, that is whether to provide high or low velocities of discharge from the diffuser section of the outfall. Unfortunately, the conclusions stated in the report are vague; mention being made that at the outfall sites examined there was no apparent advantage in producing a high jet velocity at the outlet ports. It also argues that because extra costs are involved in the need for a pumping system to produce high velocities, and extra land space required for storage, it is on balance better to use low discharge velocities.

WRc has continued with its research and has now produced, in 'draft' form, a design guide[43] which hopefully will be used for the design of all future outfalls. It is surprising that the United Kingdom which has been constructing outfalls for over a hundred years has only recently had published a design guide, whereas countries, such as New Zealand[61] have had guides for many years. The new WRc design guide has been written to assist engineers in the design and construction of efficient outfalls in order to achieve the standards and objectives laid down by the European Community. The guide covers the philosophy of outfall design, the environmental characteristics and impact predictions, the arrangement of headworks, the arrangements for outfall and diffuser arrangements and general hydraulic design. Incorporated within this document is a state of the art review of the methods of outfall design which includes several of the works cited and discussed earlier in this chapter.

CHAPTER 3

UNDERLYING THEORY AND NEW DEVELOPMENTS

3.1 Single Port Outfall

3.1.1 Analysis of a Single Port Outfall Under Wave Action

As a wave passes over the diffuser section of an outfall, changes in pressures acting on the diffuser occur, which causes fluctuations in the rate of sewage flows leaving the system. This change in pressure varies depending upon such factors as wave height and the ratio of wavelength to water depth (see section 3.2.5) - and is usually referred to as the attenuation of pressure. For this initial analysis it will be assumed that the wavelength to water depth ratio is such that the effluent discharge system will operate in a shallow water regime, and that the whole of the pressure exerted by the wave action will act upon the outfall. It will be seen later that this is a condition that leads to the greatest fluctuations in the rate of discharge and can, in consequence, be described as the worst case.

To begin the analysis, an outfall such as that shown in figure 3.1 is to be examined; this is a basic outfall arrangement in which flows enter the screening chamber at a constant rate prior to being discharged to the piped section of the outfall comprising a single outlet port at its downstream end. It is worth mentioning at this point that this technique of examining the behaviour of a single port outfall was previously undertaken by Henderson[27] as part of his investigation of the wider issues relating to multiport diffusers; the

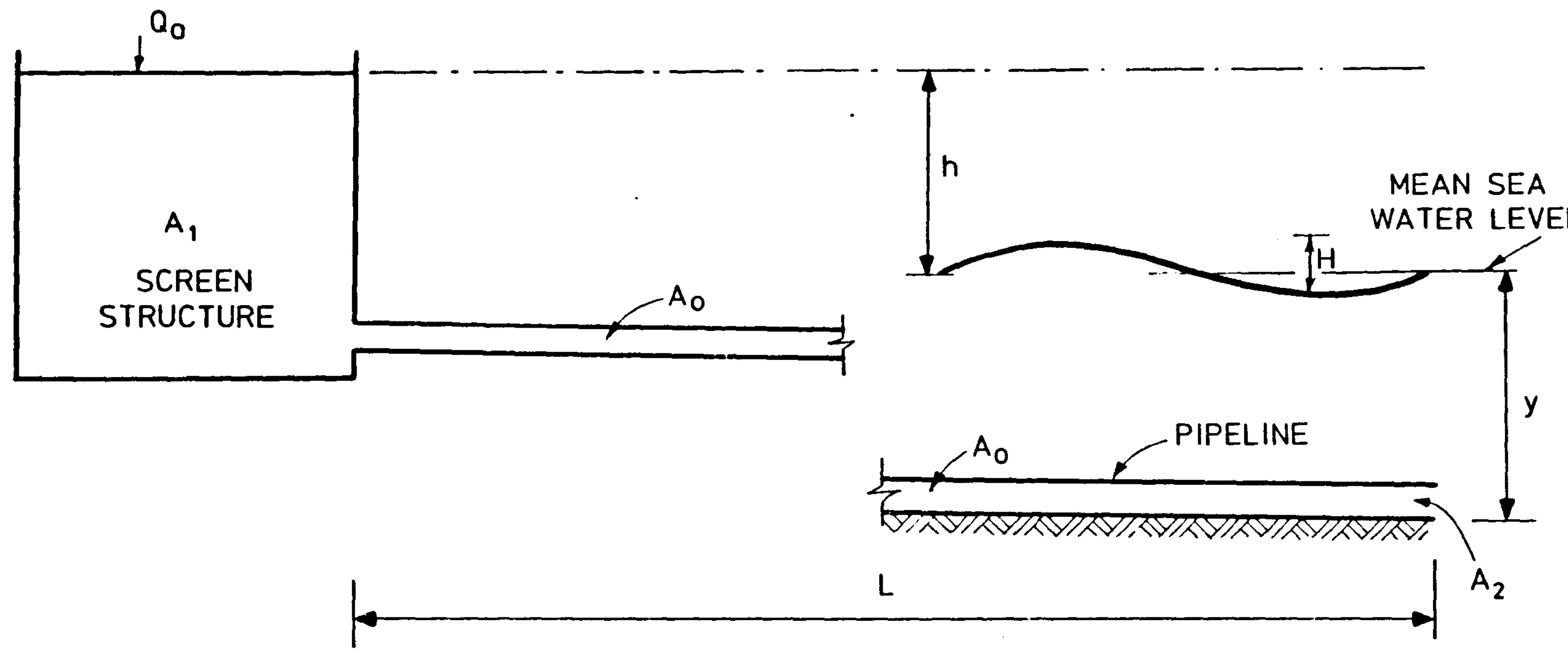

FIGURE 3.1. OUTFALL FOR INITIAL ANALYSIS

authors research of a multiport diffuser is described later in section 3.2 of this thesis. From Figure 3.1 the following symbols are defined:-

H_w - waveheight

h - difference in water levels between mean sea level and the water level within the screen structure

A_1 - area of screen structure

A_2 - area of outlet port

A_0 - area of outfall pipe

y - depth of sea water

T - wave period

L - length of outfall pipe and

Q_0 - steady flow into screen structure.

Taking figure 3.1 and applying the Bernoulli equation between the water level in the screen structure and the mean sea water level under steady conditions (no wave action) it can be seen that

$$h = \left[\frac{fL}{D} + \frac{A_o^2}{A_2^2}\right] \frac{V^2}{2g} \qquad (3.1)$$

where f - Darcy-Weisbach friction factor

D - pipe diameter and

V - velocity of flow in pipe

In equation (3.1) the first term (fL/D) represents the head lost due to frictional resistance within the pipe and the second term (A_0^2/A_2^2) gives the head lost at the exit of the pipe. For this simple analysis it was assumed the density of inflow into the outfall was equal to the density of the receiving water.

If waves act upon the end of the pipeline it can be seen from Figure 3.1 that the difference between the head in the screen structure and mean sea water level must vary as the waveheight varies, hence the difference in head between the screen structure and sea water level is given by

$$h - \frac{H_W}{2} \sin \frac{2\pi t}{T} \tag{3.2}$$

where t = the instantaneous time at a particular point during the wave period.

It is therefore necessary to ensure that the total head obtained from expression (3.2) is of sufficient magnitude to overcome the frictional resistance within the pipeline, supply on adequate velocity head at the outlet port and provide any acceleration head that may be required within the pipeline.

3.1.2 Calculation of Acceleration Head

If it is assumed that the liquid passing down the outfall pipe is incompressible then the assumption can also be made that within the pipeline a column of water will behave like a rigid rod; hence any change brought about at one end of the pipeline will immediately be transmitted to the other end, (see Webber[57]).

Figure 3.2 shows a uniform pipeline of length L and cross-sectional area A, connected to a reservoir or surge tank. The headloss due to friction is given by h_{Lf}. The discharge from the pipe is controlled by a valve (the increase in pressure due to wave action passing over the end of the outfall has a similar effect) at the downstream end of the pipeline. The mass of water in motion at any time is given by ρAL, where ρ is the density of the water. During a period of flow adjustment, caused by the closing of the valve, the

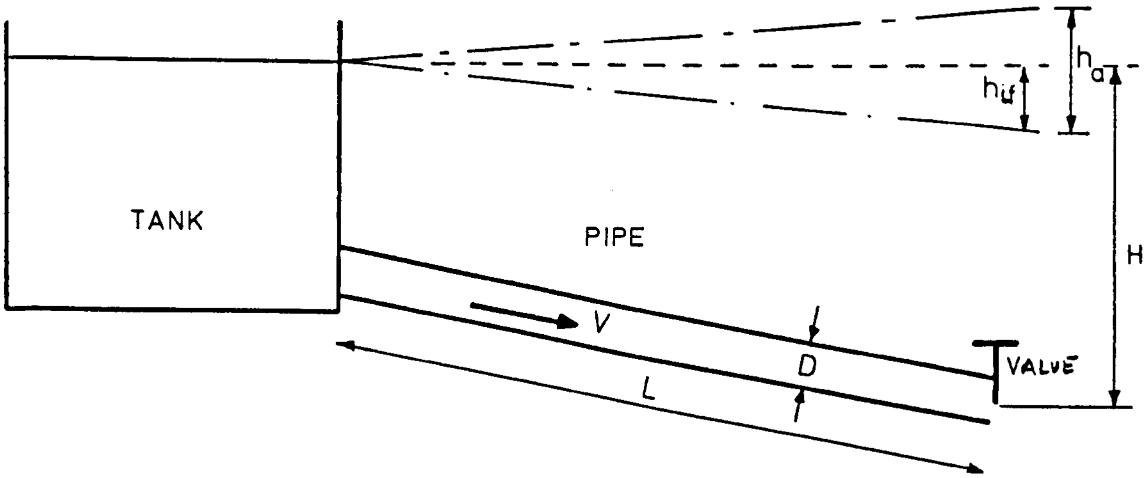

Figure 3.2

instantaneous velocity is V and the retardation is given by -dV/dt (negative because in this case +dv/dt would be seen as an acceleration term). Thus in accordance with Newtons second law of motion the pressure force at the valve is given by

$$\Delta p \ A = - \ \rho AL \frac{dV}{dt}$$

where Δp is the surge pressure superimposed onto the normal pressure. The dynamic, or acceleration, head term (h_a) at the valve is given by

$$h_a = \frac{\Delta p}{\rho g} = - \frac{L}{g}\frac{dV}{dt} \qquad (3.3)$$

3.1.3 Formulation of General Equation

From the foregoing analysis it can be deduced that the dynamic equation of motion for the outfall shown in figure 3.1 is (Henderson[27])

$$h - \frac{H_w}{2} \sin \left[\frac{2\pi t}{T}\right] = \left[\frac{fL}{D} + \frac{A_0{}^2}{A_2{}^2}\right] \frac{V^2}{2g} + \frac{L}{g}\frac{dV}{dt} \qquad (3.4)$$

and from the equation of continuity

$$Q_0 = A_1 \frac{dh}{dt} + A_0 V \qquad (3.5)$$

3.1.4 Solution of Equations 3.4 and 3.5

Equations (3.4) and (3.5) can be solved using either a simplified method such as that used by Henderson[27] or by using a numerical solution which is described below. In the simplified method Henderson obtained equation (2.12) which computes the extra storage required at the upstream end of an outfall as waves pass over its downstream end. Use of numerical techniques is more versatile as it permits the systematic variation of the parameters used in equations (3.4) and (3.5) so enabling the user to determine the optimum design for the outfall.

(a) The initial numerical model derived here was based on Escande's[31] finite difference method.

Using equation (3.5) initially, and letting $Q_0 = A_0V_0$ it follows that

$$V = V_0 - \frac{A_1}{A_0}\frac{dh}{dt} \tag{3.6}$$

Equation 3.4 can be rewritten as

$$h - \frac{H_w}{2}\sin\left[\frac{2\pi t}{T}\right] = \frac{f'V^2}{2g} + \frac{L}{g}\frac{dV}{dt} \tag{3.7}$$

where $f' = \dfrac{fL}{D} + \dfrac{{A_0}^2}{{A_2}^2}$

As friction will always act in the opposite direction to the motion of the fluid equation (3.7) can be rewritten as

$$h - \frac{H_w}{2}\sin\left[\frac{2\pi t}{T}\right] = \frac{f'V|V|}{2g} + \frac{L}{g}\frac{dV}{dt} \tag{3.8}$$

Differentiating equation (3.6) leaves an expression for the acceleration of the fluid within the main pipe, which is

$$\frac{dV}{dt} = -\frac{A_1}{A_0}\frac{d^2h}{dt^2}$$

and so by substituting for both V and dV/dt in equation (3.8) and by letting u equal dh/dt and du/dt equal d^2h/dt^2 the main equation for use in Escandes finite difference is obtained, as

$$h - \frac{H_W}{2} \sin\left[\frac{2\pi t}{T}\right] = \frac{f'}{2g} (V_0 - \frac{A_1}{A_0} u) \left| (V_0 - \frac{A_1}{A_0} u) \right| - \frac{L}{g} \frac{A_1}{A_0} \frac{du}{dt} \tag{3.9}$$

By rearranging equation (3.9) and replacing the differentials dt and du by small but finite differences, Δt and Δu respectively, equation (3.9) becomes

$$\Delta u = \frac{f' \ A_0 \ \Delta t}{2L \ A_1} (V_0 - \frac{A_1}{A_0} u) \left| (V_0 - \frac{A_1}{A_0} u) \right| - \frac{g \ A_0 \ \Delta t}{L \ A_1} h$$

$$+ \frac{g \ A_0 \ H_W}{2L \ A_1} \Delta t \sin(\frac{2\pi t}{T}) \tag{3.10}$$

Equation (3.10) is used to investigate theoretically the effects wave action has on an outfall. It is solved for successive time steps of Δt within the computer program called FINDIF2 VFORTRAN, described in Appendix D. For each iteration the values of surge velocity and surge height within the screen structure are increased as follows:-

$$u = u + \Delta u$$

$$\Delta h = u \quad \Delta t$$

$$h = h + \Delta h.$$

(b) The second numerical method of dealing with equations (3.4) and (3.5) is to use Runge-Kutta forward integration.

The necessary equations required for using this method are outlined below.

If a function is given such that

$$y'' = f(x,y,y')$$

where y' and y" are time differentials, then it can be solved using an iterative procedure by utilising the following equations

$$k1 = \frac{b^2}{2}\,[f(x,y,y')]$$

$$k2 = \frac{b^2}{2}\,[f(x + \frac{1}{2}\,b,\; y + \frac{b}{2}\,y' + \frac{k1}{4},\; y' + \frac{k1}{b})]$$

$$k3 = \frac{b^2}{2}\,[f(x + \frac{1}{2}\,b,\; y + \frac{b}{2}\,y' + \frac{k1}{4},\; y' + \frac{k2}{b})]$$

$$k4 = \frac{b^2}{2}\,[f(x + b,\; y + by' + k3,\; y' + \frac{2}{b}\,k3)]$$

$$\Delta y = \frac{1}{3}\,(k1 + k2 + k3)$$

$$\Delta y' = \frac{1}{3b}\,(k1 + 2k2 + 2k3 + k4)$$

Therefore,

$$y(x + b) = y(x) + b(y'(x)) + \Delta y$$

and

$$y'(x + b) = y'(x) + \Delta y'$$

where b is the step length for each iteration. The starting point for this analysis is equation (3.9) which is rearranged to give

$$\frac{d^2h}{dt^2} = \frac{A_0\ f'}{2L\ A_1}\ (V_0 - \frac{A_1}{A_0}\frac{dh}{dt})\,|(V_0 - \frac{A_1}{A_0}\frac{dh}{dt})| + \frac{g\ A_0\ H_w}{2L\ A_1}\ \sin(\frac{2\pi t}{T})$$

$$- \frac{g\ A_0\ h}{L\ A_1} \tag{3.11}$$

Equation 3.11 is then substituted into the Runge-Kutta equations to give values for k1 to k4.

$$k1 = \frac{(dt)^2}{2}\ [\frac{A_0\ f'}{2L\ A_1}\ (V_0 - \frac{A_1}{A_0}\frac{dh}{dt})\,|(V_0 - \frac{A_1}{A_0}\frac{dh}{dt})|$$

$$+ \frac{g\ A_0\ H_w}{2L\ A_1}\ \sin(\frac{2\pi t}{T}) - \frac{g\ A_0\ h}{L\ A_1}]$$

$$k2 = \frac{(dt)^2}{2}\ [\frac{A_0\ f'}{2L\ A_1}\ (V_0 - \frac{A_1}{A_0}\ (\frac{dh}{dt} + \frac{k1}{dt}))\ \ |(V_0\ \frac{A_1}{A_0}\ (\frac{dh}{dt} + \frac{k1}{dt}))|$$

$$+ \frac{g\ A_0\ H_w}{2L\ A_1}\ \sin\ (\frac{2\pi(t + \frac{dt}{2})}{T}) - \frac{g\ A_0}{L\ A_1}\ \ (h + \frac{dt\ \frac{dh}{dt}}{2} + \frac{k1}{4})]$$

$$k3 = \frac{(dt)^2}{2}\ [\frac{A_0\ f'}{2L\ A_1}\ (V_0 - \frac{A_1}{A_0}\ (\frac{dh}{dt} + \frac{k2}{dt}))\,|(V_0 - \frac{A_1}{A_0}\ (\frac{dh}{dt} + \frac{k2}{dt}))|$$

$$+ \frac{g\ A_0\ H_w}{2L\ A_1} \sin(\frac{2\pi(t + \frac{dt}{2})}{T}) - \frac{g\ A_0}{L\ A_1} (h + \frac{dt\ x \frac{dh}{dt}}{2} + \frac{k1}{4})]$$

$$k4 = \frac{(dt)^2}{2} [\frac{A_0\ f'}{2L\ A_1} (V_0 - \frac{A_1}{A_0} (\frac{dh}{dt} + \frac{2k3}{dt})) | (V_0 - \frac{A_1}{A_0} (\frac{dh}{dt} + \frac{2k3}{dt})) |$$

$$+ \frac{g\ A_0\ H_w}{2L\ A_1} \sin(\frac{2\pi(t + dt)}{T}) - \frac{g\ A_0}{L\ A_1} (h + \frac{dt\ x\ dh}{dt} + k3)]$$

As in the previous finite difference method, small time steps of dt are required for a satisfactory solution to be obtained from the equations k1 to k4.

Computer program FINDIF VFORTRAN (Appendix D) was written to solve the equations k1 to k4 and the results were compared with those obtained using Escandes finite difference method. The results were utilised in the production of the paper by Ali, Burrows and Mort[5] - a copy of which is included in Appendix F.

3.1.5 Boundary Conditions

Before either set of equations can be used in a mathematical model, a set of equations have to be obtained to model the boundary conditions at the upstream and downstream ends of the outfall.

The upstream boundary condition is determined by the amount of liquid in the screen structure while the downstream condition is determined by the instantaneous water depth over the outfall. The initial conditions within the outfall (time (t) = 0) are assumed to be steady, and the waveheight acting over the outfall set to zero. The flow rate passing through the system is equal to Q_0 and so from equation (3.7) it can be deduced that

$$h = \frac{f' V^2}{2g}$$

where h represents the driving head required to overcome the friction head in the pipeline, and provide a constant discharge at the downstream end.

It was found from preliminary applications of the computer programs that a time step (dt) of between 1/5 and 1/10 of the ambient wave period produced the best results within a reasonable time limit, if the time step selected was too large some of the minor oscillations were omitted and the oscillatory motion within the outfall would not be completely defined. (See appendix D and paper by Ali, Burrows and Mort[5] given in appendix F).

3.2 Multiport Outfall

3.2.1 Analysis of a Multiport Outfall

The analysis of a multiport outfall is more complex than that of a single-port system, because each riser on the manifold will be subject to different driving heads as waves pass across the system. Furthermore, it may be envisaged that should individual risers consist of several separate outlet ports, then each port will be subjected to various increases or decreases in wave pressure, which will dictate instantaneous discharge. However, these differences should be small due to the limited spatial separations and hence these effects can be neglected in analysis of the complete outfall system. Because there would be a need to analyse each riser individually, it is not feasible to employ the earlier technique described in Section 3.1.1. Moreover it would be difficult to understand the behaviour of an outfall whose multiport system is subjected to wave action. In addition effluent output is dependent on the upstream head which is probably different for each of the adjacent risers.

Mathematically modelling a multiport manifold is complex, requiring the application of continuity and momentum equations for unsteady flow within the system. The approach adopted for a solution to the problem is similar to that followed by Larsen(35). The derivation of the equations used in the model is given below.

3.2.2 Equation of Motion

The equation of motion is derived by the application of Newtons second law of motion, in the axial direction, to the element of fluid shown in Figure 3.3, (see Streeter and Wylie(53)).

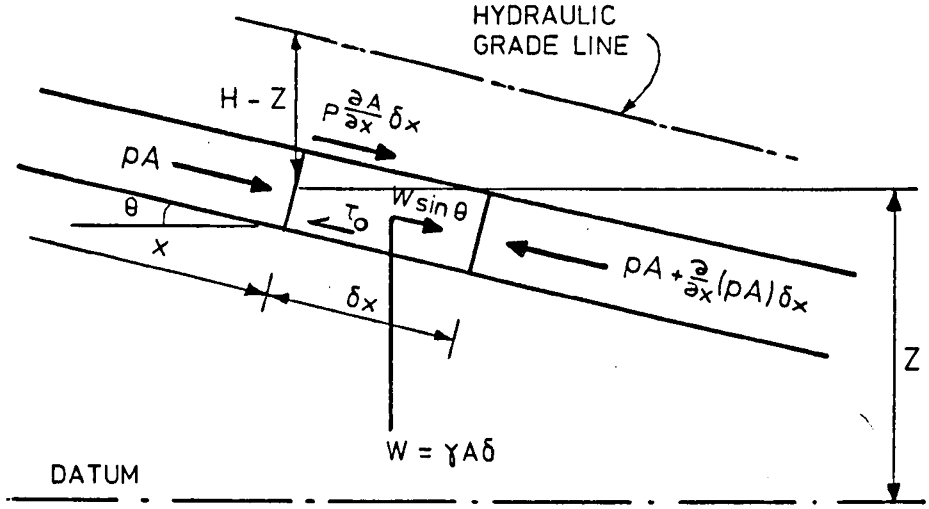

Definition sketch showing forces acting on an element of fluid within the outfall pipe

Figure 3.3

Applying Newtons second law of motion to the free body gives

$$pA - [pA + \frac{\partial}{\partial x}(pA)\ \delta x] + p\frac{\partial A}{\partial x}\ \delta x + \gamma A\ \delta x\ \sin\theta - \tau_0\ \pi D\ \delta x$$

$$= \rho A\ \delta x\ \frac{dV}{dt} \qquad (3.12)$$

where p = pressure

A = cross sectional area of body

γ = specific weight of fluid (= ρg)

ρ = density of liquid

τ_0 = wall shear stress

D - pipe diameter

V - velocity of fluid in pipe

t - time and

θ - inclination of pipe to horizontal.

Equation (3.12) is divided through by the mass of the element, $\rho A \delta x$, to give

$$-\frac{1}{\rho}\frac{\partial p}{\partial x} + g \sin \theta - \frac{4 \tau_0}{\rho D} = \frac{dV}{dt} \tag{3.13}$$

The pipe pressures can be expressed in terms of the elevation of the hydraulic grade line; so

$$p = \rho g(H - z) \tag{3.14}$$

which leads to

$$\frac{\partial p}{\partial x} = \rho g(\frac{\partial H}{\partial x} - \frac{\partial z}{\partial x}) \tag{3.15}$$

From figure 3.3 $\partial z/\partial x = - \sin \theta$ and so by substituting equation (3.15) into equation (3.13) the equation of motion becomes

$$g \frac{\partial H}{\partial x} + \frac{4 \tau_0}{\rho D} + \frac{dV}{dt} = 0 \tag{3.16}$$

In the case of steady turbulent flow

$$\tau_0 = \rho f \frac{V^2}{8} \tag{3.17}$$

where f = Darcy-Weisbach friction factor, and the assumption is made that the friction factor in unsteady flow is the same as in steady flow. So the equation of motion becomes

$$g \frac{\partial H}{\partial x} + \frac{dV}{dt} + \frac{f\ V^2}{2D} = 0 \tag{3.18}$$

Since friction always acts in the opposite direction to the equation of motion, V^2 must be written as $V|V|$ to provide the correct sign. So by introducing this into equation (3.18) and expanding the acceleration term the equation of motion for use in this analysis becomes

$$g \frac{\partial H}{\partial x} + V \frac{\partial V}{\partial x} + \frac{\partial V}{\partial t} + \frac{f\ V|V|}{2D} = 0 \tag{3.19}$$

3.2.3 Equation of Continuity

The equation of continuity for the unsteady flow situation is applied to the control volume of fluid shown in figure 3.4.

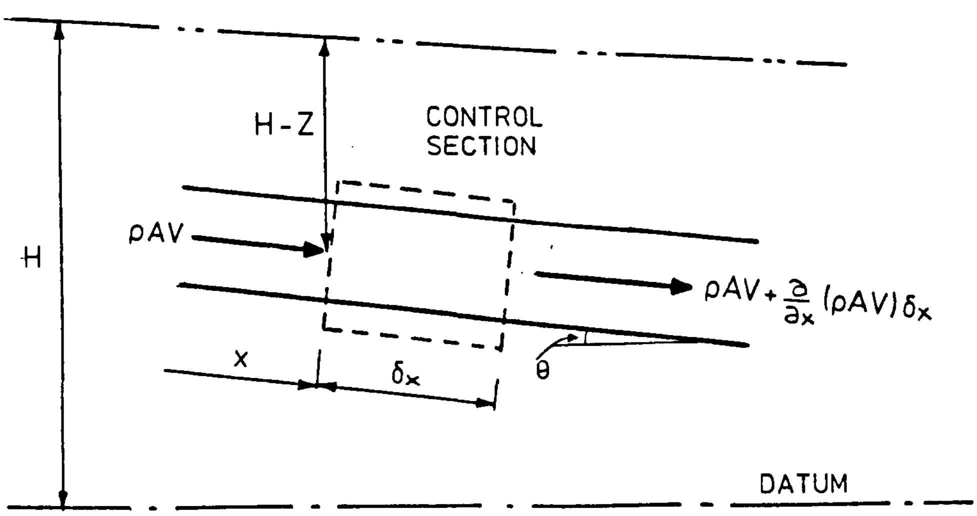

Control volume for derivation of continuity equation

Figure 3.4

The continuity equation obtained from the control volume is given by

Rate at which mass enters the control volume

= Rate at which mass leaves the volume

+ Rate of increase of mass within the volume

and in equation form

$$\rho AV = [\rho AV + \frac{\partial}{\partial x}(\rho AV)\,\delta x] + \frac{\partial}{\partial t}(\rho A\ \delta x) \tag{3.20}$$

in which δx is not a function of t. Equation (3.20) can be reduced to give

$$-\frac{\partial}{\partial x}(\rho AV)\,\delta x = \frac{\partial}{\partial t}(\rho A\ \delta x)$$

By expanding this equation and dividing through by the mass, $\rho A\ \delta x$ leaves

$$\frac{V}{A}\frac{\partial A}{\partial x} + \frac{1}{A}\frac{\partial A}{\partial t} + \frac{V}{\rho}\frac{\partial \rho}{\partial x} + \frac{1}{\rho}\frac{\partial \rho}{\partial t} + \frac{\partial v}{\partial x} = 0 \tag{3.21}$$

Now

$$\frac{1}{A}\frac{dA}{dt} = \frac{1}{A}\frac{\partial A}{\partial x}\frac{dx}{dt} + \frac{1}{A}\frac{\partial A}{\partial t} = \frac{V}{A}\frac{\partial A}{\partial x}\quad\frac{1}{A}\frac{\partial A}{\partial t} \tag{3.22}$$

therefore $\{dA/dt/A\}$ can be substituted into equation (3.21) in place of the first two terms. Similarly it can be shown that $\{(d\rho/dt)/\rho\}$ can be substituted for the third and fourth terms, so equation (3.21) becomes

$$\frac{1}{A}\frac{dA}{dt} + \frac{1}{\rho}\frac{d\rho}{dt} + \frac{\partial v}{\partial x} = 0 \tag{3.23}$$

The first term of equation (3.23) deals with elasticity of the wall and its rate of deformation as the pressure within the pipe changes and the second term takes into account the compressibility of the liquid.

Initially whilst looking at outfall pipes in general, it was not anticipated that compressibility would be a major factor in the behaviour of the fluid; so this is now considered more closely. If a pipe is flowing full of water, considered incompressible, and the wall of the pipe is perfectly rigid then if a decrease in fluid velocity at the downstream end of the pipe occurred, (caused for example by an increase in pressure due to wave action or a valve being closed), all the particles of fluid within the pipe would have to decelerate together. From Newtons second law of motion the force acting on the valve or other constriction at closure is given by

$$F = m\frac{dV}{dt}$$

where F = force and

m = mass of fluid

and so if the closure was instantaneous then dt $\rightarrow$ 0 and the force would become infinite. This indicates that deceleration of the fluid within a pipe does not take place instantaneously and that the fluid within the pipe must be to some extent compressible. This is shown in the following diagram which demonstrates how the fluid in the pipe reacts on sudden closure of a valve.

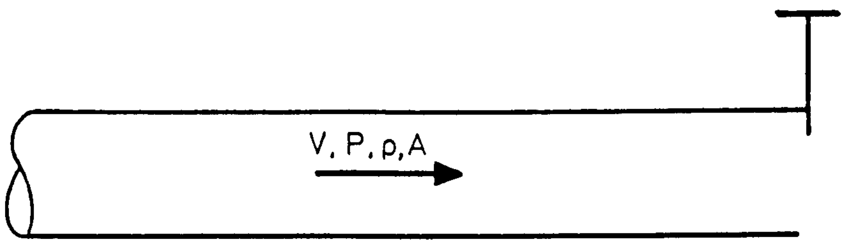

a) Initial conditions: valve open

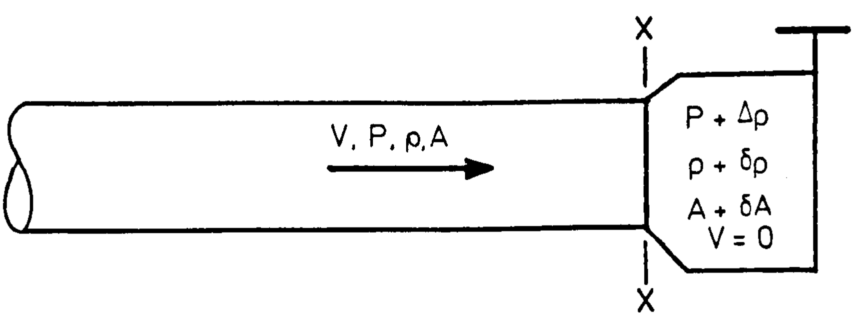

b) Valve just closes

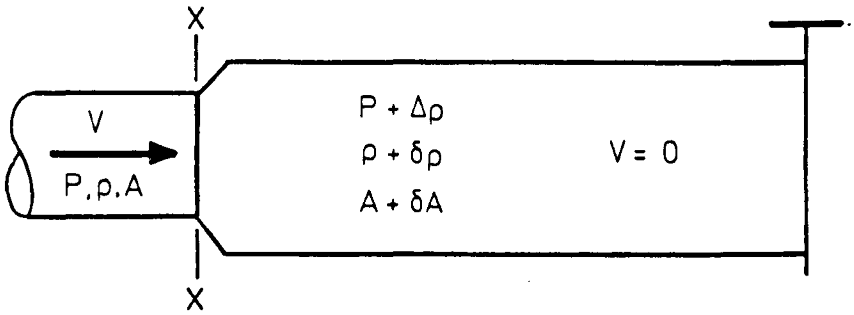

c) A short time later

Figure 3.5

Just before closure of the valve the pipe is flowing full of water (figure 3.5a) moving with a velocity, V; if the valve is now shut the fluid immediately next to the valve is brought to rest whilst the fluid upstream continues to flow as if nothing has happened. Consequently, the fluid next to the valve is compressed slightly and its pressure is increased. To accommodate this increase in pressure the pipe, which is no longer assumed to be perfectly rigid, expands. The next element of fluid now finds an increased pressure in front of it and so it too comes to rest, is then compressed and expands the pipe slightly. This process continues until all the fluid in the pipe has been brought to rest. The line across the pipe, denoted by x-x in figure 3.5 represents a discontinuity and is usually termed the pressure wave or pressure transient.

In the case of wave action acting upon the end of the pipe the fluid within the pipe may not actually come to rest. In this case it is a reduction in the velocity of flow which causes the pressure transient as shown in Fig. 3.6.

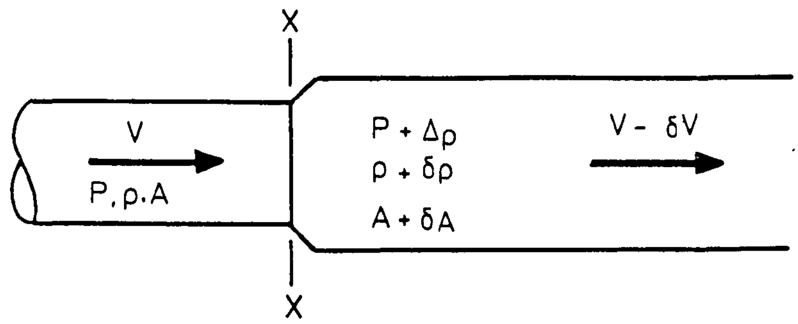

Diagram Showing Pressure Transient as Wave Pressure

Over the End of the Pipe Increases

Figure 3.6

After deriving equation (3.23) it can be deduced that values have to be obtained for the speed at which the pressure wave passes along the pipe as this will govern rate of deformation of the pipe.

As previously mentioned, the first term of equation (3.23) deals with the elasticity of the pipe wall and its rate of deformation with pressure. From Fig. 3.7 it can be deduced that the rate of change of tensile force per unit length is given by

$$\frac{D}{2}\frac{dp}{dt}$$

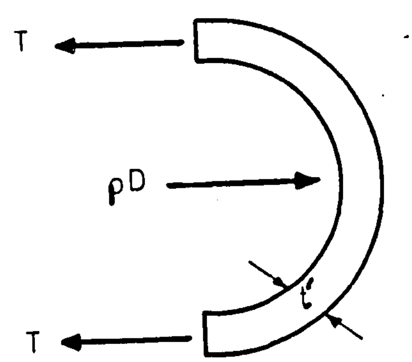

Tensile Force in Pipe Wall

Figure 3.7

Dividing this by the wall thickness gives the rate of change of unit stress

$$[(\frac{D}{2t'}) \frac{dp}{dt})]$$

and dividing by the Young's modulus of elasticity for the pipe wall gives the rate of unit strain,

$$\text{rate of unit strain} = (\frac{D}{2t'E}) \frac{dp}{dt}$$

where E = Young's modulus of elasticity.

Multiplying this by the radius gives the radial extension and so by multiplying the radial extension by the perimeter the rate of area increase is obtained, viz

$$\frac{dA}{dt} = \frac{D}{2t'E} \frac{dp}{dt} \frac{D}{2} \pi D$$

hence

$$\frac{1}{A} \frac{dA}{dt} = \frac{D}{t'E} \frac{dp}{dt} \tag{3.24}$$

The compressibility of a liquid is given by its bulk modulus of elasticity

$$k = - \frac{dp}{(\frac{dV_L}{V_L})} = \frac{dp}{(\frac{d\rho}{\rho})}$$

where V_L = volume

and k = bulk modulus of elasticity

and the rate of change of density divided by density gives

$$\frac{1}{\rho}\frac{d\rho}{dt} = \frac{1}{k}\frac{dp}{dt} \tag{3.25}$$

Substituting the values obtained in equation (3.24) and (3.25) into equation (3.23) gives

$$\frac{1}{k}\frac{dp}{dt}\left(1 + \frac{kD}{Et'}\right) + \frac{\partial V}{\partial x} = 0 \tag{3.26}$$

By dividing equation (3.26) through by $\rho(1 + kD/Et')$ and setting

$$a^2 = \frac{\left(\frac{k}{\rho}\right)}{\left(1 + \left(\frac{k}{E}\right)\left(\frac{D}{t'}\right)\right)}$$

equation (3.26) becomes

$$\frac{1}{\rho}\frac{dp}{dt} + a^2\frac{\partial V}{\partial x} = 0 \tag{3.27}$$

The equation which gives a^2 is sometimes written as

$$a^2 = \frac{\left(\frac{k}{\rho}\right)}{\left(1 + \left(\frac{k}{E}\right)\left(\frac{D}{t'}\right)C_1\right)}$$

where C_1 is unity for a pipeline with expansion joints. The value of 'a' is defined as the speed with which the pressure wave is transmitted along the pipe. From Fig. 3.4 it can be seen that

$$p = \rho g(H - z)$$

therefore

$$\frac{dp}{dt} = V \frac{\partial p}{\partial x} + \frac{\partial p}{\partial t} = V\rho g \left(\frac{\partial H}{\partial x} - \frac{\partial z}{\partial x}\right) + \rho g \left(\frac{\partial H}{\partial t} - \frac{\partial z}{\partial t}\right)$$

The change of ρ with respect to x or t is much less than the change of H with respect to x or t, so ρ is considered constant; also as pipes are generally fixed in position $\partial z/\partial t = 0$ and $\partial z/\partial x = -\sin\theta$; hence

$$\frac{1}{\rho}\frac{dp}{dt} = Vg \left(\frac{\partial H}{\partial x} + \sin\theta\right) + g \frac{\partial H}{\partial t} \qquad (3.28)$$

and the continuity equation for a compressible liquid in an elastic pipe is obtained by substituting for $1/\rho \; dp/dt$ in equation (3.27) leaving

$$\frac{a^2}{g}\frac{\partial v}{\partial x} + V \frac{\partial H}{\partial x} + \frac{\partial H}{\partial t} + V \sin\theta = 0 \qquad (3.29)$$

3.2.4 Solution of equations (3.19) and (3.29)

Equations (3.19) and (3.29), the equations of motion and continuity, are used in the mathematical model to determine the effects that wave action has on a complete outfall system so enabling unsteady flow analysis. These equations open the way for calculating the velocity of flow inside each individual riser and the hydraulic head across the system. The equations are solved using the method of characteristics[53] solution which is outlined below.

The two equations are combined and rearranged using an unknown multiplier λ so that they become

$$[\frac{\partial H}{\partial x}(V + \lambda g) + \frac{\partial H}{\partial t}] + \lambda\ [\frac{\partial v}{\partial x}(V + \frac{a^2}{g\lambda}) + \frac{\partial v}{\partial t}] + V \sin\theta$$

$$+ \lambda\ f\ \frac{v|v|}{2D} = 0 \qquad (3.30)$$

The equation has been arranged in such a way that the first term, would be equal to dH/dt if

$$\frac{dx}{dt} = V + \lambda g \qquad (3.31)$$

and similarly the second term in brackets would equal dV/dt if

$$\frac{dx}{dt} = V + \frac{a^2}{g\lambda} \qquad (3.32)$$

As equations (3.31) and (3.32) must be equal then

$$V + \lambda g = V + \frac{a^2}{g\lambda}$$

implying that

$$\lambda = \pm \frac{a}{g}$$

By substituting for λ in the above equations, four equations (called characteristic equations) are obtained such that

$$\left.\begin{aligned} &\frac{dH}{dt} + \frac{a}{g}\frac{dv}{dt} + V \sin\theta + \frac{af\, v|v|}{2gD} = 0 \\ &\frac{dx}{dt} = V + a \end{aligned}\right] \quad \beta+$$

$$\left.\begin{aligned} &\frac{dH}{dt} - \frac{a}{g}\frac{dv}{dt} + V \sin\theta - \frac{af\, v|v|}{2gD} = 0 \\ &\frac{dx}{dt} = V - a \end{aligned}\right] \quad \beta-$$

In the calculations to follow it is generally found that the value of 'a' is much greater than the value of V and so $dx/dt = \pm a$. The calculation using the method of characteristics can now be carried out using the rectangular mesh indicated in figure 3.8.

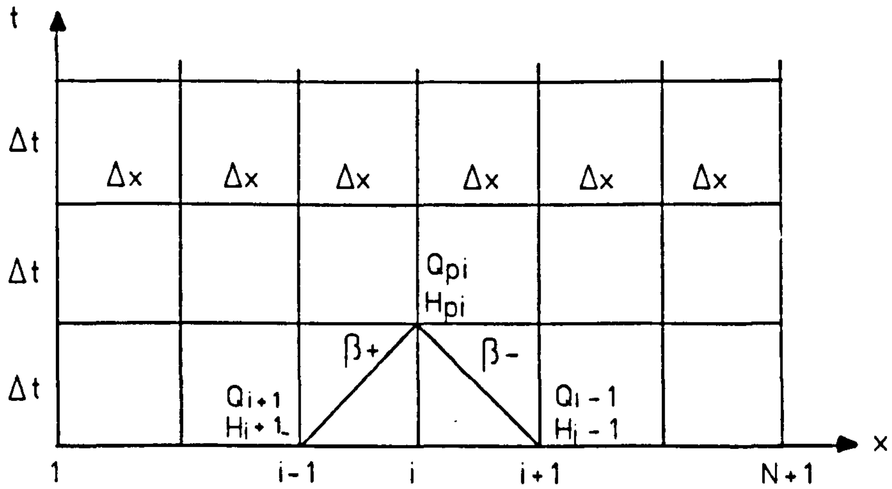

Rectangular Grid for Solution of Characteristics Equations

<u>**Figure 3.8**</u>

The horizontal lines on the grid represent the outfall pipe and the positions of points 1 to N + 1 are shown in Fig. 3.9 below.

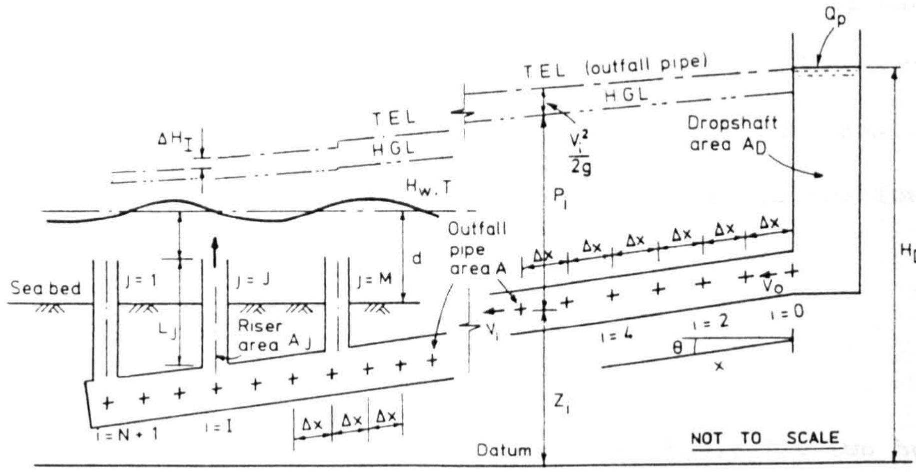

Figure showing positions of points 1 to N+1 in outfall pipeline

Figure 3.9

The mesh only calculates the conditions within the horizontal section of the outfall and the risers are dealt with separately and this is detailed later within this section. For the mesh at time t = 0 the pipe is realising its initial conditions, i.e. there is zero flow passing through the pipe or there is steady flow passing through the pipe but in each case there is no wave action acting on the system. The program then steps through values of Δt, changing the values of the conditions for points 1 through to N + 1. In the case of the mesh drawn in Fig. 3.8 the lines β+ and β- are straight as the value of 'a' is greater than the value of V. If the value of 'a' was not very much larger than V, V would remain in the dx/dt equations and the characteristic equations would be curved. They would then not necessarily meet at such a clearly defined point, as shown in Fig. 3.8. In the case of curved characteristic lines further interpolation would be required to find the point of intersection. From the diagram (figure 3.8) it can be seen that the time step of each calculation is $\Delta t = \Delta x/a$ and that at time $t = 0$ the value of H and 'a' at each grid point along the pipe must be known. Hence the solution is carried out along the characteristics, starting from known conditions and by finding new intersections so that heads and velocities are found for later times.

3.2.5 Boundary Conditions

As previously mentioned all outfall pipes have basically two boundary conditions. The upstream condition is dependent upon the type of inlet arrangement to the outfall, this may be either a gravity fed or pumped system, the downstream condition is governed by the normal pressure of the sea water caused by its density and height above the outfall and the additional pressure caused by wave action at the sea water surface. A detailed description of the boundary conditions is give below:-

(a) Upstream Boundary Conditions

The program (SFLOW FORTRAN) offers a choice of two upstream boundary conditions; they are either a pumped flow into the outfall, or a header tank allowing flow to gravitate into the outfall. The essential difference between the two upstream boundary conditions is that when the flow is pumped it is assumed that the pump generates a constant head whereas in the case of the header tank the head within the tank will vary. If the outfall to be modelled mathematically uses a pump to move the water from storage tanks to a drop shaft then the upstream boundary condition should be taken as an upstream reservoir with an area equal to that of the drop shaft.

(b) Downstream Boundary Conditions

The downstream boundary is governed by the wave condition, the sea water level and density, coupled with the number of risers contained within the manifold or diffuser system. The wave form generated by the program is that of a sinusoidal wave, the height of which varies from riser to riser depending upon the ratio of the riser spacing to wavelength. The variation in pressure acting upon each riser due to a change in wave height is obtained using the following expression:-

$$\Delta p = \rho_s \, g\eta \left[\frac{\cosh \frac{2\pi}{\lambda_L} (H_s - z)}{\cosh \frac{2\pi H_s}{\lambda_L}} \right] \tag{3.33}$$

where Δp = pressure change due to wave action

ρ_s = density of sea water

λ_L = wavelength

H_s = water depth

z = distance from mean sea water level to top of riser and

$$\eta = \frac{H_w}{2} \sin 2\pi \left(\frac{x}{\lambda_L} - \frac{t}{T}\right) \text{ = water surface elevation} \tag{3.34}$$

where H_w = wave height

x = distance along the direction of propagation of the wave measured from the point directly above riser 1 (see Fig. 3.10)

t = instantaneous time

T = wave period

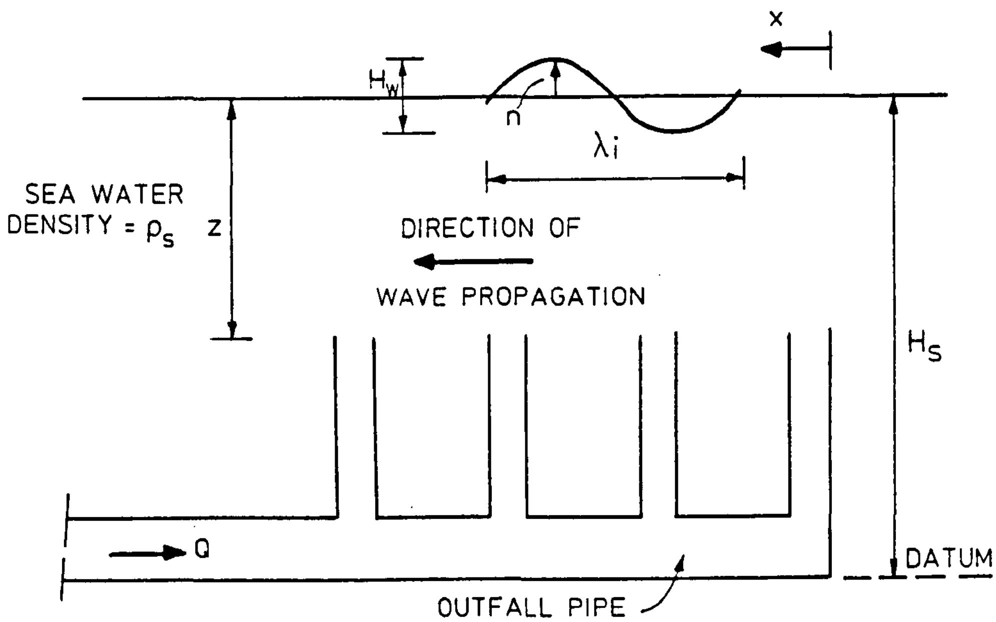

Figure 3.10

Equation (3.33) effectively reduces the change in pressure caused by the wave action as the depth to the top of the riser increases. Under a shallow water wave, one in which H_s-z/λ_L < 1/20, all the pressure caused by an increase in waveheight will act on the outfall, in intermediate depth this will vary and in deep water, H_s-z/λ_L > 1/2 very little of the pressure will act upon the outfall.

3.2.6 Modelling of Individual Risers

a) Velocity in Risers

The risers themselves are not modelled mathematically using the finite difference mesh shown in figure 3.8, instead an inertia method is used (usually termed lumped inertia, Wylie and Streeter[64]) as the speed with which the pressure wave passes through a short narrow pipe is substantially quicker than for the main pipe. Due to the high speed of the pressure wave and the short length of the riser pipe the change in flow within a riser pipe is almost instantaneous along its length as the pressure changes over the outlet port. The lumped inertia method uses the initial equation

$$F_1 - F_3 - F_f - F_w = \frac{\gamma A_2 L_2}{g} \frac{dv}{dt} \qquad (3.35)$$

where referring to figure 3.11

F_1 = pressure force at section (1)

F_3 = pressure force at section (3)

F_f = frictional force on fluid caused by wall shear stress

F_w = force due to weight of fluid

γ = weight of fluid

The remaining symbols are derived in figure 3.11.

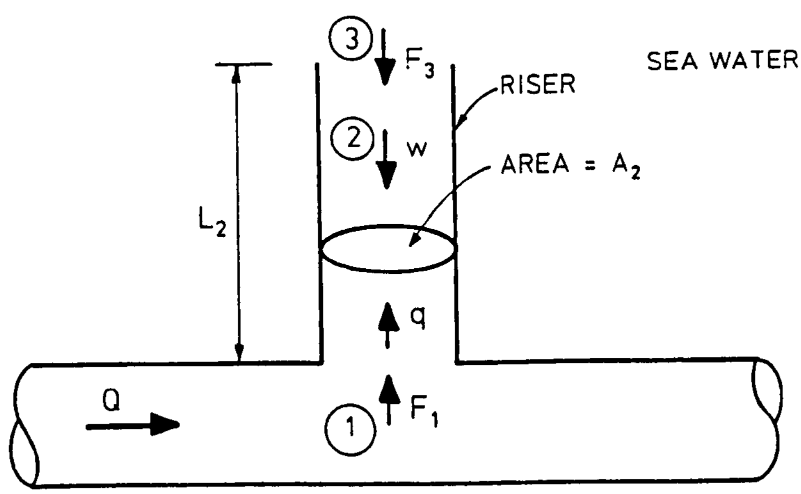

Figure 3.11

b) Riser/Main pipe connection

One of the more important areas of mathematical modelling within the outfall structure is the junction between the individual risers of the manifold and the main outfall pipe itself.

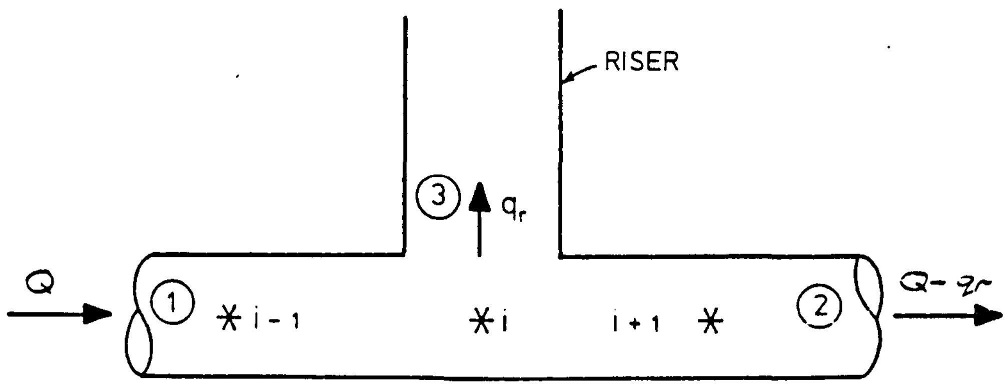

Diagram Showing Main Pipe to Riser Connector

Figure 3.12

Where from figure 3.12 q_r − flow in riser

$*$ − the calculation points which correspond with the mesh shown in figure 3.8.

At a connection such as the one shown in figure 3.12 above, it is essential that the continuity equation and equation of momentum be satisfied at all times; the method used by Streeter and Wylie[53] to calculate this particular type of boundary conditions is to assume that there is a constant head loss across the intersection. This may be a valid assumption for the analysis of long pipelines but when relatively short risers form the junctions and there is a relatively short length of pipe between them, it is obvious from the Bernoulli equation that there is a rise in the pressure head across the junction, as shown in Fig. 3.13, if the main outfall pipe remains a constant diameter throughout. The rise in pressure head is not as large as that calculated from the Bernoulli equation due to additional 'energy' losses caused by a disruption to the flow field as some of the fluid enters the riser. If no correction is made to accommodate the change in pressure head then the numerical model will produce inaccurate results.

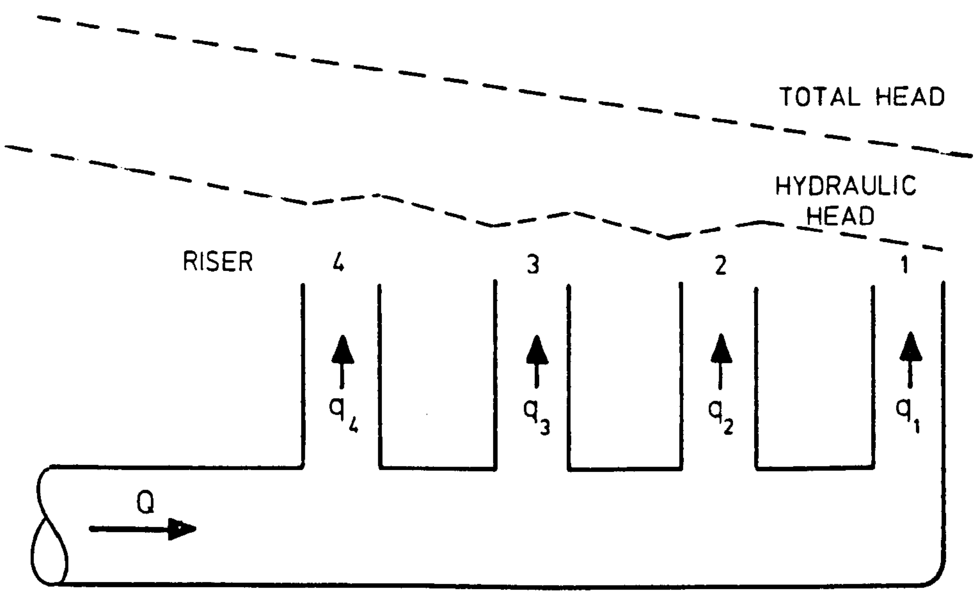

Diagram Showing how Hydraulic Head Varies Across a Manifold which is Attached to a Pipe of Constant Cross Section

<u>Figure 3.13</u>

To overcome this problem of unbalanced flow many outfalls are tapered towards the end riser, but because this was not the case with the model, the analysis had to be changed to accommodate the actual system. If the equations had not been corrected the analysis would have produced incorrect flow rates within the individual risers. With reference to Fig. 3.12 the equations used for calculating the discharge and hydraulic head at a 'riser-outfall' intersection are given by Streeter and Wylie(53) as

$$Qp_i = - \frac{Hp_i}{CH} + \frac{Cp_1}{CH} \tag{3.36}$$

$$- Qp_{i+1} = - \frac{Hp_i}{CH} + \frac{C_m}{CH} \tag{3.37}$$

$$- q_{pr} = - \frac{Hp_i}{C} + \frac{C_1}{C} \tag{3.38}$$

where Hp_i = common hydraulic head at intersection

Qp_i, Qp_{i+1} = flow rates at points i and i+1 respectively

$CH = \frac{a}{gA}$

A = area of outfall tunnel and

$C = \frac{2 L_r}{g A_r \Delta t}$

where L_r = length of riser

A_r = area of riser and

Δt = time step for calculations.

The values of C_p, C_m and C_1 are calculated using the following equations

$$C_p = H_{i-1} + Q_{i-1} \; [CH_{i-1} - R_{i-1} \; |Q_{i-1}|]$$

$$C_m = H_{i+1} + Q_{i+1} \; [R_{i+1} \; |Q_{i+1}| - CH_{i+1}]$$

and $C_1 = H_T - H_B + q_r \; [R_R \; |q_r| - C]$

where with reference to Fig. 3.12

H_{i-1}, H_{i+1} = the hydraulic heads at points (i-1) and (i+1) respectively one time step previous

Q_{i-1}, Q_{i+1} = the flow rates at points (i-1) and (i+1) respectively one time step previous

R_{i-1}, R_{i+1} = the pipe friction losses and are given by

$$R_{i-1} = \frac{f_{i-1}\ \Delta x}{2gD\ A_{i-1}^{2}}$$

and
$$R_{i+1} = \frac{f_{i+1}\ \Delta x}{2gD\ A_{i+1}^{2}}$$

where f = friction factor.

For the equation to calculate C_1

H_T = the hydraulic head at the top of the riser one time step previously

H_B = the hydraulic head at the bottom of the riser one time step previously and

R_R = the friction losses due to flow in the riser and is given by

$$R_R = \frac{f\ L_r}{2gd\ A_r^{2}}$$

where d = diameter of riser pipe.

So from these equations it can be seen that C_p, C_m and C_1 are calculated from the values obtained for the parameters one time step earlier. Equation (3.37) is modified to take into account the change in head across a riser/main pipe junction, and so becomes

$$-Qp_{i+1} = -\frac{Hp_i}{CH} + \frac{C_m}{CH} - \frac{H_I}{CH} \tag{3.39}$$

where H_I is the change in head across the junction.

H_I increases or decreases depending upon the conditions within the outfall and the iterative procedure for the calculation is repeated. If the outfall being modelled is tapered through the diffuser section then the value of H_I is set to zero as it is assumed that the tapering should balance the the flow rate through the risers under steady state conditions.

3.2.7 Outstanding Limitations of the theoretical modelling

Introduction of a density difference between the discharging fluid and the heavier sea water creates no serious difficulty in the numerical model until a point is reached where internal driving heads at certain sections become inadequate and saline intrusion into the system results. At this point the numerical model becomes inadequate and a mass balance model must be added to describe the dispersion of the saline influx through the diffuser manifold. The resulting changes in fluid densities within the outfall system will affect the hydrodynamics of the system.

As observed, both in the field and in the laboratory, there is a great resistance to mixing between the two fluids and stratification normally occurs in the main outfall pipe as a consequence of saline intrusion. This in turn leads to the formation of a saline wedge. This, therefore, may entail a knowledge of the characterisation of a saline wedge, as this may have an influence on the flow hydrodynamics within the outfall pipe.

3.3 Saline Wedges

3.3.1 Analysis of Saline Wedges in Pipes

To complement the previous work on oscillations within an outfall it is essential to predict the length to which the saline wedge will extend once it has penetrated the outfall tunnel. The initial method of investigating this was to determine the profiles and lengths of saline wedges in open ended outfall pipes.

Although work has been carried out by various researchers into the effects of saline wedges within open ended pipes, it has been mainly experimental observations that have been made with little or no theoretical work being produced to model the effects (see Chapter 2). It was therefore relevant to undertake an investigation into the theoretical mechanics of a salt wedge before carrying out experimental investigations so that an attempt could be made to compare the theoretical predictions with the experimental results.

The mathematical model is derived here and draws from references cited in part 1 of Chapter 2. Definition sketches for the analysis are shown in Fig. 3.14, where the notations are

ρ_1, ρ_2 - respective densities of upper and lower layers ($\rho_2 > \rho_1$)

V_1, V_2 - respective velocities

d_1, d_2 - respective depths of upper and lower layers

z - height of pipe invert above datum

S_0 - slope of outfall pipe

τ_0 - wall shear stress

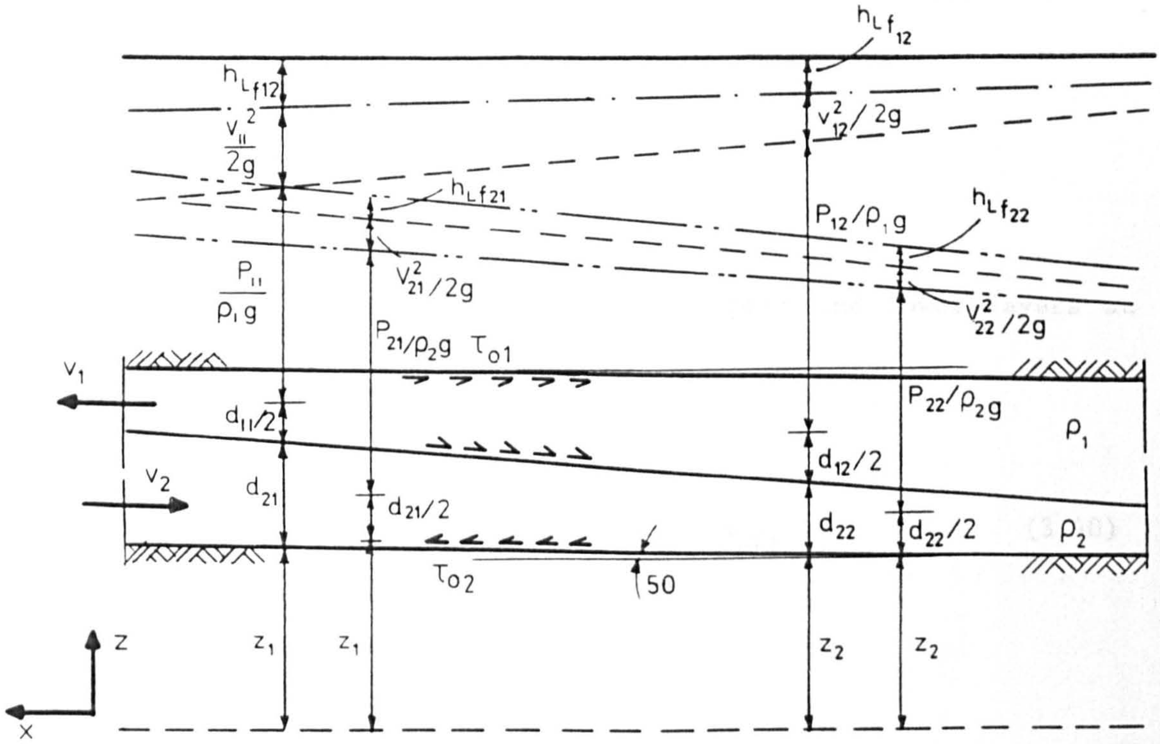

FIGURE 3.14a

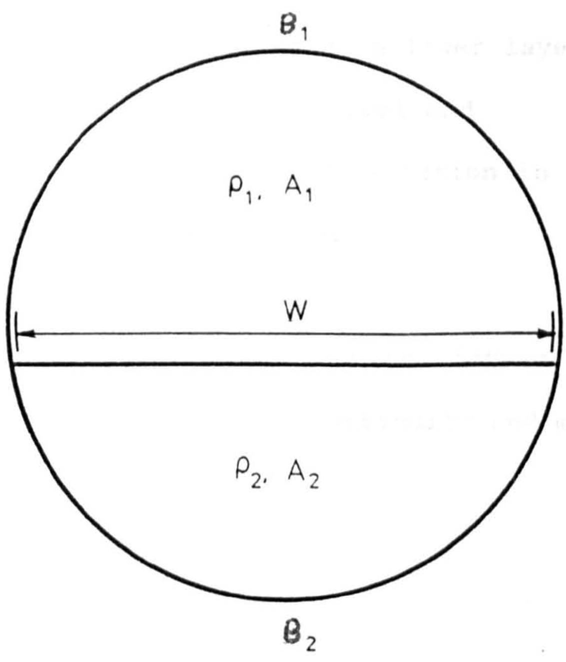

FIGURE 3.14b

FIGURES FOR USE IN SALINE WEDGE ANALYSIS

τ_i = interfacial shear stress

P_1, P_2 = pressure in fresh and salt water respectively

A_1, A_2 = area of fresh and salt water respectively

W = width of interface between two layers

B_1, B_2 = respective perimeter lengths.

Taking the total energy equations for the upper and lower layers at section 1 in Fig. 3.11a it is found that

$$H_1 = \frac{P_{11}}{\rho_1 g} + \frac{V_{11}^2}{2g} + \frac{1}{2} d_{11} + d_{21} + z_1 + h_{Lf1} \tag{3.40}$$

and

$$H_2 = \frac{P_{21}}{\rho_2 g} + \frac{V_{21}^2}{2g} + \frac{1}{2} d_{21} + z_1 + h_{Lf2} \tag{3.41}$$

where H_1 = total energy head at upstream end of pipe

H_2 = total energy head in lower layer, taken originally as the sea water level and

h_{Lf1}, h_{Lf2} = head losses due to friction in the upper and lower layers respectively .

As mentioned earlier within this chapter, for calculations involving the flow of water the equations of continuity and momentum must at all times be satisfied.

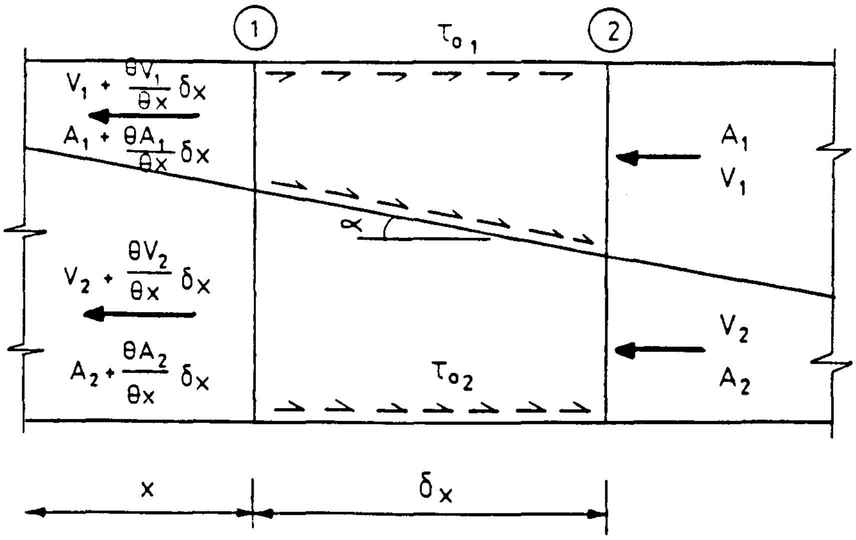

Figure 3.15

From Fig. 3.15 the equation of continuity for the upper layer is given as

$$V_1 A_1 = (V_1 + \frac{\partial V_1}{\partial x}\ \delta x)(A_1 + \frac{\partial A_1}{\partial x}\ \delta x) \tag{3.42}$$

and so by expanding and neglecting second order terms

$$A_1 \frac{\partial V_1}{\partial x} + V_1 \frac{\partial A_1}{\partial x} = 0 \tag{3.43}$$

and similarly for the lower layer

$$A_2 \frac{\partial V_2}{\partial x} + V_2 \frac{\partial A_2}{\partial x} = 0 \tag{3.44}$$

The next stage is to look at the momentum equations for each layer, these are found by applying Newtons second law of motion to the element of fluid which is δx long and lies between boundaries (1) and (2) in Fig. 3.15. For the upper layer

$$p_1A_1 - [(p_1 + \frac{\partial p_1}{\partial x}\delta x)(A_1 + \frac{\partial A_1}{\partial x}\delta x)] + p_1\frac{\partial A_1}{\partial x}\delta x$$

$$+ \gamma(A_1 + \frac{\partial A_1}{\partial x}\delta x)\delta x \cos\beta - \tau_{01}\ \delta x(B_1 + \frac{\partial B_1}{\partial x}\delta x)$$

$$- \tau_i\ \delta x(W + \frac{\partial W}{\partial x}\delta x)\cos\alpha = Q\rho((V_1 + \frac{\partial V_1}{\partial x}\delta x) - V_1) \qquad (3.45)$$

By expanding equation (3.45) and neglecting second order terms the equation becomes

$$- A_1\frac{\partial p}{\partial x} - \rho_1 g(A_1 + \frac{\partial A_1}{\partial x}\delta x)(\frac{1}{2}\frac{\partial d_1}{\partial x} + \frac{\partial d_2}{\partial x} + \frac{\partial z}{\partial x}) - T_1 = Q\rho\frac{\partial V_1}{\partial x}$$

(3.46)

where $T_1 = \tau_0(B_1 + \frac{\partial B_1}{\partial x}\delta x) + \tau_i(W + \frac{\partial W}{\partial x}\delta x)$

and $\cos\alpha = 1$ and $\cos\beta = \frac{1}{2}\frac{\partial d_1}{\partial x} + \frac{\partial d_2}{\partial x} + \frac{\partial z}{\partial x}$

The derivation of the angles α and β is given in Appendix C.

Taking equation (3.46) and letting $Q = V_1A_1$ and then dividing through by $\rho_1 A_1 g$ leaves

$$- \frac{1}{\rho_1 g}\frac{\partial p_1}{\partial x} - \frac{1}{A_1}(A_1 + \frac{\partial A_1}{\partial x}\delta x)(\frac{1}{2}\frac{\partial d_1}{\partial x} + \frac{\partial d_2}{\partial x} + \frac{\partial z}{\partial x})$$

$$- \frac{T_1}{\rho_1 g\ A_1} = \frac{V_1}{g}\frac{\partial V_1}{\partial x} \qquad (3.47)$$

The equation of momentum for the lower layer is given as

$$p_2A_2 - [(p_2 + \frac{\partial p_2}{\partial x}\delta x)(A_2 + \frac{\partial A_2}{\partial x}\delta x)] + p_2\frac{\partial A_2}{\partial x}\delta x$$

$$- \rho_2 g(A_2 + \frac{\partial A_2}{\partial x}\delta x)\delta x \cos\beta_2 - \tau_0\ \delta x(B_2 + \frac{\partial B_2}{\partial x}\delta x)$$

$$- \tau_i(W + \frac{\partial W}{\partial x}\delta x)\delta x \cos\alpha = Q_2\rho_2((V_2 + \frac{\partial V_2}{\partial x}\delta x) - V_2) \tag{3.48}$$

and expanding and eliminating second order differentials produces

$$-A_2\frac{\partial p_2}{\partial x} - \rho_2 g(A_2 + \frac{\partial A_2}{\partial x}\delta x)(\frac{1}{2}\frac{\partial d_2}{\partial x} + \frac{\partial z}{\partial x}) - T_2 = Q_2\rho_2\frac{\partial V_2}{\partial x} \tag{3.49}$$

where $T_2 = \tau_{02}(B_2 + \frac{\partial B_2}{\partial x}\delta x) + \tau_i(W + \frac{\partial W}{\partial x}\delta x)$

and $\cos\alpha = 1$ and $\cos\beta_2 = (\frac{1}{2}\frac{\partial d_2}{\partial x} + \frac{\partial z}{\partial x})$

By letting $Q_2 = V_2A_2$ and dividing through by ρ_2A_2g leaves

$$-\frac{1}{\rho_2 g}\frac{\partial p_2}{\partial x} - \frac{1}{A_2}(A_2 + \frac{\partial A_2}{\partial x}\delta x)(\frac{1}{2}\frac{\partial d_2}{\partial x} + \frac{\partial z}{\partial x}) - \frac{T_2}{\rho_2 g\,A_2} = \frac{V_2}{g}\frac{\partial V_2}{\partial x} \tag{3.50}$$

Equations (3.47) and (3.50) are the momentum equations for the upper and lower layers in a form in which they are ready to use for further analysis.

If a saline wedge develops within a pipe it is obvious that the pressure across the interface of the two liquids must be constant and so from Fig. 3.14

$$P_1 + \frac{1}{2}\rho_1 g\, d_1 = P_2 - \frac{1}{2}\rho_2 g\, d_2$$

Differentiating this equation with respect to x leaves

$$\frac{\partial p_1}{\partial x} + \frac{1}{2}\rho_1 g\frac{\partial d_1}{\partial x} = \frac{\partial p_2}{\partial x} - \frac{1}{2}\rho_2 g\frac{\partial d_2}{\partial x}$$

Substituting for $\partial p_2/\partial x$ into equation (3.50) and rearranging leaves

$$\frac{\partial p_1}{\partial x} = -\frac{1}{2}\rho_1 g\frac{\partial d_1}{\partial x} - \frac{1}{2}\rho_1 g\frac{\partial d_2}{\partial x} - \frac{\rho_2 g}{A_2}\left(A_2 + \frac{\partial A_2}{\partial x}\delta x\right)\left(\frac{1}{2}\frac{\partial d_2}{\partial x} + \frac{\partial z}{\partial x}\right)$$

$$- \frac{T_2}{A_2} - \rho_2 V_2\frac{\partial V_2}{\partial x} \qquad (3.51)$$

Substituting for $\partial p_1/\partial x$ in equation (3.47) gives

$$-\frac{1}{\rho_1 g}\left[-\frac{1}{2}\rho_1 g\frac{\partial d_1}{\partial x} - \frac{1}{2}\rho_2 g\frac{\partial d_2}{\partial x} - \frac{\rho_2 g}{A_2}\left(A_2 + \frac{\partial A_2}{\partial x}\delta x\right)\left(\frac{1}{2}\frac{\partial d_2}{\partial x} + \frac{\partial z}{\partial x}\right)\right.$$

$$\left.- \frac{T_2}{A_2} - \rho_2 V_2\frac{\partial V_2}{\partial x}\right] - \frac{1}{A_1}\left(A_1 + \frac{\partial A_1}{\partial x}\delta x\right)\left(\frac{1}{2}\frac{\partial d_1}{\partial x} + \frac{\partial d_2}{\partial x} + \frac{\partial z}{\partial x}\right) - \frac{T_1}{\rho_1 g\, A_1}$$

$$- \frac{V_1}{g}\frac{\partial V_1}{\partial x} \tag{3.52}$$

upon expansion this becomes

$$\frac{1}{2}\frac{\partial d_1}{\partial x} + \frac{1}{2}\frac{\rho_2}{\rho_1}\frac{\partial d_2}{\partial x} + \frac{\rho_2}{\rho_1 A_2}(A_2 + \frac{\partial A_2}{\partial x}\delta x)(\frac{1}{2}\frac{\partial d_2}{\partial x} + \frac{\partial z}{\partial x}) + \frac{T_2}{\rho_1 g\, A_2}$$

$$+ \frac{\rho_2}{\rho_1 g} V_2 \frac{\partial V_2}{\partial x} - \frac{1}{A_1}(A_1 + \frac{\partial A_1}{\partial x}\delta x)(\frac{1}{2}\frac{\partial d_1}{\partial x} + \frac{\partial d_2}{\partial x} + \frac{\partial z}{\partial x}) - \frac{T_1}{\rho_1 g\, A_1}$$

$$= \frac{V_1}{g}\frac{\partial V_1}{\partial x} \tag{3.53}$$

Taking the equations of continuity for the upper and lower layers it can be found from equation (3.43) that

$$\frac{\partial A_1}{\partial x} = - \frac{A_1}{V_1}\frac{\partial V_1}{\partial x} \tag{3.54}$$

and from equation (3.44) that

$$\frac{\partial V_2}{\partial x} = \frac{V_2}{A_2}\frac{\partial A_2}{\partial x} \tag{3.55}$$

and substituting for $\partial A_1/\partial x$ and $\partial v_2/\partial x$ in equation (3.53) gives

$$\frac{1}{2}\frac{\partial d_1}{\partial x} + \frac{1}{2}\frac{\rho_2}{\rho_1}\frac{\partial d_2}{\partial x} + \frac{\rho_2}{\rho_1 A_2}(A_2 + \frac{\partial A_2}{\partial x}\delta x)(\frac{1}{2}\frac{\partial d_2}{\partial x} + \frac{\partial z}{\partial x}) + \frac{T_2}{\rho_1 g\ A_2}$$

$$- \frac{\rho_2}{\rho_1}\frac{V_2{}^2}{gA_2}\frac{\partial A_2}{\partial x} - \frac{1}{A_1}(A_1 - \frac{A_1}{V_1}\frac{\partial V_1}{\partial x}\delta x)(\frac{1}{2}\frac{\partial d_1}{\partial x} + \frac{\partial d_2}{\partial x} + \frac{\partial z}{\partial x}) - \frac{T_1}{\rho_1 g\ A_1}$$

$$= \frac{V_1}{g}\frac{\partial V_1}{\partial x} \tag{3.56}$$

Restricting attention now to a stationary salt wedge, it follows that $V_2 = 0$ and substituting this into equation (3.56) and rearranging

$$\frac{1}{2}\frac{\partial d_1}{\partial x} + \frac{1}{2}\frac{\rho_2}{\rho_1}\frac{\partial d_2}{\partial x} + \frac{\rho_2}{\rho_1}(1 + \frac{1}{A_2}\frac{\partial A_2}{\partial x}\delta x)(\frac{1}{2}\frac{\partial d_2}{\partial x} + \frac{\partial z}{\partial x}) + \frac{T_2}{\rho_1 g\ A_2}$$

$$- (1 - \frac{1}{V_1}\frac{\partial V_1}{\partial x}\delta x)(\frac{1}{2}\frac{\partial d_1}{\partial x} + \frac{\partial d_2}{\partial x} + \frac{\partial z}{\partial x}) - \frac{T_1}{\rho_1 g\ A_1} = \frac{V_1}{g}\frac{\partial V_1}{\partial x} \tag{3.57}$$

Substituting small but finite differences for the differentials produces

$$\frac{1}{2}\frac{\Delta d_1}{\Delta x} + \frac{1}{2}\frac{\rho_2}{\rho_1}\frac{\Delta d_2}{\Delta x} + \frac{\rho_2}{\rho_1}A_{s2}(\frac{1}{2}\frac{\Delta d_2}{\Delta x} + S_0) - \frac{T_2}{\rho_1 g\ A_2}$$

$$- A_{s1}(\frac{1}{2}\frac{\Delta d_1}{\Delta x} + \frac{\Delta d_2}{\Delta x} + S_0) - \frac{T_1}{\rho_1 g\ A_1} = \frac{V_1}{g}\frac{\Delta V_1}{\Delta x} \tag{3.58}$$

where $A_{s1} = (1 - \frac{\Delta V_1}{V_1})$

$A_{s2} = (1 + \frac{\Delta A_2}{A_2})$ and

$$S_0 = \frac{\Delta z}{\Delta x} = \text{pipe slope.}$$

Then rearranging equation (3.58) leaves an equation for Δx in the form

$$\Delta x = \frac{\left[\frac{\Delta d_1}{2} + \frac{\rho_2}{2\rho_1} \Delta d_2 + \frac{\rho_2}{2\rho_1} A_{S2} \Delta d_2 - \frac{1}{2} A_{S1} \Delta d_1 - A_{S1} \Delta d_2 - \frac{V_1}{g} \Delta V_1\right]}{\left[\frac{T_1}{\rho_1 g A_1} - \frac{T_2}{\rho_1 g A_2} + A_{S1} S_0 - \frac{\rho_2}{\rho_1} A_{S2} S_0\right]} \tag{3.59}$$

3.3.2 Shear Stress Parameters

The shear stress parameters estimate the head losses within the flowing layer caused by the wall and interfacial friction acting upon it. The wall shear stresses for the upper and lower layers are given as

i) for the upper layer

$$\tau_{01} = f \frac{\rho_1}{8} |V_1| V_1 \tag{3.60}$$

ii) and for the lower layer as

$$\tau_{02} = f \frac{\rho_2}{8} |V_2| V_2 \tag{3.61}$$

where f = friction factor.

The friction factor is determined by using the Colebrook-White equation which is written as

$$\frac{1}{\sqrt{f}} = -2.0 \log\left[\frac{k}{14.8R} + \frac{2.51}{R_e\sqrt{f}}\right] \tag{3.62}$$

where k = roughness of the pipe

R_e = Reynolds number of flowing layer and

R = hydraulic radius of flowing layer.

The interfacial shear stress is given as

$$\tau_i = f_i \frac{\bar{\rho}}{8} |V_1 - V_2| (V_1 - V_2) \tag{3.63}$$

for the upper flowing layer, and as

$$\tau_i = f_i \frac{\bar{\rho}}{8} |V_2 - V_1| (V_2 - V_1) \tag{3.64}$$

for the stagnant lower layer

where f_i = interfacial friction factor and

$$\bar{\rho} = \frac{\rho_1 + \rho_2}{2}$$

As noted in Section 2.1 there are many expressions derived from field and laboratory data for the value of the interfacial friction factor, but as no data is available for the interfacial friction factor within a pipe then the values of friction factor had to be treated with caution.

3.3.3 Boundary Conditions

There are two boundary conditions taken for this mathematical model; these are (i) the upstream condition and (ii) the exit condition.

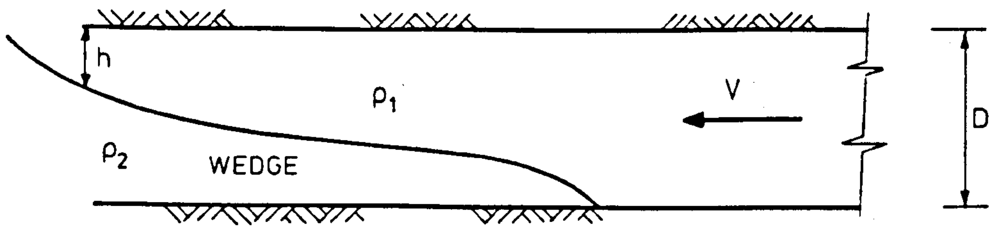

Horizontal Outfall Pipe Showing Assumed Position of Saline Wedge

Figure 3.16

At the upstream boundary condition it is assumed that the height of the wedge is zero and so the pipe is flowing full of sewage. At the exit to the pipe, which is taken as the downstream condition, an expression has to be found for calculating the value of h as shown on Fig. 3.16. The problem to be confronted at the exit of the pipe is the high curvature as the fluid with the lower density is acted on by buoyancy effects and redirects itself towards the sea surface. This emerging flow then form the plumes around which Brookes[11] and others have carried out research work on the trajectories of circular jets. The boundary condition required for the saline wedge model is the height, h, of the flow stream at exit and the local curvature within the pipe. A detailed analytical study of this was recently undertaken by Ali[4] in an unpublished derivation and is reproduced here in full.

ii) Analytical Study of Exit Condition

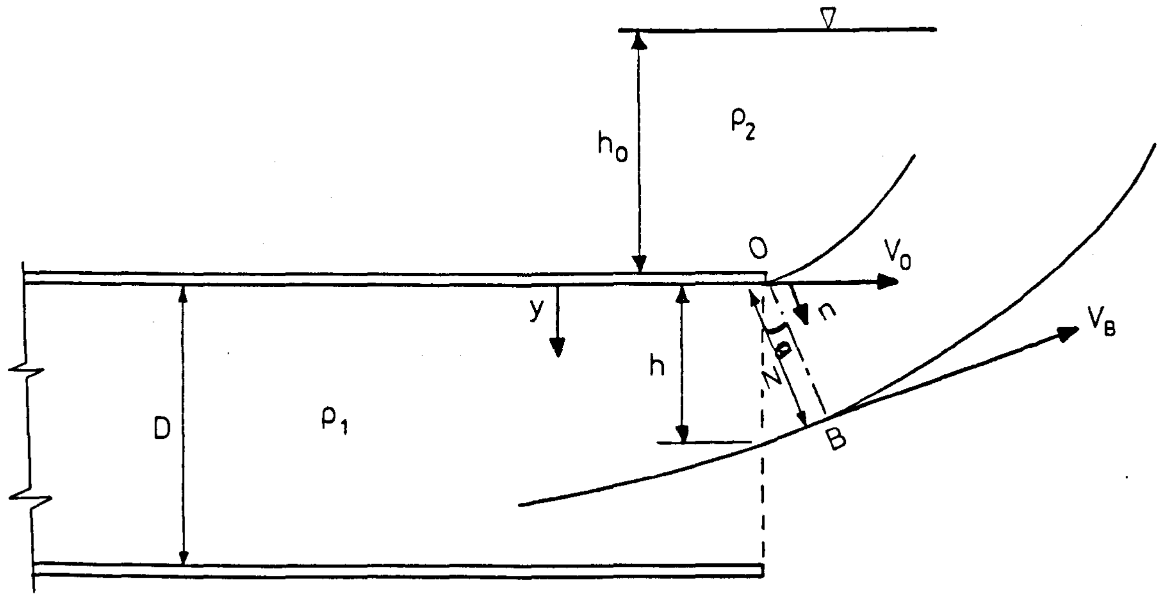

Diagram showing boundary conditions at exit of pipe

Figure 3.17

Figure 3.17 shows the flow conditions at the downstream end of an open ended outfall. In the region being investigated it is assumed that the shape of the exit jet from just inside the pipe to just past the exit remains unaltered. Assuming irrotational flow at section OB gives

$$\frac{\partial v}{\partial n} = -\frac{v}{r} \qquad (3.65)$$

where v = local tangential velocity

r = local radius of curvature and

n = normal distance from 0.

It is next assumed that the local radius of curvature (r) varies linearly with n, hence

$$r = R_0 + mn \tag{3.66}$$

where R_0 = average radius of curvature at 0 and

m = constant.

Substituting for r in equation (3.65) and rearranging gives

$$\frac{\partial v}{v} = - \frac{\partial n}{(R_0 + mn)} \tag{3.67}$$

and by integrating this with respect to n

$$\ell n \ v = - \frac{1}{m} \ell n \ (R_0 + mn) + k \tag{3.68}$$

where k = constant of integration.

From Fig. 3.17 it can be seen that when $n = 0$, $v = v_0$ and so

$$k = \ell n \ v_0 + \frac{1}{m} \ell n \ R_0$$

Substituting for k in equation (3.7.8) and simplifying leaves

$$\frac{v}{v_0} = [\frac{R_0}{(R_0 + mn)}]^{1/m} \tag{3.69}$$

The variation of the length of normal N with h is given as

$$h = \int_0^N \cos \theta \ dn \tag{3.70}$$

and the variation of θ with n, which is assumed to be linear, is

$$\theta = \theta_0 + k_2 n \tag{3.71}$$

This equation is differentiated to give $d\theta = k dn$ and substituting for dn in equation (3.70) gives

$$h = \frac{1}{k} \int_{\theta_0}^{\theta_B} \cos \theta \, d\theta$$

$$= \frac{1}{k} [\sin \theta_B - \sin \theta_0] \tag{3.72}$$

where $\theta_B = \theta_0 + kN$.

The next stage is to investigate the discharge equation for the flowing upper layer leaving the pipe. If it is assumed that θ is small then it can also be assumed that $h = N$. The area of flow leaving the pipe is determined with reference to Fig. 3.18.

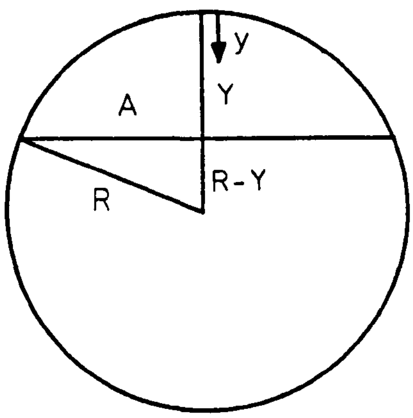

Figure 3.18

The area of the upper segment of the circle is given by

$$A = \frac{D^2\ 2 \cos^{-1}\ (\frac{R - y}{R})}{8} - \frac{D^2 \sin\ (2 \cos^{-1}\ (\frac{R - y}{R}))}{8} \tag{3.73}$$

where D = diameter of pipe

R = radius of pipe and

y = normal distance measured from the top of the pipe.

Equation (3.73) gives an exact result for the area of flow, but the overall equation is difficult to handle so by using a series expansion equation (3.73) becomes

$$\frac{A}{\bar{A}} = a_0(\frac{y}{D})^3 + b_0(\frac{y}{D})^2 + c_0(\frac{y}{D}) \tag{3.74}$$

where $\bar{A}$ = total pipe cross sectional area

a_0 = -1.1622

b_0 = 1.7416 and

c_0 = 0.4196.

The values of a_0, b_0 and c_0 are the constants obtained when equation (3.74) is derived from first principles.

Differentiating equation (3.74) with respect to y gives

$$dA = \frac{\bar{A}}{D}\ [a\ (\frac{y}{D})^2 + b(\frac{y}{D}) + c]dy \tag{3.75}$$

where $a = -3.4866$

$b = 3.4832$ and

$c = 0.4196$.

The velocity distribution across the outlet area is given by equation (3.69) and by putting n = y equation (3.69) becomes

$$V = V_0 [\frac{R_0}{(R_0 + my)}]^{1/m} \tag{3.76}$$

hence the discharge through a differential area, dA, is given by

$$dQ = \frac{V_0 R_0^{1/m} \bar{A}}{D(R_0 + my)^{1/m}} [a(\frac{Y}{D})^2 + b(\frac{Y}{D}) + c]dy \tag{3.77}$$

therefore the total discharge is given by

$$Q = \frac{V \bar{A} R^{1/m}}{D} \int_0^h \frac{a(\frac{Y}{D})^2 + b(\frac{Y}{D}) + c}{(R_0 + my)^{1/m}} dy \tag{3.78}$$

This equation can be integrated by putting $\varphi = y/D$, and so making dy = Dd and dy = $Dd\varphi$ yielding

$$Q = V_0 \bar{A} (\frac{R_0}{D})^{1/m} \int_0^{\varphi_B} \frac{(a\varphi^2 + b\varphi + c)}{(\bar{R} + m\varphi)^{1/m}} d\varphi \tag{3.79}$$

where $\varphi_B = \frac{h}{D}$ and $\bar{R} = \frac{R_0}{D}$.

By putting

$$I = \int_0^{\varphi_B} \frac{a\varphi^2 + b\varphi + c}{(\bar{R} + m\varphi)^{1/m}} d\varphi$$

the final equation for the flow rate through the section is

$$Q = V_0 \bar{A} (\frac{R_0}{D})^{1/m} I. \tag{3.80}$$

The equation for I can be solved in the following way; putting

$$I = aI_1 + bI_2 + cI_3$$

leaves

$$I_1 = \int_0^{\varphi_B} \frac{\varphi^2 \, d\varphi}{(\bar{R} + m\varphi)^J}$$

$$I_2 = \int_0^{\varphi_B} \frac{\varphi \, d\varphi}{(\bar{R} + m\varphi)^J}$$

and $$I_3 = \int_0^{\varphi_B} \frac{d\varphi}{(\bar{R} + m\varphi)^J}$$

where $J = \frac{1}{m}$.

The equations for I_1, I_2 and I_3 are now in a standard format and so an explicit solution can be obtained for I.

$$I = \frac{a}{m^3(J - 3)\lambda^{J-3}} + \frac{(\frac{2a\varphi_B}{m} - b)}{m^2(J - 2)\lambda^{J-2}} - \frac{\bar{R}(\frac{a\bar{R}}{m} - b)}{m^2(J - 1)\lambda^{J-1}}$$

$$+ \frac{C\lambda^{1-J}}{m(1 - J)} + \frac{a}{m^3(J - 3)\bar{R}^{J-2}} - \frac{(\frac{2a\bar{R}}{m} - b)}{m^2(J - 2)\bar{R}^{J-2}}$$

$$+ \frac{\frac{a\bar{R}^2}{m} - b\bar{R}}{m^2(J - 1)\bar{R}^{J-1}} - \frac{C\bar{R}^{1-J}}{m^2(J - 1)\bar{R}^{J-1}} - \frac{C\bar{R}^{1-J}}{m(1 - n)}$$

where $\lambda = \bar{R} + m\varphi$.

The next stage of the analysis is to look at the total energy head at the end of the pipe. With reference to figure 3.17 the total energy head at point B relative to the pipe invert can be given by

$$H = \frac{V_B{}^2}{2g} + \frac{P_B}{\rho_1 g} + (D - h) \tag{3.81}$$

where ρ_1 = density of sewage

V_B = velocity at point B and

P_B = pressure at point B.

If any centrifugal pressure corrections are ignored then the pressure at point B is given by

$$p_B = \rho_2 g(h + h_0) \tag{3.82}$$

where ρ_2 = density of sea water

h = depth of flow at exit and

h_0 = depth of sea water to top of pipe.

Substituting for p_B from equation (3.82) into equation (3.81) gives

$$H = \frac{V_B^2}{2g} + \frac{\rho_2}{\rho_1}(h_0 + h) + (D - h)$$

therefore V_B becomes

$$V_B = [2g(H - \frac{\rho_2}{\rho_1}(h_0 + h) - (D - h)]^{1/2} \tag{3.83}$$

Applying the energy equation to point 0 on figure 3.17 gives

$$H = \frac{V_0^2}{2g} + \frac{P_0}{\rho_1 g} + D \tag{3.84}$$

Once again ignoring the centrifugal pressure effects P_0 can also be given by

$$P_0 = \rho_2 g\, h_0$$

Substituting for P_0 into equation (3.84) leads to

$$H = \frac{V_0^2}{2g} + \frac{\rho_2}{\rho_1} h_0 + D$$

and therefore an expression for V_0 can be found

$$V_0 = [2g(H - \frac{\rho_2}{\rho_1} h_0 - D)]^{1/2} \tag{3.85}$$

hence by combining equations (3.69), (3.83) and (3.85) the following expression for the velocities are obtained

$$\frac{V_B}{V_0} = [\frac{H - \frac{\rho_2}{\rho_1}(h_0 + h) - (D - h)}{(H - \frac{\rho_2}{\rho_1} h_0 - D)}]^{1/2} = [\frac{R_0}{(R_0 + mh)}]^{1/m} \tag{3.86}$$

Using the equations for velocity and flow rate (equations 3.80 and 3.86) and an initial estimate for the boundary condition, a calculated downstream boundary condition was obtained by iteration until the theoretical and experimental flow rates were equal. The saline wedge problem could then be solved by computer to determine the length and profiles of saline wedges which will form in open ended pipes. This analysis for the end condition is only valid for pipes which are laid to within a few degrees either way from the horizontal.

In a vertical riser there is no change in the angle of exit of the buoyant plume and this analysis is the invalidated for this situation. From experimentation the flow appears to exit from a vertical riser in a manner similar to that shown in Figure 3.19.

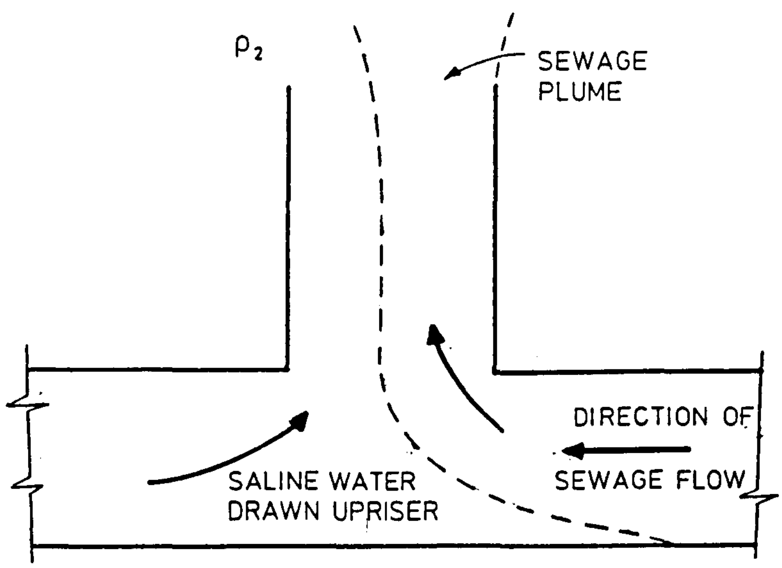

Figure 3.19

3.3.4 Numerical Models

Four computer models were developed using the equations derived in this chapter. These are; two models for looking at a single port outfall - one using Escandes finite difference method, called FINDIF VFORTRAN, and one using Runge-Kutta forward integration method called FINDIF2 VFORTRAN; a model representing the effects of wave action on a multi-riser outfall, called SFLOW VFORTRAN; and finally a model for the description of saline wedges within an open ended outfall pipe called SALWED VFORTRAN. A listing of the programs along with their respective flow diagrams can be found in Appendix D of this report. Results of application of these models and their comparison against experimental observation follows in Sections 6 and 7.

CHAPTER 4

EXPERIMENTAL APPARATUS

4.1 Experimental Apparatus

4.1.1

The model outfall testing rig was designed for versatility to enable the implementation of a variety of experiments into different aspects of outfall behaviour. The principal components of the model were a header tank, a small stilling basin which incorporated a 'V' notch for measuring small flow rates, an inflow manifold, a venturi for the measurement of larger flows and a 5 metre long perspex pipe representing the outfall. Provision had been made with the perspex pipe to facilitate the connection of riser pipes, thereby enabling the development of a multiple riser/diffuser arrangement. The outfall system was installed within a wave flume as illustrated in Fig. 4.1. A description of the various components comprising the model is outlined below.

4.1.2 Header Tank

This was located so that its base was at a height of 3.5 metres above the outfall pipe and its dimensions were such that it held approximately 1700 litres of water. The water level can be maintained using mains water supply. The elevation of the header tank was governed by the presence of an existing structural steel support frame. If the outfall was to be operated in its inverted position (i.e. with saline water instead of fresh water being discharged from the header tank, see section 5) then the tank was regularly refilled with salt water for each set of experiments - the density of the salt water being measured using a hand held digital density meter.

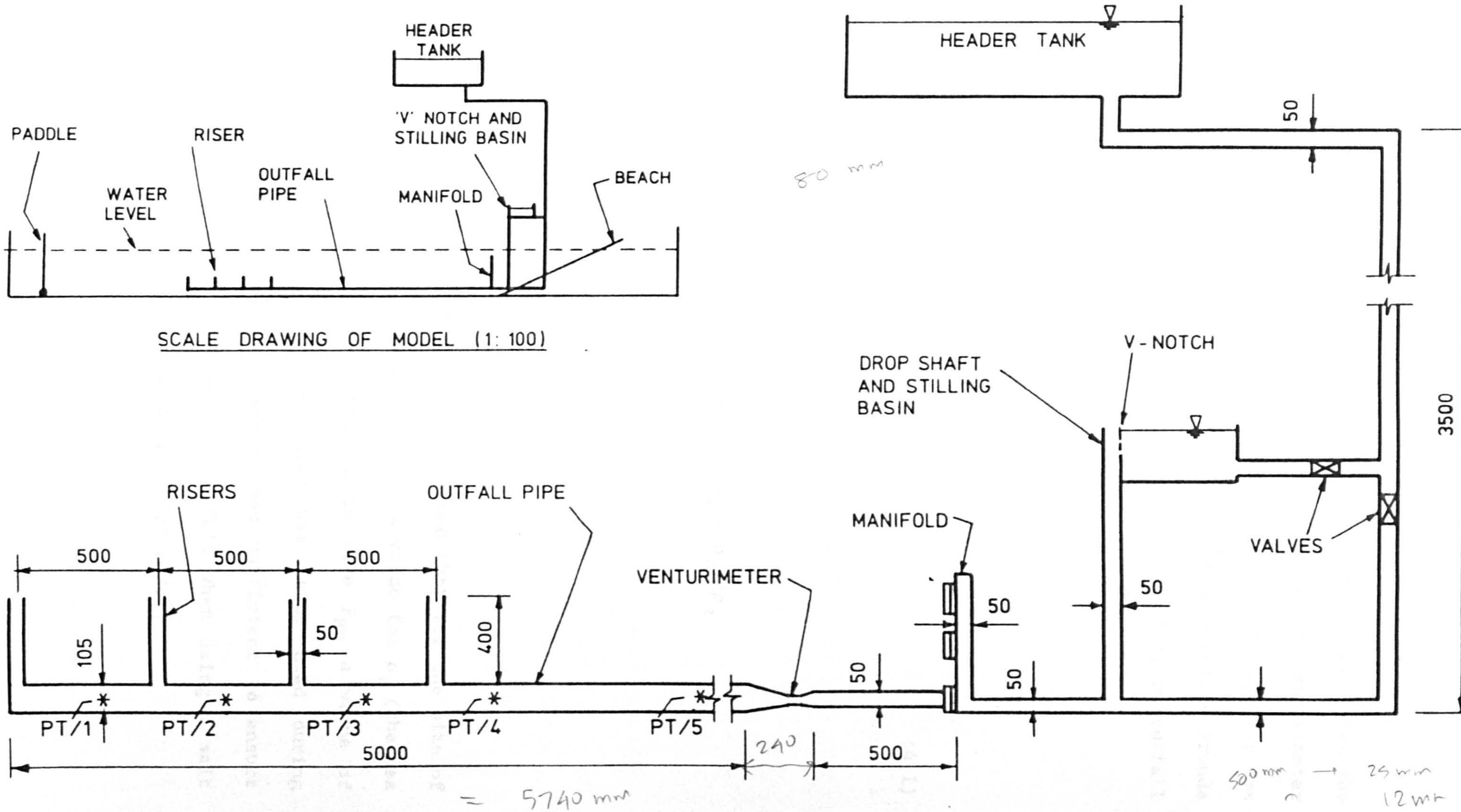

FIGURE 4.1. OUTFALL TESTING APPARATUS

From the header tank the flow of water could be directed to either the stilling basin and 'V' notch arrangement or through the venturimeter depending on the required rate of flow. The maximum flow capacity was approximately 2.5 litres/second (l/s) which gave a densimetric Froude number greater than unity for an open ended outfall, i.e. an outfall without risers.

The densimetric Froude number is calculated from

$$F_{RD} = V/\sqrt{\epsilon \; g \; D} \tag{4.1}$$

where F_{RD} = densimetric Froude number

V = velocity of flow

ϵ = density factor and is given by $(\rho_2 - \rho_1)/\rho_2$

g = acceleration due to gravity

D = pipe diameter

ρ_1 = fresh water density and

ρ_2 = density of salt water.

For a given flow rate of 2.5 l/s it can be found that for the size of outfall pipe that was used (see section 4.1.5) a value for ρ_1 (the sea water density) of 1080 kg/m^3 was required to give F_{RD} a value of unity. This is a very high value which was never used during experimentation. Hence the flow capacity was sufficient to ensure that there was enough water to purge the outfall when using a salt water density similar to that of sea water (1025 kg/m^3).

4.1.3 Stilling Basin and 'V'-Notch

This arrangement was used for the measurement of small flow rates. The whole assembly, as shown in Fig. 4.2, was constructed from perspex; the stilling basin had dimensions of 500mm x 300mm x 250mm deep and the 'V' notch was set at an angle of 20° and was 200mm high, (see Appendix B). Water levels within the stilling basin were controlled by both an inflow valve and a variable overflow weir which was fabricated as a sector weir, see plate 4.15. From the stilling basin the flow was conveyed to the inflow pipe manifold.

4.1.4 Inflow Pipe Manifold

This was assembled from a 50mm bore PVC pipe and it allowed the outfall pipe to be positioned and operated at one of three levels. The upper level was used when the outfall was operated in its inverted position and the lower level used during the outfalls operation in its normal position; this position offers the greatest receiving water depths and is the only position in which the vertical risers could be used. However, early experiments were undertaken with the outfall installed in its upper position on the manifold and the risers pointing vertically down, these experiments are described in section 5. Diagrammatic sketches of the manifold and outfall positions are shown in Fig. 4.3.

4.1.5 Outfall Pipe

This was connected to the inlet manifold with a transition piece as the pipe and the manifold connections had different diameters. The transition piece incorporated a venturimeter for the measurement of the larger flow rates which were passed through the system. The outfall pipe was constructed from perspex and is 5m long with a bore of 105mm. The pipe, when located in the normal position on the bottom

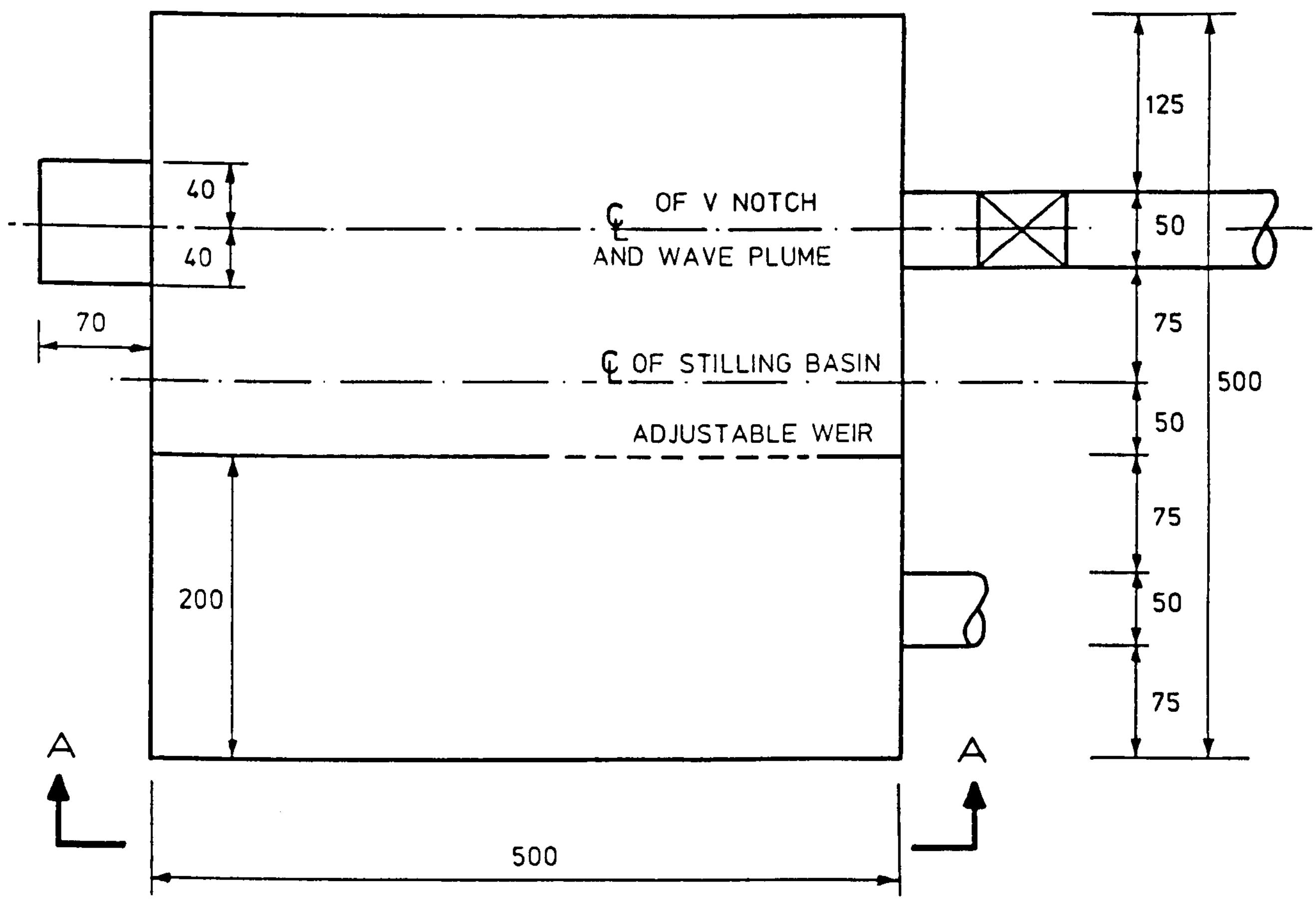

FIGURE 4.2A STILLING BASIN - GENERAL LAYOUT

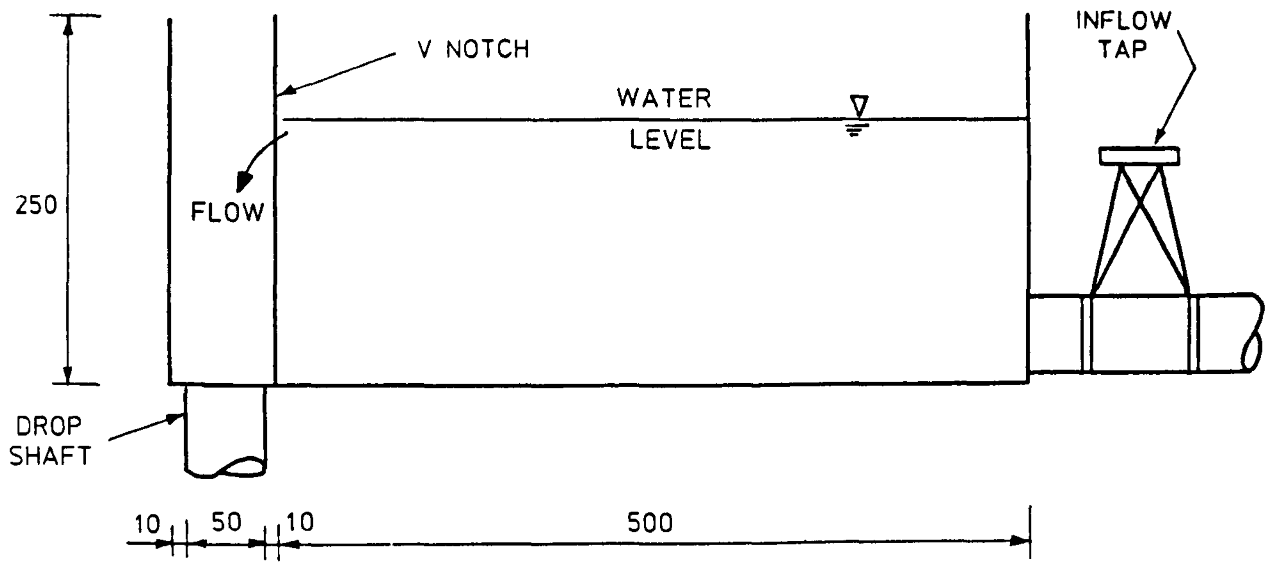

SECTION A - A

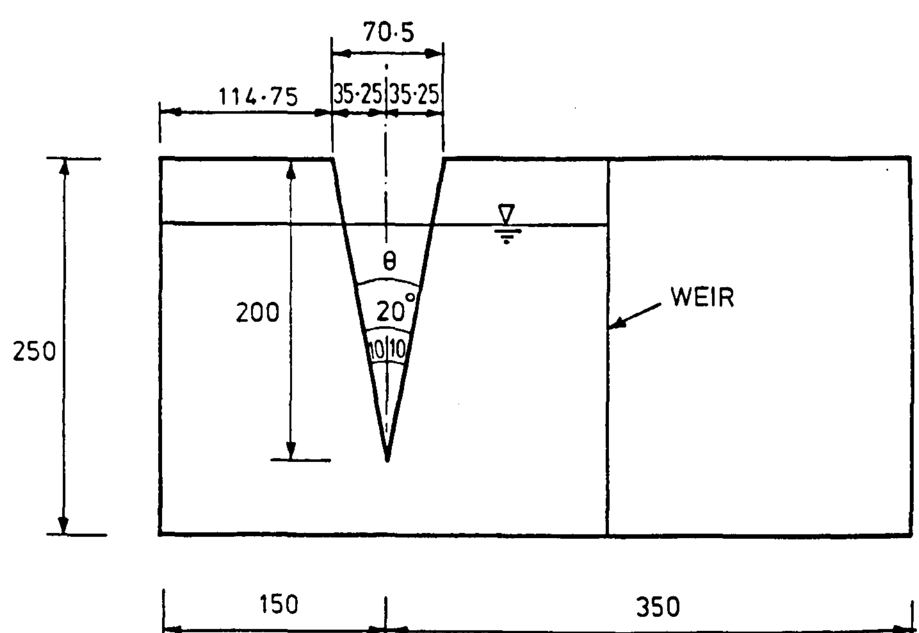

FIGURE 4.2B. V NOTCH AND FRONT PLATE OF STILLING BASIN

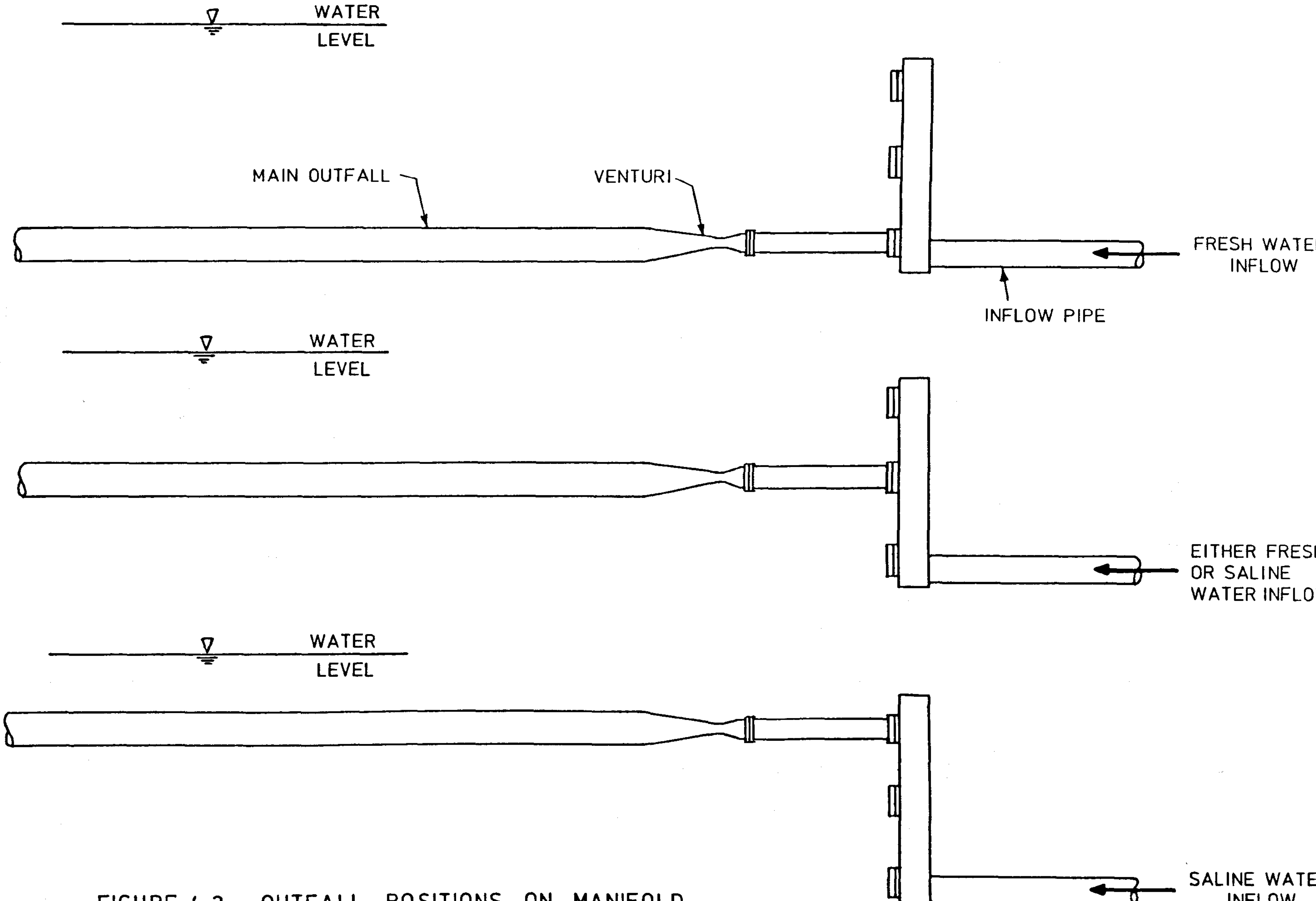

FIGURE 4.3. OUTFALL POSITIONS ON MANIFOLD

of the wave flume, had connectors attached to it at 500mm centres at soffit level, so that a riser/diffuser arrangement could be fitted. This facility enabled observation of the effects of wave action on either an open ended outfall or one with a diffuser system.

Pressure tappings were also located along the pipe at 500mm intervals, spaced midway between the riser connections. These consisted of tappings on both sides of the pipe at each measurement section, see Fig. 4.16. One side was connected to a multi-tube oil/water inverted 'U' tube manometer which provided approximate visual recordings of pressure changes, whilst the other side of the pipe had electronic pressure transducers installed which accurately recorded small and fluctuating pressures. The transducer system was connected to the Departmental Data General Eclipse computer which collected and analysed the data received during operation of the model.

All riser sections used with the model were constructed from 50mm bore perspex pipe, each being 400mm in length.

4.1.6 <u>The Venturimeter</u>

Figure 4.4 shows the venturimeter which was designed to measure the larger flow rates and in addition allow the larger diameter outfall pipe to be connected to the smaller diameter manifold pipe. As water leaves the manifold it passes through a 500mm length (10 pipe diameters) of pipe to ensure that near uniform streamline flow is attained before the flow passes into the venturimeter. The flow then passed into a throat of 25mm diameter before finally discharging to the 105mm bore section, which is the same diameter as that of the main outfall (all diameters are measured internally). The short length of pipe preceeding the venturimeter is the minimum length recommended to

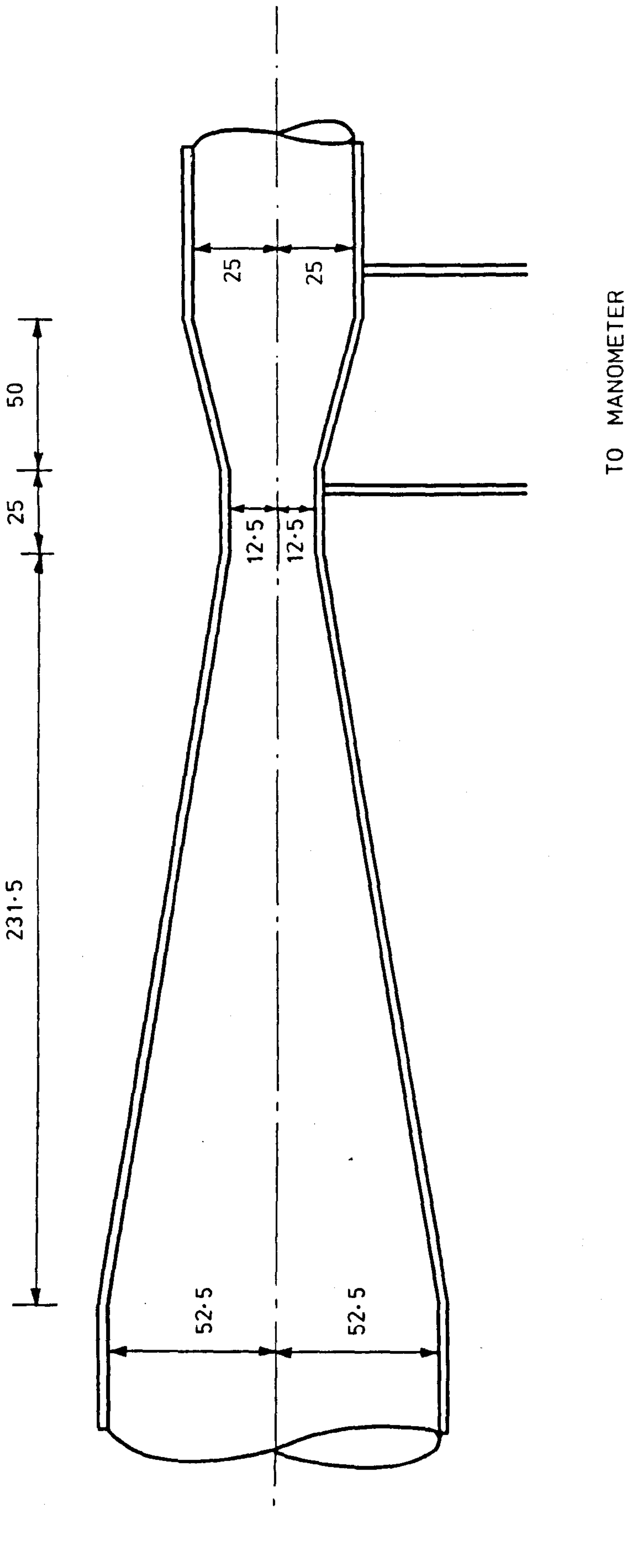

FIGURE 4.4. VENTURIMETER

ensure accurate results from the venturimeter. The throat of the venturimeter also acts as a control on the upstream migration of any saline wedge forming within the outfall by virtue of the high velocity at this section. This ensures that the flow rate being measured is only fresh water being discharged and not a mixture of both fresh and salt water as often occurs near or within the diffuser manifold section. It is worth mentioning that the use of the venturimeter as a practical method of reducing saline intrusion has been suggested by Charlton[16].

4.1.7 The Wave Flume

The outfall pipe was installed within, and discharged to, a wave flume 12 metres long by 0.75 metres wide and operates with a water depth of up to 0.920m (920mm). This placed the water surface at approximately 340mm above the top of the risers when the outfall was used in its normal position and 720mm above the open end of the risers when the outfall was operated in the inverted position.

The wave generator was constructed by a specialist firm, Keelavite Hydraulics, and it can generate either a regular sine wave or a random wave spectrum. The height and frequency of regular sine wave was controlled by the operator at the wave paddle operating console, whereas randomly generated wave spectra were specified and controlled using the Departmental Eclipse computer forming part of the control data aquisition facility. The random wave spectrum is generated by first running a program described in Appendix 1, which creates a wave spectrum for the paddle using the Pierson-Moskowitz spectrum. The output from this program is converted into a series of small paddle movement steps which are passed down a series of cables from the computer to the control console for the paddle; this produces the signal which the wave paddle follows. In general waves up to 150mm in height with periods in the range 0-5 seconds were employed and either surface piercing wave gauges or pressure transducers were used to measure wave heights.

4.2 Design of Outfall

4.2.1 The main outfall pipe

Perhaps the most vital part of the apparatus was the pipe which models the main outfall and riser/diffuser system. Consequently, great care was taken when designing this part of the apparatus. However, despite being meticulous on this point of detail, a few problems did arise which could not, unfortunately, be readily overcome, as they were inherent within the model.

The main outfall pipe was modelled by using a perspex tube having an internal diameter of 105mm. It was also decided that a minimum of four risers be attached to the discharge end of the outfall and that this would prove adequate for experiments to examine the effects of various physical factors on the diffuser section. The model itself was not physically scaled from any existing prototype outfall as it was an exploratory model to investigate a variety of hydraulic effects upon the outfall system. Nevertheless, to put the results obtained into a meaningful perspective a comparison does have to be made between the model and prototype outfalls.

The model scaling was performed using similar densimetric Froude numbers, the equation for F_{RD} is given in equation 4.1 and the equation for similar densiometric Froude numbers is given as

$$\frac{V_m}{\sqrt{\epsilon_m\ g\ D_m}} = \frac{V_p}{\sqrt{\epsilon_p\ g\ D_p}} \tag{4.2}$$

where suffix m indicates model and p indicates prototype. It was decided to use this rather than Reynolds number similarity because it was felt that gravitational rather than shear effects would be more important.

Calculations carried out in Appendix B show that the apparatus can operate with a flow rate in excess of 4.0 l/s. Knowing this and taking into account the possibility of unforeseen losses, and the fact that this flow rate will cause the main tank density to quickly reduce, it was decided to use 2.0 l/s as the design flow rate. The following assumptions were then made for application of equation 4.2:-

(i) the prototype pipe diameter was taken as 2.7m; and
(ii) the model salt water density would be 1016 kg/m^3 and the sea water density is 1025 kg/m^3.

This second assumption gave values for ϵ_p and ϵ_m as 0.0244 and 0.0157 respectively. By rearranging equation 4.2 an expression for V_p is obtained such that

$$V_p = \frac{V_m \sqrt{\epsilon_p\ g\ D_p}}{\sqrt{\epsilon_m\ g\ D_m}} \tag{4.3}$$

For the model it is found that for a flow rate of 2.0 l/s and a model diameter of 105mm the velocity, V_m, is 0.23 m/s. By substituting this into equation 4.3, V_p is found to be 1.45 m/s, which represents a flow rate of 8.3 m^3/s (8300 l/s). The prototype pipe diameter of 2.7m was deliberately chosen as this is the size of the proposed outfall for the new Liverpool Sewage treatment works. The flow rates which the North West Water Authority based its calculations on are as follows:-

Minimum flow for phase 1 of construction	= 1.5 m^3/s
Minimum flow for phase 2 of construction	= 1.8 m^3/s
Dry weather flow	= 4.0 m^3/s
Maximum flow	= 13.0 m^3/s

It can therefore be seen that the model flow rate of 2.0 l/s gives a value equivalent to approximately twice the dry weather flow of the Liverpool S.T.W. This indicates that the results produced by the experimental model will give a reasonable indication of what happens in a prototype outfall as the hydraulic characteristics will be similar.

The length scale of the outfall was found by dividing the prototype diameter (D_p) by the model diameter and it gave a value of

$$\frac{D_p}{D_m} = 25.71$$

The length of the model outfall is 5 metres so the equivalent prototype length is given by

$$5.0 \times 25.71 = 128.6\text{m}$$

This value of 128.6 metres is small when compared to the lengths of prototype outfalls but as it was the diffuser section which was of principal importance in this study, the length of the model was considered adequate.

The spacing of risers on prototype outfalls can range upwards from as little as 2 metres up to much higher values depending upon the required conditions for dilution and dispersion. For the Weymouth and Portland outfall[49] risers where positioned at 50 metre centres. On the model the riser spacing was 0.5 metres (500mm) which corresponds to a prototype spacing of 12.8 metres, within the range of values for typical outfalls.

The diameters of risers on outfalls also vary a great deal, as dictated by the design for good effluent diffusion and dispersion. In practice, they generally have diameters of between 400 and 600mm . The model outfall has a riser diameter of 50mm which corresponds to a prototype value of 1.28 metres. This is larger than the risers generally installed on prototype outfalls. To model the risers so that they had equivalent prototype values would have meant the use of 23mm diameter pipes to be used on the model - these would have given an equivalent prototype diameter of 600mm. This diameter of model riser pipe would have made the measurement of velocities within the riser impractical with the equipment then available.

The scaling factor of 25.71 when applied to water depth gives a prototype water depth above the top of the risers of just over 8 metres. This is probably shallower than the normal depth over outfalls but it enabled the investigation of a larger range of wave conditions within the wave tank, which would affect the internal pipe hydraulics. Increasing water depth leads to the attenuation of wave induced pressure fluctuations for waves of shorter period and there was a restriction on the largest wave periods considered as a result of standing wave formation in the flume.

If the outfall pipe itself had been modelled using a scaling factor of such a value that the model riser diameters, of 50mm, would have an equivalent prototype diameter then several problems would have presented themselves in the construction and operation of the model. The resulting increase in flow rates required would have caused delivery problems with the intended supply system.

From the publication by Miller[39] it can be found that using four risers of 23mm diameter a flow balance would be achieved at the higher range of experimental flow rates but in the case of the model using 50mm risers this is not so. Consequently, the flow through the risers had to be balanced and this is discussed in the next section (4.2.2).

It was eventually decided to use 50mm diameter riser pipes, 400mm in length (which corresponds to a prototype length of 10.28 metres) for the following reasons

(i) model risers of 50mm diameter had previously been used by Charlton et al[17] at Dundee University; and

(ii) this size not only enabled velocity probes to be used within the riser but would also reduced the problematic effect of wall shear on measurements taken within the riser.

4.2.2 Flow Balancing

In practice, particularly in tunnelled outfalls, the manifold section is designed to have a decrease in its cross-sectional area after several riser/diffuser positions as indicated in Fig. 4.5:-

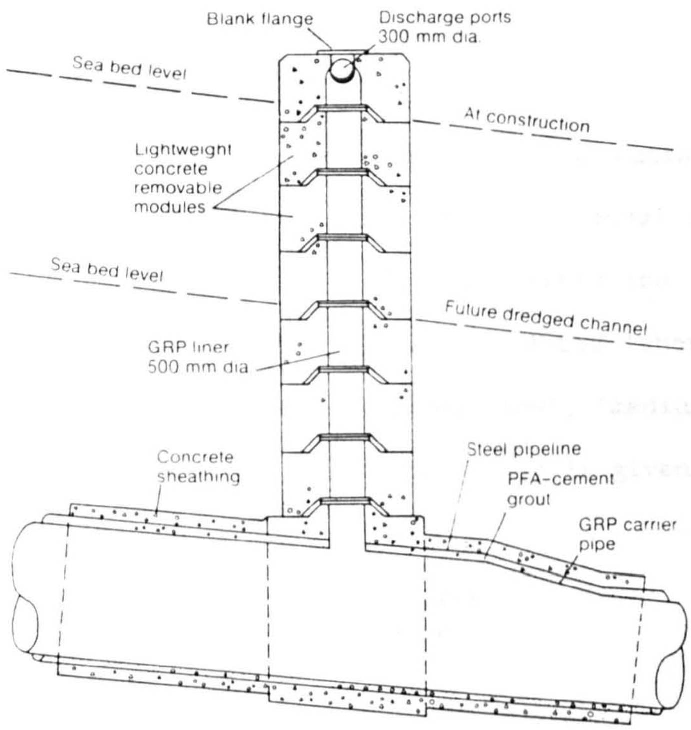

Figure Showing Change in Cross-Sectional Area of Manifold After Riser Position

Figure 4.5

This type of arrangement is used to enable the outfall to maintain self cleansing flow velocities along its length and to ensure that the hydraulic head is maintained at a sufficient level to provide an equal rate of flow through the risers. As the series of experiments being considered for this study looked at various aspects of general flow behaviour, it was decided early on in the programme to adopt a uniform diameter for the outfall pipe. The riser flows were later balanced by inserting orifice plates into the base of each riser.

The calculations for balancing the outfall system were performed with reference to the work on minor head losses at pipe junctions by Miller[39]. In addition the November 1986 WRC Engineering publication[43] on outfall design may also be used to advantage, although it was not available for the early stages of this research programme which began in the Autumn of 1985.

A comprehensive set of design parameters for the outfall model was prepared which should enable the establishment of equal rates of flow through all risers. However, Miller[39] highlights the likelihood of varying flow distributions, which is quantified for 'short', 'medium' and 'long' manifold lengths with associated 'low', 'medium' and 'high' branch loss ratios. The branch loss ratios (L_R) is given by

$$L_R = \frac{\text{Total branch cross-sectional area}}{\text{Manifold cross-sectional area}}$$

For the outfall model adopted it was established that the branch loss ratio approximated to 0.91 and as the overall manifold length was short, the theoretical flow distribution through the risers is given by application of the procedure as being high at the seaward riser and low in the landward riser. This is shown in Fig. 4.6.

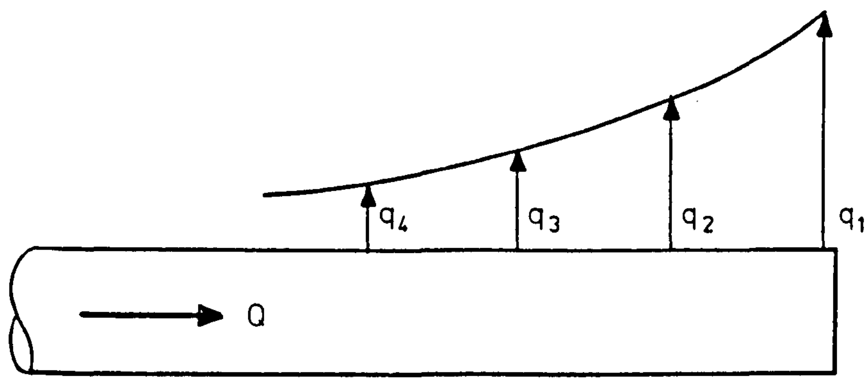

Flow Distribution For High Branch Loss Ratio

($L_R \approx 1.0$)

Figure 4.6

To achieve uniformly distributed flows across the manifold system, a loss ratio of approximately 0.5 is required. This would necessitate the installation of four risers each with an internal diameter of approximately 36mm, an arrangement that would lead to difficulties in attempting to measure flow velocities in the riser.

Even after completing the design appraisal using Miller's techniques, problems will still be expected to arise with the precise balance of flows on the experimental model because some of the parameters used will be subject to slight changes, for example the salt water density. The complete calculation set for the flow balance appears in Appendix B, which also details the final in-situ tuning of orifice insertions required to effect the necessary flow balance in the experimental facility under the design flow rate.

4.2.3 Diffuser Ports

A final series of experiments were conducted towards the end of the study period into the effects of wave action on the manifold when flow constricting in the form of diffuser heads with smaller diameter ports are fixed to the top of each riser pipe. Two different riser heads were looked at for experimental purposes:-

(i) the first was the initial proposal for the Weymouth and Portland outfall in which riser pipes of 400mm diameter were to have a diffuser head which incorporated two ports of 250mm diameter -this gave a ratio of port area (A_p) to riser area (A_r) of 0.78; and

(ii) the second was the designed diffuser head for the Great Grimsby outfall. This had risers of 500mm diameter and each diffuser head had two ports of 300mm diameter. This gave an A_p/A_r ratio of 0.72.

It was decided that a ratio of A_p/A_r should be set at 0.72. The experimental diffuser head therefore consisted of two ports, with each port being 30mm diameter (Fig. 4.14).

4.3 Measuring Devices

4.3.1 'V' Notch

The 'V' notch, for outfall flow measurement, was initially designed using the relevant British Standard, BS3680[9] Part 4a. The notch adopted had an angle of 20° (see Fig. 4.2b) selected to ensure an acceptable range of upstream head measurements under the range of experimental flow rates, as detailed more fully in Appendix B. Once the 'V' notch had been constructed it was calibrated, in accordance with the normal equation, given below, by adopting the procedure laid down in Section 5.1.2. The equation for calculating the height of a 'V' notch is given by

$$h^{5/2} = \frac{Q}{(\frac{8}{15} C_d \sqrt{2g} \tan \frac{\theta}{2})} \tag{4.4}$$

where h = height of water over 'V' notch

Q = flow rate

C_d = coefficient of discharge

θ = total angle of 'V' notch.

4.3.2 Inlet Manifold and Venturimeter

The inlet manifold section of the outfall model was required to enable the outfall to be positioned at one of three different levels, in order that a variety of experiments could be undertaken. A typical example of the need for this versatility is illustrated when the outfall was modelled in the inverted position, the inlet manifold was then employed to hold the outfall and prevent the ingress of fresh water into the pipes upstream of the manifold.

One serious problem encountered whilst using these two pieces of operational equipment, (the 'V' notch and the manifold) was that when the flow rate passing through the 'V' notch was high, it tends to form a vortex when passing into the downstream pipe and so draws air with it into the outfall system. When the outfall is modelled in its correct position, i.e. with the risers pointing upwards any entrained air will discharge through the first open riser it reaches; if, however, the outfall is inverted air will gather along the soffit of the pipe causing experimental impediment.

In the first situation, there is the likelihood that air rising up the outfall port would cause discrepancies in the readings registered by the ultrasonic velocity probe as well as possibly modifying the flow properties. In the second case trapped pockets of air would create constrictions in the pipe leading to a significant loss of effective operational area resulting in serious experimental errors. This latter condition could, however, be readily overcome by fitting air release valves to the soffit of the pipe.

The prevention of air entrainment occurring in the system during experiments with high flow rates was achieved by using the main venturimeter which was free from such problems. The venturimeter was not of standard specification and was designed as described in Appendix B. Its calibration is outlined in Section 5.1.3.

4.4 Instrumentation

4.4.1 Pressure Measurement

Two types of pressure measuring devices were used during the course of experimental work, they were:-

(i) an oil/water manometer; and
(ii) electronic pressure transducers.

The oil/water manometer system was a purpose built multi-pipe inverted 'U' tube arrangement fitted to a scale graduated at 5mm intervals. The principal use for this device was to allow observation of the distribution of mean pressures within the outfall pipe, since the system would not respond adequately to the high frequency oscillations induced by waves. As it turned out during experiments little attempt was made to use this system. The oil used in the manometer was chosen to have a specific gravity close to unity (the specific gravity of water) to maximise the sensitivity of the instrument, so that small changes in pressure produces relatively large movement on the manometric scale. (The specific gravity was approximately 0.9).

Some problems did occur when using the manometer, not least the difficulty of making accurate measurements manually. This proved especially difficult during periods of wave action as the inertia of water in the manometer pipes ensured that there was a delay between the time at which the pressure change acted on the pipe and the corresponding deflection on the scale.

The electronic pressure transducer system was more extensively used because of its ability to automatically record instantaneous pressures, with the signals being fed to the data acquisition system and stored on computer files for subsequent analysis. For these reasons it was clearly advantageous to adopt the use of electronic measuring devices for the experiment.

The pressure transducers used were type PDCR42 and are manufactured by Druck Ltd, a photograph of one is shown in Fig. 4.7. One difficulty when using electronic transducers is that whilst the front face of the device is in contact with the fluid, care has to be taken to ensure the back of the transducer is also kept dry otherwise it will become irreparably damaged. To avoid this happening each transducer is mounted within individual housings attached to the side of the pipe as

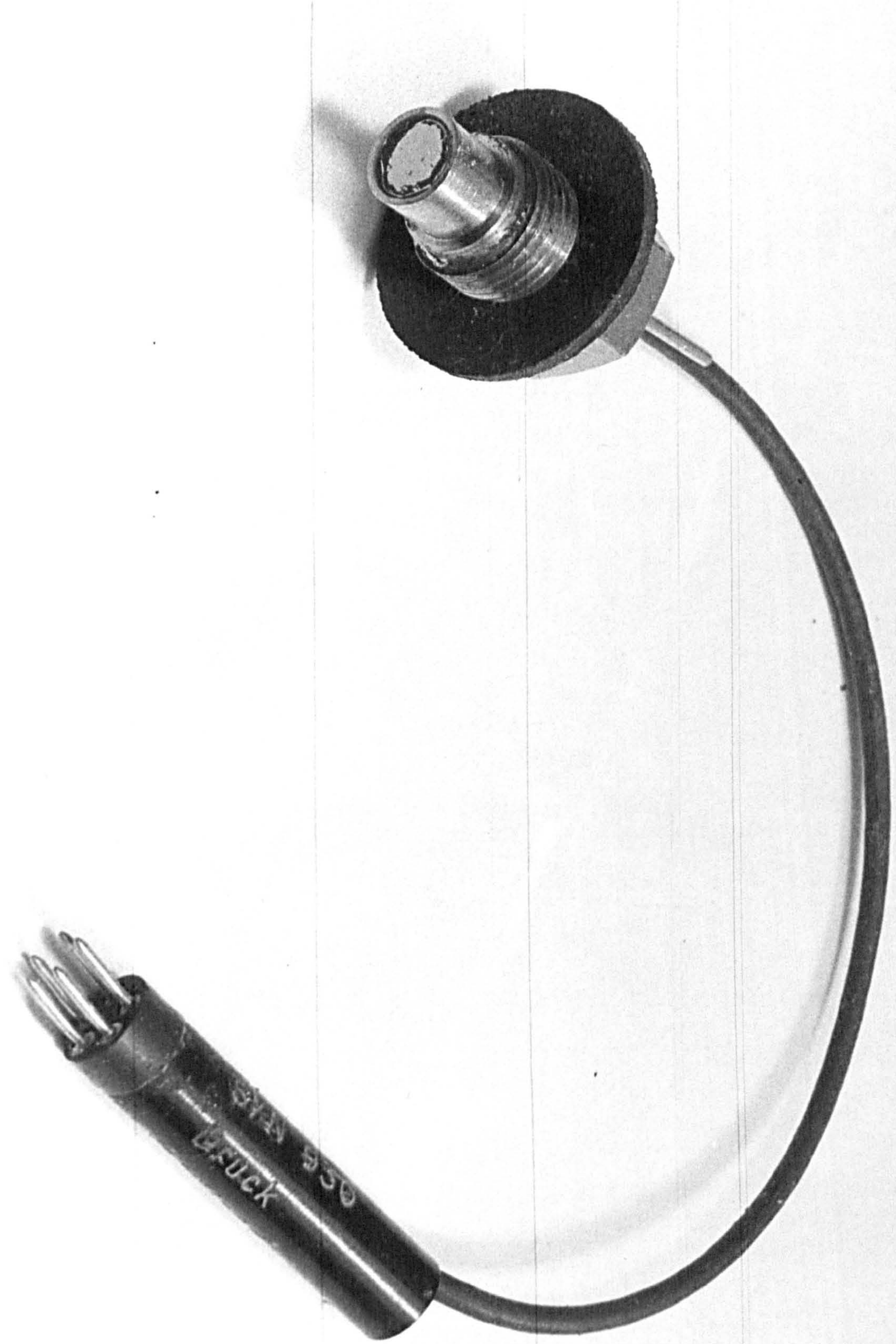

FIGURE 4.7. PRESSURE TRANSDUCER

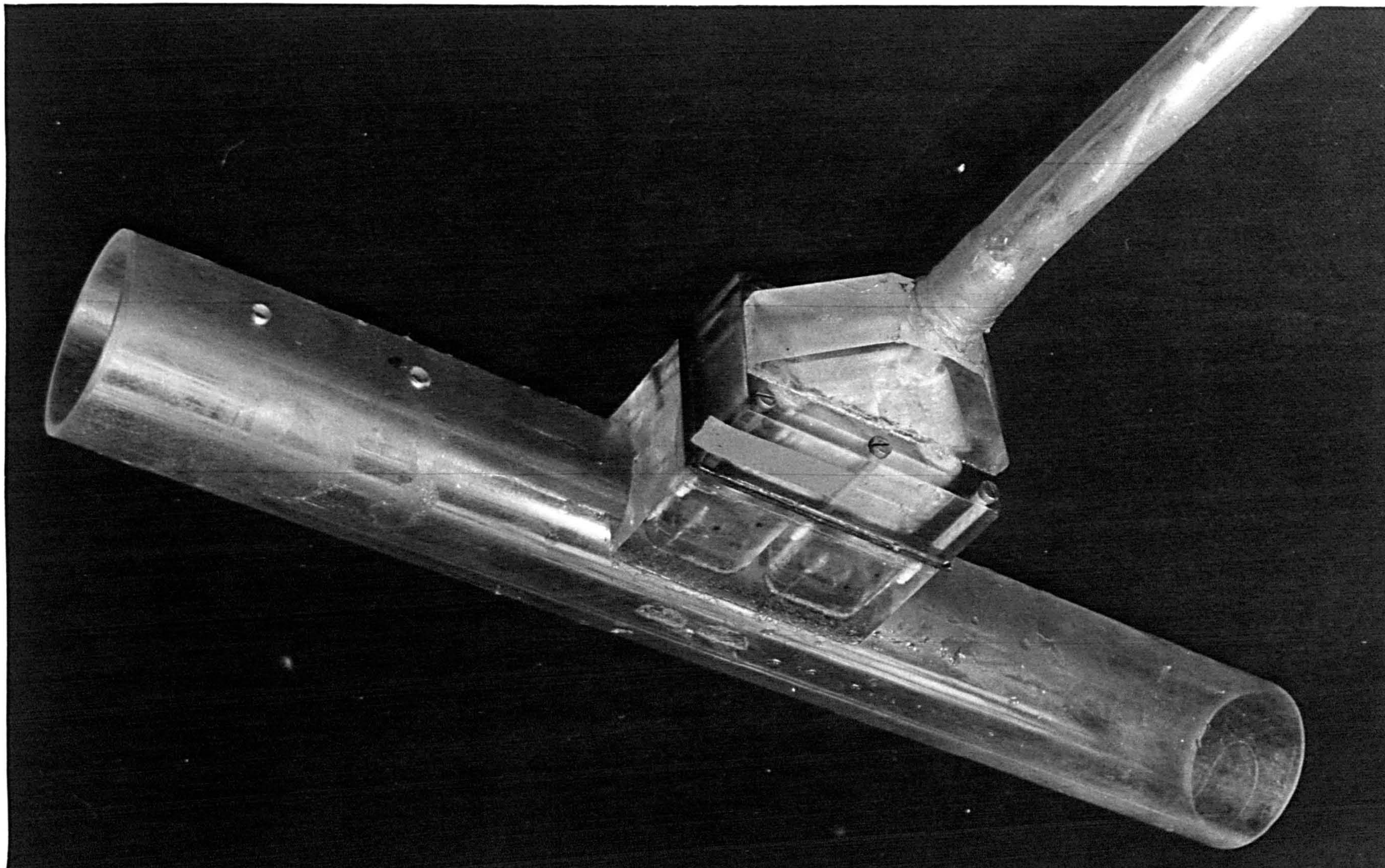

FIGURE 4.8. VIEW SHOWING TYPICAL TRANSDUCER HOUSING (HERE FIXED TO SIDE OF NOVEL VELOCITYMETER)

shown in Fig. 4.8. The electrical leads from the transducer were then passed out of the tank through a hose attached to the back of the housing. This method of protecting the transducers was very effective and proved satisfactory for the measurement of pressure along the pipe for either salt or fresh water tests.

The transducer operates by picking up a change in electrical signal as the diaphragm at the front of the transducer moves, as this is only a small signal it has to be amplified before the data acquisition system can record it, so each transducer is connected to an individual amplifier, manufactured by Fylde Ltd, and then the signal from the amplifier is recorded by the data system. Before any measurements are recorded the transducers have to be set to zero for the initial conditions; this is carried out by fitting a bridge circuit, also manufactured by Fylde, in line with the amplifier and transducer.

4.4.2 Wave Measurement

The measurement of the wave height and period within the tank was required in order that the change in pressure with time across the top of the manifold/diffuser system could be calculated. During initial testing and experimentation the wave tank was filled with fresh water and Churchill (capacitance) wave gauges were installed to measure wave height (see Fig. 4.9). These gauges proved very successful in operation and were linked to the data acquisition system so the results could be stored on computer file. One difficulty with this type of wave gauge arises when both fresh and saline water is introduced to the system causing stratification. The gauges operate by using capacitance generated by liquid lying between two parallel wires, and as the level of liquid rises, a corresponding increase in reading is recorded on the monitors.

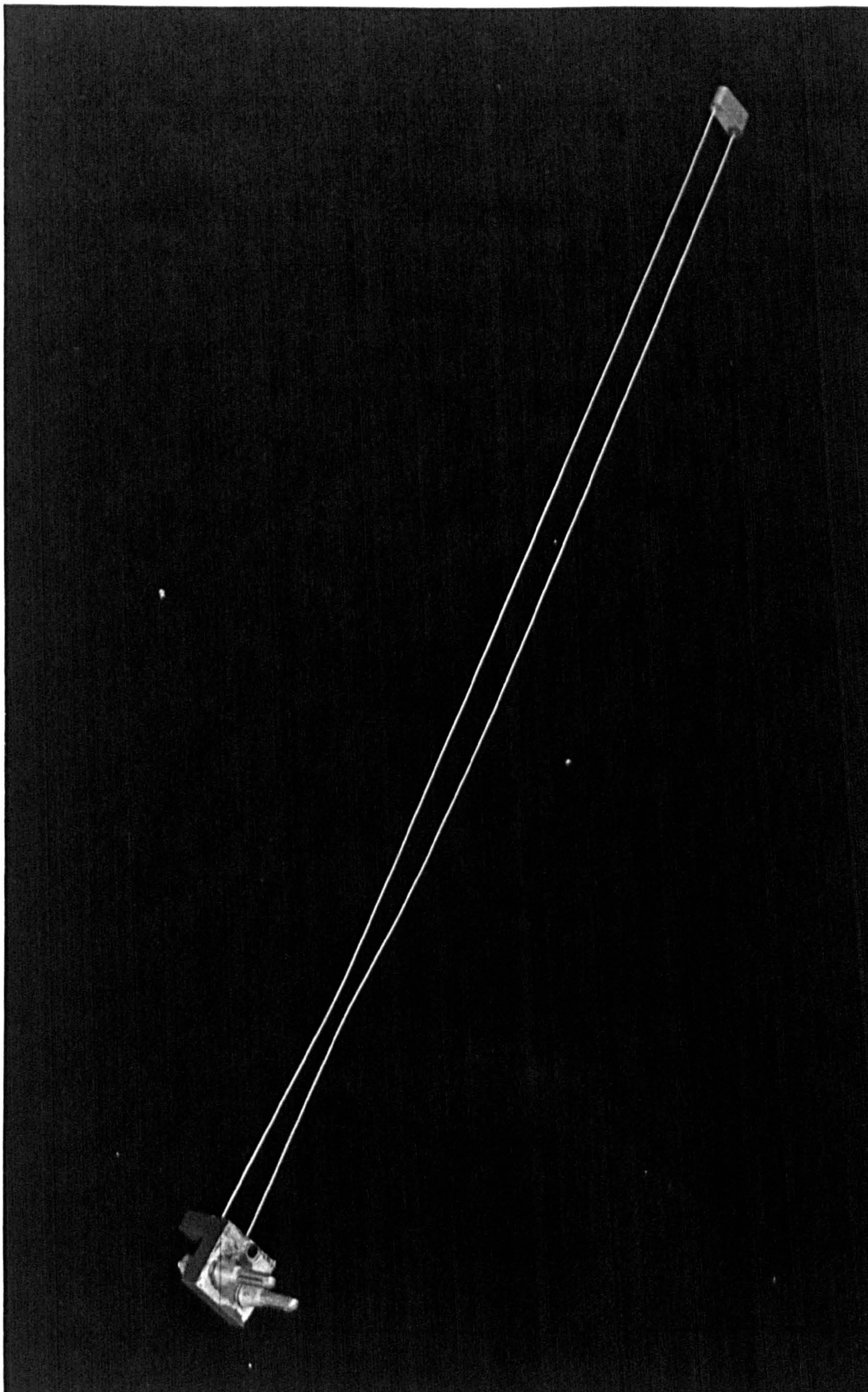

FIGURE 4. 9. CHURCHILL WAVE GAUGE

When salt water is used in the wave tank and fresh water is discharged from the outfall a layer of fresh water forms across the top of the salt water and causes varying changes of capacitance at the wave gauges, in consequence true readings of wave heights cannot be obtained. In an attempt to overcome the problem other techniques of measuring wave height were considered, and one finally selected was the use of a pressure transducer located at an elevation as close to the water surface as possible whilst being submerged at all times during tests for the entire range of regular and random wave trains. This method gave a change in pressure which corresponded to a change in waveheight above that point. The position of the transducer, close to the trough of the wave was chosen to prevent errors caused by reductions in pressure due to depth attenuation. The transducer was calibrated as outlined in Section 5.1.4.

The transducer was mounted inside a water-tight container with only the front membrane exposed to liquid; connections were made between the transducer and the bridge and amplifier, and the whole system was connected to the data acquisition system. During the performance of an experiment it was found that the change in density and change in water level above the transducer were negligible and so this system of wave measurement proved most satisfactory.

4.4.3 Density Measurement

The density of the saline water held within the main wave tank or in the header tank (during experiments when the pipe was in the inverted position) was measured using a hand held density meter which is manufactured by Paar Scientific. This instrument enabled measurements to be taken during experiments to ensure that the density of water within the tank did not change dramatically during a series of experimental runs. The density meter was also equipped with a thermometer to enable the operator to check the temperatures in both the header tank and the main tank were equal. This ensured that thermal stratification within the pipe was kept to a minimum and so the only stratification would be due to a change in density.

Density measurements were taken over a grid of points along the wave tank at the surface, at a set depth below the surface and also at a draw-off point located at the base of the tank to detect possible stratification within the tank. If the water in the tank was stratified then a pump was used to circulate and mix the water until the density was considered uniform. The same pump was used to circulate the water if salt had been added in order to increase the receiving water density. When saline water was required from the header tank, when the outfall was modelled in its inverted position, salt and water were mixed using a stirrer powered by a small motor.

4.4.4 Velocity Measurements

One of the most difficult areas of measurement proved to be that of obtaining velocities within individual risers of the manifold system. Various methods were tried, the details of each being outlined below.

(i) Video method

Initially a video camera and a flat screen video monitor were used to track the movement of dye released into each riser. The dye was injected using a hypodermic needle, positioned at the midpoint of the riser section and supplied with potassium permanganate dye, of equal density to the receiving water, from small header tanks positioned along the side of the main tank. A predetermined scale was fixed to the back of each riser and the video camera was used to record the movement of the dye during an experimental run. The time taken for the dye to move over various distances could be recorded on the video display unit by a stop watch incorporated within the camera. The velocity was then calculated by re-running the tape in slow motion and recording the time taken for the dye to move between two points on the scale. This method was reasonable for obtaining an approximate mean value of the flow rate within the riser but it was impossible to estimate instantaneous velocities as waves passed over the manifold system. Another problem with this technique is that over a period of time the dye disperses into the rest of the fluid so rendering it impossible to conduct visual analysis.

(ii) Miniature propeller meter

The miniature propeller meter was used so that the instantaneous velocity of flow within the riser could be determined as a wave passed over the manifold system. The device used was a special type instrument fitted with a 90° angle change on its shaft so that flow velocities perpendicular to the water surface could be measured (see Fig. 4.10). This was positioned over the top of the riser and the experiment was performed. During the experimental run it was found to be difficult to determine the orientation of the flow, i.e. whether it was either positive (discharging) or negative (intrusive), additionally, because the instrument was positioned over the top of the riser and not within the pipe section, there was doubt as to whether the measured velocity was the actual velocity of flow within the riser or a mixture of the velocity of flow and the particle velocity caused by wave action. The propeller meter system was consequently abandoned because of the problems outlined above and the

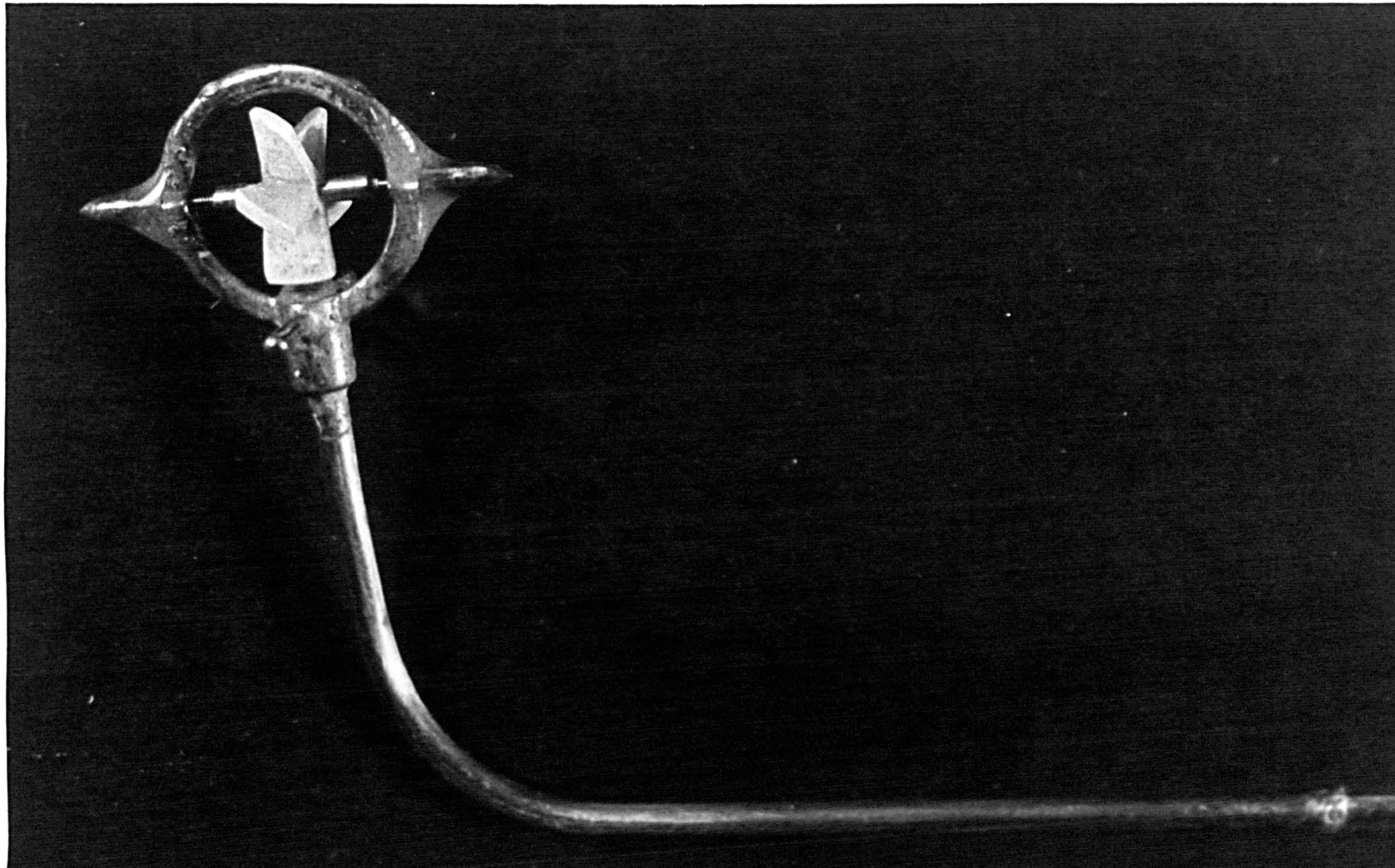

FIGURE 4.10. PROPELLER METER WITH 90° TURN IN SHAFT

additional drawback that the propeller system was unable to respond to rapid changes in velocity, so rendering it of little use for the planned wave action tests.

(iii) Ultrasonic probe

The ultrasonic probe had the capability of measuring both positive and negative flows in three directions (see Fig. 4.11). For this experimental study only the vertical direction (Z) was required. When this probe was placed at the top of the riser in early trials, it was found that the uncertainty regarding the velocity information still remained but the probe itself responded quickly to changes in flow rate.

The method which was eventually adopted was to drill two small holes in the riser to receive the vertical velocity probes of the meter. By using this method it was certain that the velocity measured was that within the riser and not a combination of other possible velocity components. The velocity meter output was connected to the data acquisition system so that all the readings could be stored on file.

(iv) Pitot method

The method used for obtaining riser velocities outlined in section (iii) was the technique used for most of the experiments reported. However, it was decided to investigate a novel system of measuring velocity using a dual pitot arrangement connected to electronic pressure transducers. The reason for this was that in an ideal situation each riser would have its own velocity meter and within the department the equipment was available to install this type of velocity meter within each riser, whilst no funds were available for the purchase of multiple ultrasonic probes.

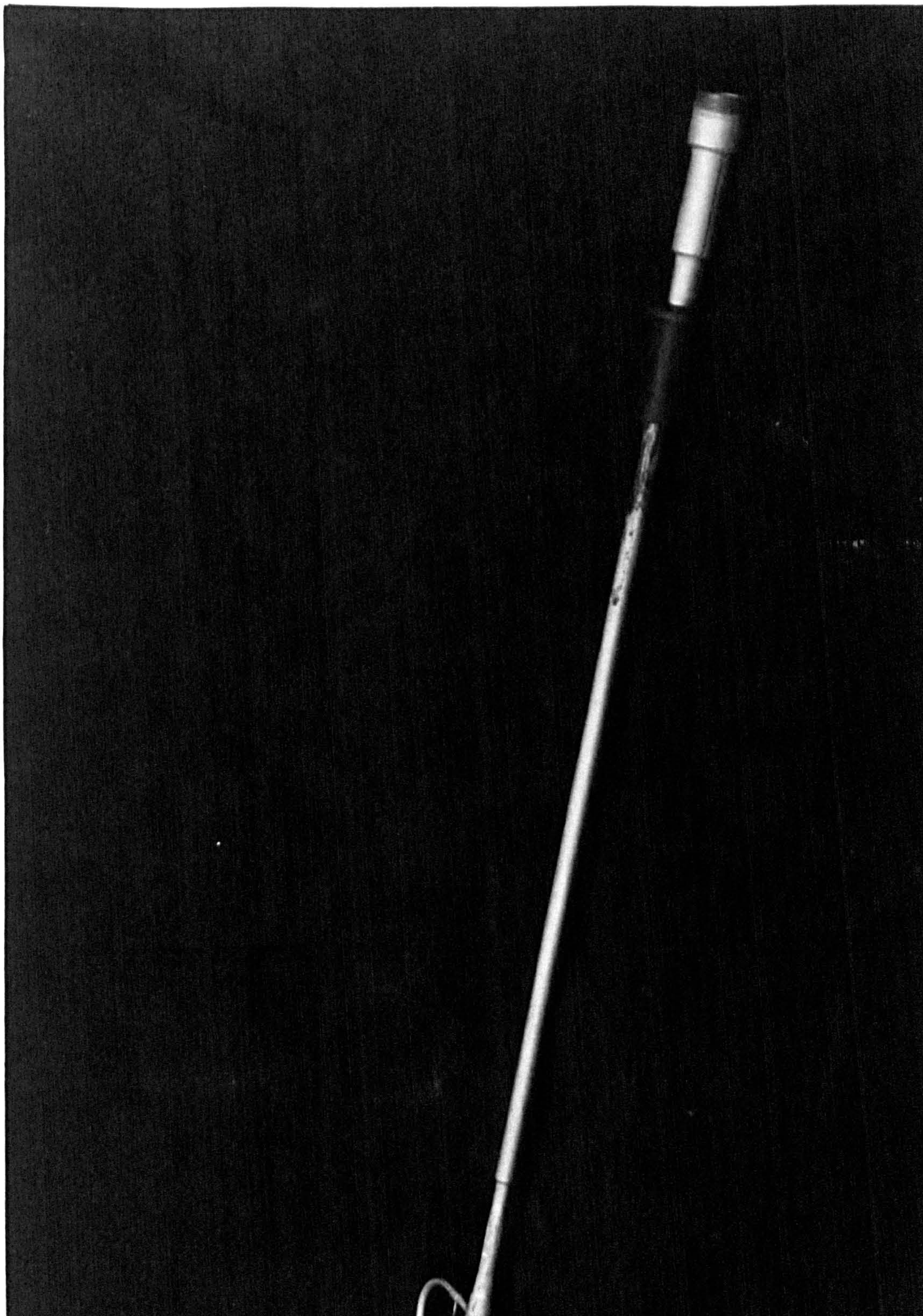

FIGURE 4.11. ULTRASONIC VELOCITY PROBE

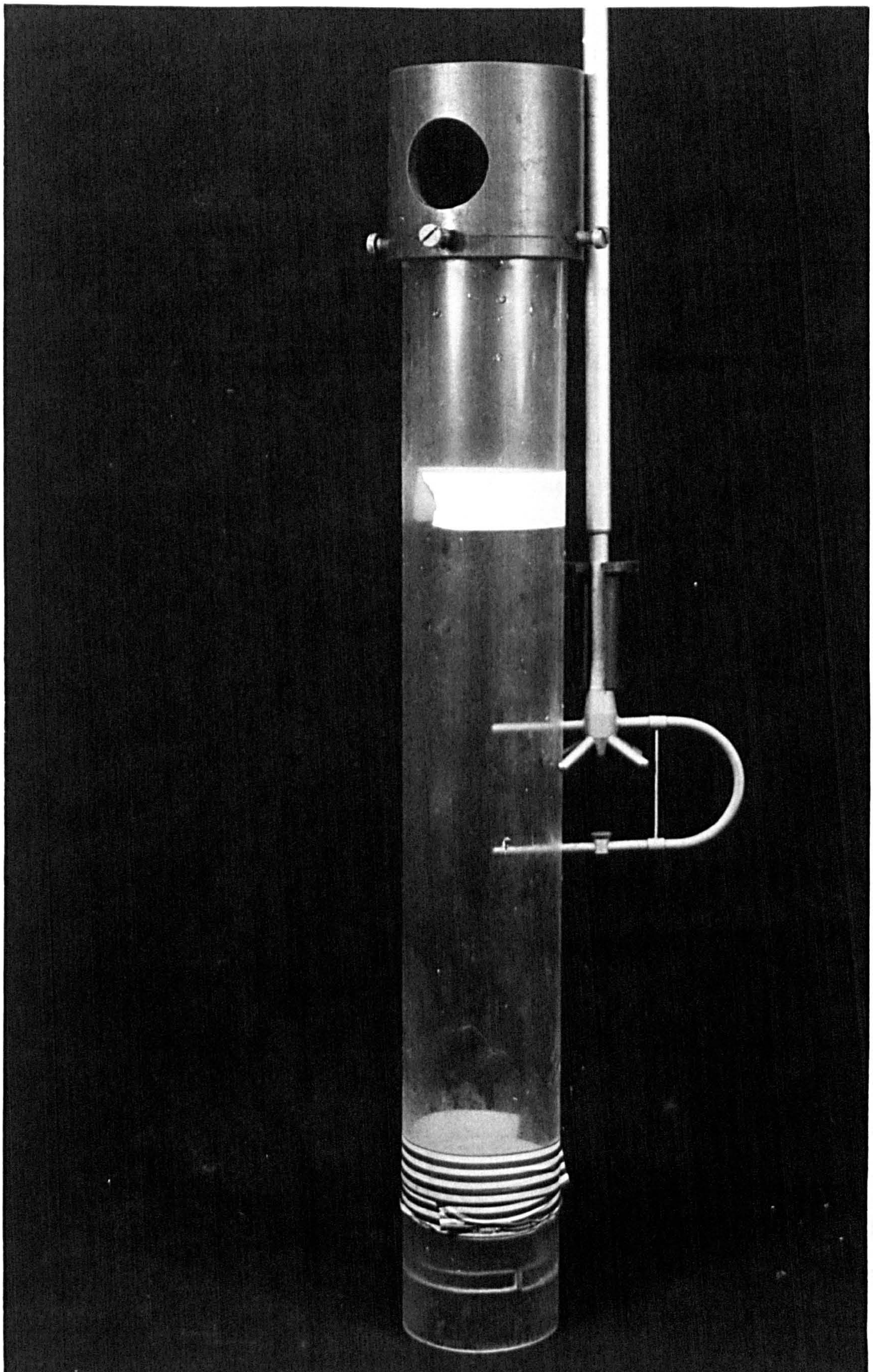

FIGURE 4.12. POSITION OF ULTRASONIC VELOCITY PROBE INSIDE RISER

This velocity meter development entailed construction of a riser and placing two small diameter pitot tubes within it, each tube positioned in such a way as to be pointing in opposite directions along the line of flow, see Fig. 4.13. Each pitot tube was connected to a small reservoir attached to the side of the riser and each of the reservoirs had a side wall incorporating a pressure transducer, the whole unit being enclosed in a water tight container to prevent damage by moisture. The velocity of flow from the riser at any instant was calculated from the change in pressure indicated by the pressure transducers. This arrangement of the apparatus enabled the determination of the flow velocity, in both the positive and negative directions, from the change in pressure recorded on the transducers.

4.4.5 Data Acquisition

The data obtained from the experiments was collected automatically using the Department of Civil Engineering Data General Eclipse computer. The analogue to digital acquisition system stored and analysed information using a variety of existing programs and some written specifically for this project. Each individual component of the apparatus, such as the wave gauges, pressure transducers and the velocity meter, was connected to one channel of the computer for the collection of data. The computer can record up to 32 channels of information at any one time and all the channels are read simultaneously. The computer can read the channels at a speed of up to 100 readings/second (100 Hz) but it was found that a speed of 20 Hz was adequate for the experiments performed for this project, and the number of channels required varied between 8 and 12.

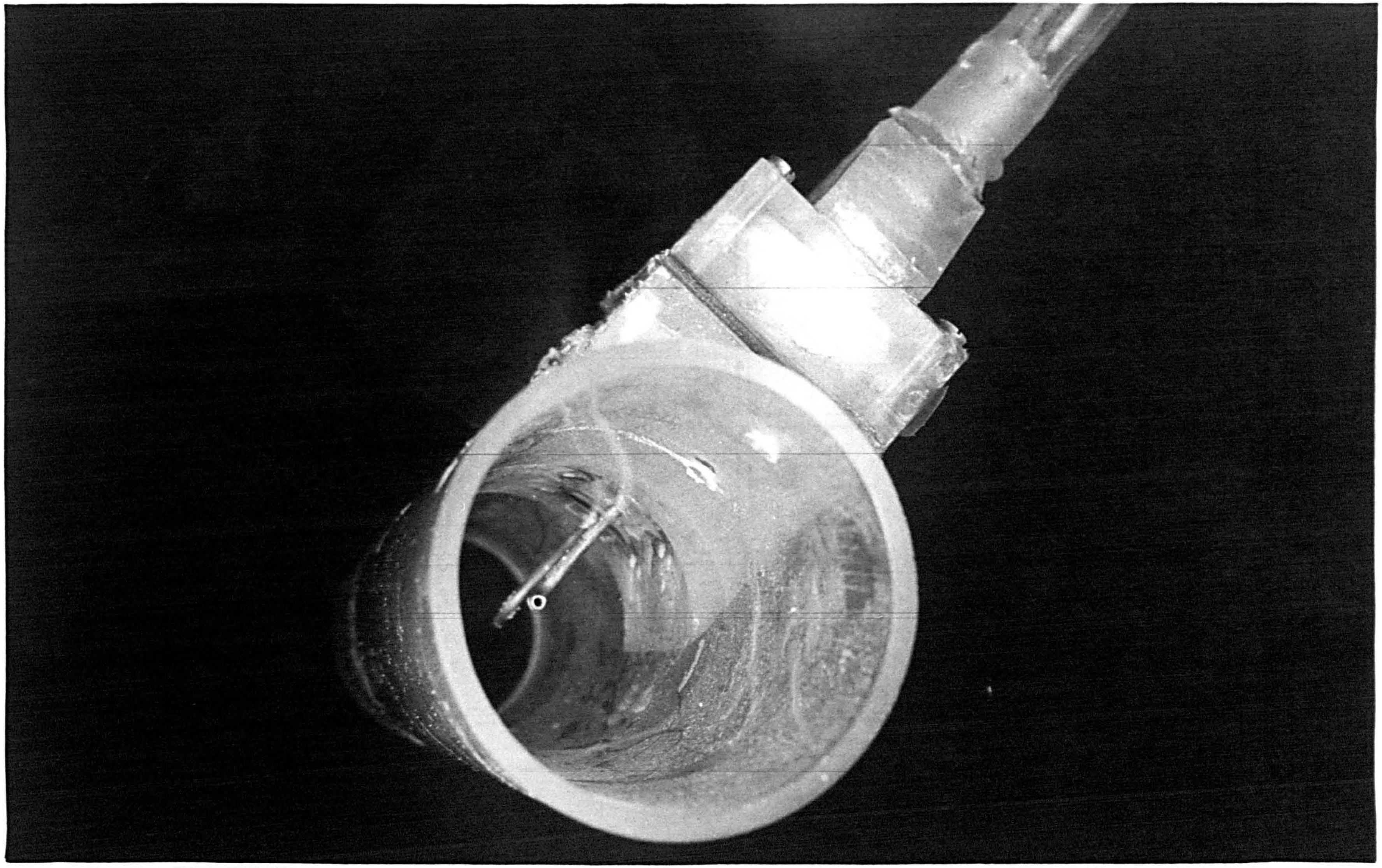

FIGURE 4. 13A VIEW INSIDE NOVEL VELOCITYMETER

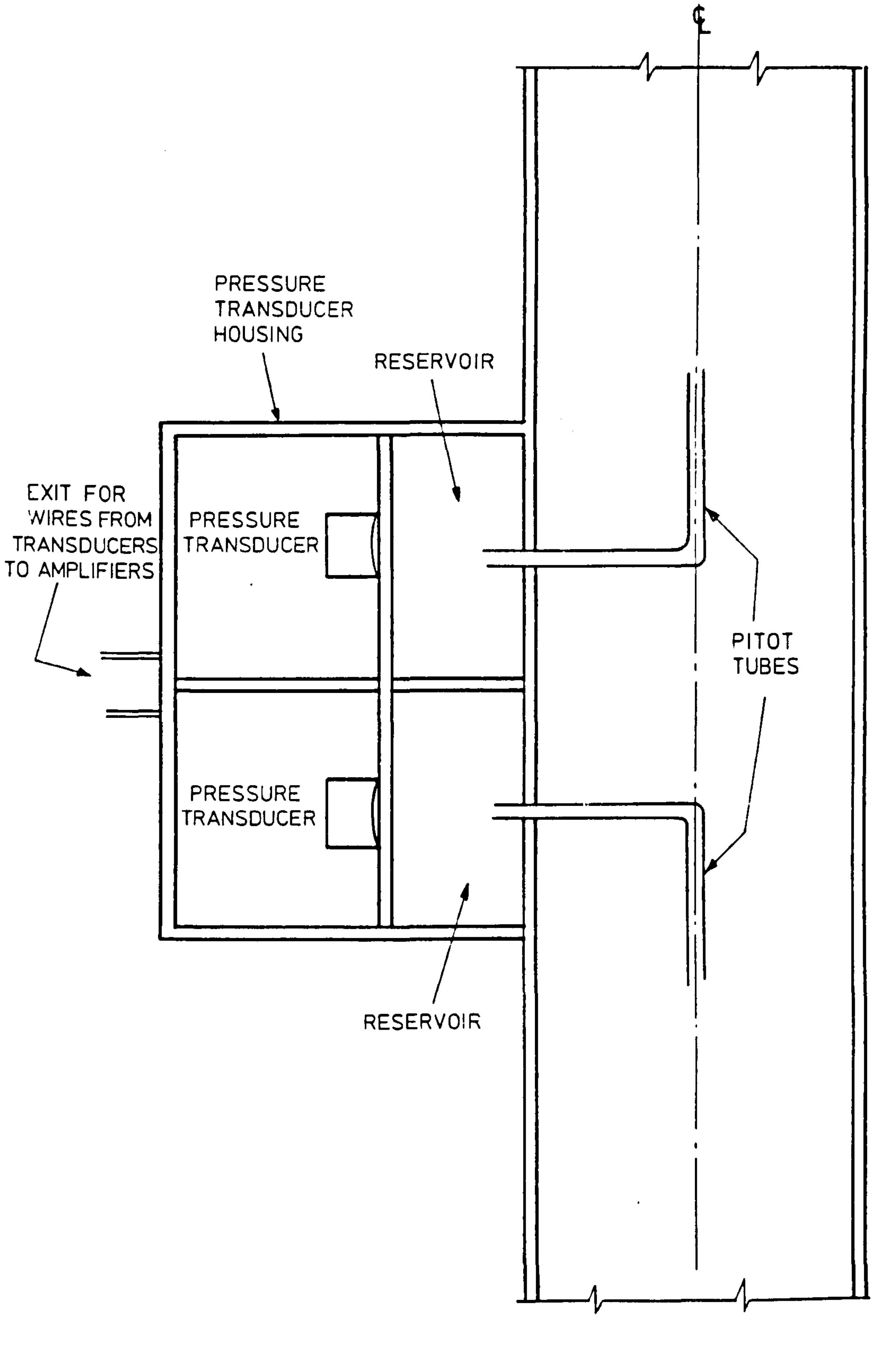

FIGURE 4.13B DIAGRAM OF NOVEL VELOCITY METER

In addition to collecting the data, the computer also had a digital to analogue converter which was used along with the program outlined in Appendix A to generate a random wave signal for the paddle in the wave tank. This enabled experiments to be undertaken to establish the effects that real sea conditions might have on an outfall. The random wave signal from the computer was fed to the paddle console which in turn drives the paddle; if regular waves were used then the wave period and waveheight were selected by the operator and the wave generator produced a sine wave using the selected values directly.

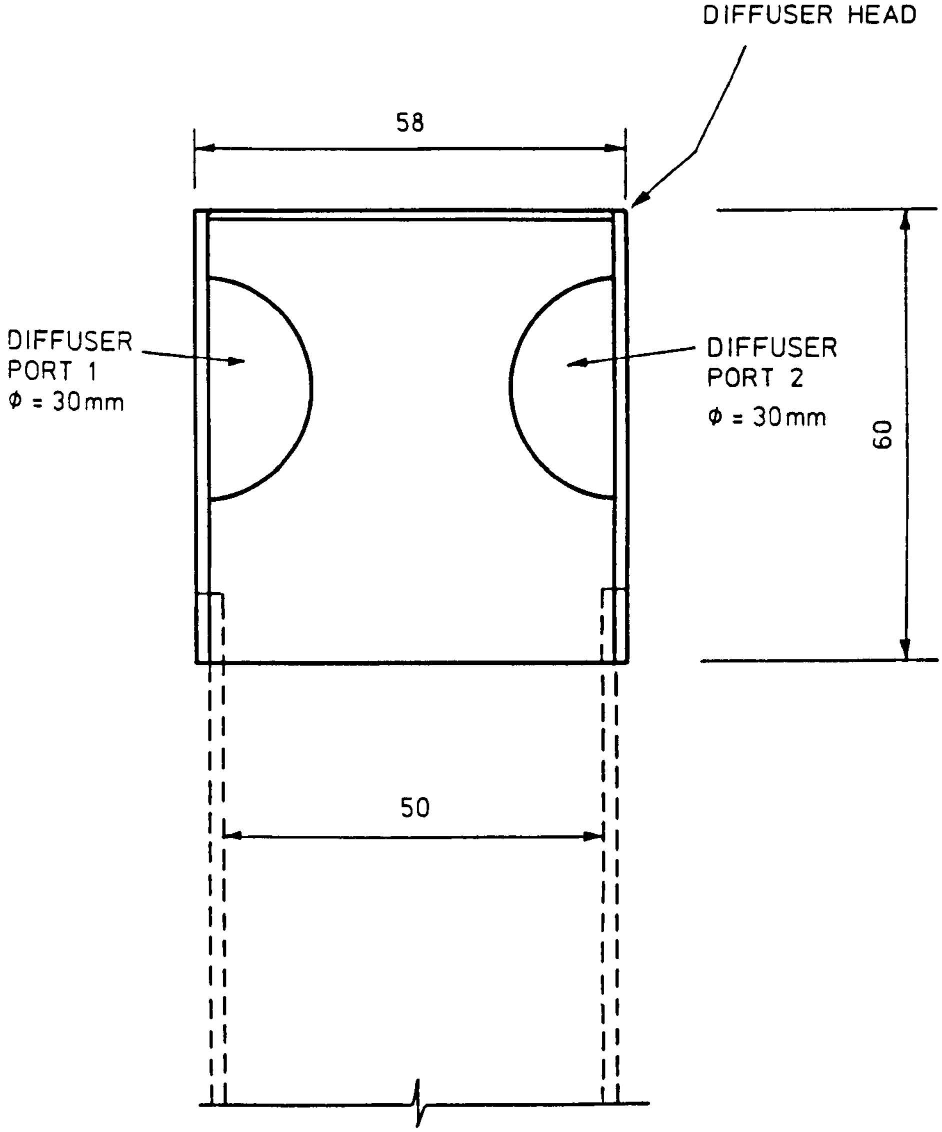

FIGURE 4.14. DIAGRAM OF DIFFUSER HEAD

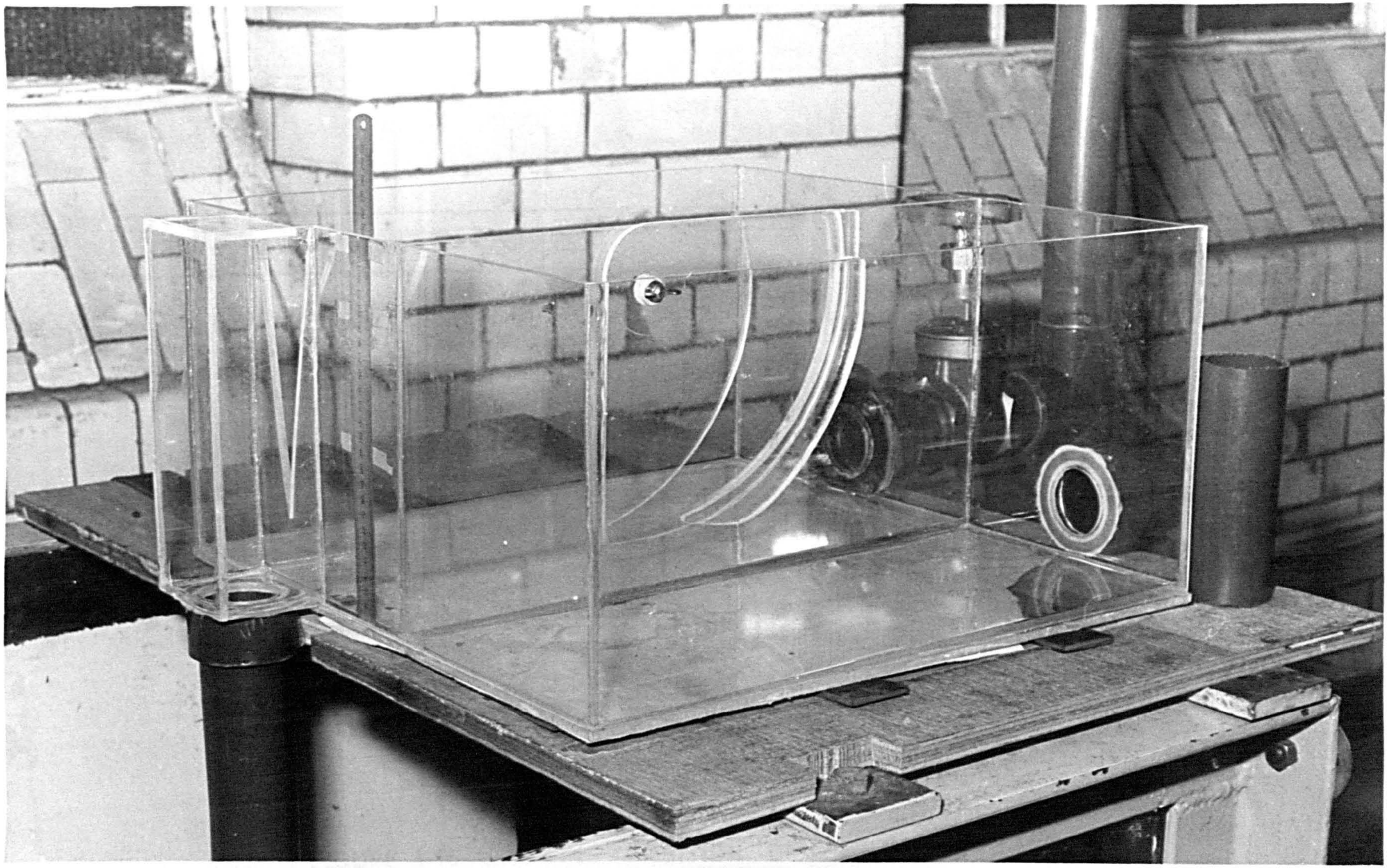

FIGURE 4.15. STILLING BASIN AND 'V' NOTCH

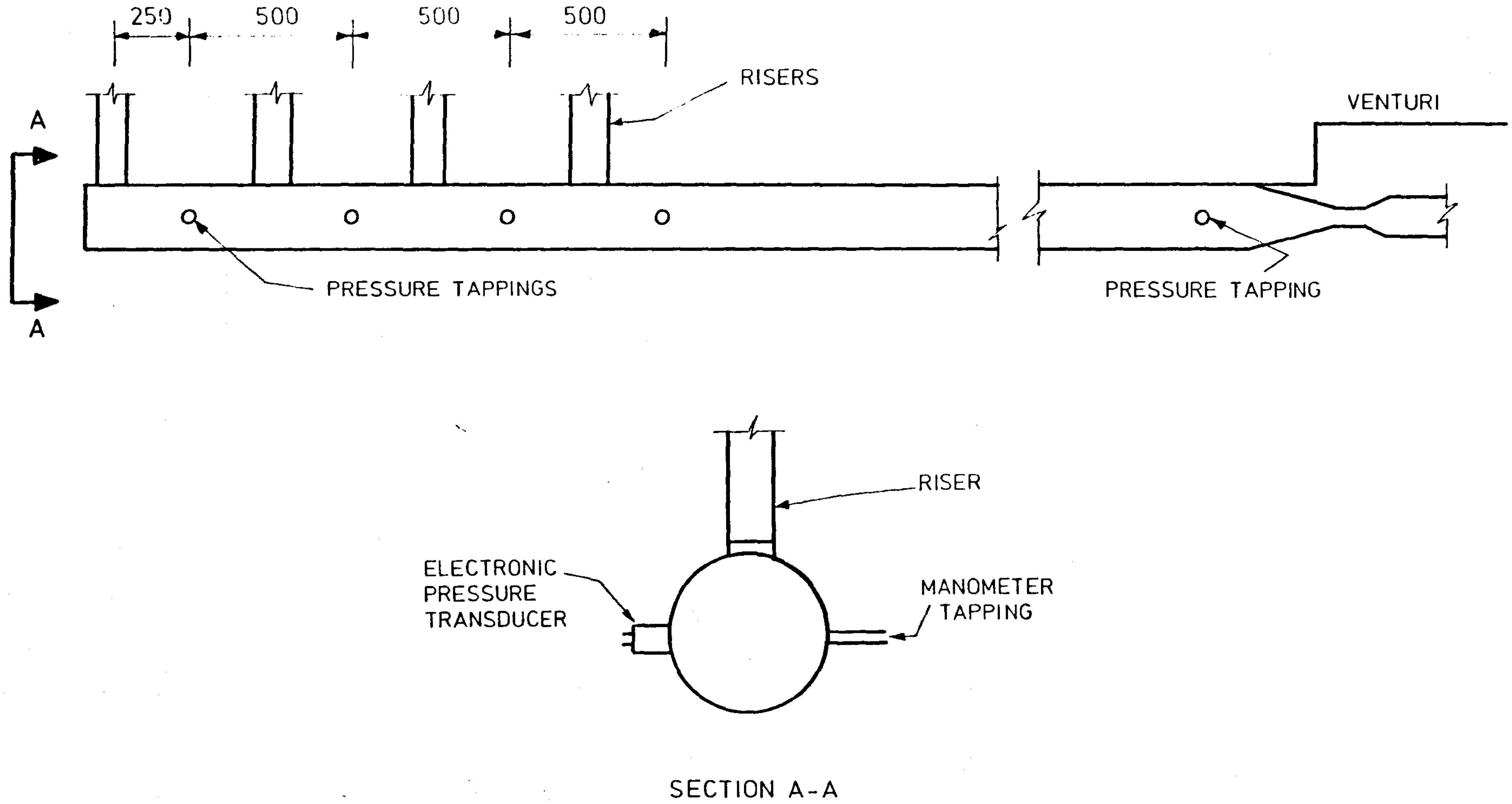

FIGURE 4.16 SHOWING POSITION OF PRESSURE TAPPINGS ALONG OUTFALL PIPE.

CHAPTER 5

EXPERIMENTAL PROCEDURE

5.1 Calibration

5.1.1 General Outline

The experimental results discussed herein were taken from either the new outfall model as described in Chapter 4, or from a smaller model detailed by Porter[47]. The new outfall model was used for both flow distribution studies and saline wedge experiments, whereas the smaller model was used specifically for collecting data on saline wedges and plume characteristics. This section is wholly concerned with procedures undertaken on the larger model.

The model was designed to be versatile so that various experiments could be performed to determine the effect of a range of physical factors influencing outfall operation. The intention was that this would eventually produce an overall picture which would provide knowledge of how outfalls performed during their operating periods.

Before work could commence, however, the physical components of the outfall had to be calibrated to ensure that reliable results were obtained. The procedure for calibrating the various components is outlined below.

5.1.2 Calibration of the 'V'-Notch

The 'V'-notch was calibrated twice, firstly in isolation and secondly in its final operating position over the outfall drop shaft. In the first instance, the V-notch was positioned over a tank and water was allowed to fill the stilling basin; once a steady head above the base of the V-notch had been established volumetric flow measurements were conducted using the collecting tank.

The V-notch and stilling basin arrangement was subsequntly placed in its final operating position on the outfall test rig and recalibrated. This was performed by installing a 'U' shaped riser in the most downstream part of the outfall model, to facilitate volumetric measurements as illustrated in Fig. 5.1.

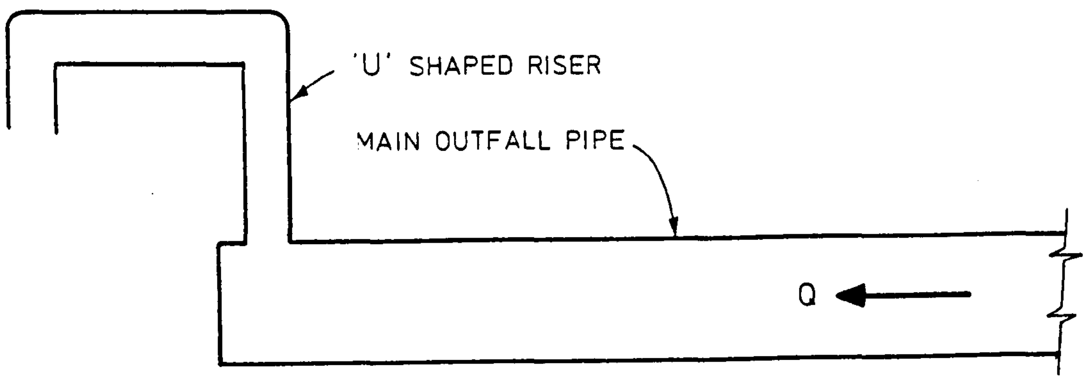

Figure 5.1

Before readings could be recorded for the calibration the system was allowed to discharge for a short period to ensure that initial flow surges had decayed and steady flow was passing through the outfall. The range of operational flows for the V-notch was 0 to 1.0 l/s -above this value too much air was drawn into the system, as discussed earlier in Chapter 4.

5.1.3 Calibration of the Venturimeter

Because of its non-standard geometry a volumetric calibration of the venturimeter was performed insitu using the same apparatus as used above for the calibration of the V-notch. In this case the rate of flow was controlled by a valve linked to the main header tank over range from 0 to 2.0 l/s. Once the flow had stabilised head differences were measured on a water manometer.

The results were plotted to produce head/discharge relationships which enables accurate estimation of the flow rate during experimental tests. These are presented in graphical form in figures 5.2 and 5.3.

5.1.4 Calibration of Electronic Instruments

Electronic measuring systems were calibrated before test runs using algorithms developed for, and built into, the data acquisition and processing system. In the case of pressure measurements and wave gauge readings the calibration was achieved by varying the depth of water in the wave tank over a known range. At each change in level the computed pressures (kN/m^2) and water levels are input and related to the analogue signals received from the transducer and wave gauges respectively. Once complete the analogue signals are automatically converted to digital signals before storage. The data acquisition system then calculates the required calibration factor to convert the digital readings to analogue values.

In the case of ultrasonic velocity measurement, calibration was performed by electronically changing the potential across the velocity probe. The same packages were used on the data acquisition system for

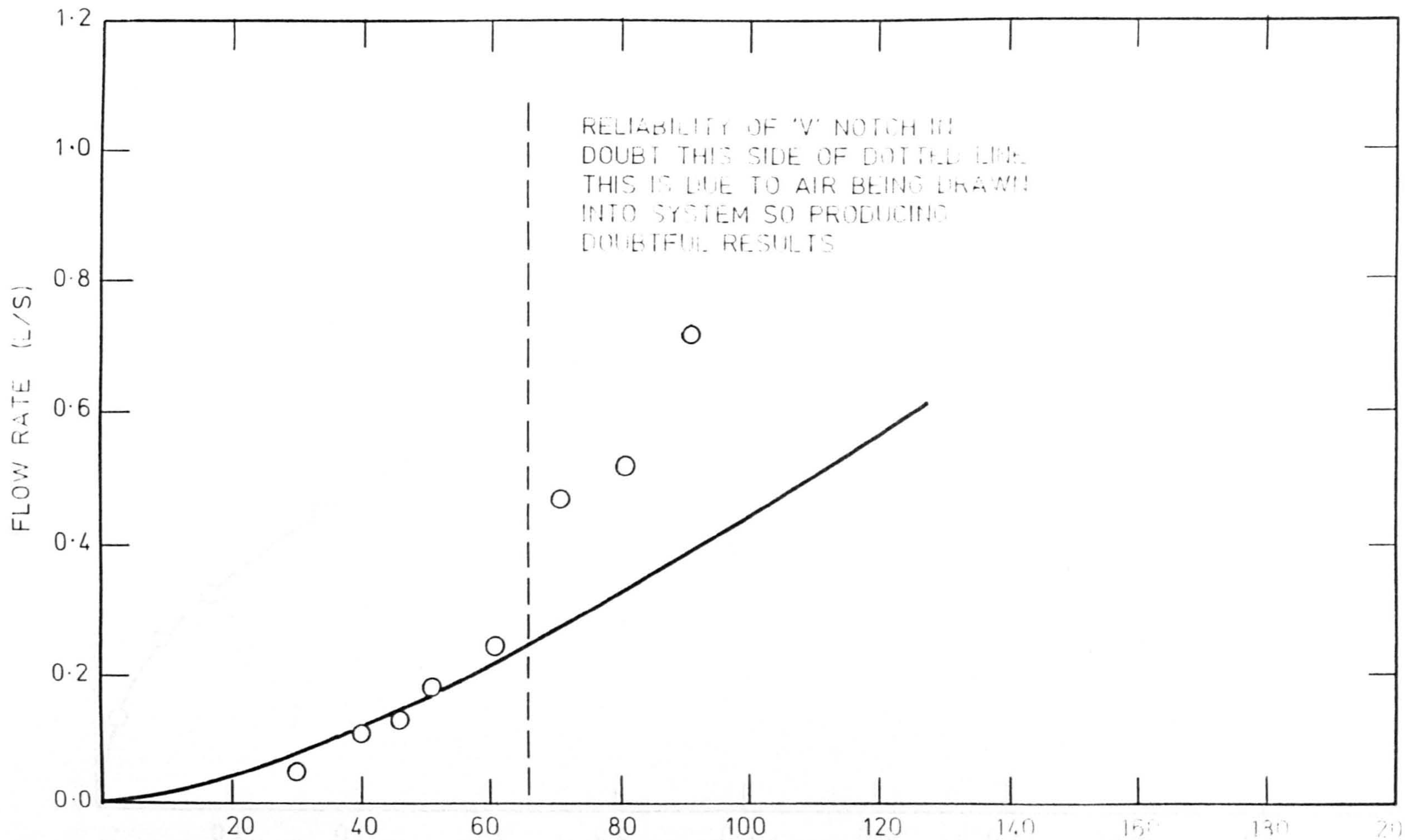

FIGURE 5.2. CALIBRATION FOR 'V' NOTCH

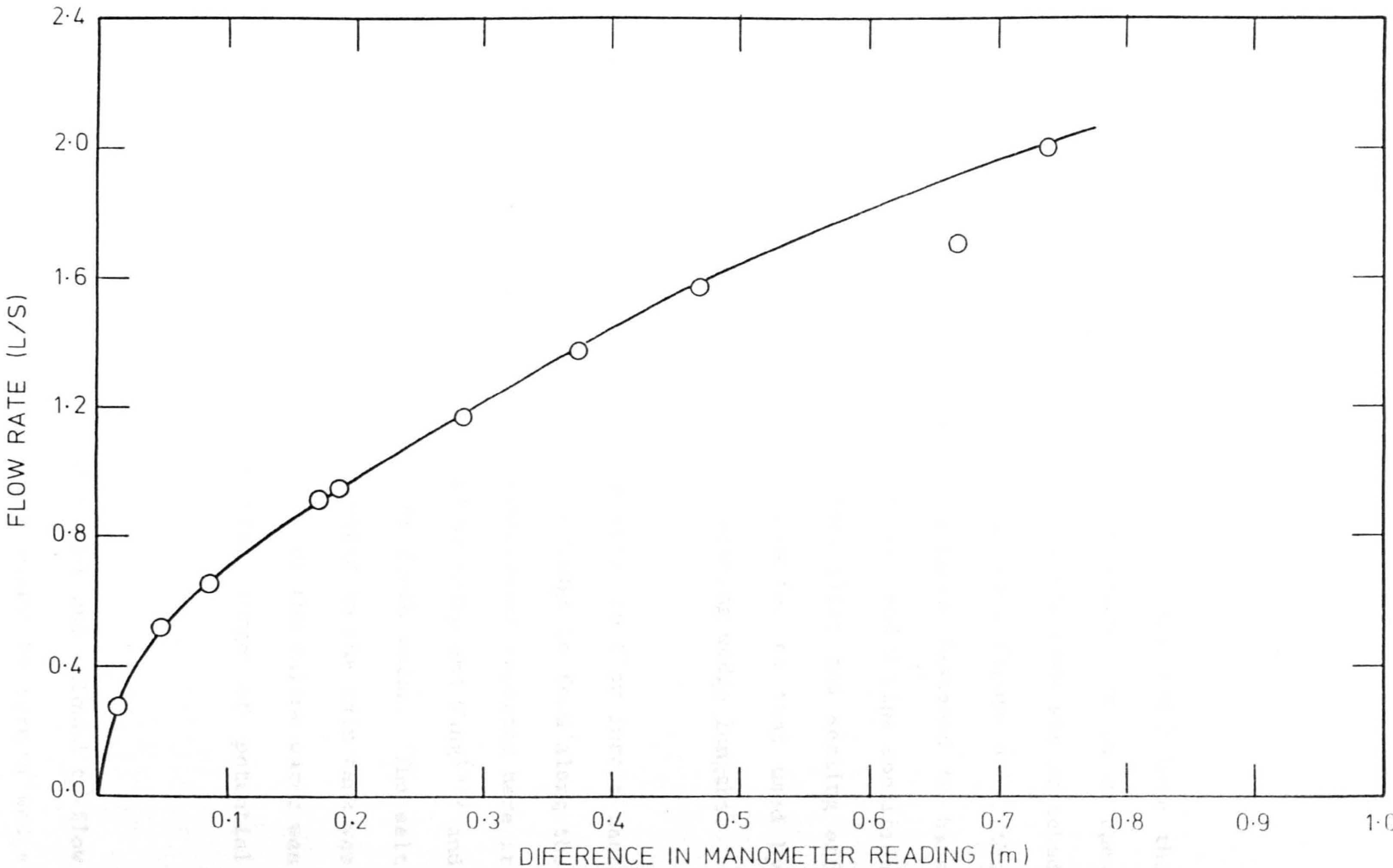

FIGURE 5.3. CALIBRATION CURVE FOR VENTURIMETER

the calibration as were utilised for the other electronic components. The velocity meter was then checked in known flows of water and the calibration was generally found to be good.

5.2 Experimentation

5.2.1 Series 1 - Saline Wedge Experiments

The initial series of experiments using the outfall model were the measurements of the lengths of saline wedges which form in an open ended pipe. For these experiments the main outfall pipe was attached to the centre mounting of the inlet manifold (see figure 4.3), the remainder of the pipe being supported by hangers fastened to bars placed across the top of the wave tank. The open ended pipe condition was created by removing the downstream flange plate and sealing off the riser ports and creating a similar situation to that used by Charlton[12,21] and Sharp and Wang[51] for measuring wedge lengths.

Charlton's experiments[12,21] allowed fresh water to flow into a tank of salt water therefore permitting the saline wedge to form along the bottom of the pipe. However, for initial experiments reported here it was decided to follow the procedure employed by Sharp and Wang[51] and to permit saline water to flow into a tank of fresh water. The salt water was mixed in the header tank and the water in the main tank was kept at a density of 1000 kg/m^3. The density of the saline water was varied between experiments to cover a wide range of potential significance.

The salt water was released from the header tank and allowed to flow through the main pipe where it induced fresh water to form a wedge along the top of the pipe as sketched in figure 5.4.

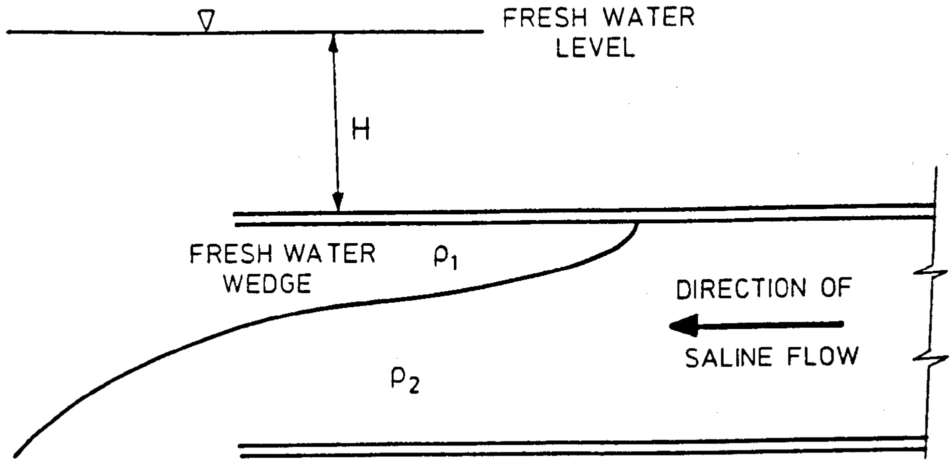

Diagram showing position of fresh water wedge

in an open ended pipe

Figure 5.4

The water level in the main tank was kept constant by drawing off the salt water through a valve located in the bottom of the tank. To measure the length of the wedge a scale was attached to the side of the pipe which was graduated in 50mm intervals; to define more clearly the position of the wedge a red dye (Rhodamine B liquid) was mixed into the saline solution whilst in the header tank. The principal disadvantage with this method is that the water within the main tank eventually becomes discoloured and prevents the scale on the pipe from being read; consequently at frequent intervals the main tank was completely emptied, cleaned and refilled with fresh water. Velocity readings within the stratified flowing layer were measured using a propeller type velocity meter. This was installed within the pipe through a specially designed outfall port cap so that it would be free to move vertically, allowing a velocity profile through the layers to be obtained.

The results produced from these tests were compared with those published by Charlton et al[12] using a smaller diameter pipe. A more extensive examination has recently been undertaken by Porter[47] in a complementary study to the present one, in which he investigates both wedge and length profiles, as well as novel diffuser sections.

The effects of wave action on wedge lengths was looked at in several exploratory tests but it proved to be difficult to obtain instantaneous results from within the pipe as the wedge was seen to oscillate in length.

5.2.2 Series 2 - Experiments Performed on an Inverted Outfall

Before any experiments could be performed using the manifold system it was important to ensure that under design flow conditions all risers discharged at an equal rate - this is the situation for which most outfalls are designed. Head loss computations (see Section 4 and Appendix B) to establish the necessary flow constrictions, using orifice tubes, to achieve this balance proved insufficient and fine tuning by trial was necessitated - this involved the removal or addition of small sections of orifice tube. Once this had been completed the base of each riser was marked to ensure the correct positioning in all experiments.

The experiments for series 2 were performed with the outfall positioned at the top of the inlet manifold and the risers pointing downwards towards the base of the wave tank. Risers where placed in the four downstream ports and the end of the pipe was sealed with a flange plate. Then the header tank was filled with saline water and the wave tank with fresh water. The initial experiments where performed with waves passing over the manifold which was under shutdown conditions, i.e. Q = 0; the velocity was measured using dye tracing techniques outlined in Section 4.4.4(i). It should be noted that the dye used should have the same density as the receiving water otherwise velocity measurements could be subject to errors due to the buoyancy of the liquid introduced. The mean velocity and overall direction of flow could therefore, be determined for each riser from the results.

The next set of experiments within this section dealt with the normal operation of flow passing through the system. For these the salt water was allowed to flow through the pipe and discharge to the fresh water regime with the velocity measured by dye tracing techniques. Two problems occurred with this experiment that rendered the results unsatisfactory and these where

i) air gathered along the top of the pipe which restricted the area of flow in the main pipe and

ii) the dye used in measuring the velocity dispersed too quickly for the velocity to be measured.

The first problem was overcome by installing two valves which removed the air from the pipe and the second problem was overcome in subsequent test series by use of a velocity probe for direct measurement.

The most serious drawback with the dye trace method is its inability to record instantaneous velocities within the risers as the progression of wave crests and troughs pass over the system. It is also impossible to synchronise the velocities with pressure measurements taken within the pipe.

For all these experiments a sinusoidal wave pattern was generated using the wave paddle generator system for which waveheight and periods could be specified. The actual heights in the tank were measured using Churchill wave gauges attached to the eclipse computer system. In all the experiments the water level was maintained at a constant level by drawing off water from the bottom of the tank as experiments proceeded.

Overall these experiments were useful in that they gave an early insight into the effects of wave action on an outfall and pointed the direction for the main experimental studies.

5.2.3 Series 3 - Outfall in Upright Position Under Shutdown Conditions

For operation in the more conventional position the outfall was attached to the lower connection on the inlet manifold and the ultrasonic probe was used to accurately record time varying velocities in the risers under wave action.

This series of experiments which looked at the outfall during shutdown conditions, was carried out for several different wave heights and periods and the wave tank was either filled with fresh or salt water. Because only one ultrasonic probe was available the experiment had to be carried out four times to enable the measurement of flows in each riser in turn. The probe was positioned through holes in the side of a riser, see figure 4.12, and the holes in the remaining risers were blocked off by dummy probe arms. Once the velocity-meter had been positioned results were recorded by activating the computer data collection program; the results from each instrument being recorded for a duration of 100 seconds at a sampling rate of 20 readings/second (20 Hz). The results were then analysed and plotted using purpose written programs within the computer system.

5.2.4 Series 4 - Outfall in Upright Position with Flow Passing Through the Manifold System (Normal operating conditions - no waves)

Series 4 experiments examined what effect varying outfall flow rates have on the flow distribution within the manifold/riser system of an outfall. The aim was to extend the earlier reported work of Charlton[17,19] and Wilkinson[60]. For all experiments the outfall was positioned in its conventional (upright) position, the main wave tank was filled with salt water and the header tank contained fresh water. Saline water within the wave tank was circulated using a submersible pump to ensure the removal of density stratification. Both tanks of water were allowed to stand for several hours so that each would have approximately equal temperature thereby avoiding thermal stratification. Again four tests were completed for each varying set of conditions so that the velocity fluctuations in all four risers could be recorded.

The experiment was carried out by establishing a flow rate over the V-notch or through the venturimeter, then allowing this to continue until the velocity in the riser being measured had reached a steady value, the pressure of water above the manifold system was kept constant by the removal of salt water from the base of the tank. The pressure was gauged from the pressure transducer used for surface elevation measurement. Once the system had achieved a steady balance the data collection system was activated.

Due to the large volume of the wave tank it was found that when small flow rates where discharged from the outfall, volume and density changes within the wave tank were small. After each set of four experiments, the wave tank and outfall model were left for several hours to stabilise and then the water in the wave tank was remixed to ensure an overall uniform density. The results obtained were analysed using similar procedures to those described in Section 5.2.3.

5.2.5 Series 5 - Effects of Wave Action on a Discharging Outfall System

Series 5 experiments were designed to investigate the effects that wave action has upon the manifold/riser system whilst the outfall is discharging. Experiments where carried out in the same way as outlined in Section 5.2.4, except that after the flow had stabilised and before the data collection system was activated waves were generated to pass over the outfall, for the required 100 second run period. The waves were of a sinusoidal form and target values of heights and periods were specified. The flow rates used in both Sections 5.2.4 and 5.2.5 ranged from 0.1862 l/s up to the design flow rate of 2.0 l/s.

5.2.6 Series 6 - Effects of Wave Action on an Outfall with Diffuser Heads Fitted to the Risers

The experimental procedures outlined in Sections 5.2.4 and 5.2.5 were repeated to investigate the effects of variations in flow and wave action on riser flow distribution when diffuser heads are fitted to the tops of the riser pipes.

CHAPTER 6

SALINE WEDGE RESULTS

6.1 Introduction

The major part of the work reported here is concerned with the effects of two density flow regimes within pipes. Because of this it was felt at an early stage that a greater understanding of the mechanism and formation of saline wedges within conduits was required if reliable means of numerically modelling flows through multi-riser systems are to be developed in circumstances where stratification is present.

To examine the form of saline wedges two experimental models were used. The first was an open-ended pipe of 105mm diameter enclosed within the wave flume described earlier in Section 5.2.1. The second was a 50mm diameter pipe which discharged into a tank of saline water[47]. Rhodamine B liquid dye was introduced to show more clearly the position of the wedge; however, the injection of the dye did create some problems as outlined in Section 5.2.1. and in this respect the 50mm diameter pipe was less troublesome because it was located outside of the tailwater tank. Consequently, the detailed profile measurements of saline wedges were restricted to the 50mm pipe, and wedge lengths only were recorded using the larger model facility. Wedge length data produced by Charlton et al[12] employing an 88mm diameter perspex pipe, was utilized for comparison purposes, and proved to be useful during the calibration of the associated numerical models.

6.2 Results of Series 1 Experiments

6.2.1 Saline Wedge Lengths

The experimental results for wedge lengths in the larger (105mm) diameter pipe are shown in Figure 6.1 and are compared with the results obtained by Charlton(12). All experiments were performed in a horizontal pipe and the density of saline water was varied for the different tests.

Figure 6.1 shows the results plotted in the dimensionless form $^L/D$ against the densimetric Froude number (F_{RD}); where L is the wedge length and D is the pipe diameter. The densimetric Froude number is obtained from

$$F_{RD} = \frac{Q/A_p}{\sqrt{E\ g\ D}} \qquad (6.1)$$

where Q = flow rate through the outfall pipe

A_p = area of pipe

E = density factor = $(\rho_2 - \rho_1)/\rho_2$

g = acceleration due to gravity and

D = pipe diameter

It can be seen that a trend is followed by all of the results; that is as the densimetric Froude number increases, the value of $^L/D$ decreases. They also show that as the value of F_{RD} tends towards unity, the value of $^L/D$ tends towards zero indicating that the wedge will be purged from the pipe. Conversely, the Froude number falls towards zero when the wedge length becomes infinite; in other words the length of the wedge will frequently be constrained by both the length and position of the outfall.

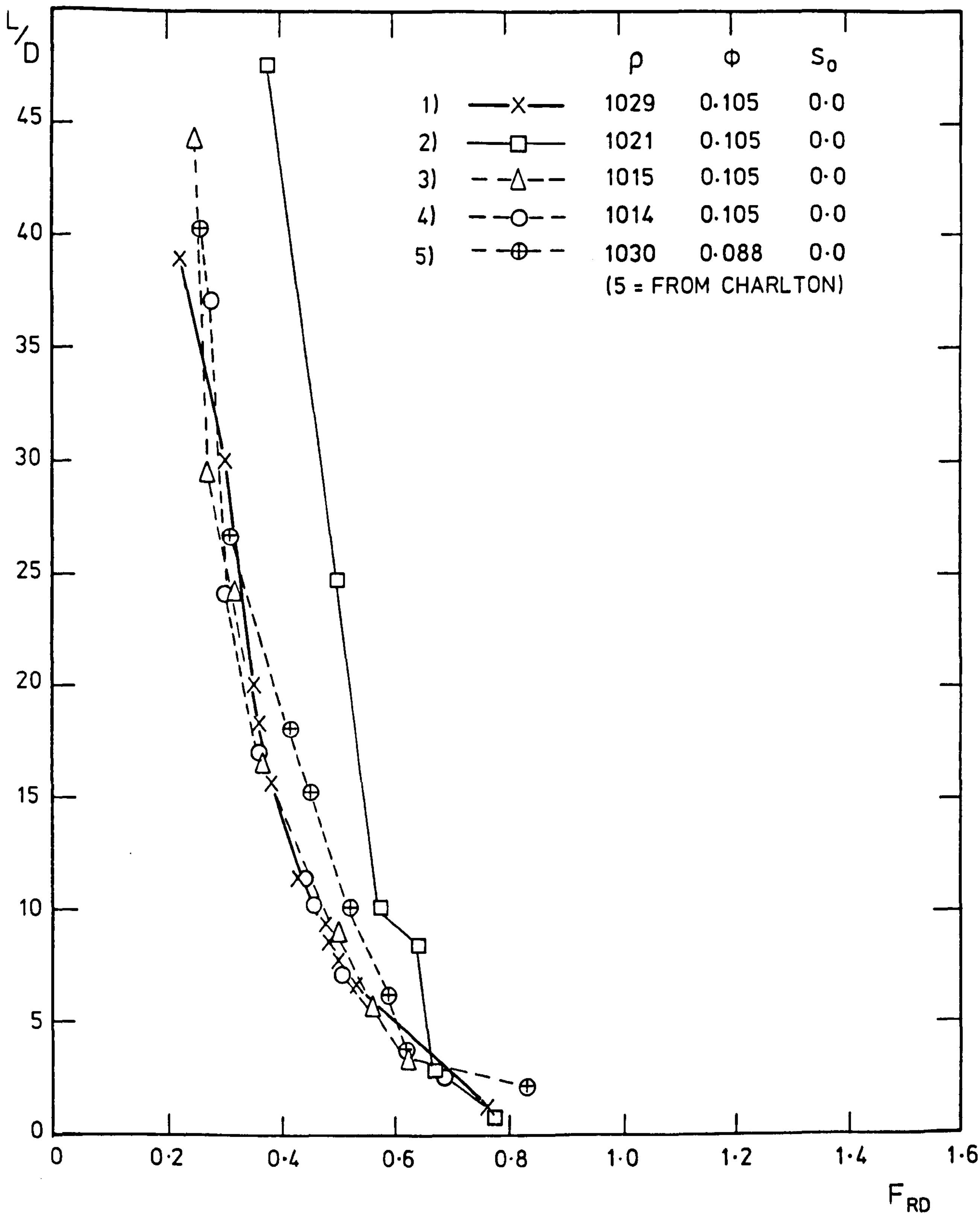

FIGURE 6.1. VALUES OF L/D AGAINST F_{RD} FOR SERIES 1 EXPERIMENTS

The set of results produced when using a sea water density of 1021 kg/m^3 and a pipe diameter of 105mm show a marked deviation from other results. This is possibly attributable to experimental error since all other results follow a consistent pattern.

It should be noted that Charlton[12] and Davies et al[21] in their equivalent plots use a value of (2 F_{RD}) for the horizontal axis, following from work carried out by Keulegan[34]. This was termed by Keulegan as the river flow parameter and used to describe the depth of the salt wedge at a river mouth. By a combination of both experimental and field data it was possible to determine the effect of an open channel on the profile of saline wedge. The use of this factor in relation to pipes is open to question and Davies et al[21] note that there are potential pitfalls in applying two dimensional open channel results to a three dimensional problem. This is considered later in Section 6.5.

6.2.2 Velocity Profiles

Whilst the experiments for determining wedge lengths and profiles were underway, it was decided that velocity profiles should also be recorded to justify assumptions made during theoretical developments reported upon in Section 3.3. The theoretical assumption was that the flow in the saline layer was zero, and the velocity in the moving upper layer had a uniform distribution. The results produced were used to determine the required calibration of the velocity dependent components in the mathematical model.

Initial experiments were performed using a sea water density of 1026 Kg/m^3 and a flow rate of 0.41 l/s, giving a densimetric Froude number of 0.293. Velocity meters were inserted at three positions, 500mm, 1500mm and 2500mm from the open end of the pipe. Figure 6.2 shows that velocity profiles steepen towards the open-end of the outfall in the upper layer, hence the maximum velocity increases. It is interesting to note that as the velocity profile narrows it steepens near the pipe wall and the slope tends to be more gradual nearer the wedge, suggesting that there could be a positive velocity within the wedge caused by interfacial shear. This however, is thought to be small because the velocity probe was unable to trace any movement within the saline layer. The velocity meter could not accurately record values below about 1 cm/sec; also, velocity values within the interfacial region are subject to small errors due to interfacial wave action.

The velocity profiles in Figure 6.3 indicate the variation in velocity between the toe of the wedge and the exit of the flowing layer from the outfall pipe. Figure 6.3 shows the results for a flow rate of 0.537 l/s and a seawater density of 1015 kg/m^3. These give densimetric Froude number of 0.503 and a Reynolds number (not densimetric) of 5712, indicating a turbulent flow regime. Figure 6.3 also shows that at the toe of the wedge, the velocity profile is similar to that expected for a turbulent flow regime and as the flow passes over the wedge, the velocity profile steepens.

The final results are presented in Figure 6.4 for a flow rate of 0.427 l/s and a seawater density of 1022 kg/m^3. These give values for the Reynolds and densimetric Froude numbers of 4542 and 0.331 respectively. All profiles show results that are consistent with turbulent flow characteristics, indicating similar trends to the previous results given in Figures 6.2 and 6.3.

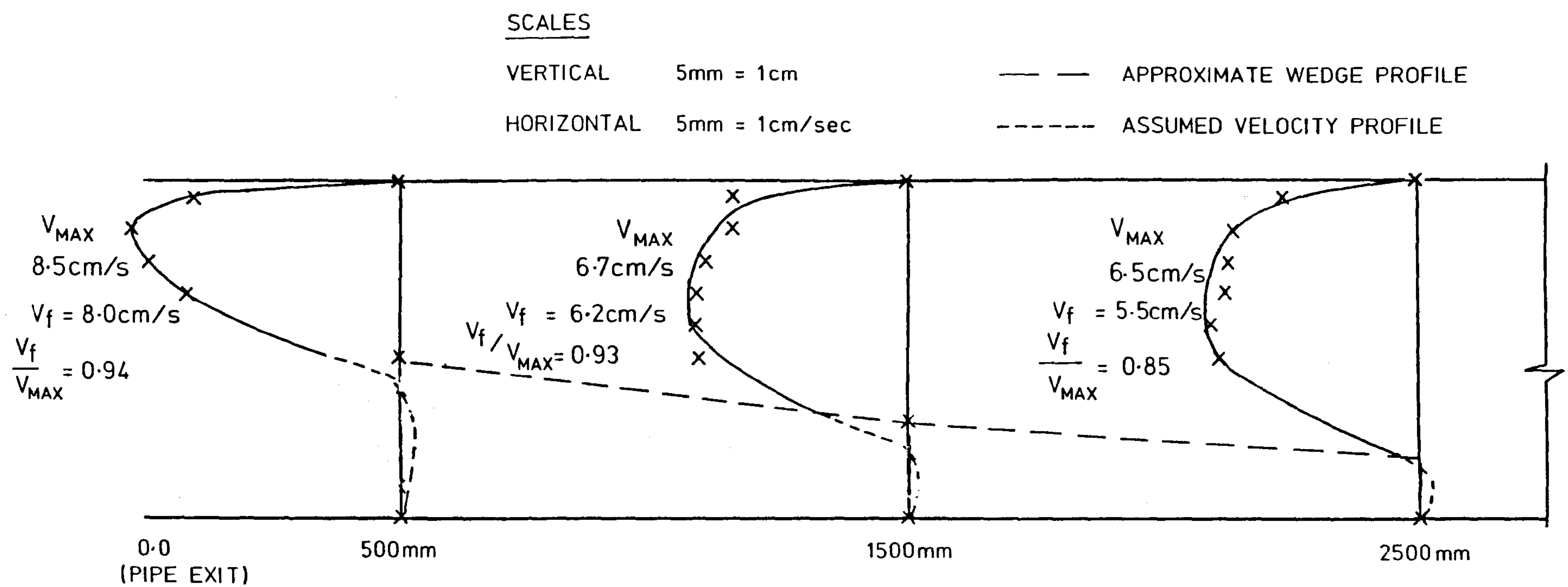

FIGURE 6.2. VELOCITY PROFILES IN PIPE FOR $\rho = 1026 kg/m^3$ AND FLOW RATE = 0·41 L/S

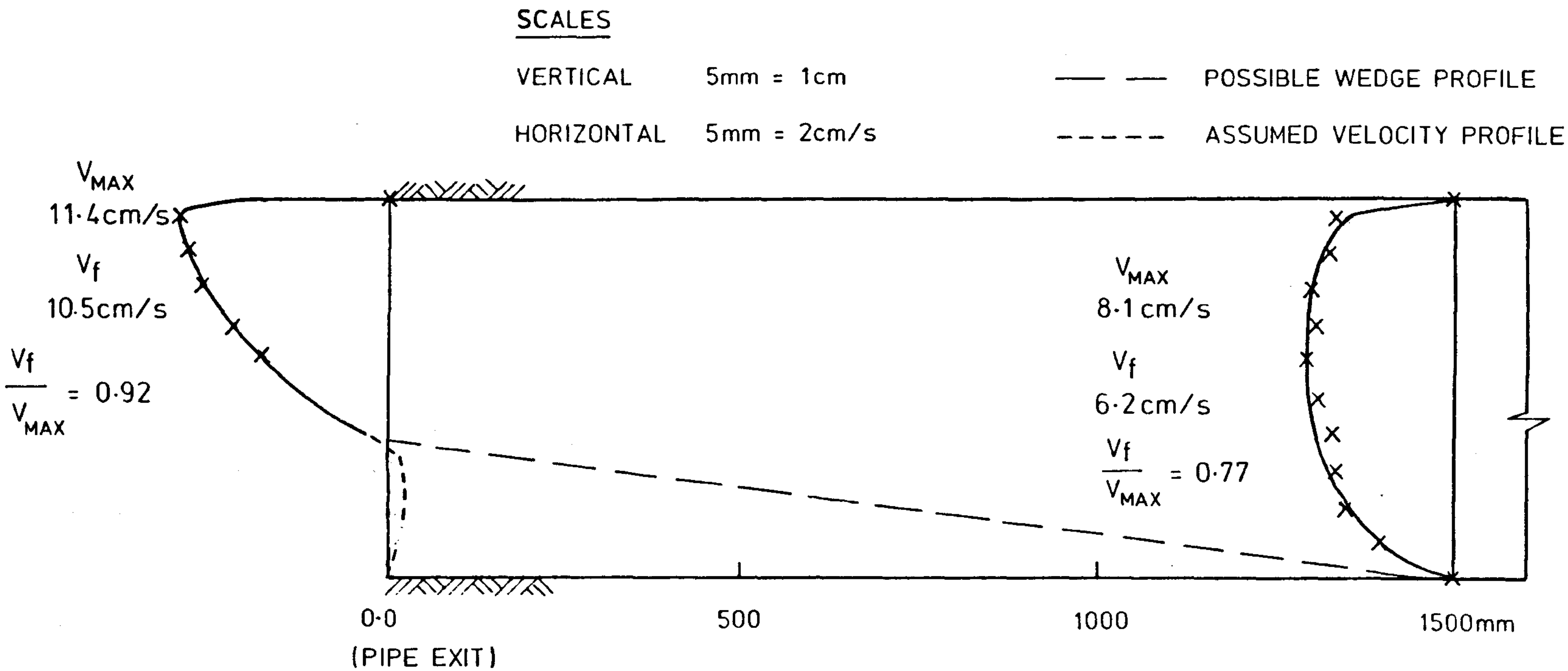

FIGURE 6.3. VELOCITY PROFILES IN PIPE FOR ρ = 1015kg/m^3 AND FLOW RATE = 0·537L/S

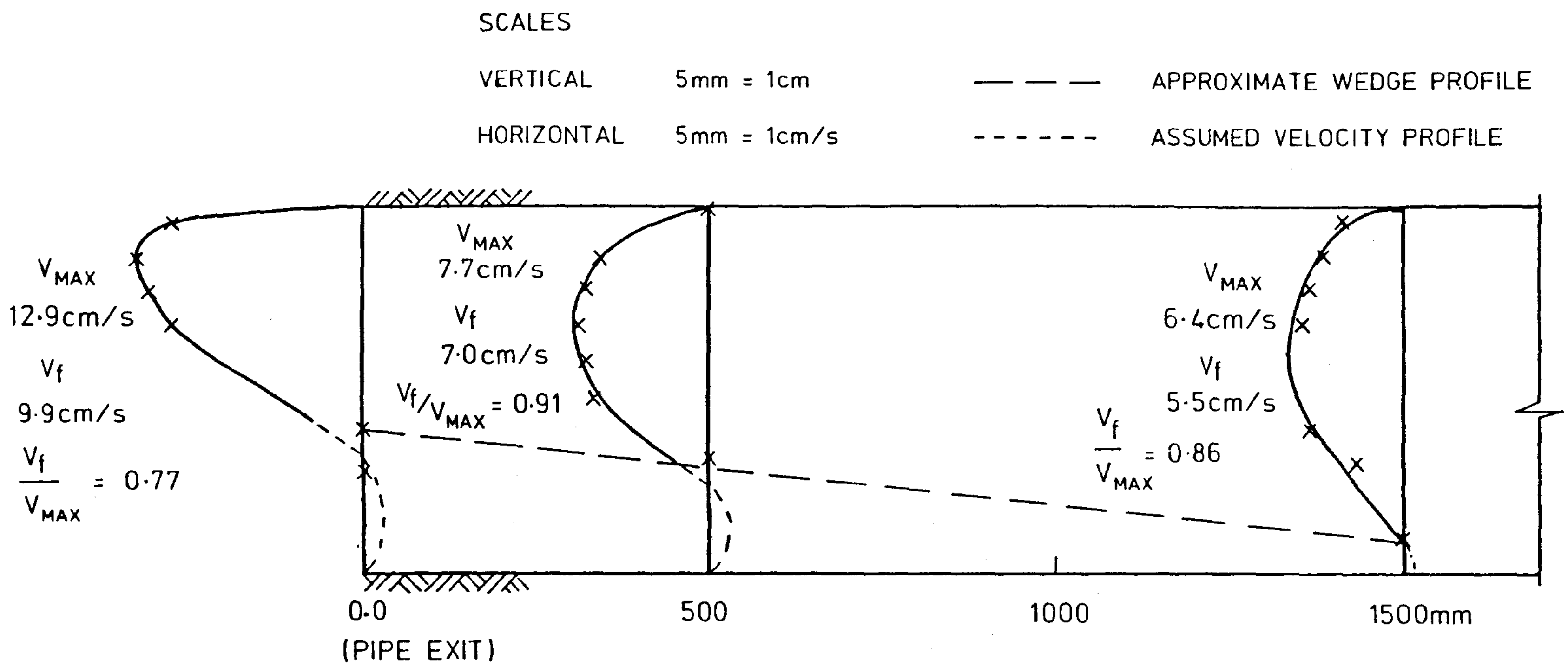

FIGURE 6.4. VELOCITY PROFILES IN PIPE FOR $\rho = 1022 kg/m^3$ AND FLOW RATE = 0·427 L/S

The experimental results of velocity profiles show that as the flow reaches the outlet point of the pipe the velocity profile becomes more peaked. However the ratio of V_f/V_{max} does not show this. The possible explanations are

i) experimental error in determining V_{max} using the propellor meter
ii) the calculation of V_f required an accurate valuation of the depth of flow. As the depth of flow was constantly changing due to interfacial wave action it seems feasible that an accurate value was not obtained
iii) towards the outlet section of the pipe the velocity of the flowing layer will have both horizontal and vertical components. As the propellor meter only measured the horizontal flow this could also lead to errors in measuring V_{max}.

6.2.3 Wedge Profiles

Wedge profile experiments were conducted in the smaller 50mm diameter pipe both by the author and by Porter[47]. The results obtained are discussed more fully by Porter and are utilised in this report for calibration of the numerical model.

6.3 Numerical Model

6.3.1 Introduction

The application of the numerical model for obtaining saline wedge lengths and profiles is based on Equation (3.59) which is

$$\Delta x = \frac{\left[\frac{\Delta d_1}{2} + \frac{\rho_2}{2\rho_1} \Delta d_2 + \frac{\rho_2}{2\rho_1} A_{s2} \Delta d_2 - \frac{1}{2} A_{s1} \Delta d_1 - A_{s1} \Delta d_2 - \frac{V_1}{g} \Delta V_1\right]}{\left[\frac{T_1}{\rho_1 g A_1} - \frac{T_2}{\rho_1 g A_2} + A_{s1} S_o - \frac{\rho_2}{\rho_1} A_{s2} S_0\right]}$$

(6.2)

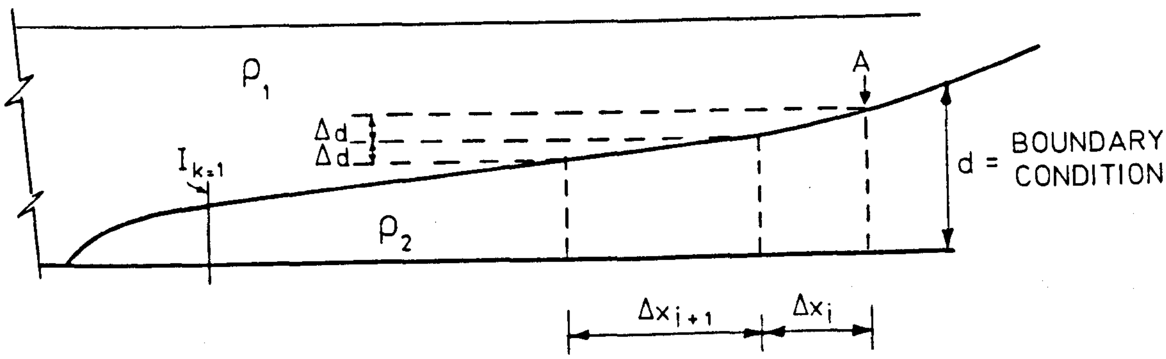

Sketch showing Calculation steps for numerical model

Figure 6.5.

The notation used in equation (6.2) is given in Section 3.3 and details of the numerical model are provided in Appendix D.

The saline wedge occurs as a result of seawater/freshwater contact, and one of the governing factors determining the shape of the wedge is the shear stress acting at the interface of the two fluids, each of different densities. Wall and interfacial shear stresses are given by equations (6.3) and (6.4) respectively;

$$\tau_o = f \frac{\rho}{8} \quad V_1 |V_1| \tag{6.3}$$

and $$\tau_i = f_i \frac{\bar{\rho}}{8} \quad (V_1 - V_2)|(V_1 - V_2)| \tag{6.4}$$

The symbols have previously been defined in Section 3.3.2 herein. The equation used for obtaining 'f' in the mathematical model was Colebrook-White, utilizing a Reynolds number based on the hydraulic radius of the flowing layer so that

$$R_e = \frac{V_1 \, R}{\nu} \tag{6.5}$$

where R = hydraulic radius.

Modelling the interfacial friction factor (f_i) also creates problems; from Section 2.1 it has been noted that several researchers have derived empirical relationships for the magnitude of the interfacial friction factor, and that they generally offer different values. Moreover the relationships have been deduced for flows in open channels and estuaries, and to date no research has been found relating to interfacial friction factors for flow in pipelines.

It is known that at the pipe wall friction factors and shear stresses depend on the boundary layer along the wall[32]. Hence it can be assumed that the magnitude of interfacial shear stress will depend upon the various processes taking place at the boundary between the salt wedge and the flow of fresh water.

This is a highly complex situation and generally it is found that equations for numerically modelling this condition have been derived empirically from experimental data. The equation used to determine the friction factor in the numerical model used herein is that developed by Dick and Marselak (see Smith and Elsayed[52]); the equation is given as

$$f_i = 0.316/R_e^{0.25} \tag{6.6}$$

where $R_e = 4 \frac{V_1}{\nu_1} \left[\frac{A_1}{B_1 + W}\right]$

This equation is the same as that given in Section 2.1 except that the suffixes have been changed so that '1' represents the upper flowing layer. Dick and Marselak obtained their equation for a lower flowing layer, (when the salt water layer was in motion with a static upper layer), but Smith and Elsayed[51] mention that it would be reasonable to assume that the relationship for the interfacial friction factor would still hold if the parameters were changed to suit an upper flowing layer. As this friction factor was found from open channel flow experiments, it was expected that some corrections may need to be made because of possible different flow conditions within a pipe and that of an open channel.In both the pipe and channel situations the velocity of flow will increase as the area decreases but in the pipe situation any interfacial effects are subject to variation as the pipe width changes. Up until the spring point the width of the wedge increases, once this point is passed the width of the wedge will decrease to the pipe exit. This will not occur in an open channel or rectangular conduit as the width remains constant.

The numerical modelling procedure computes the wedge profile in the following manner,

i) the depth of the wedge of salt water at the pipe exit is determined using the theoretical equations in Section 3.3.3,

ii) the value for Δd, as shown in Figure 6.5 is obtained by dividing the depth of the salt wedge at the pipe exit by 50 to ensure an acceptable resolution for the results,

iii) the value of Δx is then calculated for each interval of Δd using equation (6.2)

iv) graphical plots are then produced showing the saline wedge profiles.

6.3.2 Boundary Conditions

The boundary conditions used within the numerical model play an important role in determining the calculated length of the saline wedge, as well as providing an accurate prediction of the wedge profile. The way in which the numerical model is developed involves realistic predictions of salt wedge height at the exit of the pipe to ensure a reasonable calculation of wedge profile and length. Therefore, initial calculations were made using the numerical model to compare theoretical and experimental boundary conditions, and the results are shown in Table 6.1, together with the theoretical and experimental wedge lengths. The theoretical boundary conditions are obtained from the equations in Section 3.3.3. Figures 6.6 and 6.7, lines (a) and (c) show a comparison of the boundary condition at the pipe exit in respect of the 50 mm diameter conduit. It can be seen from both Table 6.1 and Figures 6.6 and 6.7 that there is very little difference between the theoretical and experimental boundary condition (height of the salt wedge) at the pipe exit. The difference between the theoretical and experimental salt wedge heights at the boundary is, apart from one result, between 0 and 7 mm. Errors could be due to experimental error as interfacial waves could cause these differences in the height of the salt wedge. Consequently it was decided to leave the boundary condition equations in their original form as shown in Section 3.3.3.

Flow Rate (L/S)	Seawater Density (kg/m^3)	Densimetric Froude Number (F_{RD})	Numerical Wedge Height at Pipe Exit (cm) (D_1)	Experimental Wedge Height at Pipe Exit (cm) (D_2)	Numerical Wedge Length (m) (L_1)	Experimental Wedge Length (m) (L_2)	% Difference in Wedge Height $\left(\frac{D_1 - D_2}{D_2}\right)$	% Difference in Wedge Length $\left(\frac{L_2 - L_1}{L_2}\right)$
0.125	1044	0.443	3.2	3.2	2.13	1.05	0%	-39%
0.105	1026	0.480	3.2	3.5	2.21	1.50	8.6%	-8.6%
0.167	1041	0.612	2.9	3.0	0.801	0.85	3.3%	-20%
0.175	1033	0.712	2.7	3.0	0.622	0.95	10.0%	5.8%
0.197	1042	0.714	2.7	2.0	0.717	0.35	-35%	-141%
0.210	1036	0.819	2.5	1.0	0.437	0.15	-150%	-385%
0.197	1028	0.868	2.4	2.0	0.375	0.35	-20%	-102%

Results for 50 mm diameter pipe

Table 6.1

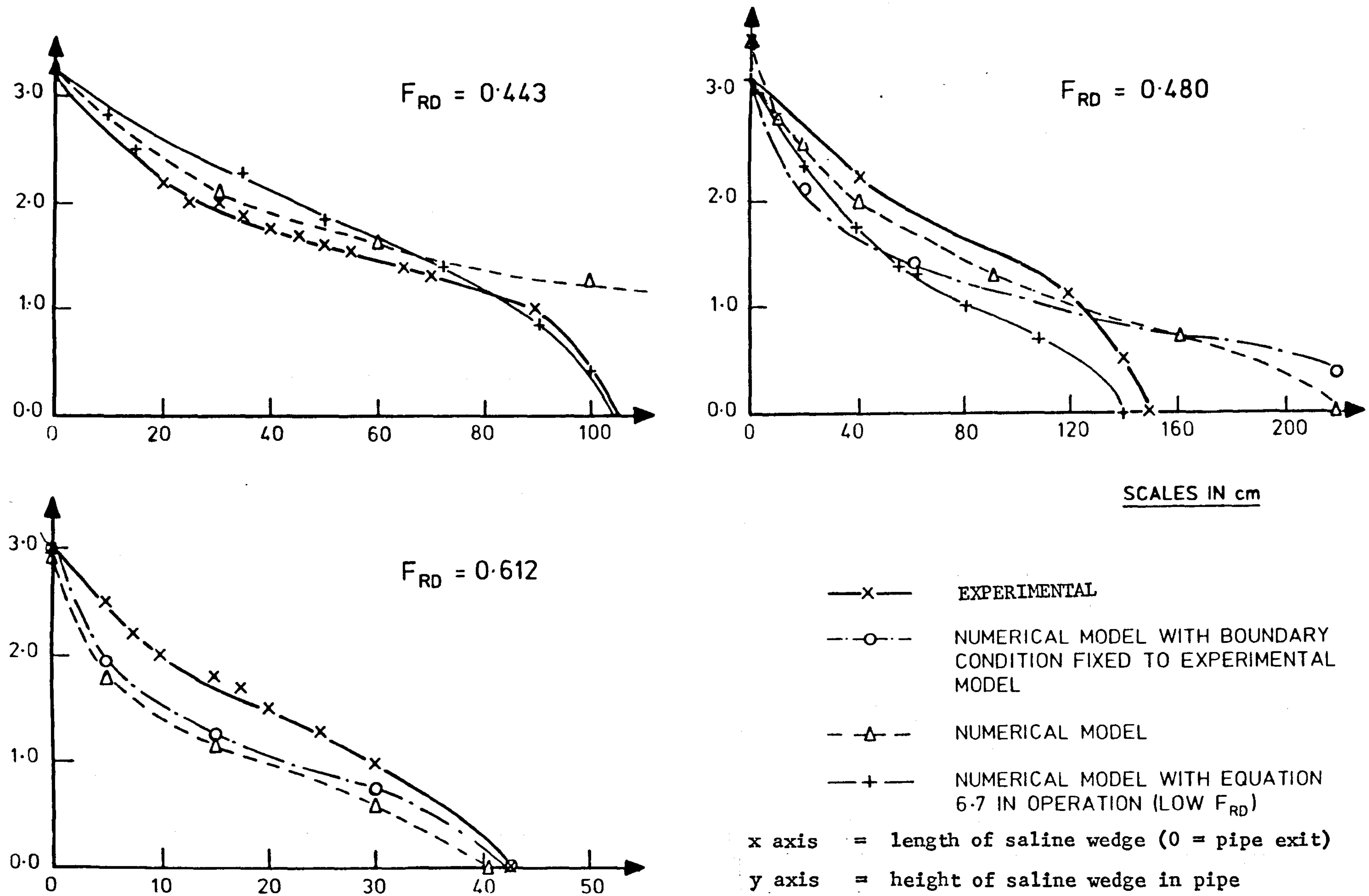

FIGURE 6. 6 . EXPERIMENTAL AND THEORETICAL WEDGE PROFILES

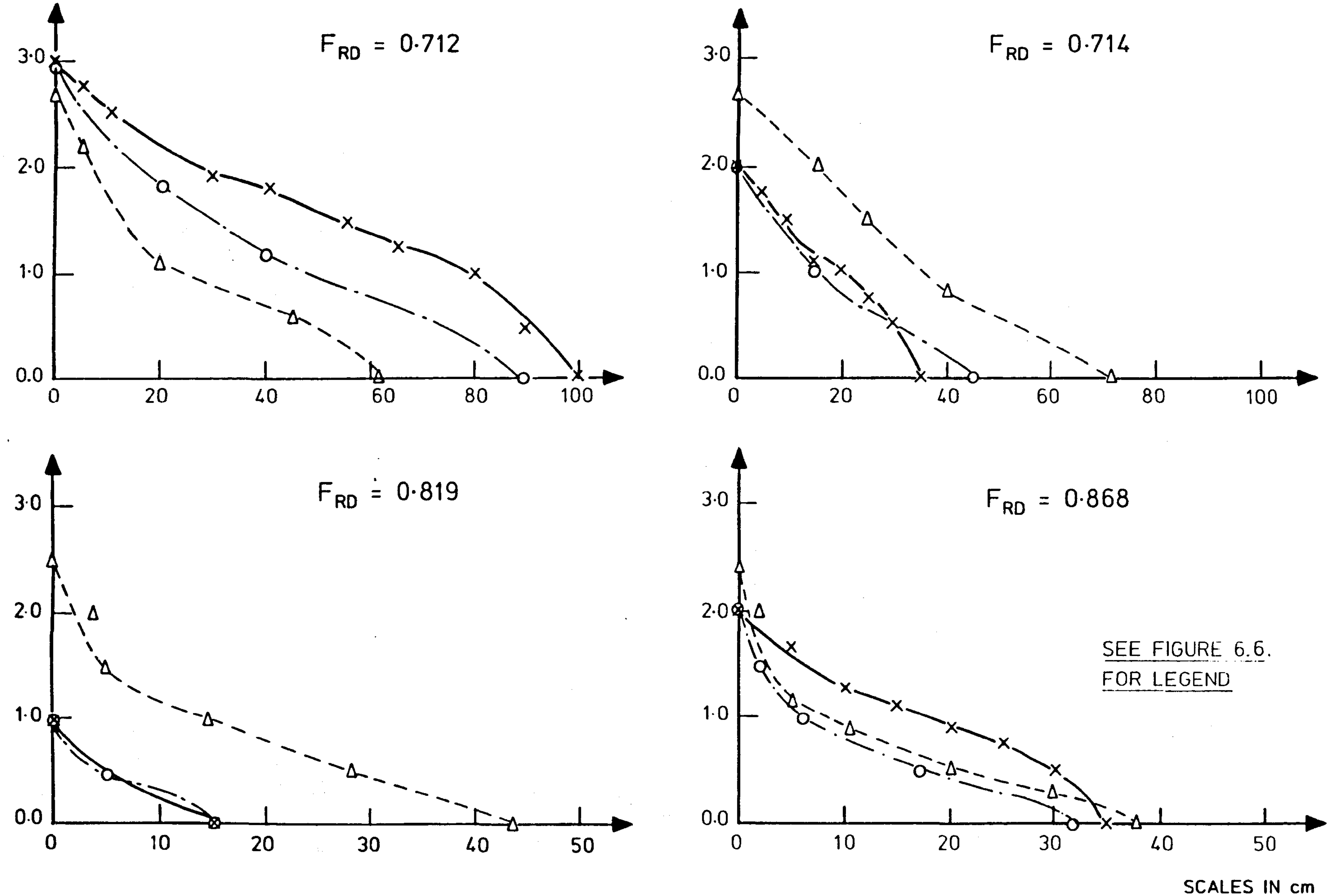

FIGURE 6.7 EXPERIMENTAL AND THEORETICAL WEDGE PROFILES

6.3.3 Application of the Numerical Model

When the numerical model was employed in its original form using equation (6.2) throughout, it was found that this equation became unstable at the pipe exit; which was due to the steep curvature of the saline wedge at this point. The upward curvature is caused by the buoyancy of the freshwater which, on exit from the pipe at the seabed, forms a plume and disperses upwards towards the surface. These plumes are referred to as buoyant jets and are discussed in more detail by Brook s[11] and Wright[61,62].

The instability of equation (6.2) is due to the rapid change in the saline wedge characteristics. The numerical model calculates the value of Δx by taking plane sections through the pipe. At the downstream end of the pipe this is inadequate and the original analysis becomes invalid. To improve this analysis the streamlines could have been modelled using curvi-linear Bernoulli's equation, demonstrated by Ali and Ridgeway[6]. Before adopting this technique it was felt that more experimental data would be required. Therefore, to enable partial completion of the study, the numerical model was altered empirically to reflect the change in wedge profile.

The empirical routine was developed in the following way. Initially the boundary condition in the numerical model was set equal to the experimental value for the relevant flow conditions. Calculations using equation (6.2) were performed from the boundary condition to a point A (the transition point shown in Figure 6.5). At this point equation (6.2) gave sensible results for the value of Δx. Assuming the numerical model took N steps of Δd to reach point A then the wedge length from point A to the pipe exit was obtained by multiplying N by the first positive value of Δx.

It was also assumed that for every change in Δd up to point A the horizontal distance for each interval was the first sensible value of Δx. On comparison with experimental data it was found that a more accurate result was found by dividing the value of Δx by 15. This empirical numerical procedure was then retained for deriving the downstream wedge profile. From point A the wedge length was calculated using equation (6.2) in its original form. The extent of the instability experienced with equation (6.2) at the downstream end of the wedge was found to be between 10 and 20 % of the computed wedge length, with very few results falling outside this range.

6.3.4 Reappraisal of Numerical Model

6.3.4.1 Velocity Profiles/Friction Aspects

Daly and Harleman[15] show that for a pipe flowing full, the velocity distribution is such that the ratio of mean velocity to maximum velocity approximates to 0.8 in respect to turbulent flow. The results given in Figures 6.2 to 6.4 show asymmetrical distribution vertically through the pipe and indicate that the ratio of mean velocity (V_f) to maximum velocity (V_{max}) ranges from approximately 0.8 at the toe of the wedge to about 0.9 before the flow exits from the pipe, although these results could well be subject to errors as outlined in section 6.2.2.

Another condition which will cause the velocity profiles to change is the effect of interfacial waves within the pipe. These waves were visually apparent during the experimental procedures for the Series 1 experiments. They appear as small undulations at the toe of the wedge gradually increasing as they move along the length of the wedge towards the exit port. This creates difficulties in measuring the wedge height at the exit port . It should be noted that these internal waves are not caused by external waves passing along the sea surface, but arise from turbulence within the flow whilst steady external conditions exist.

The presence of waves at the interface must increase the effect of interfacial friction and may also induce localised turbulence around the saline/fresh water interface, whilst fresh water flowing near the smooth pipe wall will probably remain unaffected. Due to a lack of experimental data demonstrating interfacial velocities and forces it was not possible to improve the model formulation for these processes.

6.3.4.2 Upstream Wedge Condition

Figures 6.6 and 6.7 show wedge profiles from both experimental and numerical data based on the 50 mm pipe. The figures show the results obtained using two different boundary conditions.

One boundary condition is defined by the theoretical equations in Section 3.3.3, the other being fixed and equal to the experimental condition. For the higher Froude numbers it can be seen that when boundary conditions are the same, the wedge profiles and lengths between the experimental and theoretical results are similar. For low Froude number situations the numerical and experimental profiles are of a similar shape until approaching the toe of the wedge when marked differences occur between the results. It was therefore resolved that the only remaining problem was to predict the form of the wedge toe more accurately.

The existing numerical model predicts that the toe of the wedge is formed by the asymptotic approach of the liquid interface to the pipe invert, and this is shown in Figure 6.8 line A below:

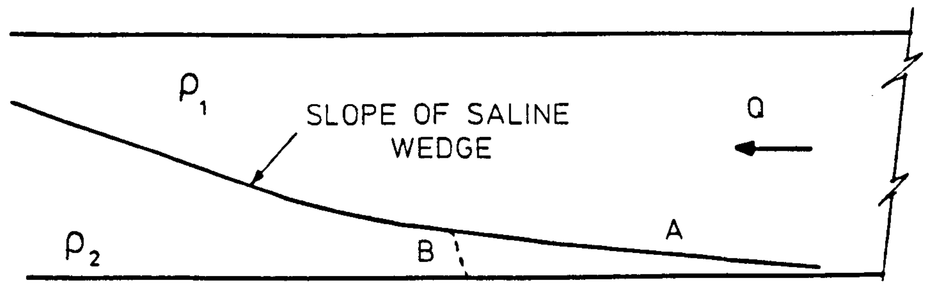

Sketch showing predicted slope of wedge

Figure 6.8

From earlier experimental observations it was discovered that the toe of the wedge was generally steep and turbulent as sketched in Figure 6.8 line B.

The steep slope of the wedge is caused by turbulence and is referred to by Viollet[56] as a 'shock' and occurs when flows of differing velocities and densities meet. No reference can be found of this phenomenon in open channel flow research, which leads the writer to the conclusion that the condition is more pronounced in pipe flow. However Simpson [65] makes reference to this in the case of gravity currents.

In order to model the steeper slope at the toe of the wedge it was necessary to increase the interfacial friction factor during the final steps of the interactive procedure. In effect the numerator of Equation (6.6) would change and the equation for f_i would then become

$$f_i = (k_i \times 0.316)/R_e^{0.25} \qquad (6.7)$$

An intuitive solution for the value of k_i was obtained in the following way. The theoretical procedures adopted to calculate the wedge height at the pipe exit were discontinued(only for the purpose of calibration to model the toe) and the boundary condition was set to equal to the experimental value for the 50 mm pipe. This eliminated the effect of disparities between the theoretical and experimental downstream boundary condition before attempting an assessment. The numerical model then generated the wedge length and profile.

Following several trials Equation (6.8) was developed to give an appropriate adjustment for the interfacial friction factor as the wedge approached the pipe invert.

$$k_i = [(I_k - A_k) \times 0.5] + 0.5 \qquad (6.8)$$

where k_i = multiplication factor used in Equation (6.7)

I_k = step number of iteration of wedge profile calculation, see Figure 6.5 and

A_k = integer as outlined below.

This calculates the increase in friction factor in a way which avoids discontinuity occurring at the toe of the wedge and results are shown in Figures 6.6 and 6.7. The graphs are drawn for when F_{RD} is equal to 0.443 and 0.480. The value of 'A_k' varies depending upon the densimetric Froude number (F_{RD}). For a value of $F_{RD} < 0.45$, the value of A_k was taken as 30 and Equation 6.8 was valid for $I_k > 30$. For a value of $F_{RD} > 0.45$, the value of A_k was taken as 40 and the equation valid for $I_k > 40$. When the value of F_{RD} was greater than 0.5 the value of k was taken as 1 on the basis of the calibration data available.

By increasing the interfacial friction factor in Equation (6.7) the procedure is expected to represent more realistically the complex processes occurring within the pipe, and in the absence of more extensive experimental evidence it is considered adequate.

6.3.5 Calibration for Larger Diameter Pipes

The numerical model was supplied with data used for the Series 1 experiments (see Section 6.2.1) to establish if it could produce equivalent wedge length results. Table 6.2 shows the initial outcome and demonstrates that large discrepancies exist between the experimental and the theoretical wedge length values.

On investigation it was found that when the boundary conditions from Section 3.3.3 were applied to the larger diameter pipes the results produced for the wedge height at the pipe exit were too large. For example, large densimetric Froude numbers gave wedge heights greater than half the pipe diameter which, from experimental observations, is misleading. This in turn gave rise to computed wedge lengths being greater than the experimental results.

From various tests carried out it was found that by multiplying the boundary condition result by the factor D/50, where D is the pipe diameter in millimetres, and 50 is the diameter of the pipe from which the base calculations were produced, the computed wedge lengths then approached values similar to those obtained experimentally. The results are shown in Figures 6.9 to 6.13 and discussed in Section 6.3.6.

6.3.6 Comparison of L/D against F_{RD} for Large diameter pipes

Figures 6.9 to 6.13 inclusive show comparisons of L/D against F_{RD} for both experimental and numerical model results. The numerical data has been obtained from the theoretical model after calibration, as well as from the equation produced by Davies et al[21]. From Figures 6.9 to 6.13 it can be seen that at high densimetric Froude numbers the margin between numerical and experimental data tends to be small whilst at low Froude numbers the error tends to be larger.

Figure 6.10 shows the largest deviation between the experimental and theoretical results which reinforce conclusions made in Section 6.2.1, namely that there was an error in determining experimental wedge lengths in this case.

Large deviations at lower Froude numbers are probably caused by a combination of errors in determining the exact experimental wedge lengths, and the inability of the numerical model to accurately determine the toe of the wedge.

Equation 2.2 (given in Section 2.1) is the expression developed by Davies et al[21] for obtaining wedge lengths and was obtained empirically from experimental data. As mentioned in Section 2.1 there was an error in the equation giving the value of 'k'. The equation for 'k' should be

$$k = 0.054 \exp[-3.69 (\ln (2 F_{RD}))^2] \qquad (6.9)$$

and using this in conjunction with Equation (2.2) gives the third of the three lines shown in Figures 6.9 to 6.13.

Table 6.2

	Q L/S	ρ kg/m³	Diameter mm	F_{RD}	Exp Length	Comp. Length	% Diff. $(\frac{Exp - TH}{Exp})$
1.	0.32	1029	105	0.217	4.40	13.71	-212
2.	0.25	1030	88	0.259	3.60	7.63	-112
3.	0.28	1014	105	0.271	3.90	12.41	-218
4.	0.335	1015	105	0.314	2.55	8.07	-217
5.	0.45	1021	105	0.357	5.0	4.12	17.6
6.	0.37	1014	105	0.358	1.85	5.79	-213
7.	0.40	1030	88	0.415	1.60	2.53	-58
8.	0.64	1029	105	0.434	1.20	2.14	-78
9.	0.45	1014	105	0.436	1.20	3.03	-152
10.	0.52	1014	105	0.504	1.00	2.35	-135
11.	0.75	1029	105	0.508	0.825	1.52	-84
12.	0.60	1015	105	0.562	0.80	1.207	-51
13.	0.72	1021	105	0.571	1.05	0.898	-14
14.	0.6	1030	88	0.622	0.80	0.99	-24
15.	0.675	1015	105	0.632	0.65	0.543	17
16.	0.71	1014	105	0.688	0.35	0.163	29
17.	1.12	1029	105	0.759	0.15	0.005	97
18.	0.97	1021	105	0.770	0.10	0.0004	100
19.	0.8	1030	88	0.830	0.40	0.19	53

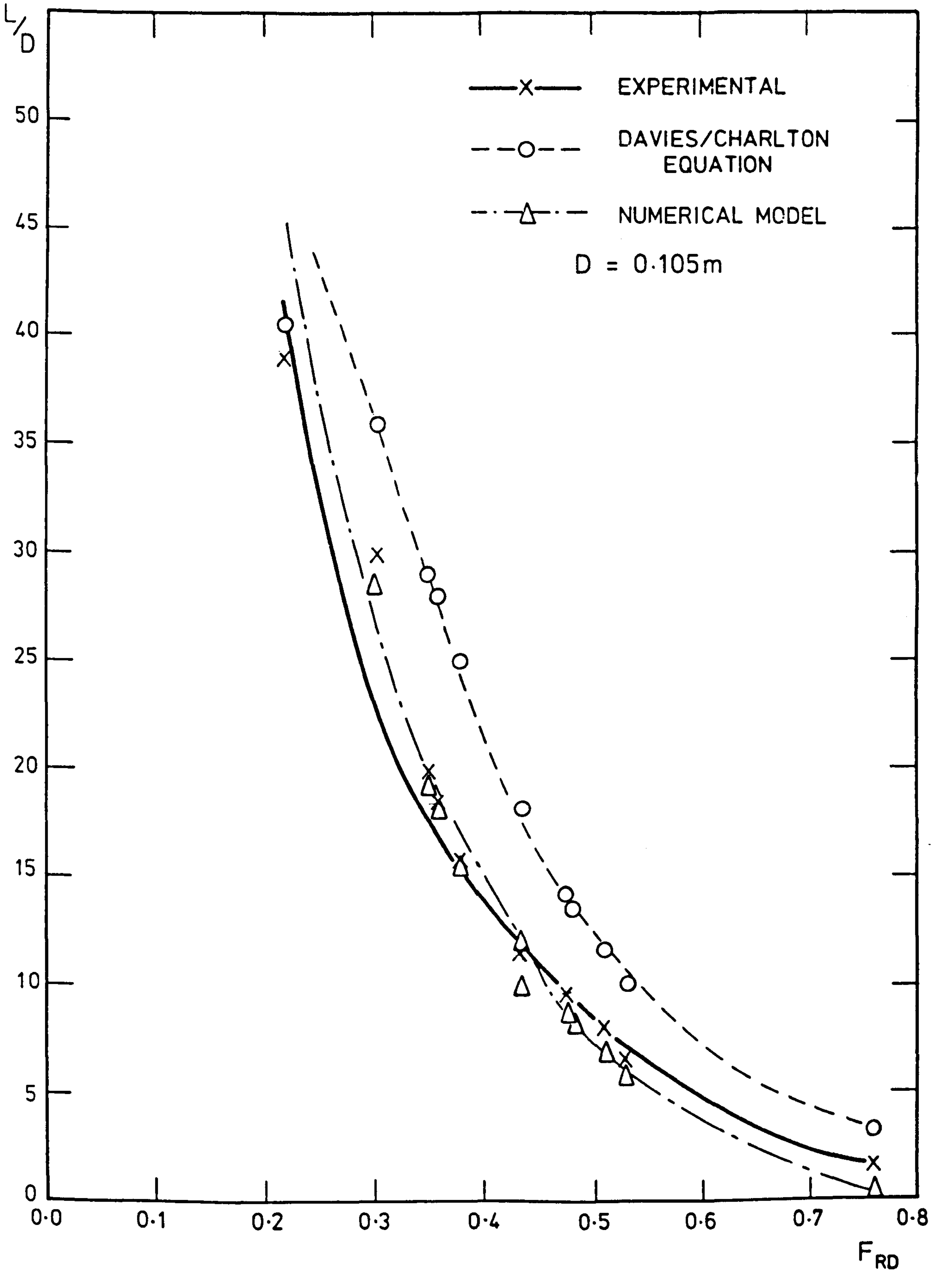

FIGURE 6.9. COMPARISON OF EXPERIMENTAL AND NUMERICAL MODELS FOR $\rho = 1029 kg/m^3$

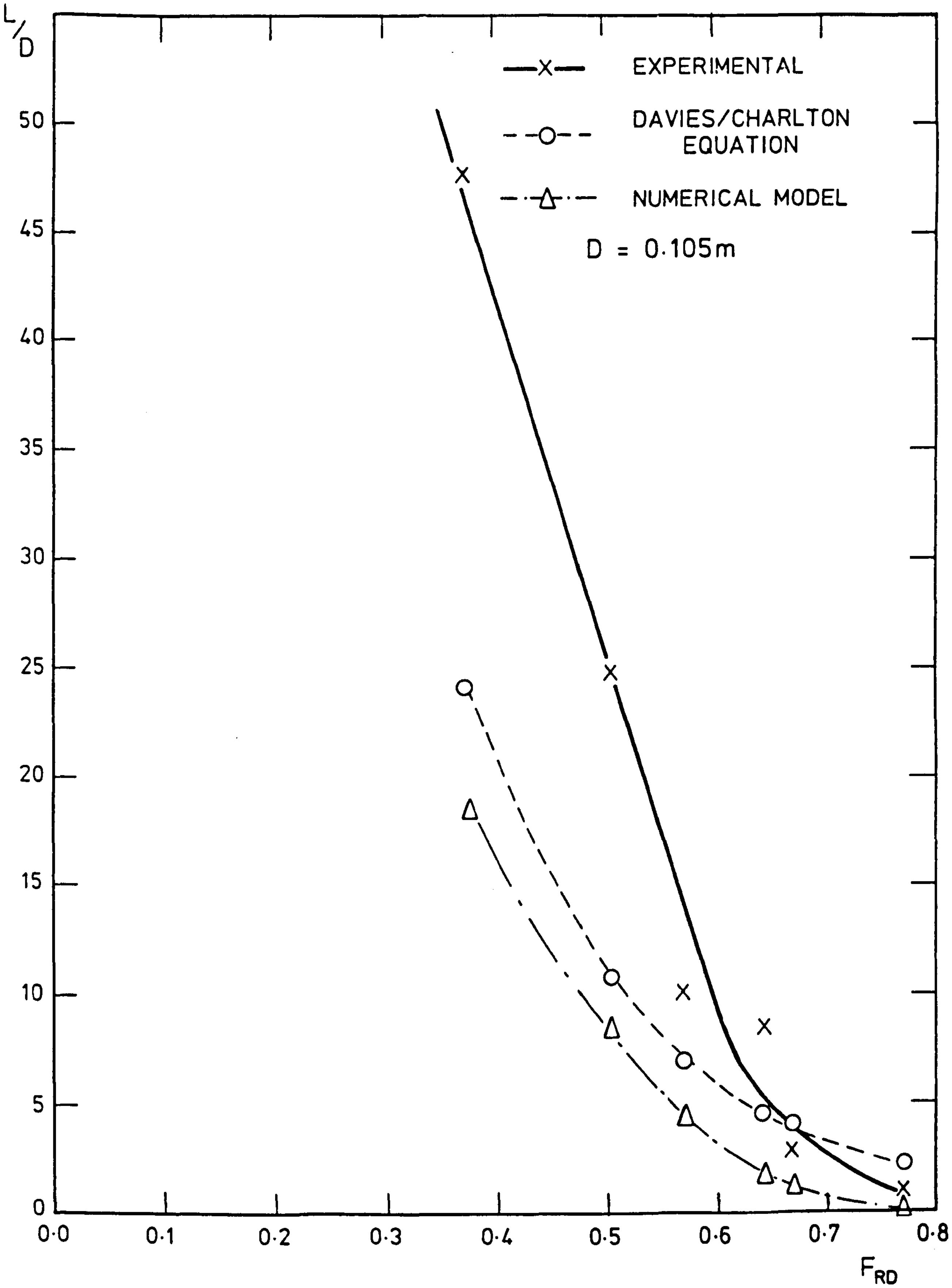

FIGURE 6.10 COMPARISON OF EXPERIMENTAL AND NUMERICAL MODELS FOR $\rho = 1021 kg/m^3$

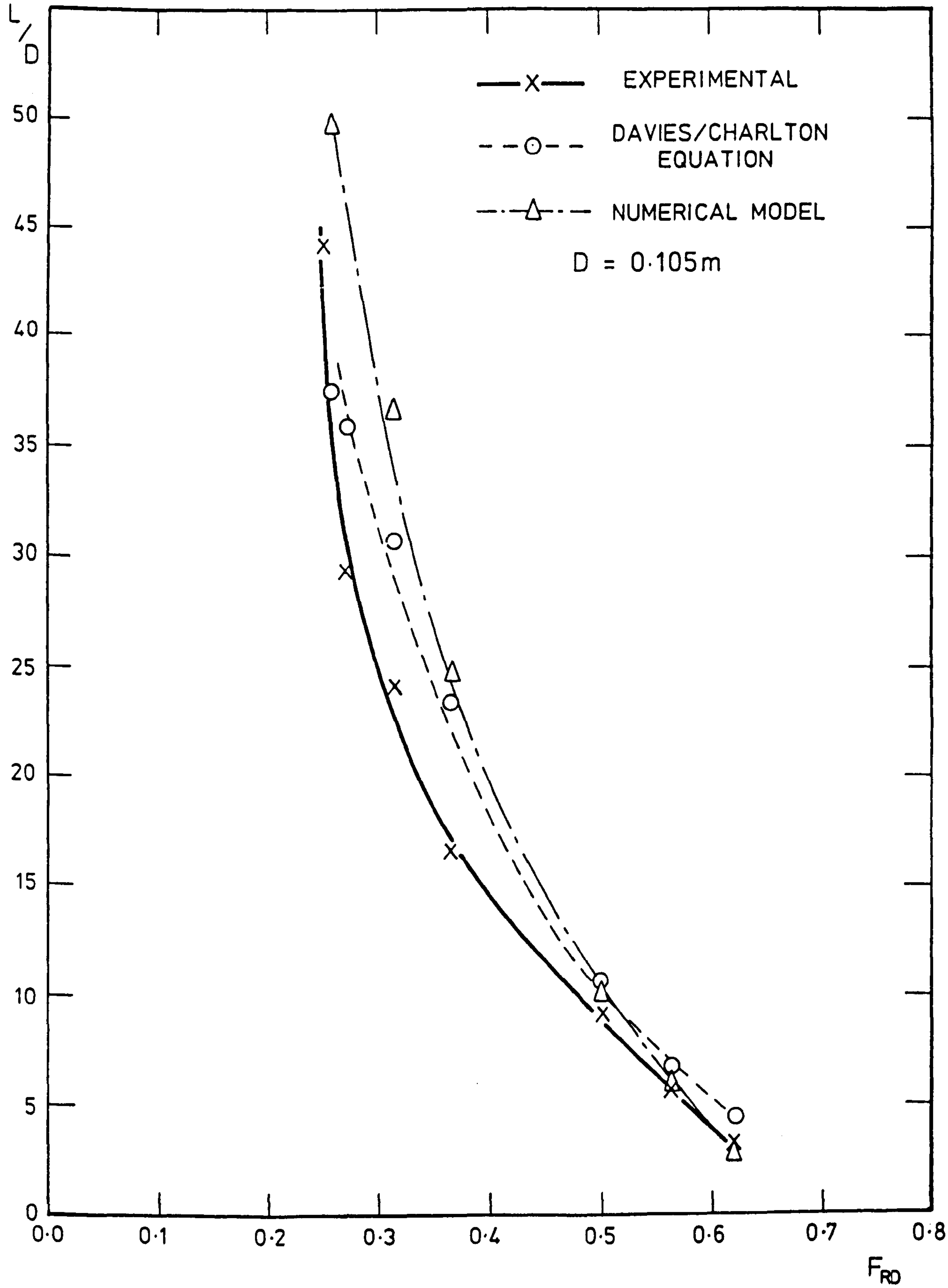

FIGURE 6.11. COMPARISON OF EXPERIMENTAL AND NUMERICAL MODELS FOR $\rho = 1015 kg/m^3$

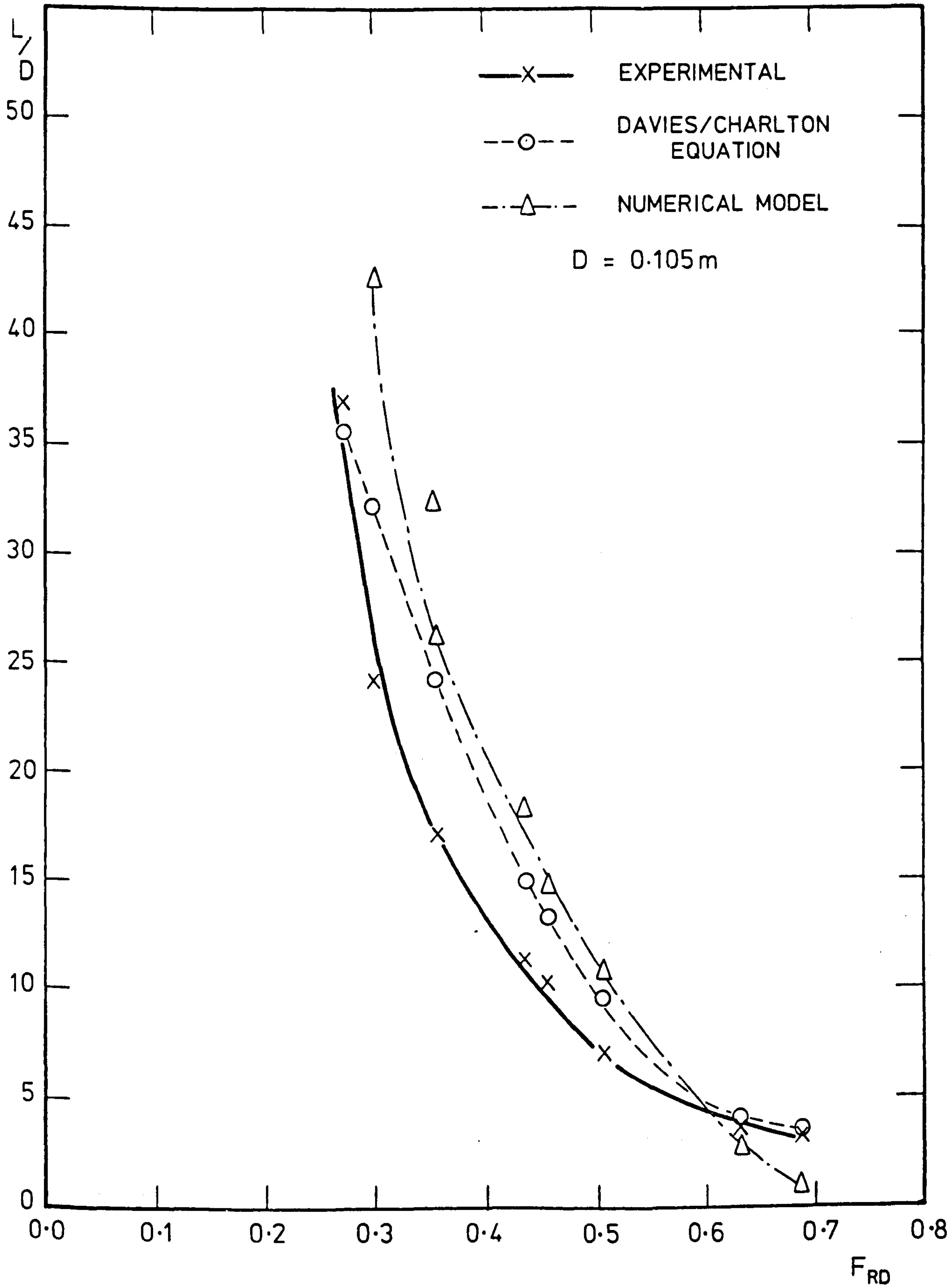

FIGURE 6.12 COMPARISON OF EXPERIMENTAL AND NUMERICAL MODELS FOR $\rho = 1014 kg/m^3$.

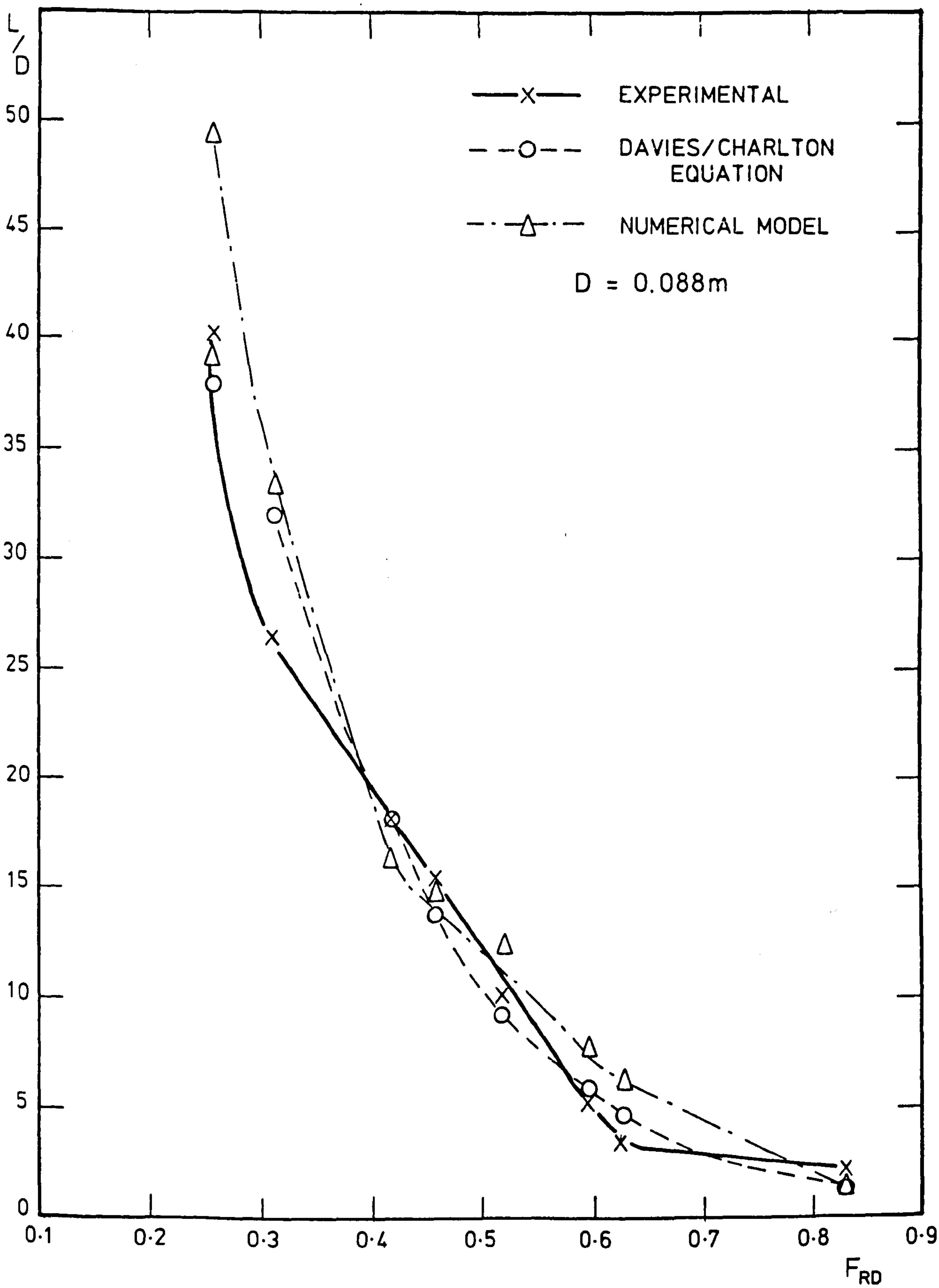

FIGURE 6.13 COMPARISON OF EXPERIMENTAL AND NUMERICAL MODELS FOR $\rho = 1030 kg/m^3$ (Charltons results)

Figures 6.9 to 6.13 demonstrate that the numerical model in its present state calculates similar values for the lengths of saline wedges as those obtained experimentally. However, the use of an empirically-derived scaling factor is important as this factor adjusts the numerically calculated boundary condition upon which the remaining numerical calculations hinge. The effect of this on the profile of the saline wedge is uncertain as no experimental data was obtained for wedge profiles in larger diameter pipes.

6.4 Numerical Model

6.4.1 Status of Numerical Model

From the foregoing, it has been found that the numerical model is able to predict wedge lengths (for all conditions) and profiles (for 50 mm diameter pipe only) similar to those obtained experimentally, although discrepancies occur throughout. These are due in part to experimental errors, coupled with the outstanding difficulties of numerically modelling stratified flow in pipes. Consequently more research is required to investigate the effects of boundary conditions in different pipe sizes, to determine how the wall and interfacial shear stresses vary along the saline wedge, as well as the conditions affecting the toe of the wedge.

The numerical model in its present form produces diagramatic print outs showing profiles of the saline wedges for various conditions, see Figure 6.14. The first graph on Figure 6.14 shows the change in pipe roughness, the symbol key giving the heights of pipe roughness in metres. This

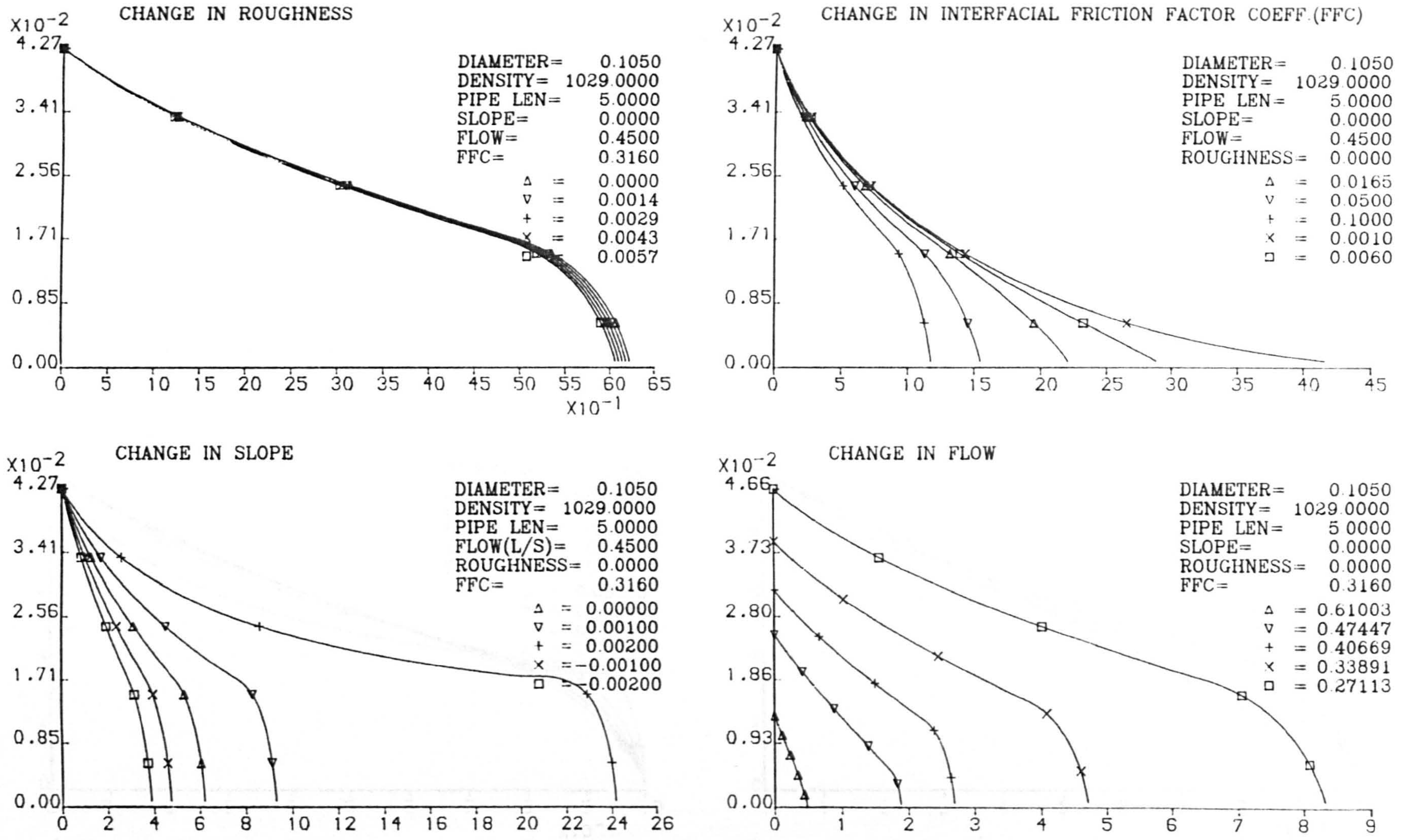

X AXIS= WEDGE LENGTH, Y AXIS=WEDGE DEPTH

FIGURE 6.14 GRAPH OF WEDGE PROFILES

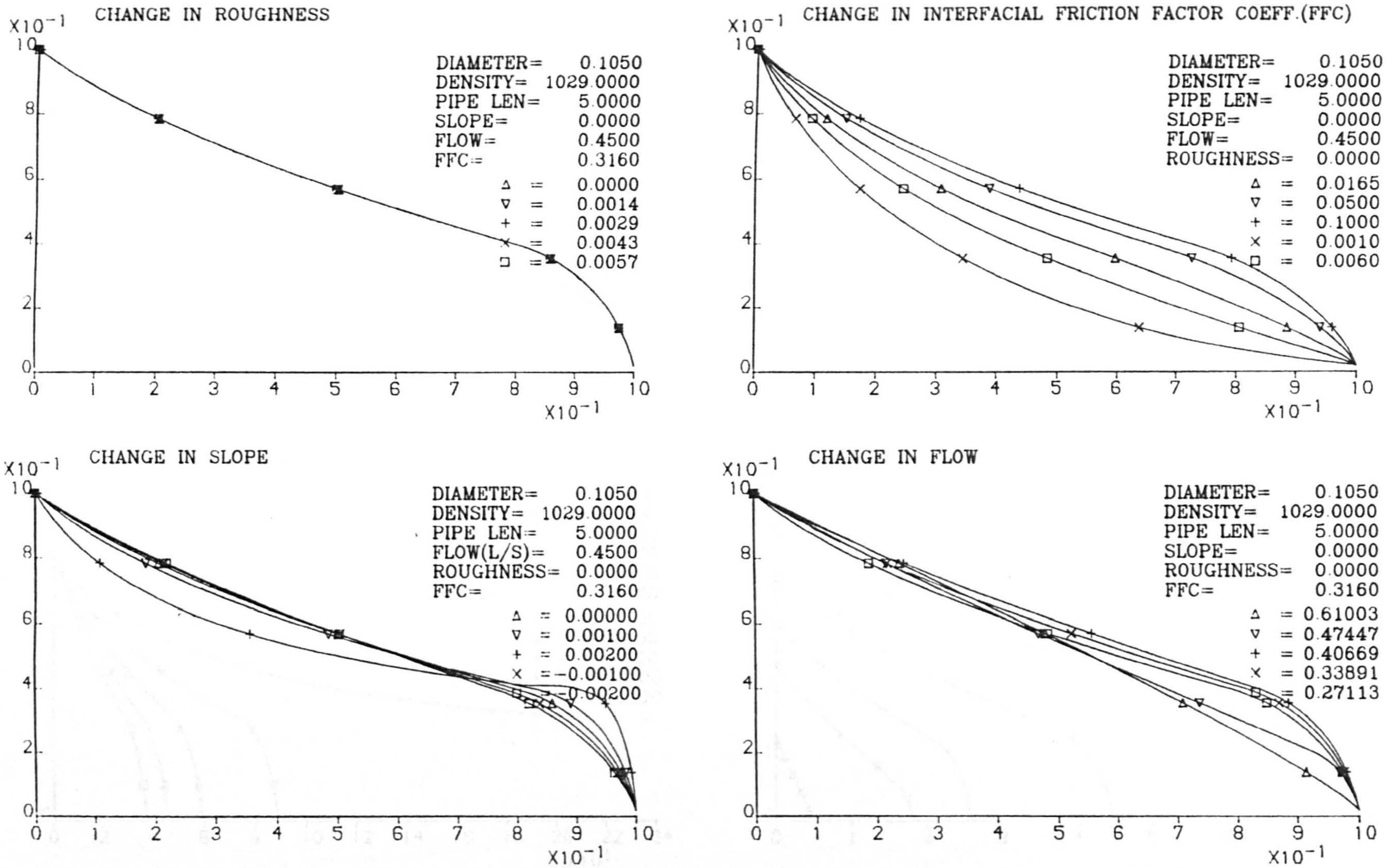

X AXIS= X/L, Y AXIS=Y/YMAX

FIGURE 6.15 X/L AGAINST Y/YMAX

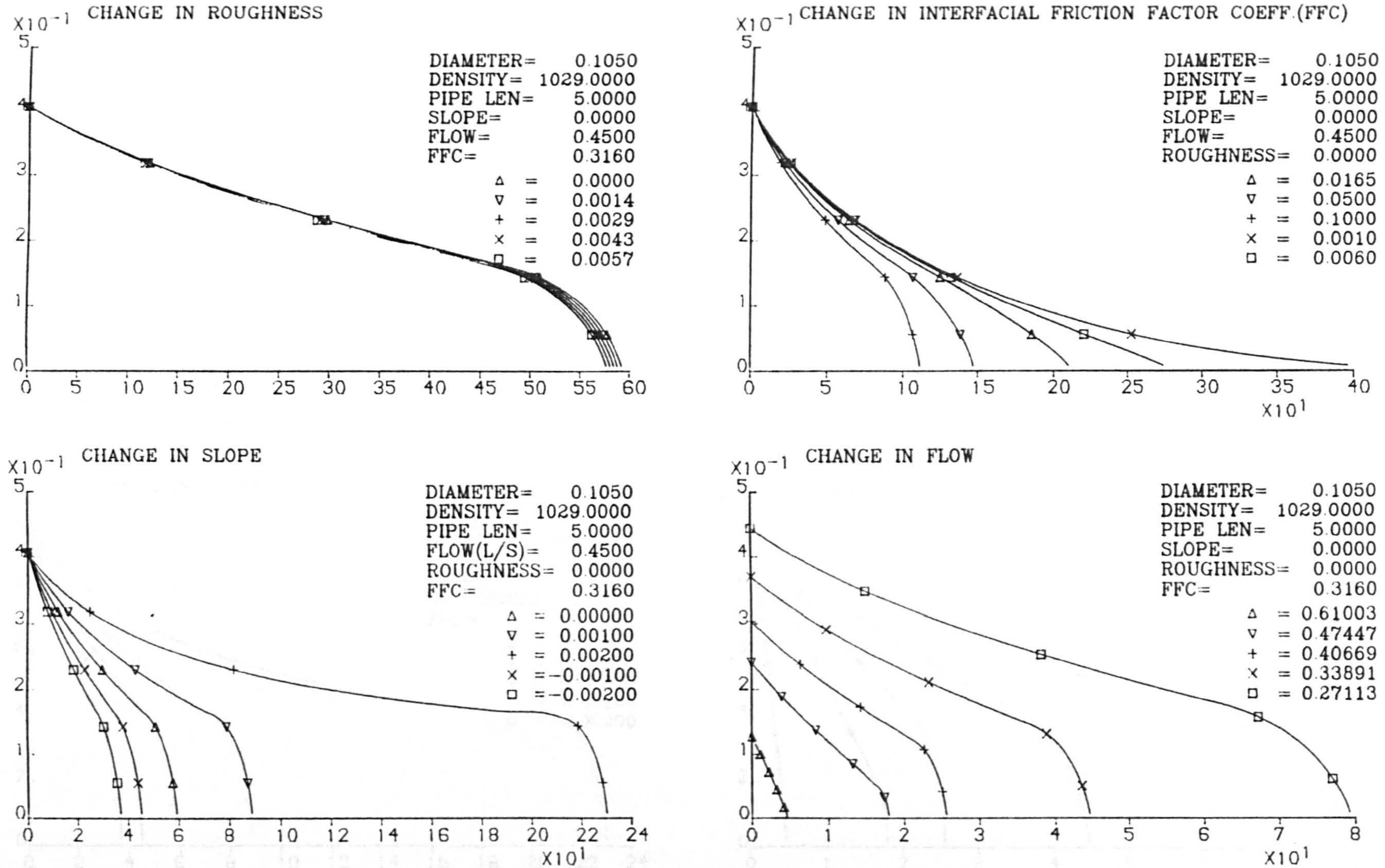

X AXIS= X/D, Y AXIS=Y/D

FIGURE 6.16 X/D AGAINST Y/D

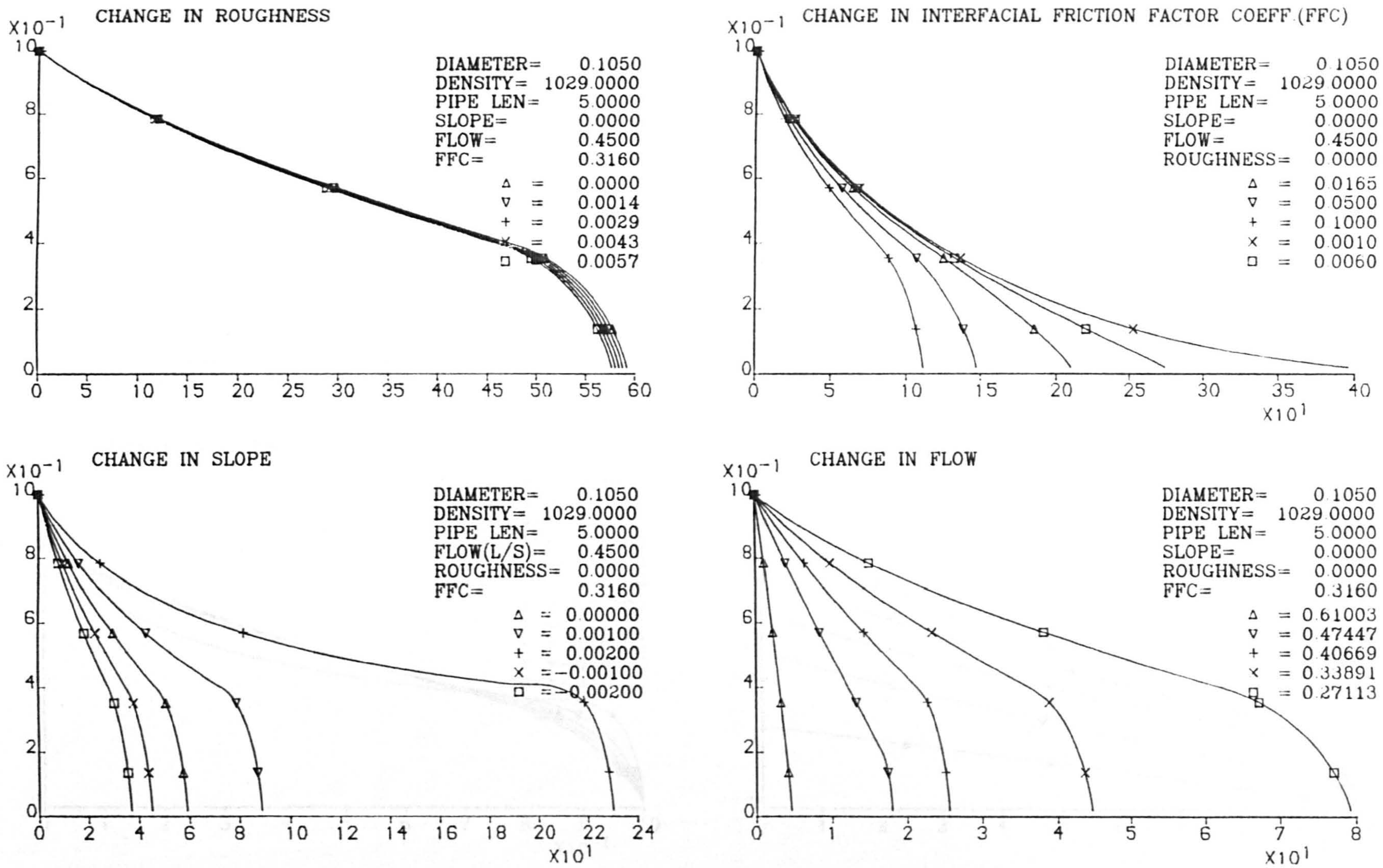

X AXIS= X/D, Y AXIS=Y/YMAX

FIGURE 6.17 X/D AGAINST Y/YMAX

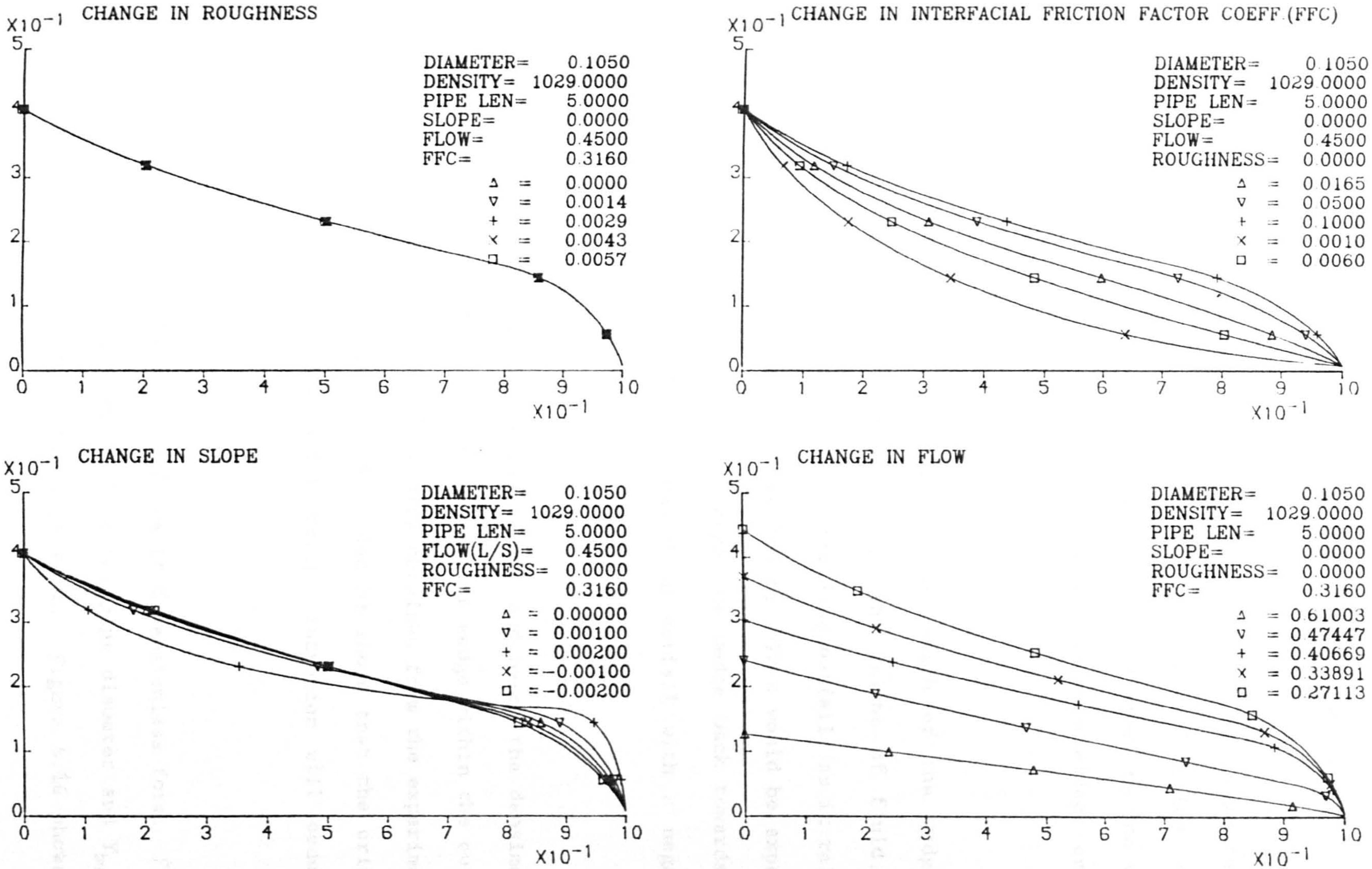

X AXIS= X/L, Y AXIS=Y/D

FIGURE 6.18 X/L AGAINST Y/D

demonstrates that there is little change in the saline wedge profile as the pipe roughness increases; this in turn suggests that the value of the wall shear stress only has a small effect on the wedge profile.

The second diagram shows how a change in the value of the numerator of equation (6.6), given in Figure 6.14 as the Interfacial Friction Factor coefficient, affects the saline wedge profile. Here changes to the value of the interfacial friction coefficient have a noticable effect on the wedge profile.

The change in slope of the pipe affects the length of the wedge by altering the direction of the force due to the weight of fluid. A positive slope (this is the usual case in tunnelled outfalls as it relates to a backfall) shows an increase in wedge length. This would be expected as the weight of the salt water will force the wedge back towards the headworks dropshaft. As would be expected an outfall with a negative slope has a decreased wedge length.

The final figure shows that as the flow rate, and hence the densimetric Froude number increases, the length of the saline wedge within the outfall decreases. This is expected as the results obtained from the experimental model demonstrate this same effect and it can be shown that the critical densimetric Froude number below which saline intrusion will occur is unity[15].

Figures 6.15 to 6.18 show the same profiles in dimensionless form. Figure 6.15 shows X/D against Y/Y_{max}, where D is the pipe diameter and Y_{max} is the value of the wedge height at the pipe exit. Figure 6.16 shows X/D against Y/D and Figure 6.17 shows X/L against Y/Y_{max}, where L is the original length of the saline wedge. The final computer diagram, Figure 6.18, shows how X/L varies against Y/D.

6.4.2 Uses of the Numerical Model

The numerical model, at present, is a combination of theoretical and empirical procedures which have been tuned to model wedge profiles within a 50 mm diameter pipe and wedge lengths, with associated profiles, in larger diameter pipes. Due to the combination of procedures and lack of experimental data, on larger diameter pipes, with which the numerical model could be tested the number of possible applications is restricted. It could be used to provide an estimate of wedge lengths and profiles within an open ended outfall pipe and accurate results of wedge profiles in a 50 mm diameter tube could also be obtained. However until more rigorous testing is undertaken the results obtained for larger diameter pipes must be treated with caution.

6.5 Comparison with Open Channel Data

Apart from work performed by Sharp and Wang(51) and Davies et al(12,21), all earlier investigations undertaken on saline wedges have been targeted on the two dimensional open channel situation. Both theoretical and experimental work has been carried out and, consequently, it would seem appropriate for open channel results to be compared with pipe flow results.

A saline wedge in an open channel usually takes the profile shown in figure 6.19 below:-

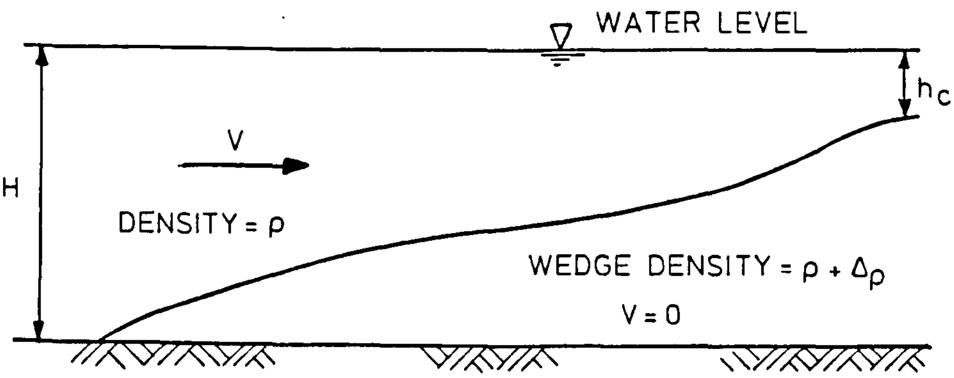

Shape of Wedge in an Open Channel

Figure 6.19

Figure 6.19 is taken from Harleman[26] and it is shown that at the downstream end of the channel the flowing layer forms a critical depth as it passes over the top of the wedge. The water surface in channels is not physically restricted by a rigid boundary, unlike the case in conduits, but the wedge shape will change in a channel depending upon the total driving head of water.

Both Sharp and Wang[51] and Davies et al[21] compare their experimental results with those obtained from open channel experiments undertaken by other researchers. Sharp and Wang[51] compare their experimental work with a theoretical equation derived by Polk and Benedict[46]; this uses both wall and interfacial friction factors and the densimetric Froude number. For comparison they employ the pipe diameter instead of the water depth, H, for producing the length scales - this demands considerable care due to the crucial role of the Froude number in open channel calculations.

Davies et al[21] however use the hydraulic radius as the single length scale in the formulation of the densimetric Froude number. This would appear to be the more logical approach to the problem as it defines both the open channel flows and pipe flows in a similar form.

The method used by Davies et al[21] is outlined as follows. If the densimetric Reynolds number (R_{eD}) and the densimetric Froude number are re-defined in terms of D_* such that

$$(R_{eD})* = \frac{V_* \; D_*}{\nu_o} \tag{6.10}$$

and
$$(F_{RD})* = \frac{V_o}{(g' \; D_*)^{1/2}} \tag{6.11}$$

then for pipe geometry D_* equals the pipe diameter D, therefore, the Reynolds and Froude numbers also remain unchanged and $L/D_* = L/D$. For an open channel of depth H and width B then

$$D_* = \frac{4BH}{(B + 2H)}$$

and the densimetric Reynolds and Froude numbers become

$$(R_{eD})_* = (R_{eD}) \; (D_*/H)^{3/2} \tag{6.12}$$

and
$$(2F_{RD})_* = (2F_{RD}) \; (H/D_*)^{1/2} \tag{6.13}$$

and
$$L/D_* = (L/H) \; (H/D_*) \tag{6.14}$$

In a similar manner to Davies et al[21], results were obtained from plots by Keulegan[34] and converted to equivalent results for comparison with pipe flow, using the above equations. Two sets of data from open channel results were used and compared against two sets of pipe flow data which had similar values of $(R_{eD})_*$. The plots are shown in Figure 6.20 and it is clear that wedge lengths in open channels are greater than those in pipes for similar densimetric Froude numbers.

Figure 6.21 compares saline wedge profiles in an open channel with those in a pipe using similar densimetric Froude numbers. The Figure shows that for the Froude number adopted, the wedge profile of the pipe is steeper at the toe than that in the channel, and also the height of the wedge in the pipe at the exit is greater. (In Figure 6.21, h_s is the height of the saline wedge and K is the depth of flow upstream of the saline wedge).

The use by Sharp and Wang[51] of the equation derived by Polk and Benedict[46] appears to give accurate estimations as to the length of the wedge forming in the pipe. The equation given[46] is

$$\begin{aligned}\frac{fL}{H} &= \frac{2}{F^2}\,(1 - F^{8/3}) + \frac{8\alpha}{3F^2}\,(1 - F^{6/3}) \\ &+ \frac{4\alpha\,(1+\alpha)}{F^2}\,(1 - F^{4/3}) + \frac{8}{F^2}\,[\alpha\,(1+\alpha)^2 - F^2]\,(1 - F^{2/3}) \\ &+ \frac{8\alpha}{F^2}\,[(1+\alpha)^3 - F^2]\,[\ln\alpha - \ln(1 + \alpha - F^{2/3})] \qquad (6.15)\end{aligned}$$

where f = wall friction coefficient

L = wedge length

H = depth of channel

F = densimetric Froude number ($= F_{RD}$)

and α = ratio between interfacial and wall friction coefficient.

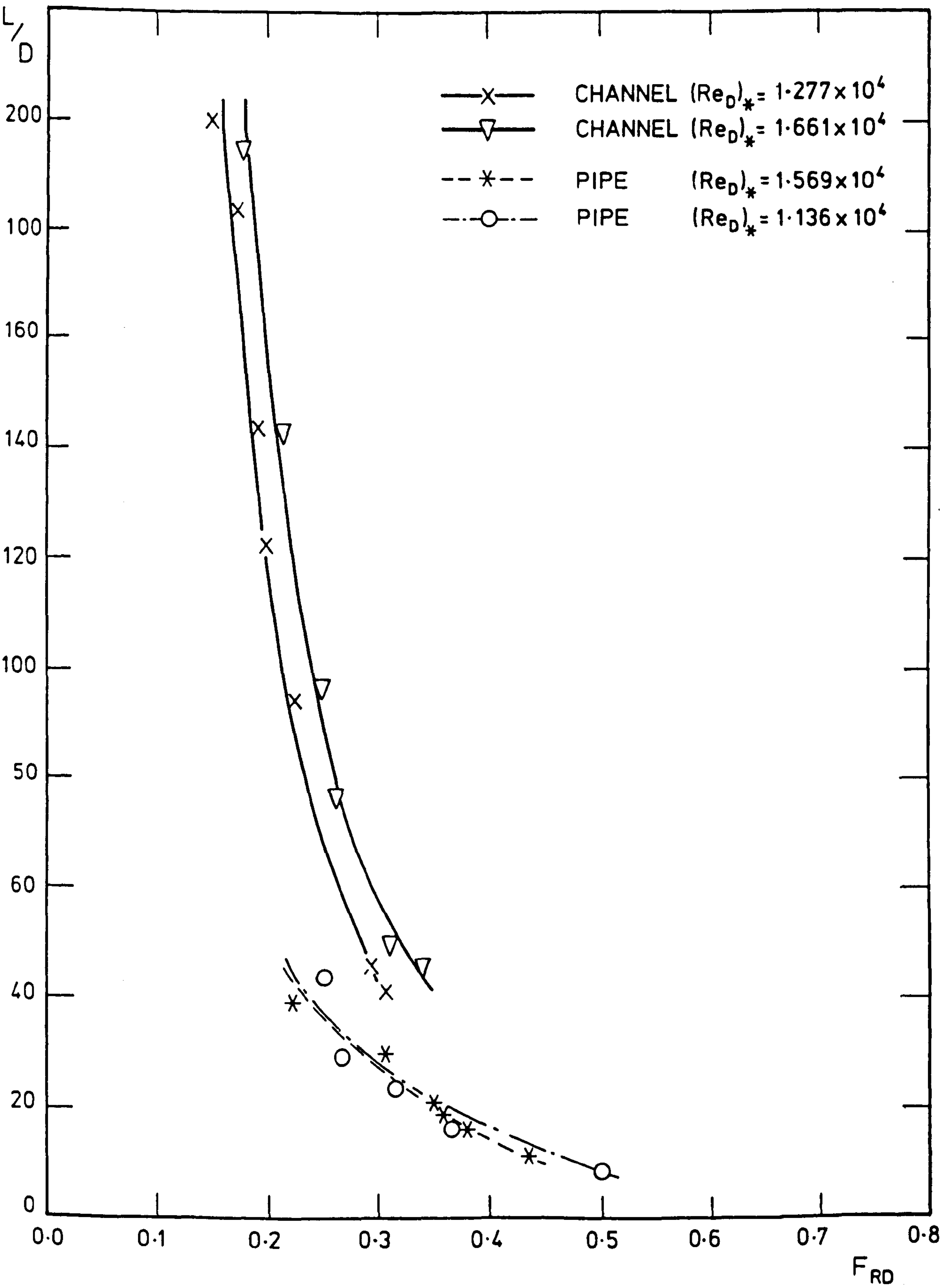

FIGURE 6.20 COMPARATIVE PLOTS OF (L/D_*) AGAINST $(F_{RD})_*$ FOR OPEN CHANNEL AND PIPE FLOW

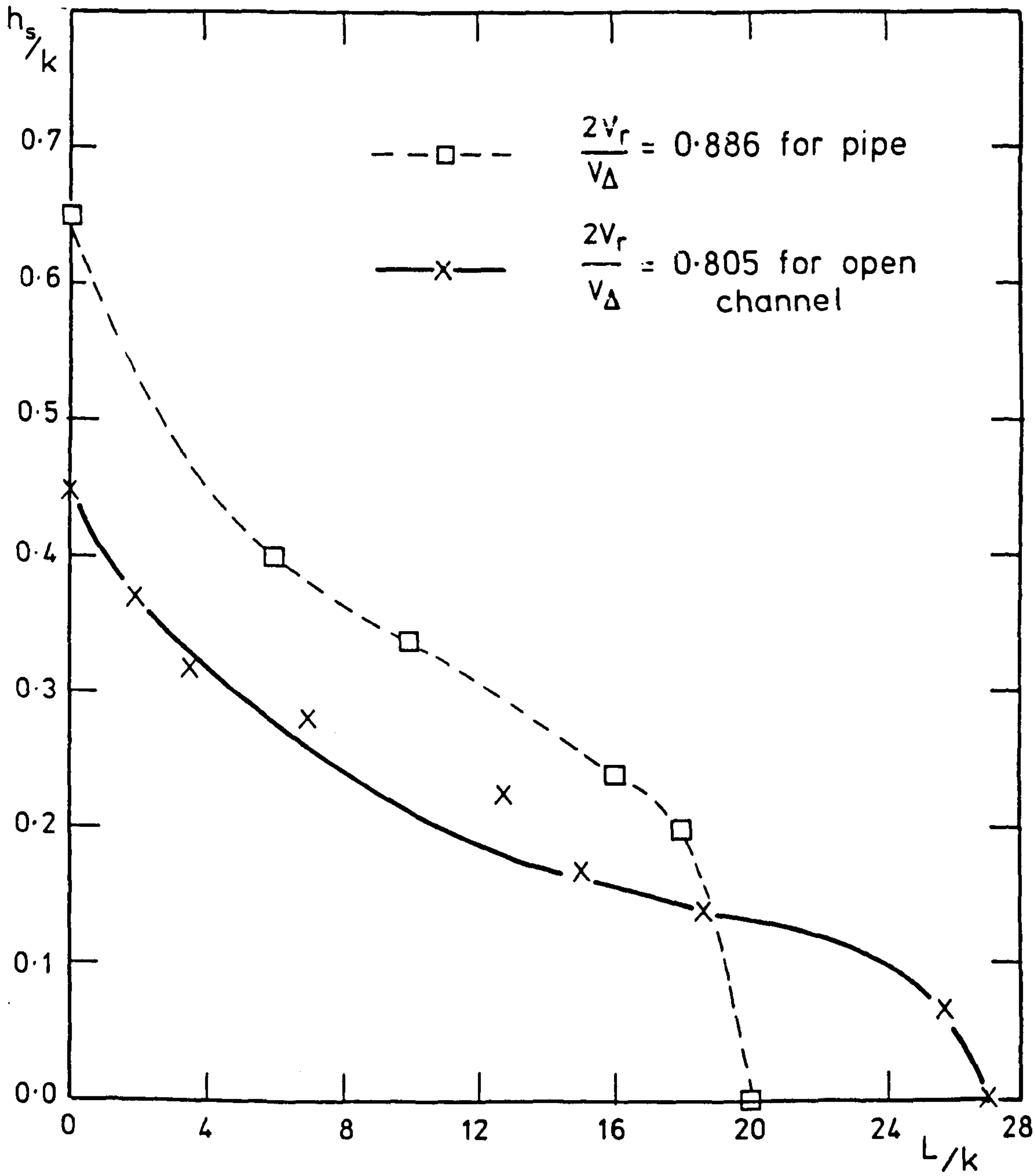

FIGURE 6. 21 $\frac{hs}{k}$ AGAINST $\frac{L}{k}$ WHERE k FOR PIPE = 5·0cm AND k FOR OPEN CHANNEL = 22·5 cm

Sharp and Wang[51] assumed the value of H to equal the diameter of the pipe and calculated the densimetric Froude number using Equation (6.1). However attempts to reproduce Sharp and Wangs results using Equation (6.15) have been unsuccessful as seen below in Table 6.3.

F_{RD}	α	$\frac{fL}{D}$ from Sharp and Wang	$\frac{fL}{D}$ from equation 6.15
0.6	0.2	2.5	0.5
0.6	0.45	6.0	0.28

Table 6.3

The matter has not been resolved because Sharp and Wang did not indicate how the translation from channels to pipes was undertaken, or how the boundary conditions were defined.

6.6 Summary

1) The theoretical model was successfully fitted to the experimental results obtained from the 50 mm diameter model pipe, but entailed the use of:-

a) intuitive adjustments to numerical computational routine near to the pipe exit to avoid instability arising in Equation (6.2), and

b) incorporation of further empirical adjustments to the interfacial friction factor near the toe of the wedge to reflect the observed steepness of the wedge in this region at lower densimetric Froude numbers.

2) Application of the calibrated numerical model to larger diameter experimental model results proved inadequate, and ensuing wedge lengths were found in many cases to be over estimated by a factor closely related to the scale ratio between the larger model and the 50 mm pipe. The cause of this has not been resolved because the measurement of exit boundary conditions was not possible for this test series. Consequently, more extensive studies for the determination of boundary conditions are needed before the numerical model can be adequately tested and validated for more general use.

CHAPTER 7

INVESTIGATION OF FLOW THROUGH MULTI-RISER OUTFALL SYSTEMS

7.1 Preliminary Results

The experimental work documented deals primarily with the effect of wave action on marine outfalls with multi-riser systems. Initial work undertaken to examine wave action on single port systems has been described in an earlier publication by Ali, Burrows and Mort[5], a copy of which is contained in Appendix F. The theoretical models used for single port outfall investigation are outlined in Appendix D, with the theoretical equations shown in Section 3.1. Previous work on this subject is reported upon by Henderson[27].

Early results, from experimental and numerical modelling, indicate that upstream oscillations induced by wave action increase as the cross-sectional area of the inlet drop shaft decreases. It was also noted that oscillations decrease as the rate of flow increases. Another important observation was that the time period of oscillation within the inlet shaft can be approximated by the following equation:-

$$T = 2\pi \sqrt{\frac{L\,A_1}{g\,A}} \qquad (7.1)$$

T - time period of oscillation

L - outfall length

A_1 - area of dropshaft and

A - area of outfall pipe

The above definitions are shown in Figure 3.1, and the equation is similar to that for calculating oscillations in a variety of other systems.

Henderson[27] dealt with the problem by assuming that the worst condition occurred when a wave crest was positioned across the entire diffuser system (see Figure 7.1).

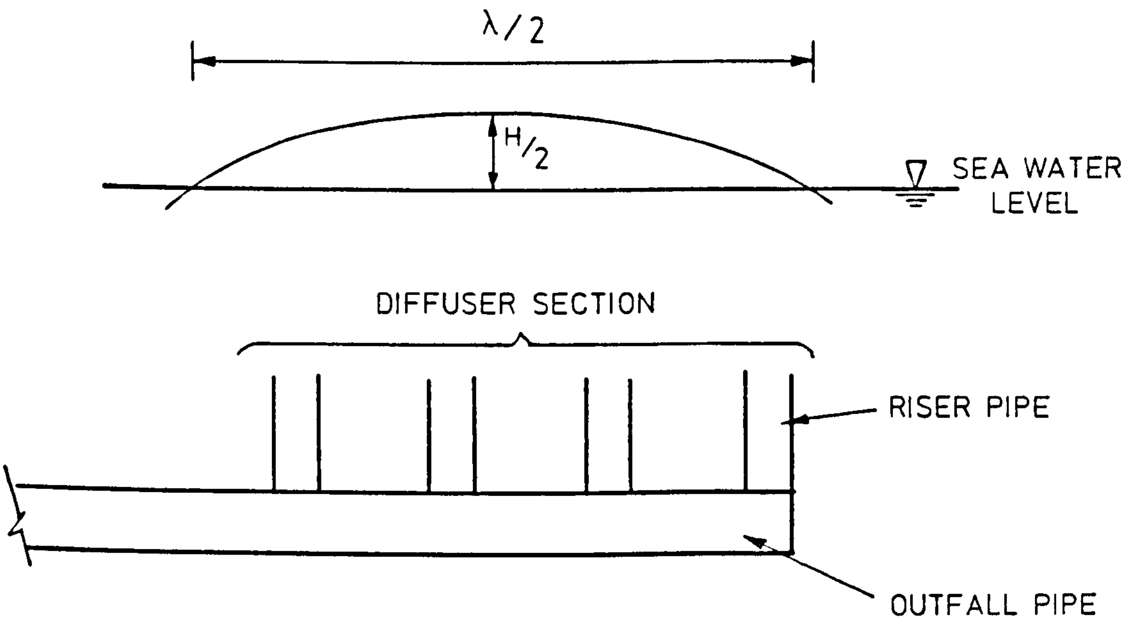

Figure 7.1

This assumption may have been valid for the problem Henderson was concerned with (the worst effect on an outfall diffuser system) but it does neglect to take account of oscillations of flow within individual risers and the effect that this may have on the overall efficiency of the outfall system. To investigate these problems a more rigorous testing facility was designed and constructed, and a more refined numerical model developed.

7.2 Wave action on a Multi-riser outfall

The main aim of this thesis was to investigate the effects that wave action has on an outfall during both its operational and closedown periods. To pursue this study an experimental model was designed and constructed, as outlined in Chapter 4 and experiments as outlined in Sections 5.2.2 to 5.2.6 were performed. A numerical model was also developed using the unsteady flow equations of motion and continuity, equations (3.19) and (3.29) respectively, so that this could be calibrated and utilized to model a wide variation of conditions affecting an outfall. A further development of the model is its possible use in modelling prototype outfalls as described in Section 7.7.3.

The following sections deal with the results and conclusions from both the experiments and numerical models.

7.2.1 Experimental and Numerical Results

Figures E1 to E83 inclusive (found in Appendix E) show the experimental and mathematical results produced during this research programme. Tables E1 to E39 indicate the mean, minimum and maximum velocities within outfall risers for the complete range of experiments performed.

Figures E1 to E20 are experimental velocity and pressure results obtained using an outfall without diffuser caps. Figures E21 to E38 are the corresponding numerical model results. Figures E39 to E65 show the experimental velocity and pressure graphs for an outfall with diffuser caps fitted, and a velocity graph for the corresponding wave conditions without diffuser caps fitted. Figures E66 to E83 are the numerical results obtained for an outfall with diffuser caps fitted. On the individual graphs the term WA and W indicate wave action and the terms NO WA and NW indicate no wave action.

7.2.2 Multi-riser outfall systems under shut-down conditions

7.2.2.1 Initial Experiments - Series 2

The first series of experiments were performed with the outfall model in its inverted position, and injected dye was used to track the direction of flow. It should be noted that the use of the model in the inverted position was essentially for test purposes only, and that quantitative results were not recorded because the performance of the model in this mode tended to be unsatisfactory on occasions. This was mainly caused by the collection of air along the soffit of the pipe. However, when performing satisfactorily, the model revealed, via the dye trace, signs of saline intrusion which was clearly generated by wave action, together with oscillatory velocity patterns within the risers, in both the zero flow condition and when salt water was passed through the system. (NOTE In the inverted position, salt water represents the sewage flow).

Series 3 experiments were undertaken in the same way as series 2, but with the outfall model in its normal operating position. Initial tests concentrated on shut-down conditions in order to investigate the effect of wave action alone on internal flows.

The velocity of induced flows in risers was estimated by recording the speed of the dye trace within the riser after its injection at the midpoint of the riser pipe. This method proved to be unsatisfactory for the accurate determination of riser flows and, in consequence, was only used as a qualitative indicator of general riser motion, thus enabling identification of the intrusive or discharging condition. Table E1 lists a set of results collected for a range of wave conditions.

When studying Table E1 it can be seen that there is no consistent pattern in respect of flow conditions in the risers, but what does emerge is that limited flow circulation takes place. Table E1 also indicates that under shut-down conditions, the mechanism which causes intrusion is particularly unstable. It was noted during experimental runs that some risers behave irregularly and would change their direction of flow over a short period of time. In other cases the dye trace indicated that the flow was entirely oscillatory within the riser, this being indicated by a zero in the table.

7.2.2.2 Initial Experiments Using Ultrasonic Flowmeter

This is an extension of the Series 3 experiments under shut-down conditions. The results produced during the initial series of experiments are listed in Table E2 (riser velocities) and Table E3 (outfall pressures).

Table E2 indicates that the velocity within the risers embody large wave induced fluctuations about mean inflow or outflow velocities. It is also clear from Table E2 that a continuity balance does not exist for the measurements taken and the reasons for this are outlined in Section 7.2.2.3.

The largest mean velocity observed was 3.5mm/sec which, when using the scaling factor given by Equation (4.3), gives a prototype velocity of 0.015m/sec in a 600mm diameter riser. This equates to a rate of flow of only 4.3 l/sec through the riser in the prototype system, and circulatory flows are, in consequence, likely to be of very low magnitude. Instantaneous flow rates, both discharging and intrusive, will be significantly larger. For example, taking a model velocity of 0.045m/s and using Equation 4.3; it is found that this gives an equivalent prototype velocity of 0.19m/s in a 600mm diameter riser.

From the results shown in Table E2 it can be observed that velocities above and below 0.045m/s are encountered in the risers during intrusive and discharging conditions. It is therefore possible that suspended particles could be transported into the diffuser under the flow rates encountered. From the limited range of tests completed at this stage, it was deduced that wave periods between 1.0 and 1.5 seconds appear to generate the strongest internal circulations. These waves have lengths ranging between 1.56 and 3.51 metres in the flume, which in turn will exhibit significant phase lags between instantaneous pressures over the various risers, (see Section 7.7).

The wave pressure results given in Table E3 show that pressures oscillate as waves pass over the outfall. It should be noted that the pressure at the upstream and of the pipe (pressure point 5) has a maximum and minimum difference equivalent in magnitude to the differences shown at the other four pressure points, thereby indicating that the fluctuations extend backwards along the outfall pipe and into the outfall shaft.

Figures E1 and E2 show graphical outputs for riser velocities and pressures along the centreline of the outfall pipe, for the experiment involving a wave height of 4.1cm and a wave period of 2.22 seconds. Looking first at Figure E1, the mean velocities deviate little from the zero value indicating that very weak internal circulations take place. The oscillatory instantaneous velocity ranges from a discharging condition of 4cm/sec to an intrusive condition of 4cm/sec. No evidence of larger period oscillations, equivalent to those found in a single port outfall (see Ali, Burrows, Mort[4]; Appendix F) were detected in these results.

Figure E2 is the graphical output of pressure fluctuations under the same wave conditions as for the velocity graph in Figure E1. The pressure graphs for pressure points 1 to 4 in the diffuser section, show cyclical pressure oscillations at the wave frequency, but the upstream pressure transducer at pressure point 5, gives a distorted output. The distortions are probably caused by turbulence at this section resulting from changes in water level in the drop-shaft and varying flow conditions due to the close proximity of the venturimeter.

Large oscillations in pressure are generated by long wavelengths producing very little pressure attenuation from the surface down to riser head elevation. The wavelength for a period of 2.22 seconds is 5.78m indicating that at some instances in time, all risers will be acted upon simultaneously by an increase in pressure (see Figure 7.1). More importantly, however, is that there is always a significant pressure lag between the most seaward and landward risers due to movement of the wave (Figure 7.2).

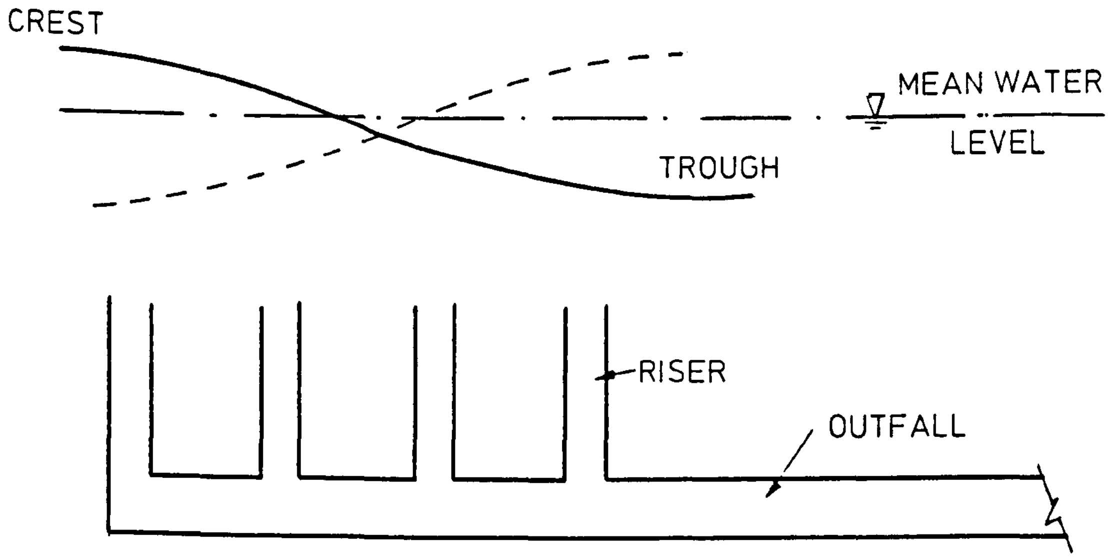

Figure 7.2

The average change in pressure along the centre line of the main outfall pipe, under the diffuser section, was found by taking the differences between the maximum and minimum pressure values at pressure points 1 to 4. For a wave height of 4.2 cm and wave period of 2.22 seconds (see Figure E2) the average change in pressure was found to be 0.26 kN/m^2. Assuming the wave to be in shallow water the theoretical change in pressure at the pipe centreline caused by the wave passing from a trough to a crest is 0.4 kN/m^2. This indicates that only 65% of the total wave pressure appears to act at the pipe centreline.

7.2.2.3 Errors and Discrepancies with Experimental Results

As mentioned earlier, Table E2 indicates clearly that a continuity balance between the four risers does not exist. The reason for this is largely due to the fact that each set of velocities produced for a single wave condition, are prepared from results produced during four different experimental runs. As mentioned in Chapter 5, the velocity meter was moved from riser to riser for each set of experiments. Consequently, there is no guarantee that all conditions were identical, although every effort was made to ensure that conditions were similar.

The probe was very sensitive to density changes, and this became a problem when two different densities of water were used. The largest change in the setting of the probe was found to be 1cm/s leading to possible errors in velocity measurement and there was also an instability within the device of approximately 3 - 5 mm/s. The velocity values recorded on intrusive risers will not be subject to the larger instability because they are not influenced by changing fluid densities, whereas the discharging risers will under some conditions have a mixture of densities depending on the local scale of mixing from any saline wedge present.

Because the velocity meter was moved between the risers the velocity traces do not provide an instantaneous record of the flows in the different risers. The graphs therefore record the flows within the individual risers and so provide an estimate as to how the diffuser system is acting.

7.3 Multi-riser outfall systems under normal operation

The results reported here are for series 4 and 5 experimental groups referred to in Chapter 5. A total of nine different rates of flow were used and these ranged between 0.1862 l/s to the design flow rate of 2.0 l/s. For each discharge rate, the effect of five different wave conditions were examined.

7.3.1 Experimental results (outfalls without diffuser caps)

Tables E4 through to E21 summarise the statistics of velocity fluctuations within individual risers, together with the variations of pressure within the pipeline for both still water and the various wave conditions. Figures E3 to E20 inclusive, show sampling time histories of riser velocities, as well as pressures in the pipeline for a waveheight of 0.066m and a waveperiod of 1.429 seconds.

In all cases it can be observed that at various discharge rates, intrusive conditions occur in the seaward risers, and that as the flow increases the number of risers subject to intrusive conditions decreases. Under the design flow condition of 2.0 l/s, Table E20 and Figure E20 both indicate that all risers have been purged of seawater.

The instantaneous velocity within the risers is dependent upon a combination of flow rate and wave action. From Tables E4 to E20 inclusive, it can be seen that the largest fluctuations are caused by longer wave periods - hence longer wavelengths, and Figures E3 to E20 show the magnitude of these fluctuations for one of the longer wave periods.

In general, the riser velocity plots show that if a riser was operating in the reverse flow mode during steady flow conditions, wave action over the system increased the intrusive velocity thereby allowing more seawater to be drawn into the outfall.

The time traces showing the changes in pressure along the centreline of the pipe are cyclic, with distortions appearing at the peaks, except in the case of pressure point 5 which is distorted at all times. The distortions are probably caused by turbulence within the pipeline due to varying flow conditions; in the case of the pressure point 5 the problem is exacerbated by the proximity of the venturimeter.

All mean velocity results for these experiments are superimposed on each other as shown in Figure 7.3. The percentage change of mean velocity against steady flow state mean velocity is shown in Figure 7.4. These show how the mean velocity of individual risers varies with wave action.

An interesting feature which appears on Figure 7.3 is that before a riser can be purged of seawater, its neighbouring landward side riser must have a velocity approaching 0.2 m/s. In addition, it was observed that whilst a riser is being purged, the adjacent seaward riser usually allowed higher volumes of seawater to enter the system. This indicates that during the purging process, strong local mechanisms appear to exist affecting the rate at which seawater is drawn into the outfall.

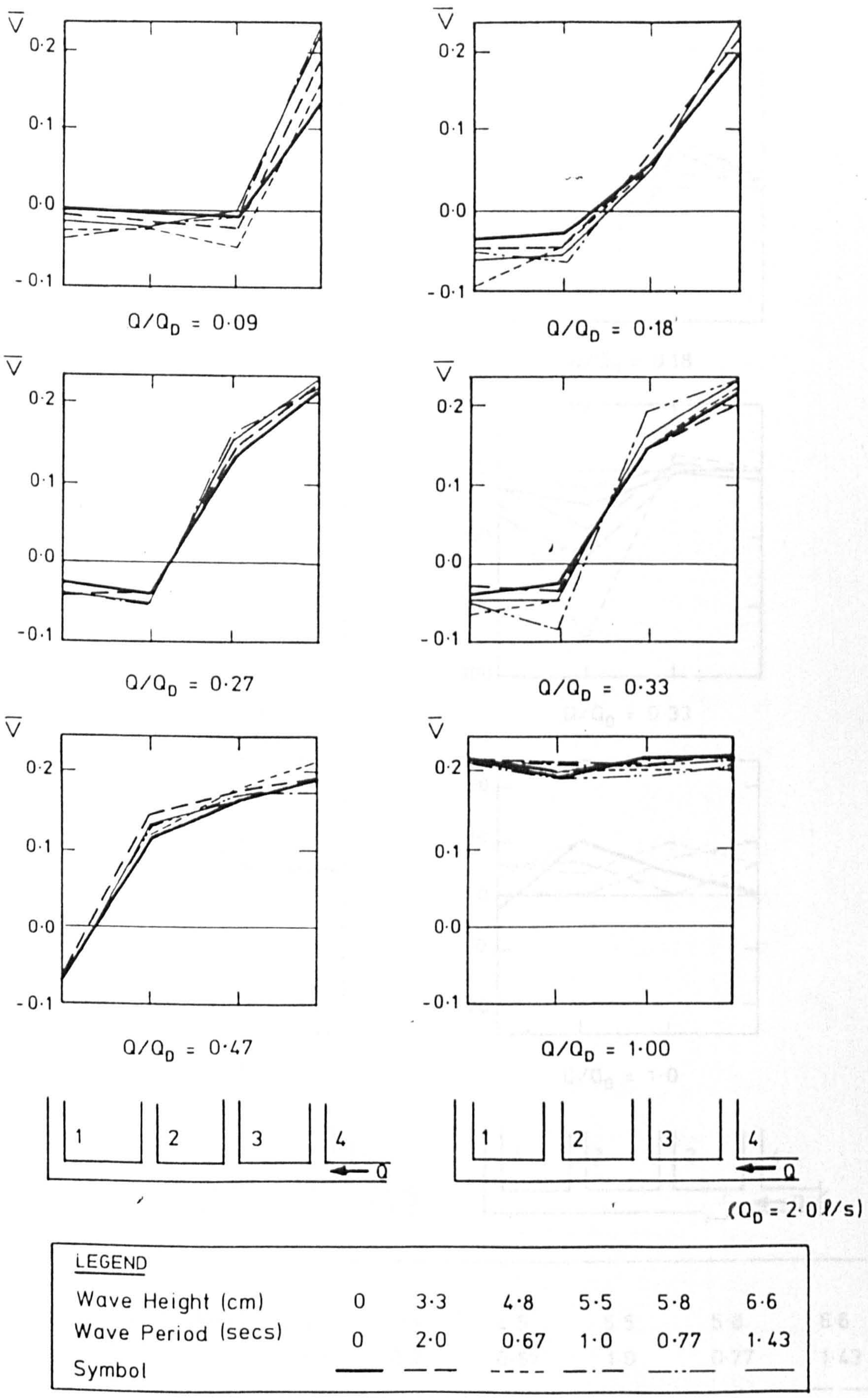
V̄
0·2
0·1
0·0
- 0·1
Q/Q_D = 0·09
Q/Q_D = 0·18
Q/Q_D = 0·27
Q/Q_D = 0·33
Q/Q_D = 0·47
Q/Q_D = 1·00
1
2
3
4
Q
(Q_D = 2·0 ℓ/s)
LEGEND
Wave Height (cm) 0 3·3 4·8 5·5 5·8 6·6
Wave Period (secs) 0 2·0 0·67 1·0 0·77 1·43
Symbol

FIGURE 7.3

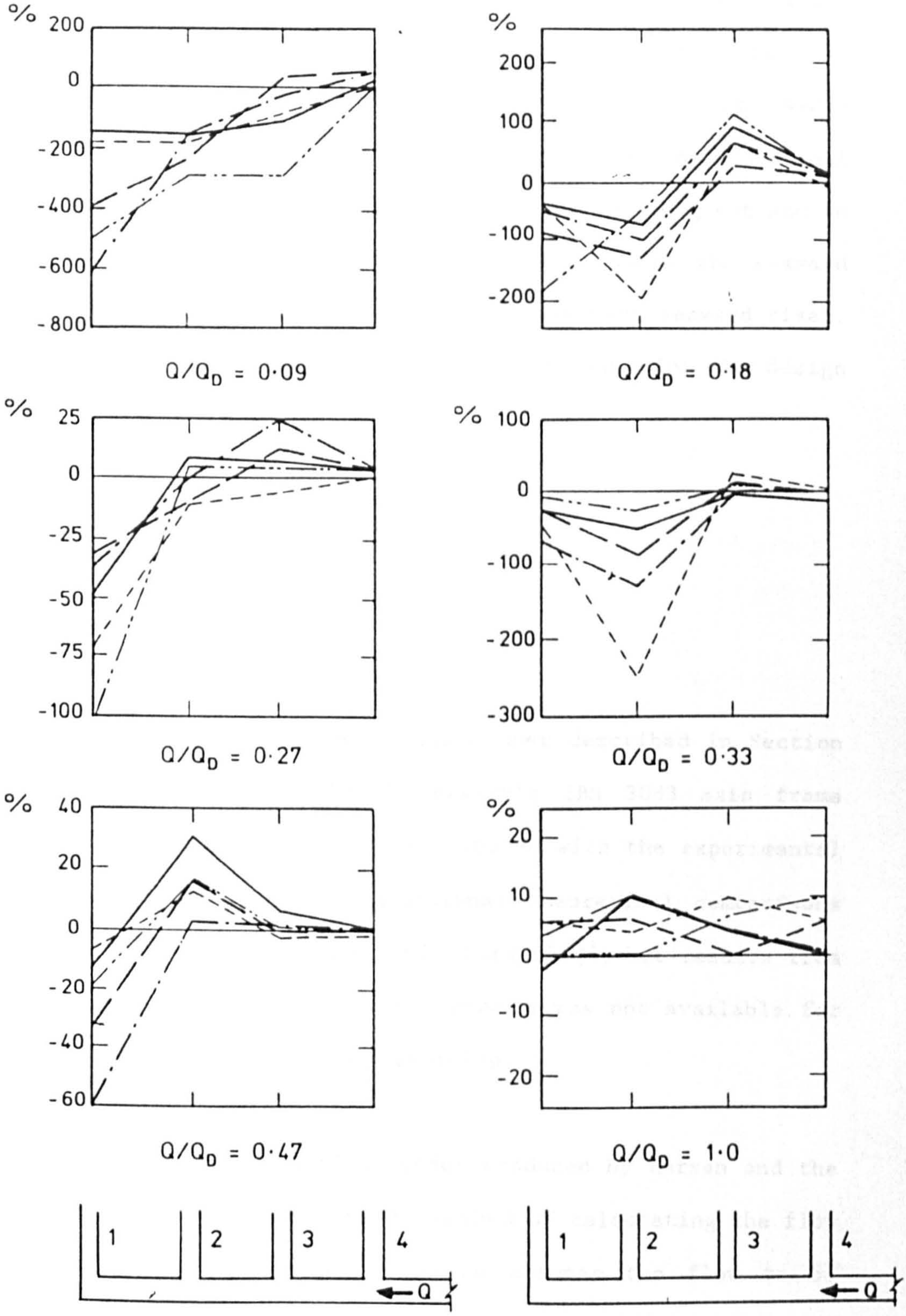

LEGEND

Wave Height, (cm)	3·3	4·5	5·5	5·8	6·6
Wave Period, (secs)	2·0	0·67	1·0	0·77	1·43
Symbol					

FIGURE 7.4

This apparent purging velocity of 0.2 m/s appears to be the critical velocity at which the headloss of the flow moving up the riser is equal to that caused by the flow acting against the saline wedge within the outfall. If the flow rate is then increased the additional flow cannot move up the riser as the headloss will be too great and so the additional flow will force the saline wedge towards the seaward risers and hence begin the process of purging the next seaward riser. This flow velocity is similar to the calculated value for the design flow rate.

7.4 Numerical Model and Results

7.4.1 Numerical Model

The numerical model was developed in the manner described in Section 3.2. The model was run on the University's IBM 3083 main frame computer and all results produced were compared with the experimental values outlined in Section 7.3. Additional theoretical comparisons were obtained from the model developed by Larsen[35], but results from this can not be shown because computer hardware was not available for producing output from the comparison exercise.

The difference between the numerical model produced by Larsen and the one developed for this research was the method of calculating the flow rate around the diffuser section. Larsen assumes the flow to be wholly incompressible within the diffuser and, in consequence, uses equations similar to those in Section 3.1, for motion and continuity, (equations 3.4 and 3.5), to calculate flows in the risers and intermediate pipe sections. He then uses the method of characteristics to determine the flows along the main section of the intermediate pipe sections. He then uses the method of characteristics to determine the flows along the main section of the outfall (Figure 7.5).

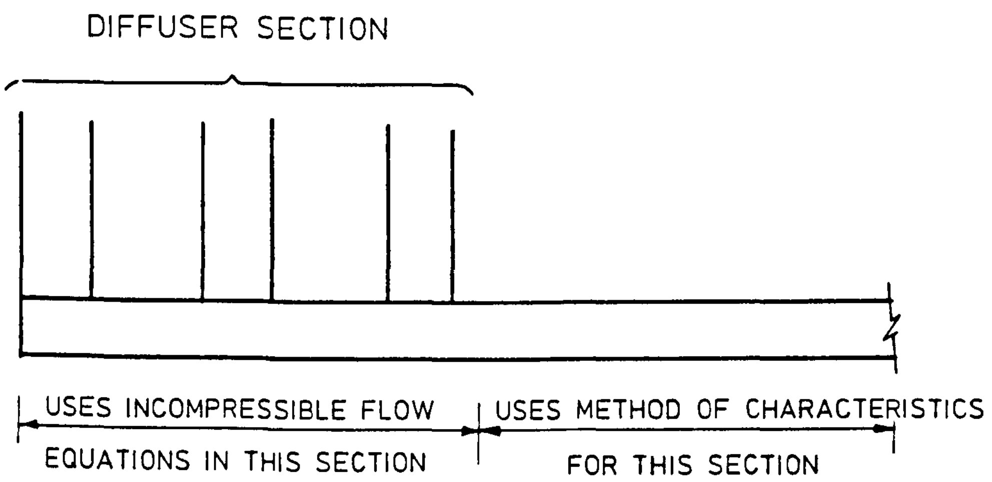

Diagram showing basis of equation in Larsen's model.

Figure 7.5

For the model developed at Liverpool, the flow is assumed to be compressible within the entire section of the main outfall pipe and incompressible within the individual risers, as outlined in Section 3.2.

7.4.2 Calibration of Numerical Model

The numerical model developed at Liverpool was calibrated by varying within justifiable physical limits, headloss factors inside the riser/outfall 'T' junctions. Initially the numerical model calculates the headloss requirements within each riser pipe so that during design steady state flow conditions (2.0 l/s) there was equal discharge between all four risers. The headloss within each riser consists of an entry and exit loss and a frictional headloss caused by wall shear stress. However, when the numerical model was being operated during unsteady flow conditions, but at design discharge, the exit and entry headloss coefficients remained at a constant value and the wall shear stress friction factor was varied using the Colebrooke-White equation[56]. By keeping the entry headloss coefficient constant an error is built into the model because, as demonstrated by Miller[38], when the ratio of flow rate entering the riser to the flow rate passing along the main pipe changes so does the headloss coefficient. One way to overcome this is to build a headloss database into the model. However using Millers[38], headloss diagrams may also lead to discrepancies as the data was obtained from experiments using high Reynolds numbers whereas an outfall tends to operate at low Reynolds numbers.

From the experimental model it was observed that once the flow rate dropped below the design flow condition saline intrusion occurred. This led to the formation of a saline wedge within the main outfall pipe and a more complicated process of flow distribution. The numerical model now becomes inadequate as it does not contain the required mass balance equations which take account of any mixing, nor does it have the ability to recreate the flow conditions as the fresh water passes over the saline wedge. To enable the numerical model to be used for comparing experimental data, and to investigate other outfall conditions, it had to be altered using empirical adjustments. To do this one set of experimental data was obtained and the numerical model was adjusted until the numerical results were similar to the experimental data. Two adjustments to the numerical were made and both were made to the riser sections. The first adjustment was to set the density of water within an intrusive equal to that of the seawater, the numerical model recognised an intrusive riser as the velocity result was negative.

When the numerical model calculated the velocity in the riser to be a positive discharge of fresh water the density of water within the riser was changed to 1000 kg/m^3 and under zero flow rate conditions all the water within the outfall was set to equal the seawater density.

The second stage was to make minor adjustments to the entry headloss coefficients at the base of the individual risers until the numerical and experimental results for the one condition were similar.

The numerical model in this adjusted condition was then compared with further experimental results without any more adjustments being made.

7.4.3 Numerical model results

Figures E21 to E38 inclusive show the numerical model output for the nine different rates of flow during periods of still water, and when waves of heights of 6.6cm and periods of 1.429 secs are passed over the system. By comparing the numerical model results with those produced experimentally, Figure 7.6, it can be seen that the behaviour is comparable. Figure 7.6 illustrates the numerical and experimental mean flow velocities within risers subject to wave action, over a range of six different discharge rates. A major discrepancy arising is when $Q/Q_o = 0.09$; the numerical model depicts riser 2 to be discharging whilst the experimental model shows it to be intrusive. When analysing the theoretical model results it was

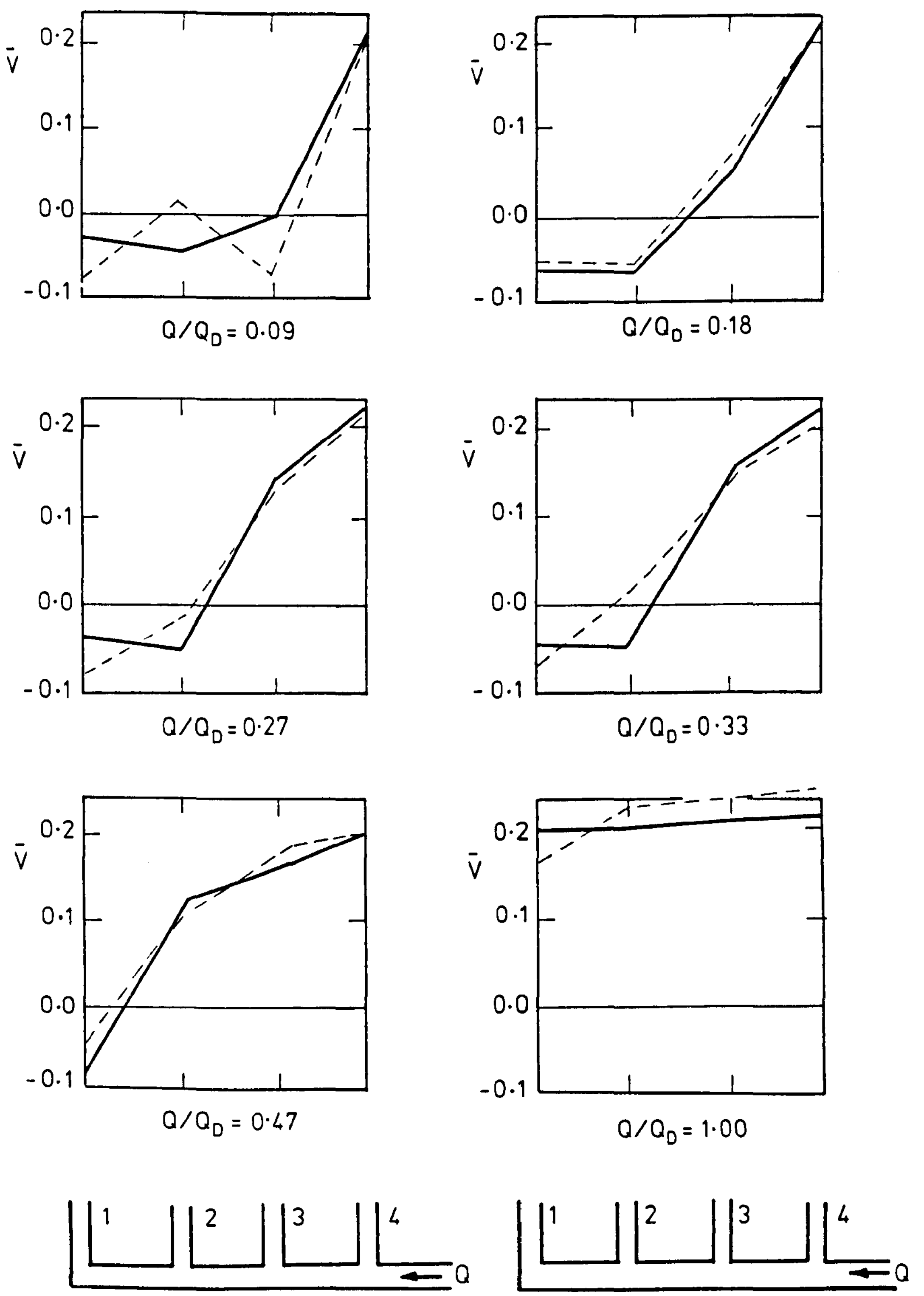

(WAVEHEIGHT = 0·066m,   WAVEPERIOD = 1·429secs, Q_D = 2·0L/S)

LEGEND :-

THEORETICAL MODEL RESULTS - - - - -

EXPERIMENTAL MODEL RESULTS ———

FIGURE 7.6   COMPARISON OF EXPERIMENTAL AND THEORETICAL VELOCITY RESULTS discovered that the discrepancy is caused by internal circulation between risers 1 and 2. When $Q/Q_o = 0.09$ all freshwater discharges from the manifold via riser 4, whilst drawing seawater in through riser 3. A smaller discrepancy is apparent when $Q/Q_o = 0.33$. In this case the mathematical model shows riser 3 to be in the process of purging, whereas the experimental results indicate it to be in an intrusive condition.

The discrepancies will be due to the method by which the numerical model calculates the purging process, and this is performed in the following way. Initially there is zero flow and the wave action is allowed to build up, so creating small amounts of salt water circulation within the diffuser system. The fresh water flow rate is then gradually introduced into the system and this is slowly increased over a series of time steps until the required discharge is attained. As the flow rate is being increased the fresh water begins to pass along the main outfall pipe, and eventually begins to discharge through the most landward riser. As it discharges the density value within the riser is changed to 1000 kg/m^3; the other risers will still have seawater within them. Once the critical velocity is reached (where the headloss along the pipe and up the riser are equal) the flow will then move along the pipe and begin to purge the next riser. The process then continues until a mean velocity equilibrium exists.

It can be seen that the results produced by the numerical model compare favourably with those produced experimentally, but problems do exist with the numerical model. The principal difficulty is that, under certain flow conditions, when no wave action occurs, the numerical results indicate the flow within the risers to be oscillating. This is seen to be an inherent instability with the model and whilst several attempts were made to eradicate the problem none were wholly successful. The graphical output obtained from the numerical model demonstrates that during periods of wave action the inherent instability has no effect on the result as the oscillations in velocity are equivalent to the wave period. Moreover, no account was taken for the mixing process of salt and freshwater within the outfall, or for changes in flow characteristics caused by the developing saline wedge. In consequence more research is needed to refine the theoretical model, and this is outlined in Section 8.2.

7.5 The effects of wave action on an outfall manifold with diffuser heads attached

7.5.1 Introduction

The results discussed so far have been concerned with the effects of wave action on open-ended risers. In practice, however, risers are frequently capped with diffuser heads to aid both dilution and dispersion of the discharging effluent. In addition, a well designed diffuser system will alleviate unacceptable 'boils' and surface 'slicks' at sea level.

In addition the capping of risers increases the headloss within the riser and so the results obtained will be similar to the effects of using either longer risers or narrower risers, which have a similar increase in headloss.

In order that the numerical model can take into consideration situations where diffuser caps have been installed, it had to be re-calibrated, and this was done with the aid of the experimental model which produced the required data.

The experimental model had fitted to it replica diffuser caps, similar to those used on the Grimsby long sea outfall as shown in Figure 4.14. The calculation used in the design of the caps is given in Section 4.

7.5.2 Experimental Results (Diffuser Caps Fitted)

Figures E39 to E65 show the effect that diffuser caps have on general flow characteristics within individual risers. The discharge rates used were the same as those employed for producing the results contained in Section 7.3, and the sample chosen for comparison was that derived from a waveheight and period of 0.058 metres and 0.769 secs. respectively. The mean velocity results, together with maximum and minimum values, are given in Tables E22 to E39; the results obtained from the pressure transducers are also given.

Figure 7.7 attempts to clarify the comparison between experimental velocity results within the risers when diffuser caps are fitted and when they are not. It shows that lower flow rates are needed to purge the riser which in turn ensures a reduction in the amount of seawater entering the system.

However, it is interesting to note that whilst all risers are discharging at a Q/Q_o value of 0.47, it does not follow that the outfall is completely purged. The situation shown in Figure 7.8 below, may well have developed:-

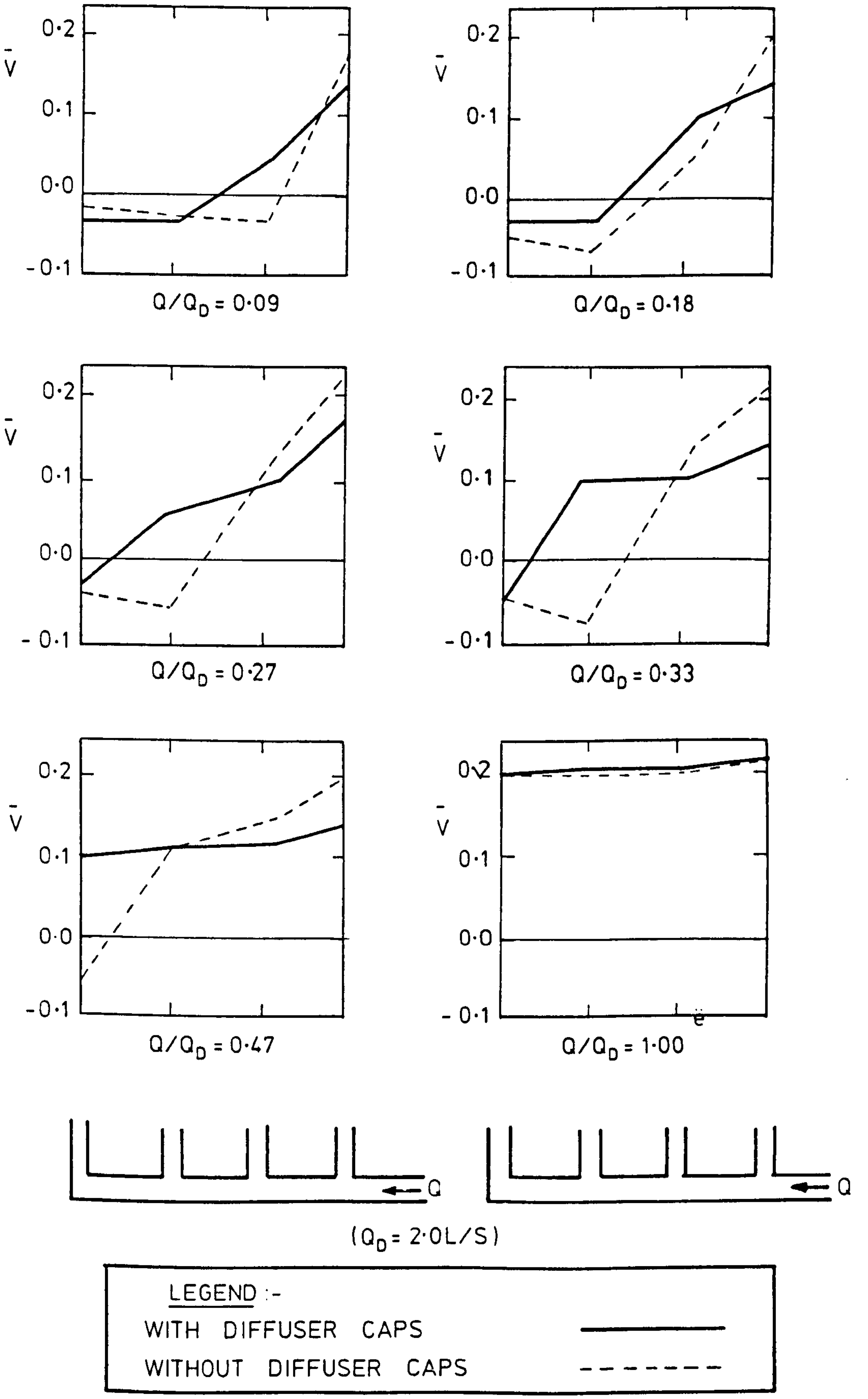

FIGURE.7.7 COMPARISON OF EXPERIMENTAL VELOCITY RESULTS BEFORE AND AFTER DIFFUSER CAPS ARE INSTALLED

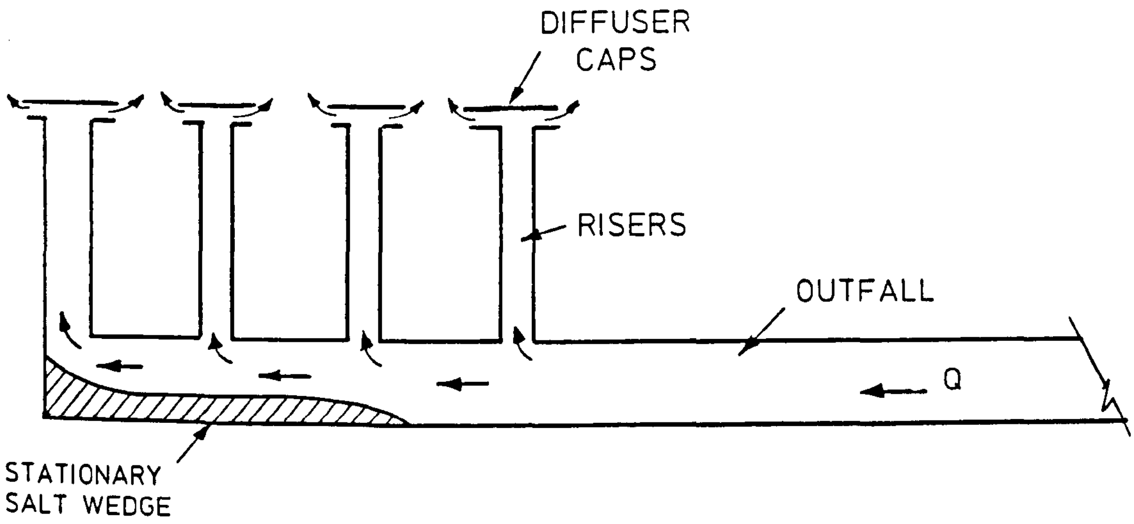

Figure 7.8

Figure 7.8 shows fresh water passing over the salt wedge leading to a purging of all four risers, but offering little or no indication of the extent of saline intrusion within the manifold. Should the saline wedge not be fully purged at frequent intervals, sediment ingress and deposition is likely to occur, eventually causing a blockage in the pipe. The absence of diffuser heads does allow easier determination of the limits of application of a saline wedge because its toe will usually be near to the most landward riser - once this riser has been purged. It is appreciated however, that in addition to providing more efficient dispersion characteristics, the use of diffuser heads has the distinct advantage of reducing the ingress of seawater. One possible method of preventing saline intrusion is to install mechanical non-return values on the diffuser ports as outlined in Section 2.

7.6 Numerical Model Results

The theoretical model was calibrated for the new set of experimental results, which take account of attached diffuser caps in a way similar to that described in Section 7.4.2. The data produced by the theoretical model are given in Figures E66 to E83 inclusive. The instability problem mentioned in Section 7.4.3. is still present and could not be satisfactorily eradicated.

Figure 7.9 shows a comparison between mean velocity results within the risers obtained from the experimental and theoretical models. It can be seen that, whilst small discrepancies exist, the mathematical model predicted the behaviour of the experimental model quite well. Once it was established that the theoretical model produced satisfactory results, it was extended as outlined in Section 7.7.

7.7 Appraisal of the numerical model

The results given in previous sections demonstrate that the calibrated mathematical model produces satisfactory results. Therefore an obvious extension of this work should be to vary the data relating to outfall parameters and wave conditions, and to investigate the results the mathematical model produces. The following sections contain a summary of further work undertaken using the numerical model.

7.7.1 Varying the riser diameter and length

As mentioned in Section 4.2.1 the riser diameter chosen for the experimental model represented a diameter which was larger than those used on actual outfalls. It was suggested in Section 4.2.1 that a

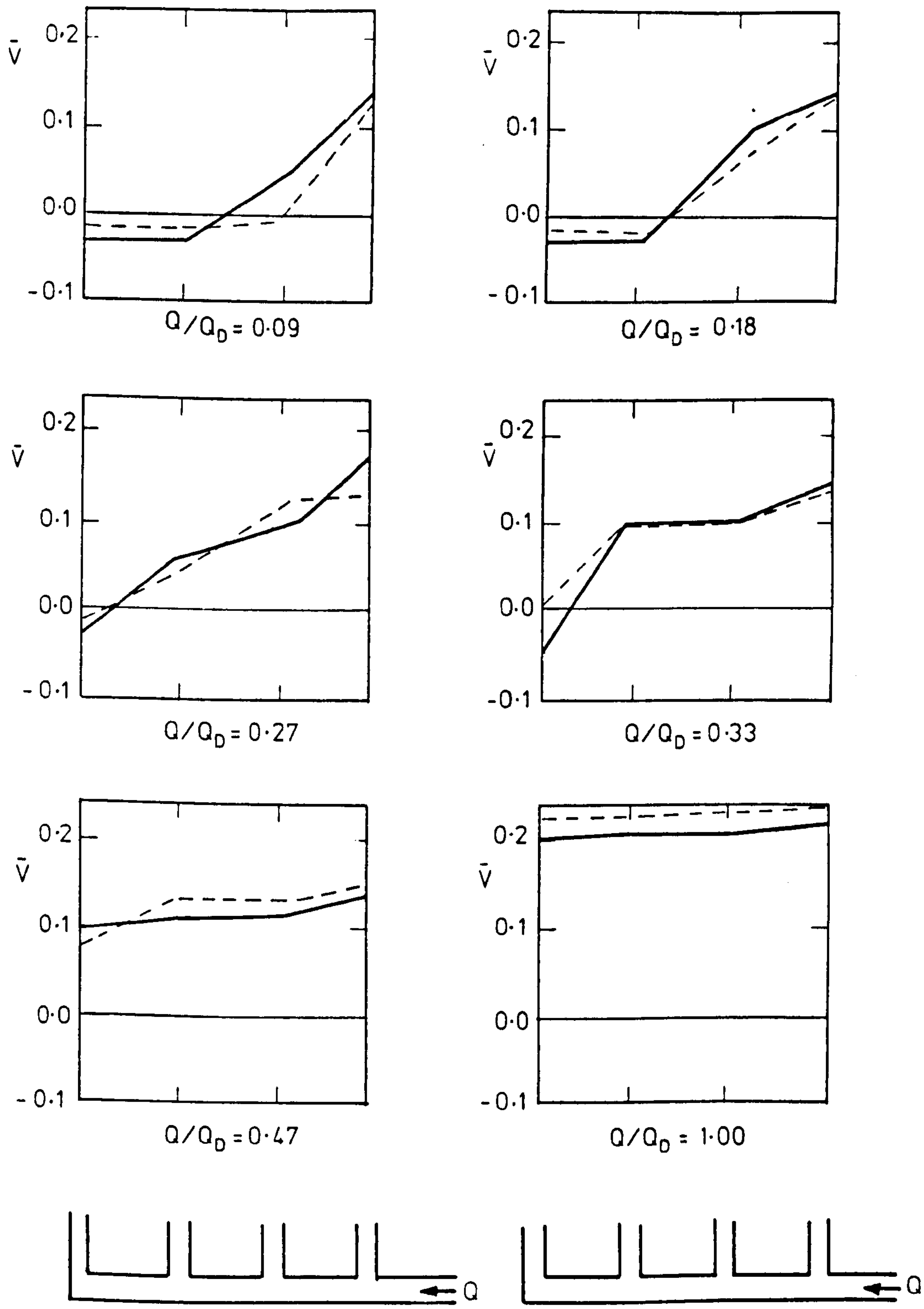

$(Q_D = 2·0L/S)$

LEGEND:-

EXPERIMENTAL ————

THEORETICAL - - - - - -

FIGURE 7.9 COMPARISON OF EXPERIMENTAL AND THEORETICAL VELOCITY RESULTS WITH DIFFUSER CAPS INSTALLED model riser diameter of 23mm would enable better representation of the general outfall system, and that a model diameter of around 35mm would lead to a more balanced system.

Figures 7.10 and 7.11 show the consequence of a change in diameter of the riser. Both are subject to identical wave conditions and discharge rates, as well as having diffuser caps fitted to the riser outlets. Table 7.1 shows the differences in mean velocity results.

From Table 7.1 it can be seen that as the riser diameter decreases the average velocity increases and the distribution of flow through the risers becomes more even. Figure 7.12 shows the effect of a low discharge rate upon a system comprising smaller riser diameters. For this situation Riser 1 is shown to be in an intrusive condition, whilst the remaining risers discharge. This may be compared with Figure E22 which shows similar conditions with a riser diameter of 0.05m. This indicates that as riser diameters decrease, the amount of seawater entering the system, via the intrusive process, also decreases.

	Riser diameter (m)	
Riser	0.035	0.05
1	0.175	0.015
2	0.175	0.09
3	0.175	0.011
4	0.175	0.011

Mean velocity results (m/s) for change in riser diameter

(riser length = 0.040 m)

Table 7.1

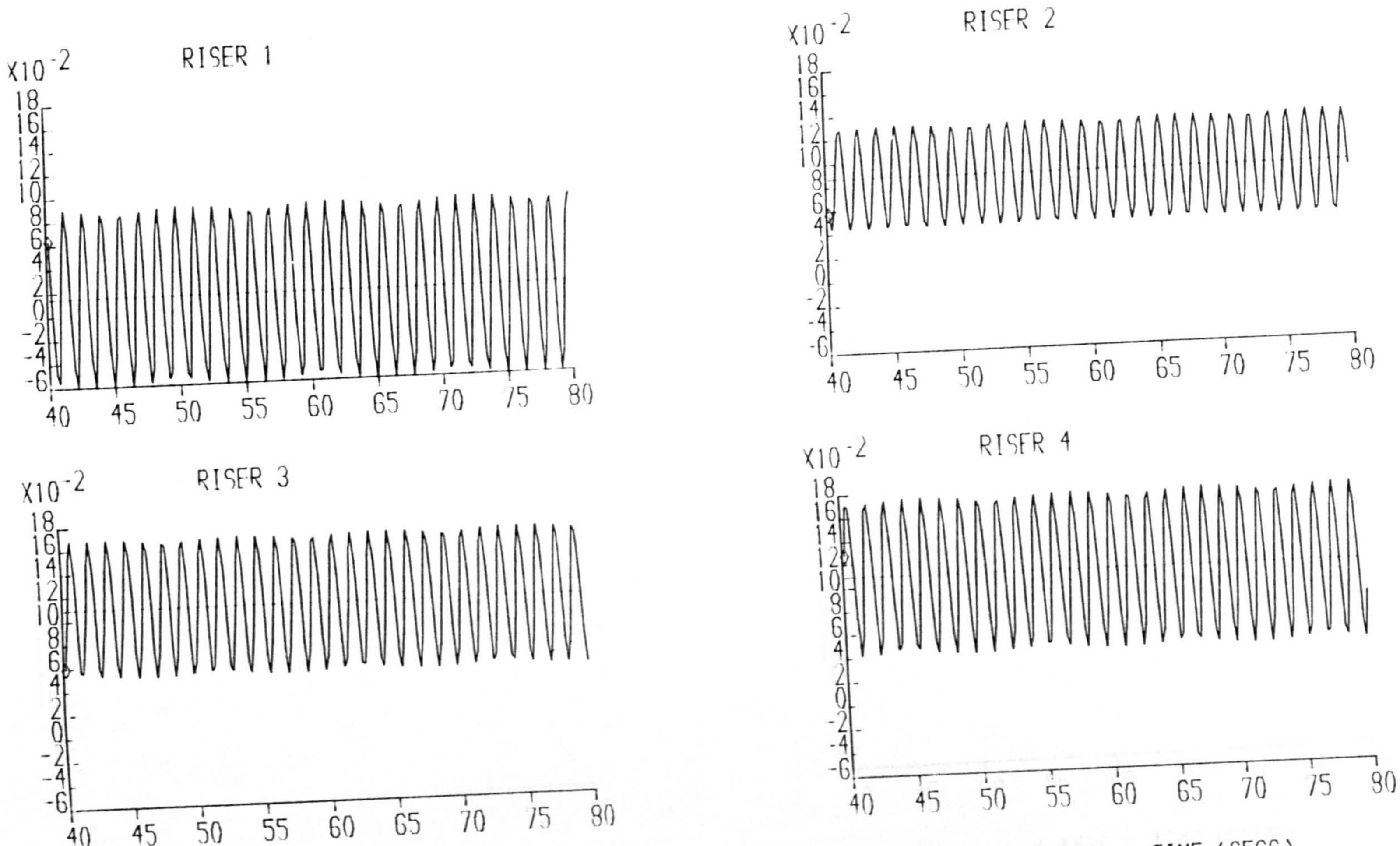

X-AXIS = TIME (SECS)

Y-AXIS = RISER VELOCITY (M/S),

WAVEHEIGHT= 0.06000 WAVEPERIOD= 1.42600 FLOW RATE= 0.00063

RISER DIAMETER = 0·05m RISER LENGTH = 0·4m

FIGURE 7.10

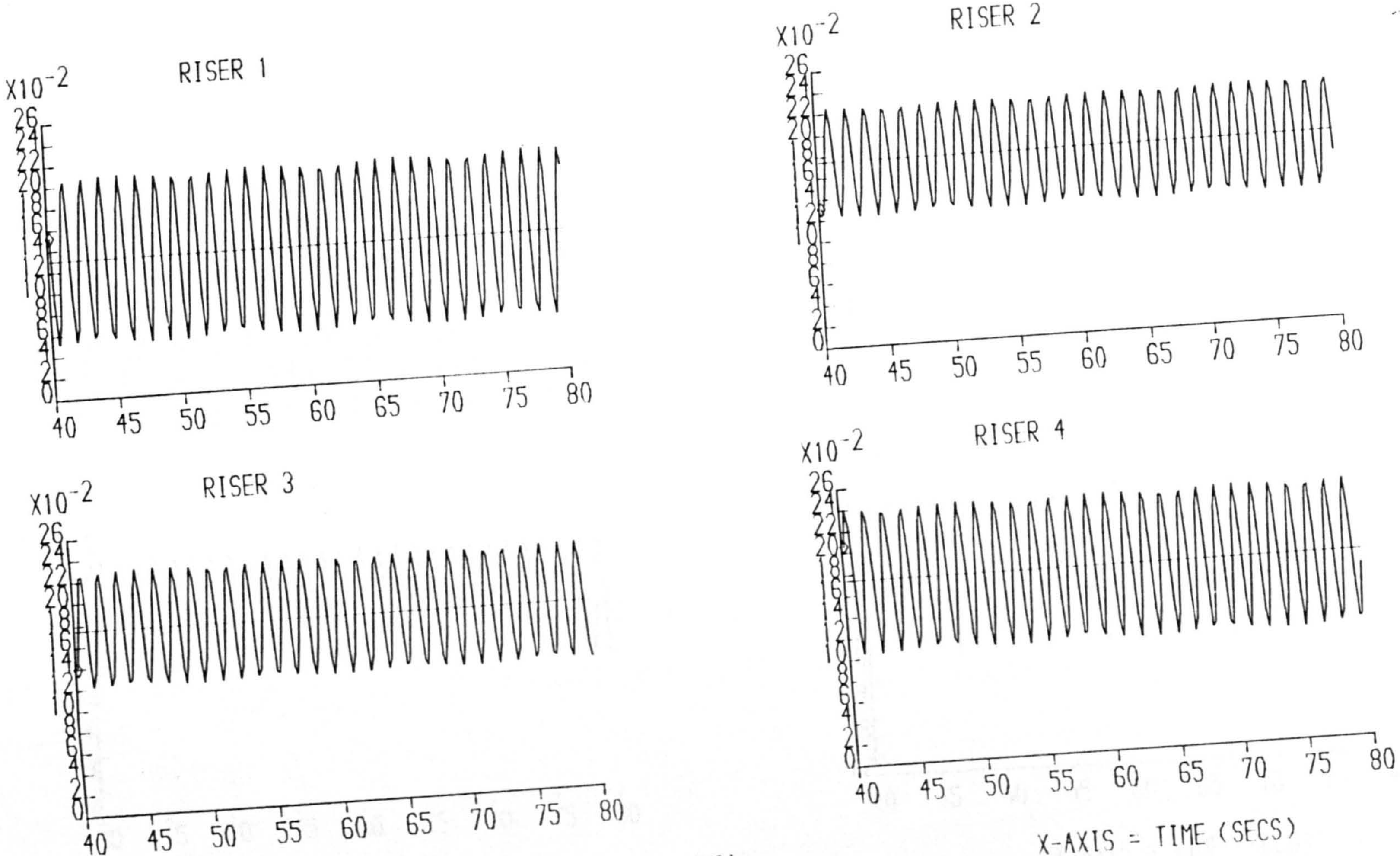

X-AXIS = TIME (SECS)

Y-AXIS = RISER VELOCITY (M/S),

WAVEHEIGHT= 0.06000 WAVEPERIOD= 1.42600 FLOW RATE= 0.00063

RISER DIAMETER = 0·035 m RISER LENGTH = 0·4 m

FIGURE 7.11

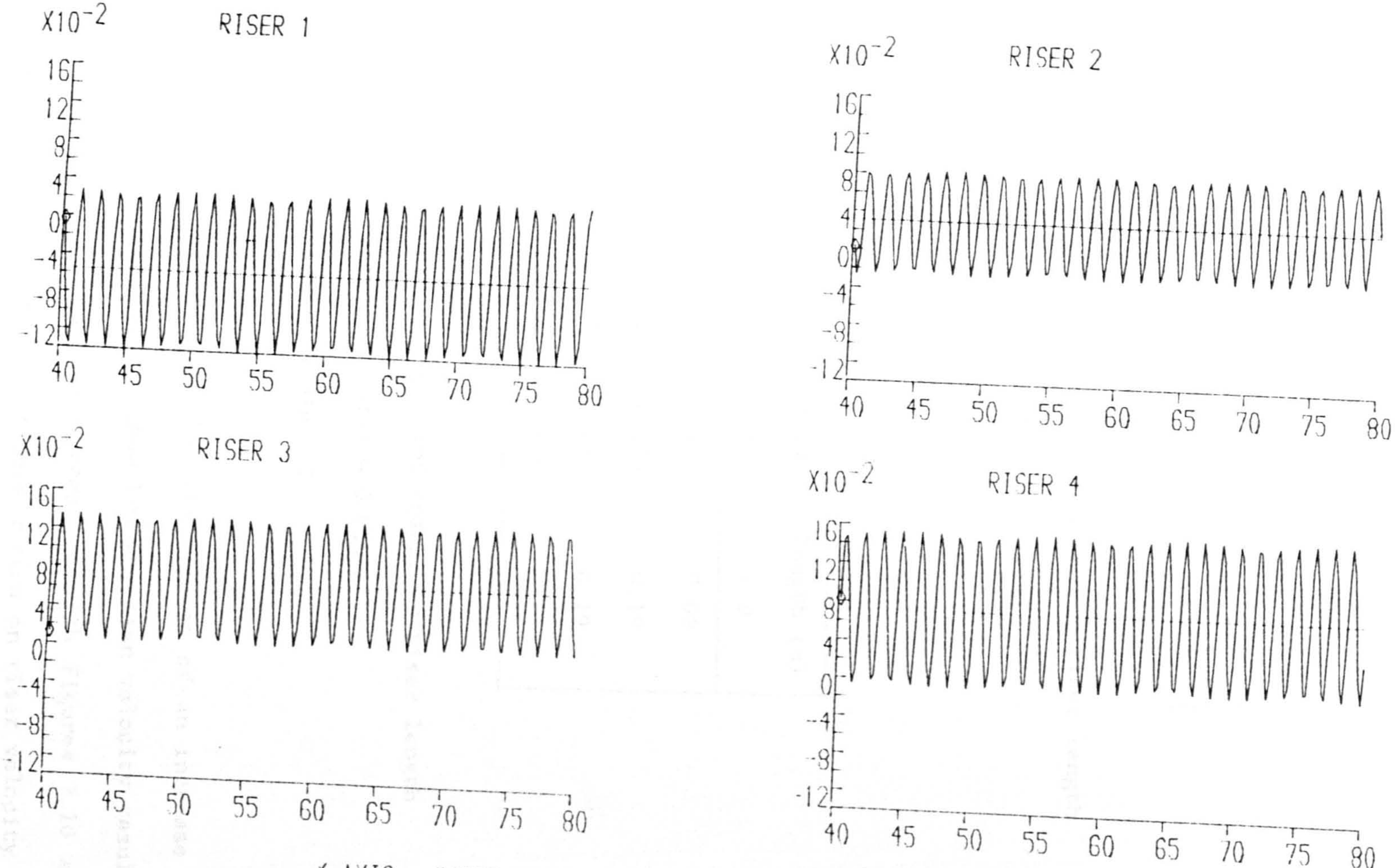

Y-AXIS = RISER VELOCITY (M/S),

X-AXIS = TIME (SECS)

WAVEHEIGHT= 0.06000 WAVEPERIOD= 1.42600 FLOW RATE= 0.00019

RISER DIAMETER = 0·035m RISER LENGTH = 0·4m

FIGURE 7.12

Riser	Riser Length (m) 0.40	1.0
1	0.015	-0.03
2	0.09	0.03
3	0.11	0.16
4	0.11	0.16

Mean velocity results (m/s) for change in riser length

(riser diameter = 0.05 m)

Table 7.2

Riser	Riser Length (m) 0.40	1.0
1	0.130	0.09
2	0.175	0.19
3	0.175	0.19
4	0.175	0.19

Mean velocity results (m/s) for change in riser length

(riser diameter = 0.035 m)

Table 7.3

Figures 7.13 and 7.14 demonstrate the consequences of an increase in riser length. Tables 7.2 and 7.3 show how the mean velocity results vary with a change in length. When compared with Figures 7.10 and 7.11 it is clear that the effects of wave action on riser velocity is

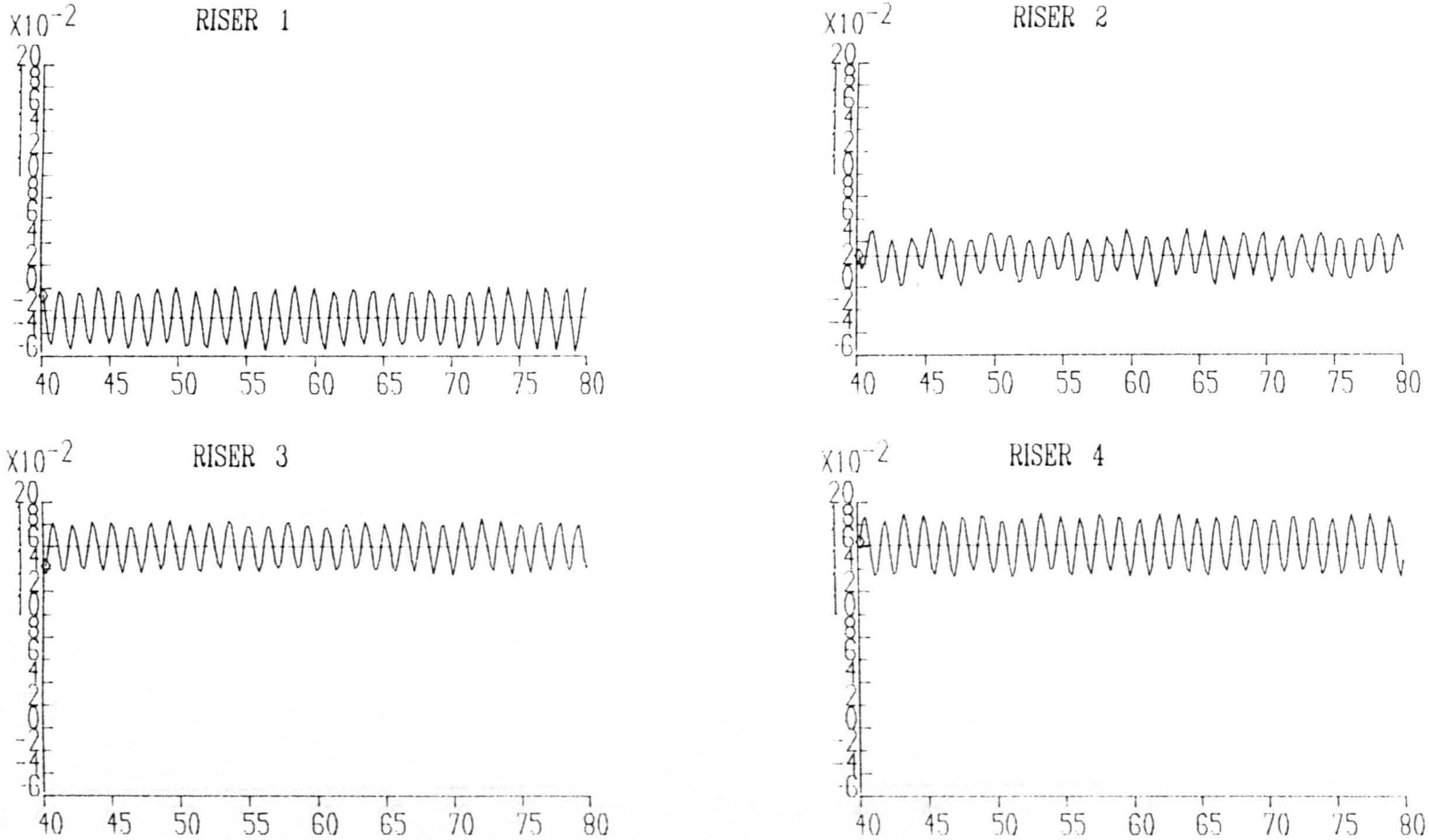

Y-AXIS = RISER VELOCITY (M/S). X-AXIS = TIME (SECS)

WAVEHEIGHT= 0.06000 WAVEPERIOD= 1.42600 FLOW RATE= 0.00063

RISER DIAMETER = 0·05m RISER LENGTH = 1·0m

FIGURE 7.13

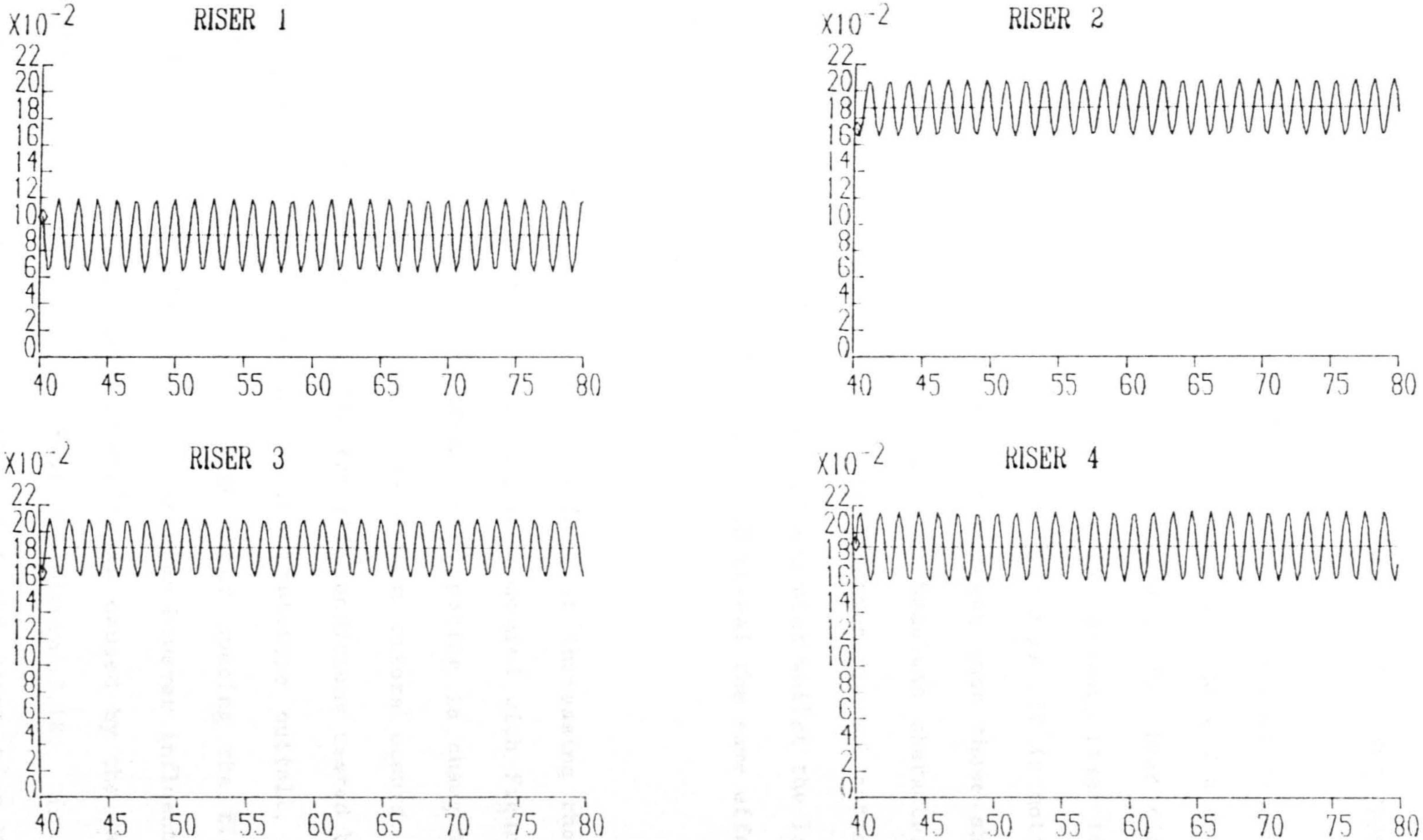

Y-AXIS = RISER VELOCITY (M/S), X-AXIS = TIME (SECS)

WAVEHEIGHT = 0.06000 WAVEPERIOD = 1.42600 FLOW RATE = 0.00063

RISER DIAMETER = 0·035m RISER LENGTH = 1·0m

FIGURE 7.14

reduced. This may be expected because the difference in pressure between the centreline of the outfall and longer risers will be less when subjected to the action of waves.

7.7.2 Increase in the Number of Risers and change in Riser spacing

Figures 7.15 and 7.16 show how discharge through outfall ports is affected by an increase in the number of risers. Table 7.4 shows the variation in mean velocity results for a change in riser diameter. Assuming the seaward riser to be No 1 and the landward riser to be No 8, with a design maximum discharge rate of 2.0ℓ/s, it is noticeable that all risers are purging at velocities lower than those shown in Figure 7.10. This is due to a change in headloss characteristics within the numerical model. However, similar behavioural patterns do emerge in that the seaward risers draw-in seawater whilst the landward risers are purging. Figures 7.16A and 7.16B reveal the same effect but where riser diameters are 0.035m.

Figure 7.17 and Table 7.5 show the effect of increasing the riser spacings from 0.5m to 0.75m. This may be compared with Figure 7.10 and serves to demonstrate that when riser spacing is changed, very little change in mean flow velocities within risers occurs. This outcome would appear to be specific for the conditions tested because numerical model results obtained for the prototype outfall, Figure 7.20, show that when there is a large riser spacing the flow has little effect in drawing in seawater. It does however influence the oscillations of velocity. This condition is caused by the ratio of wavelength to riser spacing, as shown in Figure 7.18. In Figure 7.18A, the riser spacing is such that when the crest of a wave is above one riser the trough is above the adjacent riser. In the second

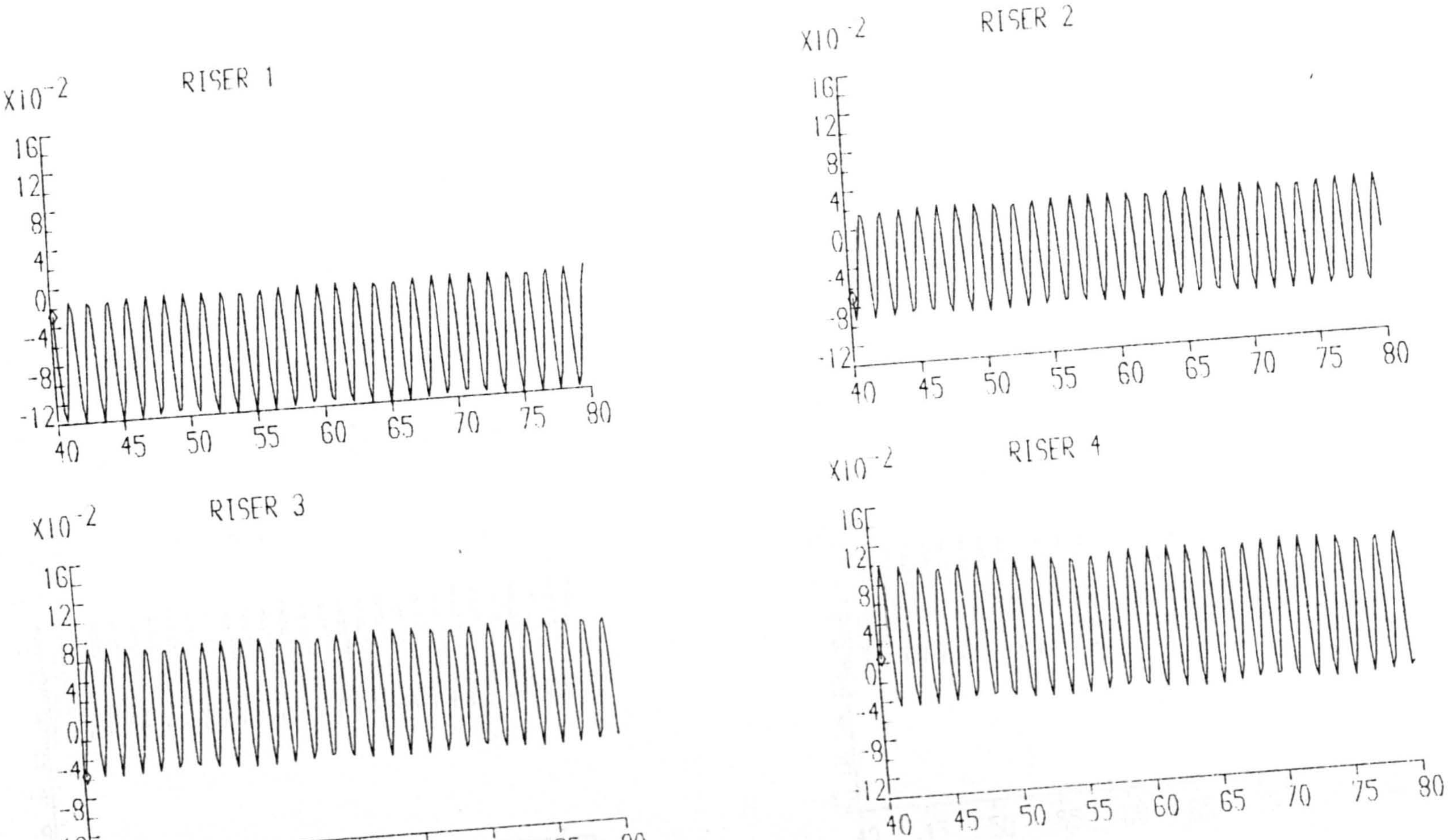

X-AXIS = TIME (SECS)

Y-AXIS = RISER VELOCITY (M/S),

FLOW RATE= 0.00063

WAVEHEIGHT= 0.06000 WAVEPERIOD= 1.42600

RISER DIAMETER = 0·05m RISER LENGTH = 0·4m

FIGURE 7.15A

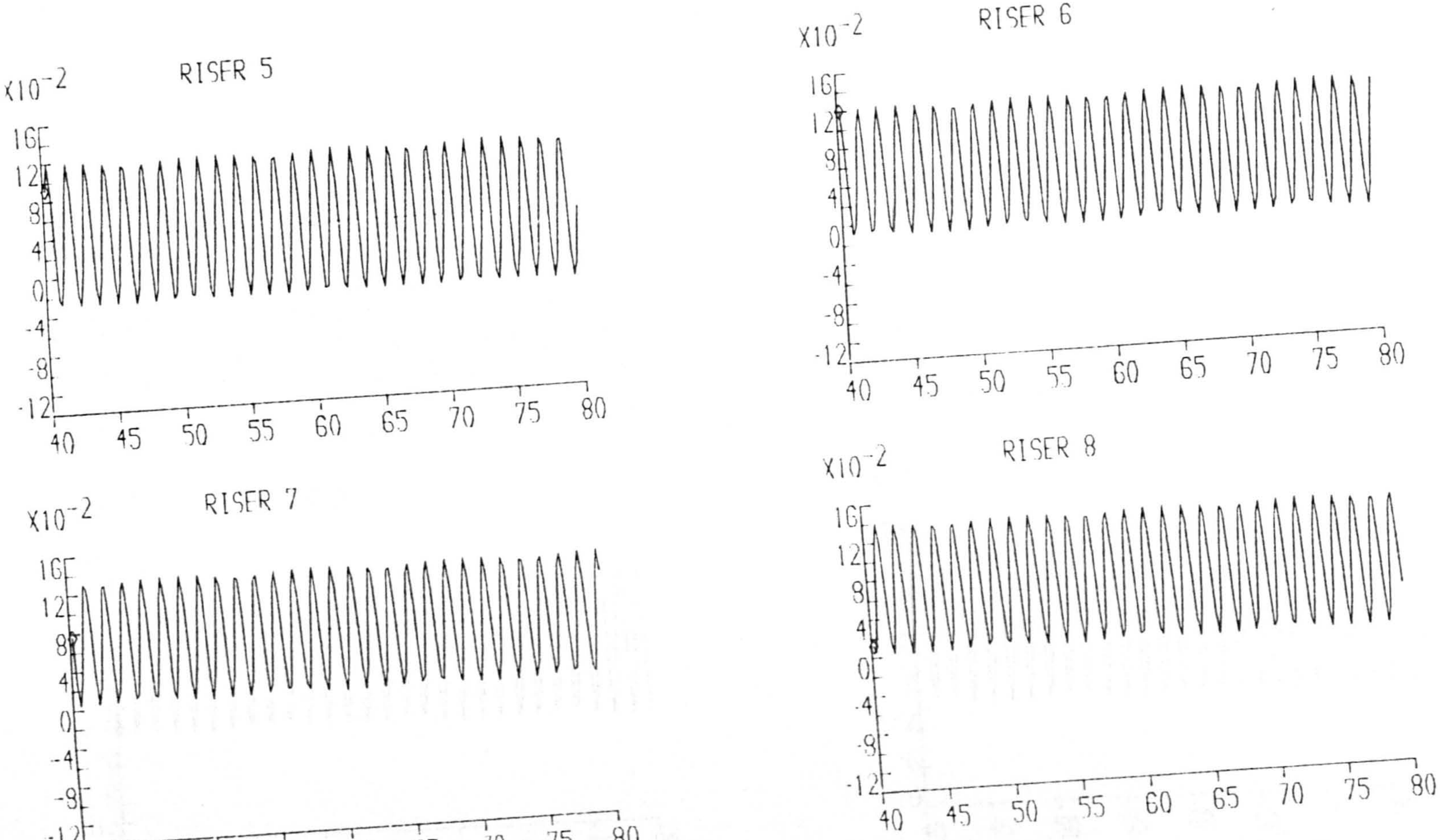

X-AXIS = TIME (SECS)

Y-AXIS = RISER VELOCITY (M/S), FLOW RATE= 0.00063

WAVEHEIGHT= 0.06000 WAVEPERIOD= 1.42600

RISER DIAMETER = 0·05m RISER LENGTH = 0·4m

FIGURE 7.15B

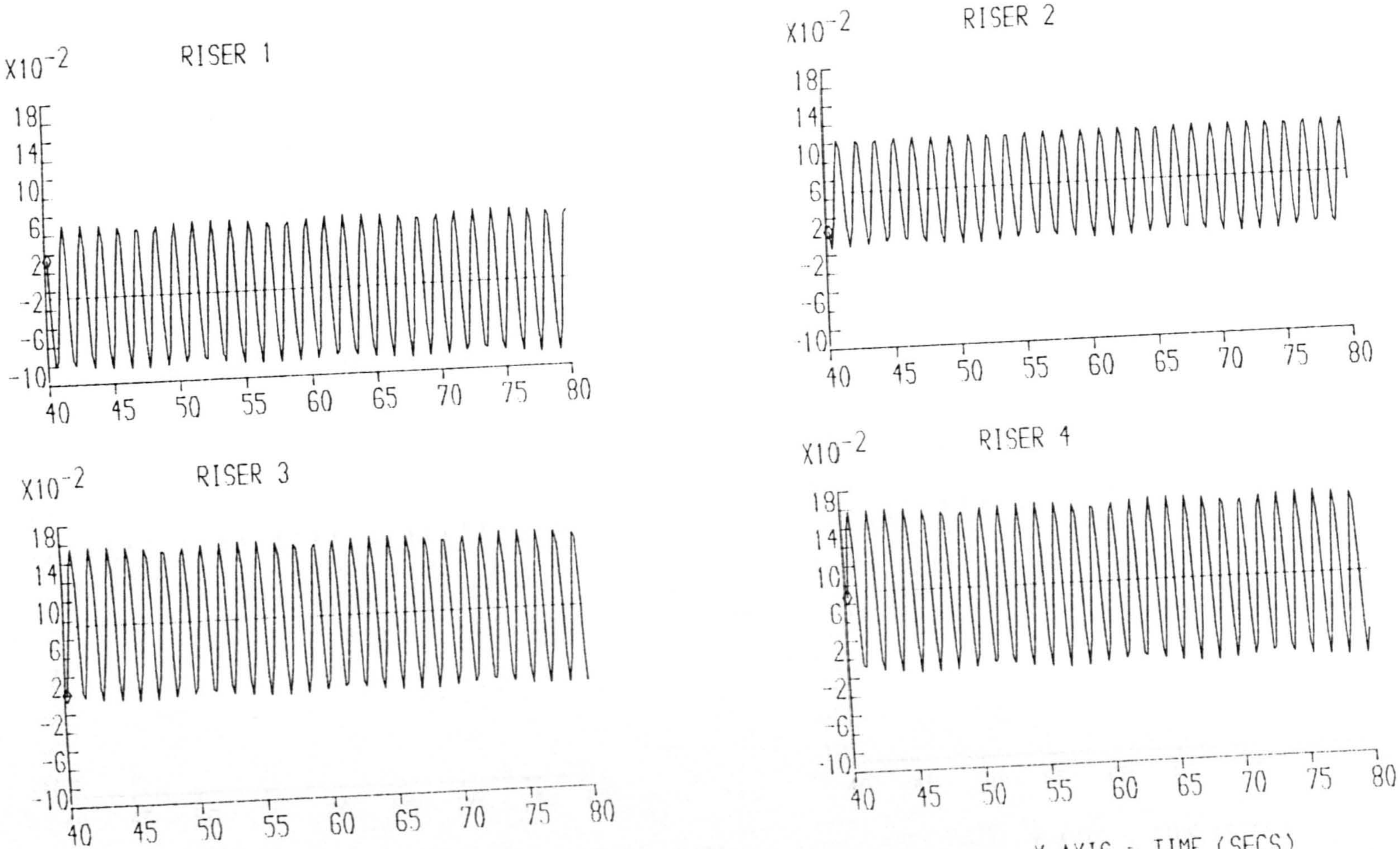

Y-AXIS = RISER VELOCITY (M/S), X-AXIS = TIME (SECS)

WAVEHEIGHT= 0.06000 WAVEPERIOD= 1.42600 FLOW RATE= 0.00063

RISER DIAMETER = 0·035m RISER LENGTH = 0·4m

FIGURE 7.16A

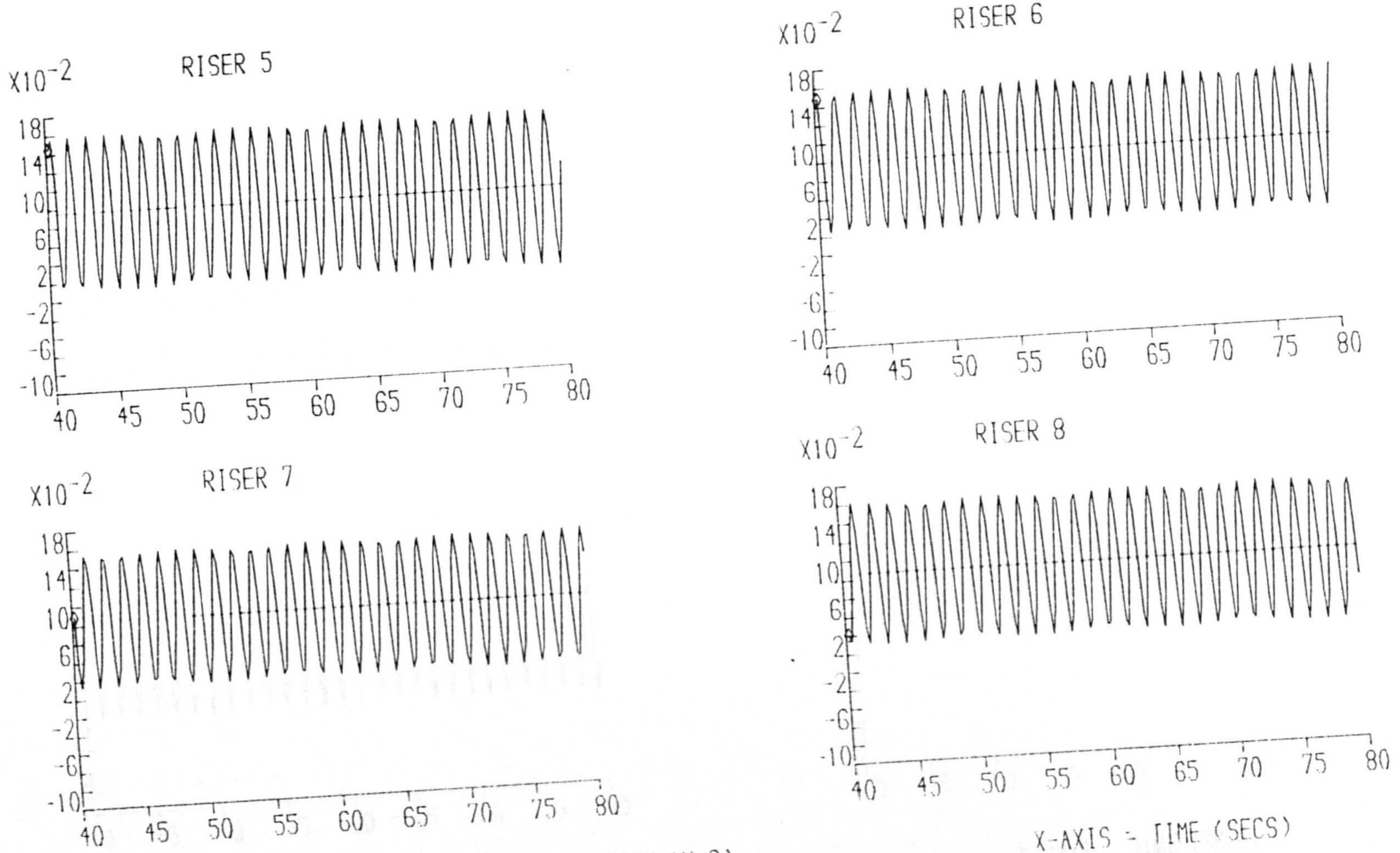

Y-AXIS = RISER VELOCITY (M/S),

WAVEHEIGHT= 0.06000

WAVEPERIOD= 1.42600

FLOW RATE= 0.00063

RISER DIAMETER = 0·03m

RISER LENGTH = 0·4m

FIGURE 7.16B

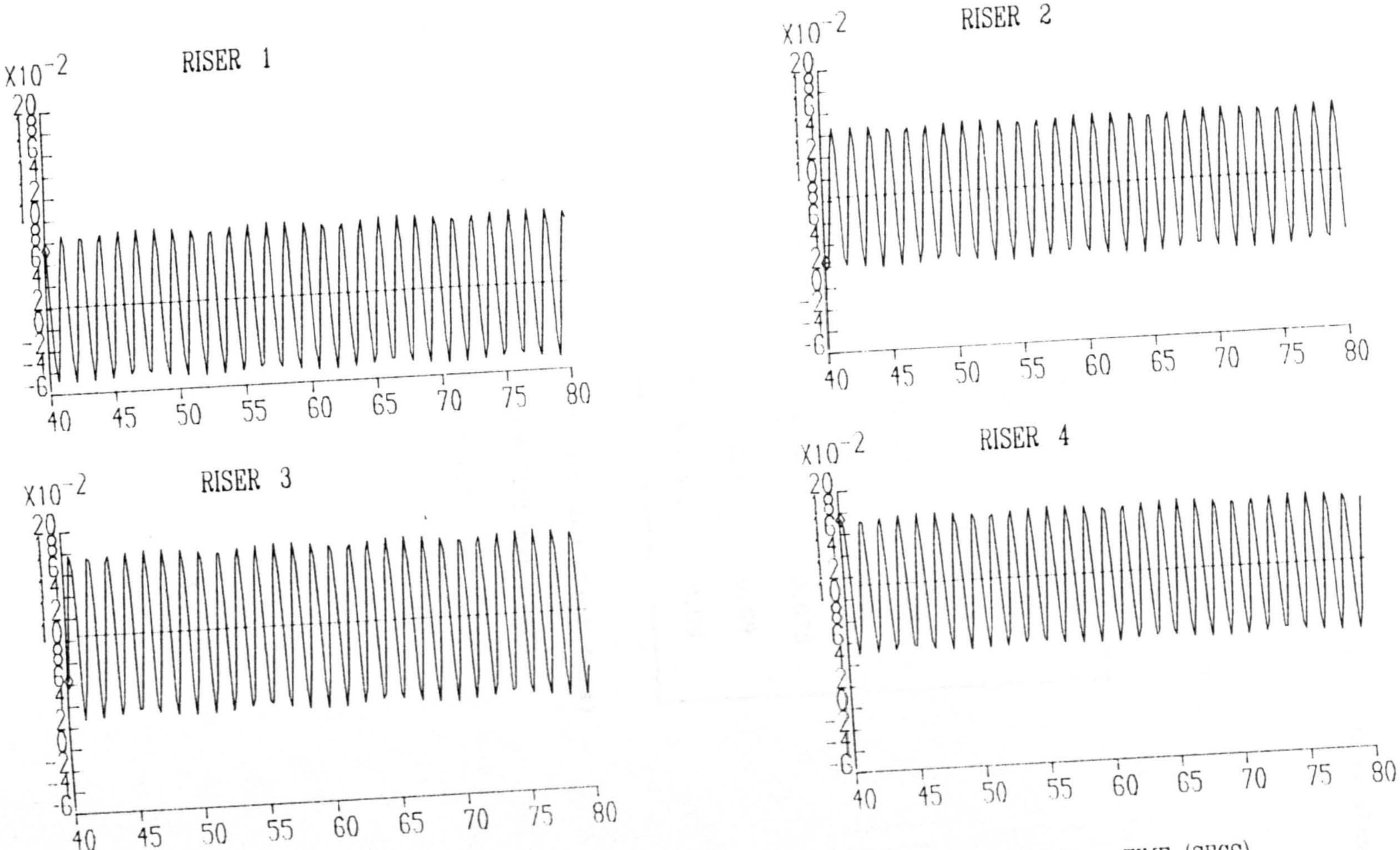

X-AXIS = TIME (SECS)

Y-AXIS = RISER VELOCITY (M/S).

WAVEHEIGHT= 0.06000 WAVEPERIOD= 1.42600 FLOW RATE= 0.00063

RISER DIAMETER = 0·05m RISER LENGTH = 0·4m RISER SPACING = 0·75m

FIGURE 7.17

case depicted by Figure 7.18B, the first riser is shown to be immediately below the crest of the wave whilst the adjacent riser is close to the wave node point. For the situation shown in Figure 7.17, the riser spacing is 0.75m and the wavelength is approximately 3.0m and, in consequence, the situation occurring is similar to that shown in Figure 7.18B.

	Riser diameter (m)	
Riser	0.035	0.05
1	-0.03	-0.06
2	0.07	-0.02
3	0.095	0.03
4	0.095	0.05
5	0.10	0.06
6	0.10	0.075
7	0.105	0.09
8	0.105	0.09

Mean velocity results in each riser (m/s)

for an eight riser diffuser system

Table 7.4

	Riser Spacing (m)	
Riser	0.50	0.75
1	0.015	0.02
2	0.09	0.085
3	0.11	0.105
4	0.11	0.115

Mean velocity results (m/s) for a change in riser spacing

(riser diameter = 0.05 m)

Table 7.5

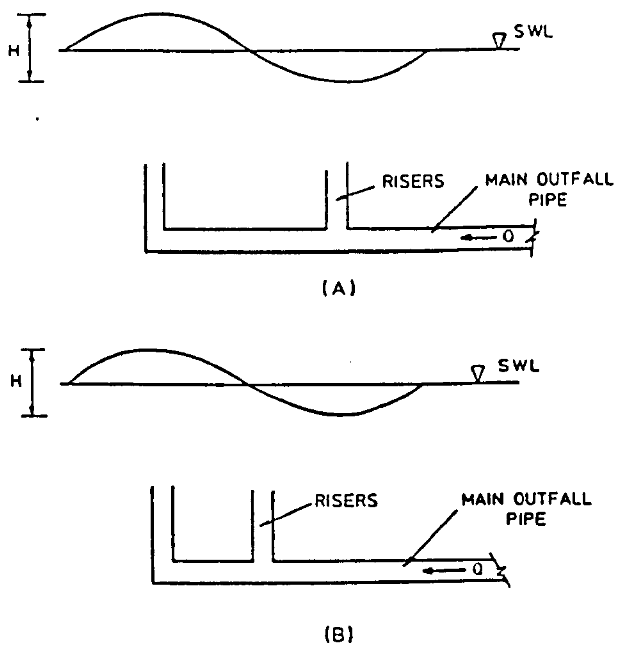

Changes in ratio of riser spacing to Wavelength

Figure 7.18

Figure 7.10 shows the results when risers are spaced at 0.5m intervals and clearly shows that this causes a difference in the level of oscillatory motion in the risers.

7.7.3 Prototype Outfall Modelling

One aim of this research programme was to attempt to produce a numerical procedure which could ultimately be used to model prototype marine outfalls so ensuring that wastewater is discharged in the best practical manner. Whilst the numerical model is not fully perfected (as discussed previously) a trial application was considered relevant. The trial outfall chosen was the proposed Bombay Long Sea outfall which is shortly to be designed by Binnie and Partners (Consulting Engineers). The sketch in Figure 7.19 illustrates how the outfall may look, since detail designs have not yet been prepared. A principal design parameter for the proposed outfall is that it will have a maximum discharge rate of $24.0 m^3/sec$.

Figures 7.20A and 7.20B show the values of velocity in all risers under quiescent conditions when the flow rate was approximately 1.0 m^3/s. It can be seen that under these conditions there are no oscillations and that the risers are too far apart to be affected by the flow condition in an adjacent riser. Hence flow is not drawn into the diffuser through the seaward risers, (riser 1 being the most seaward and 8 being the most landward riser).

Under the action of waves, Figures 7.21A and B, it can be seen that there is a mean discharge, with large oscillations through the landward risers. In the seaward risers (risers 1 to 4) there are large oscillations in flow velocity and there is evidence of seawater circulation within the system, especially between risers 1 and 2. The large velocities, up to 3 m/s for these particular wave conditions, could carry sediment into the outfall if this is not guarded against.

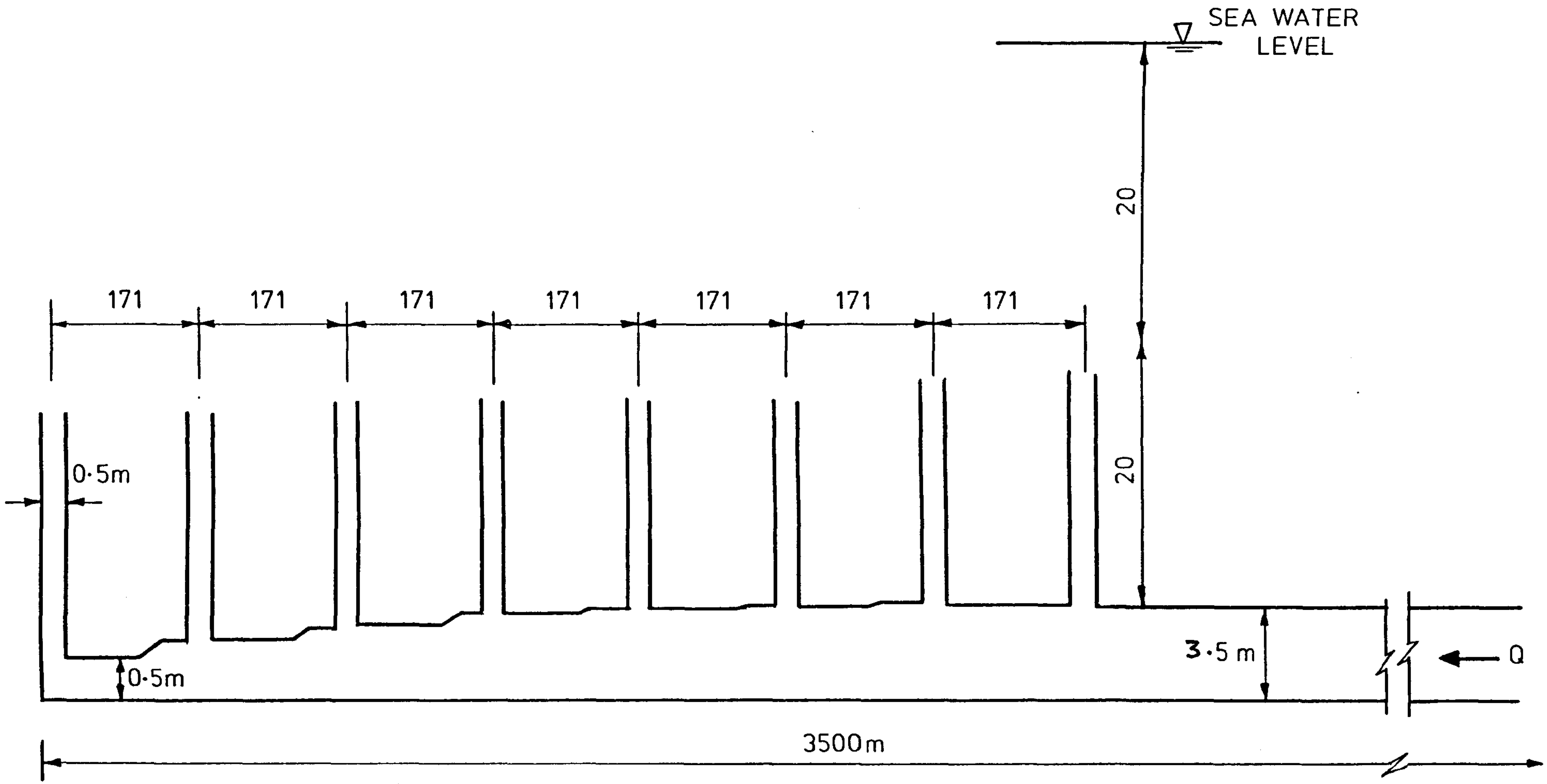

FIGURE 7 19 SHOWING PROPOSED . BOMBAY OUTFALL

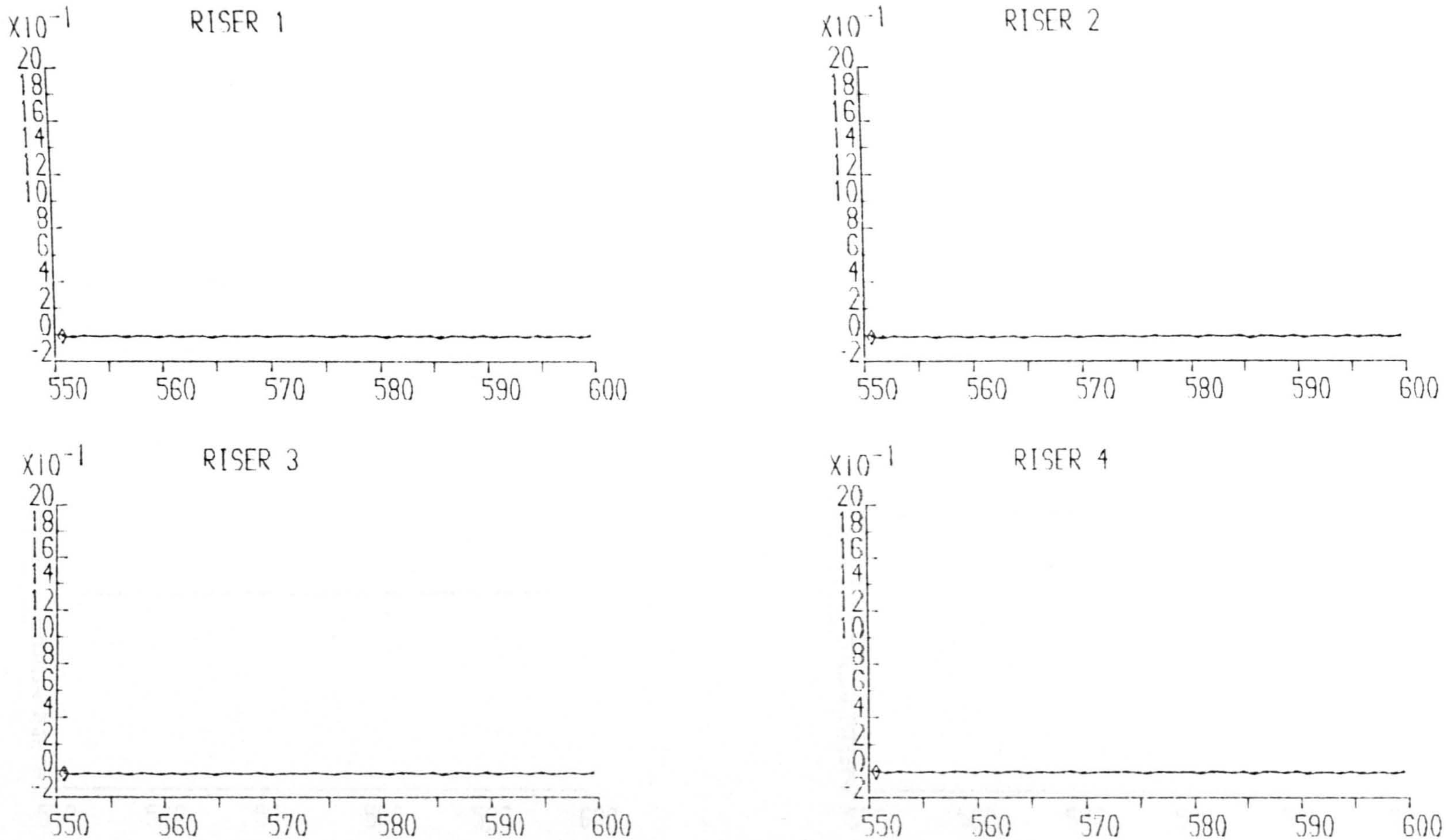

Y-AXIS = RISER VELOCITY (M/S), X-AXIS = TIME (SECS)

WAVEHEIGHT= 0.00000 WAVEPERIOD= 12.00000 FLOW RATE= 6.00000

FIGURE 7.20A

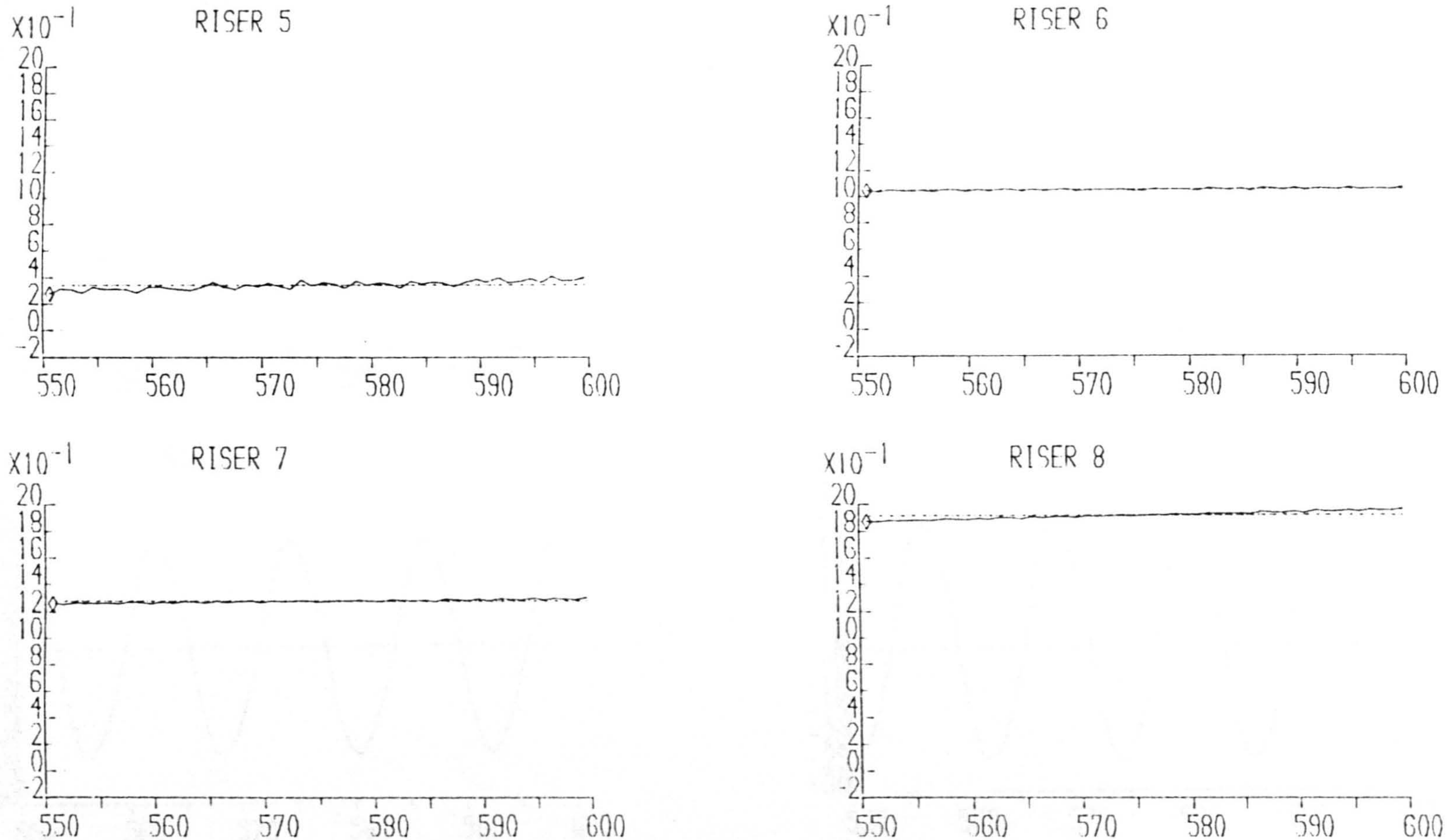

Y-AXIS = RISER VELOCITY (M/S), X-AXIS = TIME (SECS)

WAVEHEIGHT= 0.00000 WAVEPERIOD= 12.00000 FLOW RATE= 0.00000

FIGURE 7.20B

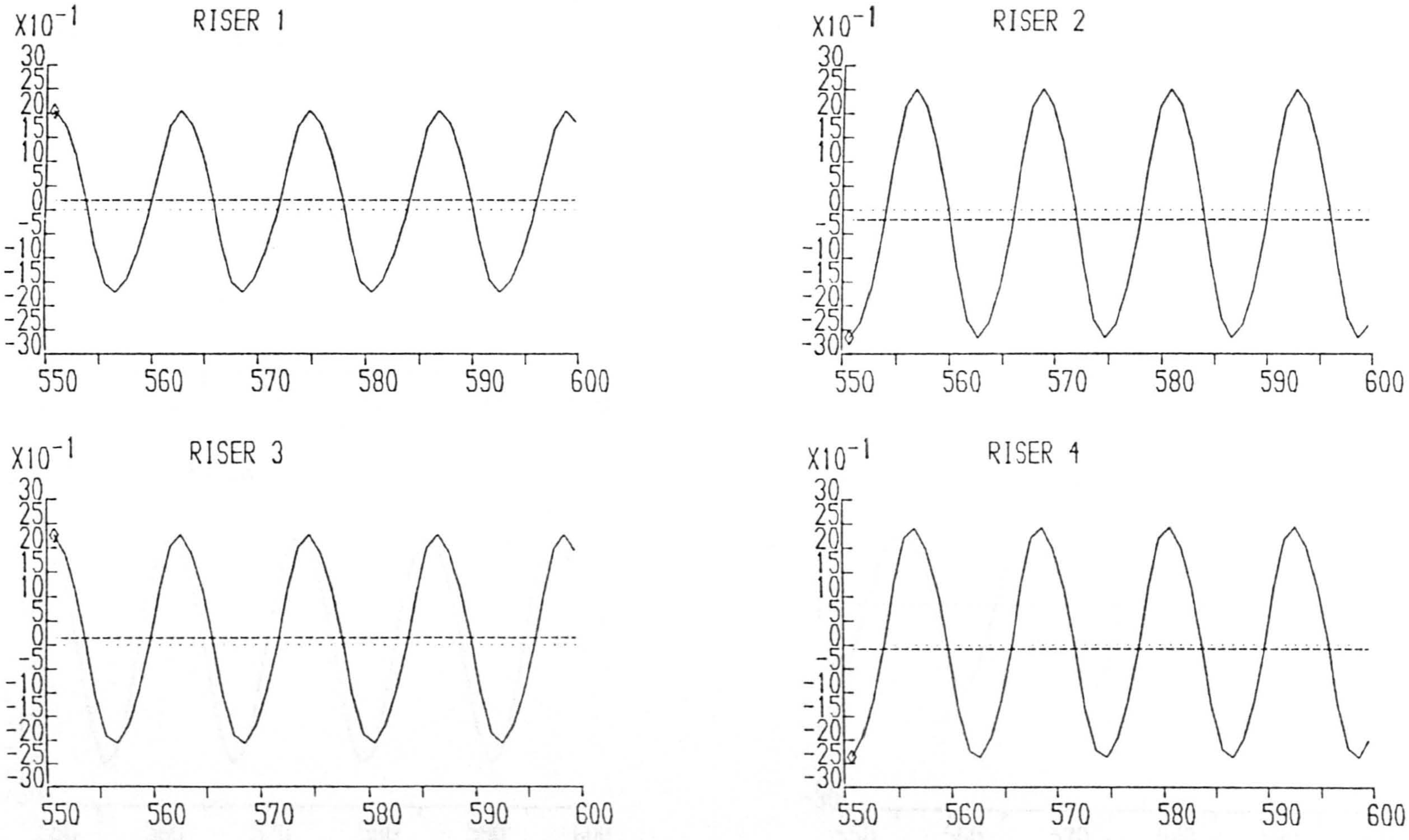

Y-AXIS = RISER VELOCITY (M/S), X-AXIS = TIME (SECS)

WAVEHEIGHT= 8.00000 WAVEPERIOD= 12.00000 FLOW RATE= 6.00000

FIGURE 7.21A

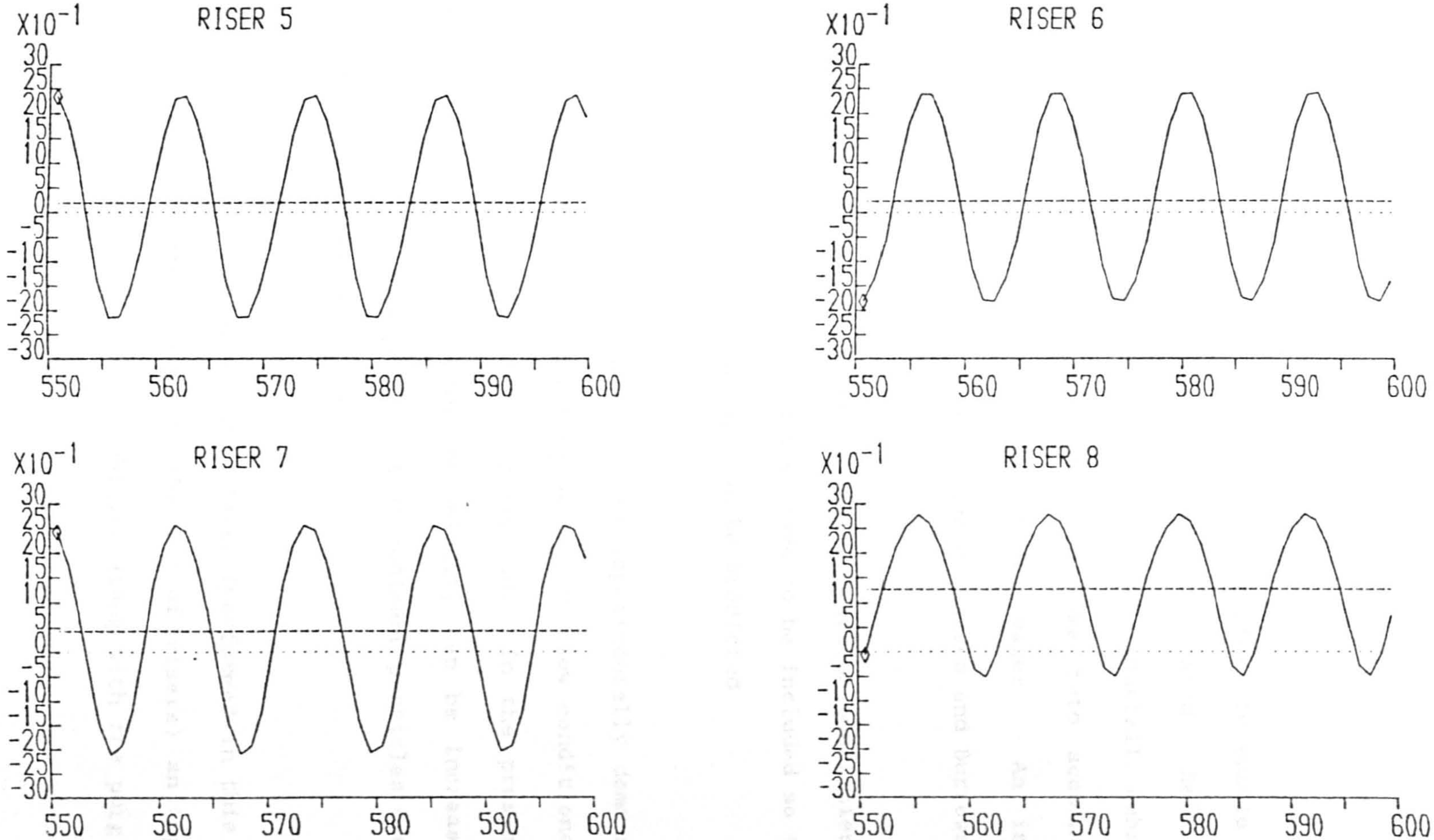

Y-AXIS = RISER VELOCITY (M/S), X-AXIS = TIME (SECS)

WAVEHEIGHT= 8.00000 WAVEPERIOD= 12.00000 FLOW RATE= 6.00000

FIGURE 7.21B

7.8 Summary

From the foregoing discussion it can be concluded that the numerical model is at present able to reproduce the experimental results obtained and also be used to predict the effects that other sea conditions will have on outfall behaviour.

To do this it does contain empirical headloss factors to enable it to operate whilst salt water is present within the system. Before the model can be used to accurately predict the outfall behaviour computational routines must be included to take into account the mixing process between the salt and fresh water. An initial investigation into this has since been made by Larsen and Burrows(37).

In conjunction with this a database providing headloss coefficients at the main pipe/riser junctions would also have to be included so that a complete picture of outfall behaviour can be predicted.

The results obtained both numerically and experimentally demonstrate that when an outfall is not operating at design flow conditions then there can be a problem with saline intrusion. In the presence of certain wave conditions the intrusive velocity can be increased to such a level that it becomes possible that sediment particles could be transported into the outfall.

By increasing the headloss within the risers (performed in this study by the addition of diffuser caps to the top of risers) an improved flow balance between the risers is achieved along with the purging of salt water from the seaward risers at a lower flow rate. This could however create the problem of a permanent wedge remaining in the main outfall pipe.

CHAPTER EIGHT

CONCLUSIONS AND RECOMMENDATIONS

8.1 Conclusions

8.1.1 Saline Wedge Investigations

(i) The experimental results demonstrating how the ratio of saline wedge length over pipe diameter varies as the densimetric Froude number changes, show a consistent trend. In all cases the wedge lengths increase as the densimetric Froude number decreases.

(ii) Output from the numerical model developed for saline wedge analysis compared favourably with the experimental results of wedge profiles obtained from the 50 mm diameter outfall model. However, to achieve this empirical adjustements had to be made to both the toe of the wedge and the shape of the wedge at the exit of the pipe, these were described in Sections 6.3.4.2 and 6.3.3.

(iii) The numerical procedure was also used to model saline wedge lengths in larger diameter pipes. To enable it to produce results similar to the experimental results an additional empirical factor was used during the calculation of the saline wedge boundary condition. As Figures 6.9 to 6.13 demonstrate, the use of the additional empirical factor enables the numerical model to produce saline wedge length results similar to the experimental data obtained. The results also agree with those obtained using the empirical relationship developed by Davies et al[21].

The numerical procedure used for modelling large diameter pipes has not been rigorously tested against saline wedge profile data as none was available and so any further results on pipes with diameters greater than 50 mm must be treated with caution.

8.1.2 Effects of wave action on a multi-riser system

(i) During either shut down or low flow periods of a marine outfall, some surface wave conditions can trigger circulatory flows within the diffuser system. The mean flow rates within risers are usually small, but the instantaneous velocities can be high and frequently cause oscillation of water level in the outfall drop-shaft.

(ii) Should the rate of flow passing through the outfall be less than that for which it was designed, then seawater circulation is very likely to be induced into the outfall manifold - a phenomenon which has been clearly demonstrated by Wilkinson[58,60] using a two - riser system, and by Charlton et al[17,18,19].

(iii) During conditions of low flow, the effect of wave action is to increase seawater intrusion into the outfall, via the risers. The wave conditions which cause this show noticeable pressure fluctuations at the elevation of the diffuser ports (i.e. shallow water conditions).

(iv) The instantaneous values of velocities within risers during periods of saline intrusion can be large and may well be a major contributory cause of the problems relating to the transportation of marine sediments into an outfall system.

(v) The numerical model developed for examining the effects of waves on outfalls produced results which compared favourably with those obtained from the physical model experiments. To do this, however, empirical factors were included to enable the model to reproduce the effects of saline intrusion. These empirical factors are described in Section 7.4.2. The numerical model replicates closely the intrusive mechanisms within the outfall but it did not consistently yield closely matching velocities.

(vi) The placing of diffuser caps on outfall risers reduces the effect that wave action has on flow velocities within the risers. In addition, the caps enable risers to be purged of sea water at lower rates of effluent discharge, thereby reducing the volume of sea water drawn into the system.

(vii) The numerical model was also used to investigate the effects of changes in riser diameter, riser length and the spacing between the risers. The results of these tests demonstrated that as the diameter of the risers decreased the velocity within the risers became more balanced. As the riser length increased the oscillation of velocity within the system decreased. Both situations cause the headloss within the diffuser system to increase, and this will generally cause the flow through the risers to become more balanced[39]. The reduction in oscillations caused by the use of longer risers will be due to an increase in inertia within the pipe along with an increase in the velocity of flow required to successfully purge the riser.

A small change in the riser spacing had a very small effect on the intrusive velocity conditions but the oscillation of velocity changed. This indicates that the oscillations within the outfall system could be a function of the wavelength to riser spacing ratio.

(viii) The numerical model was finally used to examine a prototype long sea outfall, as described in Section 7.7.3. The results produced must be treated with caution due to the empirical factors used within the numerical model. The results obtained from this exercise show that when the riser spacing is large then intrusive conditions within the risers, under steady sea conditions, is negligible. It also demonstrated that under the wave condition tested (waveheight = 8 m and waverperiod = 12 secs) large oscillatory velocities developed within the riser which could carry sediment into the system. The wave condition used also induced a small amount of circulation between the two seaward risers.

8.2 Recommendations for further work

8.2.1 Experimental Model

More work is needed to examine the effect of modifying the geometry of the outfall diffuser systems, such as varying the spacings between risers and altering the headlosses within the risers (by reducing the diameter or increasing the length), and investigating how wave action will then affect the flow rates within the outfall system. There is also a need to examine in detail the effects of sediment transport within the outfall. This is because any permanent deposition of sediment is likely to constrict the pipe area and so change the flow characteristics of the outfall. Deposition of sediment is more likely to occur under conditions were there is a permanent saline wedge along the pipe invert as this has a zero velocity and particles will fall through it and remain on the pipe invert. Unless the wedge is flushed from the system deposits of sediment will build up until they become irremoveable - this may have occured in the North Wirral Outfall(42).

The model could also be used to investigate how well mechanical devices placed at the riser outlet ports operate under various wave conditions. The types of mechanised valve which could be investigated are the 'Duck-Bill' valve(15) and the 'Poppet' type valve(25).

8.2.2 Numerical Model

Improvements to the model are required, particularly in relation to the calculation of head losses, coupled with the way in which saline intrusion is dealt with. Firstly, it would clearly be advantageous to include a database for various headloss characteristics such as those located at the 'T' junctions between the riser and the manifold, in order that the model can select the headloss condition at each stage of the calculation. Secondly, the model could be improved to take account of saline intrusion when the outfall is being analysed. This could be accomplished by incorporating the saline wedge model into the present outfall/diffuser model which would alter the flow conditions by reducing the area of flow within the main outfall pipe. Alternatively, algorithms could be used to vary the cross-sectional area of the outfall pipe. Opportunities could also be taken to determine the extent of saline and fresh water mixing within the outfall, because this appears (from experimental observations) to have significant effect on the discharge performance of the structure. It is known that Larsen and Burrows[37] have very recently included this feature into a numerical model using mass balance equations.

At present the numerical model calculations are based on a line of points along the centreline of the main outfall pipe. This does not give a completely accurate picture of the flow velocity variation within the pipe. This could be overcome by using a mesh type arrangement (similar to that used by Viollet[56]) as shown in Figure 8.1.

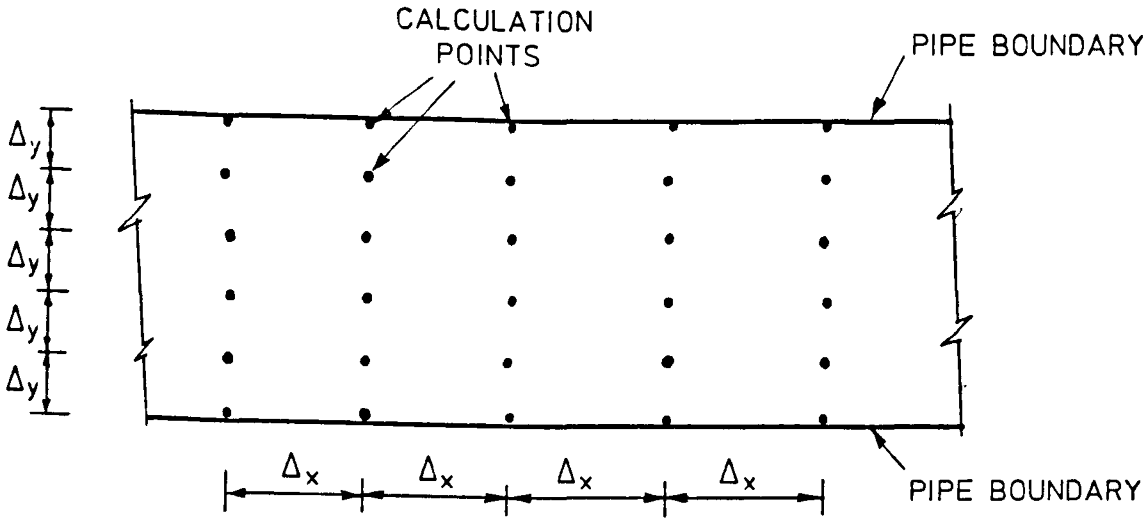

Possible mesh system for calculation of outfall hydraulics

Figure 8.1

This type of numerical procedure would operate by calculating the velocity at each point at every incremental time step. By using the mesh an accurate prediction of the position of the saline wedge, if one existed could be obtained, and an improved estimate of the flow condition of the fresh water around it could be calculated.

<u>References</u>

1) ABRAHAM, G. KARELSE, M., and Van OS, A.G.; "On the Magnitude of Interfacial Shear of Subcritical Stratified Flows in Relation with Interfacial Stability". Journal of Hyd. Res. 17. 1979 No. 4 pp 273-287.

2) ACRIVOS, A., BABCOCK, B.D. and PIGFORD, R.L.; "Flow Distribution in Manifolds". Chemical Engineering Science 1959. Vol. 10, pp 112-124.

3) AGG, A.R.; "Application of Coastal Pollution Research 3 -Initial Dilution". WRc Technical Report TR92, Oct. 1978.

4) ALI, K.H.M., Personal Communication, Department of Civil Engineering, University of Liverpool.

5) ALI, K.H.M., BURROWS, R., and MORT, R.B.; "Investigation of Wave Induced Oscillations in Sewage Outfalls". 5th Symposium of Coastal and Ocean Management, Seattle, USA, 1987.

6) ALI, K.H.M., and RIDGEWAY, A.; "The Circular Free Overfall". Water Power and Dam Construction, May 1977, pp 42-45.

7) ALMQUIST, C.W. and STOLZENBACH, K.D.; "Staged Multiport Diffusers". Proc. ASCE, Journal of Hydraulics Div. Vol. 106 HY2, Feb. 1980. pp 285-302.

8) BATA, G.L.; "Recirculation of Cooling Water in Rivers and Canals". Proc. ASCE, Journal of Hydraulics Div. Vol. 83 HY6 June 1957.

9) BENNETT, N.J.; "Initial Dilution : A Practical Study of the Hastings Long Sea Outfall". Proc. ICE, Part 1, Feb. 1981. Paper No. 8426, pp 113-122.

10) British Standard, BS 3680 Part 4a.

11) BROOKS, N.H.; "Synthesis of Stratified Flow Phenomenon for Design of Outfalls". 2nd Int. Symposium on Stratified Flows, NIT, Norway 1980, pp 809-831.

12) CHARLTON, J.A.; Private Memo.

13) CHARLTON, J.A.; "Salinity Intrusion into Multiport Sea Outfalls". Proc. 18th Int. Conference on Coastal Engineering. Capetown 1982, pp 2376-2385.

14) CHARLTON, J.A.; "Hydraulic Modelling of Saline Intrusion into Sea Outfalls". Int. Conference on Hydraulic Modelling of Civil Engineering Structures, Coventry, England, Sept. 1982, pp 349-356.

15) CHARLTON, J.A.; "Sea Outfalls" From 'Developments in Hydraulic Engineering 3' edited by P. NOVAK. Published by Elesevier, Amsterdam, 1985, pp 79-127.

16) CHARLTON, J.A.; "The Venturi as a Saline Intrusion Control for Sea Outfalls". Proc. ICE Part 2 1985 (Dec.) Paper No. 8980, pp 697-704.

17) CHARLTON, J.A., DAVIES, P.A. and BETHUNE, G.H.M.; "Seawater Intrusion and Purging in Multiport Sea Outfalls". Proc. ICE, Part 2 1987. Paper No. 9132, pp 263 - 274.

18) CHARLTON, J.A., DAVIES, P.A. and BETHUNE, G.H.M.; Discussion on "Purging of Saline Wedges from Ocean Outfalls". by D.L. WILKINSON, Proc. ASCE, Journal of Hydraulic Engineering, August 1987, pp 1077-1082.

19) CHARLTON, J.A., DAVIES, P.A., BETHUNE, G.H.M. and M^c^DONALD, L.M.; "Hydraulic Model Studies and Field Monitoring of Saline Intrusion in Long Sea Outfalls". Int. Symposium on Modelling Environmental Flows, ASCE, New York, 1985, pp 89-91.

20) DAILY, J.W. and HARLEMAN, D.R.F.; "Fluid Dynamics". Published by Addison-Wesley Publishing Company Inc. USA, 1966.

21) DAVIES, P.A., CHARLTON, J.A. and BETHUNE, G.H.M.; "A Laboratory Study of Primary Saline Intrusion in a Circular Pipe". Journal of Hydraulic Research, Vol. 26, No. 1, 1988, pp 33-48.

22) ELLISON, T.H. and TURNER, J.S.; "Mixing of Dense Fluid in a Turbulent Pipe Flow". Journal of Fluid Mechanisms, August 1960, pp 514-544.

23) ELSAYED, E.E.M.; "Buoyancy Effects on Mixing Characteristics of Staged Diffuser". Int. Conference on the Hydraulic Modelling of Civil Engineering Structures, England, Sept. 1982, pp 325-337.

24) GRACE, R.A.; "Sea Outfalls - A Review of Failure, Damage and Impairment Mechanisms". Proc. ICE No. 8766, Feb. 1985.

25) HANSON, L.E. et al; "San Francisco Ocean Outfall Port Valve Development". Proc. 1980 Hydraulics Speciality Conference, ASCE, Chicago, Il. USA, pp 51-61.

26) HARLEMAN, D.R.F.; "Stratified Flow". Chapter 26 from 'Handbook of Fluid Dynamics' edited by V.L. STREETER, Published by M^{c}Graw Hill Inc.

27) HENDERSON, F.M.; "The Effect of Wave Action on the Flow in the Proposed Ocean Outfall of a Sewage Line, Napier". A report to Messrs. Steven and Fitzmaurice, Consulting Engineers, Christchurch, New Zealand, May 1967.

28) HINO, M., HUNG, S.N. and NAKAMURA, K.; "Entrainment and Friction at the Interface of Salt Wedge". 2nd Int. Symposium on Stratified Flows. NIT, Trondheim, Norway 1980, pp 763-782.

29) HOLLEY, E.R. and WADDELL, K.M.; "Stratified Flow in Great Salt Lake Culvert". Proc. ASCE, Hydraulics Division, Vol. 102, HY7, July 1976, pp 969-985.

30) ISAACSON, M.S., KOH, R.C.Y. and BROOKES, N.H.; "Plume Dilution for Diffusers with Multiport Risers". Proc. ASCE, Journal of Hydraulic Engineering, Vol. 109, No. 2, Feb. 1983, pp 199-220.

31) JAEGAR, C.; "Fluid Transients". Published by Blackie and Son Ltd., Glasgow and London, 1977.

32) JENSEN, B.L., SUMER, B.M. and FREDSOE, J.; "Transition to Turbulence at High Reynolds Numbers in Oscillating Boundary Layers". Prog. Rep. 66, February 1988, Tech. Univ. of Denmark.

33) KEULEGAN, G.H.; "Interfacial Instability and Mixing in Stratified Flows". Journal of Research of the National Bureau of Standards, Vol. 43, 1949.

34) KEULEGAN, G.H.; "The Mechanism of an Arrested Saline Wedge". Chapter 11 from 'Estuary and Coastline Hydrodynamics' edited by A.T. IPPEN, Published by McGraw-Hill Inc. 1966.

35) LARSEN, T.; "Influence of Waves on the Hydraulics of Sea Outfalls". 20th Int. Conference on Coastal Engineering, Nov. 1986, Taipei, Taiwan.

36) LARSEN, T.; "Sea Outfall Design based in a Stochastic Transport/ Dispersion Model". Symposium on Modelling of Environmental Flows, Arr by ASME and ASCE, Boston, November 1983.

37) LARSEN, T. and BURROWS, R.; "Wave Induced Saline Intrusion in Sea Outfalls". IAHR XXIII Congress, Ottawa, Canada, August 1989.

38) "Mathematical Modelling for the Cowes Sea Outfall"; Tunnels and Outfall Engineering, June 1987.

39) MILLER, D.S.; "Internal Flow Systems". BHRA Fluid Engineering, 1978.

40) MUNRO, D.; "Comparison of Sea Outfall Designs Providing High and Low Jet Velocities from Diffusers". WRc enquiry report ER 773, Sept. 1980.

41) MUNRO, D.; "Seawater Exclusion from Tunnelled Outfalls Discharging Sewage". WRc Environment, Report 7M, 1981.

42) NCE Report on North Wirral Outfall. New Civil Engineer, 3 May 1984.

43) NEVILLE-JONES, P.J.D. and DORLING, C. (Editors) "Outfall Design Guide for Environmental Protection". WRc Engineering, Nov. 1986.

44) PALMER, N.H.; "Seawater Entry into Tunnelled Sewage Outfalls". BHRA, TRC 1137, Oct. 1975.

45) PARTHENIADES, E.,DERMISSIS, V. and MEHTA, A.J.; "Graphs of Saline Wedges in Estuaries". ASCE Civil Engineering, Jan. 1980, pp 90-92.

46) POLK, E.M., BENEDICT, B.A. and PARKER, F.L.; "Cooling Water Density Wedges in Streams". Proc. ASCE, Journal of the Hydraulics Division, Vol. 97, No. HY10, Paper 8446, Oct. 1971, pp 1639-1652.

47) PORTER, G.B.; M.Eng. Thesis, University of Liverpool.

48) RAMAMURTHY, A.S. and SATISH, M.G.; "Internal Hydraulics of Diffusers with Uniform Lateral Moment Distribution". Proc. ASCE, Journal of Environmental Eng., Vol. 113, No. 3, June 1987, pp 449-463.

49) ROBERTS, D.G.M. et al; "Weymouth and Portland Marine Treatment Scheme - Tunnel Outfall and Marine Treatment Works". Proc. ICE Part 1, 1984 (Feb.), Vol. 76, Paper No. 8749, pp 117-144.

50) SCHIJF, J.B. and SCHONFELD, J.C.; "Theoretical Considerations on the Motion of Salt and Fresh Water". Proceedings of the Minnesota Int. Hydr. Conv., Sept 1953, pp 321-333.

51) SHARP, J.J. and WANG, C.; "Arrested Wedge in Circular Tube". Proc. ASCE, Journal of Hydraulics Division, Vol. 100, HY7, July 1974, pp 1085-1088.

52) SMITH, A.A. and ELSAYED, E.; "Gradually Varied Stratified Flows". 2nd Int. Symposium on Stratified Flows, NIT, Trondheim, Norway, 1980, pp 595-608.

53) STREETER, V.L. and WYLIE, E.B.; "Fluid Mechanics". Published by McGraw Hill Book Company 1975.

54) VAN DER KUUR, P.; "Lock with Devices to Reduce Salt Intrusion". Proc. ASCE, Journal of Waterway, Port and Coastal Engineering, Vol. 111, No. 6, Nov. 1985, pp 1009-1021.

55) VIGLIANI, P.G. et al; "An Investigation of the Initial Dilution of Sewage Discharged through Submarine Diffusers". Prog. Water Technology, Vol. 12, No. 1, pp 321-337.

56) VIOLLET, P.L.; "Observation and Numerical Modelling of Density Currents Resulting from Thermal Transients in a Non-Rectalinear Pipe". Journal of Hydraulic Research, Vol. 25, No. 2, 1987.

57) WEBBER, N.B.; "Fluid Mechanics for Civil Engineers". Published by Chapman and Hall, London, 1971.

58) WILKINSON, D.L.; "Circulation Blocking of Tunnelled Ocean Outfalls". 8th Australian Fluid Mechanics Conference, University of Newcastle, NSW 1983, pp 9C.1-9C.5.

59) WILKINSON, D.L.; "Purging of Saline Wedges from Ocean Outfalls". Proc. ASCE, Journal of Hydraulics Engineering, Vol. 110, No. 12, Dec. 1984, pp 1815-1829.

60) WILKINSON, D.L.; "Seawater Circulation in Sewage Outfall Tunnels". Proc. ASCE, Journal of Hydraulic Engineering, Vol. 111, No. 5, May 1985, pp 846-858.

61) WILLIAMS, B.L. (Editor); "Ocean Outfall Handbook". Water and Soil Miscellaneous Publication No. 76.

62) WRIGHT, S.J.; "Mean Behaviour of Buoyant Jets in a Crossflow". Proc. ASCE, Journal of Hydraulics Division, Vol. 103, No. 5.

63) WRIGHT, S.J.; "Buoyant Discharge from Outfall Diffuser into Stratified Fluid". 2nd Int. Symposium on Stratified Flows, NIT, Trondheim, Norway, 1980.

64) WYLIE, E.B. and STREETER, V.L.; "Fluid Transients". Published by McGraw Hill Book Company, 1975.

65) SIMPSON, J.E.; "Gravity Currents". Published by Ellis Horwood.

66) BURROWS, R and MORT, R.B.; "Wave Action on multi-riser Marine Outfalls". Published by BHRA (Information Services). See Appendix F.

APPENDIX A

This appendix details the computer program (MORT1 FORTRAN) which is used to generate random waves within the departmental wave flume. This enables the calculation of the regular wave trains (of given height and period) in a step sequence which, when superimposed, make up the random sea state described by the Pierson-Moskowitz spectrum. The program is based on the summation of equal energy slices through the spectra where energy (E) is given by

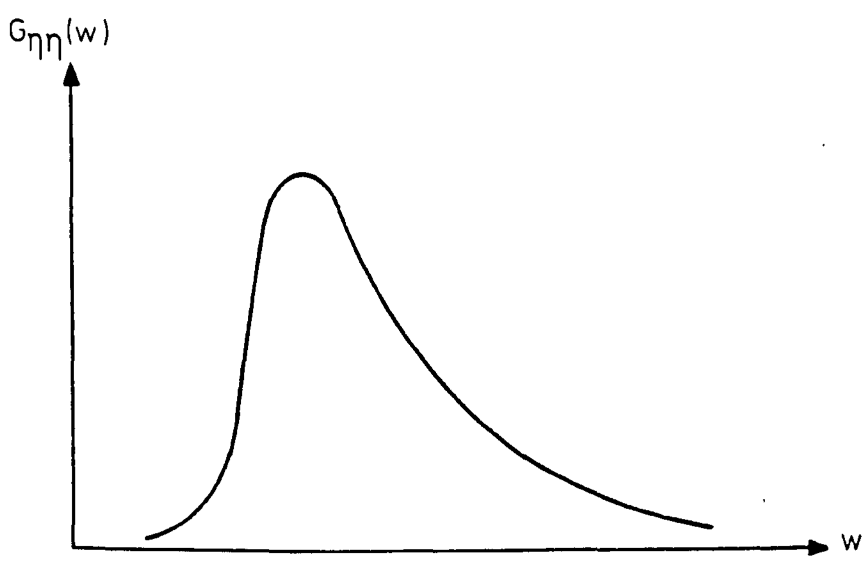

Figure A1 - Sketch of Pierson-Moskowitz Spectrum

$$E = \frac{1}{2} \rho_2 \, g \, a^2 \qquad \text{(A1)}$$

where ρ_2 = sea water density

g = acceleration due to gravity and

a = wave amplitude (= half the waveheight).

From equation (A1) it can be seen that

$$E \propto a^2$$

A typical trace for a random wave can be represented in terms of η, the instantaneous surface elevation relative to still water level.

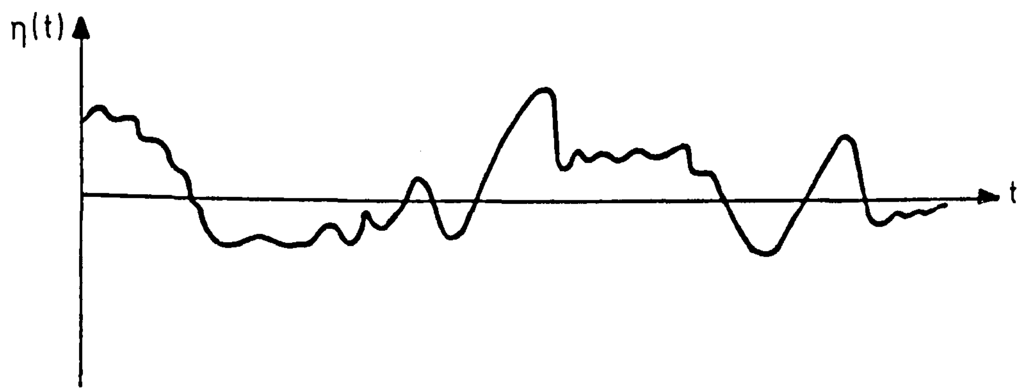

Figure A2 - Diagram Showing Surface Elevation

It is known that the surface elevation η can be given by

$$\eta(x,t) = \sum_{i=1}^{n} a_i \cos (k_i x - \omega_i t + \alpha_i) \tag{A2}$$

where k = wave number

ω = wave frequency

α = random phase

From equation (A2) it can be seen that the random wave train is essentially a superposition of sinusoidal waves.

The values for k, ω and α used in equation (A2) can be found from

$$k = \frac{2\pi}{\lambda}$$

where λ = wavelength

$$\omega = \frac{2\pi}{T}$$

where T = wave period

and α is found from the probability function shown in Fig. A3.

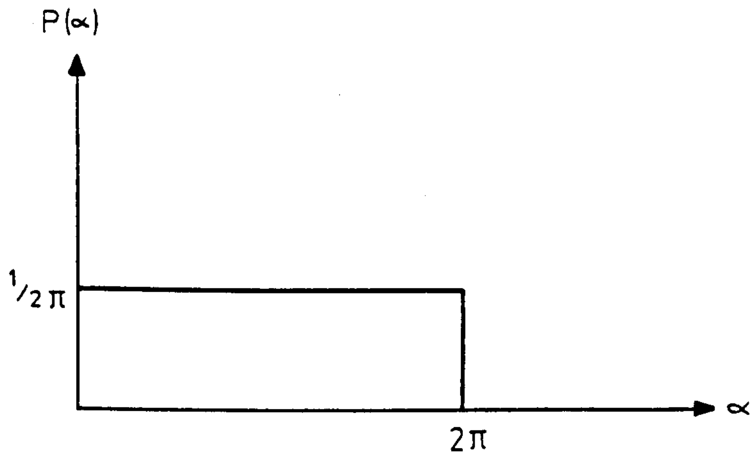

Figure A3

From wave kinematics it can also be shown that

$$\omega_i^2 = g\, k_i \tanh k_i d$$

where d = water depth

The Pierson-Moskowitz spectrum shown in Figure A1 is redrawn in Figure A4 showing the approximated spectrum that is calculated by the program.

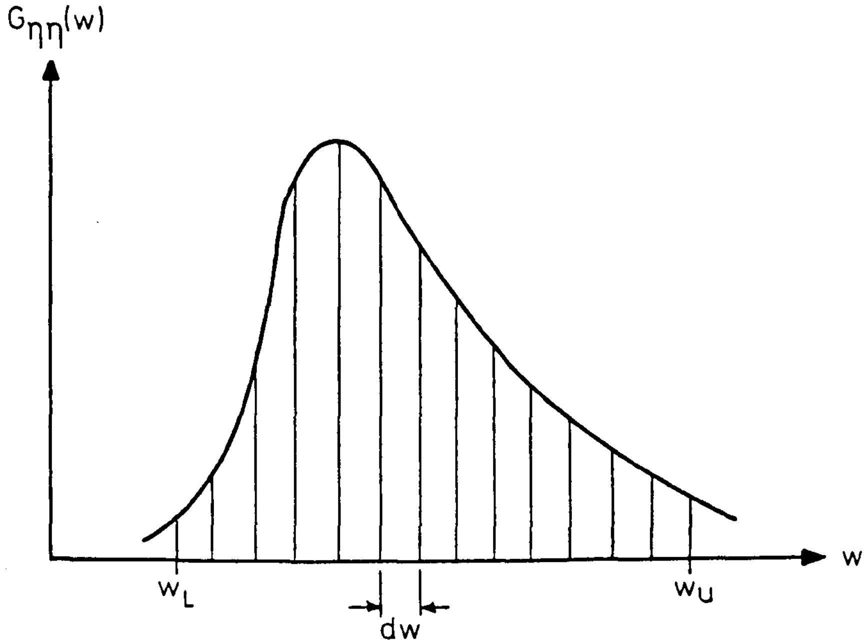

Figure A4

An expression for $G_{\eta\eta}(\omega)$ is given such that

$$G_{\eta\eta}(\omega) = \frac{Ag^2}{\omega^5} \exp\left[\frac{-B\,\omega_0^{\,4}}{\omega^4}\right] \tag{A3}$$

where A = 0.0081

B = 0.74 and

ω_0 = g/u

where u = the wind speed at 19.5 metres above sea water level.

From wave analysis it can also be derived that

$$\int_0^x G\eta(\omega)\ d\omega = \sigma_\eta^{\ 2}$$

and $$G_\eta(\omega_i)d\omega = \frac{a_i^{\ 2}}{2} \tag{A4}$$

The program requires information concerning the upper and lower frequency values, ω_u and ω_ℓ respectively, and by using a cumulative spectrum method it calculates values of the surface elevation. Equal values of variance $(\sigma_n^{\ 2})$ are used throughout the procedure. The cumulative spectrum is given by

$$Q_\eta(\omega_j) = \int_0^{\omega_j} G_\eta(\omega)d\omega \tag{A5}$$

and the spectrum is shown in Figure A5.

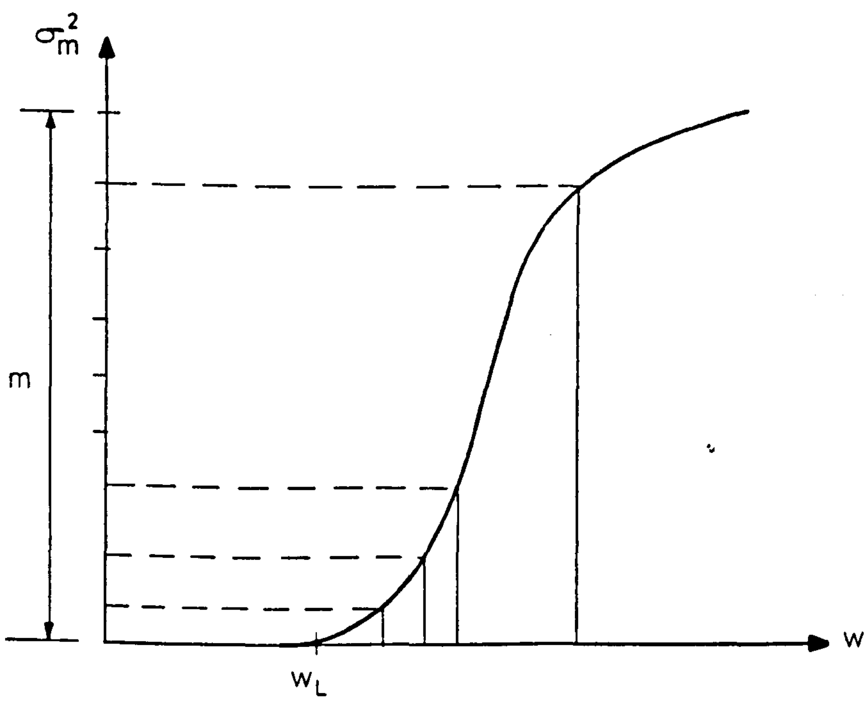

Figure A5

It is known that

$$\frac{a_i^{2}}{2} = \frac{\sigma_\eta^{2}}{m}$$

and so the equation for surface elevation becomes

$$\eta(x,t) = \sqrt{\frac{2}{m}}\,\sigma_\eta \sum_{i=1}^{m} \cos\,(k_i x - \omega_i t + \alpha_i)$$

and by using this method the computer calculates a series of random waveheights and periods which are then converted to paddle strokes using an experimentally obtained constant.

The constant is obtained by setting up a sinusoidal wave in the tank which has the maximum waveheight required, and then by using an oscilloscope the output voltage passing from the console to the paddle to generate this waveheight can be obtained. This procedure is then carried out for several smaller waveheights and an average value of voltage/waveheight can be obtained. This value was used as the initial estimate for the constant in the program. The program was then run and the generated random wave signal was played out to an oscilloscope. The constant was subsequently refined until the required spectrum was obtained.

It should be noted that the lower and upper limits for ω, i.e. ω_ℓ and ω_u were set at 4 standard deviations from the mean frequency in each direction.

```
C     MORT1.FR IS THE FIRST PART OF RANDOM WAVE GENERATION CONTROL SIGNAL
C     PROGRAM SIMULATION BY SUMMATION OF EQUAL ENERGY SLICES
C       FILE IN RANP1 IN 64 WORD BLOCKS
        DIMENSION SPP(1001),SPT(201,2),HW(201,2),WN(201),IBUF(64)
        DIMENSION RP(201),SINA(201),SINB(201),COSA(201),COSB(210)
   5    FORMAT(30A2)
  10    FORMAT(//////////)
  20    FORMAT(1P4E12.3)
        NJ=1001
        NI=NJ-1
        TYPE" INPUT FILE TITLE "
        CALL FOPEN(2,'RANP1',128,'B')
        READ(11,5)(IBUF(I),I=1,30)
        WRITE BINARY(2) IBUF
        ACCEPT "NO. OF COMPONENTS ",NC,"SEQUENCE LENGTH ",NL
        ACCEPT "NO. OF COMPONENTS ABOVE 85% LEVEL ",NCB
        ACCEPT "LOWER AND UPPER SNN LIMITS RADS/SEC ",WL,WU
        ACCEPT "NO. OF 1/100 SEC STEPS ",NT
        ACCEPT "GRAV CONST ",G,"WATER DEPTH ",H
        ACCEPT "HINGED MODE FACTOR (-1.0 PISTON) ",AK
        DW=(WU-WL)/NI
        DT=NT/100.0
C       MOSCOWITZ SPECTRUM
        ACCEPT "ALPHA ",A1,"BETA ",B1,"WIND SPEED ",UW
        WO=G/UW
        AG2=A1*G*G
        BW=-B1*(WO**4)
        W=WL
        DO 1035 I=1,NJ
        W4=W**4
        SPP(I)=AG2*EXP(BW/W4)/(W4*W)
 1035   W=W+DW
C       CALCULATE STAND. DEVIATION OF SURFACE ELEVATION
        SUM=0.0
        DO 1040 I=2,NI,2
 1040   SUM=SUM+4.0*SPP(I)+2.0*SPP(I+1)
        SUM=SQRT((SUM+SPP(1)-SPP(NJ))*DW/3.0)
        TYPE "STD DEV FOR SNN ",SUM
        ACCEPT "SNN O/P INT OR 0 ",KK
        IF(KK.EQ.0)GOTO 900
        CALL OPM(SPP,KK,DW,WL,NJ)
C       SPP NOW HOLDS TARGET SPECTRUM SNN
  900   ACCEPT "START TIME ",TS,"NO. OF ADDITIONAL H(W) VALUES OR 0 ",NH
        ACCEPT "NO. OF STD DEV OF STROKE FOR CLIPPING ",NS
        IF(NH.EQ.0)GOTO 1050
        TYPE "FREQUENCY RADS/SEC              H(W)     "
        DO 1045 I=1,NH
        ACCEPT HW(I,1),HW(I,2)
 1045   CONTINUE
        ACCEPT "LOWER & UPPER H(W) LIMITS RADS/SEC ",WLH,WUH
C       CALCULATE NORMAL LINEAR TRANSFER FUNCTION
 1050   W=WL
        DO 1055 I=1,NJ
        AA=W*W*H/G
        J=1
```

```
      R1=2.0*AA
 501  Y2=TANH(R1)
      R2=AA/Y2
      IF(ABS((R2-R1)/R2).LE.0.001)GOTO 502
      IF (J.GT.1000)GOTO 503
      J=J+1
      R1=R2
      GOTO 501
 503  TYPE " TANHSOL ",R1,R2,W
 502  TO=R2
      R=SQRT(1.0-(AA/TO)**2)
      HP=2.0*(AA**2)/(TO**3-TO*AA*AA+AA*TO)
      HH=HP*(AA-1.0+R)/(AA*AK)
      IF(AK.GT.0.0)HP=HH
      SPP(I)=SPP(I)/(HP*HP)
 1055 W=W+DW
C     APPLY ADDITIONAL H(W) IF REQD.
      IF(NH.EQ.0)GOTO 1200
      W=WL
      NK=NH-1
      DO 1080 I=1,NJ
      IF(W.LT.WLH.OR.W.GT.WUH)GOTO 1085
      DO 1090 J=1,NK
      K=J
      IF(W.LE.HW(J+1,1).AND.W.GE.HW(J,1))GOTO 1095
 1090 CONTINUE
      GOTO 9002
 1095 HA=HW(K,2)+(HW(K+1,2)-HW(K,2))*(W-HW(K,1))/(HW(K+1,1)-HW(K,1))
      GOTO 1100
 1085 HA=1.0
 1100 SPP(I)=SPP(I)*HA*HA
 1080 W=W+DW
C     FINAL STROKE SPECTRUM HELD IN SPP. CALCULATE STD DEV OF STROKE
 1200 SUM=0.0
      ACCEPT "SPP O/P INT OR 0 ",KK
      IF(KK.EQ.0)GOTO 901
      CALL OPM(SPP,KK,DW,WL,NJ)
  901 DO 1205 I=2,NI,2
 1205 SUM=SUM+4.0*SPP(I)+2.0*SPP(I)
      SUM=(SUM+SPP(1)-SPP(NJ))*DW/3.0
      SC=SQRT(SUM)
      SLIM=NS*SC
      NCA=NC-NCB
      NCA1=NCA+1
      NCA2=NCA+2
      ASA=0.85*SUM/NCA
      ASB=0.15*SUM/NCB
      DSA=SQRT(2.0*ASA)
      DSB=SQRT(2.0*ASB)
      TYPE "STROKE STD DEV=",SC,"LIMIT=",SLIM
      TYPE "     DSA,DSB    ",DSA,DSB
      SCFA=1.000E+05
      SCFB=1.7000E+5
      SCFC=1.422E+03
      SCFD=1.008E+03
      TYPE "SCALES LESS THAN 0.015  0.030   0.108   0.152  "
      TYPE "INPUT AMP VOLTAGE  10V     5V      RT2V     1V"
      WRITE(10,20)SCFA,SCFB,SCFC,SCFD
      ACCEPT "SCALE FACTOR ",SCF
C     CONVERT SPP TO CUMULATIVE SPECTRUM
      DW2=DW/2.0
      SS=SPP(1)
      SPP(1)=0.0
      DO 1210 I=2,NJ
      ST=(SS+SPP(I))*DW2
      SS=SPP(I)
```

```
 [illegible]  SPP(I)=SPP(I-1)+ST
      ACCEPT "SPP AND O/P INT OR 0 ",KK
      IF(KK.EQ.0)GOTO 902
      CALL OPM(SPP,KK,DW,WL,NI)
C     FIND FREQUENCIES AT JUNCTIONS OF SLICES
 902  NC1=NC+1
      WN(NC1)=WU
      WN(1)=WL
      SUM=ASO
      DO 1250 I=2,NCA1
      W=WL
      DO 1255 J=1,NI
      K=J
      IF(SUM.GE.SPP(J).AND.SUM.LE.SPP(J+1))GOTO 1260
 1255 W=W+DW
      GOTO 9003

 1260 WN(I)=W+DW*(SUM-SPP(K))/(SPP(K+1)-SPP(K))
 1250 SUM=SUM+ASA
      SUM=SUM-ASA+ASB
      DO 1251 I=NCA2,NC
      W=WL
      DO 1256 J=1,NI
      K=J
      IF(SUM.GE.SPP(J).AND.SUM.LE.SPP(J+1))GOTO 1261
 1256 W=W+DW
      GOTO 9003
 1261 WN(I)=W+DW*(SUM-SPP(K))/(SPP(K+1)-SPP(K))
 1251 SUM=SUM+ASB
      DO 1265 I=2,NC1
      WW=WN(I-1)
 1265 WN(I-1)=(WW+WN(I))/2.0
C     PHASE ANGLE UNIFORM BETWEEN 0 &2PI
      SEED=0.312567489
      PI2=8.0*ATAN(1.0)
      DO 1270 I=1,NC
      TMP=29.0*SEED
      JJJ=TMP
      SEED=TMP-JJJ
 1270 RP(I)=PI2*SEED
      ACCEPT "RP AND WN O/P OR 0 ",KK
      IF(KK.EQ.0)GOTO 903
      CALL OPM(WN,KK,DW,WL,NC)
      CALL OPM(RP,KK,DW,WL,NC)
 903  DO 1275 I=1,NC
      ARG1=WN(I)*(TS-DT)+RP(I)
      ARG2=WN(I)*DT
      SINA(I)=SIN(ARG1)
      COSA(I)=COS(ARG1)
      SINB(I)=SIN(ARG2)
 1275 COSB(I)=COS(ARG2)
      ICNT=1
      JCNT=1
      XM=0.0
      XM2=0.0
C     START SIMULATION
      DO 2000 I=1,NL
      SUMA=0.0
      DO 2005 J=1,NCA
      CS=COSA(J)*COSB(J)-SINA(J)*SINB(J)
      SS=SINA(J)*COSB(J)+COSA(J)*SINB(J)
      SUMA=SUMA+CS
      COSA(J)=CS
 2005 SINA(J)=SS
      SUMB=0.0
      DO 2006 J=NCA1,NC
```

```
      CS=COSA(J)*COSB(J)-SINA(J)*SINB(J)
      SS=SINA(J)*COSB(J)+COSA(J)*SINB(J)
      SUMB=SUMB+CS
      COSA(J)=CS
2006  SINA(J)=SS
      ARG=SUMA*DSA+SUMB*DSB
      IF(ABS(ARG).LT.SLIM)GOTO 2020
      TYPE ARG
      ARG=SIGN(SLIM,ARG)
      TYPE ARG
2020  XM=XM+ARG
      XM2=XM2+ARG*ARG
      IBUF(ICNT)=ARG*SCF
      ICNT=ICNT+1
      IF(ICNT.LE.64)GOTO 2000
      WRITE BINARY(2) IBUF
      TYPE JCNT
      JCNT=JCNT+1
      ICNT=1
2000  CONTINUE
      IF(ICNT.GT.64.OR.ICNT.EQ.1)GOTO 2010
      DO 2015 I=ICNT,64
2015  IBUF(I)=0
      WRITE BINARY(2) IBUF
      TYPE JCNT
2010  TYPE SIMULATION FINISHED
      XM=XM/NL
      SA=SQRT(XM2/(NL-1))
      TYPE "MEAN STROKE ",XM," STROKE STD DEV ",SA
      WRITE(10,10)
      CALL FCLOS(2)
      STOP
      GOTO 9009

9002  TYPE "INTERPOLATION ERROR ADDN H(W) ",W
      GOTO 9009
9003  TYPE "INTERPOLATION ERROR FOR WN(I) ",SUM
9009  CALL FCLOS(2)
      WRITE(10,10)
      STOP
      END


      SUBROUTINE OPM(A,I,D,WS,N)
      DIMENSION A(1001)
      W=WS
      WRITE(10,10)
      K=I-1
      DO 100 J=1,N
      K=K+1
      IF(K.NE.I)GOTO 100
      K=0
      WRITE(10,20)
100   W=W+D
      WRITE(10,30)
10    FORMAT(///,23H   FREQUENCY    VALUE    ,/)
20    FORMAT(1P2E14.5)
30    FORMAT(////)
      RETURN
      END
```

APPENDIX B

DESIGN OF COMPONENTS FOR OUTFALL TEST FACILITY

1. Design Calculations for 'V' Notch (BS 3680)

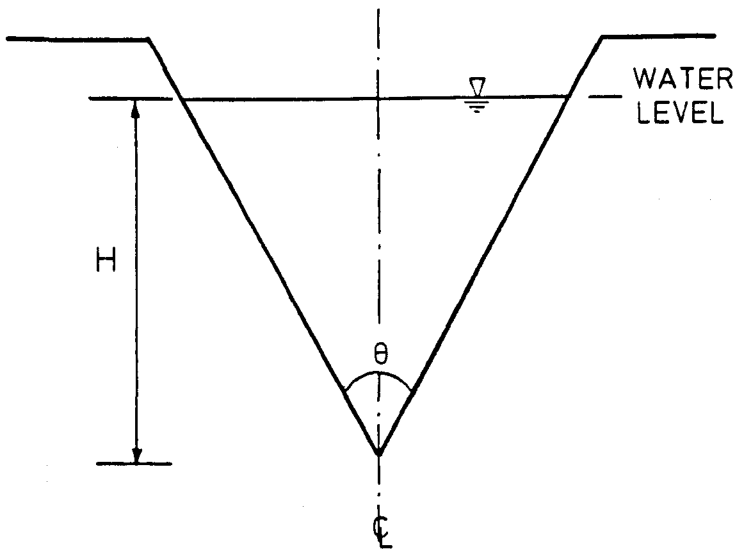

Figure B.1

For a notch the flow rate is given as

$$Q_t = \frac{8}{15} C_d \sqrt{2g} \tan \frac{\theta}{2} H^{5/2} \qquad \text{(B1)}$$

where C_d = coefficient of discharge

g = acceleration to gravity

Q_t = flow rate

θ = angle of V notch and

H = water level above V notch.

A coefficient of discharge, C_d, is inserted into equation (B1) to take into account losses in pressure head as the flow passes over the V notch and other assumptions in the underlying theory. If it is assumed that the velocity of approach to the V notch is negligible then Figure 8 from BS 3680 part 4a can be used to determine C_d.

As the V notch was not required to take the full design flow rate it was decided to use a Q_T value of 0.0015 m^3/s (1.5 litres/s) which is 75% of the design flow rate. From calculations using equation B1 it was eventually found that a V notch with an angle of 20° would be adequate as it gave a head above the V notch of approximately 130mm.

2. Design of Venturimeter

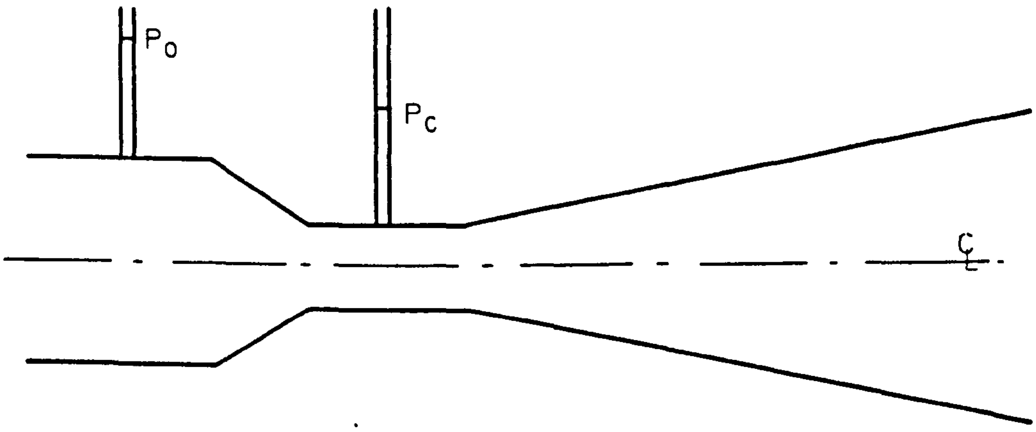

Sketch Showing Venturimeter

Figure B2

The venturimeter was designed for a flow rate of 2.0 L/s as this was the design flow rate of the outfall system. The equation for the flow rate through a venturi is

$$Q = \frac{C_d \sqrt{2g}\ (\frac{\pi}{4})\ D_0{}^2}{(1 - m^2)^{1/2}} \left(\frac{P_0 - P_c}{W}\right)^{1/2} \tag{B2}$$

where Q = flow rate

C_d = coefficient of discharge

D_c = diameter of throat

P_c = pressure at throat

P_0 = pressure upstream of throat

D_0 = diameter upstream of throat

W = specific weight of water (= ρg) and

m = $(D_c/D_0)^2$.

C_d was taken as 0.95 and $((P_0 - P_c)/W)$ was equivalent to the value of H on the manometer (where H is difference in manometer levels) hence

$$Q = \frac{0.95\sqrt{2g}\ (\frac{\pi}{4}) D_c{}^2}{(1 - m^2)^{1/2}} H^{1/2} \tag{B3}$$

Substituting the design flow rate in equation B3 and using D_0 equal to 50mm, (equal to the inflow pipe diameter) it was found that a throat diameter (D_c) of 25mm gave a value of H.of 88cm. This was adopted as the throat diameter as the value of the H lay within the bounds required for acceptable accuracy of the manometer system.

The subsequent calibration of the Venturimeter is shown in figure 5.3. It was found that the actual coefficient of discharge (C_d) was approximately 0.98.

3. Calculation for Appropriate Maximum Flow Rate Through System

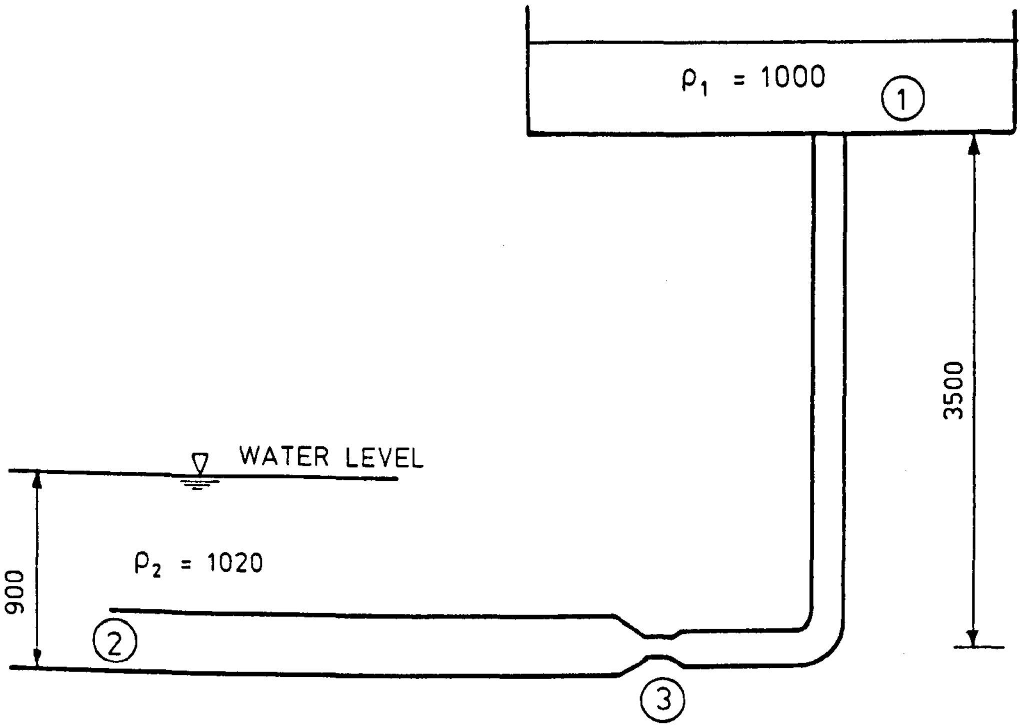

Figure Showing General Sketch of Outfall Arrangement

Figure B3

Two types of freshwater supply systems were considered initially. They were i) a header tank and ii) a pumped supply system.

Most prototype outfalls are fed from a dropshaft so it was decided that one should be incorporated into the model. This meant that if a pumped system was used the pump would have to lift the water from a sump to the level of the dropshaft and then discharge it into the outfall. Hence it was just as convenient to fix a header tank to the top of the dropshaft and fill this from the mains supply.

To determine whether the system was adequate to provide the required flow rates Bernoulli's equation is applied between Sections (1) and (2) shown in figure B3. In the limit when the tank is at the point of completely draining and accounting for minor and pipe friction losses, Bernoulli's equation gives

$$3.5 = \frac{\rho_2}{\rho_1} + \frac{V_2^{\,2}}{2g} + \frac{f_1 L_1 Q_1^{\,2}}{2g\ D_1 A_1^{\,2}} + \frac{f_2 L_2 Q_2^{\,2}}{2g\ D_2 A_2^{\,2}} + \frac{k\ V_1^{\,2}}{2g} \qquad \text{(B4)}$$

where ρ_2,ρ_1 = seawater and freshwater densities respectively

h = height of seawater

V_2 = velocity of flow at exit

f_1,f_2 = pipe friction factors for the small and large pipe diameters respectively

L_1,L_2 = respective lengths of pipe

D_1,D_2 = respective pipe diameters

Q_1,Q_2 = flow rates in the two different pipe diameters

A_1,A_2 = areas of respective pipes and

k = minor losses at bends and expansions.

Approximate values of k where obtained from Miller(37) and taken as the following

k for bends = 0.5

k at pipe inlet = 0.6

k at expansion of Venturi = 10.0

k at pipe exit = 1.0

k to cover any other losses = 2.0

Therefore total value of k is 14.1. At a flow rate of 2.0 L/s the velocity in the 50mm pipe is 1.02 m/s and the velocity in the 105mm pipe is 0.231 m/s. This gives values of Reynolds numbers for both pipes of approximately 4.474×10^4 and 2.126×10^4 respectively. Hence from the Moody diagram[39] for smooth pipes the values of f_1 and f_2 are given as 0.022 and 0.025 respectively. At this stage the value of 2.0 L/s was still arbitary and it was felt as prudent to let f_1 and f_2 equal to 0.025. By substituting all the values into equation (B4) the following expression is obtained

$$3.5 - \frac{1020}{1000} \times 0.9 + \frac{Q_2^{\,2}}{2g\ A_2^{\,2}} + \frac{0.025 \times 5.5 \times Q_1^{\,2}}{2g\ D_1\ A_1^{\,2}}$$

$$+ \frac{0.025 \times 5 \times Q_2^{\,2}}{2g\ D_2\ A_2^{\,2}} + \frac{13.1\ Q_1^{\,2}}{2g\ A_1^{\,2}} + \frac{1.0\ Q_2^{\,2}}{2g\ A_2^{\,2}} \qquad \text{(B5)}$$

As Q_1 equals Q_2 in equation B5 this can be rearranged to give a value for Q of 3.49 litres/sec. This demonstrated that the apparatus would be adequate for the flow rates required.

As the header tank was not kept at a constant head of water it was important to determine the drop in the head of water during an experimental run. An experimental run lasted 100 seconds so it was expected that the drop in head would take place over a period of time of approximately 110 seconds.

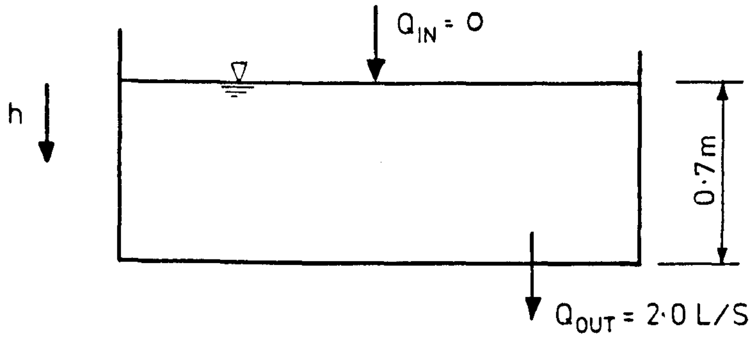

Diagram of header tank

Figure B4

The dimensions of the header tank were 1.67 x 1.52 metres with an initial water level of 0.7m. Initial conditions are such that at T = 0 the flow rate Q is 2.0 ℓ/s and from continuity the following equation holds

$$Q_{in} = A_T \frac{dh}{dt} + Q_{OUT} \tag{B6}$$

$$Q_{OUT} = - A_T \frac{dh}{dt}. \tag{B7}$$

where A_T = area of header tank and

Q_{OUT} = flow into pipe.

For a time interval dt it can be assumed that the quantity of flow leaving the header tank is dq, therefore, equation B7 can be written as

$$dq = -dh\ A_T \tag{B8}$$

The equation for flow through an orifice is given as

$$Q = A_0\ C_d\sqrt{2gh} \tag{B9}$$

where A_0 = area of orifice and

C_d = coefficient of discharge,

hence for a flow rate of 2.0 ℓ/s to discharge from the orifice for a water level of 0.7m the value of (A_0 C_d) must be equal to 5.397 x $10^{-4}m^2$. Also, from equation B9 it must hold that the flow rate for an interval of time, dt is given by

$$dq = A_0\ C_d\sqrt{2gh}\ dt \tag{B10}$$

By substituting for dq in equation B8, and then rearranging and integrating the following expression is obtained for the change in h,

$$H_1^{1/2} - H_2^{1/2} = \frac{A_0\ C_d\ T\sqrt{2g}}{2\ A_T} \tag{B11}$$

where H_1 = initial level of water in tank

H_2 = final level of water in tank and

T = total time of operation.

This gives a value for H_2 of 0.62m, a drop of 8cm for the total run.

B.1 Critical appraisal of flow supply system

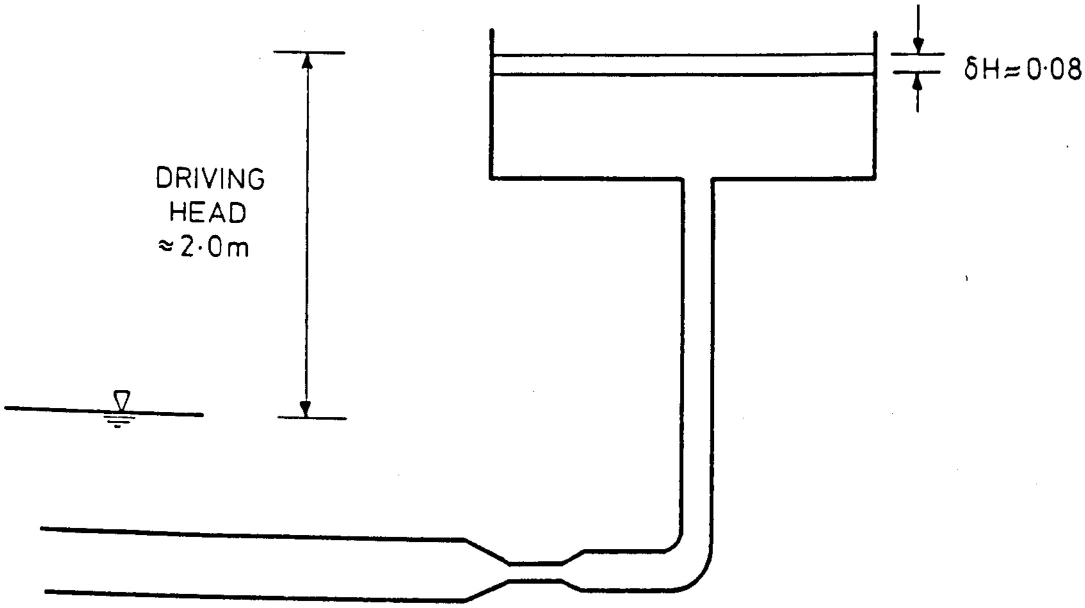

Figure B5

From initial calculation $\delta H \approx 0.08$m (8cm) for a 100 second test at a flow rate of 2.0 L/s.

$$\therefore \text{ percentage change in head} = \left[\frac{\delta H}{H}\right] \times 100 \approx 4\%$$

$$\text{Now } H = \frac{\sum K_i V^2}{2g} = (\textstyle\sum k)Q^2 = k'Q^2$$

where k_i = loss coefficients for pipes bends and entrances

$$\text{hence } \frac{dH}{dQ} = 2k'Q = 2\left[\frac{H}{Q}\right]$$

$$\therefore \left[\frac{dH}{H}\right] = 2\left[\frac{dQ}{Q}\right]$$

$$\therefore \frac{dQ}{Q} = \frac{1}{2}\left[\frac{dH}{H}\right]$$

∴ % change in Q will be 1/2 x 4% i.e. 2% under maximum operating flow.

As most of the flow rates investigated are lower than this then the system was deemed satisfactory.

4 Balancing the Manifold System

4.1 Introduction

As the flow passes into the manifold section of an outfall and is discharged at each riser, changes occur in the pressure and head losses within the pipe which leave a situation in which the flow passing through the risers is not necessarily equal.

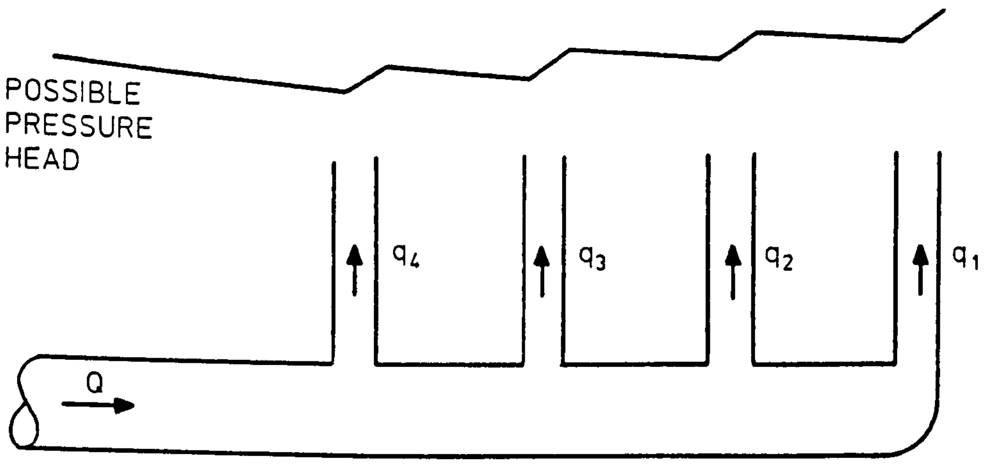

Sketch showing possible pressure head for manifold

Figure B6

The diagram shown in figure B6 indicates that for the pressure head shown the maximum flow rate would occur in riser 1 and the minimum in riser 4 when the full design flow rate was passing through the system. In order to prevent this and balance the flow orifice plates were designed and placed in each riser. The following section demonstrates how the analysis was performed; all the calculations follow those shown in Miller[39].

If the estimated flow to purge the risers in the manifold system is taken as being 2.0 ℓ/s, it is this figure which is used to estimate the friction factor within the risers and main pipe.

For main outfall pipe

$$\text{velocity} = \frac{\text{flow rate}}{\text{pipe area}} = 0.231 \text{ m/s}$$

and Reynolds number = 2.2×10^{-4}. From reference to a Moody diagram[39] the friction factor in the main pipe is 0.025. Similarly for the individual risers it was found that a friction factor of 0.026 was required (both calculations were made on the assumption that the pipe was smooth).

In its original state the outfall risers were not balanced and an estimate has to be made of the initial flow distribution. Basing this on tables and diagrams in Miller[39] an initial estimate was made as follows

$q_1 = 0.65$ L/s

$q_2 = 0.55$ L/s

$q_3 = 0.45$ L/s

$q_4 = 0.35$ L/s.

Utilising the design charts by Miller[39] a better estimate for the flow through each riser can be calculated as follows:-

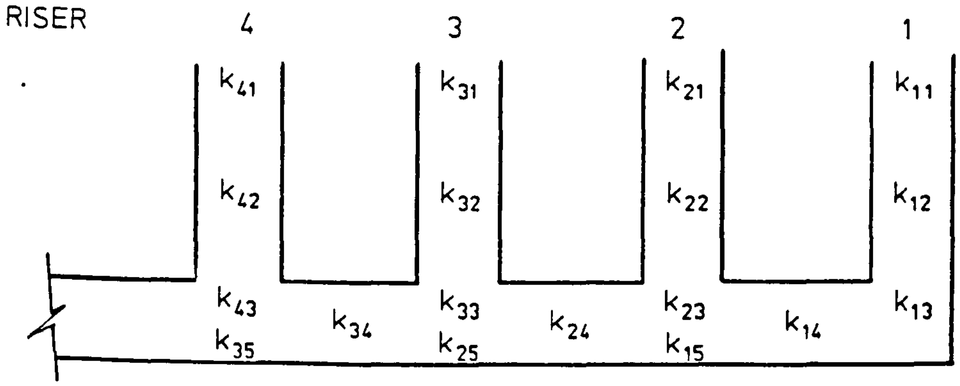

Definition of headloss components

(from Miller[39])

Figure B7

All calculations performed from Miller[39], and all values obtained from tables in same publication. Taking riser 1

$k_{11} = 1.0$

$k_{12} = \frac{fL}{D_R} = 0.208 = (\frac{0.026 \times 0.4}{0.05})$

$k_{13} = 8.0$

$k_{14} = \frac{fL}{D_2} = 0.119 = (\frac{0.025 \times 0.5}{0.105})$

$k_{15} = 0.04$

Total loss coefficient (k')

$$k' = (1 + 0.208)\ (\frac{0.65 \times 10^{-3}}{0.23})^2 + (8 + 0.119)(0.65 \times 10^{-3})^2$$

$$+ (0.04(0.65 \times 10^{-3} + 0.55 \times 10^{-3})^2)$$

$= 1.314 \times 10^{-5}$

From riser 2

$$k_{21} = 1.0$$

$$k_{22} = 0.208$$

$$k_{23} = 3.5$$

$$k' = (1 + 0.208)\left(\frac{0.55 \times 10^{-3}}{0.23}\right)^2 + (3.5\ (1.20 \times 10^{-3})^2)$$

$$= 1.1948 \times 10^{-5}$$

As the headloss from riser 1 does not equal the headloss from riser 2 try $q_2 = 0.58$ ℓ/s - this has the effect of changing k_{23}

$$k_{23} = 3.75$$

$$k' = (1 + 0.208)\left(\frac{0.58 \times 10^{-3}}{0.23}\right)^2 + (3.75\ (1.23 \times 10^{-3})^2)$$

$$= 1.3355 \times 10^{-5}$$

As this value of k' is within approximately 2% of the k' value for riser 1 let

$$q_1 = 0.65 \text{ and } q_2 = 0.58.$$

The head loss value from riser 2 to riser 3 gives

$$k_{24} = 0.119$$

$$k_{25} = -0.03$$

$$k' = 1.3355 \times 10^{-5} + (0.119\ (1.23 \times 10^{-3})^2) - (0.03\ (1.23 \times 10^{-3} + 0.45 \times 10^{-3})^2)$$

$$= 1.345 \times 10^{-5}$$

For riser 3

$$k_{31} = 1.0,\ k_{32} = 0.208,\ k_{33} = 1.6$$

$$k' = (1 + 0.208)\left(\frac{0.45 \times 10^{-3}}{0.23}\right)^2$$

$$+ (1.6\ (1.23 \times 10^{-3} + 0.45 \times 10^{-3})^2)$$

$$= 0.140 \times 10^{-6}$$

As this is not equal to 1.34×10^{-5} let $q_3 = 0.56$ which sets $k_{33} = 1.9$ and

$$k' = (1 + 0.208)\left(\frac{0.56 \times 10^{-3}}{0.23}\right)^2$$

$$+ (1.9\ (1.23 \times 10^{-3} + 0.56 \times 10^{-3})^2)$$

$$= 1.3249 \times 10^{-5}$$

As this is within 2% of 1.3450×10^{-5} let $q_3 = 0.56$

From riser 3 to riser 4

$$k_{34} = 0.119,\ k_{35} = -0.02$$

$$k' = 1.3249 \times 10^{-5} + (0.119(1.23 \times 10^{-3} + 0.56 \times 10^{-3})^2)$$

$$- (0.02\ (1.79 \times 10^{-3} + 0.35 \times 10^{-3})^2)$$

$$= 1.3539 \times 10^{-5}$$

For riser 4

$$k_{41} = 1.0,\ k_{42} = 0.208,\ k_{43} = 1.3$$

$$k' = (1 + 0.208)\left(\frac{0.35 \times 10^{-3}}{0.23}\right)^2 + (1.3\ (2.14 \times 10^{-3})^2)$$

$$= 8.757 \times 10^{-6}$$

As this is not close to 1.3539×10^{-5} try a flow rate of $q_4 = 0.50$ which gives a k_{43} value of 1.5.

$$k' = (1 + 0.208)\left(\frac{0.50 \times 10^{-3}}{0.23}\right)^2 + (1.5(2.29 \times 10^{-3})^2)$$

$$= 1.3575 \times 10^{-5}$$

As this lies within 2% of 1.3539×10^{-5} let $q_4 = 0.5$. Therefore the total calculated flows are

$q_1 = 0.65$

$q_2 = 0.58$

$q_3 = 0.56$ and

$q_4 = 0.50$

These give a total of 2.29 so to bring the total to 2.0 L/s all the values are factored by 2.0/2.29 which gives $q_1 = 0.57$ L/s, $q_2 = 0.51$ L/s, $q_3 = 0.49$ L/s and $q_4 = 0.43$ L/s.

4.2 Balancing of flows in risers

As the flows through each riser are not equal the diameter and length of orifice plates to balance the flows are then determined. If flows are balanced each riser will be discharging at a rate of 0.5 L/s, and the calculations are performed in the opposite direction to those carried out in section 4.1.

For riser 4

$$k_{41} = 1.0,\ k_{42} = 0.208 \text{ and } k_{43} = 1.5$$

$$k' = ((1 + 0.208)(\frac{0.50 \times 10^{-3}}{0.23})^2) + (1.5(2 \times 10^{-3})^2)$$

$$= 1.1709 \times 10^{-5}$$

From riser 4 to riser 3

$$k_{35} = -0.03,\ k_{34} = 0.119$$

$$1.1709 \times 10^{-5} = y + (0.119(1.5 \times 10^{-3})^2) - (0.03(2.0 \times 10^{-3})^2)$$

$$k = 1.156 \times 10^{-5}$$

For riser 3

$$k_{31} = 1.0, \; k_{32} = 0.208 \text{ and } k_{33} = 2.5$$

$$k = 1.156 \times 10^{-5} = ((1 + 0.208)(\frac{0.5 \times 10^{-3}}{0.23})^2)$$

$$+ (2.5(1.5 \times 10^{-3})^2) + (j(0.5 \times 10^{-3})^2)$$

$$j = 0.906$$

where j in this section is a loss coefficient.

From Miller[39]

$$j = 0.906 = (0.8 \times 0.5) + (0.026 \times \frac{L}{0.044} \times \frac{1}{0.78^2}) \qquad \text{(B12)}$$

where 0.8 and 0.5 are values obtained from tables 14.3 and 14.5 from reference (39), L is the length of the orifice, 0.044 is the orifice diameter, 0.026 is the friction factor and 0.18 is the area ratio.

Length of orifice = 28mm

For riser 2

from riser 3 to 2

$$k_{24} = 0.119,\ k_{25} = -0.03$$

$$k' = 1.156 \times 10^{-5} = j + (0.119(1.0 \times 10^{-3})^2)$$

$$- (0.03(1.5 \times 10^{-3})^2)$$

$$j = 1.157 \times 10^{-5}$$

For riser 2

$$k_{21} = 1.0,\ k_{22} = 0.208,\ k_{23} = 5.6$$

$$k' = 1.157 \times 10^{-5} = (1.208(\frac{0.5 \times 10^{-3}}{0.23})^2) + (5.5(1.0 \times 10^{-3})^2)$$

$$+ (j(0.5 \times 10^{-3})^2)$$

$$j = 1.205$$

From equation B12 the length of orifice required for riser 2 is 44mm.

From riser 2 to riser 1

$$k' = 1.157 \times 10^{-5} = j + (0.119(0.5 \times 10^{-3})^2)$$

$$- (0.02(1.0 \times 10^{-3})^2)$$

$$j = 1.150 \times 10^{-5}$$

For riser 1

$$k_{11} = 1.0,\ k_{12} = 0.208,\ k_{13} = 21$$

$$k' = 1.150 \times 10^{-5} = (1.205(0.5 \times 10^{-3})^2) + (20(0.5 \times 10^{-3})^2)$$

$$+ (j(0.5 \times 10^{-3})^2)$$

$$j = 2.16$$

From equation B12 this gives an orifice length of 97mm.

The graph showing the head losses in reference (39) indicates that for the above requirements the conditions are out of the ranges shown on the graph. Hence the value of 21 is only an estimate.

The orifice tubes for these calculated lengths were then inserted into the risers of the experimental model and tested. Refinements took place until the experimental model behaved satisfactorily. It was found that the lengths of the orifice tubes required in the experimental model where 10mm, 30mm and 70mm for risers 3, 2 and 1 respectively. One possible reason for the differences in orifice sizes is that Millers work was carried out at high Reynolds numbers and as this model uses low Reynolds numbers discrepancies may occur.

APPENDIX C

DERIVATION OF ANGLES OF INTERFACE AND UPPER FLOW

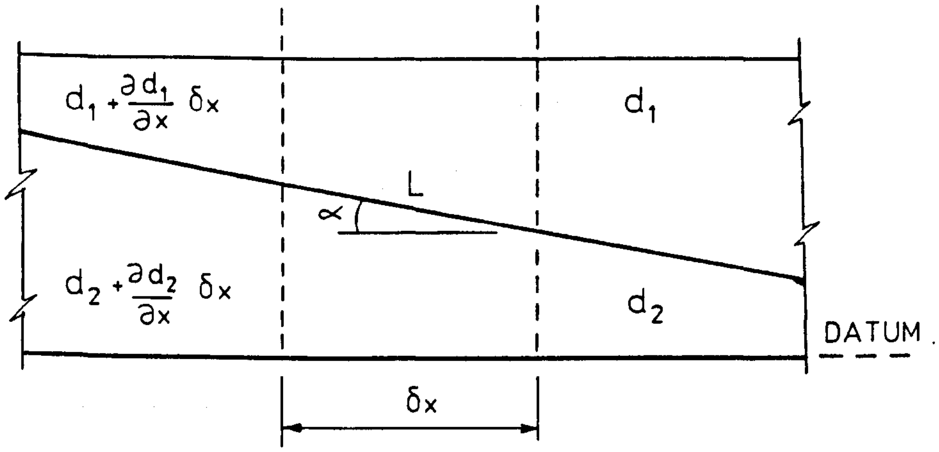

Figure C1

For angle α at interface of fluids.

From datum at base of pipe to interface, the change in level of interface is given by

$$d_2 + \frac{\partial d_2}{\partial x}\,\delta x - d_2 = \frac{\partial d_2}{\partial x}\,\delta x \qquad \text{(C1)}$$

Length of interface, L, is given by

$$L = \sqrt{(\delta x)^2 + (\frac{\partial d_2}{dx}\,\delta x)^2} \qquad \text{(C2)}$$

$$= \delta x \sqrt{1 + (\frac{\partial d_2}{\partial x})^2} \qquad \text{(C3)}$$

$$\approx \delta x \qquad \text{(C4)}$$

therefore $\cos \alpha = \delta x / \delta x = 1$

For angle β

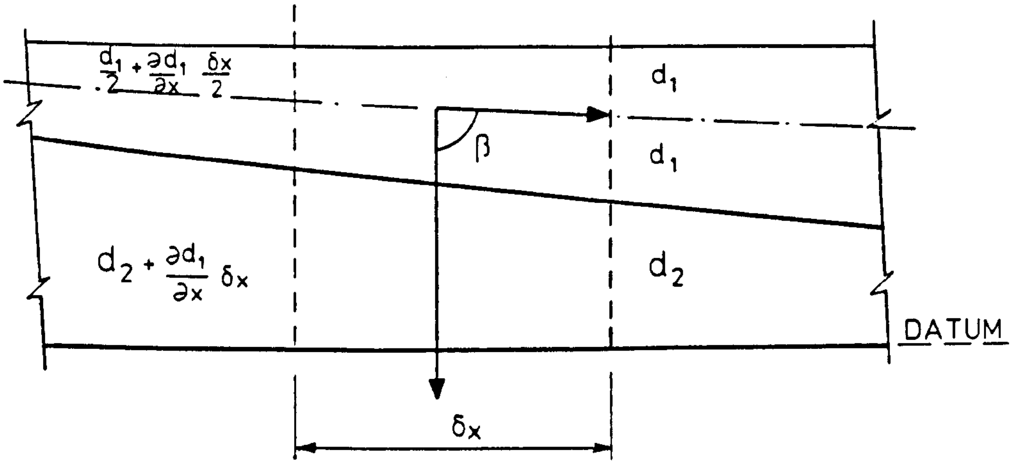

Figure C2

From datum the change in level of the central line of the upper layer is given by

$$\frac{d_1}{2} + \frac{\partial d_1}{\partial x} \frac{\delta x}{2} - \frac{d_1}{2} + d_2 + \frac{\partial d_2}{\partial x} \delta x - d_2 \tag{C5}$$

$$= \frac{1}{2} \frac{d\partial_1}{\partial x} \delta x + \frac{\partial d_2}{\partial x} \delta x \tag{C6}$$

$$L_2 = \sqrt{\delta x^2 + (\frac{1}{2} \frac{\partial d_1}{\partial x} \delta x + \frac{\partial d_2}{\partial x} \delta x)^2} \tag{C7}$$

$$L_2 \approx \delta x \tag{C8}$$

$$\cos \beta = \frac{1}{2} \frac{\partial d_1}{\partial x} + \frac{\partial d_2}{\partial x} \tag{C9}$$

APPENDIX D

COMPUTER PROGRAMS

Program 1 - FINDIF VFORTRAN: this calculates the effects of wave action on an open ended outfall pipe.

FINDIF VFORTRAN uses the Runge-Kutta forward integration method to analyse the problem of a single port outfall. The aim of the program is to calculate the surge in the screen structure and the velocity within the pipe as a wave passes over the open end of the outfall. The initial stage of the program requires information regarding the physical properties of the outfall and the receiving water. Hence the information required is the outfall cross-sectional area, $A\varphi$, the area of the surge tank, A1, the area of the open end of the outfall, A2, the length of the outfall, ZL, the roughness of the outfall pipe, ROV, the constant flow rate into the outfall surge tank, Q2, the height of the waves, H2, the time period of the waves, T, and the diameter of the main outfall pipe, D. The constant flow rate passing into the outfall screen structure represents the flow rate passing from an outfall headworks into the head of a prototype outfall. The program then requests the step length of the computation, DT, and the total time of the outfall flow simulation. As mentioned in Chapter 3 it was found that the value of the time step has to be kept between $^1/_5$ and $^1/_{10}$ of the ambient wave period.

The program first computes constants to be used within the main calculations, it calls subroutine FRIFAC which determines the friction factor using the Colebrook-White equation for the particular flow rate given, this is then assumed to be constant for the main calculations. The other constants calculated are

$$ZK = \left(\frac{fL}{D} + \left(\frac{A_0^{\,2}}{A_2^{\,2}}\right)\right)$$

$$F1 = \frac{A_0 \times k}{2 \times L \times A1}$$

$$F2 = \frac{A_1}{A_0}$$

$$F3 = \frac{g\ A_0}{L \times A_1}$$

$$F4 = \frac{g\ A_2\ H_2}{2L\ A_1}$$

and $$YT = \frac{2k\ V_0^{\,2}}{2g}$$

The symbol definitions are given in the format, they are found in Chapter 3. YT is the value of the level of water within the inlet structure which would enable flow Q to pass down the pipe under steady state conditions (i.e. zero wave action). This represents the head required for the flow to overcome friction within the pipe and produce a velocity V_0.

The initial boundary conditions are set such that the level of water in the surge tank equals YT and the flow rate through the outfall equals V_o. The main calculations are then performed using the Runge-Kutta integration routines given in Chapter 3.

At each computation point (time step Δt) the values of the velocity of surge and height of surge within the screen structure are output along with the velocity of flow within the pipe. A flow diagram for this computational routine and a listing of the computer program are given on the proceeding pages.

Typical output is shown in the paper entitled "Investigation of Wave Induced Oscillations in Sewage Outfalls" in appendix F.

FINDIF VFORTRAN - Flow diagram

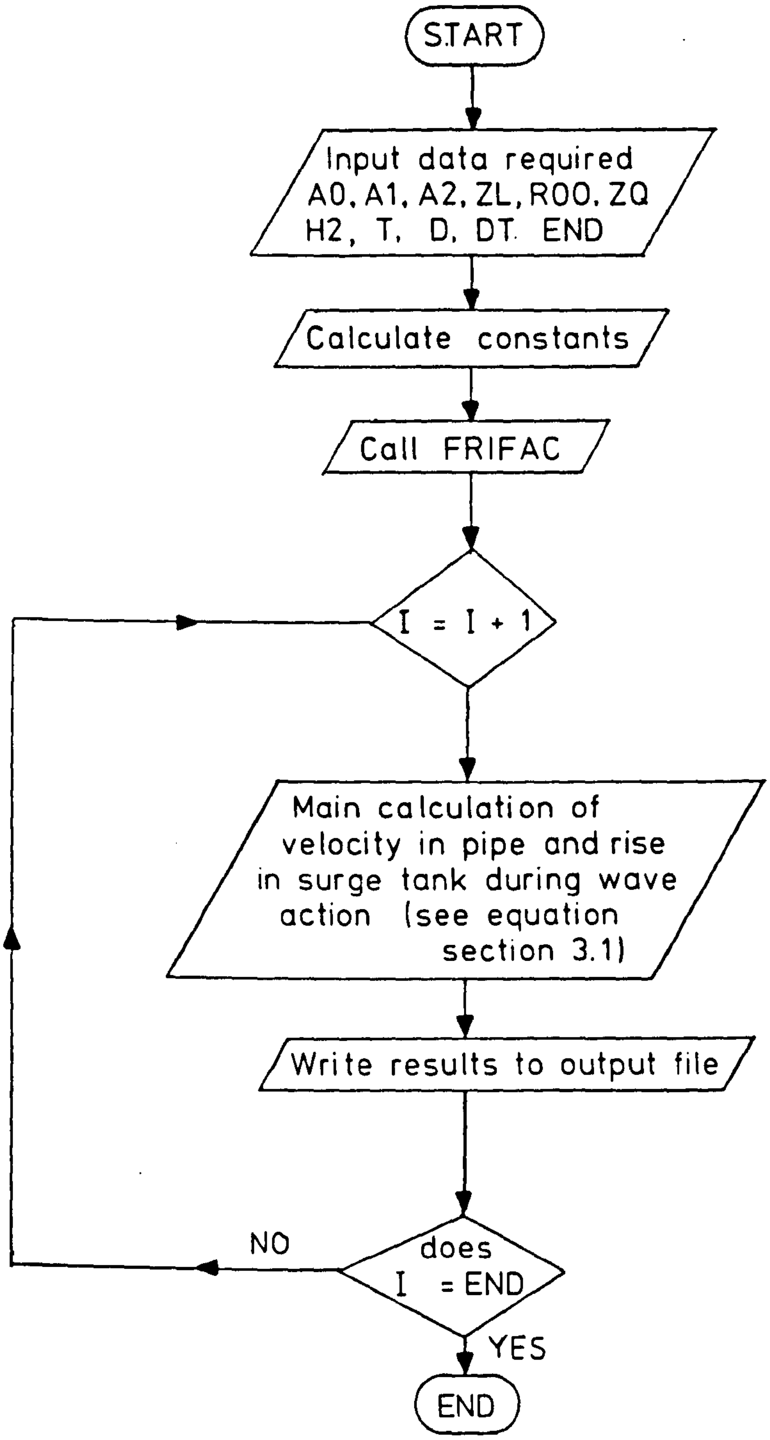

```
C     ******************************************************************
C     *                                                                *
C     *    THIS PROGRAM, "FINDIF FORTRAN" ,USES RUNGE                  *
C     *    KUTTA FORWARD INTEGRATION TO CALCULATE THE                  *
C     *    EFFECTS WAVE ACTION ON THE UPSTREAM END OF                  *
C     *    AN OUTFALL.                                                 *
C     *                                                                *
C     *    THE PROGRAM CALCULATES THE SURGE WITHIN THE                 *
C     *    SCREEN STRUCTURE,THE SURGE VELOCITY AND THE                 *
C     *    PIPE VELOCITY.                                              *
C     *                                                                *
C     ******************************************************************

C     A0=AREA OF OUTFALL
C     A1=AREA OF SCREEN ,STRUCTURE
C     A2=AREA OF RISER PORT
C     ZL=LENGTH OF OUTFALL
C     FF=PIPE FRICTION FACTOR
C    ROU=PIPE ROUGHNESS IN METRES
C     ZQ=FLOW IN CUMECS INTO SCREEN STRUCTURE
C      H=WAVE HEIGHT
C      T=TIME PERIOD OF WAVES
C      D=OUTFALL DIAMETER
C     DT=TIME STEP
C    END=FINAL TIME
C      U=VELOCITY OF SURGE WITHIN SCREEN STRUCTURE
C     GG=ACCN. DUE TO GRAVITY
C      Y=VALUE OF SURGE
C     DY=CHANGE IN SURGE

C     *****"INPUT VALUES REQUIRED TO RUN PROGRAM"***********
      WRITE(6,1)
    1 FORMAT(43H INITIAL VALUES OF A0,A1,A2,ZL,ROU,ZQ,H,T,D)
      READ(3,*)A0,A1,A2,ZL,ROU,ZQ,H2,T,D
      WRITE(6,2)
    2 FORMAT(40H INPUT VALUES OF STEP LENGTH & END VALUE)
      READ(5,*)DT,END


C     *****"CALCULATE CONSTANTS "****************************
      II=INT(END/DT)
      PI=4.0*ATAN(1.0)
      GG=9.81
      V0=ZQ/A0
      P=PI*D
      T2=0.0
      CALL FRIFAC(ROU,D,V0,A0,P,T2,FF)
      WRITE(6,*)FF
      ZK=(FF*ZL/D)+((A0**2.0)/(A2**2.0))
      F1=(A0*ZK)/(2.0*ZL*A1)
      F2=A1/A0
      F3=(GG*A0)/(ZL*A1)
      F4=(GG*A0*H2)/(2.0*ZL*A1)
      YT=(ZK*(V0**2.0))/(2.0*GG)


C     *****"BOUNDARY CONDITIONS"****************************
      T2=0.0
      Y=YT
      I=0
      DY=0.0
      U=0.0
      WRITE(9,16)ZL
   16 FORMAT(19H LENGTH OF OUTFALL=,F8.3,7H METRES)
      WRITE(9,17)H2
   17 FORMAT(19H DESIGN WAVEHEIGHT=,F5.3,7H METRES)
```

```
      WRITE(9,25)
   25 FORMAT(' INITIAL VALUES OF I,T2,U,Y,V0 ')
      WRITE(9,10)I,T2,U,Y,V0
      WRITE(9,24)
   24 FORMAT(' ****************************************************** ')
      WRITE(9,29)
   29 FORMAT(4X,1HI,6X,4HTIME,5X,8HVEL. OF ,2X,
     &10H VALUE OF ,7X,8H VEL. IN)
      WRITE(9,299)
  299 FORMAT(21X,5HSURGE,5X,11HOSCILLATION,7X,4HPIPE)

C     *****"MAIN CALCULATION"************************************
      DO 3 I=1,II
      ZK1=((DT**2)/2.0)*(F1*(V0-F2*DY)*ABS(V0-F2*DY)+F4*SIN(2.0*PI*T2/
     &)-F3*Y)
      ZK2=((DT**2)/2.0)*(F1*(V0-F2*(DY+ZK1/DT))*ABS(V0-F2*(DY+ZK1/DT))
     &+F4*SIN(2.0*PI*(T2+DT/2.0)/T)-(F3*(Y+DT*DY/2.0+ZK1/4.0)))
      ZK3=((DT**2)/2.0)*(F1*(V0-F2*(DY+ZK2/DT))*ABS(V0-F2*(DY+ZK2/DT))
     &+F4*SIN(2.0*PI*(T2+DT/2.0)/T)-(F3*(Y+DT*DY/2.0+ZK1/4.0)))
      ZK4=((DT**2)/2.0)*(F1*(V0-F2*(DY+2.0*ZK3/DT))*ABS(V0-F2*(DY+2.0*
     &ZK3/DT))+F4*SIN(2.0*PI*(T2+DT)/T)-(F3*(Y+DT*DY+ZK3)))
      DH=(ZK1+ZK2+ZK3)/3.0
      DDH=(ZK1+2.0*ZK2+2.0*ZK3+ZK4)/(3.0*DT)
      Y=Y+(DT*DY)+DH
      DY=DY+DDH
      U=DY
      VP=(ZQ-(A1*U))/A0
      Q9=VP*A0
      WRITE(9,10)I,T2,U,Y,VP
   10 FORMAT(I5,1X,F10.5,2X,F10.7,3X,F10.7,5X,F10.7)
      WRITE(10,56)Y
   56 FORMAT(F10.5)
      WRITE(11,56)T2
      T2=T2+DT
    3 CONTINUE
      STOP
      END
      SUBROUTINE FRIFAC(ROW,D,U,UA,P,T2,AY)
C     THIS SUBROUTINE USES THE COLEBROOK-WHITE EQN. TO CALCULATE
C     THE FRICTION FACTOR FOR FLOWING LAYER, NOT INTERFACE.
C     ROW=PIPE ROUGHNESS,D=PIPE DIAMETER,U=VELOCITY
C     UA=AREA,P=PERIMETER,T2=INTERFACE BETWEEN 2 LAYERS,
C     AY=CALCULATED FRICTION FACTOR
      DIMENSION ZU(2000)
      RR=UA/(P+T2)
      REN=4.0*U*RR/1.1E-06
      DO 10 JJ=1,2000
      ZU(JJ)=0.0
   10 CONTINUE
      ZUU=0.0
      I=0
      AA=0.0
      ZUL=0.0
      ZKK=0.0
      I=1
      ZU(1)=0.0
      ZU(2)=5.0
   20 I=I+1
      AA=ZU(I)
      ZX=-2.0*LOG10((ROW/(14.83*RR))+(2.51/(REN*SQRT(AA))))
      ZY=1.0/(SQRT(AA))
      ZKK=ZX-ZY
      IF(ZKK.LE.0.1E-12.AND.ZKK.GE.-0.1E-12)GOTO 30
      IF(ZKK.GT.0.0)GOTO 40
      IF(ZKK.LE.0.0)GOTO 50
```

```
40 ZUU=ZU(I)                                                          FIN01330
   ZU(I+1)=(ZUU+ZUL)/2.0                                              FIN01340
   GOTO 20                                                            FIN01350
50 ZUL=ZU(I)                                                          FIN01360
   ZU(I+1)=(ZUU+ZUL)/2.0                                              FIN01370
   GOTO 20                                                            FIN01380
30 AY=AA                                                              FIN01390
   RETURN                                                             FIN01400
   END                                                                FIN01410
```

Program 2 - FINDIF2 VFORTRAN

FINDIF2 VFORTRAN uses Escandés finite difference method to analyse the problems when wave action acts on a single port outfall. The aims of the program and the information required are the same as for FINDIF VFORTRAN. The flow diagram is also the same as that for FINDIF VFORTRAN.

```
C     ***********************************************************
C     *                                                         *
C     *    THIS PROGRAM, "FINDIF2 FORTRAN" USES ESCANDES        *
C     *    FINITE DIFFERENCE METHOD TO CALCULATE THE            *
C     *    EFFECTS WAVE ACTION ON THE UPSTREAM END OF           *
C     *    AN OUTFALL.                                          *
C     *                                                         *
C     *    THE PROGRAM CALCULATES THE SURGE WITHIN THE          *
C     *    SCREEN STRUCTURE,THE SURGE VELOCITY AND THE          *
C     *    PIPE VELOCITY.                                       *
C     *                                                         *
C     ***********************************************************

C     A0=AREA OF OUTFALL
C     A1=AREA OF SCREEN STRUCTURE
C     A2=AREA OF RISER PORT
C     ZL=LENGTH OF OUTFALL
C     FF=PIPE FRICTION FACTOR
C     ZQ=FLOW IN CUMECS INTO SCREEN STRUCTURE
C      H=WAVE HEIGHT
C      T=TIME PERIOD OF WAVES
C      D=OUTFALL DIAMETER
C     DT=TIME STEP
C    END=FINAL TIME
C      U=VELOCITY OF SURGE WITHIN SCREEN STRUCTURE
C     GG=ACCN. DUE TO GRAVITY
C      Y=VALUE OF SURGE
C     DY=CHANGE IN SURGE

C     *****"INPUT VALUES REQUIRED TO RUN PROGRAM"***********
      DIMENSION AQ(7)
      WRITE(6,1)
    1 FORMAT(43H INITIAL VALUES OF A0,A1,A2,ZL,ROU,ZQ,H,T,D)
      READ(3,*)A0,A1,A2,ZL,ROU,H2,T,D
      READ(4,*)(AQ(I),I=1,1)
      WRITE(6,2)
    2 FORMAT(40H INPUT VALUES OF STEP LENGTH & END VALUE)
      READ(5,*)DT,END


C     *****"CALCULATE CONSTANTS "****************************
      DO 100 JI=1,7
      ZQ=AQ(JI)
      II=INT(END/DT)
      PI=4.0*ATAN(1.0)
      GG=9.81
      V0=ZQ/A0
      P=PI*D
      T2=0.0
      CALL FRIFAC(ROU,D,V0,A0,P,T2,FF)
      WRITE(6,*)FF
C     ZK=(FF*ZL/D)+((A0**2.0)/(A2**2.0))
      ZK=(FF*ZL/D)+6
      F1=(A0*ZK)/(2.0*ZL*A1)
      F2=A1/A0
      F3=(GG*A0)/(ZL*A1)
      F4=(GG*A0*H2)/(2.0*ZL*A1)
      YT=(ZK*(V0**2.0))/(2.0*GG)

C     *****"BOUNDARY CONDITIONS"*****************************
      T2=0.0
      Y=YT
      I=0
      DU=0.0
      DY=0.0
      U=0.0
```

```
      WRITE(9,16)ZL
   16 FORMAT(19H LENGTH OF OUTFALL=,F8.3,7H METRES)
      WRITE(9,17)H2
   17 FORMAT(19H DESIGN WAVEHEIGHT=,F5.3,7H METRES)
      WRITE(9,25)
   25 FORMAT(' INITIAL VALUES OF I,T2,U,Y,VO ')
      WRITE(9,10)I,T2,U,Y,VO
      WRITE(9,24)
   24 FORMAT(' ************************************************** ')
      WRITE(9,29)
   29 FORMAT(4X,1HI,6X,4HTIME,5X,8HVEL. OF ,2X,
     &10H VALUE OF ,7X,8H VEL. IN)
      WRITE(9,299)
  299 FORMAT(21X,5HSURGE,5X,11HOSCILLATION,7X,4HPIPE)

C     *****"MAIN CALCULATION"**********************************
      DO 3 I=1,II
      DU=F1*(VO-(F2*U))*ABS(VO-(F2*U))*DT-F3*Y
     &*DT+F4*SIN(2.0*PI*T2/T)*DT
      WRITE(12,*)I,DU
      U=U+DU
      WH=H2*SIN(2.0*PI*T2/T)
      WRITE(35,56)WH
      VP=(ZQ-(A1*U))/A0
      DY=U*DT
      Y=Y+DY
      Q9=VP*A0
C     ABB=VP/VO
C     ABC=Y/YT
      WRITE(9,10)I,T2,U,Y,VP
   10 FORMAT(I5,1X,F10.5,2X,F10.7,3X,F10.7,5X,F10.7)
      WRITE(10,56)Y
   56 FORMAT(F10.5)
      WRITE(11,56)T2
      T2=T2+DT
    3 CONTINUE
  100 CONTINUE
      STOP
      END
      SUBROUTINE FRIFAC(ROW,D,U,UA,P,T2,AY)
C     THIS SUBROUTINE USES THE COLEBROOK-WHITE EQN. TO CALCULATE
C     THE FRICTION FACTOR FOR FLOWING LAYER, NOT INTERFACE.
C     ROW=PIPE ROUGHNESS,D=PIPE DIAMETER,U=VELOCITY
C     UA=AREA,P=PERIMETER,T2=INTERFACE BETWEEN 2 LAYERS,
C     AY=CALCULATED FRICTION FACTOR
      DIMENSION ZU(2000)
      RR=UA/(P+T2)
      REN=4.0*U*RR/1.1E-06
      DO 10 JJ=1,2000
      ZU(JJ)=0.0
   10 CONTINUE
      ZUU=0.0
      I=0
      AA=0.0
      ZUL=0.0
      ZKK=0.0
      I=1
      ZU(1)=0.0
      ZU(2)=5.0
   20 I=I+1
      AA=ZU(I)
      ZX=-2.0*LOG10((ROW/(14.83*RR))+(2.51/(REN*SQRT(AA))))
      ZY=1.0/(SQRT(AA))
      ZKK=ZX-ZY
      IF(ZKK.LE.0.1E-12.AND.ZKK.GE.-0.1E-12)GOTO 30
      IF(ZKK.GT.0.0)GOTO 40
```

```
      IF(ZKK.LE.0.0)GOTO 50
   40 ZUU=ZU(I)
      ZU(I+1)=(ZUU+ZUL)/2.0
      GOTO 20
   50 ZUL=ZU(I)
      ZU(I+1)=(ZUU+ZUL)/2.0
      GOTO 20
   30 AY=AA
      RETURN
      END
```

Program 3 - SALWED VFORTRAN: Calculates length and profiles of saline wedges.

SALWED VFORTRAN uses a finite difference method to determine the shape characteristics and length of a saline wedge within an open ended outfall pipe using the theory derived in section 3. The program calculates the characteristics of the wedge for four different sets of conditions covering changes in pipe slope, flow rate, pipe roughness and interfacial friction factor coefficients. The program loops through each of these in the sequence given above.

It initially reads in data from one of the data files which contains the information regarding either flow rate, or pipe slope, or pipe roughness or interfacial friction coefficient and then reads in information regarding pipe diameter, density of receiving water, pipe length and sea water level. It then reads in the data for variables which remain constant for that particular calculation, i.e. if the data file being read was a series of different flow rates the constant values would be pipe roughness, slope and interfacial friction coefficient. Dimensionless parameters arising from the data are also computed for use in the graph plotting procedures.

Next the program asks the operator whether or not all the information from the calculations are to be put into the output file, if the operator types yes (i.e. types Y) all the information regarding velocity, wetted perimeters, shear stress values and other values used in the calculation are written to the output file.

The program then calls the subroutine FLOWD, which calculates the depth of fresh water at the outlet point, (the downstream end of the pipe) using the equations derived in section 3.2.5. This gives the boundary condition at the exit of the pipe and is the basis for the calculation. (This boundary condition is also determined by the Froude number as outlined in section 6.1.6.) Following the determination of the boundary condition the program enters subroutine STAT which uses a finite difference method to calculate the profile and length of the wedge within the outfall pipe. The calculations are performed by taking a constant value of Δd and obtaining the corresponding value of Δx for each step (see Figure 6.5).

Once this calculation has been performed subroutine INFO is called; this collects data from the calculation procedures and stores it in a series of arrays to enable plotting and other forms of output. If all the data has not been worked through the INFO returns to STAT which returns to the main program to obtain more data files; but if all the calculations have been completed the results are output in the form of graphical plots.

SALWED VFORTRAN -

Flow diagram

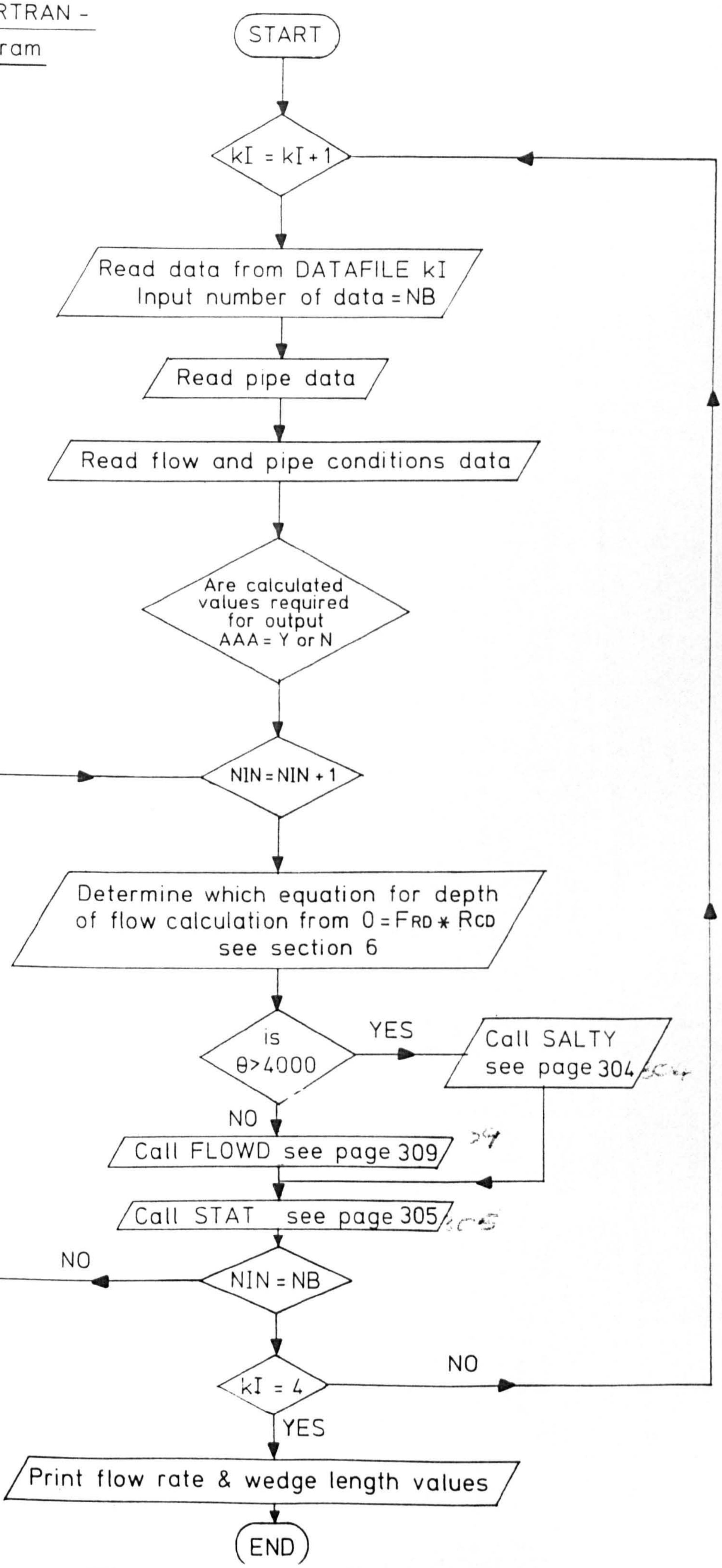

Subroutine SALTY

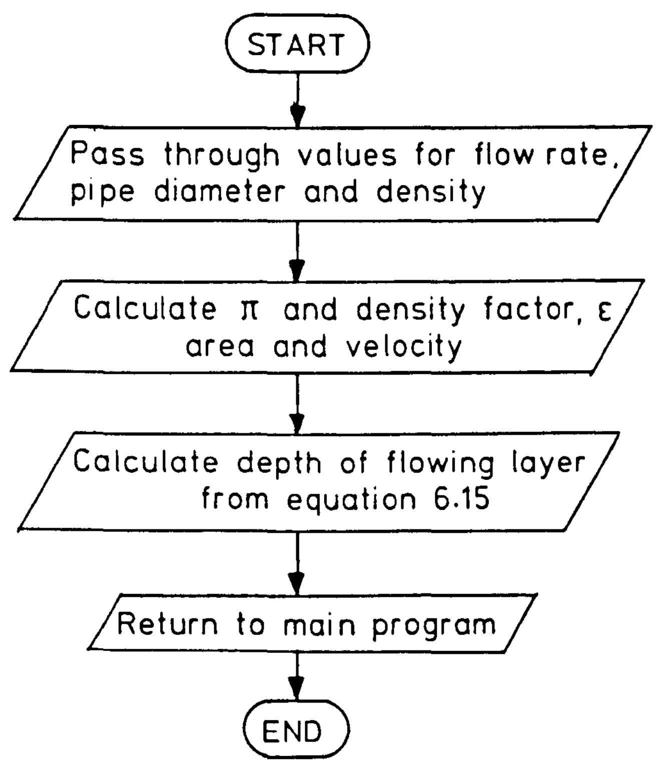

Subroutine STAT

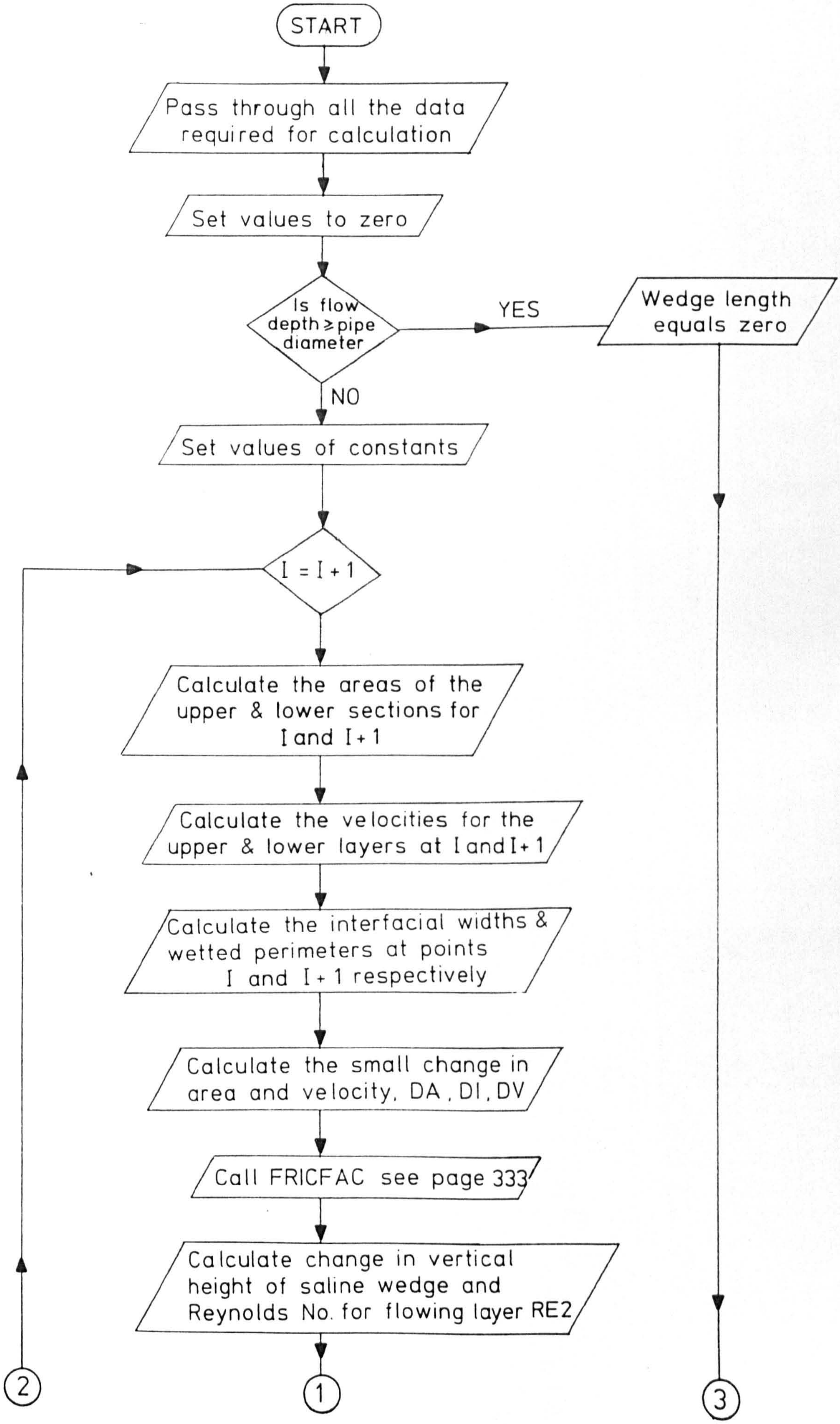

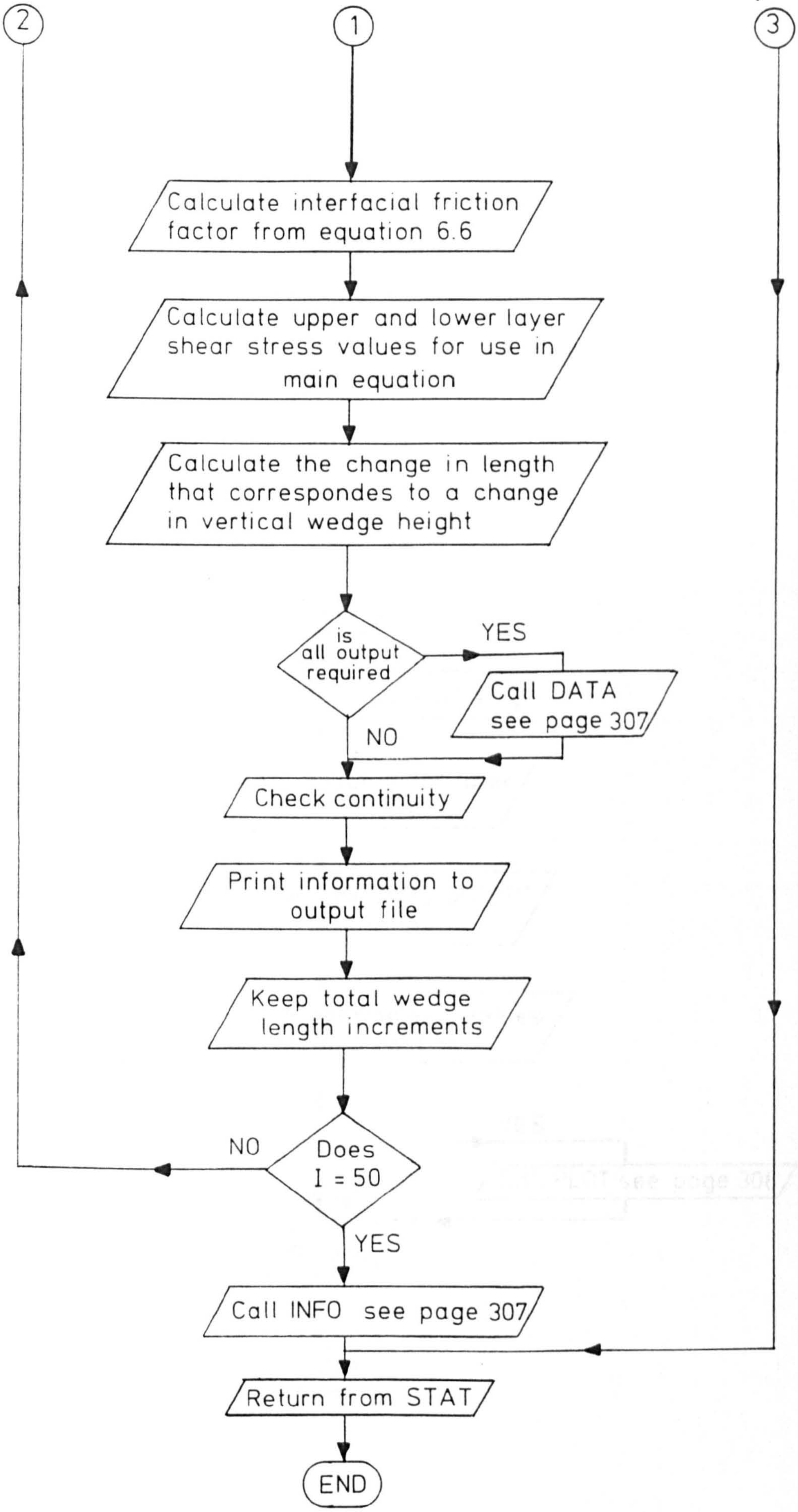
2
1
3
Calculate interfacial friction factor from equation 6.6
Calculate upper and lower layer shear stress values for use in main equation
Calculate the change in length that correspondes to a change in vertical wedge height
is all output required
YES
Call DATA see page 307
NO
Check continuity
Print information to output file
Keep total wedge length increments
NO
Does I = 50
YES
Call INFO see page 307
Return from STAT
END

Subroutine DATA

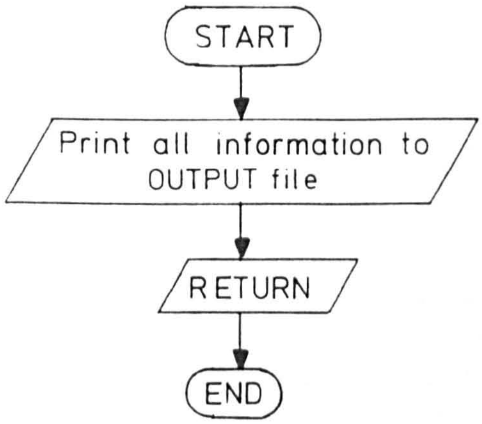

Subroutine INFO

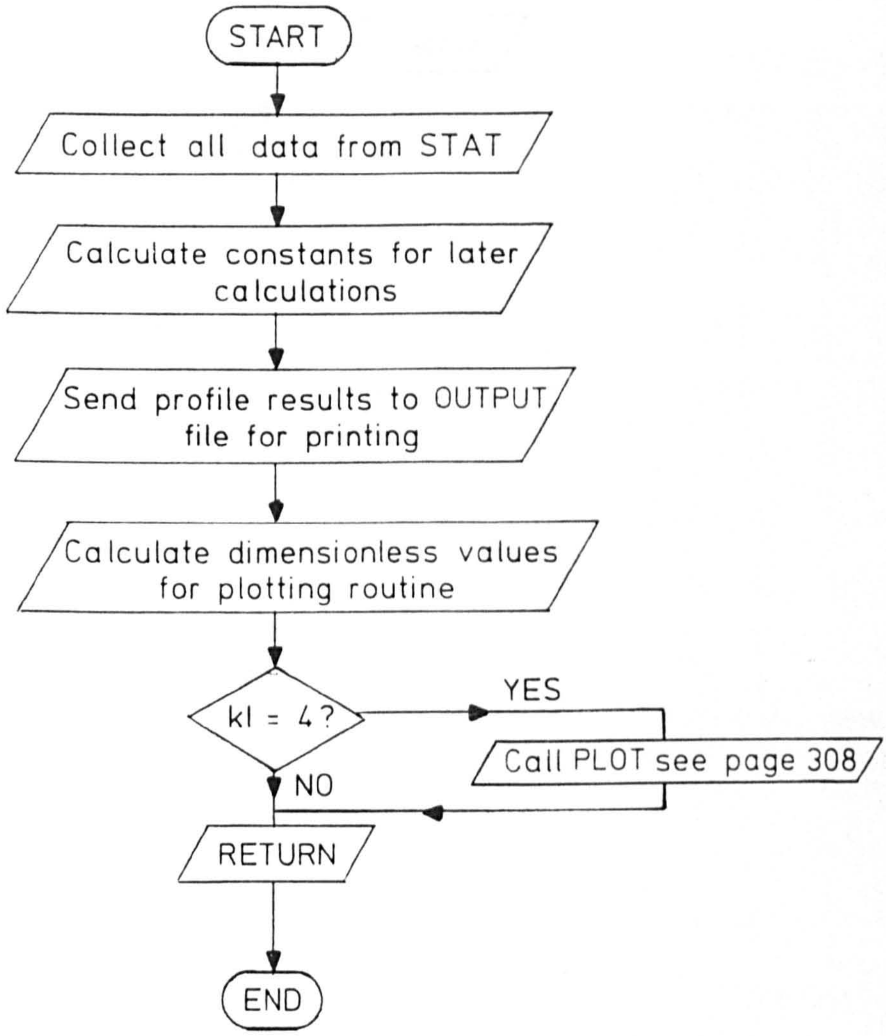

Subroutine PLOT

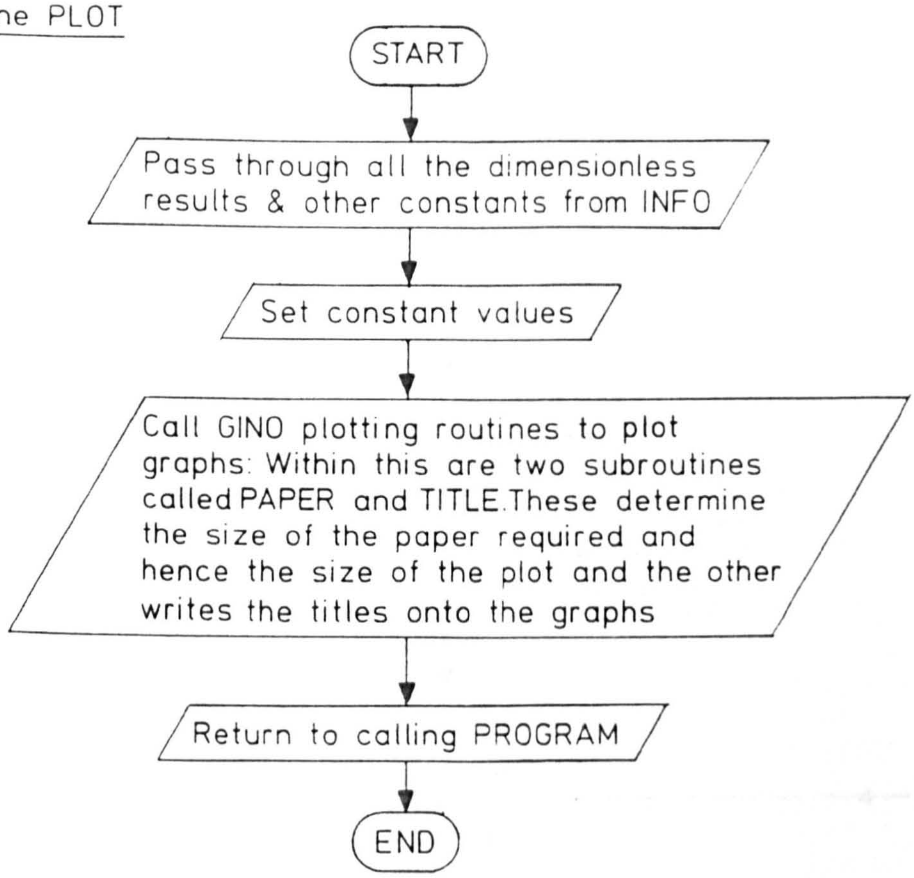

Subroutine FLOWD

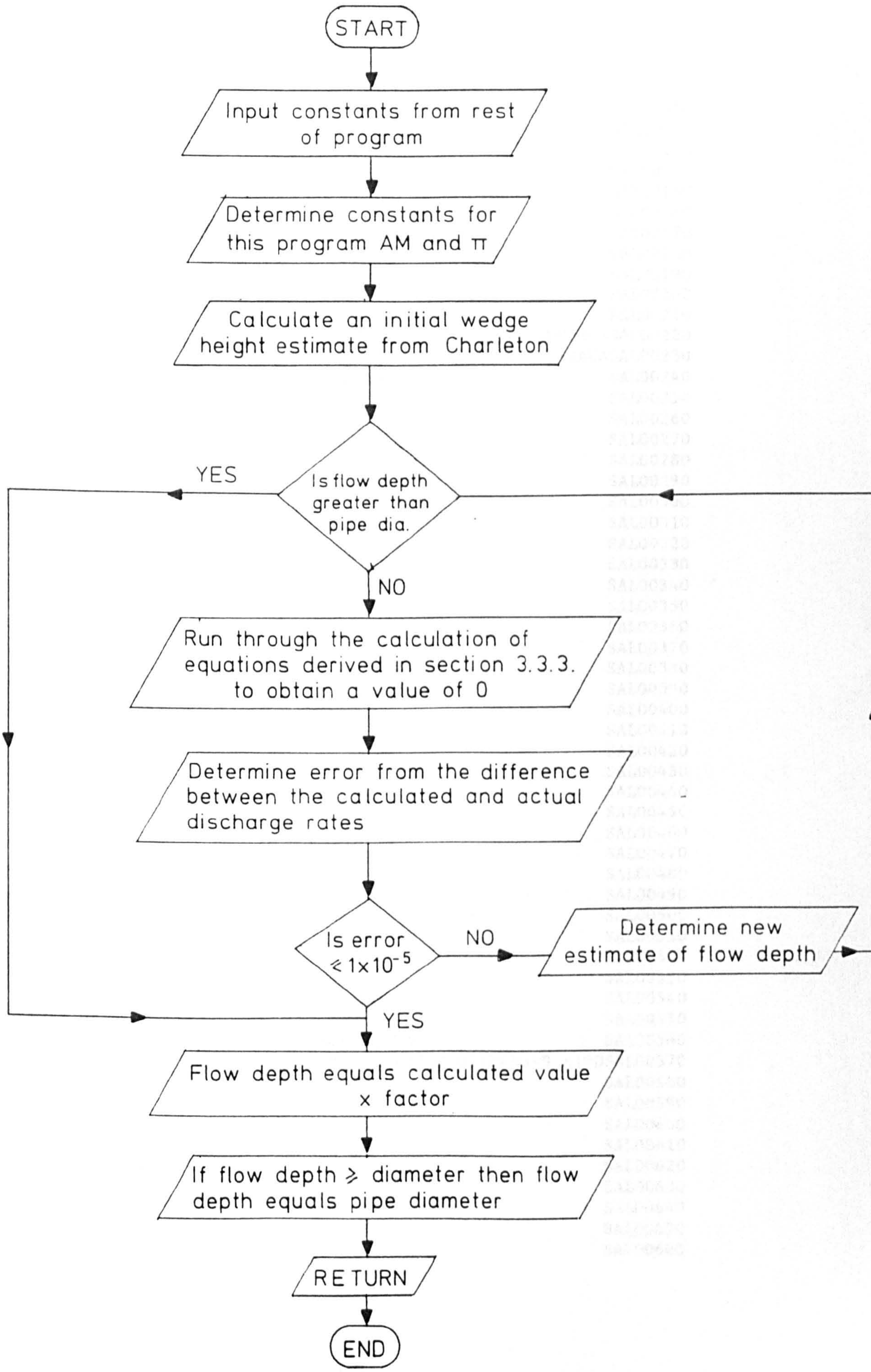

```
C       **************************************************
C       *                                                *
C       *     PROGRAM SALWED VFORTRAN CALCULATES         *
C       *     THE LENGTH OF A SALINE WEDGE WITHIN        *
C       *     EITHER A PIPE OR A RECTANGULAR OPEN        *
C       *     CHANNEL.                                   *
C       *                                                *
C       *     PLOTS 4 GRAPHS/PAGE                        *
C       **************************************************
C
C       Q=  FLOW RATE THROUGH PIPE
C       D=  PIPE DIAMETER
C       SZ= SLOPE OF PIPE
C       ZK= PIPE ROUGHNESS
C       ZL= PIPE LENGTH  .
C
        DIMENSION DD(20),Q(20),ZZZ(15),ZQ(20)
        CHARACTER*1 AAA
C       INPUT INITIAL VALUES
        CALL CLEAR
        WRITE(6,56)
   56   FORMAT(' INPUT FLOW(CUMECS),DIAMETER OF PIPE,SLOPE( ZERO=HORIZON
       &L,-VE=SLOPES UP FROM '/' LAND, +VE=SLOPES DOWN FROM LAND) ,SEAWA
       &R DENSITY,PIPE ROUGHNESS, AND '/' PIPELENGTH ')
        DO 998 KI=1,4
        READ(30+KI,*)NB
        READ(30+KI,*)(Q(NA),NA=1,NB)
        DO 1999 NZ=1,5
        NXY=NXY+1
        ZQ(NXY)=Q(NZ)
        WRITE(16,1974)
 1974   FORMAT(' ZQ(NXY),NXY AT START ')
        WRITE(16,*)ZQ(NXY),NXY
 1999   CONTINUE
        READ(4,*)DP,DEN,ZL,SWL
        ZZZ(1)=DP
        ZZZ(2)=DEN
        ZZZ(3)=ZL
        IF(KI.EQ.1)THEN
        PRINT*,' INPUT Q1,ZK '
        READ(5,*)Q1,ZK
        FFIT=0.316
        ZZZ(4)=Q1*1000.0
        ZZZ(5)=ZK
        ZZZ(6)=FFIT
        ELSE IF(KI.EQ.2)THEN
        PRINT*,' INPUT SO,ZK '
        READ(5,*)SO,ZK
        FFIT=0.316
        ZZZ(7)=SO
        ZZZ(8)=ZK
        ZZZ(9)=FFIT
C       CREATE DIMENSIONLESS FACTORS
        DO 5555 IL=6,10
        PI=4.0*ATAN(1.0)
        PRINT*,' IL=',IL,' ZQ(IL)=',ZQ(IL),' DEN=',DEN
        ZQ(IL)=(ZQ(IL)/(PI*(DP**2)/4.0))/(SQRT(((DEN-1000.0)/DEN)*9.81*D
       &)
        PRINT*,' DEN=',DEN,' ZQ(IL)=',ZQ(IL)
        WRITE(16,2648)
 2648   FORMAT(' ZQ(IL),IL AT 5555 ')
        WRITE(16,*)ZQ(IL),IL
 5555   CONTINUE
C
        ELSE IF(KI.EQ.3)THEN
        PRINT*,' INPUT SO,Q1 '
```

```
      READ(5,*)SO,Q1
      FFIT=0.316
      ZZZ(10)=SO
      ZZZ(11)=Q1*1000.0
      ZZZ(12)=FFIT
C     CREATE DIMENSIONLESS FACTORS
      DO 5556 KLM=11,15
      ZQ(KLM)=ZQ(KLM)/DP
      WRITE(16,1978)
 1978 FORMAT(' ZQ(KLM),KLM AT 5556 ')
      WRITE(16,*)ZQ(KLM),KLM
 5556 CONTINUE
      DO 5557 LG=1,20
      WRITE(16,*)LG,ZQ(LG)
 5557 CONTINUE
C
      ELSE IF(KI.EQ.4)THEN
      PRINT*,' INPUT SO,Q1,ZK '
      READ(5,*)SO,Q1,ZK
      ZZZ(13)=SO
      ZZZ(14)=Q1*1000.0
      ZZZ(15)=ZK
      ENDIF
  179 PI=4.0*ATAN(1.0)
      AZ=D
  281 I=0
      CALL CLEAR
      WRITE(6,87)
   87 FORMAT(' ARE VALUES OF FRICTION FACTORS, PERIMETERS ETC. REQD? ')
      READ(5,83)AAA
   83 FORMAT(A1)
      DO 78 NIN=1,NB
      IF(KI.EQ.1)THEN
      SO=Q(NIN)
      ELSE IF(KI.EQ.2)THEN
      Q1=Q(NIN)
      ELSE IF(KI.EQ.3)THEN
      ZK=Q(NIN)
      ELSE IF(KI.EQ.4)THEN
      FFIT=Q(NIN)
      ENDIF
      D=DP
      CALL FLOWD(Q1,DEN,D,SWL,AY)
      WRITE(16,7890)
 7890 FORMAT(' JUST BEFORE ENTERING STAT ')
      DO 7894 IKL=1,20
      WRITE(16,*)IKL,ZQ(IKL)
 7894 CONTINUE
      CALL STAT(Q1,D,SO,AY,DEN,ZK,D2,ZL,AAA,NB,NIN,Q,FFIT,ABB,ZZZ,KI,Z
     &,AY2)
      DD(NIN)=D2
   78 CONTINUE
  998 CONTINUE
      WRITE(7,71)
   71 FORMAT(17X,10H FLOW RATE,2X,13H WEDGE LENGTH)
      DO 72 IZ=1,NB
      IF(DD(IZ).LE.-ZL)GOTO 75
      WRITE(7,73)Q(IZ),DD(IZ)
   73 FORMAT(14X,F12.6,2X,F12.6)
      GOTO 72
   75 WRITE(7,88)Q(IZ)
   88 FORMAT(14X,F12.6,2X,'SALINE WEDGE > PIPE LENGTH ')
   72 CONTINUE
   99 STOP
      END
C
```

```
C
C     ***********************************************
C     *  SUBROUTINE STAT CALCULATES THE            *
C     *  LENGTH OF THE SALINE WEDGE IN A PIPE      *
C     ***********************************************
C
      SUBROUTINE STAT(Q1,D,SO,A1,DEN,ROU,D2,ZL,AAA,NB,NIN,Q
     &,FFIT,ABB,ZZZ,KI,ZQ,AY2)
      COMMON/DATA1/DPH1,DPH2,FF,FFI,TORIN,TORU,TOR
      COMMON/DATA2/TORB,TORA,DXU,DXL,UA1,ABC,U11
      COMMON/DATA3/DV,DAB,PE1,DX,T2,CHEC1,I
      DIMENSION BA(500),DF(500),AX(500),Q(20),ZZZ(15),ZQ(20)
      CHARACTER*1 AAA,ABB
      WRITE(16,1957)
 1957 FORMAT(' LQ,ZQ(LQ) AT START OF STAT ')
      DO 2514 LQ=1,20
      WRITE(16,*)LQ,ZQ(LQ)
 2514 CONTINUE
      DO 1 MM=1,51
      BA(MM)=0.0
  1   CONTINUE
      TORIN=0.0
      TORU=0.0
      J=0
      IF(A1.EQ.D)GOTO 6
      A2=D-A1
      YMAX=A2
      DA2=A2/51.0
      R=D/2.0
C     SET DELTA CHANGE IN DEPTH OF FLOWING LAYER
      DO 3 IJ=1,51
      BA(IJ)=D-A2
      IF(BA(IJ).GT.D)BA(IJ)=D
      A2=A2-DA2
  3   CONTINUE
      PI=4.0*ATAN(1.0)
      D2=0.0
      DX=0.0001
      WRITE(7,427)Q1,D,SO
 427  FORMAT(' Q1=',F12.6,' D=',F12.6,' SO=',F12.6)
      KA=0
      DO 4 I=1,50
      WRITE(7,431)I
 431  FORMAT(' I=',I3)
C     LEAVE LAST THREE SECTIONS AS THEY ARE UNSTABLE
C     UA1= AREA OF FLOWING LAYER AT POSITION I
C     UA2= AREA OF FLOWING LAYER AT POSITION I+1
      ABC=BA(I)
      UA1=((D)**2.0*2.0*ACOS((R-BA(I))/R)/8.0)-((D)**
     &2.0*SIN(2.0*ACOS((R-BA(I))/R))/8.0)
      UA2=((D)**2.0*2.0*ACOS((R-BA(I+1))/R)/8.0)-((D)**
     &2.0*SIN(2.0*ACOS((R-BA(I+1))/R))/8.0)
      AREAT=PI*(D**2)/4.0
      A21=AREAT-UA1
      A22=AREAT-UA2
      DA2=A21-A22
C     U11,U12= RESPECTIVE VELOCITIES AT SECTIONS I & I+1
      U11=Q1/UA1
      U12=Q1/UA2
      U21=0.0
      U22=0.0
      EPS=(DEN-1000.0)/DEN
      FRD=(Q1/AREAT)/SQRT(EPS*9.81*D)
      AYD=(D-BA(I))/2.0
C     T2,T3= RESPECTIVE INTERFACIAL WIDTHS AT SECTIONS I & I+1
      T2=2.0*(SQRT(R**2-(R-BA(I))**2))
```

```
      DEF=R**2-(R-BA(I+1))**2
      IF(DEF.LE.0.1E-10.AND.DEF.GE.-0.1E-10)DEF=0.0
      T3=2.0*(SQRT(DEF))
      DTT=T2-T3
C     PE1,PE2= RESPECTIVE PERIMETER LENGTHS AT SECTIONS I & I+1
      PE1=D*ACOS((R-BA(I))/R)
      PE2=D*ACOS((R-BA(I+1))/R)
      DPE=PE1-PE2
      AYP=(D-BA(I))/2.0
      DA=UA1-UA2
      DV=U11-U12
      DV2=U21-U22
C     FRIFAC CALCULATES WALL FRICTION FACTOR FOR FLOWING LAYER
      CALL FRIFAC(ROU,D,U11,UA1,PE1,T2,FF)
      DAB=BA(I)-BA(I+1)
      RE2=(4.0*U11/1.14E-06)*(UA1/(PE1+T2))
C     FFI= INTERFACIAL FRICTION FACTOR
      IF(FRD.LE.0.45)THEN
      NM=30
      ELSE
      NM=40
      ENDIF
      IF(I.LE.NM.OR.FRD.GE.0.5)THEN
      FFI=FFIT/(RE2**0.25)
      ELSE
      DDF=(REAL(I-NM)*0.5)+0.5
      FFI=DDF*FFIT/(RE2**0.25)
  209 ENDIF
      WRITE(7,679)FF,FFI
  679 FORMAT(' FF=',F10.6,' FFI=',F10.6)
      TORIN=FFI*((DEN+1000.0)/2.0)*U11*ABS(U11)/8.0
C     TORINL=0.0
      TORINL=FFI*((DEN+1000.0)/2.0)*(1.0*U11)*ABS(1.0*U11)/8.0
C     TORIN=0.0
C
      TORU=1.0*FF*1000.0*(U11)*ABS(U11)/8.0
      TORUW=1.0*FF*1000.0*(U11)*ABS(U11)/8.0
C     TOR= NONDIMENSIONAL SHEAR FACTOR
      TOR1=((TORU*(PE1+(DPE/1.0)))+(TORIN*(T2+DTT/1.0)))/(9810.0*UA2)
      TOR2=(TORINL*(T2+DTT/1.0))/(9810.0*A22)
 1256 WRITE(7,284)TOR1,TOR2,TOR3
  284 FORMAT(' TOR1=',F10.6,' TOR2=',F10.6,' TOR3=',F10.6)
      TORA=TORU*PE1
      TORB=TORIN*T2
      DAB2=DAB*(-1.0)
   10 DPH2=(-DAB2*DEN*9.81)-(9.81*DEN*SO*AT)
      DPH1=DPH2
      WA1=(U11/U12)**2
      DELTA=(1.0-(DEN/1000.0))*DAB2
      VELA=U11*DV*AAY/9.81
      AS=1.0-(DV/(1.0*U11))
      AS2=1.0+(DA2/(1.0*A22))
C
C
      AAY=1.0
      FAC=1.0
      DXU=(DAB*(1.0)/2.0)+((DEN/2000.0)*DAB2)+((DEN/2000.0)*AS2*DAB2)
     &-(0.5*AS*DAB)-(AS*DAB2)-(AAY*U11*DV/9.81)
C
      IF(DXU.GE.0.0.AND.KA.EQ.0)GOTO 235
      IF(DXU.GE.0.0)GOTO 234
      KA=KA+1
      GOTO 4
  234 DXL=TOR1+((DEN/1000.0)*TOR2)-((DEN/1000.0)*AS2*SO)+(AS*SO)
      KA=KA+1
      DX=DXU/DXL*(-15.0)
```

```
      DO 238 IK=1,KA
      AX(IK)=DX
      D2=D2+DX
      DF(IK)=D2
  238 CONTINUE
      KA=0
      GOTO 4
C
C     PRINT*,' DXU=',DXU
C
  235 HF=0.0
      DXL=TOR1+((DEN/1000.0)*TOR2)-((DEN/1000.0)*AS2*SO)+(AS*SO)
C     PRINT*,' DXL=',DXL
      DX=(DXU/DXL)/(-1.0)
      AX(I)=DX
      DENFR=U12/SQRT(((DEN-1000.0)/DEN)*9.81*(UA2/(PE2+T3)))
      DENFR2=U12/SQRT(((DEN-1000.0)/DEN)*9.81*BA(I+1))
      WRITE(7,437)DENFR,DENFR2
  437 FORMAT(' DENFR=',F12.6,' DENFR2=',F12.6)
      IF(AAA.EQ.'N')GOTO 89
      CALL DATA
C     CHECKS THE VALUE OF DX USING CONTINUITY
   89 CHEC1=(U11*DA/DX)+(UA1*DV/DX)
      IF(CHEC1.GE.0.00001.AND.CHEC1.LE.-0.00001)GOTO 9999
      WRITE(7,425)DXU,DXL,DX
  425 FORMAT(' DXU=',F12.6,1X,' DXL=',F12.6,1X,' DX=',F12.6)
      WRITE(7,424)UA1,UA2,T2
  424 FORMAT(' UA1=',F12.6,1X,' UA2=',F12.6,1X,' T2=',F12.6)
      WRITE(7,429)U11,U12,DV
  429 FORMAT(' U11=',F12.6,1X,' U12=',F12.6,1X,' DV=',F12.6)
      WRITE(7,433)AS,DAB,DEN
  433 FORMAT(' AS=',F12.6,1X,' DAB=',F12.6,1X,' DEN=',F12.6)
      WRITE(7,434)PE1,PE2
  434 FORMAT(' PE1=',F12.6,1X,' PE2=',F12.6)
      D2=D2+DX
      WRITE(7,428)D2
  428 FORMAT(' D2=',F12.6)
      DF(I)=D2
    4 CONTINUE
C     INFO CALCULATES THE NONDIMENSIONAL RESULTS
      CALL INFO(DF,BA,Q1,DEN,D,D2,AX,YMAX,NB,NIN,Q,ABB,ZZZ,KI,ZQ)
      GOTO 5
    6 D2=0.0
    5 RETURN
 9999 END

      SUBROUTINE FRIFAC(ROW,D,U,UA,P,T2,AY)
C     THIS SUBROUTINE USES THE COLEBROOK-WHITE EQN. TO CALCULATE
C     THE FRICTION FACTOR FOR FLOWING LAYER, NOT INTERFACE.
C     ROW=PIPE ROUGHNESS,D=PIPE DIAMETER,U=VELOCITY
C     UA=AREA,P=PERIMETER,T2=INTERFACE BETWEEN 2 LAYERS,
C     AY=CALCULATED FRICTION FACTOR
      DIMENSION ZU(2000)
      RR=UA/(P+T2)
      REN=1.0*U*RR/1.1E-06
C     IF(REN.LE.2100)GOTO 523
      DO 10 JJ=1,2000
      ZU(JJ)=0.0
   10 CONTINUE
      ZUU=0.0
      I=0
      AA=0.0
      ZUL=0.0
      ZKK=0.0
      I=1
      ZU(1)=0.0
```

```
      ZU(2)=5.0                                                         SAL03310
   20 I=I+1                                                             SAL03320
      AA=ZU(I)                                                          SAL03330
      ZX=-2.0*LOG10((ROW/(14.83*RR))+(2.51/(REN*SQRT(AA))))             SAL03340
      ZY=1.0/(SQRT(AA))                                                 SAL03350
      ZKK=ZX-ZY                                                         SAL03360
      IF(ZKK.LE.0.1E-12.AND.ZKK.GE.-0.1E-12)GOTO 30                     SAL03370
      IF(ZKK.GT.0.0)GOTO 40                                             SAL03380
      IF(ZKK.LE.0.0)GOTO 50                                             SAL03390
   40 ZUU=ZU(I)                                                         SAL03400
      ZU(I+1)=(ZUU+ZUL)/2.0                                             SAL03410
      GOTO 20                                                           SAL03420
   50 ZUL=ZU(I)                                                         SAL03430
      ZU(I+1)=(ZUU+ZUL)/2.0                                             SAL03440
      GOTO 20                                                           SAL03450
   30 AY=AA                                                             SAL03460
      GOTO 524                                                          SAL03470
C 523 AY=64.0/REN                                                       SAL03480
C     PRINT*,' AY=',AY                                                  SAL03490
 524  RETURN                                                            SAL03500
      END                                                               SAL03510
      SUBROUTINE DATA                                                   SAL03520
      COMMON/DATA1/DPH1,DPH2,FF,FFI,TORIN,TORU,TOR                      SAL03530
      COMMON/DATA2/TORB,TORA,DXU,DXL,UA1,ABC,U11                        SAL03540
      COMMON/DATA3/DV,DAB,PE1,DX,T2,CHEC1,I                             SAL03550
      WRITE(7,*)I                                                       SAL03560
      WRITE(7,51)CHEC1                                                  SAL03570
   51 FORMAT(' CHECK FOR CONTINUITY=',F12.7)                            SAL03580
      WRITE(7,9951)DPH1,DPH2                                            SAL03590
 9951 FORMAT('DPH1=',F10.6,'DPH2=',F10.6)                               SAL03600
 9952 WRITE(7,951)FF,FFI                                                SAL03610
 951  FORMAT( 'FF=',F10.7,2X,'FFI=',F10.7)                              SAL03620
      WRITE(7,998)TORIN,TORU,TOR                                        SAL03630
 998  FORMAT( 'TORIN=',F10.7,2X,'TORU=',F10.7,2X,'TOR=',F10.7)          SAL03640
      WRITE(7,997)TORB,TORA                                             SAL03650
 997  FORMAT( 'TORB=',F10.7,2X,'TORA=',F10.7)                           SAL03660
      WRITE(7,455)DXU,DXL,UA1                                           SAL03670
      WRITE(7,456)ABC,U11                                               SAL03680
      WRITE(7,457)DV,DAB,PE1                                            SAL03690
      WRITE(7,458)DX,T2,DPH1                                            SAL03700
 455  FORMAT( 'DXU=',F10.6,2X,'DXL=',F10.6,2X,'AREA=',F10.6)            SAL03710
 456  FORMAT( 'BA(I)=',F10.6,2X,'U11=',F10.6)                           SAL03720
 457  FORMAT( 'DV=',F10.6,2X,'DAB=',F10.6,2X,'PE1=',F10.6)              SAL03730
 458  FORMAT( 'DX=',F10.7,2X,'T2=',F10.7,2X,'DPH1=',F10.7)              SAL03740
      RETURN                                                            SAL03750
      END                                                               SAL03760
C                                                                       SAL03770
      SUBROUTINE INFO(DF,BA,Q1,DEN,D,D2,AX,YMAX,NB,NIN,Q,ABB,ZZZ,KI,ZQSAL03780
      DIMENSION DF(100),BA(100),AX(100),BD(100),AXX(100),AXK(20,60)     SAL03790
      DIMENSION XOL(20,60),YOD(20,60),YOY(20,60),Q(20),XOD(20,60)       SAL03800
      DIMENSION BDK(20,60),QQ(20),ZZZ(15),ZQ(20)                        SAL03810
      CHARACTER*1 ABB                                                   SAL03820
      VDEL=SQRT(((DEN-1000.0)/DEN)*9.81*D)                              SAL03830
      PI=4.0*ATAN(1.0)                                                  SAL03840
      VR=Q1/(PI*(D**2)/4.0)                                             SAL03850
      AVR=VR/VDEL                                                       SAL03860
      AMU=VDEL*D/1.14E-06                                               SAL03870
      ALD=D2/D                                                          SAL03880
      WRITE(7,234)                                                      SAL03890
  234 FORMAT('RESULTS')                                                 SAL03900
      WRITE(7,236)Q1                                                    SAL03910
  236 FORMAT('FLOW RATE= ',F10.6,'CUMECS')                              SAL03920
      IF(ABB.EQ.'S')GOTO 867                                            SAL03930
      WRITE(7,866)Q(NIN)                                                SAL03940
  866 FORMAT(' SLOPE OF PIPE=',F12.7)                                   SAL03950
  867 WRITE(7,53)YMAX                                                   SAL03960
```

```
   53 FORMAT(' AT X=0.0 WEDGE HEIGHT=',F12.6)
      WRITE(7,52)
   52 FORMAT('RESULTS FOR WEDGE PROFILE ')
      WRITE(7,237)
  237 FORMAT('DIST. FROM EXIT',5X,'WEDGE HEIGHT',10X,'DIFF')
      BD(1)=YMAX
      AXX(1)=0.0
      WRITE(7,238)AXX(1),BD(1),AX(1)
      DO 239 I=2,51
      AXX(I)=DF(I-1)
      BD(I)=D-BA(I)
      WRITE(7,238)AXX(I),BD(I),AX(I)
  238 FORMAT(F10.7,10X,F10.7,10X,F10.7)
  239 CONTINUE
      WRITE(7,553)
  553 FORMAT('DIMENSIONLESS RESULTS ')
      WRITE(7,240)
  240 FORMAT(6X,'Q',11X,'L/D',10X,'VR/VDEL',5X,'VDEL*D/MU')
      WRITE(7,242)Q1,ALD,AVR,AMU
  242 FORMAT(F10.6,4X,F10.6,4X,F10.6,4X,F10.4)
      NON=NIN+((KI-1)*5)
      PRINT*,' NON=',NON
      XOL(NON,1)=0.0
      YOD(NON,1)=YMAX/D
      YOY(NON,1)=1.0
      XOD(NON,1)=0.0
      AXK(NON,1)=0.0
      BDK(NON,1)=YMAX
      DO 563 JJ=2,51
      BDK(NON,JJ)=BD(JJ)
      AXK(NON,JJ)=AXX(JJ)*(-1.0)
      XOL(NON,JJ)=AXX(JJ)/D2
      YOD(NON,JJ)=BD(JJ)/D
      YOY(NON,JJ)=BD(JJ)/YMAX
      XOD(NON,JJ)=AXX(JJ)/(-D)
  563 CONTINUE
      IF(NIN.NE.NB)GOTO 9999
      IF(ABB.EQ.'S')GOTO 999
      DO 995 IJ=1,NB
      QQ(IJ)=Q(IJ)/SQRT(((DEN-1000.0)/DEN)*9.81*(D**5))
  995 CONTINUE
      IF(KI.NE.4)GOTO 9999
C     CALL PLOTTING ROUTINE
  999 CALL PLOT(XOD,XOL,YOD,YOY,NB,Q,AXK,BDK,QQ,ABB,ZZZ,ZQ)
 9999 RETURN
      END
      SUBROUTINE PLOT(XOD,XOL,YOD,YOY,NB,Q,AXK,BDK,QQ,ABB,ZZZ,ZQ)
C     THIS SUBROUTINE PLOTS THE GRAPHS OF RESULTS
C     BY THE SALINE WEDGE PROGRAM.
      DIMENSION XOL(20,60),YOD(20,60),YOY(20,60),XOD(20,60)
      DIMENSION X(60),Y(60),YYH(20,60),Q(20),XXH(20,60),KAK(4)
      DIMENSION BDK(20,60),AXK(20,60),QQ(20),ZZZ(15),ZQ(20)
      CHARACTER*1 ABB
      NN=51
      SS=0.0
      SSS=0.0
      AA=0.0
      CALL GINO
      CALL SAVDRA
C
C     GRAPH OF WEDGE HEIGHT AGAINST WEDGE LENGTH TO SHOW PROFILE
C
      CALL PAPER(AXILX,AXILY,TX,TY,ZX5,ZX6)
      CALL CHASIZ(2.0,2.0)
      NPIC=1
      CALL PICBEG(NPIC)
```

```
      DO 614 NY=1,4
      SS=0.0
      AA=0.0
      PRINT*,' NY=',NY
      DO 601 KJ=((NY-1)*5)+1,((NY-1)*5)+5
      DO 601 KL=1,51
      IF(SS.LE.AXK(KJ,KL))SS=AXK(KJ,KL)
      IF(AA.LE.BDK(KJ,KL))AA=BDK(KJ,KL)
  601 CONTINUE
      PRINT*,' SS=',SS
      IF(NY.EQ.1)THEN
      CALL AXIPOS(1,(TX+ZX5+ZX5),(TY+ZX6),AXILX/2.0,1)
      CALL AXIPOS(1,(TX+ZX5+ZX5),(TY+ZX6),AXILY/2.0,2)
      ELSE IF(NY.EQ.2)THEN
      CALL AXIPOS(1,(TX+ZX5+ZX5+AXILX/2.0+20.0),(TY+ZX6),AXILX/2.0,1)
      CALL AXIPOS(1,(TX+ZX5+ZX5+AXILX/2.0+20.0),(TY+ZX6),AXILY/2.0,2)
      ELSE IF(NY.EQ.3)THEN
      CALL AXIPOS(1,(TX+ZX5+ZX5),(TY+ZX6+AXILY/2.0+20.0),AXILX/2.0,1)
      CALL AXIPOS(1,(TX+ZX5+ZX5),(TY+ZX6+AXILY/2.0+20.0),AXILY/2.0,2)
      ELSE IF(NY.EQ.4)THEN
      CALL AXIPOS(1,(TX+ZX5+ZX5+AXILX/2.0+20.0),(TY+ZX6+AXILY/2.0+20.0
     &AXILX/2.0,1)
      CALL AXIPOS(1,(TX+ZX5+ZX5+AXILX/2.0+20.0),(TY+ZX6+AXILY/2.0+20.0
     &AXILY/2.0,2)
      ENDIF
      CALL AXISCA(1,10,0.0,SS,1)
      CALL AXIDRA(1,1,1)
      CALL AXISCA(3,5,0.0,AA,2)
      CALL AXIDRA(1,-1,2)
      III=1
      DO 620 II=((NY-1)*5)+1,((NY-1)*5)+5
      DO 610 JJ=1,51
      Y(JJ)=BDK(II,JJ)
      X(JJ)=AXK(II,JJ)
  610 CONTINUE
      SXA=0.0
      DO 625 JU=1,51
      SXA=SXA+X(JU)
 625  CONTINUE
      IF(SXA.LE.0.0)GOTO 620
      CALL GRASYM(X,Y,NN,III,10)
      CALL GRACUR(X,Y,NN)
      III=III+1
  620 CONTINUE
      XP=(TX+ZX5+ZX5+TX+ZX5+ZX5+AXILX)/2.0
      YP=(TY+ZX6+TY+ZX6+AXILY)/2.0
      CALL TITLE(ZQ,ZZZ,NY,AXILX,AXILY,TX,TY,ZX5,ZX6)
  614 CONTINUE
      CALL MOVTO2((TX+ZX5+AXILX/2.0),(TY-ZX6/3.0+4.0))
      CALL HERHOL(' X AXIS= WEDGE LENGTH, Y AXIS=WEDGE DEPTH*.',-1)
      CALL CHASIZ(3.0,3.0)
      CALL MOVTO2((TX+ZX5+AXILX/2.0),(TY-ZX6/3.0-4.0))
      CALL HERHOL(' GRAPH OF WEDGE PROFILES*.',-1)
      CALL PICEND
      CALL PICCLE
C
C     END OF PROFILE GRAPH
C
      CALL CLEAR
      PRINT*,' FOUR DIFFERENT TYPES OF DIMENSIONLESS PLOTS ARE '
      PRINT*,' AVAILABLE, THEY ARE '
      PRINT*,' 1) X/D  V.  Y/YMAX '
      PRINT*,' 2) X/D  V.  Y/D    '
      PRINT*,' 3) X/L  V.  Y/YMAX '
      PRINT*,' 4) X/L  V.  Y/D    '
      PRINT*,' 0) NONE OF THESE   '
```

```
      PRINT*,' INPUT THE TOTAL NUMBER OF GRAPHS = '
      READ(3,*)NJI
      IF(NJI.EQ.0)GOTO 56
      PRINT*,' INPUT THE CORRESPONDING GRAPH NO. AS GIVEN ABOVE '
      DO 515 JMK=1,NJI
      PRINT*,' JMK=',JMK
      READ(3,*)KAK(JMK)
 515  CONTINUE
C
      DO 55 NYYY=1,NJI
      NYY=KAK(NYYY)
      PRINT*,' NYY=',NYY
      CALL PAPER(AXILX,AXILY,TX,TY,ZX5,ZX6)
      CALL CHASIZ(2.0,2.0)
      NPIC=NPIC+1
      PRINT*,' NPIC=',NPIC
      CALL PICBEG(NPIC)
      SSS=0.0
      AA=0.0
      IF(NYY.EQ.1)THEN
      DO 566 IU=1,20
      DO 566 JU=1,60
      XXH(IU,JU)=XOD(IU,JU)
      YYH(IU,JU)=YOY(IU,JU)
 566  CONTINUE
      ELSE IF(NYY.EQ.2)THEN
      DO 567 IU=1,20
      DO 567 JU=1,60
      XXH(IU,JU)=XOD(IU,JU)
      YYH(IU,JU)=YOD(IU,JU)
 567  CONTINUE
      ELSE IF(NYY.EQ.3)THEN
      DO 568 IU=1,20
      DO 568 JU=1,60
      XXH(IU,JU)=XOL(IU,JU)
      YYH(IU,JU)=YOY(IU,JU)
 568  CONTINUE
      ELSE IF(NYY.EQ.4)THEN
      DO 569 IU=1,20
      DO 569 JU=1,60
      XXH(IU,JU)=XOL(IU,JU)
      YYH(IU,JU)=YOD(IU,JU)
 569  CONTINUE
      ENDIF
      DO 987 NYZ=1,4
      SSS=0.0
      AA=0.0
      DO 201 IJ=((NYZ-1)*5)+1,((NYZ-1)*5)+5
      DO 201 IK=1,51
      IF(XXH(IJ,IK).GT.SSS)SSS=XXH(IJ,IK)
      IF(YYH(IJ,IK).GT.AA)AA=YYH(IJ,IK)
  201 CONTINUE
C
      IF(NYZ.EQ.1)THEN
      CALL AXIPOS(1,(TX+ZX5+ZX5),(TY+ZX6),AXILX/2.0,1)
      CALL AXIPOS(1,(TX+ZX5+ZX5),(TY+ZX6),AXILY/2.0,2)
      ELSE IF(NYZ.EQ.2)THEN
      CALL AXIPOS(1,(TX+ZX5+ZX5+AXILX/2.0+20.0),(TY+ZX6),AXILX/2.0,1)
      CALL AXIPOS(1,(TX+ZX5+ZX5+AXILX/2.0+20.0),(TY+ZX6),AXILY/2.0,2)
      ELSE IF(NYZ.EQ.3)THEN
      CALL AXIPOS(1,(TX+ZX5+ZX5),(TY+ZX6+AXILY/2.0+20.0),AXILX/2.0,1)
      CALL AXIPOS(1,(TX+ZX5+ZX5),(TY+ZX6+AXILY/2.0+20.0),AXILY/2.0,2)
      ELSE IF(NYZ.EQ.4)THEN
      CALL AXIPOS(1,(TX+ZX5+ZX5+AXILX/2.0+20.0),(TY+ZX6+AXILY/2.0+20.0
     &AXILX/2.0,1)
      CALL AXIPOS(1,(TX+ZX5+ZX5+AXILX/2.0+20.0),(TY+ZX6+AXILY/2.0+20.0
```

```
     &AXILY/2.0,2)
      ENDIF
      CALL AXISCA(1,10,0.0,SSS,1)
      CALL AXIDRA(1,1,1)
C
      CALL AXISCA(2,5,0.0,AA,2)
      CALL AXIDRA(1,-1,2)
C
      IIJ=1
C     PRINT*,' PLOTTING GRAPHS.'
      DO 300 II=((NYZ-1)*5)+1,((NYZ-1)*5)+5
      DO 200 JJ=1,51
      Y(JJ)=YYH(II,JJ)
      X(JJ)=XXH(II,JJ)
  200 CONTINUE
      SXA=0.0
      DO 245 JU=1,51
      SXA=SXA+X(JU)
 245  CONTINUE
      IF(SXA.LE.0.0)GOTO 300
      CALL GRASYM(X,Y,NN,IIJ,10)
      CALL GRACUR(X,Y,NN)
      IIJ=IIJ+1
  300 CONTINUE
C
      XP=(TX+ZX5+ZX5+TX+ZX5+ZX5+AXILX)/2.0
      YP=(TY+ZX6+TY+ZX6+AXILY)/2.0
C
      CALL TITLE(ZQ,ZZZ,NYZ,AXILX,AXILY,TX,TY,ZX5,ZX6)
  987 CONTINUE
      IF(NYY.EQ.1)THEN
      CALL MOVTO2((TX+ZX5+AXILX/2.0+3.0),(TY-ZX6/3.0+4.0))
      CALL HERHOL(' X AXIS= X/D, Y AXIS=Y/YMAX*.',-1)
      CALL CHASIZ(3.0,3.0)
      CALL MOVTO2((TX+ZX5+AXILX/2.0),(TY-ZX6/3.0-4.0))
      CALL HERHOL(' X/D AGAINST Y/YMAX*.',-1)
C
      ELSE IF(NYY.EQ.2)THEN
      CALL MOVTO2((TX+ZX5+AXILX/2.0+3.0),(TY-ZX6/3.0+4.0))
      CALL HERHOL(' X AXIS= X/D, Y AXIS=Y/D*.',-1)
      CALL CHASIZ(3.0,3.0)
      CALL MOVTO2((TX+ZX5+AXILX/2.0),(TY-ZX6/3.0-4.0))
      CALL HERHOL(' X/D AGAINST Y/D*.',-1)
C
      ELSE IF(NYY.EQ.3)THEN
      CALL MOVTO2((TX+ZX5+AXILX/2.0+3.0),(TY-ZX6/3.0+4.0))
      CALL HERHOL(' X AXIS= X/L, Y AXIS=Y/YMAX*.',-1)
      CALL CHASIZ(3.0,3.0)
      CALL MOVTO2((TX+ZX5+AXILX/2.0),(TY-ZX6/3.0-4.0))
      CALL HERHOL(' X/L AGAINST Y/YMAX*.',-1)
C
      ELSE IF(NYY.EQ.4)THEN
      CALL MOVTO2((TX+ZX5+AXILX/2.0+3.0),(TY-ZX6/3.0+4.0))
      CALL HERHOL(' X AXIS= X/L, Y AXIS=Y/D*.',-1)
      CALL CHASIZ(3.0,3.0)
      CALL MOVTO2((TX+ZX5+AXILX/2.0),(TY-ZX6/3.0-4.0))
      CALL HERHOL(' X/L AGAINST Y/D*.',-1)
      ENDIF
      CALL PICEND
      CALL PICCLE
  55  CONTINUE
  56  CALL DEVEND
      END
      SUBROUTINE PAPER(AXILX,AXILY,TX,TY,ZX5,ZX6)
      CHARACTER*1 RR
C     DEFINES PAPER SIZE FOR GINO
```

```
      WRITE(6,10)
   10 FORMAT(49H DEFINE PAPER SIZE A0,A1,A2,A3,A4,OWN=0,1,2,3,4,5)
      READ(5,*)IN
      IF(IN.EQ.5) THEN
      WRITE(6,20)
   20 FORMAT(23H INPUT PAPER SIZE X & Y)
      READ(3,*)XX,YY
      ELSE
      IF(IN.EQ.0) THEN
      X=1188.0
      Y=840.0
      ELSE IF(IN.EQ.1) THEN
      X=840.0
      Y=594.0
      ELSE IF(IN.EQ.2) THEN
      X=594.0
      Y=420.0
      ELSE IF(IN.EQ.3) THEN
      X=420.0
      Y=297.0
      ELSE IF(IN.EQ.4) THEN
      X=297.0
      Y=210.0
      END IF
      WRITE(6,30)
   30 FORMAT(39H IS PAPER VERTICAL OR HORIZONTAL=V OR H)
      READ(5,40)RR
   40 FORMAT(A1)
      IF(RR.EQ.'H') THEN
      XX=X
      YY=Y
      ELSE
      XX=Y
      YY=X
      END IF
      END IF

C     DEFINE AREAS FOR WINDOW
      XN=XX+10.0
      YN=YY+10.0

      CALL DEVPAP(XX,YY,0.0)
      CALL WINDO2(0.0,XN,0.0,YN)


C     DEFINE DRAWING AREA
C     CALL MOVTO2(0.0,0.0)
C     CALL LINTO2(XX,0.0)
C     CALL LINTO2(XX,YY)
C     CALL LINTO2(0.0,YY)
C     CALL LINTO2(0.0,0.0)

      ZY1=YY*15.0/100.0
      ZY2=YY*8.0/100.0
      ZX1=YY*8.0/100.0
      ZX2=YY*2.0/100.0

      IF(RR.EQ.'V')GOTO 50

C     CALL MOVTO2(ZX1,ZY2)
C     CALL LINTO2(XX-ZX2,ZY2)
C     CALL LINTO2(XX-ZX2,YY-ZY1)
C     CALL LINTO2(ZX1,YY-ZY1)
C     CALL LINTO2(ZX1,ZY2)
      ZX6=ZX1
      ZX5=ZX1
```

```
      TX=ZX1
      TY=ZY2

      AXILX=(XX-ZX1-ZX2)*72.0/100.0
      AXILY=(YY-ZY1-ZY2)*66.0/100.0
      GOTO 60

   50 CALL MOVTO2(ZY1,ZX1)
      CALL LINTO2(XX-ZY2,ZX1)
      CALL LINTO2(XX-ZY2,YY-ZX2)
      CALL LINTO2(ZY1,YY-ZX2)
      CALL LINTO2(ZY1,ZX1)
      ZX6=ZX1
      ZX5=ZX22
      TX=ZY1
      TY=ZX1

      AXILX=(XX-ZY1-ZY2)*72.0/100.0
      AXILY=(YY-ZX1-ZX2)*66.0/100.0
   60 RETURN
      END
      SUBROUTINE TITLE(ZQ,ZZZ,NY,AXILX,AXILY,TX,TY,ZX5,ZX6)
      DIMENSION ZZZ(15),ZQ(20)
      CALL HERALF(3)
      IF(NY.EQ.1)THEN
      DO 1111 I=1,5
      N2=NY*I
      CALL MOVTO2((TX+ZX5+AXILX/2.0-3.0),(TY+ZX6-(FLOAT(I)*3.2)+1.0
     &+AXILY/3.0))
      CALL SYMBOL(I)
      CALL MOVTO2((TX+ZX5+AXILX/2.0-1.0),(TY+ZX6-(FLOAT(I)*3.2)
     &+AXILY/3.0))
      CALL CHASTR(' =')
      CALL MOVTO2((TX+ZX5+AXILX/2.0+1.0),(TY+ZX6-(FLOAT(I)*3.2)
     &+AXILY/3.0))
      CALL HERFIX(ZQ(N2),9,5)
 1111 CONTINUE
      DO 1112 II=1,6
      CALL MOVTO2((TX+ZX5+AXILX/2.0-19.0),(TY+ZX6+20.0-(FLOAT(II)*3.2)
     &+AXILY/3.0))
      IF(II.EQ.1)THEN
      CALL HERHOL(' DIAMETER=*.',-1)
      ELSE IF(II.EQ.2)THEN
      CALL HERHOL(' DENSITY=*.',-1)
      ELSE IF(II.EQ.3)THEN
      CALL HERHOL(' PIPE LEN=*.',-1)
      ELSE IF(II.EQ.4)THEN
      CALL HERHOL(' FLOW(L/S)=*.',-1)
      ELSE IF(II.EQ.5)THEN
      CALL HERHOL(' ROUGHNESS=*.',-1)
      ELSE IF(II.EQ.6)THEN
      CALL HERHOL(' FFC=*.',-1)
      ENDIF
      CALL MOVTO2((TX+ZX5+AXILX/2.0+1.0),(TY+ZX6+20.0-(FLOAT(II)*3.2)
     &+AXILY/3.0))
      CALL HERFIX(ZZZ(II),9,4)
 1112 CONTINUE
      CALL MOVTO2((TX+ZX5+ZX5+7.0),(TY+ZX6+AXILY/2.0+5.0))
      CALL HERHOL(' CHANGE IN SLOPE*.',-1)
C
      ELSE IF(NY.EQ.2)THEN
      DO 1113 I=1,5
      N2=((NY-1)*5)+I
      CALL MOVTO2((TX+ZX5+20.0+AXILX),(TY+ZX6-(FLOAT(I)*3.2)+1.0
     &+AXILY/3.0))
      CALL SYMBOL(I)
```

```
      CALL MOVTO2((TX+ZX5+20.0+AXILX+2.0),(TY+ZX6-(FLOAT(I)*3.2)
     &+AXILY/3.0))
      CALL HERHOL(' =*.',-1)
      CALL MOVTO2((TX+ZX5+20.0+AXILX+4.0),(TY+ZX6-(FLOAT(I)*3.2)
     &+AXILY/3.0))
      CALL HERFIX(ZQ(N2),9,5)
 1113 CONTINUE
      DO 1114 II=1,6
      CALL MOVTO2((TX+ZX5+AXILX+3.0),(TY+ZX6+20.0-(FLOAT(II)*3.2)
     &+AXILY/3.0))
      IF(II.EQ.1)THEN
      CALL HERHOL(' DIAMETER=*.',-1)
      NH=1
      ELSE IF(II.EQ.2)THEN
      CALL HERHOL(' DENSITY=*.',-1)
      NH=2
      ELSE IF(II.EQ.3)THEN
      CALL HERHOL(' PIPE LEN=*.',-1)
      NH=3
      ELSE IF(II.EQ.4)THEN
      CALL HERHOL(' SLOPE=*.',-1)
      NH=7
      ELSE IF(II.EQ.5)THEN
      CALL HERHOL(' ROUGHNESS=*.',-1)
      NH=8
      ELSE IF(II.EQ.6)THEN
      CALL HERHOL(' FFC=*.',-1)
      NH=9
      ENDIF
      CALL MOVTO2((TX+ZX5+20.0+AXILX+4.0),(TY+ZX6+20.0-(FLOAT(II)*3.2)
     &+AXILY/3.0))
      CALL HERFIX(ZZZ(NH),9,4)
 1114 CONTINUE
      CALL MOVTO2((TX+ZX5+ZX5+AXILX/2.0+27.0),(TY+ZX6+AXILY/2.0+5.0))
      CALL HERHOL(' CHANGE IN FLOW*.',-1)
C
      ELSE IF(NY.EQ.3)THEN
      DO 1115 I=1,5
      N2=((NY-1)*5)+I
      CALL MOVTO2((TX+ZX5+AXILX/2.0-5.0),(TY+ZX6-(FLOAT(I)*3.2)+1.0
     &+AXILY))
      CALL SYMBOL(I)
      CALL MOVTO2((TX+ZX5+AXILX/2.0-3.0),(TY+ZX6-(FLOAT(I)*3.2)
     &+AXILY))
      CALL HERHOL(' =*.',-1)
      CALL MOVTO2((TX+ZX5+AXILX/2.0+1.0),(TY+ZX6-(FLOAT(I)*3.2)
     &+AXILY))
      CALL HERFIX(ZQ(N2),9,4)
 1115 CONTINUE
      DO 1116 II=1,6
      CALL MOVTO2((TX+ZX5+AXILX/2.0-19.0),(TY+ZX6+20.0-(FLOAT(II)*3.2)
     &+AXILY))
      IF(II.EQ.1)THEN
      CALL HERHOL(' DIAMETER=*.',-1)
      NH=1
      ELSE IF(II.EQ.2)THEN
      CALL HERHOL(' DENSITY=*.',-1)
      NH=2
      ELSE IF(II.EQ.3)THEN
      CALL HERHOL(' PIPE LEN=*.',-1)
      NH=3
      ELSE IF(II.EQ.4)THEN
      CALL HERHOL(' SLOPE=*.',-1)
      NH=10
      ELSE IF(II.EQ.5)THEN
      CALL HERHOL(' FLOW=*.',-1)
```

```
      NH=11
      ELSE IF(II.EQ.6)THEN
      CALL HERHOL(' FFC=*.',-1)
      NH=12
      ENDIF
      CALL MOVTO2((TX+ZX5+AXILX/2.0+1.0),(TY+ZX6+20.0-(FLOAT(II)*3.2)
     &+AXILY))
      CALL HERFIX(ZZZ(NH),9,4)
 1116 CONTINUE
      CALL MOVTO2((TX+ZX5+ZX5+7.0),(TY+ZX6+AXILY/2.0+20.0+AXILY/2.0
     &+5.0))
      CALL HERHOL(' CHANGE IN ROUGHNESS*.',-1)
C
      ELSE IF(NY.EQ.4)THEN
      DO 1117 I=1,5
      N2=((NY-1)*5)+I
      CALL MOVTO2((TX+ZX5+20.0+AXILX),(TY+ZX6-(FLOAT(I)*3.2)+1.0
     &+AXILY))
      CALL SYMBOL(I)
      CALL MOVTO2((TX+ZX5+20.0+AXILX+2.0),(TY+ZX6-(FLOAT(I)*3.2)
     &+AXILY))
      CALL HERHOL(' =*.',-1)
      CALL MOVTO2((TX+ZX5+20.0+AXILX+4.0),(TY+ZX6-(FLOAT(I)*3.2)
     &+AXILY))
      CALL HERFIX(ZQ(N2),9,4)
 1117 CONTINUE
      DO 1118 II=1,6
      CALL MOVTO2((TX+ZX5+AXILX+3.0),(TY+ZX6+20.0-(FLOAT(II)*3.2)
     &+AXILY))
      IF(II.EQ.1)THEN
      CALL HERHOL(' DIAMETER=*.',-1)
      NH=1
      ELSE IF(II.EQ.2)THEN
      CALL HERHOL(' DENSITY=*.',-1)
      NH=2
      ELSE IF(II.EQ.3)THEN
      CALL HERHOL(' PIPE LEN=*.',-1)
      NH=3
      ELSE IF(II.EQ.4)THEN
      CALL HERHOL(' SLOPE=*.',-1)
      NH=13
      ELSE IF(II.EQ.5)THEN
      CALL HERHOL(' FLOW=*.',-1)
      NH=14
      ELSE IF(II.EQ.6)THEN
      CALL HERHOL(' ROUGHNESS=*.',-1)
      NH=15
      ENDIF
      CALL MOVTO2((TX+ZX5+20.0+AXILX+4.0),(TY+ZX6+20.0-(FLOAT(II)*3.2)
     &+AXILY))
      CALL HERFIX(ZZZ(NH),9,4)
 1118 CONTINUE
      CALL MOVTO2((TX+ZX5+ZX5+AXILX/2.0+20.0+5.0),(TY+ZX6+AXILY/2.0
     &+20.0+AXILY/2.0+5.0))
      CALL HERHOL(' CHANGE IN INTERFACIAL FRICTION FACTOR COEFF.(FFC)
     &*.',-1)
      ENDIF
      RETURN
      END
C
      SUBROUTINE FLOWD(Q1,DEN,D,YO,AY)
C     THIS PROGRAM IS USED TO FIND THE HEIGHT OF A SALINE
C     WEDGE AT THE END OF AN OPEN ENDED PIPE. DR. ALI'S THEORY.
C     YO=SEA WATER LEVEL ABOVE PIPE INVERT
      AM=1.639
      PI=4.0*ATAN(1.0)
```

```
      NH=11
      ELSE IF(II.EQ.6)THEN
      CALL HERHOL(' FFC=*.',-1)
      NH=12
      ENDIF
      CALL MOVTO2((TX+ZX5+AXILX/2.0+1.0),(TY+ZX6+20.0-(FLOAT(II)*3.2)
     &+AXILY))
      CALL HERFIX(ZZZ(NH),9,4)
 1116 CONTINUE
      CALL MOVTO2((TX+ZX5+ZX5+7.0),(TY+ZX6+AXILY/2.0+20.0+AXILY/2.0
     &+5.0))
      CALL HERHOL(' CHANGE IN ROUGHNESS*.',-1)
C
      ELSE IF(NY.EQ.4)THEN
      DO 1117 I=1,5
      N2=((NY-1)*5)+I
      CALL MOVTO2((TX+ZX5+20.0+AXILX),(TY+ZX6-(FLOAT(I)*3.2)+1.0
     &+AXILY))
      CALL SYMBOL(I)
      CALL MOVTO2((TX+ZX5+20.0+AXILX+2.0),(TY+ZX6-(FLOAT(I)*3.2)
     &+AXILY))
      CALL HERHOL(' =*.',-1)
      CALL MOVTO2((TX+ZX5+20.0+AXILX+4.0),(TY+ZX6-(FLOAT(I)*3.2)
     &+AXILY))
      CALL HERFIX(ZQ(N2),9,4)
 1117 CONTINUE
      DO 1118 II=1,6
      CALL MOVTO2((TX+ZX5+AXILX+3.0),(TY+ZX6+20.0-(FLOAT(II)*3.2)
     &+AXILY))
      IF(II.EQ.1)THEN
      CALL HERHOL(' DIAMETER=*.',-1)
      NH=1
      ELSE IF(II.EQ.2)THEN
      CALL HERHOL(' DENSITY=*.',-1)
      NH=2
      ELSE IF(II.EQ.3)THEN
      CALL HERHOL(' PIPE LEN=*.',-1)
      NH=3
      ELSE IF(II.EQ.4)THEN
      CALL HERHOL(' SLOPE=*.',-1)
      NH=13
      ELSE IF(II.EQ.5)THEN
      CALL HERHOL(' FLOW=*.',-1)
      NH=14
      ELSE IF(II.EQ.6)THEN
      CALL HERHOL(' ROUGHNESS=*.',-1)
      NH=15
      ENDIF
      CALL MOVTO2((TX+ZX5+20.0+AXILX+4.0),(TY+ZX6+20.0-(FLOAT(II)*3.2)
     &+AXILY))
      CALL HERFIX(ZZZ(NH),9,4)
 1118 CONTINUE
      CALL MOVTO2((TX+ZX5+ZX5+AXILX/2.0+20.0+5.0),(TY+ZX6+AXILY/2.0
     &+20.0+AXILY/2.0+5.0))
      CALL HERHOL(' CHANGE IN INTERFACIAL FRICTION FACTOR COEFF.(FFC)
     &*.',-1)
      ENDIF
      RETURN
      END
C
      SUBROUTINE FLOWD(Q1,DEN,D,Y0,AY)
C     THIS PROGRAM IS USED TO FIND THE HEIGHT OF A SALINE
C     WEDGE AT THE END OF AN OPEN ENDED PIPE. DR. ALI'S THEORY.
C     Y0=SEA WATER LEVEL ABOVE PIPE INVERT
      AM=1.639
      PI=4.0*ATAN(1.0)
```

```
C                                                                       SAL09250
C     INITIAL ESTIMATE FROM CHARLTON                                    SAL09260
C     WH=HEIGHT OF FLOWING LAYER                                        SAL09270
      R=D/2.0                                                           SAL09280
      AREA=PI*(D**2)/4.0                                                SAL09290
      VV=Q1/AREA                                                        SAL09300
      WH2=0.0                                                           SAL09310
      WH=(VV**2)/(9.81*((DEN-1000.0)/1000.0))                           SAL09320
      WHH=D                                                             SAL09330
C                                                                       SAL09340
 10   IF(WH.GT.D)GOTO 60                                                SAL09350
      UA1=((D)**2.0*2.0*ACOS((R-WH)/R)/8.0)-((D)**                      SAL09360
     &2.0*SIN(2.0*ACOS((R-WH)/R))/8.0)                                  SAL09370
      VBAR=Q1/UA1                                                       SAL09380
C     H=TOTAL ENERGY HEAD AT END OF PIPE                                SAL09390
      H=((VBAR**2)/(2.0*9.81))+(((DEN*9.81*Y0)-(DEN*9.81*(D-WH))-       SAL09400
     &(0.5*1000.0*9.81*WH))/(1000.0*9.81))+WH/2.0+(D-WH)                SAL09410
      V0=SQRT(2.0*9.81*(H-D-(DEN*(Y0-D)/1000.0)))                       SAL09420
      VB=SQRT(2.0*9.81*(H-D+WH-(DEN*(Y0-D+WH)/1000.0)))                 SAL09430
      A0=PI*(D**2)/4.0                                                  SAL09440
      R0=AM*((VB/V0)**AM)*WH/(1.0-((VB/V0)**2))                         SAL09450
      AN=1.0/AM                                                         SAL09460
      THI=WH/D                                                          SAL09470
      RB=R0/D                                                           SAL09480
      ALAM=R+AM*THI                                                     SAL09490
      ALP=-3.4866                                                       SAL09500
      B=3.4832                                                          SAL09510
      C=0.4196                                                          SAL09520
      AI1=(-ALP/((AM**3)*(AN-3.0)*(ALAM**(AN-3.0))))+((                 SAL09530
     &(2.0*ALP*THI/AM)-B)/((AM**2)*(AN-2.0)*(ALAM**(AN-2.0))))          SAL09540
     &-(RB*((ALP*RB/AM)-B)/((AM**2)*(AN-1.0)*(ALAM**(AN-1.0))))         SAL09550
      AI2=(C*(LAM**(1.0-AN))/(AM*(1.0-AN)))+(ALP/((AM**3)*(AN-3.0)*(RBSAL09560
     &(AN-3.0))))-(((2.0*ALP*RB/AM)-B)/((AM**2)*(AN-2.0)*(RB**(AN-2.0)SAL09570
     &)                                                                 SAL09580
      AI3=(((ALP*(RB**2)/AM)-(B*RB))/((AM**2)*(AN-1.0)*(RB**(AN-1.0)))SAL09590
     &(C*(RB**(1.0-AN))/((AM**2)*(AN-1.0)*(RB**(AN-1.0))))-             SAL09600
     &(C*(RB**(1.0-AN))/(AM*(1.0-AN)))                                  SAL09610
      AI=AI1+AI2+AI3                                                    SAL09620
C                                                                       SAL09630
      QD=V0*A0*((R0/D)**(AN))*AI                                        SAL09640
      ERR=QD-Q1                                                         SAL09650
      IF(ABS(ERR).LE.0.1E-05)GOTO 60                                    SAL09660
      IF(ERR.GE.0.0)THEN                                                SAL09670
      WH2=WH                                                            SAL09680
      WH=(WH2+WHH)/2.0                                                  SAL09690
      GOTO 10                                                           SAL09700
      ELSE                                                              SAL09710
      WHH=WH                                                            SAL09720
      WH=(WHH+WH2)/2.0                                                  SAL09730
      GOTO 10                                                           SAL09740
      ENDIF                                                             SAL09750
 60   FRDL=((DEN-1000.0)/DEN)*9.81*D                                    SAL09760
      FRDT=Q1/(PI*(D**2)/4.0)                                           SAL09770
      FRD=FRDT/SQRT(FRDL)                                               SAL09780
      FAC=D/0.05                                                        SAL09790
      AY=WH*FAC                                                         SAL09800
C     AY=0.030                                                          SAL09810
      IF(AY.GT.D)AY=D                                                   SAL09820
      RETURN                                                            SAL09830
      END                                                               SAL09840
```

Program 4 - SFLOW VFORTRAN - performs an analysis of multi-riser systems.

SFLOW27 VFORTRAN uses the method of characteristics approach to solve the equations of motion and continuity derived in section 3 of the report. The aim of the program is to mathematically model the effects that wave action has on the internal hydraulics of a multi-riser outfall system.

The program begins by requesting information regarding the outfall design and the receiving water conditions, the information required is listed as follows

The outfall length	(TOL)
Diameter of dropshaft	(DS)
The pipe roughness	(ROU)
The sea water level	(SWL)
The sea water density	(DEN1)
The spacing of the risers	(RPL)
The total number of risers	(NOR)
Waveheight	(HW)
Waveperiod	(T)
Time for the end of run	(END)
Slope of outfall	(SO)
Riser diameter	(DR)
Riser length	(RL)
Design flow	(TOQ)
Expected flow	(TOQQ)
Bulk modulus of water	(BMW)

Thickness of wall of outfall pipe (TP)

Thickness of wall of riser pipe (TR)

Young's modulus of main pipe material (EP)

and Young's modulus of riser pipe material (ER)

The data input subroutine requests all this information, along with the main pipe diameter between risers for those cases where the outfall is tapered. Also information concerning riser length and diameter is put into an array as the risers may not all have the same length or diameter, the information being requested in turn for each riser beginning with the most seaward one. The bulk modulus of the water along with the thickness and elasticity of the pipe materials is required to calculate the speed of the pressure pulse wave within the outfall system, see section 3.2.3.

The program initially calls the data collection subroutine which requests the data to be input into the program. This subroutine also calls the subroutine WAVEL which calculates the wavelength of the sine wave passing over the outfall system; this does not handle or produce random wave forms. The wavelength is calculated from

$$L = \frac{gT^2}{2\pi} \tanh \left(\frac{2\pi d}{L}\right)$$

where L = wavelength

g = acceleration due to gravity

and d = sea water depth and equals (SWL).

Subroutine DATA also calls subroutine SPEED which calculates the speed of the internal pressure wave through the risers and the main body of the outfall pipe.

The main program then calls subroutine RISFRI - this calculates the friction conditions within the riser system to ensure that the flow will balance under design flow conditions. This subroutine calls FRIFAC to calculate the friction factors for the outfall components under the full flow conditions and it also calls RISERV which sets the initial flow conditions within the individual risers. If the operator requests the flow to be present before the wave action begins the subroutine RISFRI calls MOFC, which is the main calculation subroutine. If however the operator requires no wave action to be present before the flow begins the program returns to the main subroutine which then sets the initial values in the pipe for zero flow conditions. This then calls subroutine MOFC and the calculations begin.

Subroutine MOFC calculates the head and velocity at the predetermined calculation points and within the risers during the passage of waves across the diffuser section of the outfall. This progresses through the various calculations until the specified simulation time is complete. Because the time step used in the calculation is small, the main calculation loop in MOFC repeats itself many times therefore output has to be restricted; this is achieved by specification of output time steps required at the data input stage of the program execution. The output is written to a file called SFLOW OUTPUT and information is also passed to a subroutine called COLDAT. This collects and assembles the data into a suitable form for plotting, which is initiated through program PLOT when all the calculations are complete. Output from the model is shown in Section 7.

Program - SFLOW VFORTRAN

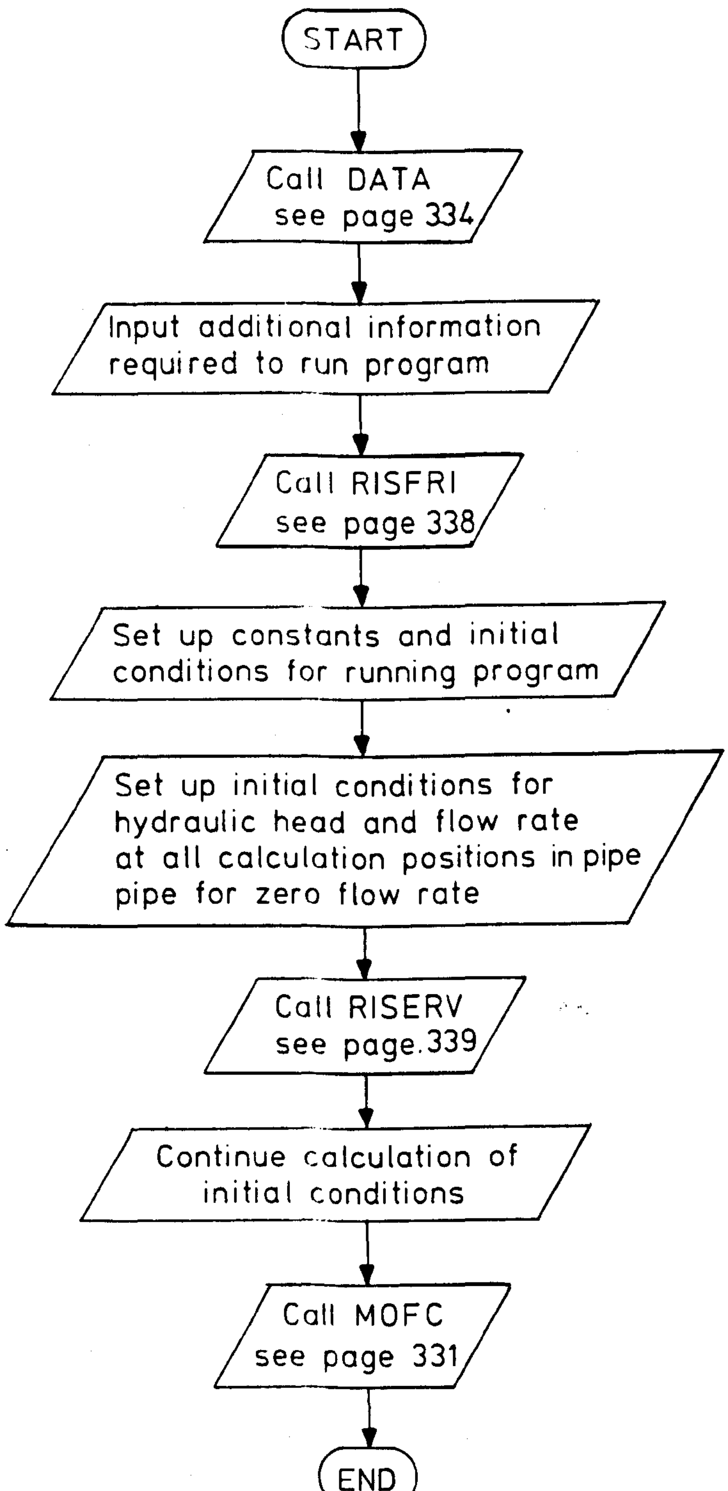

Subroutine MOFC

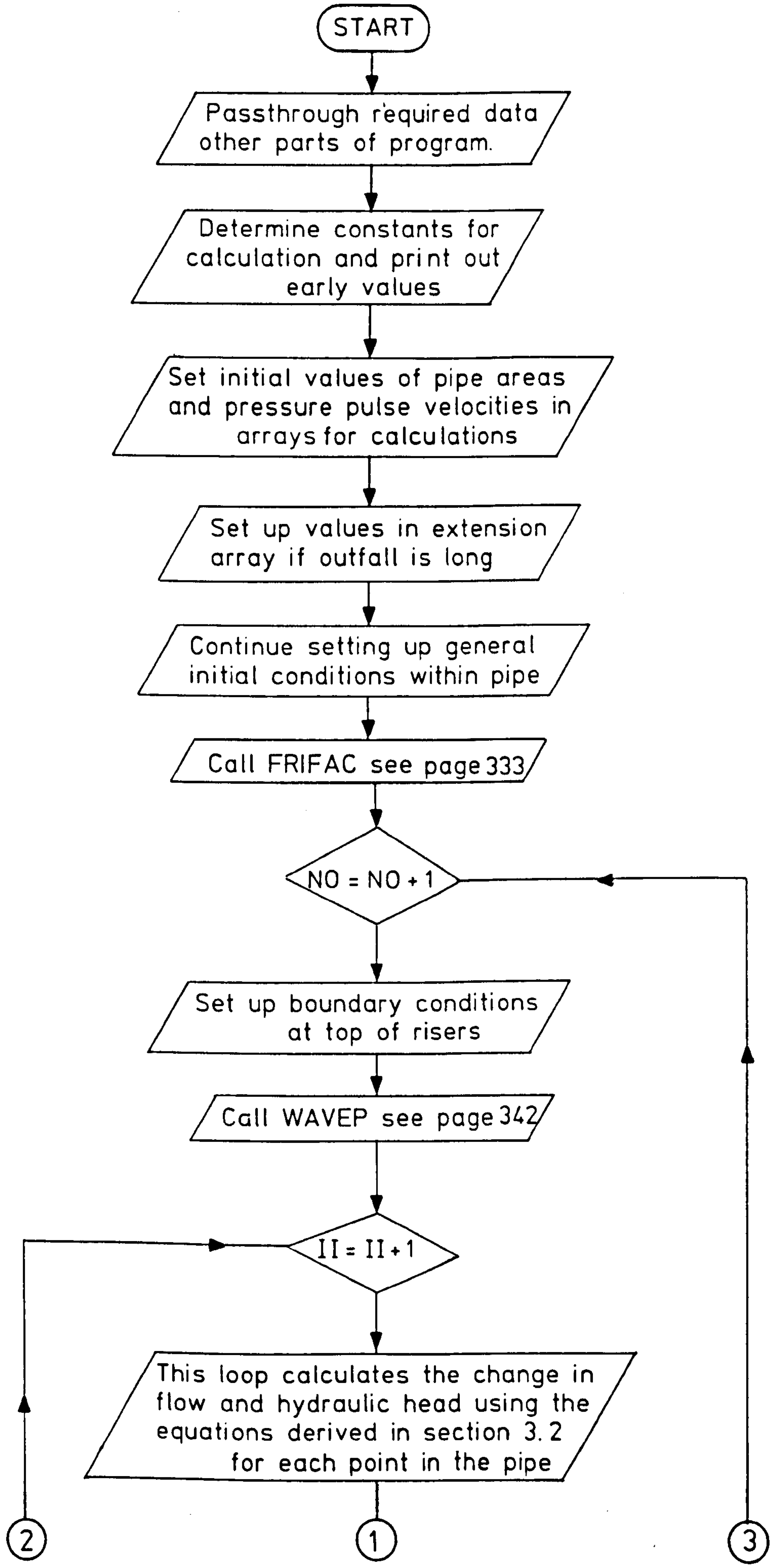

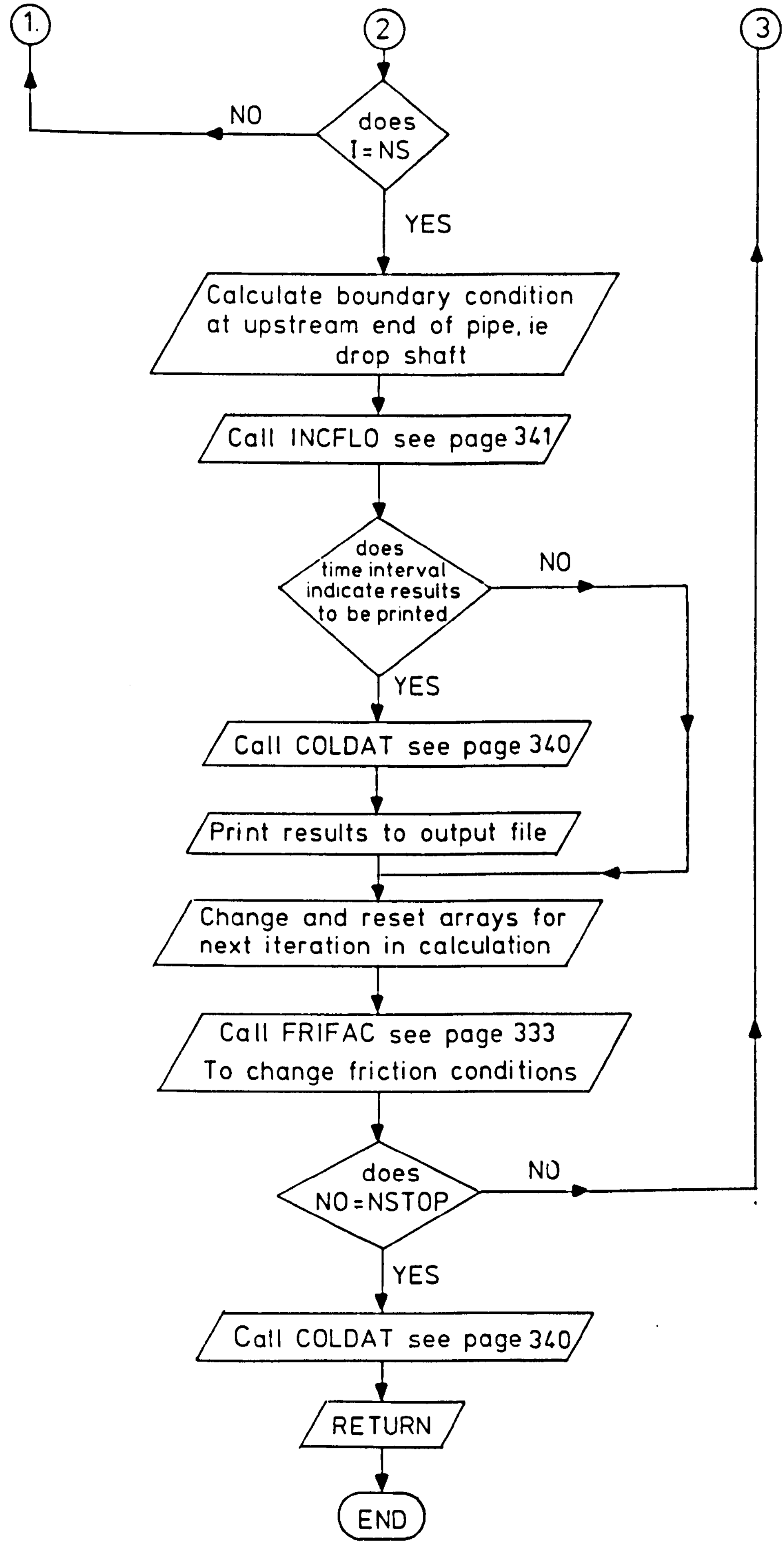
1.
2
3
NO
does
I=NS
YES
Calculate boundary condition
at upstream end of pipe, ie
drop shaft
Call INCFLO see page 341
does
time interval
indicate results
to be printed
NO
YES
Call COLDAT see page 340
Print results to output file
Change and reset arrays for
next iteration in calculation
Call FRIFAC see page 333
To change friction conditions
does
NO=NSTOP
NO
YES
Call COLDAT see page 340
RETURN
END

Subroutine FRIFAC

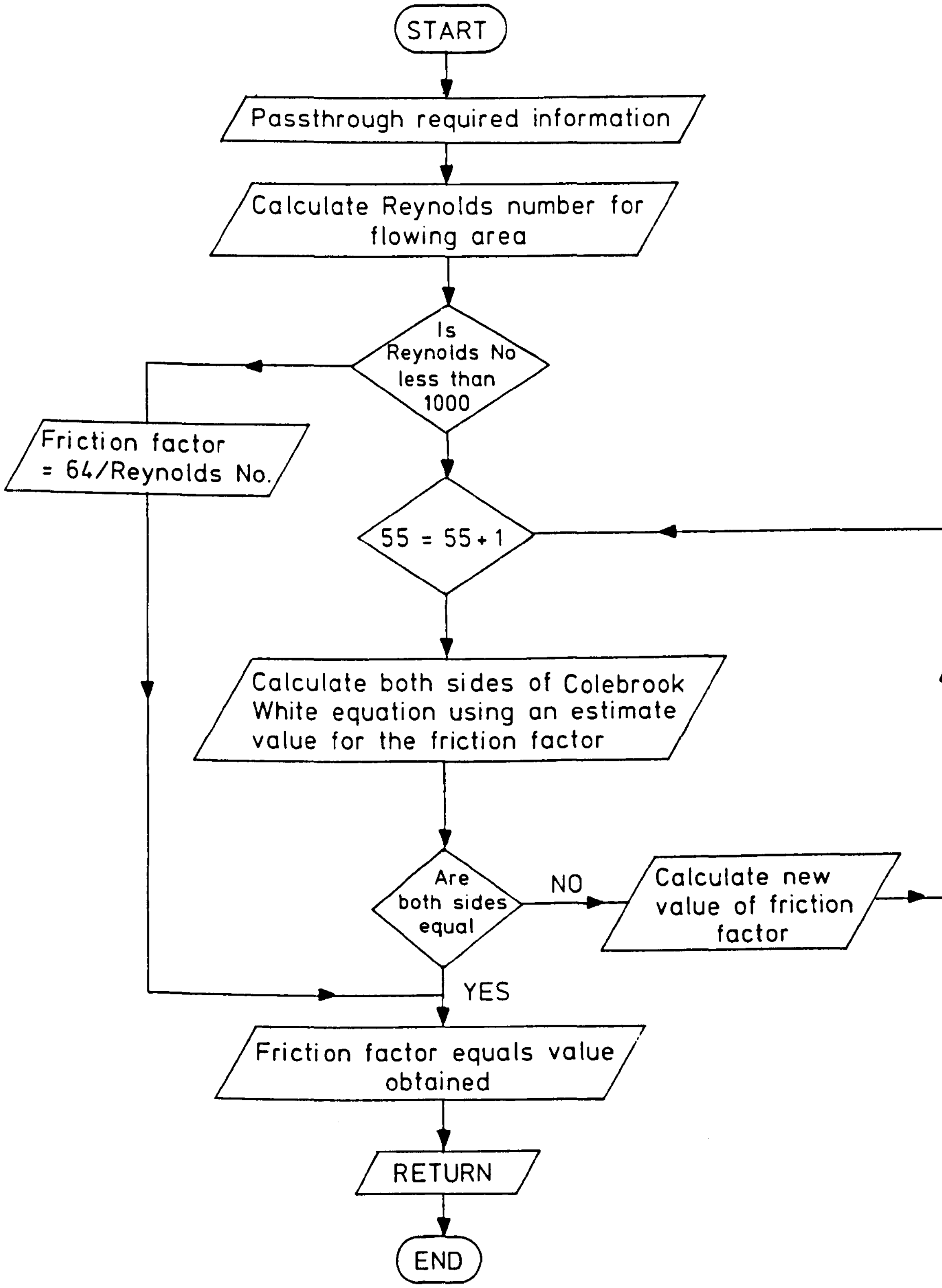

Subroutine DATA

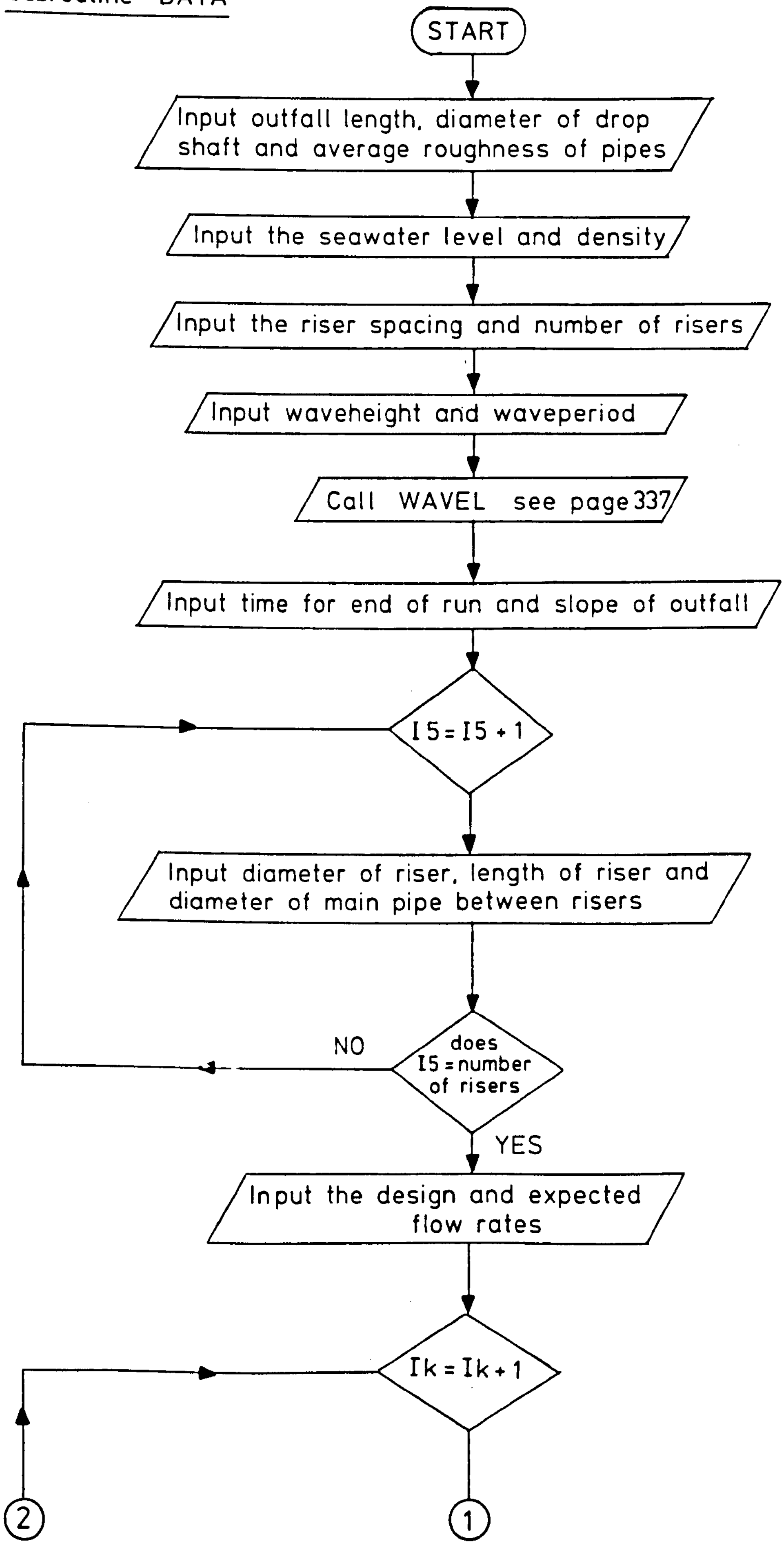

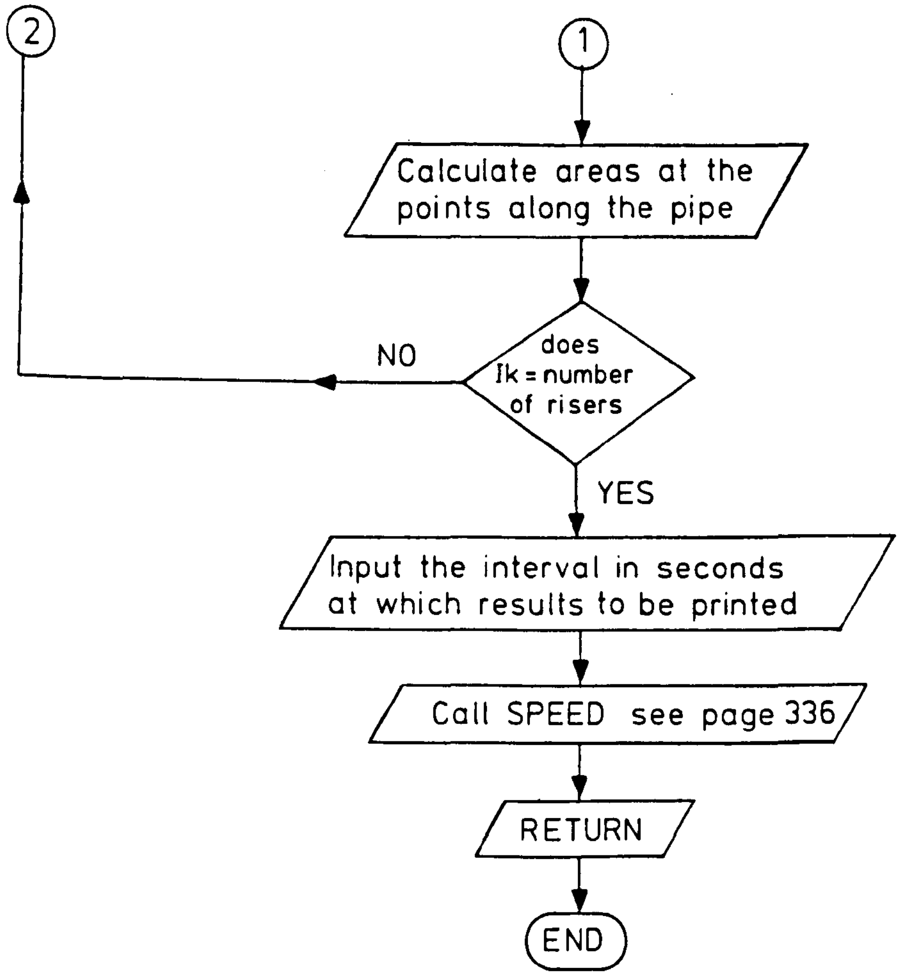
2
1
Calculate areas at the points along the pipe
does Ik = number of risers
NO
YES
Input the interval in seconds at which results to be printed
Call SPEED see page 336
RETURN
END

Subroutine SPEED

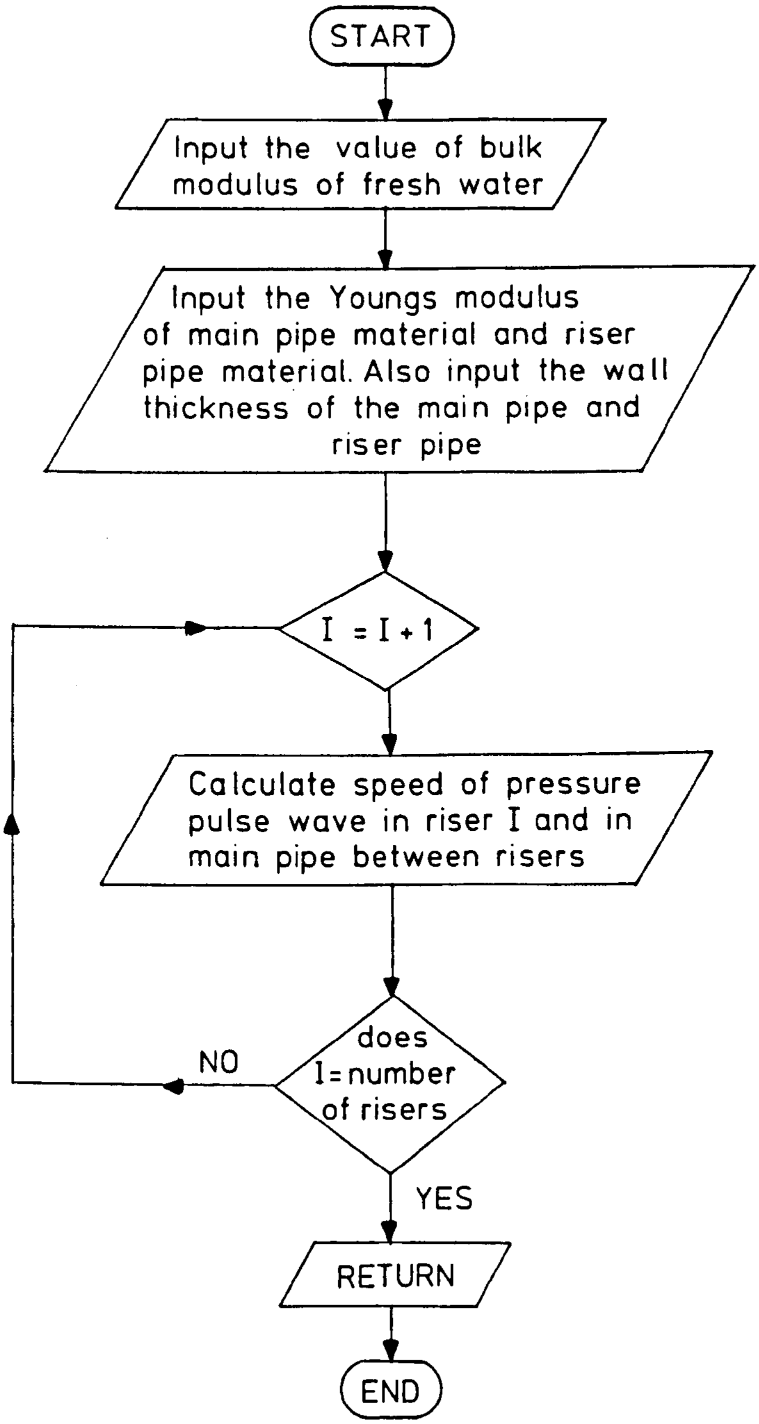

Subroutine WAVEL

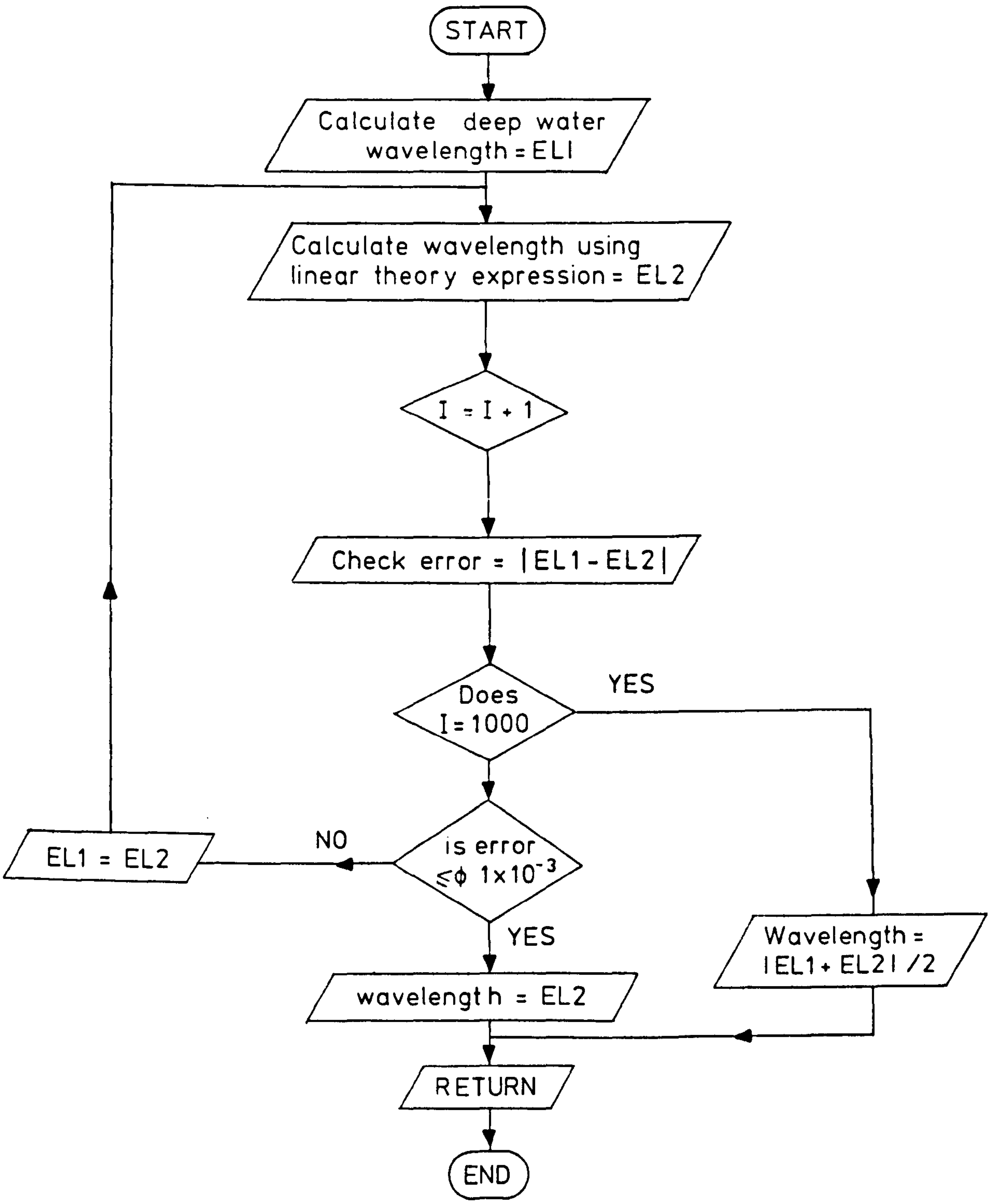

Subroutine RISERI

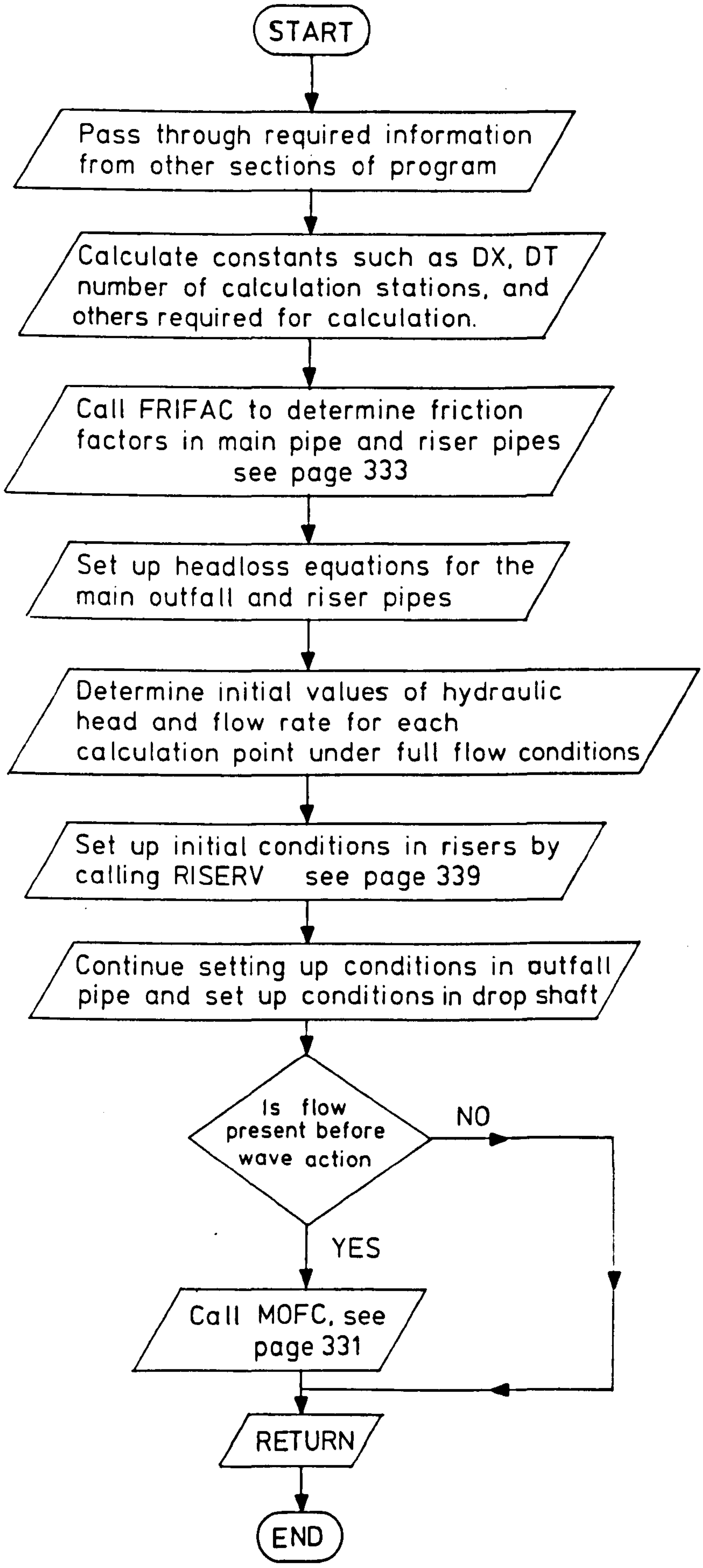

Subroutine RISERV

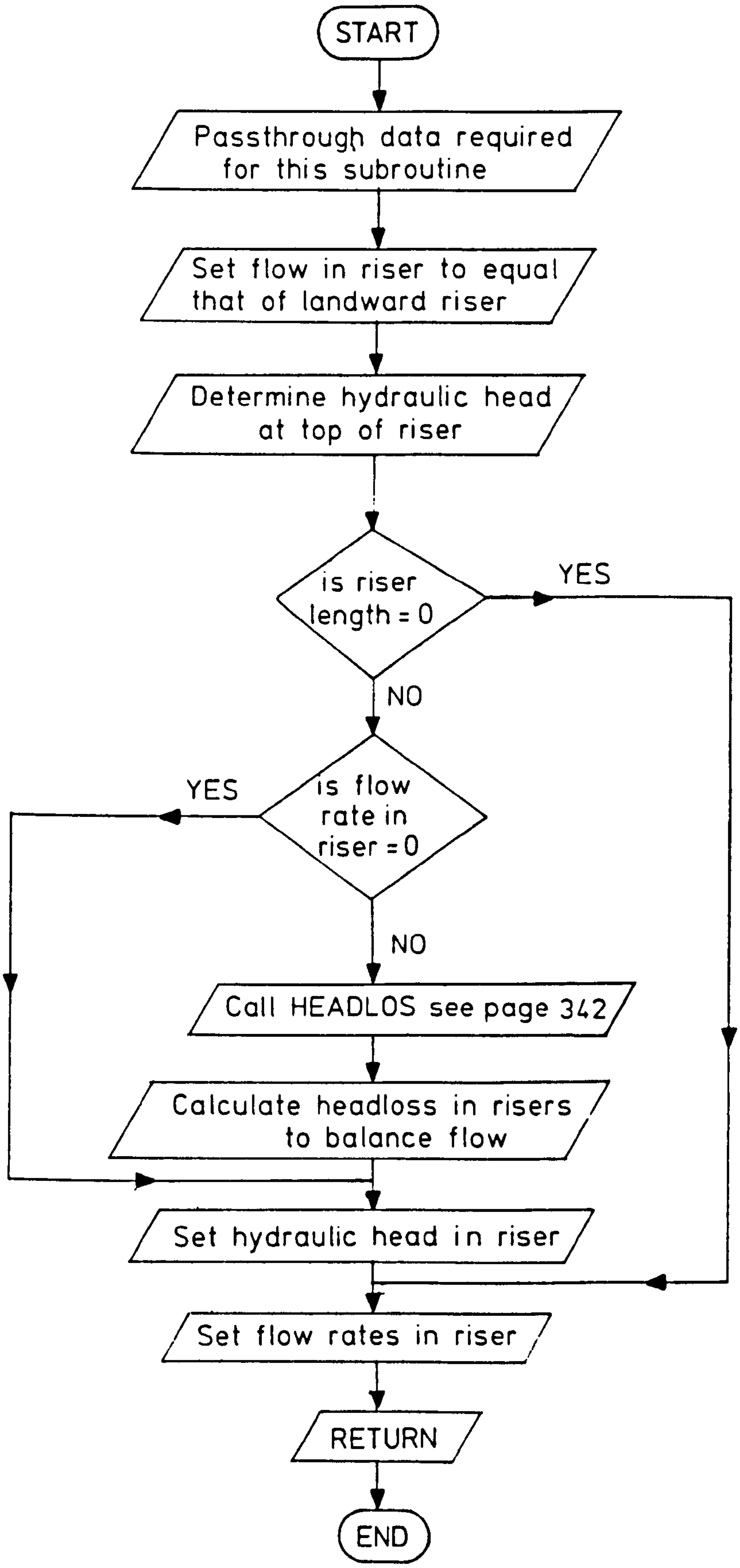

Subroutine COLDAT

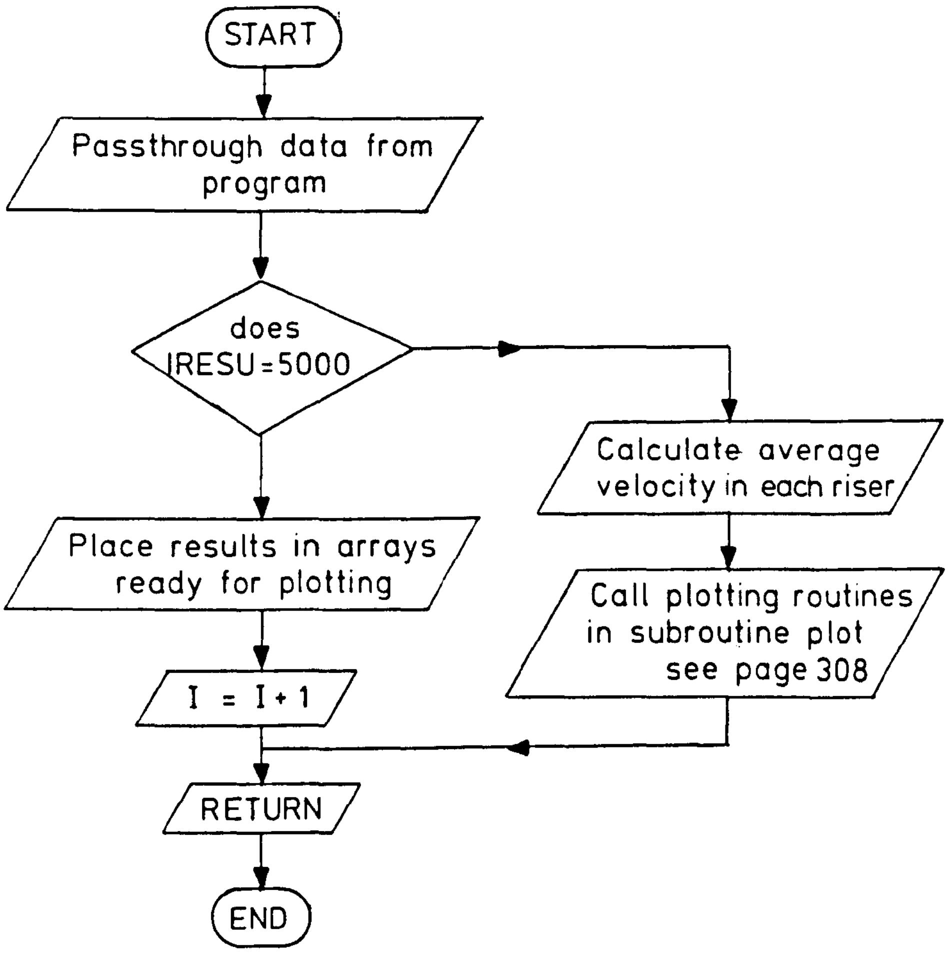

Subroutine INCFLO.

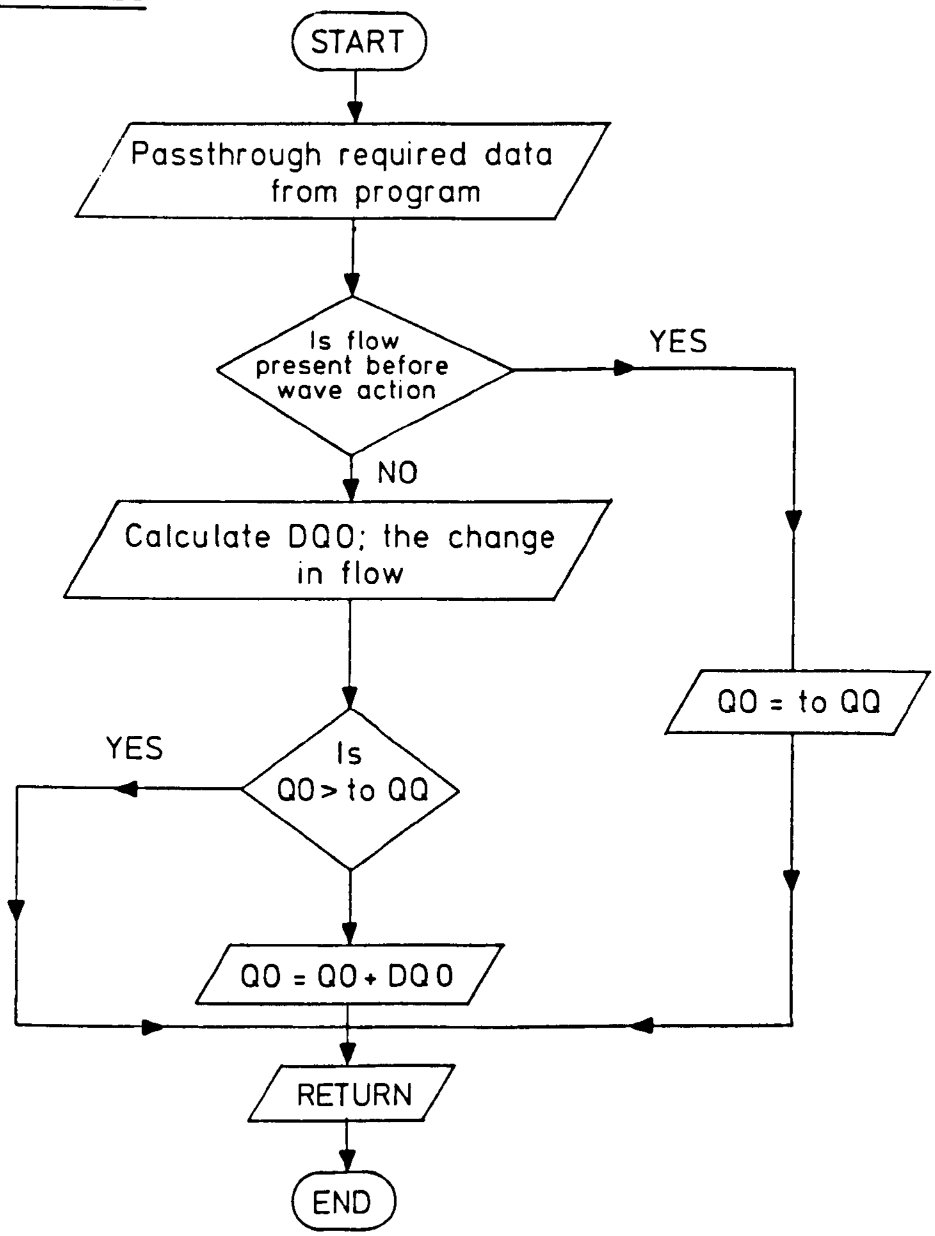

Subroutine WAVEP.

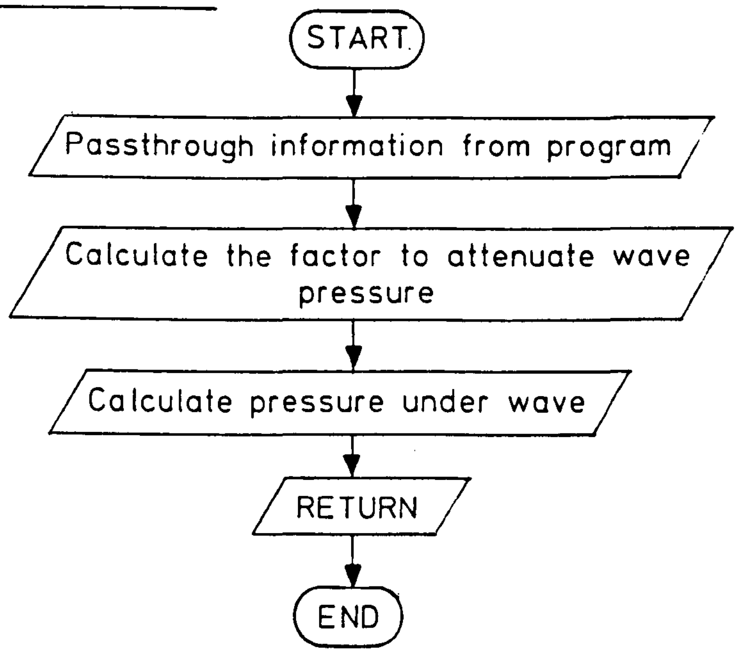

Subroutine HEALOS

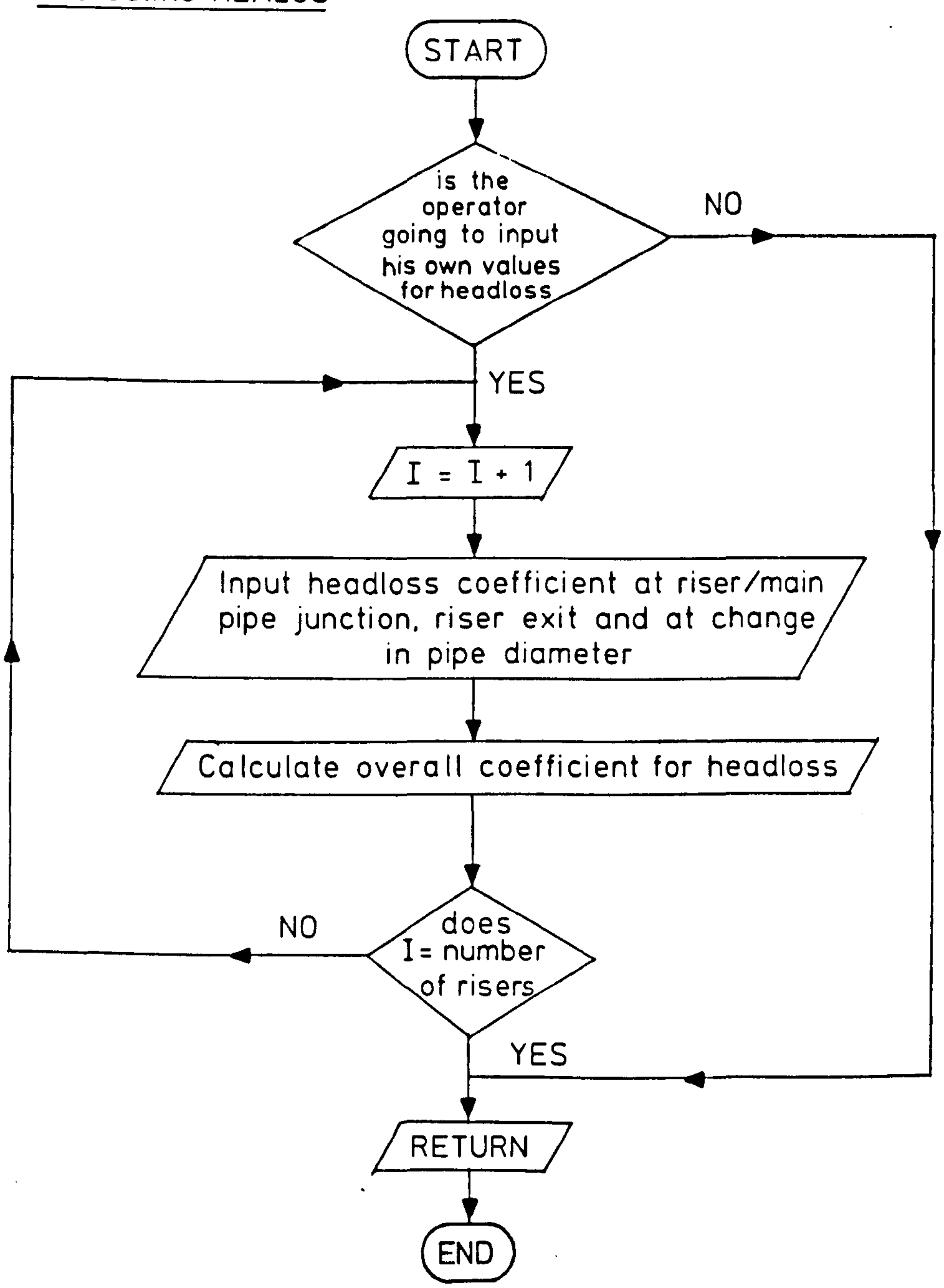

```
C     ****************************************************************
C     *                                                              *
C     *   PROGRAM SFLOW27 CALCULATES THE HEAD AND FLOW               *
C     *   CHARACTERISTICS WITHIN AN OUTFALL PIPE DURING              *
C     *   THE BUILD UP OF FLOW IN THE PIPE AND THE                   *
C     *   PASSAGE OF WAVES ACROSS THE RISER MANIFOLD.                *
C     *   CALCULATES THE DISCONTINUITY ACROSS RISER.                 *
C     *   PLOTS 4 TO A PAGE                                          *
C     ****************************************************************
C
C     ****************************************************************
C     *     SUBROUTINE SFLOW CALCULATES THE INITIAL                  *
C     *     CONDITIONS WITHIN A PIPE DURING STEADY                   *
C     *     OR ZERO FLOW                                             *
C     ****************************************************************
C
      DIMENSION QPO(500),H(500),Q(500),HP(500),QP(500),YEK(500)
      DIMENSION RH(15,2),RQ(15,2),DQ(500),UQ(500),YH(15,2)
      DIMENSION HH(500),QQ(500),UQQ(500),DQQ(500),RR(15),AJ(15)
      DIMENSION DD2(500),AREAP2(500)
      CHARACTER*1 TFG,TFH
C     CALCULATION FOR STEADY FLOW
C     NOR=NO. OF RISER PORTS
C     AREAP=AREA OF OUTFALL PIPE
C     AREARP=AREA OF RISER PORT
C     QPO=RISER FLOW FROM EACH PORT
C     RPL=DISTANCE BETWEEN RISER PORTS
C     TOL=TOTAL LENGTH OF OUTFALL
C     FF=PIPE FRICTION FACTOR
C     SWL=LEVEL OF SEAWATER ABOVE LEVEL OF C/L OF OUTFALL PIPE
C     DEN=SEAWATER DENSITY
C     TOQ=TOTAL FLOW IN MAIN OUTFALL
C     RL=RISER LENGTH
C     SO=PIPE SLOPE(-VE SLOPE UPWARDS)
C     RISERS ARE ASSUMED TO BE VERTICAL
C
      COMMON/DATA1/AREAP(500),AREARP(15),AREAS,RPL,TOL,DD(500),
     &ROU,SWL,DEN,NOR
      COMMON/DATA2/HW,T,WL,END,SO,DR(15),RL(15),A(500),DEN1,
     &AA(15),TOQ,TOQQ,CH(500),CH2(15),C2(15)
      CALL DATA(ARESU,AJ)
      RPQ=TOQ/FLOAT(NOR)
      PRINT*,' IS FLOW PRESENT BEFORE WAVE ACTION '
      READ(5,4)TFG
    4 FORMAT(A1)
      PRINT*,' IS FLOW TO BE PUMPED '
      READ(5,4)TFH
      IF(TFH.EQ.'Y')THEN
      PRINT*,' INPUT CONSTANT PUMPING HEAD '
      READ(5,*)PH
      ELSE
      ENDIF
      IF(TFG.EQ.'N')DEN=DEN1
      CALL RISFRI(RR,RPQ,R,TFG,ARESU,AJ,TFH,PH)
      DX=RPL/3.0
      DT=DX/AJ(NOR)
      DX2=DT*AA(NOR)
      NPTR=2
      N=INT(TOL/DX)
      NS=N+1
      IF(NS.GT.500)NS=500
      NY=INT(RPL/DX)
      IF(NY.LT.1)NY=1
      PI=4.0*ATAN(1.0)
      TQ=0.0
      T2=0.0
```

```
      P=PI*D                                                            SFL00670
      P2=PI*DR(NOR)                                                     SFL00680
C     CALCULATION OF INITIAL VALUES                                     SFL00690
      NRIS=NOR                                                          SFL00700
      RH(NOR,1)=((DEN/1000.0)*SWL)-((RQ(NOR,1)**2)/(2.0*9.81*           SFL00710
     &(AREARP(NOR)**2)))                                                SFL00720
      RH(NOR,NPTR)=RH(NOR,1)-((RL(NOR)+DD(1)/2.0)*(DEN/1000.0))-        SFL00730
     &(RR(NOR)*(RQ(NOR,1)**2)*RL(NOR))                                  SFL00740
      RQ(NOR,NPTR)=RQ(NOR,1)                                            SFL00750
      TQ=0.0                                                            SFL00760
      NK=((NOR-1)*NY)+1                                                 SFL00770
      UQ(NK)=0.0                                                        SFL00780
      DQ(NK)=0.0                                                        SFL00790
      H(NK)=RH(NOR,1)                                                   SFL00800
      H(NK+1)=H(NK)+(SO*DX)                                             SFL00810
      Q(NK+1)=0.0                                                       SFL00820
      DO 2450 IL=1,NK-1                                                 SFL00830
      DO 2451 KJ=1,NOR                                                  SFL00840
      IF((NK-IL).EQ.(1+(KJ-1)*NY))GOTO 2452                             SFL00850
      IF((NK-IL).EQ.((KJ-1)*NY))GOTO 2455                               SFL00860
 2451 CONTINUE                                                          SFL00870
      H(NK-IL)=H(NK-IL+1)-(SO*DX)                                       SFL00880
      Q(NK-IL)=0.0                                                      SFL00890
      GOTO 2450                                                         SFL00900
 2452 H(NK-IL)=H(NK-IL+1)-(SO*DX)                                       SFL00910
      UQ(NK-IL)=0.0                                                     SFL00920
      NRIS=NRIS-1                                                       SFL00930
      INN=NK-IL                                                         SFL00940
      LE=NS-IL                                                          SFL00950
      PRINT*,' RISERV CALLED FROM LINE 96 '                             SFL00960
      CALL RISERV(H,RH,RQ,RR,DX2,TQ,NPTR,INN,NRIS,LE)                   SFL00970
      DQ(NK-IL)=0.0                                                     SFL00980
      GOTO 2450                                                         SFL00990
 2455 H(NK-IL)=H(NK-IL+2)+((Q(NK-IL+2)**2)/                             SFL01000
     &(2.0*9.81*(AREAP(NS-NK+IL-2)**2)))-                               SFL01010
     &((DQ(NK-IL+1)**2)/(2.0*9.81*(AREAP(NS-NK+IL-2)**2)))              SFL01020
     &-(R*(Q(NK-IL+2)**2))-(R*(DQ(NK-IL+1)**2))                         SFL01030
      Q(NK-IL)=0.0                                                      SFL01040
 2450 CONTINUE                                                          SFL01050
      DO 2464 KL=1,NOR-1                                                SFL01060
      RH(KL,1)=RH(NOR,1)                                                SFL01070
      RH(KL,NPTR)=RH(NOR,NPTR)                                          SFL01080
      RQ(KL,1)=RQ(NOR,1)                                                SFL01090
      RQ(KL,NPTR)=RQ(NOR,NPTR)                                          SFL01100
 2464 CONTINUE                                                          SFL01110
      DO 2453 IK=NK+2,NS                                                SFL01120
      H(IK)=H(IK-1)+(SO*DX)                                             SFL01130
      Q(IK)=0.0                                                         SFL01140
 2453 CONTINUE                                                          SFL01150
C     HF=LEVEL OF WATER IN UPSTREAM TANK                                SFL01160
      HF=(1.0/9810.0)*(9810.0*H(NS))                                    SFL01170
C     INITIAL CONDITIONS IN RISERS                                      SFL01180
      DO 25 II=1,NS                                                     SFL01190
      HH(II)=H(NS-II+1)                                                 SFL01200
      QQ(II)=Q(NS-II+1)                                                 SFL01210
      UQQ(II)=UQ(NS-II+1)                                               SFL01220
      DQQ(II)=DQ(NS-II+1)                                               SFL01230
      AREAP2(II)=AREAP(NS-II+1)                                         SFL01240
      DD2(II)=DD(NS-II+1)                                               SFL01250
   25 CONTINUE                                                          SFL01260
      DO 252 MP=1,NS                                                    SFL01270
      AREAP(MP)=AREAP2(MP)                                              SFL01280
      DD(MP)=DD2(MP)                                                    SFL01290
  252 CONTINUE                                                          SFL01300
      DO 40 I=1,NS                                                      SFL01310
      WRITE(9,41)I,H(I),Q(I),HH(I),QQ(I)                                SFL01320
```

```
   41 FORMAT(2X,I5,1X,F12.6,1X,F12.6,1X,F12.6,1X,F12.6)
   40 CONTINUE
      DO 5296 LA=1,NS
      YEK(LA)=0.0
 5296 CONTINUE
      QO=0.0
      CALL MOFC(R,RR,FF,HH,QQ,NY,QPO,HF,RH,RQ,UQQ,DQQ,ARESU,
     &TFG,YEK,AJ,QO,TFH,PH)
      STOP
      END
      SUBROUTINE MOFC(R,RR,FF,H,Q,NY,QPO,HF,RH,RQ,UQ,DQ,ARESU,
     &TFG,YEK,AJ,QO,TFH,PH)
C
C     ******************************************************
C     *      SUBROUTINE M OF C CALCULATES THE CHANGES     *
C     *      IN HEAD & VELOCITY WITHIN THE PIPE DURING    *
C     *      PERIODS OF WAVE PASSAGE.                     *
C     ******************************************************
C
      COMMON/DATA1/AREAP(500),AREARP(15),AREAS,RPL,TOL,DD(500),
     &ROU,SWL,DEN,NOR
      COMMON/DATA2/HW,T,WL,END,SO,DR(15),RL(15),A(500),DEN1,
     &AA(15),TOQ,TOQQ,CH(500),CH2(15),C2(15)
      DIMENSION H(500),Q(500),HP(500),QP(500),DQP(500),RA(15)
      DIMENSION RH(15,2),RQ(15,2),RHP(15,2),RQP(15,2),UQP(500)
      DIMENSION DQ(500),UQ(500),HC(15),RR(15),WLK(500),DHP(500)
      DIMENSION DH(500),YEK(500),AJ(15),AREAP2(500),AREAPA(3000)
      DIMENSION QA(3000),CHA(3000),HPA(3000),HA(3000),QPA(3000),DSA(15
      DIMENSION CHE(500),CH2E(500)
      CHARACTER*1 TFG,TFH
      PRINT*,' DEN=',DEN
      PI=4.0*ATAN(1.0)
      NAKL=1
      DO 2244 JKL=1,NOR
      RA(JKL)=RR(JKL)
 2244 CONTINUE
      DX=RPL/3.0
      T2=0.0
      P=PI*D
      PRINT*,' WAVELENGTH=',WL
      PRINT*,' HF= ',HF
      PRINT*,' H(1)= ',H(1)
C     PRINT*,' ARESU= ',ARESU
      PRINT*,'QO=',QO
      PRINT*,' R=',R
      N=INT(TOL/DX)
      NS=N+1
      IF([illegible])NS1=NS
      IF(NS.GT.500)NS1=500
C
      DO 789 IU=1,NS1
      AREAP2(IU)=AREAP(NS-IU+1)
  789 CONTINUE
      DO 785 KU=1,NS1
      AREAP(KU)=AREAP2(KU)
  785 CONTINUE
C     RL=RISER LENGTH
      N1=0
      N2=0
      DO 231 IJ=1,NOR
      N1=N2+1
      N2=NS-((NOR-IJ)*NY)
      DO 232 KZ=N1,N2
      A(KZ)=AJ(NOR-IJ+1)
  232 CONTINUE
  231 CONTINUE
```

```
      DO 203 KJ=1,NS1                                                   SFL01990
      CHE(KJ)=A(KJ)/(9.81*AREAP(KJ))                                    SFL02000
      CH(KJ)=A(KJ)/(9.81*AREAP(KJ))                                     SFL02010
 203  CONTINUE                                                          SFL02020
      IF(NS.LE.500)GOTO 204                                             SFL02030
      DO 90 IH=1,NS-500                                                 SFL02040
      AREAPA(IH)=AREAP(1)                                               SFL02050
      CHA(IH)=CH(1)                                                     SFL02060
  90  CONTINUE                                                          SFL02070
      IF(H(2).EQ.H(3))GOTO 207                                          SFL02080
C     SETS VALUES IN EXTENSION ARRAY                                    SFL02090
C     WITH FLOW                                                         SFL02100
      DO 209 JKK=1,NS-500                                               SFL02110
      HA(JKK)=H(3)+((R*Q(3)**2)*FLOAT(JKK))+(SO*DX*FLOAT(JKK))          SFL02120
      QA(JKK)=Q(3)                                                      SFL02130
 209  CONTINUE                                                          SFL02140
C                                                                       SFL02150
C     WITHOUT FLOW                                                      SFL02160
 207  DO 208 JIK=1,NS-500                                               SFL02170
      HA(JIK)=H(2)                                                      SFL02180
      QA(JIK)=Q(2)                                                      SFL02190
 208  CONTINUE                                                          SFL02200
 204  DO 202 KI=1,NOR                                                   SFL02210
      CH2(KI)=AA(KI)/(9.81*AREARP(KI))                                  SFL02220
      CH2E(KI)=AA(KI)/(9.81*AREARP(KI))                                 SFL02230
 202  CONTINUE                                                          SFL02240
      DO 201 IM=1,500                                                   SFL02250
      WLK(IM)=500.0                                                     SFL02260
      DH(IM)=H(IM)                                                      SFL02270
 201  CONTINUE                                                          SFL02280
      DT=(DX/A(NS))                                                     SFL02290
      DX2=DT*AA(NOR)                                                    SFL02300
C     ANPTR=(RL(NOR)/DX2)+1.0+0.5                                       SFL02310
C     NPTR=INT(ANPTR)                                                   SFL02320
      NPTR=2                                                            SFL02330
      DX2=RL(NOR)/FLOAT(NPTR-1)                                         SFL02340
      DX2=0.0                                                           SFL02350
      DO 401 LI=1,NOR                                                   SFL02360
      C2(LI)=(2.0*RL(LI))/(9.81*AREARP(LI)*DT)                          SFL02370
 401  CONTINUE                                                          SFL02380
      PRINT*,' DX=',DX                                                  SFL02390
      PRINT*,' DX2=',DX2                                                SFL02400
      PRINT*,' DT=',DT                                                  SFL02410
      NSTOP=INT(END/DT)                                                 SFL02420
      DO 60 I=1,NOR                                                     SFL02430
      DO 60 K=1,NPTR                                                    SFL02440
      WRITE(9,221)I,K,RH(I,K),RQ(I,K),RR(I)                             SFL02450
 221  FORMAT(1X,I3,1X,I3,1X,F12.6,1X,F12.6,2X,F14.5)                    SFL02460
  60  CONTINUE                                                          SFL02470
C     MAIN CALCULATION                                                  SFL02480
      RESU=0.0                                                          SFL02490
      NOC2=0                                                            SFL02500
      IF(TOQ.EQ.TOQQ)GOTO 2368                                          SFL02510
C     CHANGE FRICTION DEPENDING ON FLOW                                 SFL02520
      DO 2367 IS=1,NOR                                                  SFL02530
      P2=PI*DR(IS)                                                      SFL02540
      T2=0.0                                                            SFL02550
      UV=RQ(IS,1)/(FLOAT(NOR)*AREARP(IS))                               SFL02560
      IF(UV.EQ.0.0)GOTO 2367                                            SFL02570
      CALL FRIFAC(ROU,DR(IS),UV,AREARP(IS),P2,T2,FFF)                   SFL02580
      PRINT*,' FFF=',FFF                                                SFL02590
      DSA(IS)=FFF/(2.0*9.81*(AREARP(IS)**2))                            SFL02600
      RR(IS)=RR(IS)-RR(NOR)+DSA(IS)                                     SFL02610
2367  CONTINUE                                                          SFL02620
2368  DO 22 NO=1,NSTOP                                                  SFL02630
      NOC2=NOC2+1                                                       SFL02640
```

```
      IF(NOC2.EQ.2)NOC2=0
      IRESU=0
      JZ=0
      RESU=RESU+DT
      TC=TC+DT
C     BOUNDARY CONDITIONS
C     TAKEN FROM TOP OF RISER PORTS AND UPSTREAM END OF OUTFALL
      DO 10 KL=1,NOR
      HC(KL)=(HW/2.0)*SIN(2.0*PI*((FLOAT(KL-1)*RPL/WL)+(TC/T)))
      CALL WAVEP(HC(KL),SWL,RL(KL),WL,TC,T,DD(1),PR)
      RHP(KL,NPTR)=((DEN1*9.81*(SWL-RL(KL)-(DD(1)/2.0)))
     &+(DEN1*9.81*PR))/9810.0
C     PRINT*,' RHP(KL,NPTR)=',RHP(KL,NPTR),' PR=',PR,' KL=',KL
   10 CONTINUE
C     FOR MAIN PIPE
      DO 3 II=2,NS
      DO 4 IK=1,NOR
      IF(II.EQ.NS)GOTO 8
      IF(II.EQ.NS-((IK-1)*NY))GOTO 5
      IF(II.EQ.NS-((IK-1)*NY)+1)GOTO 6
      IF(II.EQ.NS-((IK-1)*NY)-1)GOTO 7
    4 CONTINUE
C     EXTRA POINTS ABOVE THOSE REQUIRED
      IF(NS.LT.500)GOTO 4000
      IZZ=II-2
      IF(II.EQ.3)GOTO 6000
      IF(II.EQ.NS-500)GOTO 8000
      CP=HA(IZZ-1)+QA(IZZ-1)*(CHA(IZZ-1)-R*ABS(QA(IZZ-1)))-
     &(QA(IZZ-1)*DT*SO/AREAPA(IZZ-1))
      HPA(IZZ)=0.5*(CP+HA(IZZ+1)+QA(IZZ+1)*(R*ABS(QA(IZZ+1))-
     &CHA(IZZ+1))-(QA(IZZ+1)*DT*SO/AREAPA(IZZ+1)))
      QPA(IZZ)=(CP-HPA(IZZ))/CHA(IZZ)
      GOTO 3
 6000 CP=H(2)+Q(2)*(CH(2)-R*ABS(Q(2)))-(Q(2)*DT*SO
     &/AREAP(2))
      HPA(IZZ)=0.5*(CP+HA(IZZ+1)+QA(IZZ+1)*(R*ABS(QA(IZZ+1))-
     &CHA(IZZ+1))-(QA(IZZ+1)*DT*SO/AREAPA(IZZ+1)))
      QPA(IZZ)=(CP-HPA(IZZ))/CHA(IZZ)
      GOTO 3
 8000 CP=HA(IZZ-1)+QA(IZZ-1)*(CHA(IZZ-1)-R*ABS(QA(IZZ-1)))-
     &(QA(IZZ-1)*DT*SO/AREAPA(IZZ-1))
      HP(I)=0.5*(CP+H(3)+Q(3)*(R*ABS(Q(3))-CH(3))-
     &(Q(3)*DT*SO/AREAP(3)))
      QPA(IZZ)=(CP-HPA(IZZ))/CHA(IZZ)
      GOTO 3
C
 4000 IF(NS.LE.500)GOTO 4020
      NS2=NS-NS1
      I=II-(NS-NS1)
      IF(II.EQ.2)GOTO 4031
      IF(I.EQ.3)GOTO 4032
      GOTO 4030
 4020 I=II
 4030 CP=H(I-1)+Q(I-1)*(CH(I-1)-R*ABS(Q(I-1)))-(Q(I-1)*DT*SO/AREAP(I-1
      HP(I)=0.5*(CP+H(I+1)+Q(I+1)*(R*ABS(Q(I+1))-CH(I+1))-(Q(I+1)*DT*S
     &AREAP(I+1)))
      QP(I)=(CP-HP(I))/CH(I)
      GOTO 3
 4031 CP=H(II-1)+Q(II-1)*(CH(II-1)-R*ABS(Q(II-1)))-(Q(II-1)*DT*SO
     &/AREAP(II-1))
      HP(I)=0.5*(CP+HA(1)+QA(1)*(R*ABS(QA(1))-CHA(1))-(QA(1)*DT*SO/
     &AREAPA(1)))
      QP(I)=(CP-HP(I))/CH(I)
      GOTO 3
 4032 CP=HA(NS2)+QA(NS2)*(CHA(NS2)-R*ABS(QA(NS2)))-(QA(NS2)*DT*SO
     &/AREAPA(NS2))
```

```
      HP(I)=0.5*(CP+H(I+1)+Q(I+1)*(R*ABS(Q(I+1))-CH(I+1))-(Q(I+1)*DT*SSFL03310
     &AREAP(I+1)))                                                      SFL03320
      QP(I)=(CP-HP(I))/CH(I)                                            SFL03330
      GOTO 3                                                            SFL03340
C     FOR RISER-MAIN PIPE JUNCTION                                      SFL03350
    5 I=II-(NS-NS1)                                                     SFL03360
C     R2=HEADLOSS ACROSS RISER                                          SFL03370
      R2=R                                                              SFL03380
      IF(QO.EQ.0.0)YEK(I)=0.0                                           SFL03390
      IF(QP(I-1).LE.0.0)YEK(I)=0.0                                      SFL03400
      IF(QP(I+1).LE.0.0)YEK(I)=0.0                                      SFL03410
      IF(DD(1).NE.DD(NS))YEK(I)=0.0                                     SFL03420
      DEN=DEN1                                                          SFL03430
      IF(QO.LE.TOQQ/40.0)GOTO 552                                       SFL03440
      CALL FLOSS(RR,NOR,RA,RQ,UQ)                                       SFL03450
      IF(IK.EQ.NOR)GOTO 126                                             SFL03460
      IF(RQ(IK-1,1).GT.0.0.AND.Q(I-NY+1).GT.0.0)DEN=1000.0              SFL03470
      GOTO 552                                                          SFL03480
  126 DEN=1000.0                                                        SFL03490
C                                                                       SFL03500
C                                                                       SFL03510
  552 CP1=H(I-1)+Q(I-1)*(CH(I-1)-R*ABS(Q(I-1)))-(Q(I-1)*DT*SO/AREAP(I-SFL03520
     &)                                                                 SFL03530
      C1=RH(IK,NPTR)+((RL(IK)+DD(1)/2.0)*(DEN/1000.0))-H(I)+(RR(IK)     SFL03540
     &*RL(IK)*RQ(IK,1)*ABS(RQ(IK,1)))-C2(IK)*RQ(IK,1)                   SFL03550
      CM3=H(I+1)-YEK(I)-Q(I+1)*(CH(I+1)-R*ABS(Q(I+1)))                  SFL03560
     &-(Q(I+1)*DT*SO/AREAP(I+1))                                        SFL03570
      CM3B=H(I+1)-Q(I+1)*(CH(I+1)-R2*ABS(Q(I+1)))-(Q(I+1)*DT*SO/AREAP SFL03580
     &(I+1))                                                            SFL03590
      HP(I)=((CP1/CH(I-1))+((RHP(IK,NPTR)+((RL(IK)+DD(1)/2.0)           SFL03600
     &*DEN/1000.0))/C2(IK))+(C1/C2(IK))+(CM3B/CH(I+1))-(YEK(I)/CH(I+1)SFL03610
     &/((1.0/CH(I+1))+(1.0/C2(IK))+(1.0/CH(I-1)))                       SFL03620
      RHP(IK,1)=HP(I)                                                   SFL03630
      QP(I)=0.0                                                         SFL03640
      UQP(I)=(-HP(I)/CH(I-1))+(CP1/CH(I-1))                             SFL03650
      RQP(IK,1)=(HP(I)/C2(IK))-((RHP(IK,NPTR)+((RL(IK)+DD(1)/2.0)       SFL03660
     &*DEN/1000.0))/C2(IK))-(C1/C2(IK))                                 SFL03670
      DQP(I)=((HP(I)+YEK(I))/CH(I+1))-(CM3B/CH(I+1))                    SFL03680
C     DHP(I)=HP(I)+((UQP(I)**2)/(19.62*(AREAP(I)**2)))-                 SFL03690
C    &((DQP(I)**2)/(19.62*(AREAP(I)**2)))                               SFL03700
C                                                                       SFL03710
C     PRINT*,' I=',I,' HP(I)=',HP(I)                                    SFL03720
C     PRINT*,' UQP(I)=',UQP(I),' DQP(I)=',DQP(I)                        SFL03730
C                                                                       SFL03740
      DHP(I)=HP(I)+((UQP(I)**2)/(19.62*(AREAP(I)**2)))-                 SFL03750
     &((DQP(I)**2)/(19.62*(AREAP(I)**2)))-((2.0*DQP(I)**2)/(19.62       SFL03760
     &*AREAP(I)**2))                                                    SFL03770
      YEK(I)=DHP(I)-HP(I)                                               SFL037
      GOTO 3                                                            SFL03790
    6 I=II-(NS-NS1)                                                     SFL03800
      IF(DQP(I-1).LT.0.0)DH(I-1)=H(I-1)                                 SFL03810
      CP=DH(I-1)+DQ(I-1)*(CH(I)-R*ABS(DQ(I-1)))-(DQ(I-1)*DT*SO          SFL03820
     &/AREAP(I-1))                                                      SFL03830
      HP(I)=0.5*(CP+H(I+1)+Q(I+1)*(R*ABS(Q(I+1))-CH(I+1))-(Q(I+1)*DT*SSFL03840
     &/AREAP(I+1)))                                                     SFL03850
      QP(I)=(CP-HP(I))/CH(I)                                            SFL03860
      GOTO 3                                                            SFL03870
    8 I=II-(NS-NS1)                                                     SFL03880
      DEN=DEN1                                                          SFL03890
      IF(QO.LE.TOQQ/50.0)GOTO 542                                       SFL03900
      IF(RQ(IK+1,1).LT.0.0)GOTO 542                                     SFL03910
      IF(RQ(IK-1,1).GT.0.0.AND.Q(I-NY+1).GT.0.0)DEN=1000.0              SFL03920
  542 CP1=H(I-1)+Q(I-1)*(CH(I-1)-R*ABS(Q(I-1)))-(Q(I-1)*DT*SO           SFL03930
     &/AREAP(I-1))                                                      SFL03940
      C1=RH(IK,NPTR)+((RL(IK)+DD(1)/2.0)*(DEN/1000.0))-H(I)+(RR(IK)     SFL03950
     &*RL(IK)*RQ(IK,1)*ABS(RQ(IK,1)))-C2(IK)*RQ(IK,1)                   SFL03960
```

```
      HP(I)=((CP1/CH(I-1))+((RHP(IK,NPTR)+((RL(IK)+DD(1)/2.0)
     &*DEN/1000.0))/C2(IK))+(C1/C2(IK)))/((1.0/CH(I-1))+(1.0/C2(IK)))
      RQP(IK,1)=(HP(I)/C2(IK))-((RHP(IK,NPTR)+((RL(IK)+DD(1)/2.0)
     &*DEN/1000.0))/C2(IK))-(C1/C2(IK))
      UQP(I)=(-HP(I)/CH(I-1))+(CP1/CH(I-1))
      QP(I)=0.0
      RHP(1,1)=HP(I)
      GOTO 3
    7 I=II-(NS-NS1)
      CP=H(I-1)+Q(I-1)*(CH(I-1)-R*ABS(Q(I-1)))+(Q(I-1)*DT*SO/AREAP(I-1
      HP(I)=0.5*(CP+H(I+1)+UQ(I+1)*(R*ABS(UQ(I+1))-CH(I+1))
     &-((UQ(I+1)*DT*SO)/AREAP(I+1)))
      QP(I)=(CP-HP(I))/CH(I)
    3 CONTINUE
C     FOR RISERS
C     BOUNDARY CONDITIONS
C     UPSTREAM END OF OUTFALL
      IF(TFG.EQ.'Y')GOTO 499
      IF(NO.LT.10)GOTO 49
  499 CALL INCFLO(DT,QO,TOQQ,TFG)
   49 IF(TFH.EQ.'Y')THEN
      HF=PH
      ELSE
      HF=HF+(((QO-Q(1))/AREAS)*DT)
      ENDIF
      HP(1)=HF-(1.0*(Q(1)**2)/(2.0*9.81*(AREAP(1)**2)))
      QP(1)=(HP(1)-H(2)-Q(2)*(R*ABS(Q(2))-CH(1)))/CH(1)
      IF(ARESU.EQ.0.0)GOTO 256
      IF(RESU.LE.ARESU+DT.AND.RESU.GE.ARESU-DT)GOTO 256
      GOTO 257
  256 RESU=0.0
      NAKL=NAKL+1
      PRINT*,' NAKL=',NAKL
C     PROGRAM STABALISES AFTER ABOUT 20 SECS
      IF(TC.LE.40.0)GOTO 25
      CALL COLDAT(RQP,HC,HF,TC,NOR,NPTR,IRESU,HW,T,AREARP,TOQQ)
      WRITE(9,259)TC
  259 FORMAT(' TIME=',F14.8)
      WRITE(9,452)HF
  452 FORMAT(' LEVEL OF WATER AT UPTREAM END=',F12.6)
      WRITE(9,466)QO
  466 FORMAT(' FLOW RATE INTO OUTFALL =',F14.9)
C     PRINT RESULTS
      DO 25 I=1,NS1
      DO 29 IK=1,NOR
      IF(I.EQ.NS1-((IK-1)*NY))GOTO 27
   29 CONTINUE
      IF(NS.GT.100.AND.I.GT.1)GOTO 520
      GOTO 521
  520 IF(I.LT.NS-100)GOTO 25
  521 IJ=I
      WRITE(9,26)IJ,HP(IJ),QP(IJ)
   26 FORMAT(I4,2X,F12.6,3X,F12.6)
      GOTO 25
   27 WRITE(9,28)I,HP(I),QP(I),RQP(IK,1),DQP(I),UQP(I)
      WRITE(9,288)DHP(I),RR(IK)
  288 FORMAT(F12.6,3X,F14.6)
      WRITE(9,567)HC(IK)
  567 FORMAT(' WAVEHEIGHT=',F12.7)
      DO 33 IX=1,NPTR
      WRITE(9,*)RHP(IK,IX),RQP(IK,IX)
   33 CONTINUE
   28 FORMAT(I4,1X,F12.6,1X,F12.6,1X,F12.6,1X,F12.6,1X,F12.6)
   25 CONTINUE
  257 DO 20 I=1,NS
      H(I)=HP(I)
```

```
      Q(I)=QP(I)
   20 CONTINUE
      DO 77 IY=1,NS-500
      HA(IY)=HPA(IY)
      QA(IY)=QPA(IY)
   77 CONTINUE
      DO 50 II=1,15
      DO 50 JJ=1,10
      RH(II,JJ)=RHP(II,JJ)
      RQ(II,JJ)=RQP(II,JJ)
   50 CONTINUE
      DO 51 I=1,NS
      DQ(I)=DQP(I)
      UQ(I)=UQP(I)
      DH(I)=DHP(I)
   51 CONTINUE
C     IF(RESU.LE.0.25+DT/2.0.AND.RESU.GE.0.25-DT/2.0)GOTO 121
C     IF(RESU.GT.0.0)GOTO 22
      DO 2369 IS=1,NOR
      P2=PI*DR(IS)
      DSB=DSA(IS)
      T2=0.0
      UV=RQP(IS,1)/(FLOAT(NOR)*AREARP(IS))
      IF(UV.EQ.0.0)GOTO 2369
      CALL FRIFAC(ROU,DR(IS),UV,AREARP(IS),P2,T2,FFF)
      DSA(IS)=FFF/(2.0*9.81*(AREARP(IS)**2))
      RR(IS)=RR(IS)-DSB+DSA(IS)
 2369 CONTINUE
   22 CONTINUE
      IRESU=5000
      CALL COLDAT(RQ,HC,HF,TC,NOR,NPTR,IRESU,HW,T,AREARP,TOQQ)
      RETURN
      END
      SUBROUTINE FRIFAC(ROW,D,UU,UA,P,T2,AY)
C
C     ***********************************************************
C     *   THIS SUBROUTINE USES THE COLEBROOK-WHITE             *
C     *   EQN. TO CALCULATE THE FRICTION FACTOR FOR            *
C     *   FLOWING LAYER, NOT INTERFACE.                        *
C     ***********************************************************
C
C     ROW=PIPE ROUGHNESS,D=PIPE DIAMETER,U=VELOCITY
C     UA=AREA,P=PERIMETER,T2=INTERFACE BETWEEN 2 LAYERS,
C     AY=CALCULATED FRICTION FACTOR
      DIMENSION ZU(2000)
      U=ABS(UU)
      RR=UA/(P+T2)
      REN=4.0*U*RR/1.1E-06
      IF(REN.LT.1000.0)GOTO 107
      DO 10 JJ=1,2000
      ZU(JJ)=0.0
   10 CONTINUE
      ZUU=0.0
      I=0
      AA=0.0
      ZUL=0.0
      ZKK=0.0
      I=1
      ZU(1)=0.0
      ZU(2)=5.0
   20 I=I+1
      AA=ZU(I)
      ZX=-2.0*LOG10((ROW/(14.83*RR))+(2.51/(REN*SQRT(AA))))
      ZY=1.0/(SQRT(AA))
      ZKK=ZX-ZY
      IF(ZKK.LE.0.1E-12.AND.ZKK.GE.-0.1E-12)GOTO 30
```

```
      IF(ZKK.GT.0.0)GOTO 40
      IF(ZKK.LE.0.0)GOTO 50
   40 ZUU=ZU(I)
      ZU(I+1)=(ZUU+ZUL)/2.0
      GOTO 20
   50 ZUL=ZU(I)
      IF(ZUL.LE.0.1E-10)ZUL=0.0
      ZU(I+1)=(ZUU+ZUL)/2.0
      GOTO 20
   30 AY=AA
      GOTO 986
  985 AY=0.000001
      GOTO 986
  107 AY=64.0/REN
  986 RETURN
  987 END
      SUBROUTINE DATA(ARESU,AJ)
C
C     ***********************************************************
C     *   SUBROUTINE DATA REQUESTS AND COLLECTS ALL THE         *
C     *   INFORMATION REQUIRED TO RUN THE PROGRAM.              *
C     ***********************************************************
C
      DIMENSION RPQ(10),AJ(15)
      COMMON/DATA1/AREAP(500),AREARP(15),AREAS,RPL,TOL,DD(500),
     &ROU,SWL,DEN,NOR
      COMMON/DATA2/HW,T,WL,END,SO,DR(15),RL(15),A(500),DEN1,
     &AA(15),TOQ,TOQQ,CH(500),CH2(15),C2(15)
      CALL CLEAR
      WRITE(6,10)
   10 FORMAT(' INPUT THE OUTFALL LENGTH, DIAMETER OF SURGE STRUCTURE,
     &AND ROUGHNESS ')
      READ(5,*)TOL,DS,ROU
      WRITE(6,20)
   20 FORMAT(' INPUT THE SEAWATER LEVEL AND DENSITY ')
      READ(5,*)SWL,DEN1
      DEN=1000.0
      WRITE(6,30)
   30 FORMAT(' INPUT THE RISER SPACING AND NUMBER OF RISERS ')
      READ(5,*)RPL,NOR
      CALL CLEAR
      WRITE(6,11)
   11 FORMAT(' INPUT WAVEHEIGHT AND WAVEPERIOD ')
      READ(5,*)HW,T
      CALL WAVEL(T,SWL,WL)
      WRITE(6,12)
   12 FORMAT(' TIME FOR END OF RUN AND SLOPE OF OUTFALL ')
      READ(5,*)END,SO
      PRINT*,' RISER 1= SEAWARD RISER '
      DO 200 IJ=1,NOR
      WRITE(6,14)
   14 FORMAT(' INPUT RISER DIAMETER, RISER LENGTH ')
      READ(5,*)DR(IJ),RL(IJ)
      IF(RL(IJ).EQ.0.0)RL(IJ)=0.005
      IF(IJ.EQ.NOR)GOTO 988
      WRITE(6,15)IJ,IJ+1
   15 FORMAT(' INPUT DIAMETER OF MAIN PIPE BETWEEN RISERS ',I2,'AND',I
     &)
      READ(5,*)DD(IJ)
      GOTO 200
  988 WRITE(6,16)IJ
   16 FORMAT(' INPUT DIAMETER OF MAIN PIPE BETWEEN RISER ',I2,'AND SUR
     &TANK ')
      READ(5,*)DD(IJ)
  200 CONTINUE
      CALL CLEAR
```

```
      PRINT*,' INPUT CALCULATED DESIGN FLOW & EXPECTED FLOW '
      READ(5,*)TOQ,TOQQ
      PI=4.0*ATAN(1.0)
      DX=RPL/3.0
      NS=INT(TOL/DX)+1
      NY=INT(RPL/DX)
      IF(NY.LT.1)NY=1
      DO 300 IK=1,NOR
      AREARP(IK)=PI*(DR(IK)**2)/4.0
      N1=(IK-1)*NY+1
      N2=IK*NY
      IF(IK.EQ.NOR)N2=NS
      DO 600 IJ=N1,N2
      AREAP(IJ)=PI*(DD(IK)**2)/4.0
      DD(IJ)=DD(IK)
  600 CONTINUE
  300 CONTINUE
      AREAS=PI*(DS**2)/4.0
      WRITE(6,5)
    5 FORMAT(' INPUT THE INTERVAL IN SECONDS AT WHICH RESULTS TO
     &BE PRINTED ')
      READ(5,*)ARESU
      CALL SPEED(AJ)
      RETURN
      END
      SUBROUTINE SPEED(AJ)
C
C     ***********************************************************
C     *   SUBROUTINE SPEED CALCULATES THE SPEED OF              *
C     *   PASSAGE OF THE INTERNAL WAVE WITHIN THE PIPE          *
C     ***********************************************************
C
      COMMON/DATA1/AREAP(500),AREARP(15),AREAS,RPL,TOL,DD(500),
     &ROU,SWL,DEN,NOR
      COMMON/DATA2/HW,T,WL,END,SO,DR(15),RL(15),A(500),DEN1,
     &AA(15),TOQ,TOQQ,CH(500),CH2(15),C2(15)
      DIMENSION AJ(15)
C     THIS SUBROUTINE CALCULATES THE SPEED OF THE INTERNAL WAVE
C     WITHIN THE PIPE FROM THE PROPERTIES OF FRESH WATER AND MATERIAL
C     OF CONSTRUCTION OF THE PIPE
      CALL CLEAR
      WRITE(6,1)
    1 FORMAT(' INPUT THE VALUE OF THE BULK MODULUS OF FRESH WATER (N/M
     &2) ')
      READ(5,*)BMW
      WRITE(6,2)
    2 FORMAT(' INPUT YOUNGS MODULUS OF MAIN PIPE MATERIAL AND YOUNGS M
     &[illegible] RISER PIPE '/' MATERIAL (N/M2) ')
      READ(5,*)EP,ER
      WRITE(6,3)
    3 FORMAT(' INPUT WALL THICKNESS OF MAIN PIPE AND WALL THICKNESS OF
     &RISER PIPE (M) ')
      READ(5,*)TP,TR
C     FOR MAIN PIPE
      PRINT*,' SPEED CALCULATION '
      DO 400 I=1,NOR
      AJ(I)=SQRT((BMW/1000.0)/(1.0+((BMW/EP)*(DD(I)/TP))))
      PRINT*,'I= ',I,' AJ(I)= ',AJ(I)
C     FOR RISER PIPES
      AA(I)=SQRT((BMW/1000.0)/(1.0+((BMW/ER)*(DR(I)/TR))))
  400 CONTINUE
      RETURN
      END
      SUBROUTINE WAVEL(T,D,WL)
C
C     ***********************************************************
```

```
C     *    SUBROUTINE WAVEL CALCULATES THE WAVELENGTH         *              SFL06610
C     *    TO BE USED IN THE PROGRAM.                         *              SFL06620
C     *****************************************************              SFL06630
C                                                                        SFL06640
      PI=4.0*ATAN(1.0)                                                   SFL06650
      I=0                                                                SFL06660
      EL0=(9.81*(T**2))/(2.0*PI)                                         SFL06670
      EL1=EL0                                                            SFL06680
    1 EL2=((9.81*(T**2))/(2.0*PI))*TANH((2.0*PI*0.9)/EL1)                SFL06690
      I=I+1                                                              SFL06700
      ERR=ABS(EL1-EL2)                                                   SFL06710
      IF(I.EQ.1000)GOTO 3                                                SFL06720
      IF(ERR.LE.0.1E-3)GOTO 2                                            SFL06730
      EL1=EL2                                                            SFL06740
      GOTO 1                                                             SFL06750
    2 WL=EL2                                                             SFL06760
      GOTO 4                                                             SFL06770
    3 WL=(EL1+EL2)/2.0                                                   SFL06780
    4 RETURN                                                             SFL06790
      END                                                                SFL06800
      SUBROUTINE RISFRI(RR,RPQ,R,TFG,ARESU,AJ,TFH,PH)                    SFL06810
C                                                                        SFL06820
C     *****************************************************              SFL06830
C     *    SUBROUTINE RISFRI CALCULATES THE FRICTION          *          SFL06840
C     *    CONDITIONS IN THE OUTFALL AND RISERS WHILST        *          SFL06850
C     *    THE OUTFALL IS RUNNING UNDER FULL FLOW             *          SFL06860
C     *    CONDITIONS. THIS SUBROUTINE ALSO CALLS THE         *          SFL06870
C     *    SUBROUTINE 'MOFC' IF THE CALCULATIONS ARE TO       *          SFL06880
C     *    START WITH THE OUTFALL DISCHARGING AT FULL         *          SFL06890
C     *    CAPACITY.                                          *          SFL06900
C     *****************************************************              SFL06910
C                                                                        SFL06920
      DIMENSION QPO(500),H(500),Q(500),HP(500),QP(500)                   SFL06930
      DIMENSION RH(15,2),RQ(15,2),DQ(500),UQ(500),YH(15,2),AJ(15)        SFL06940
      DIMENSION HH(500),QQ(500),UQQ(500),DQQ(500),RR(15),YEK(500)        SFL06950
      DIMENSION DD2(500),AREAP2(500)                                     SFL06960
      CHARACTER*1 TFG,TFH                                                SFL06970
      COMMON/DATA1/AREAP(500),AREARP(15),AREAS,RPL,TOL,DD(500),          SFL06980
     &ROU,SWL,DEN,NOR                                                    SFL06990
      COMMON/DATA2/HW,T,WL,END,SO,DR(15),RL(15),A(500),DEN1,             SFL07000
     &AA(15),TOQ,TOQQ,CH(500),CH2(15),C2(15)                             SFL07010
      DX=RPL/3.0                                                         SFL07020
      DT=DX/AJ(1)                                                        SFL07030
      CDD=0.9                                                            SFL07040
      CHSWL=DEN1*SWL/1000.0                                              SFL07050
      DX2=DT*AA(NOR)                                                     SFL07060
C     ANPTR=(RL(NOR)/DX2)+1.0+0.5                                        SFL07070
C     NPTR=INT(ANPTR)                                                    SFL07080
      NPTR=2                                                             SFL07090
      PRINT*,' NPTR',NPTR                                                SFL07100
      DX2=RL(NOR)/FLOAT(NPTR-1)                                          SFL07110
      DX2=0.0                                                            SFL07120
      N=INT(TOL/DX)                                                      SFL07130
      NS1=N+1                                                            SFL07140
      NS=N+1                                                             SFL07150
      IF(NS.GT.500)NS=500                                                SFL07160
      NY=INT(RPL/DX)                                                     SFL07170
      IF(NY.LT.1)NY=1                                                    SFL07180
      PI=4.0*ATAN(1.0)                                                   SFL07190
      RQ(NOR,1)=RPQ                                                      SFL07200
      UQ(1)=RPQ                                                          SFL07210
      T2=0.0                                                             SFL07220
      P=PI*DD(1)                                                         SFL07230
      P2=PI*DR(NOR)                                                      SFL07240
      U=(RQ(NOR,1)*FLOAT(NOR))/AREAP(1)                                  SFL07250
      UU=RQ(NOR,1)/AREARP(NOR)                                           SFL07260
```

```
      CALL FRIFAC(ROU,DD(1),U,AREAP(1),P,T2,FF)
      PRINT*,' FF=',FF
      CALL FRIFAC(ROU,DR(NOR),UU,AREARP(NOR),P2,T2,FFF)
      PRINT*,' FFF=',FFF
      R=(FF*DX)/(2.0*9.81*DD(1)*(AREAP(1)**2))
C     SECOND PART OF RR(NOR) TAKES HEADLOSS AT TOP OF RISER
      RR(NOR)=(FFF)/(2.0*9.81*DR(NOR)*(AREARP(NOR)**2))
     &+((1.5/(2.0*9.81*(AREARP(NOR)**2)))/RL(NOR))
     &+((10.0/(2.0*9.81*(AREARP(NOR)**2)))/RL(NOR))
      PRINT*,' RR(NOR)=',RR(NOR)
C     CALCULATION OF INITIAL VALUES
      NRIS=NOR
      RH(NOR,1)=((DEN1/1000.0)*(SWL-RL(NOR)-DD(1)/2.0))-((RQ(NOR,1)**2
     &/(2.0*9.81*(AREARP(NOR)**2)))+(RR(NOR)*RL(NOR)*(RQ(NOR,1)**2))
     &+RL(NOR)+DD(1)/2.0
      RH(NOR,NPTR)=RH(NOR,1)-RL(NOR)-DD(1)/2.0-(RR(NOR)*RL(NOR)*
     &(RQ(NOR,1)**2))
      RQ(NOR,NPTR)=RQ(NOR,1)
      TQ=TOQ-RQ(NOR,1)
      NK=((NOR-1)*NY)+1
      UQ(NK)=TOQ
      DQ(NK)=TOQ-RQ(NOR,1)
      H(NK)=RH(NOR,1)
      H(NK+1)=H(NK)+(R*(TOQ**2))+(SO*DX)
      Q(NK+1)=TOQ
      DO 2450 IL=1,NK-1
      DO 2451 KJ=1,NOR
      IF((NK-IL).EQ.(1+(KJ-1)*NY))GOTO 2452
      IF((NK-IL).EQ.((KJ-1)*NY))GOTO 2455
 2451 CONTINUE
      H(NK-IL)=H(NK-IL+1)-(R*(TQ**2))-(SO*DX)
      Q(NK-IL)=TQ
      GOTO 2450
 2452 H(NK-IL)=H(NK-IL+1)-(R*(TQ**2))-(SO*DX)
      UQ(NK-IL)=TQ
      NRIS=NRIS-1
      INN=NK-IL
      LE=NS-IL
      PRINT*,' H(INN)=',H(INN)
      PRINT*,' RISERV CALLED AT LINE 730 '
      CALL RISERV(H,RH,RQ,RR,DX2,TQ,NPTR,INN,NRIS,LE)
      DQ(NK-IL)=TQ
      GOTO 2450
 2455 PRINT*,' AREAP(NS-NK+IL+2)=',AREAP(NS-NK+IL+2)
      PRINT*,' NS=',NS
      PRINT*,' IL=',IL
      PRINT*,' NK=',NK
      H(NK-IL)=H(NK-IL+2)-((Q(NK-IL+2)**2)/
     &(2.0*9.81*(AREAP(NS-NK+IL-2)**2)))-
     &((DQ(NK-IL+1)**2)/(2.0*9.81*(AREAP(NS-NK+IL-2)**2)))-
     &(R*(Q(NK-IL+2)**2))-(R*(DQ(NK-IL+1)**2))
      Q(NK-IL)=TQ
 2450 CONTINUE
      IF(NS1.LE.500)THEN
      DO 2453 IK=NK+2,NS
      H(IK)=H(IK-1)+(R*(TOQ**2))+(SO*DX)
      Q(IK)=TOQ
 2453 CONTINUE
      ELSE
      DO 2463 IK=NK+2,NS-2
      H(IK)=H(IK-1)+(R*(TOQ**2))+(SO*DX)
      Q(IK)=TOQ
 2463 CONTINUE
      H(NS-1)=H(NS-2)+(R*(TOQ**2)*FLOAT(NS1-500))+(SO*DX*FLOAT
     &(NS1-500))
      H(NS)=H(NS-1)+(R*(TOQ**2))+(SO*DX)
```

```
      ENDIF
C
      IF(TFG.EQ.'N')GOTO 2955
C     HF=LEVEL OF WATER IN UPSTREAM TANK
      HF=(1.0/9810.0)*(9810.0*H(NS))
C     INITIAL CONDITIONS IN RISERS
      DO 25 II=1,NS
      HH(II)=H(NS-II+1)
      QQ(II)=Q(NS-II+1)
      UQQ(II)=UQ(NS-II+1)
      DQQ(II)=DQ(NS-II+1)
      AREAP2(II)=AREAP(NS-II+1)
      DD2(II)=DD(NS-II+1)
   25 CONTINUE
      DO 252 MP=1,NS
      AREAP(MP)=AREAP2(MP)
      DD(MP)=DD2(MP)
  252 CONTINUE
      DO 40 I=1,NS
      WRITE(9,41)I,H(I),Q(I),HH(I),QQ(I)
   41 FORMAT(2X,I5,1X,F12.6,1X,F12.6,1X,F12.6,1X,F12.6)
   40 CONTINUE
      DO 457 I=2,NOR
      KI=NS-((I-1)*NY)
      YEK(KI)=H(KI+1)-H(KI)
  457 CONTINUE
      QO=TOQQ
      CALL MOFC(R,RR,FF,HH,QQ,NY,QPO,HF,RH,RQ,UQQ,DQQ,ARESU
     &,TFG,YEK,AJ,QO,TFH,PH)
      GOTO 2956
 2955 RETURN
 2956 STOP
      END
      SUBROUTINE RISERV(H,RH,RQ,RR,DX2,TQ,NPTR,IN,IJ,LE)
C
C     ***************************************************************
C     *   SUBROUTINE RISERV SETS FRICTION CONDITIONS IN       *
C     *   THE RISERS AS WELL AS THE INITIAL FLOW              *
C     *   CONDITIONS                                          *
C     ***************************************************************
C
      DIMENSION RH(15,2),RQ(15,2),RR(15),H(500),HLK(15)
      CHARACTER*1 AAZ,ZXC
      COMMON/DATA1/AREAP(500),AREARP(15),AREAS,RPL,TOL,DD(500),
     &ROU,SWL,DEN,NOR
      COMMON/DATA2/HW,T,WL,END,SO,DR(15),RL(15),A(500),DEN1,
     &AA(15),TOQ,TOQQ,CH(500),CH2(15),C2(15)
      RQ(IJ,1)=RQ(NOR,1)
      CHSWL=DEN1*SWL/1000.0
      CDD=0.9
      RH(IJ,1)=((DEN1/1000.0)*(SWL-RL(NOR)-DD(1)/2.0))-((RQ(NOR,1)**2)
     &/(2.0*9.81*(AREARP(NOR)**2)))+(RR(NOR)*RL(NOR)*(RQ(NOR,1)**2))
     &+RL(NOR)+DD(1)/2.0
  851 RQ(IJ,NPTR)=RQ(IJ,1)
      PRINT*,' IN=',IN,' H(IN)=',H(IN)
      IF(RL(IJ).EQ.0.0)GOTO 701
      IF(RQ(IJ,1).EQ.0.0)GOTO 700
      CALL HEALOS(NOR,HLK,ZXC,AREARP)
      IF(ZXC.EQ.'N')GOTO 5132
      DO 5133 JKL=1,NOR
      RR(JKL)=HLK(JKL)+RR(NOR)
 5133 CONTINUE
      GOTO 900
 5132 RR(IJ)=((H(IN)-RH(IJ,1))/(RQ(IJ,1)**2))/RL(IJ)
      RR(IJ)=RR(IJ)+RR(NOR)
      PRINT*,' DD(IJ)=',DD(IJ),' DD(IJ-1)=',DD(IJ-1)
```

```
      IF(I.LT.5000)GOTO 25
   35 DO 456 JK=1,NOR
      AVRQ(JK)=TRQF(JK)/FLOAT(I)
  456 CONTINUE
      CALL PLOT(TT,HU,RQF,HCW,I,HW,T,NOR,AVRQ,TOQQ)
   25 RETURN
      END
      SUBROUTINE PLOT(TT,HU,RQF,HCW,I,HW,T,NOR,AVRQ,TOQQ)
C
C     ******************************************************
C     *    THIS SUBROUTINE PLOTS THE RESULTS OF THE         *
C     *    VELOCITIES OBTAINED WITHIN THE RISERS            *
C     ******************************************************
C
      DIMENSION TT(2000),HU(2000),RQF(15,2000),HCW(15,2000)
      DIMENSION X(2000),Y(2000),YY1(2000),YY2(2000),
     &YY3(2000),YY4(2000),AVRQ(15),YY5(2000),YY6(2000),YY7(2000),
     &YY8(2000),YY9(2000)
      NN=I
      SS=0.0
      SSS=0.0
      AA=0.0
      AB=0.0
      AC=0.0
      SL=10000.0
      AAL=10000.0
      ABL=10000.0
      ACL=10000.0
      CALL GINO
      CALL SAVDRA
      DO 601 KJ=1,15
      DO 601 KL=1,NN
      IF(SS.LE.TT(KL))SS=TT(KL)
      IF(SL.GE.TT(KL))SL=TT(KL)
      IF(AA.LE.HU(KL))AA=HU(KL)
      IF(AAL.GE.HU(KL))AAL=HU(KL)
      IF(AB.LE.RQF(KJ,KL))AB=RQF(KJ,KL)
      IF(ABL.GE.RQF(KJ,KL))ABL=RQF(KJ,KL)
      IF(AC.LE.HCW(KJ,KL))AC=HCW(KJ,KL)
      IF(ACL.GE.HCW(KJ,KL))ACL=HCW(KJ,KL)
  601 CONTINUE
      CALL PAPER(AXILX,AXILY,TX,TY,ZX5,ZX6)
      CALL CHASIZ(2.0,3.0)
      NPIC=1
      CALL PICBEG(NPIC)
      CALL AXIPOS(1,(TX+ZX5+ZX5),(TY+ZX6),AXILX,1)
      CALL AXISCA(1,10,SL,SS,1)
      CALL AXIDRA(1,1,1
      CALL AXIPOS(1,(TX+ZX5+ZX5),(TY+ZX6),AXILY,2)
      CALL AXISCA(3,5,AAL,AA,2)
      CALL AXIDRA(1,-1,2)
      PRINT*,' NN= ',NN
      DO 610 JJ=1,NN
      Y(JJ)=HU(JJ)
      X(JJ)=TT(JJ)
  610 CONTINUE
      CALL GRASYM(X,Y,NN,2,1000)
      CALL GRAPOL(X,Y,NN)
      AXILXT=0.0
      AXILYT=0.0
      CALL TITLE(NPIC,AXILX,AXILY,TX,TY,ZX5,ZX6,AXILXT,AXILYT)
      XP=(TX+ZX5+ZX5+TX+ZX5+ZX5+AXILX)/2.0
      YP=(TY+ZX6+TY+ZX6+AXILY)/2.0
      CALL PICCLE
C
C     END OF GRAPH 1
```

```
C
      DO 75 KM=1,NOR,4
      SSS=0.0
      DO 61 KP=1,NN
      YY1(KP)=RQF(KM,KP)
      YY2(KP)=RQF(KM+1,KP)
      YY3(KP)=RQF(KM+2,KP)
      YY4(KP)=RQF(KM+3,KP)
      YY5(KP)=AVRQ(KM)
      YY6(KP)=AVRQ(KM+1)
      YY7(KP)=AVRQ(KM+2)
      YY8(KP)=AVRQ(KM+3)
      YY9(KP)=0.0
   61 CONTINUE
      CALL PAPER(AXILX,AXILY,TX,TY,ZX5,ZX6)
      CALL CHASIZ(2.0,3.0)
      NPIC=NPIC+1
      CALL PICBEG(NPIC)
      AXILXT=AXILX/10.0
      AXILYT=AXILY/10.0

C     GRAPH1
C     PRINT*,' SETTING UP X AXIS-1.'
      CALL AXIPOS(1,(TX+ZX5+ZX5),(TY+ZX6),(4.0*AXILXT),1)
      CALL AXISCA(1,10,SL,SS,1)
      CALL AXIDRA(1,1,1)
C
      CALL AXIPOS(1,(TX+ZX5+ZX5),(TY+ZX6),(4.0*AXILYT),2)
      CALL AXISCA(1,10,ABL,AB,2)
      CALL AXIDRA(1,-1,2)
C
      CALL GRASYM(X,YY3,NN,6,1000)
      CALL GRAPOL(X,YY3,NN)
      CALL BROKEN(1)
      CALL GRAPOL(X,YY7,NN)
      CALL BROKEN(2)
      CALL GRAPOL(X,YY9,NN)
      CALL BROKEN(0)
C
C     GRAPH2
      CALL AXIPOS(1,(TX+ZX5+ZX5+(6.0*AXILXT)),(TY+ZX6),(4.0*AXILXT),1)
      CALL AXISCA(1,10,SL,SS,1)
      CALL AXIDRA(1,1,1)
C
      CALL AXIPOS(1,(TX+ZX5+ZX5+(6.0*AXILXT)),(TY+ZX6),(4.0*AXILYT),2)
      CALL AXISCA(1,10,ABL,AB,2)
      CALL AXIDRA(1,-1,2)
C
      CALL GRASYM(X,YY4,NN,6,1000)
      CALL GRAPOL(X,YY4,NN)
      CALL BROKEN(1)
      CALL GRAPOL(X,YY8,NN)
      CALL BROKEN(2)
      CALL GRAPOL(X,YY9,NN)
      CALL BROKEN(0)
C
C     GRAPH3
C     PRINT*,' SETTING UP X AXIS-1.'
      CALL AXIPOS(1,(TX+ZX5+ZX5),(TY+ZX6+(6.0*AXILYT)),(4.0*AXILXT),1)
      CALL AXISCA(1,10,SL,SS,1)
      CALL AXIDRA(1,1,1)
C
      CALL AXIPOS(1,(TX+ZX5+ZX5),(TY+ZX6+(6.0*AXILYT)),(4.0*AXILYT),2)
      CALL AXISCA(1,10,ABL,AB,2)
      CALL AXIDRA(1,-1,2)
C
```

```
      CALL GRASYM(X,YY1,NN,6,1000)
      CALL GRAPOL(X,YY1,NN)
      CALL BROKEN(1)
      CALL GRAPOL(X,YY5,NN)
      CALL BROKEN(2)
      CALL GRAPOL(X,YY9,NN)
      CALL BROKEN(0)
C
C     GRAPH4
C     PRINT*,' SETTING UP X AXIS-1.'
      CALL AXIPOS(1,(TX+ZX5+ZX5+(6.0*AXILXT)),(TY+ZX6+(6.0*AXILYT)),
     &(4.0*AXILXT),1)
      CALL AXISCA(1,10,SL,SS,1)
      CALL AXIDRA(1,1,1)
C
      CALL AXIPOS(1,(TX+ZX5+ZX5+(6.0*AXILXT)),(TY+ZX6+(6.0*AXILYT)),
     &(4.0*AXILYT),2)
      CALL AXISCA(1,10,ABL,AB,2)
      CALL AXIDRA(1,-1,2)
C
      CALL GRASYM(X,YY2,NN,6,1000)
      CALL GRAPOL(X,YY2,NN)
      CALL BROKEN(1)
      CALL GRAPOL(X,YY6,NN)
      CALL BROKEN(2)
      CALL GRAPOL(X,YY9,NN)
      CALL BROKEN(0)
C
      CALL TITLE(NPIC,AXILX,AXILY,TX,TY,ZX5,ZX6,AXILXT,AXILYT,KM,
     &TOQQ,HW,T)
      XP=(TX+ZX5+ZX5+TX+ZX5+ZX5+AXILX)/2.0
      YP=(TY+ZX6+TY+ZX6+AXILY)/2.0
C
      CALL PICCLE
   75 CONTINUE
      CALL DEVEND
      STOP
      END
      SUBROUTINE PAPER(AXILX,AXILY,TX,TY,ZX5,ZX6)
C
C     ***************************************************************
C     *  SUBROUTINE DEFINES THE PAPER SIZE FOR THE                  *
C     *  PLOTTING ROUTINES.                                         *
C     ***************************************************************
C
      CHARACTER*1 RR
      WRITE(6,10)
   10 FORMAT(49H DEFINE PAPER SIZE A0,A1,A2,A3,A4,OWN=0,1,2,3,4,5)
      READ(3,*)IN
      IF(IN.EQ.5) THEN
      WRITE(6,20)
   20 FORMAT(23H INPUT PAPER SIZE X & Y)
      READ(3,*)XX,YY
      ELSE
      IF(IN.EQ.0) THEN
      X=1188.0
      Y=840.0
      ELSE IF(IN.EQ.1) THEN
      X=840.0
      Y=594.0
      ELSE IF(IN.EQ.2) THEN
      X=594.0
      Y=420.0
      ELSE IF(IN.EQ.3) THEN
      X=420.0
      Y=297.0
```

```
      ELSE IF(IN.EQ.4) THEN
      X=297.0
      Y=210.0
      END IF
      WRITE(6,30)
   30 FORMAT(39H IS PAPER VERTICAL OR HORIZONTAL=V OR H)
      READ(3,40)RR
   40 FORMAT(A1)
      IF(RR.EQ.'H') THEN
      XX=X
      YY=Y
      ELSE
      XX=Y
      YY=X
      END IF
      END IF
C     DEFINE AREAS FOR WINDOW
      XN=XX+10.0
      YN=YY+10.0
      CALL DEVPAP(XX,YY,0.0)
      CALL WINDO2(0.0,XN,0.0,YN)
C     DEFINE DRAWING AREA
C     CALL MOVTO2(0.0,0.0)
C     CALL LINTO2(XX,0.0)
C     CALL LINTO2(XX,YY)
C     CALL LINTO2(0.0,YY)
C     CALL LINTO2(0.0,0.0)
C
      ZY1=YY*15.0/100.0
      ZY2=YY*8.0/100.0
      ZX1=YY*8.0/100.0
      ZX2=YY*2.0/100.0
      IF(RR.EQ.'V')GOTO 50
C     CALL MOVTO2(ZX1,ZY2)
C     CALL LINTO2(XX-ZX2,ZY2)
C     CALL LINTO2(XX-ZX2,YY-ZY1)
C     CALL LINTO2(ZX1,YY-ZY1)
C     CALL LINTO2(ZX1,ZY2)
      ZX6=ZX1
      ZX5=ZX1
      TX=ZX1
      TY=ZY2
      AXILX=(XX-ZX1-ZX2)*72.0/100.0
      AXILY=(YY-ZY1-ZY2)*66.0/100.0
      GOTO 60
   50 CALL MOVTO2(ZY1,ZX1)
C     CALL LINTO2(XX-ZY2,ZX1)
C     CALL LINTO2(XX-ZY2,YY-ZX2)
C     CALL LINTO2(ZY1,YY-ZX2)
C     CALL LINTO2(ZY1,ZX1)
      ZX6=ZX1
      ZX5=ZX2
      TX=ZY1
      TY=ZX1
      AXILX=(XX-ZY1-ZY2)*72.0/100.0
      AXILY=(YY-ZX1-ZX2)*66.0/100.0
   60 RETURN
      END
      SUBROUTINE TITLE(IPIC,AXILX,AXILY,TX,TY,ZX5,ZX6,AXILXT,AXILYT,KM
     &,TOQQ,HW,T)
C
C     ************************************************************
C     *    THIS SUBROUTINE CALLS THE TITLES FOR THE              *
C     *    OUTPUT FROM THE PLOTTING PROGRAM.                     *
C     ************************************************************
C
```

```
      DIMENSION ZZZ(15),ZQ(20)
      IF(IPIC.EQ.1)THEN
      CALL MOVTO2((TX+ZX5+ZX5+AXILX/3.0),(TY+ZX6-15.0))
      CALL CHASTR(' TIME IN SECS ')
      CALL CHAANG(90.0)
      CALL MOVTO2((TX+ZX5+ZX5-20.0),(TY+ZX6+AXILY/4.0))
      CALL CHASTR(' LEVEL OF WATER IN SURGE STRUCTURE ')
      CALL MOVTO2((TX+ZX5+ZX5+AXILX/4.0),(TY+ZX6+AXILY))
      CALL CHAANG(0.0)
      CALL CHASTR(' GRAPH TO SHOW LEVEL OF WATER IN SURGE STRUCTURE ')
      ELSE IF(IPIC.GT.1)THEN
      NPIC=IPIC-1
      CALL MOVTO2((TX+ZX5+ZX5+AXILX/5.0),(TY+ZX6-15.0))
      CALL CHASTR(' Y-AXIS = RISER VELOCITY (M/S),
     &X-AXIS = TIME (SECS) ')
C     CALL MOVTO2((TX+ZX5+ZX5+AXILX/3.0),(TY+ZX6-23.0))
C     CALL CHASTR(' FIG 2 - GRAPH SHOWING RISER VELOCITY AGAINST TIME
C    &')
      CALL MOVTO2((TX+ZX5+ZX5+AXILX/5.0),(TY+ZX6-23.0))
      CALL CHASTR(' WAVEHEIGHT= ')
      CALL MOVTO2((TX+ZX5+ZX5+(2.0*AXILX/4.0)),(TY+ZX6-23.0))
      CALL CHASTR(' WAVEPERIOD= ')
      CALL MOVTO2((TX+ZX5+ZX5+(8.0*AXILX/10.0)),(TY+ZX6-23.0))
      CALL CHASTR(' FLOW RATE= ')
      CALL MOVTO2((TX+ZX5+ZX5+AXILX/5.0+23.0),(TY+ZX6-23.0))
      CALL CHAFIX(HW,9,5)
      CALL MOVTO2((TX+ZX5+ZX5+(AXILX/2.0)+23.0),(TY+ZX6-23.0))
      CALL CHAFIX(T,9,5)
      CALL MOVTO2((TX+ZX5+ZX5+AXILX/1.0-20.0),(TY+ZX6-23.0))
      CALL CHAFIX(TOQQ,9,5)
C
      CALL MOVTO2((TY+ZX5+ZX5+AXILXT),(TY+ZX6+(4.5*AXILYT)))
      CALL CHASTR(' RISER  ')
      CALL MOVTO2((TY+ZX5+ZX5+AXILXT+14),(TY+ZX6+(4.5*AXILYT)))
      CALL CHAINT(KM+2,-5)
      CALL MOVTO2((TY+ZX5+ZX5+(7.0*AXILXT)),(TY+ZX6+(4.5*AXILYT)))
      CALL CHASTR(' RISER  ')
      CALL MOVTO2((TY+ZX5+ZX5+(7.0*AXILXT)+14),(TY+ZX6+(4.5*AXILYT)))
      CALL CHAINT(KM+3,-5)
      CALL MOVTO2((TY+ZX5+ZX5+AXILXT),(TY+ZX6+(10.5*AXILYT)))
      CALL CHASTR(' RISER  ')
      CALL MOVTO2((TY+ZX5+ZX5+AXILXT+14),(TY+ZX6+(10.5*AXILYT)))
      CALL CHAINT(KM,-5)
      CALL MOVTO2((TY+ZX5+ZX5+(7.0*AXILXT)),(TY+ZX6+(10.5*AXILYT)))
      CALL CHASTR(' RISER  ')
      CALL MOVTO2((TY+ZX5+ZX5+(7.0*AXILXT)+14),(TY+ZX6+(10.5*AXILYT)))
      CALL CHAINT(KM+1,-5)
      CALL MOVTO2((TX+ZX5+ZX5+AXILX/3.0),(TY+(2.0*ZX6)+AXILY))
      CALL CHASTR(' THEORETICAL MODEL ')
      ENDIF
      RETURN
      END
C
      SUBROUTINE WAVEP(HW,D,Y,WL,TF,T,D2,PR)
C
C     ******************************************************************
C     *   SUBROUTINE WAVEP CALCULATES THE ATTENUATED                   *
C     *   WAVE PRESSURE.                                               *
C     ******************************************************************
C
      PI=4.0*ATAN(1.0)
      PP=(COSH(2.0*PI*(D-(D-D2-Y))/WL))/(COSH(2.0*PI*D/WL))
      PR=PP*HW
      RETURN
      END
C
```

```
      SUBROUTINE HEALOS(NOR,HLK,ZXC,AREARP)
      DIMENSION HLK(15),AREARP(15)
      CHARACTER*1 ZXC
C     THIS SUBROUTINE ALLOWS THE DESIGNER TO INPUT
C     THE HEAD LOSSES AT BENDS ETC. RATHER THAN LET
C     THE COMPUTER DECIDE WHAT THEY SHOULD BE.
C     VALUES ARE USUALLY OBTAINED FROM EXPERIMENTS
C     OR PUBLICATIONS.
      PRINT*,' DO YOU WANT TO INPUT YOUR OWN VALUES FOR '
      PRINT*,' HEADLOSS . '
      READ(5,20)ZXC
   20 FORMAT(A1)
      IF(ZXC.EQ.'N')GOTO 30
      PRINT*,' HEADLOSS DUE TO FRICTION IS CALCULATED USING '
      PRINT*,' COLEBROOK-WHITE EQUATION '
      DO 10 I=1,NOR
      HL1=0.0
      HL2=0.0
      HL3=0.0
      PRINT*,' FOR RISER',I
      PRINT*,' INPUT HEAD LOSS COEF. AT RISER MAIN PIPE JUNCTION '
      READ(5,*)HL1
      PRINT*,' INPUT HEAD LOSS COEF. AT RISER EXIT '
      READ(5,*)HL2
      PRINT*,' INPUT HEAD LOSS DUE TO CHANGE IN MAIN PIPE DIAMETER '
      READ(5,*)HL3
      HLK(I)=(HL1+HL2+HL3)/(2.0*9.81*AREARP(I))
   10 CONTINUE
   30 RETURN
      END
      SUBROUTINE FLOSS(RR,NOR,RA,RQ,UQ)
      DIMENSION RR(15),RA(15),RQ(15,2),UQ(500)
C     RA HOLDS INITIAL VALUES
      J=0
      DO 50 II=1,NOR
      RR(II)=RA(II)
   50 CONTINUE
      DO 10 I=1,NOR
      IF(RQ(I,1).LE.0.0)GOTO 20
      RR(I)=1.5*RA(I-J)
      GOTO 10
   20 J=J+1
      RR(I)=0.2*RA(I)
   10 CONTINUE
      RETURN
      END
```

Appendix E

Tables and graphical output obtained from work performed for Chapter 7.

Table E1

Wave Condition H_w (cm)	T (sec)	Riser 1	Observed flows* Riser 2	Riser 3	Riser 4
6.1	1.0	0	I	I	D
6.1	0.8	I	I	0	D
6.1	0.67	0	I	I	D
5.49	2.5	0	D	I	I
7.16	2.5	D	D	I	I
9.35	2.5	D	D	I	I
9.97	3.33	D	D	D	I
5.01	5.00	0	I	D	D

Motion in risers under shutdown conditions (A = 0) from observation of dye movements.

* D = Discharging
I = intrusive
0 = zero

Table E2

Flow rate = 0.0

Velocity

Waveheight (cm) Waveperiod (s)	Riser (m/s)	V_{max} (m/s)	V_{min} (m/s)	$\bar{V}$ (m/s)	σ_v
4.1 cm	1	0.0528	-0.0523	-0.0015	0.0351
	2	0.0320	-0.0420	-0.0023	0.0221
2.2225	3	0.0370	-0.0410	-0.0019	0.0247
	4	0.0474	-0.0410	0.0031	0.0267
4.4 cm	1	0.0538	-0.0577	-0.0012	0.0347
	2	0.0370	-0.0419	-0.0028	0.0240
1.375	3	0.0454	-0.0380	0.0025	0.0258
	4	0.0562	-0.0493	0.0035	0.0346
4.4 cm	1	0.0844	-0.0690	-0.0016	0.0407
	2	0.0370	-0.0419	-0.0028	0.0231
1.33 s	3	0.0474	-0.0459	0.0011	0.0293
	4	0.0612	-0.0543	0.0031	0.0350

Table E3

Flow rate = 0.0

Pressure

Waveheight (cm) Wave period (s)	Location (See fig.) Pressure point	P_{max} (KN/m²)	P_{min} (KN/m²)	$\bar{P}$ (KN/m²)	σ_v
4.1 cm	1	8.019	7.700	7.865	0.666
	2	8.024	7.724	7.880	0.059
2.2225	3	7.963	7.780	7.868	0.057
	4	8.001	7.753	7.871	0.054
	5	7.976	7.794	7.874	0.039
4.4 cm	1	7.972	7.763	7.866	0.058
	2	7.972	7.772	7.876	0.061
1.37 s	3	7.959	7.762	7.884	0.064
	4	7.978	7.769	7.872	0.061
	5	7.952	7.780	7.871	0.046
4.4 cm	1	7.963	7.735	7.848	0.048
	2	7.968	7.749	7.859	0.054
1.33 s	3	7.969	7.734	7.852	0.063
	4	7.730	7.727	7.856	0.063
	5	7.991	7.713	7.854	0.051

Table E4

Flow rate = 0.1862 L/s

Velocity

Waveheight (cm) Waveperiod (s)	Riser	V_{max} (m/s)	V_{min} (m/s)	$\overline{V}$ (m/s)	σ_V
0.0	1	-0.0020	-0.0133	-0.0059	0.0036
	2	0.0000	-0.0222	-0.0102	0.0043
0.0	3	0.0000	-0.0316	-0.0145	0.0087
	4	0.2161	0.0434	0.1431	0.0549
3.3 cm	1	0.0687	-0.0967	-0.0143	0.0536
	2	0.0163	-0.0607	-0.0260	0.0149
2.0 s	3	0.0118	-0.0765	-0.0351	0.0242
	4	0.3098	0.1001	0.1911	0.0574
4.5 cm	1	-0.0158	-0.0493	-0.0352	0.0065
	2	-0.0178	-0.0577	-0.0387	0.0067
0.667 s	3	-0.0301	-0.0883	-0.0565	0.0123
	4	0.2210	0.0898	0.1817	0.0146
5.5 cm	1	-0.0020	-0.0923	-0.0452	0.0192
	2	0.0158	-0.0651	-0.0260	0.0193
1.0 s	3	0.0316	-0.0681	-0.0192	0.0243
	4	0.2792	0.0498	0.2146	0.0263
5.8 cm	1	0.0001	-0.0315	-0.0168	0.0071
	2	-0.0019	-0.0458	-0.0279	0.0092
0.769 s	3	-0.0103	-0.0567	-0.0330	0.0099
	4	0.2078	0.1328	0.1708	0.0132
6.6 cm	1	0.0558	-0.1238	-0.0288	0.0475
	2	0.0370	-0.1002	-0.0327	0.0383
1.429 s	3	0.0720	-0.0632	-0.0062	0.0302
	4	0.3528	0.1110	0.2166	0.0620

Table E5

Flow rate = 0.1862 L/s

Pressure

Waveheight (cm) Waveperiod (s)	Pressure Point	P_{max} (kN/m^2)	P_{min} (kN/m^2)	$\bar{P}$ (kN/m^2)	σ_P
0.0	1	7.968	7.779	7.874	0.019
	2	7.955	7.797	7.973	0.016
0.0	3	7.883	7.844	7.868	0.054
	4	7.916	7.807	7.874	0.011
	5	7.912	7.747	7.851	0.016
3.3 cm	1	7.994	7.752	7.870	0.055
	2	7.995	7.747	7.866	0.053
2.0 s	3	7.990	7.733	7.864	0.078
	4	8.002	7.734	7.872	0.080
	5	7.978	7.737	7.862	0.056
5.8	1	7.955	7.854	7.902	0.013
	2	7.954	7.865	7.910	0.011
0.769	3	7.928	7.876	7.904	0.009
	4	7.951	7.861	7.907	0.015
	5	7.953	7.834	7.896	0.019
5.5 cm	1	8.025	7.692	7.901	0.035
	2	8.003	7.740	7.899	0.022
1.0 s	3	8.009	7.776	7.880	0.026
	4	-	-	-	-
	5	7.921	7.813	7.866	0.018
4.5 cm	1	7.947	7.779	7.870	0.029
	2	7.939	7.798	7.871	0.024
0.6667 s	3	7.907	7.831	7.864	0.012
	4	7.964	7.867	7.876	0.031
	5	8.012	7.728	7.855	0.045
6.6 cm	1	8.037	7.720	7.873	0.089
	2	8.020	7.710	7.872	0.064
1.429 s	3	7.993	7.719	7.859	0.080
	4	8.009	7.741	7.875	0.077
	5	8.012	7.725	7.863	0.060

Table E6

Flow rate = 0.355 L/s

Velocity

Waveheight (cm) Waveperiod (s)	Riser	V_{max} (m/s)	V_{min} (m/s)	$\bar{V}$ (m/s)	σ_V
0.0	1	-0.0178	-0.0494	-0.0329	0.0072
	2	-0.0134	-0.0524	-0.0265	0.0097
0.0	3	0.1158	-0.0144	0.0386	0.0368
	4	0.2663	0.0537	0.2064	0.0265
3.3 cm	1	0.0498	-0.1307	-0.0438	0.0545
	2	-0.0069	-0.0809	-0.0462	0.0157
2.0 s	3	0.1446	0.0104	0.0767	0.0277
	4	0.3404	0.1224	0.2173	0.0486
4.5 cm	1	-0.0262	-0.0657	-0.0090	0.0083
	2	-0.0148	-0.0632	-0.0412	0.0082
0.6667 s	3	0.1465	0.0419	0.0793	0.0165
	4	0.2746	0.1002	0.2008	0.0203
5.5 cm	1	-0.0094	-0.0863	-0.0496	0.0197
	2	-0.0049	-0.0933	-0.0531	0.0210
1.0 s	3	0.1243	-0.0138	0.0679	0.0265
	4	0.3138	0.1431	0.2201	0.0266
5.8 cm	1	-0.0231	-0.0724	-0.0489	0.0097
	2	-0.0458	-0.1080	-0.0770	0.0111
0.769 s	3	0.1160	0.0213	0.0681	0.0169
	4	0.2581	0.1368	0.1860	0.0191
6.6 cm	1	-0.0331	-0.1542	-0.0641	0.0443
	2	-0.0212	-0.1470	-0.0602	0.0384
1.429 s	3	0.1243	-0.0069	0.0557	0.0263
	4	0.4115	0.0750	0.2377	0.0700

Table E7

Flow rate - 0.3550 L/s

Pressure

Waveheight (cm) Waveperiod (s)	Pressure Point	P_{max} (kN/m²)	P_{min} (kN/m²)	$\bar{P}$ kN/m²)	σ_P
0.0	1	7.909	7.824	7.862	0.010
	2	7.904	7.837	7.870	0.008
0.0	3	7.894	7.841	7.866	0.005
	4	7.917	7.829	7.873	0.009
	5	7.962	7.719	7.854	0.022
3.3 cm	1	7.996	7.732	7.858	0.057
	2	7.992	7.719	7.857	0.066
2.0 s	3	7.983	7.675	7.851	0.080
	4	8.008	7.720	7.867	0.084
	5	7.983	7.717	7.850	0.062
4.5 cm	1	7.917	7.784	7.847	0.021
	2	7.923	7.185	7.859	0.018
0.6667 s	3	7.887	7.820	7.852	0.010
	4	7.946	7.808	7.875	0.026
	5	7.958	7.701	7.844	0.040
5.5 cm	1	7.996	7.767	7.874	0.032
	2	7.976	7.785	7.878	0.024
1.0 s	3	7.931	7.827	7.880	0.019
	4	7.989	7.832	7.902	0.028
	5	7.990	7.738	7.860	0.034
5.8 cm	1	7.928	7.814	7.879	0.014
	2	7.937	7.837	7.886	0.012
0.769 s	3	7.924	7.841	7.885	0.011
	4	7.965	7.802	7.896	0.017
	5	7.997	7.632	7.868	0.027
6.6 cm	1	8.009	7.667	7.848	0.087
	2	8.000	7.699	7.852	0.091
1.429 s	3	7.993	7.720	7.848	0.080
	4	8.044	7.708	7.865	0.077
	5	8.094	7.638	7.839	0.064

Table E8

Flow rate = 0.4842 L/s

Velocity

Waveheight (cm) Waveperiod	Riser	V_{max} (m/s)	V_{min} (m/s)	$\bar{V}$ (m/s)	σ_V
0.0	1	0.0054	-0.0262	-0.0087	0.0053
	2	-0.0104	-0.0725	-0.0322	0.0149
0.0	3	0.1603	0.0908	0.1287	0.0121
	4	0.2896	0.1534	0.2046	0.0184
3.3 cm	1	0.0400	-0.1283	-0.0500	0.0513
	2	-0.0227	-0.0942	-0.0610	0.0142
2.0 s	3	0.1737	0.0434	0.1059	0.0278
	4	0.2635	0.1011	0.1768	0.0331
4.5 cm	1	-0.0074	-0.0578	-0.0269	0.0078
	2	-0.0040	-0.0577	-0.0261	0.0105
0.6667 s	3	0.1692	0.0947	0.1248	0.0106
	4	0.2738	0.1559	0.2030	0.0191
5.5 cm	1	0.0170	-0.0812	-0.0400	0.0216
	2	0.0022	-0.0857	-0.0406	0.0193
1.0 s	3	0.1980	0.0574	0.1256	0.0268
	4	0.2745	0.1156	0.1924	0.0268
5.8 cm	1	-0.0262	-0.0681	-0.0477	0.0087
	2	-0.0153	-0.0651	-0.0435	0.0103
0.769 s	3	0.1559	0.0641	0.1118	0.0157
	4	0.3009	0.1746	0.2270	0.0197
6.6 cm	1	0.0340	-0.1209	-0.0440	0.0424
	2	0.0173	-0.1263	-0.0555	0.0345
1.429 s	3	0.1643	0.0484	0.1058	0.0260
	4	0.3296	0.0770	0.1889	0.0553

Table E9

Flow rate = 0.4842 L/s

Pressure

Waveheight (cm) Waveperiod (s)	Pressure Point	P_{max} (kN/m²)	P_{min} (kN/m²)	$\bar{P}$ (kN/m²)	σ_P
0.0	1	7.896	7.837	7.865	0.010
	2	7.895	7.840	7.866	0.007
0.0	3	7.892	7.846	7.869	0.006
	4	7.912	7.843	7.876	0.012
	5	7.914	7.750	7.857	0.029
3.3 cm	1	8.001	7.744	7.866	0.055
	2	7.983	7.736	7.865	0.064
2.0 s	3	8.001	7.717	7.861	0.081
	4	8.016	7.695	7.866	0.084
	5	8.030	7.685	7.855	0.068
4.5 cm	1	7.977	7.784	7.882	0.026
	2	7.956	7.788	7.886	0.023
0.6667 s	3	7.930	7.843	7.888	0.014
	4	7.988	7.788	7.895	0.025
	5	8.037	7.712	7.878	0.045
5.5 cm	1	8.009	7.730	7.857	0.038
	2	7.939	7.756	7.854	0.024
1.0 s	3	7.921	7.747	7.850	0.027
	4	-	-	-	-
	5	7.931	7.732	7.840	0.027
5.8 cm	1	7.942	7.821	7.888	0.019
	2	7.948	7.842	7.899	0.015
0.769 s	3	7.942	7.864	7.909	0.011
	4	7.993	7.845	7.918	0.022
	5	8.032	7.764	7.891	0.040
6.6 cm	1	8.210	7.802	7.952	0.085
	2	8.167	7.785	7.949	0.081
1.429 s	3	8.073	7.794	7.941	0.079
	4	8.187	7.792	7.956	0.078
	5	8.096	7.789	7.942	0.061

Table E10

Flow rate = 0.531 L/s

Velocity

Waveheight (cm) Waveperiod (s)	Risers	V_{max} (m/s)	V_{min} (m/s)	$\bar{V}$ (m/s)	σ_V
0.0	1	-0.0104	-0.0419	-0.0279	0.0085
	2	-0.0291	-0.0577	-0.0442	0.0005
0.0	3	0.1850	0.0814	0.1389	0.0170
	4	0.3158	0.1603	0.2226	0.0232
3.3 cm	1	0.0592	-0.1283	-0.0414	0.0553
	2	0.0054	-0.0809	-0.0393	0.0184
2.0 s	3	0.2304	0.0222	0.1581	0.0252
	4	0.3611	0.1534	0.2343	0.0400
4.5 cm	1	-0.0316	-0.0775	-0.0574	0.0094
	2	-0.0202	-0.0733	-0.0410	0.0087
0.6667 s	3	0.1959	0.0893	0.1479	0.0144
	4	0.3246	0.1737	0.2380	0.0229
5.5 cm	1	0.0138	-0.0775	-0.0371	0.0187
	2	-0.0049	-0.0849	-0.0445	0.0170
1.0 s	3	0.2432	0.0972	0.1710	0.0270
	4	0.3266	0.1485	0.2323	0.0282
5.8 cm	1	-0.0262	-0.0725	-0.0479	0.0089
	2	-0.0178	-0.0735	-0.0494	0.0102
0.769 s	3	0.1801	0.0878	0.1283	0.0149
	4	0.3098	0.1603	0.2260	0.0249
6.6 cm	1	0.0640	-0.1210	-0.0357	0.0462
	2	0.0295	-0.1210	-0.0494	0.0331
1.429 s	3	0.2461	0.0611	0.1592	0.0400
	4	0.4000	0.1223	0.2349	0.0506

Table E11

Flow rate = 0.531 L/s

Pressure

Waveheight (cm) Waveperiod	Pressure Point	P_{max} (kN/m^2)	P_{min} (kN/m^2)	$\bar{P}$ (kN/m^2)	σ_P
0.0	1	7.913	7.850	7.883	0.009
	2	7.913	7.855	7.883	0.007
0.0	3	7.899	7.860	7.881	0.007
	4	7.917	7.834	7.867	0.011
	5	7.970	7.780	7.871	0.027
3.3 cm	1	7.978	7.755	7.862	0.056
	2	8.002	7.746	7.868	0.066
2.0 s	3	8.004	7.721	7.866	0.082
	4	8.016	7.701	7.858	0.085
	5	8.035	7.689	7.856	0.068
4.5 cm	1	7.960	7.818	7.886	0.020
	2	7.965	7.833	7.893	0.019
0.6667 s	3	7.934	7.853	7.895	0.013
	4	7.993	7.851	7.925	0.021
	5	8.022	7.773	7.884	0.036
5.5 cm	1	8.017	7.737	7.858	0.038
	2	7.940	7.772	7.856	0.025
1.0 s	3	7.939	7.774	7.859	0.025
	4	-	-	-	-
	5	7.940	7.762	7.847	0.026
5.8 cm	1	7.961	7.793	7.889	0.024
	2	7.960	7.800	7.893	0.020
0.769 s	3	7.935	7.846	7.895	0.014
	4	7.992	7.773	7.905	0.027
	5	8.027	7.720	7.880	0.045
6.6 cm	1	8.042	7.717	7.887	0.085
	2	8.046	7.734	7.899	0.088
1.429 s	3	8.053	7.750	7.904	0.090
	4	8.082	7.755	7.911	0.086
	5	8.085	7.683	7.877	0.075

Table E12

Flow rate = 0.6026 L/s

Velocity

Waveheight (cm) Waveperiod (s)	Riser	V_{max} (m/s)	V_{min} (m/s)	$\bar{V}$ (m/s)	σ_V
0.0	1	-0.0094	-0.0385	-0.0267	0.0057
	2	-0.0054	-0.0459	-0.0253	-0.0098
0.0	3	0.1737	0.0957	0.1343	0.0129
	4	0.3000	0.1401	0.2128	0.0265
3.3 cm	1	0.0370	-0.1885	-0.0809	0.0567
	2	-0.0212	-0.0947	-0.0621	0.0140
2.0 s	3	0.1978	0.0632	0.1301	0.0299
	4	0.3320	0.1199	0.2047	0.0354
4.5 cm	1	-0.0104	-0.0277	-0.0361	0.0099
	2	0.0025	-0.0375	-0.0146	0.0072
0.6667 s	3	0.1909	0.1120	0.1482	0.0146
	4	0.3276	0.1673	0.2290	0.0258
5.5 cm	1	-0.0004	-0.0867	-0.0491	0.0172
	2	0.0080	-0.0887	-0.0444	0.0193
1.0 s	3	0.2221	0.0652	0.1441	0.0278
	4	0.3021	0.1442	0.2115	0.0279
5.8 cm	1	-0.0158	-0.0617	-0.0373	0.0091
	2	-0.0252	-0.0765	-0.0499	0.0109
0.769 s	3	0.1751	0.0770	0.1250	0.0175
	4	0.2867	0.1288	0.2022	0.0246
6.6 cm	1	0.6612	-0.1150	-0.0310	0.0478
	2	0.0222	-0.1174	-0.0579	0.0374
1.429 s	3	0.2225	0.0947	0.1596	0.0275
	4	0.3769	0.1011	0.2337	0.0600

Table E13

Flow rate = 0.6026 L/s

Pressure

Waveheight (cm) Waverperiod (s)	Pressure Point	P_{max} (kN/m²)	P_{min} (kN/m²)	$\bar{P}$ (kN/m²)	σ_P
0.0	1	7.959	7.816	7.883	0.017
	2	7.944	7.814	7.878	0.015
0.0	3	7.903	7.858	7.880	0.006
	4	7.943	7.824	7.890	0.016
	5	7.997	7.742	7.867	0.038
3.3 cm	1	7.955	7.731	7.837	0.056
	2	7.954	7.729	7.843	0.063
2.0 s	3	7.976	7.673	7.821	0.080
	4	7.979	7.699	7.821	0.085
	5	8.038	7.645	7.836	0.072
4.5 cm	1	7.972	7.832	7.910	0.022
	2	7.992	7.843	7.914	0.020
0.6667 s	3	7.967	7.871	7.921	0.016
	4	8.014	7.855	7.928	0.023
	5	8.042	7.782	7.907	0.039
5.5 cm	1	8.024	7.643	7.840	0.048
	2	7.971	7.697	7.839	0.034
1.0 s	3	7.954	7.748	7.847	0.032
	4	-	-	-	-
	5	7.973	7.701	7.840	0.038
5.8 cm	1	7.954	7.823	7.889	0.019
	2	7.946	7.798	7.892	0.017
0.769 s	3	7.933	7.858	7.895	0.011
	4	7.946	7.794	7.890	0.021
	5	8.025	7.765	7.890	0.040
6.6 cm	1	8.036	7.716	7.885	0.081
	2	8.036	7.734	7.893	0.084
1.429 s	3	8.037	7.741	7.891	0.084
	4	8.066	7.753	7.907	0.080
	5	8.066	7.717	7.879	0.069

Table E14

Flow rate = 0.6310 L/s

Velocity

Waveheight (cm) Waveperiod (s)	Riser	V_{max} (m/s)	V_{min} (m/s)	$\bar{V}$ (m/s)	σ_V
0.0	1	-0.0059	-0.0311	-0.0163	0.0048
	2	-0.0019	-0.0261	-0.0152	0.0044
0.0	3	0.1742	0.0962	0.1309	0.0123
	4	0.2798	0.1485	0.2023	0.0228
3.3 cm	1	-0.0040	-0.1791	-0.0833	0.0390
	2	-0.0133	-0.1016	-0.0533	0.0210
2.0 s	3	0.2077	0.0735	0.1375	0.0303
	4	0.3222	0.1485	0.2215	0.0310
4.5 cm	1	-0.0082	-0.0501	-0.0334	0.0094
	2	-0.0062	-0.0427	-0.0256	0.0081
0.6667 s	3	0.1901	0.0875	0.1368	0.0160
	4	0.2656	0.1319	0.1874	0.0225
5.5 cm	1	0.0025	-0.0780	-0.0402	0.0178
	2	0.0138	-0.0706	-0.0361	0.0173
1.0 s	3	0.2274	0.0804	0.1603	0.0279
	4	0.2842	0.1278	0.02024	0.0272
5.8 cm	1	-0.0158	-0.0607	-0.0393	0.0084
	2	-0.0153	-0.0528	-0.0340	0.0091
0.769 s	3	0.1993	0.0770	0.1433	0.0192
	4	0.2945	0.1485	0.2139	0.0248
6.6 cm	1	0.0474	-0.1105	-0.0364	0.0436
	2	0.0316	-0.1041	-0.0402	0.0355
1.429 s	3	0.2151	0.0844	0.1453	0.0249
	4	0.3789	0.1189	0.2347	0.0543

Table E15

Flow rate = 0.6310 L/s

Pressure

Waveheight (cm) Waveperiod (s)	Pressure Point	P_{max} (kN/m^2)	P_{min} (kN/m^2)	$\bar{P}$ (kN/m^2)	σ_P
0.0	1	7.894	7.817	7.853	0.011
	2	7.887	7.822	7.857	0.009
0.0	3	7.890	7.832	7.856	0.008
	4	7.909	7.820	7.869	0.012
	5	7.987	7.709	7.846	0.039
3.3 cm	1	8.064	7.704	7.878	0.082
	2	8.033	7.688	7.857	0.084
2.0 s	3	8.040	7.703	7.866	0.086
	4	-	-	-	-
	5	7.960	7.727	7.842	0.050
4.5 cm	1	7.963	7.785	7.875	0.029
	2	7.949	7.805	7.879	0.024
0.6667 s	3	7.926	7.836	7.888	0.016
	4	7.984	7.797	7.898	0.031
	5	8.025	7.722	7.871	0.049
5.5 cm	1	8.036	7.685	7.867	0.057
	2	7.996	7.724	7.859	0.037
1.0 s	3	7.981	7.723	7.870	0.035
	4	-	-	-	-
	5	7.947	7.736	7.847	0.030
5.8 cm	1	7.943	7.776	7.875	0.023
	2	7.938	7.808	7.880	0.019
0.769 s	3	7.921	7.836	7.885	0.014
	4	7.960	7.786	7.887	0.027
	5	8.077	7.697	7.871	0.049
6.6 cm	1	7.990	7.664	7.833	0.087
	2	7.990	7.673	7.830	0.082
1.429 s	3	7.976	7.682	7.826	0.081
	4	7.973	7.690	7.827	0.077
	5	8.003	7.647	7.821	0.069

Table E16

Flow rate = 0.6547 L/s

Velocity

Waveheight (cm) Waveperiod (s)	Riser	V_{max} (m/s)	V_{min} (m/s)	$\bar{V}$ (m/s)	σ_V
0.0	1	-0.0261	-0.0473	-0.0370	0.0043
	2	-0.0104	-0.0419	-0.0251	0.0064
0.0	3	0.1801	0.1085	0.1455	0.0116
	4	0.3315	0.1559	0.2256	0.0265
3.3 cm	1	0.0592	-0.1125	-0.0301	0.0516
	2	0.0010	-0.0676	-0.0382	0.0138
2.0 s	3	0.2210	0.0844	0.1452	0.0267
	4	0.3271	0.1169	0.2042	0.0322
4.5 cm	1	-0.0094	-0.0617	-0.0380	0.0098
	2	-0.0133	-0.0493	-0.0316	0.0081
0.6667 s	3	0.2077	0.0972	0.1478	0.0175
	4	0.3296	0.1840	0.2491	0.0240
5.5 cm	1	-0.0133	-0.0992	-0.0606	0.0189
	2	-0.0158	-0.0992	-0.0579	0.0212
1.0 s	3	0.2077	0.0454	0.1448	0.0269
	4	0.3158	0.1367	0.2272	0.0302
5.8 cm	1	-0.0262	-0.0733	-0.0500	0.0098
	2	-0.0607	-0.1105	-0.0858	0.0110
0.769 s	3	0.2117	0.1002	0.1943	0.0184
	4	0.3054	0.1559	0.2256	0.0264
6.6 cm	1	0.0587	-0.1367	-0.0457	0.0531
	2	0.0316	-0.1105	-0.0459	0.0377
1.429 s	3	0.2274	0.0972	0.1637	0.0281
	4	0.3740	0.1130	0.2370	0.0572

Table E17

Flow rate = 0.6547 L/s

Pressure

Waveheight (cm) Waveperiod (s)	Pressure Point	P_{max} (kN/m^2)	P_{min} (kN/m^2)	$\bar{P}$ (kN/m^2)	σ_P
0.0	1	7.884	7.822	7.858	0.009
	2	7.879	7.826	7.856	0.007
0.0	3	7.873	7.824	7.854	0.007
	4	7.890	7.801	7.847	0.012
	5	7.958	7.667	7.845	0.035
3.3 cm	1	7.972	7.726	7.850	0.058
	2	7.986	7.718	7.858	0.065
2.0 s	3	7.996	7.717	7.859	0.083
	4	8.000	7.691	7.847	0.085
	5	8.061	8.094	7.848	0.081
4.5 cm	1	7.950	7.801	7.892	0.018
	2	7.936	7.821	7.891	0.015
0.6667 s	3	7.924	7.869	7.896	0.011
	4	7.981	7.856	7.918	0.017
	5	8.034	7.707	7.884	0.045
5.5 cm	1	7.975	7.764	7.870	0.030
	2	7.948	7.794	7.881	0.023
1.0 s	3	7.937	7.817	7.876	0.019
	4	7.958	7.801	7.881	0.026
	5	8.063	7.662	7.662	0.065
5.8 cm	1	7.961	7.802	7.880	0.022
	2	7.942	7.818	7.886	0.017
0.769 s	3	7.917	7.850	7.885	0.010
	4	7.952	7.804	7.879	0.023
	5	8.079	7.678	7.875	0.057
6.6 cm	1	8.003	7.642	7.819	0.093
	2	7.976	7.664	7.832	0.086
1.429 s	3	7.952	7.668	7.806	0.083
	4	7.976	7.679	7.813	0.082
	5	8.073	7.594	7.815	0.076

Table E18

Flow rate = 0.9441 L/s

Velocity

Waveheight (cm) Waveperiod (s)	Riser	V_{max} (m/s)	V_{min} (m/s)	$\bar{V}$ (m/s)	σ_V
0.0	1	-0.0375	-0.0854	-0.0616	0.0085
	2	0.1668	0.0804	0.1187	0.0143
0.0	3	0.2526	0.1105	0.1682	0.0215
	4	0.2955	0.1381	0.1925	0.0228
3.3 cm	1	0.0612	-0.1579	-0.0537	0.0645
	2	0.2368	0.1002	0.1576	0.0219
2.0 s	3	0.2580	0.1011	0.1788	0.0270
	4	0.3380	0.1002	0.1932	0.0414
4.5 cm	1	-0.0469	-0.0937	-0.0733	0.0096
	2	0.1747	0.0745	0.1186	0.0165
0.6667 s	3	0.2635	0.1273	0.1804	0.0204
	4	0.3113	0.1643	0.2173	0.0226
5.5 cm	1	-0.0578	-0.1460	-0.1014	0.0187
	2	0.1949	0.0632	0.1226	0.0232
1.0 s	3	0.2700	0.0789	0.1719	0.0333
	4	0.2699	0.1002	0.1754	0.0289
5.8 cm	1	-0.0336	-0.0859	-0.0649	0.0089
	2	0.1801	0.0789	0.1331	0.0194
0.769 s	3	0.2306	0.0947	0.1650	0.0227
	4	0.2886	0.1288	0.1937	0.0253
6.6 cm	1	0.0064	-0.1673	-0.0826	0.0474
	2	0.2235	0.1628	0.1370	0.0451
1.429 s	3	0.2383	0.0957	0.1684	0.0277
	4	0.3478	0.0498	0.1916	0.0610

Table E19

Flow rate = 0.9441 L/s

Pressure

Waveheight (cm) Waveperiod (s)	Pressure Point	P_{max} (kN/m²)	P_{min} (kN/m²)	$\bar{P}$ (kN/m²)	σ_P
0.0	1	7.912	7.784	7.850	0.017
	2	7.895	7.772	7.843	0.015
0.0	3	7.880	7.823	7.847	0.008
	4	7.889	7.789	7.839	0.016
	5	8.038	8.082	7.838	0.055
3.3 cm	1	7.985	7.737	7.863	0.057
	2	8.009	7.738	7.881	0.064
2.0 s	3	8.030	7.737	7.878	0.076
	4	8.049	7.729	7.886	0.084
	5	8.155	7.560	7.863	0.084
4.5 cm	1	8.017	7.807	7.896	0.028
	2	7.987	7.814	7.899	0.024
0.6667 s	3	7.957	7.864	7.910	0.015
	4	7.992	7.811	7.902	0.026
	5	8.057	7.687	7.888	0.048
5.5 cm	1	7.944	7.743	7.850	0.029
	2	7.932	7.769	7.857	0.020
1.0 s	3	7.940	7.823	7.866	0.018
	4	7.941	7.781	7.854	0.028
	5	8.059	7.611	7.839	0.069
5.8 cm	1	7.993	7.808	7.887	0.024
	2	7.971	7.791	7.887	0.022
0.769 s	3	7.932	7.835	7.889	0.014
	4	7.979	7.786	7.882	0.026
	5	8.064	7.682	7.874	0.050
6.6 cm	1	7.995	7.648	7.830	0.088
	2	7.997	7.662	7.840	0.081
1.429 s	3	7.982	7.687	7.824	0.077
	4	8.015	7.672	7.836	0.076
	5	8.100	7.517	7.815	0.086

Table E20

Flow rate = 2.0 L/s

Velocity

Waveheight (cm) Waveperiod (s)	Riser	V_{max} (m/s)	V_{min} (m/s)	$\bar{V}$ (m/s)	σ_V
0.0	1	0.3182	0.1559	0.2192	0.0258
	2	0.3089	0.1317	0.1958	0.0262
0.0	3	0.3024	0.1194	0.2157	0.0294
	4	0.3015	0.1317	0.2217	0.0287
3.3 cm	1	0.3562	0.1327	0.2116	0.0346
	2	0.3024	0.1115	0.2046	0.0357
2.0 s	3	0.2906	0.1169	0.2058	0.0260
	4	0.3158	0.1421	0.2188	0.0307
4.5 cm	1	0.3454	0.1534	0.2200	0.0267
	2	0.2980	0.1120	0.1957	0.0276
0.6667 s	3	0.2857	0.1243	0.1967	0.0232
	4	0.2847	0.1263	0.1960	0.0255
5.5 cm	1	0.2980	0.1426	0.2113	0.0245
	2	0.3064	0.1317	0.2171	0.0343
1.0 s	3	0.3138	0.1085	0.2070	0.0361
	4	0.3434	0.1317	0.2227	0.0315
5.8 cm	1	0.2926	0.1421	0.2021	0.0208
	2	0.2822	0.1002	0.1856	0.0290
0.769 s	3	0.2748	0.1327	0.1904	0.0235
	4	0.3113	0.1278	0.2053	0.0282
6.6 cm	1	0.3330	0.1367	0.2023	0.0314
	2	0.3340	0.1011	0.2125	0.0402
1.429 s	3	0.3261	0.1120	0.2170	0.0331
	4	0.3454	0.0804	0.2059	0.0496

Table E21

Flow rate = 2.0 L/s

Pressure

Waveheight (cm) Waveperiod (s)	Pressure Point	P_{max} (kN/m^2)	P_{min} (kN/m^2)	$\bar{P}$ (kN/m^2)	σ_P
0.0	1	8.023	7.773	7.938	0.020
	2	8.031	7.872	7.955	0.021
0.0	3	7.989	7.798	7.904	0.027
	4	7.991	7.810	7.904	0.028
	5	8.148	7.567	7.880	0.090
3.3 cm	1	8.015	7.691	7.858	0.052
	2	8.049	7.753	7.887	0.053
2.0 s	3	8.016	7.691	7.856	0.055
	4	7.991	7.706	7.867	0.048
	5	8.160	7.510	7.843	0.098
4.5 cm	1	8.161	7.645	7.915	0.073
	2	8.131	7.709	7.943	0.058
0.6667 s	3	8.079	7.729	7.904	0.058
	4	7.984	7.781	7.879	0.029
	5	8.207	7.549	7.872	0.097
5.5 cm	1	8.057	7.779	7.891	0.041
	2	8.055	7.775	7.906	0.032
1.0 s	3	7.992	7.729	7.868	0.037
	4	7.958	7.760	7.867	0.030
	5	8.147	7.529	7.850	0.087
5.8 cm	1	8.197	7.341	8.003	0.064
	2	8.192	7.831	8.005	0.051
0.769 s	3	8.120	7.819	7.961	0.045
	4	8.032	7.843	7.943	0.029
	5	8.212	7.583	7.903	0.093
6.6 cm	1	8.217	7.643	7.896	0.113
	2	8.192	7.673	7.924	0.098
1.429 s	3	8.114	7.668	7.891	0.082
	4	8.033	7.710	7.871	0.058
	5	8.193	7.499	7.863	0.103

Table E22

Flow rate = 0.1862 L/s

Velocity

Waveheight (cm) Waveperiod (s)	Riser	V_{max} (m/s)	V_{min} (m/s)	$\overline{V}$ (m/s)	σ_V
0.0	1	0.0000	-0.0291	-0.0140	0.0047
	2	0.0054	-0.0316	-0.0111	0.0062
0.0	3	0.1263	0.0296	0.0742	0.0170
	4	0.1446	0.0632	0.1044	0.0151
5.8 cm	1	0.0025	-0.0365	-0.0178	0.0074
	2	-0.0049	-0.0449	-0.0246	0.0080
0.769 s	3	0.1317	0.0340	0.0818	0.0161
	4	0.1643	0.0735	0.1167	0.0149

Table E23

Flow rate = 0.3550 L/s

Velocity

Waveheight (cm) Waveperiod (s)	Riser	V_{max} (m/s)	V_{min} (m/s)	$\overline{V}$ (m/s)	σ_V
0.0	1	0.0025	-0.0207	-0.0087	0.0042
	2	0.0183	-0.0133	0.0007	0.0052
0.0	3	0.1579	0.0641	0.1143	0.0158
	4	0.1717	0.0715	0.1107	0.0156
5.8 cm	1	0.0104	-0.0316	-0.0122	0.0073
	2	0.0089	-0.0311	-0.0124	0.0081
0.769 s	3	0.1515	0.0612	0.1096	0.0129
	4	0.1687	0.0498	0.1144	0.0178

Table E24

Flow rate = 0.1862 L/s

Pressure

Waveheight (cm) Waveperiod (s)	Pressure Point	P_{max} (kN/m^2)	P_{min} (kN/m^2)	$\bar{P}$ (kN/m^2)	σ_P
0.0	1	7.893	7.824	7.862	0.008
	2	7.887	7.847	7.863	0.006
0.0	3	7.874	7.835	7.857	0.007
	4	7.869	7.849	7.858	0.003
	5	7.889	7.820	7.855	0.008
5.8 cm	1	8.202	7.624	7.876	0.076
	2	8.111	7.613	7.869	0.061
0.769 s	3	8.096	7.673	7.864	0.049
	4	7.913	7.822	7.868	0.013
	5	7.988	7.722	7.855	0.036

Table E25

Flow rate = 0.3550 L/s

Pressure

Waveheight (cm) Waveperiod (s)	Pressure Point	P_{max} (kN/m^2)	P_{min} (kN/m^2)	$\bar{P}$ (kN/m^2)	σ_P
0.0	1	7.896	7.806	7.856	0.011
	2	7.879	7.819	7.848	0.007
0.0	3	7.886	7.829	7.855	0.009
	4	7.888	7.829	7.855	0.010
	5	7.910	7.803	7.854	0.016
5.8 cm	1	8.095	7.694	7.867	0.053
	2	8.057	7.726	7.869	0.042
0.769 s	3	8.001	7.737	7.867	0.035
	4	7.912	7.834	7.871	0.013
	5	7.968	7.766	7.857	0.035

Table E26

Flow rate = 0.4842 L/s

Velocity

Waveheight (cm) Waveperiod (s)	Riser	V_{max} (m/s)	V_{min} (m/s)	$\bar{V}$ (m/s)	σ_V
0.0	1	0.0024	-0.0967	-0.0176	0.0104
	2	0.1327	0.0538	0.0985	0.0134
0.0	3	0.1475	0.0454	0.1031	0.0150
	4	0.1529	0.0735	0.1053	0.0141
5.8 cm	1	-0.0020	-0.0543	-0.0297	0.0097
	2	0.1000	0.0276	0.0648	0.0125
0.769 s	3	0.1346	0.0369	0.0803	0.0172
	4	0.1662	0.0567	0.1009	0.0173

Table E27

Flow rate = 0.5310 L/s

Velocity

Waveheight (cm) Waveperiod (s)	Riser	V_{max} (m/s)	V_{min} (m/s)	$\bar{V}$ (m/s)	σ_V
0.0	1	0.0000	-0.0528	-0.0281	0.0120
	2	0.1263	0.0261	0.0895	0.0185
0.0	3	0.1485	0.0538	0.0975	0.0164
	4	0.1791	0.0696	0.1184	0.0166
5.8 cm	1	0.0094	-0.0578	-0.0247	0.0124
	2	0.1352	0.0054	0.0807	0.0214
0.769 s	3	0.1525	0.0567	0.1057	0.0164
	4	0.1895	0.0844	0.1345	0.0177

Table E28

Flow rate - 0.4842 L/s

Pressure

Waveheight (cm) Waveperiod (s)	Pressure Point	P_{max} (kN/m²)	P_{min} (kN/m²)	$\bar{P}$ (kN/m²)	σ_P
0.0	1	7.901	7.804	7.853	0.016
	2	7.897	7.817	7.853	0.012
0.0	3	7.885	7.809	7.849	0.012
	4	7.866	7.815	7.840	0.008
	5	7.928	7.759	7.842	0.020
5.8 cm	1	8.127	7.682	7.908	0.065
	2	-	-	-	-
0.769 s	3	8.043	7.691	7.885	0.041
	4	7.973	7.831	7.926	0.015
	5	8.020	7.753	7.887	0.038

Table E29

Flow rate - 0.5310 L/s

Pressure

Waveheight (cm) Waveperiod (s)	Pressure Point	P_{max} (kN/m²)	P_{min} (kN/m²)	$\bar{P}$ (kN/m²)	σ_P
0.0	1	7.896	7.777	7.843	0.016
	2	7.894	7.803	7.848	0.012
0.0	3	7.882	7.822	7.854	0.011
	4	7.923	7.817	7.865	0.020
	5	7.939	7.794	7.856	0.019
5.8 cm	1	8.011	7.795	7.914	0.029
	2	7.992	7.802	7.906	0.022
0.769 s	3	7.966	7.816	7.897	0.019
	4	7.932	7.857	7.893	0.011
	5	7.975	7.792	7.883	0.023

Table E30

Flow rate = 0.6026 L/s

Velocity

Waveheight (cm) Waveperiod (s)	Riser	V_{max} (m/s)	V_{min} (m/s)	$\bar{V}$ (m/s)	σ_V
0.0	1	-0.0020	-0.0360	-0.0176	0.0062
	2	0.1446	0.0685	0.1041	0.0133
0.0	3	0.1603	0.0587	0.0989	0.0160
	4	0.1717	0.0646	0.1125	0.0158
5.8 cm	1	0.0000	-0.0449	-0.0249	0.0076
	2	0.1317	0.0562	0.0964	0.0133
0.769 s	3	0.1663	0.0577	0.1062	0.0172
	4	0.1993	0.0789	0.1291	0.0211

Table E31

Flow rate = 0.6310 L/s

Velocity

Waveheight (cm) Waveperiod (s)	Riser	V_{max} (m/s)	V_{min} (m/s)	$\bar{V}$ (m/s)	σ_V
0.0	1	0.0064	-0.0409	-0.0175	0.0075
	2	0.1263	0.0538	0.0907	0.0128
0.0	3	0.1485	0.0641	0.1034	0.0145
	4	0.1791	0.0789	0.1182	0.0160
5.8 cm	1	0.0972	0.0212	0.0590	0.0133
	2	0.1510	0.0266	0.0971	0.0162
0.769 s	3	0.1327	0.0380	0.0880	0.0169
	4	0.1761	0.0632	0.1177	0.0191

Table E32

Flow rate = 0.6026 L/s

Pressure

Waveheight (cm) Waveperiod (s)	Pressure Point	P_{max} (kN/m²)	P_{min} (kN/m²)	$\bar{P}$ (kN/m²)	σ_P
0.0	1	7.907	7.793	7.836	0.012
	2	7.862	7.802	7.829	0.008
0.0	3	7.871	7.805	7.837	0.011
	4	7.857	7.800	7.827	0.008
	5	7.900	7.764	7.830	0.020
5.8 cm	1	8.245	7.645	7.868	0.082
	2	-	-	-	-
0.769 s	3	8.003	7.740	7.873	0.043
	4	7.919	7.834	7.873	0.013
	5	8.008	7.704	7.858	0.042

Table E33

Flow rate = 0.6310 L/s

Pressure

Waveheight (cm) Waveperiod (s)	Pressure Point	P_{max} (kN/m²)	P_{min} (kN/m²)	$\bar{P}$ (kN/m²)	σ_P
0.0	1	7.954	7.831	7.894	0.017
	2	7.954	7.857	7.903	0.014
0.0	3	7.962	7.843	7.903	0.021
	4	7.956	7.900	7.924	0.010
	5	7.973	7.808	7.885	0.025
5.8 cm	1	7.942	7.629	7.795	0.047
	2	7.917	7.682	7.808	0.035
0.769 s	3	7.900	7.732	7.825	0.029
	4	7.865	7.797	7.826	0.011
	5	7.919	7.708	7.810	0.032

Table E34

Flow rate = 0.6547 L/s

Velocity

Waveheight (cm) Waveperiod (s)	Riser	V_{max} (m/s)	V_{min} (m/s)	$\bar{V}$ (m/s)	σ_V
0.0	1	0.0138	-0.0301	-0.0063	0.0070
	2	0.1401	0.0567	0.0914	0.0147
0.0	3	0.1214	0.0400	0.0805	0.0167
	4	0.1559	0.0498	0.0901	0.0149
5.8 cm	1	-0.0069	-0.0543	-0.0307	0.0072
	2	0.1594	0.0558	0.1054	0.0145
0.769 s	3	0.1633	0.0592	0.1044	0.0169
	4	0.2052	0.0696	0.1273	0.0203

Table E35

Flow rate = 0.9441 L/s

Velocity

Waveheight (cm) Waveperiod (s)	Riser	V_{max} (m/s)	V_{min} (m/s)	$\bar{V}$ (m/s)	σ_V
0.0	1	0.1209	0.0646	0.0942	0.0088
	2	0.1603	0.0632	0.1036	0.0175
0.0	3	0.1431	0.0454	0.0936	0.0167
	4	0.1446	0.0686	0.1045	0.0142
5.8 cm	1	0.1446	0.0538	0.0927	0.0129
	2	0.1845	0.0474	0.1148	0.0231
0.769 s	3	0.1682	0.0558	0.1033	0.0189
	4	0.1983	0.0577	0.1217	0.0196

Table E36

Flow rate - 0.6547 L/s

Pressure

Waveheight (cm) Waveperiod (s)	Pressure Point	P_{max} (kN/m^2)	P_{min} (kN/m^2)	$\overline{P}$ (kN/m^2)	σ_P
0.0	1	7.906	7.781	7.838	0.018
	2	7.886	7.779	7.836	0.015
0.0	3	7.889	7.811	7.850	0.013
	4	7.865	7.828	7.845	0.006
	5	7.926	7.724	7.832	0.031
5.8 cm	1	8.149	7.609	7.892	0.059
	2	8.045	7.659	7.882	0.043
0.769 s	3	8.032	7.714	7.886	0.035
	4	7.943	7.812	7.879	0.013
	5	7.997	7.742	7.864	0.035

Table E37

Flow rate - 0.9441 L/s

Pressure

Waveheight (cm) Waveperiod (s)	Pressure Point	P_{max} (kN/m²)	P_{min} (kN/m²)	$\bar{P}$ (kN/m²)	σ_P
0.0	1	7.916	7.773	7.840	0.022
	2	7.886	7.782	7.830	0.014
0.0	3	7.874	7.777	7.832	0.014
	4	7.870	7.795	7.835	0.012
	5	7.925	7.687	7.819	0.034
5.8 cm	1	8.063	7.796	7.923	0.035
	2	8.033	7.825	7.938	0.028
0.769 s	3	8.022	7.844	7.935	0.025
	4	7.950	7.864	7.906	0.013
	5	8.033	7.747	7.883	0.041

Table E38

Flow rate = 2.0 L/s

Velocity

Waveheight (cm) Waveperiod (s)	Riser	V_{max} (m/s)	V_{min} (m/s)	$\bar{V}$ (m/s)	σ_V
0.0	1	0.2709	0.1401	0.1947	0.0187
	2	0.3158	0.1159	0.2067	0.0311
0.0	3	0.3000	0.1204	0.1922	0.0296
	4	0.3454	0.1475	0.2293	0.0296
5.8 cm	1	0.3330	0.1435	0.2039	0.0274
	2	0.3330	0.0972	0.1970	0.0326
0.769 s	3	0.3024	0.1085	0.1861	0.0297
	4	0.3015	0.1224	0.2088	0.0297

Table E39

Flow rate - 2.0 L/s

Pressure

Waveheight (cm) Waveperiod (s)	Pressure Point	P_{max} (kN/m²)	P_{min} (kN/m²)	$\bar{P}$ (kN/m²)	σ_P
0.0	1	8.154	7.983	8.072	0.026
	2	8.134	7.707	8.060	0.027
0.0	3	8.100	7.883	7.999	0.032
	4	8.053	7.849	7.946	0.032
	5	8.237	7.601	7.936	0.095
5.8 cm	1	8.286	7.978	8.130	0.044
	2	-	-	-	-
0.769 s	3	8.186	7.912	8.042	0.039
	4	8.104	7.870	7.993	0.035
	5	8.248	7.688	7.978	0.087

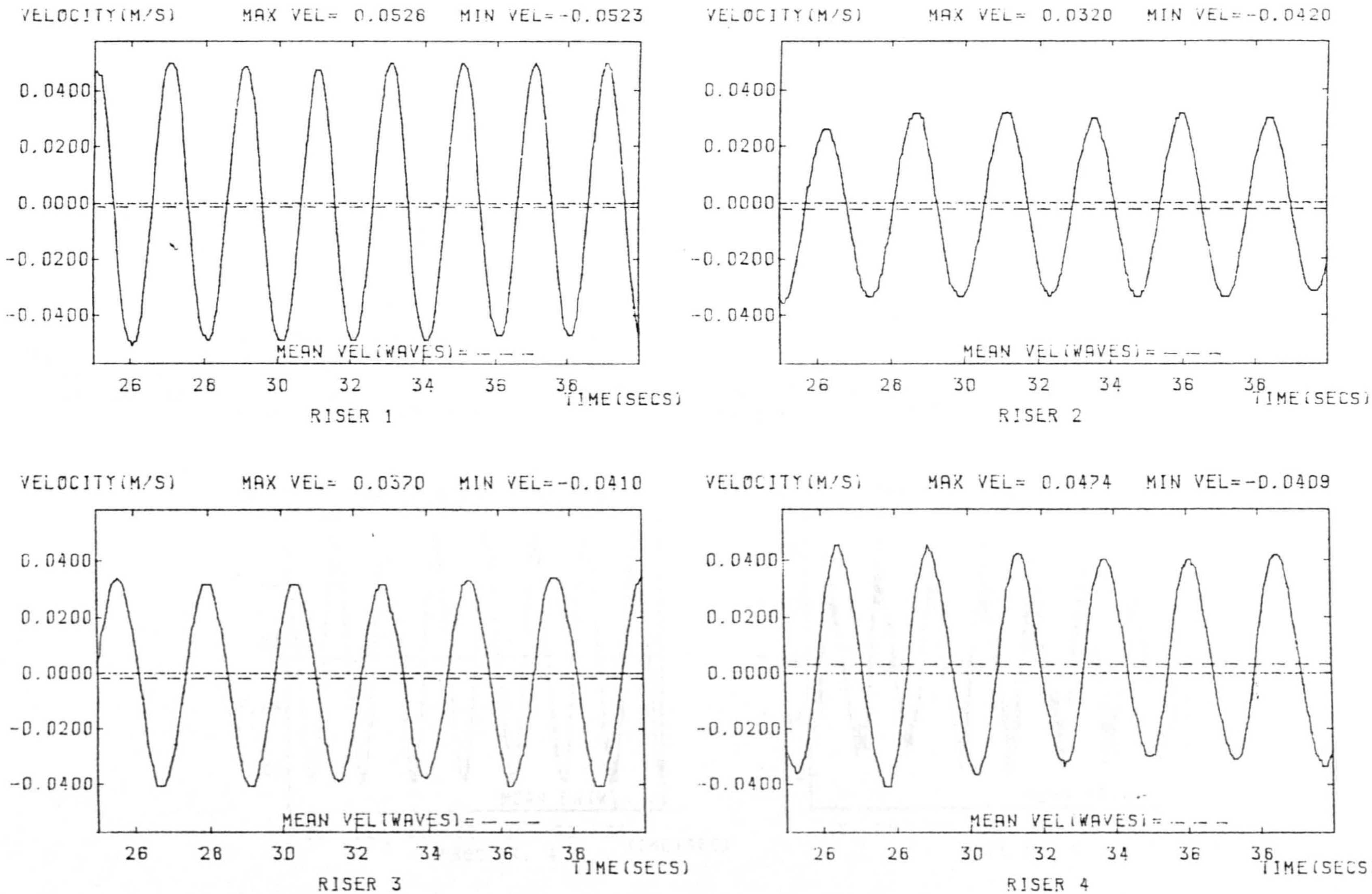

WAVEHEIGHT= 0.0410M WAVEPERIOD= 2·2200 S FLOW RATE=0.00000 L/S

FIGURE E.1

6 JUN 88 15:54:37

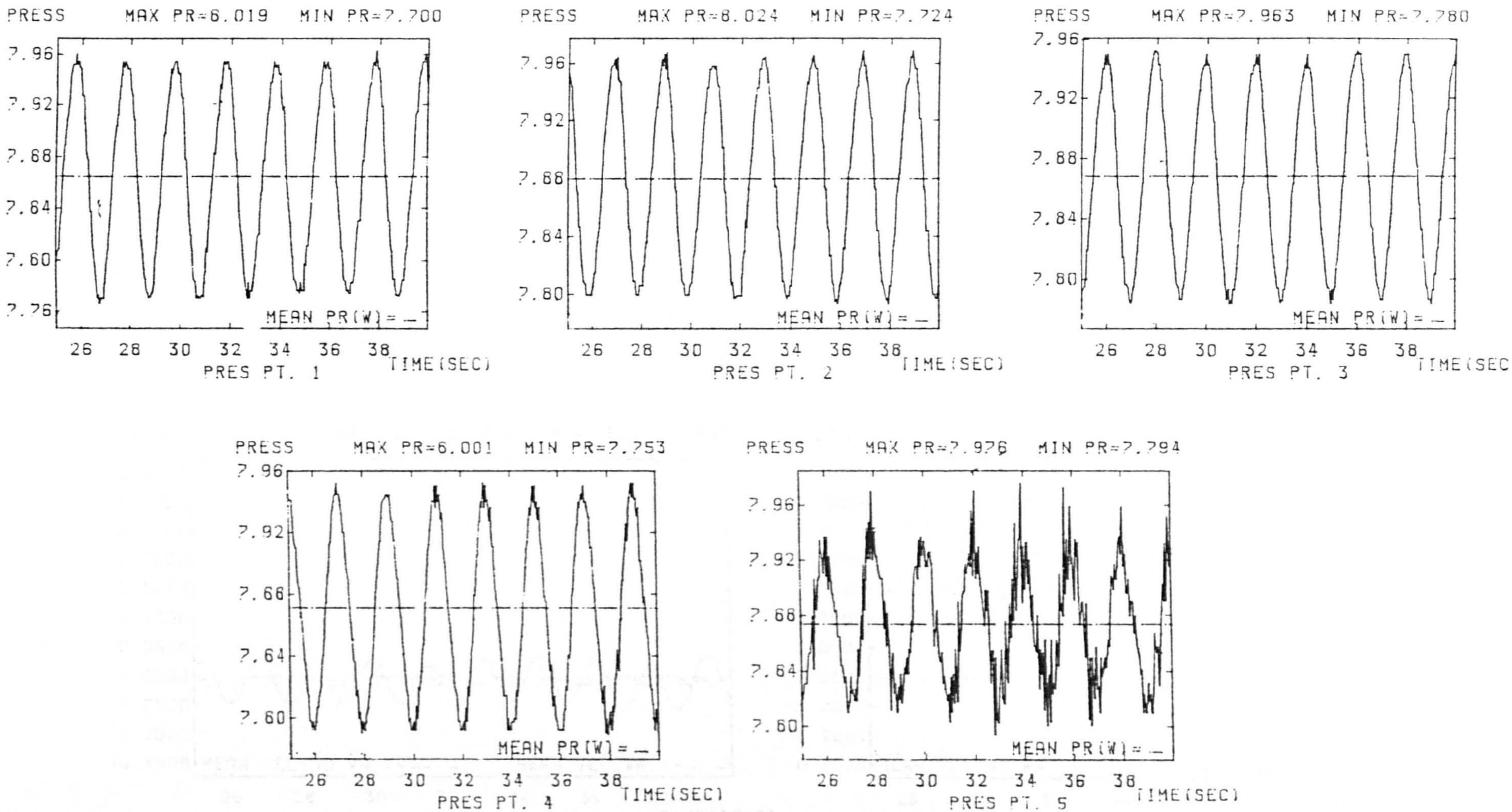

WAVEHEIGHT=0.0410 M WAVEPERIOD= 2.2200 S FLOW RATE=0.00000 L/S

FIGURE E.2

6 JUN 86 16:12:27

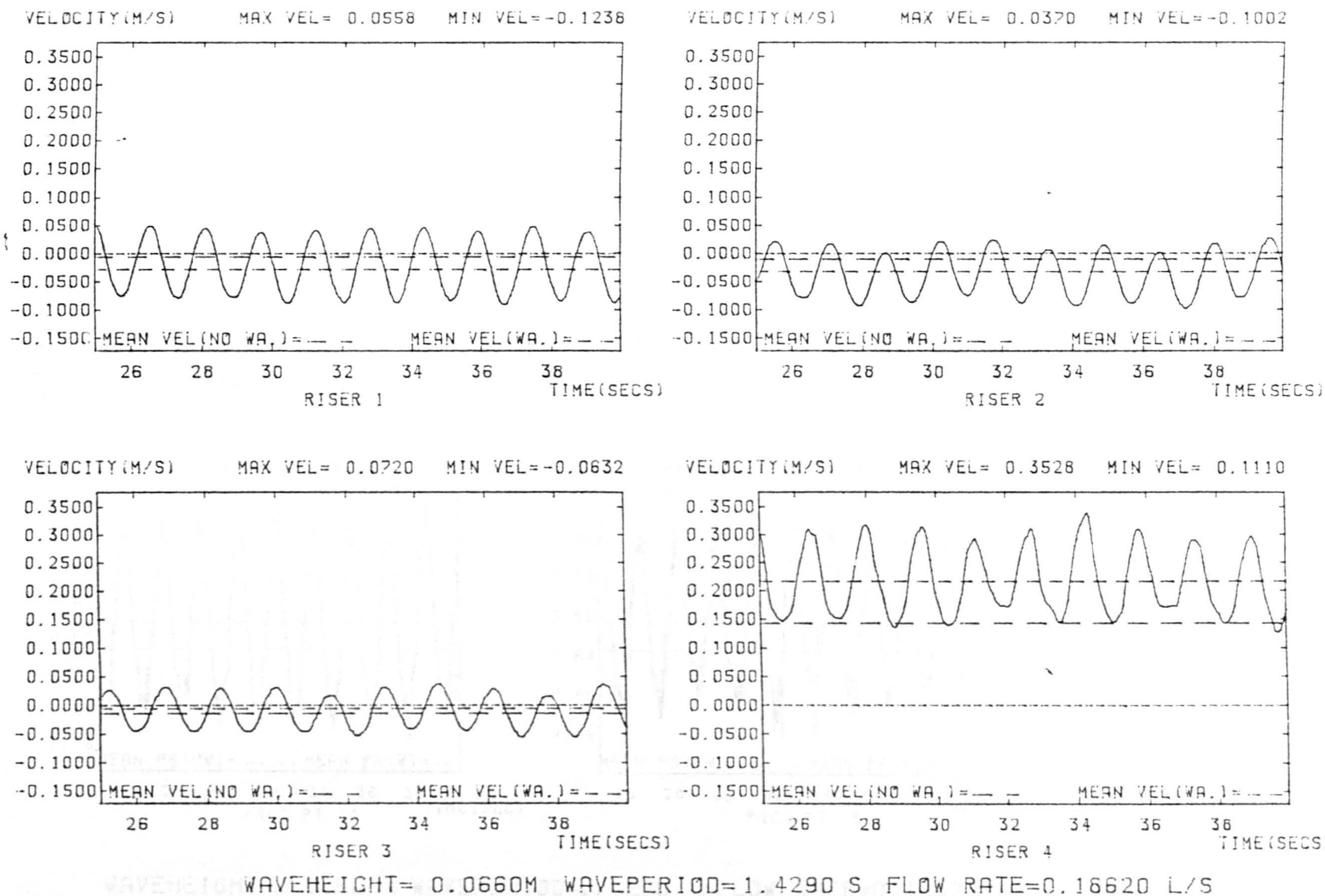

FIGURE E.3

6 JUN 86 9:26:39

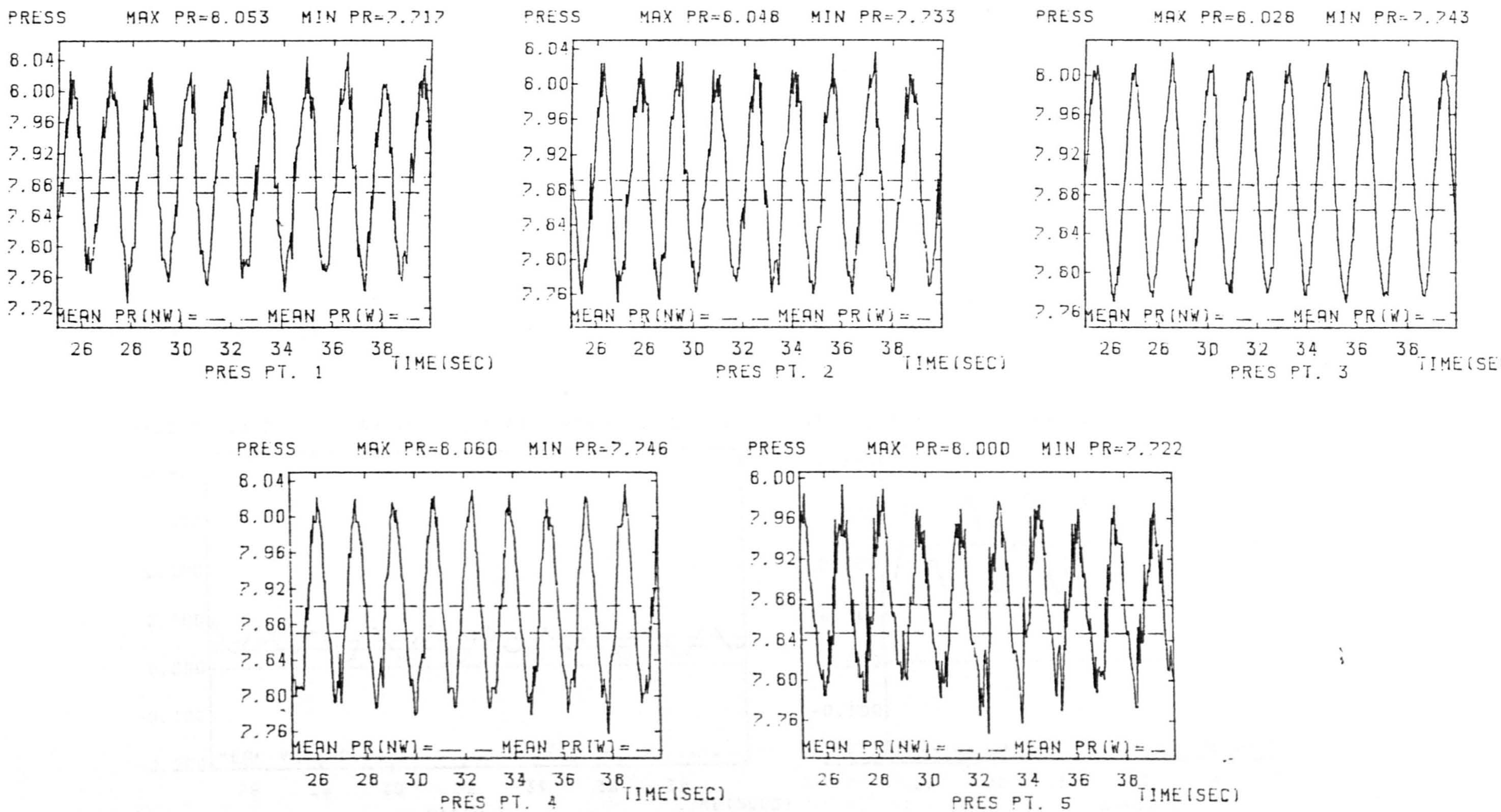

WAVEHEIGHT=0.0660 M WAVEPERIOD=1.4290 S FLOW RATE=0.18620 L/S

FIGURE E.4

6 JUN 88 15:06:22

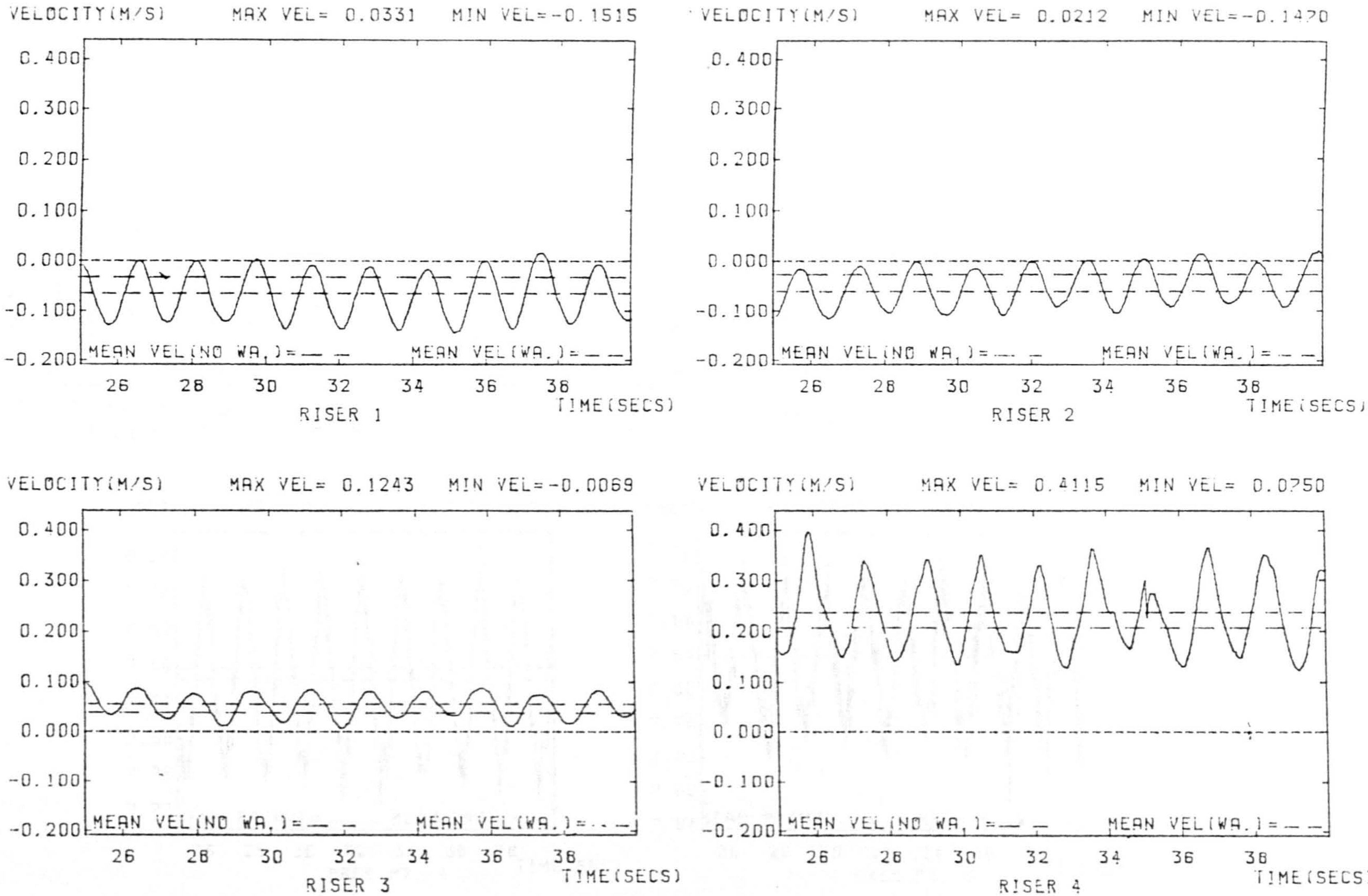

WAVEHEIGHT= 0.0660M WAVEPERIOD=1.4290 S FLOW RATE=0.35500 L/S

FIGURE E.5

6 JUN 88 10:25:43

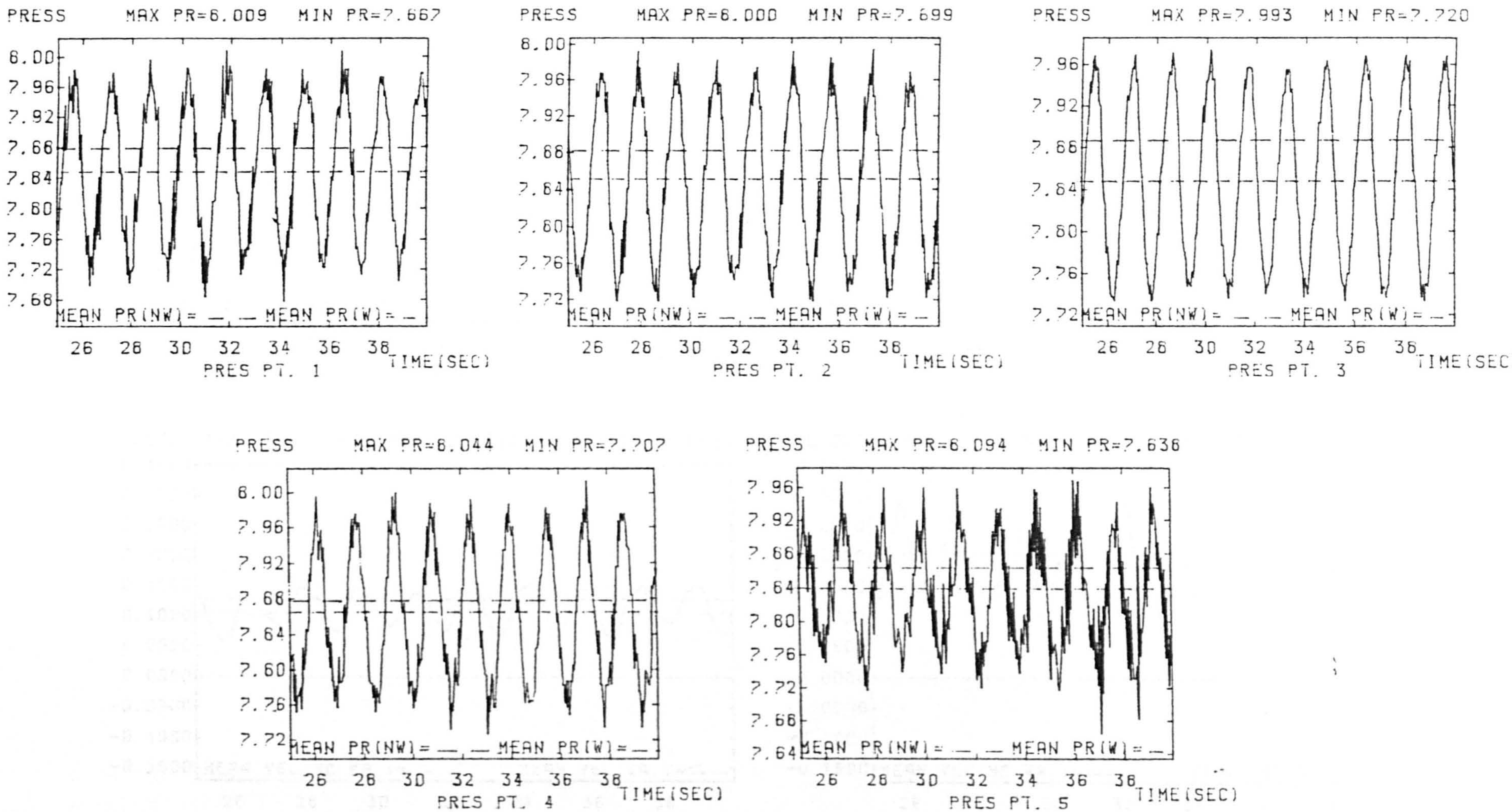

WAVEHEIGHT=0.0660 M WAVEPERIOD=1.4290 S FLOW RATE=0.35500 L/S

FIGURE E.6

6 JUN 88 15:25:31

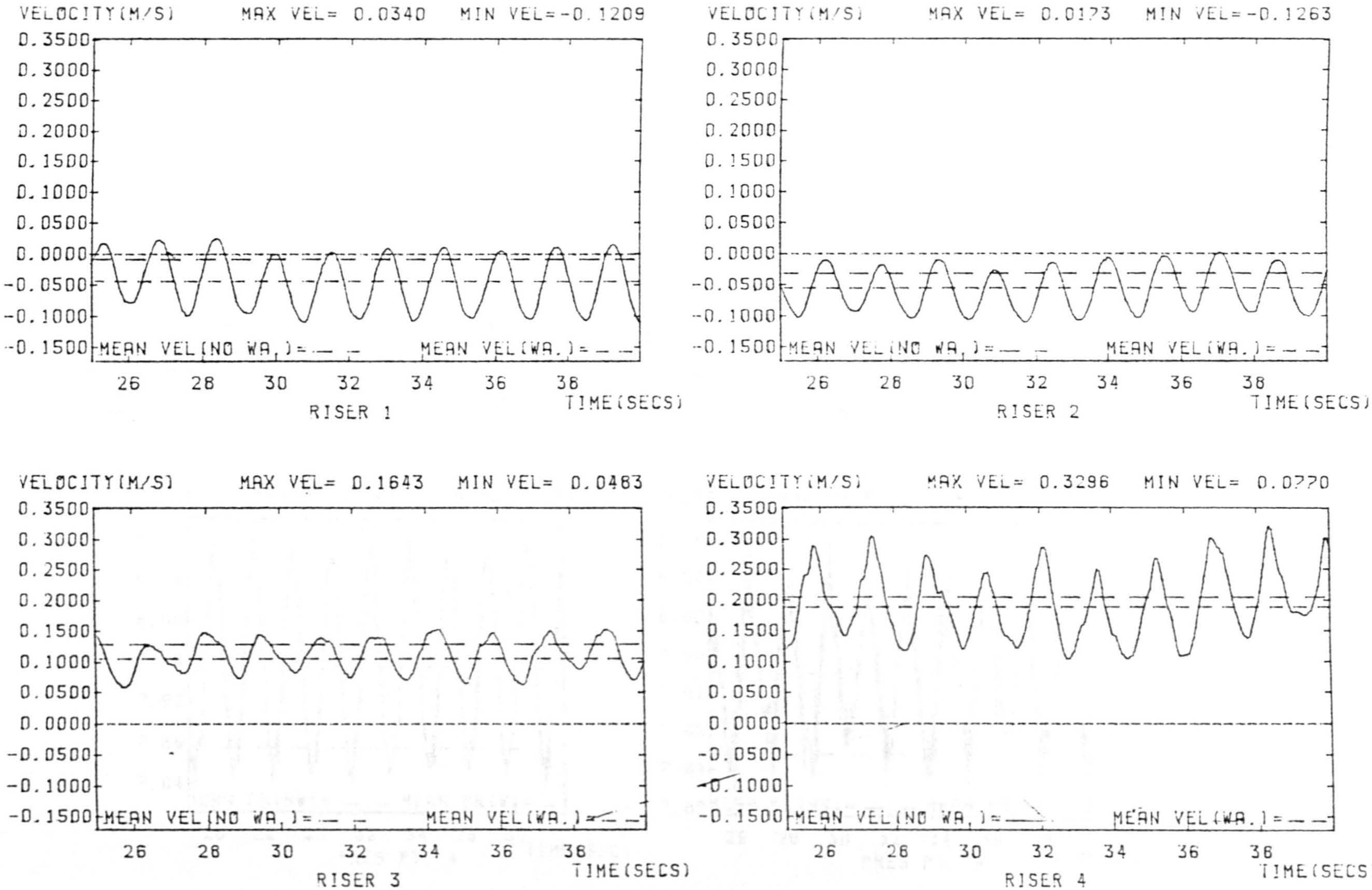

WAVEHEIGHT= 0.0660M WAVEPERIOD= 1.4290 S FLOW RATE=0.48420 L/S

FIGURE E.7

10 JUN 88 10:59:56

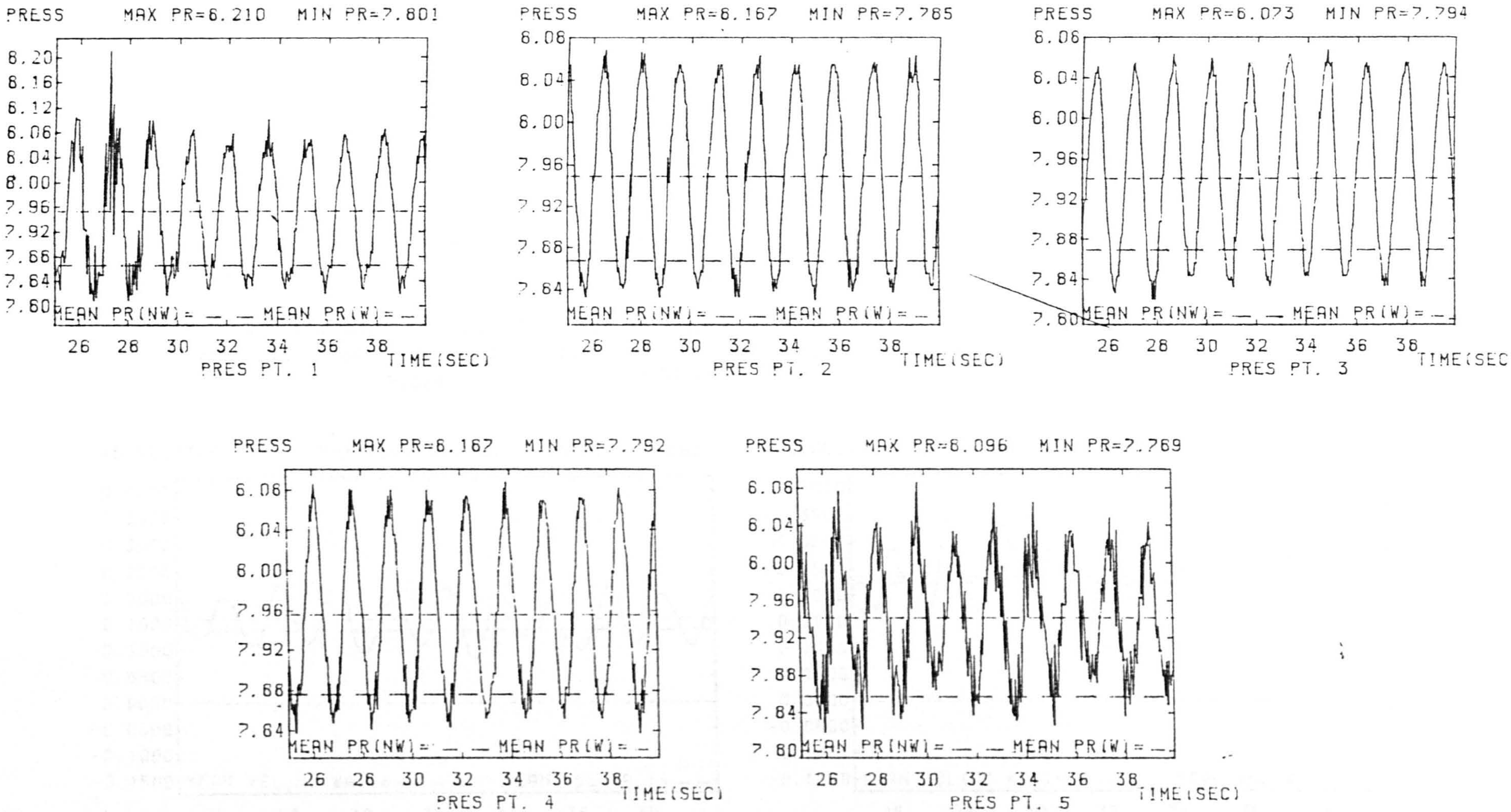

WAVEHEIGHT=0.0660 M WAVEPERIOD=1.4290 S FLOW RATE=0.46420 L/S

FIGURE E.8

..JUN 88 10:39:06

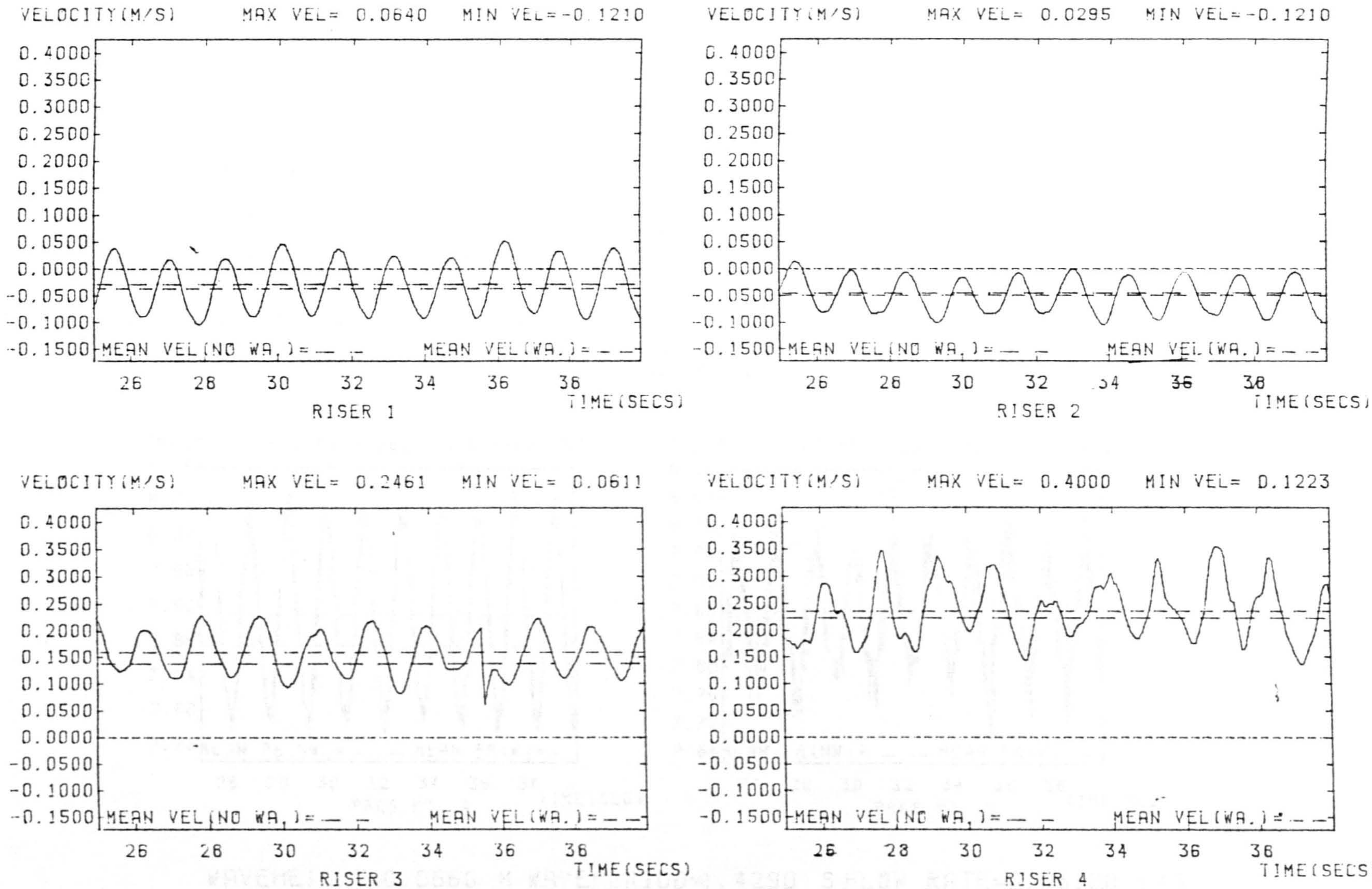

WAVEHEIGHT= 0.0660M WAVEPERIOD=1.4290 S FLOW RATE=0.53100 L/S

FIGURE E.9

0 JUN 88 12:31:18

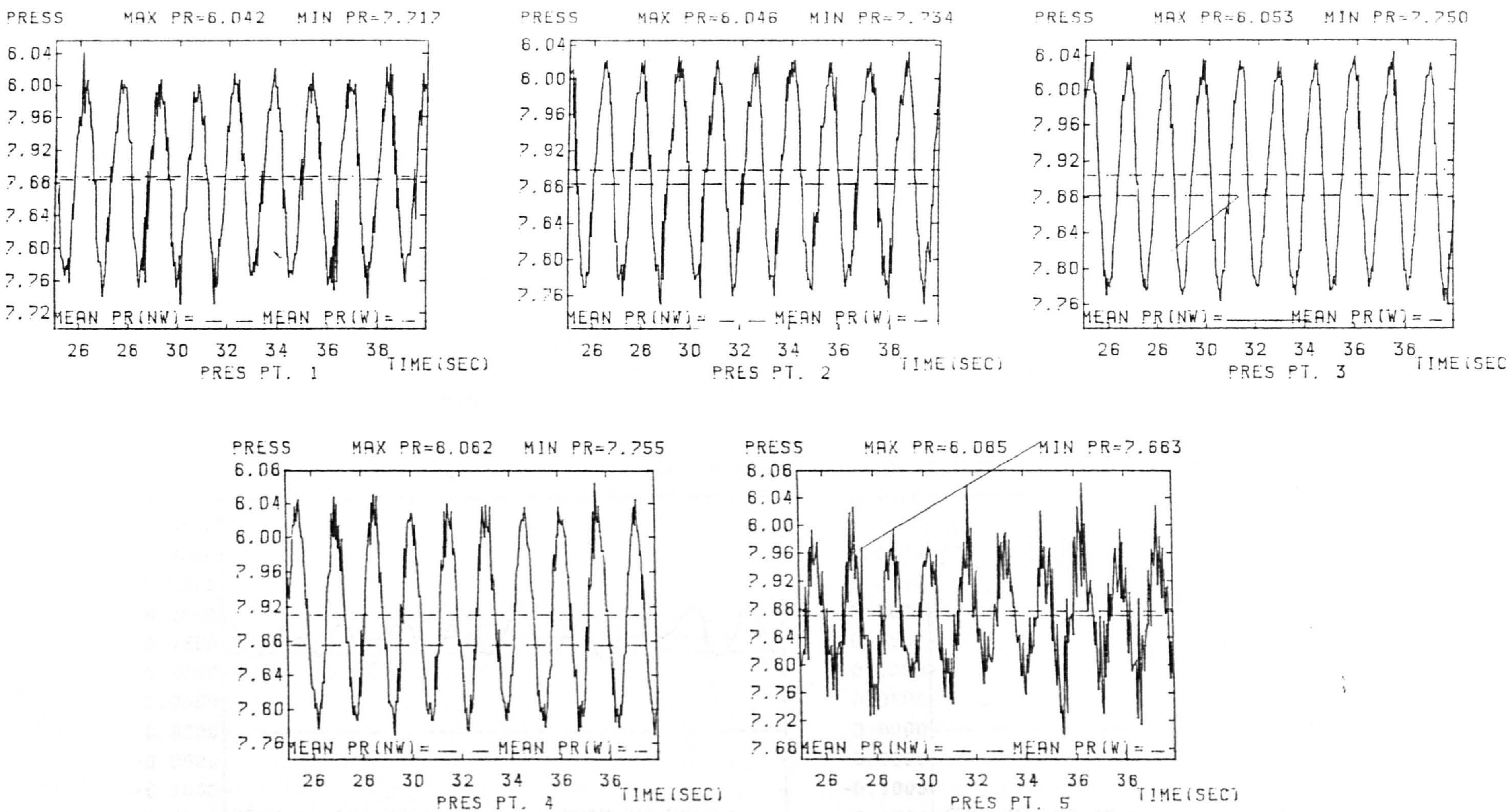

WAVEHEIGHT=0.0660 M WAVEPERIOD=1.4290 S FLOW RATE=0.53100 L/S

FIGURE E.10

10 JUN 88 11:26:16

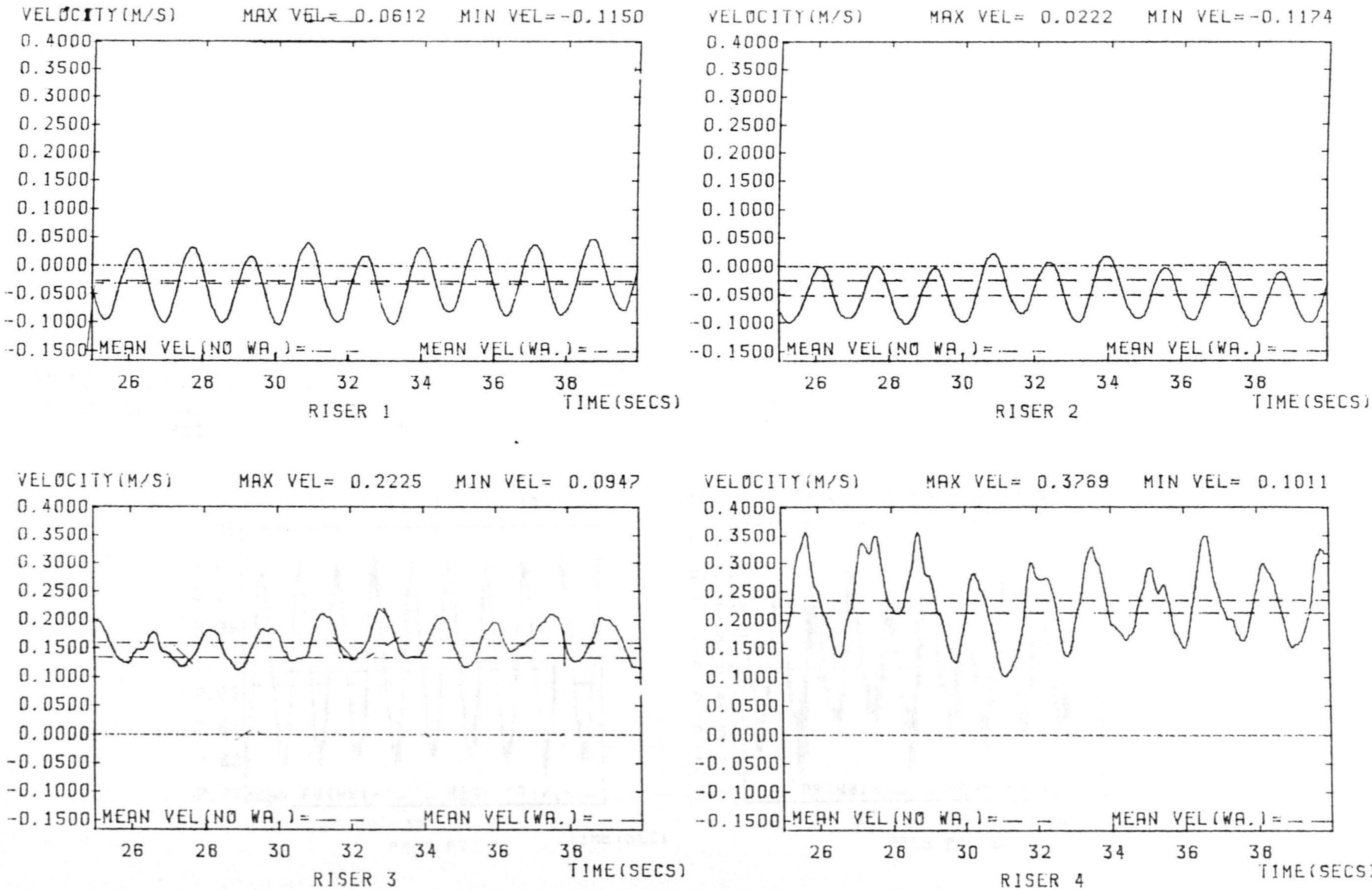

WAVEHEIGHT= 0.0660M WAVEPERIOD=1.4290 S FLOW RATE=0.60260 L/S

10 JUN 88 13:36:49

FIGURE E11

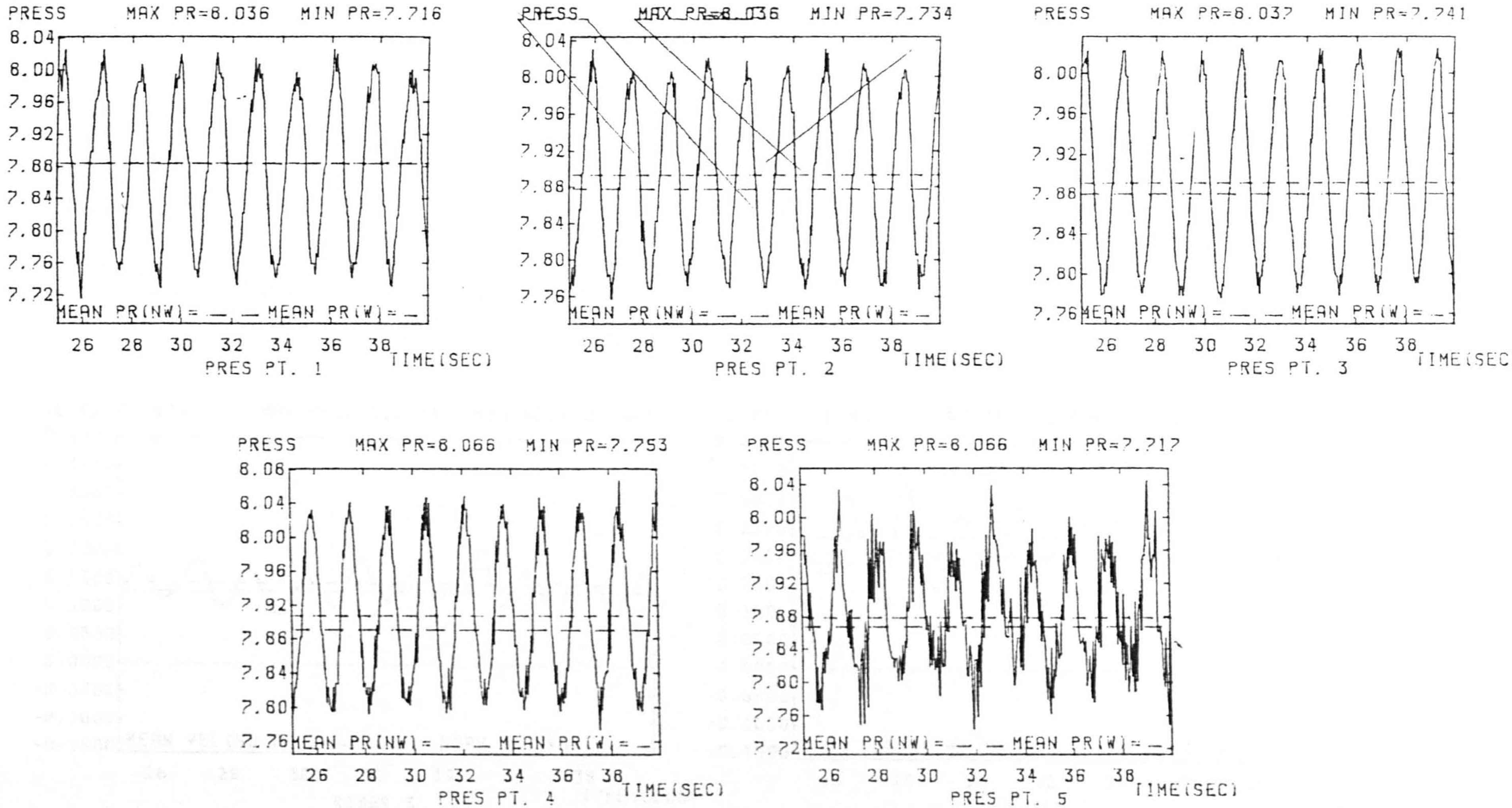

WAVEHEIGHT=0.0660 M WAVEPERIOD=1.4290 S FLOW RATE=0.60260 L/S

FIGURE E.12

10 JUN 88 12:59:58

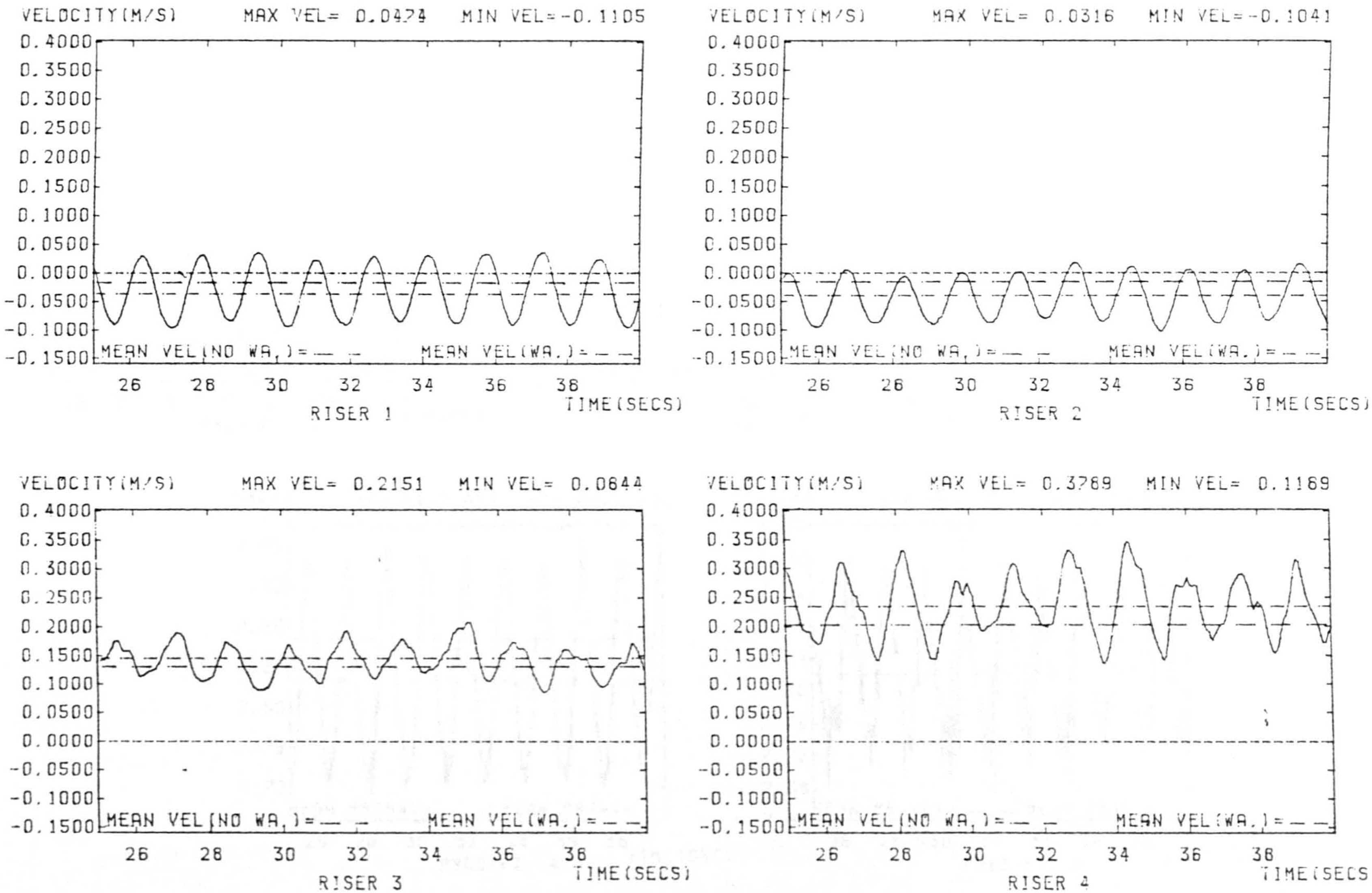

WAVEHEIGHT= 0.0660M WAVEPERIOD=1.4290 S FLOW RATE=0.63100 L/S

FIGURE E.13

10 JUN 86 16:02:43

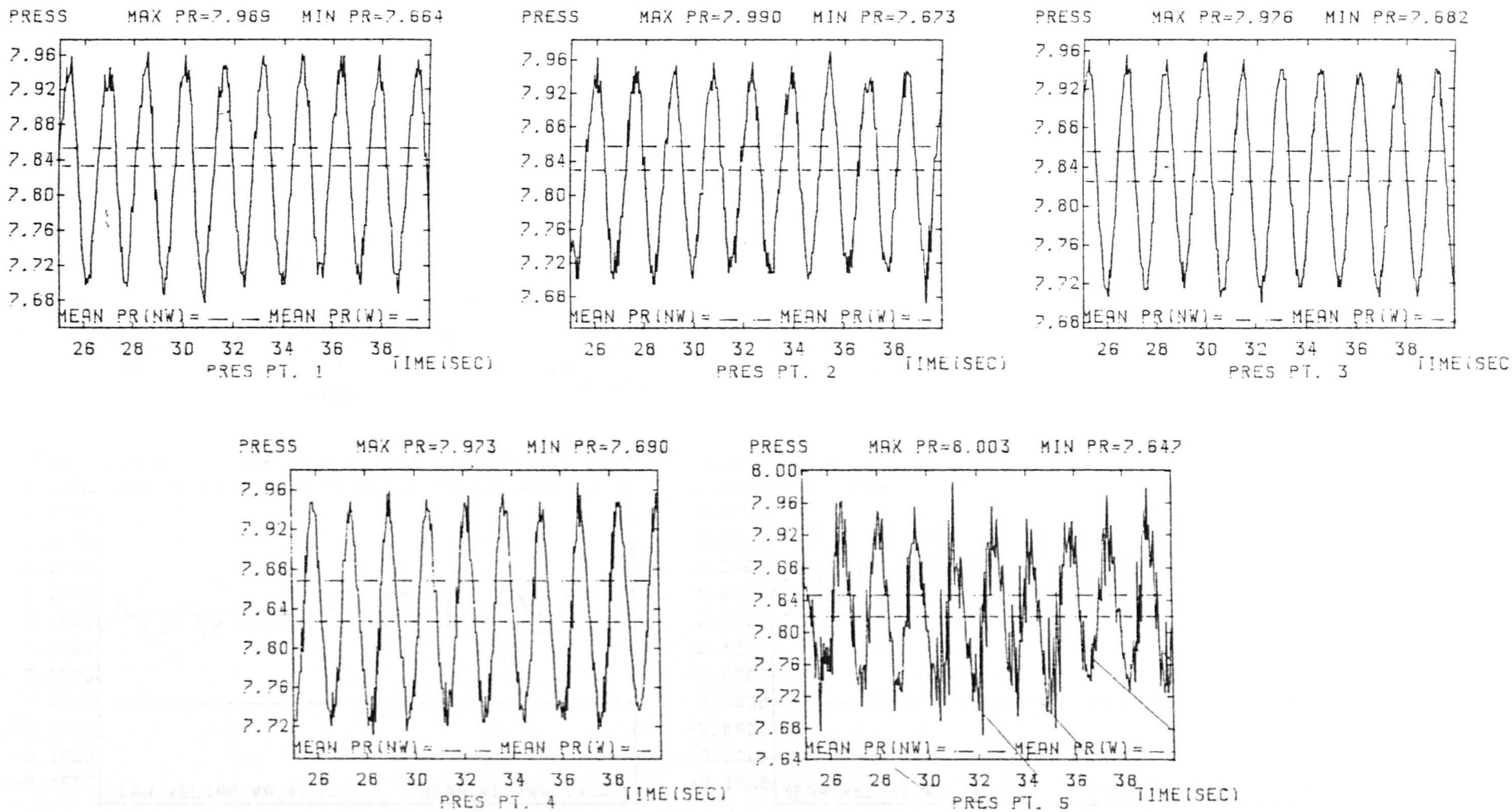

WAVEHEIGHT=0.0660 M WAVEPERIOD=1.4290 S FLOW RATE=0.63100 L/S

FIGURE E.14

10 JUN 88 14:26:57

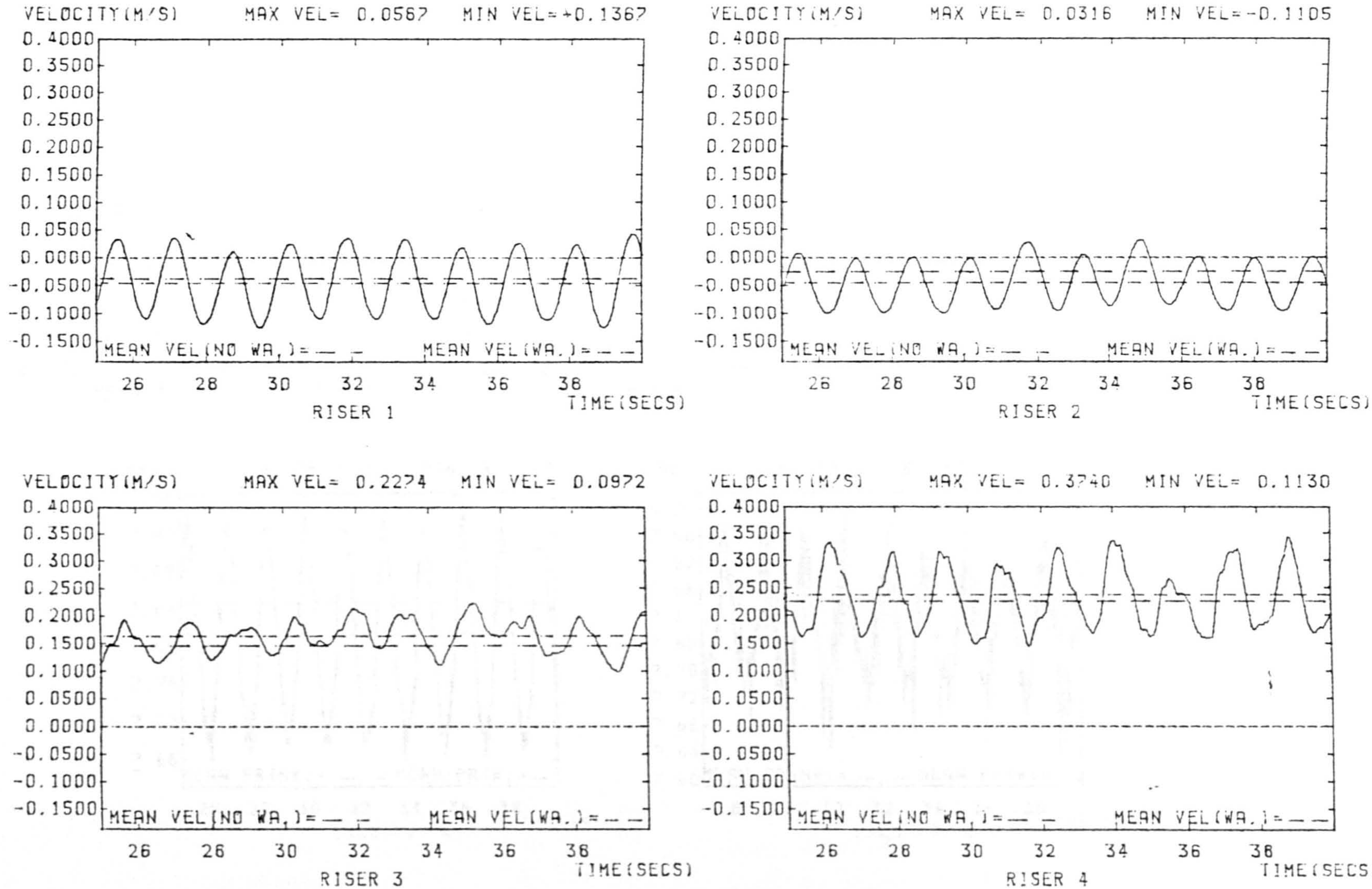

WAVEHEIGHT= 0.0660M WAVEPERIOD=1.4290 S FLOW RATE=0.65470 L/S

FIGURE E.15

10 JUN 88 16:24:19

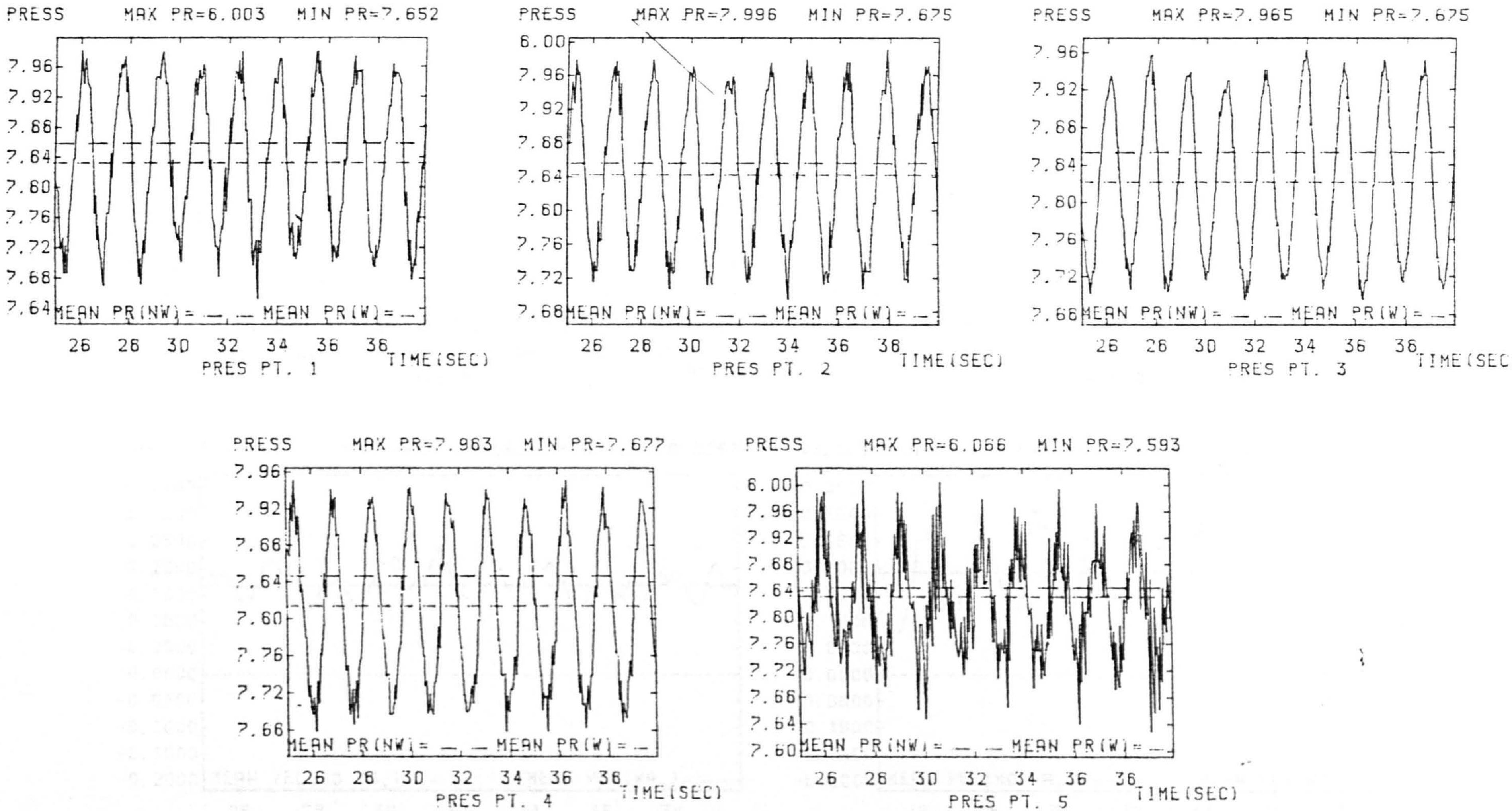

WAVEHEIGHT=0.0660 M WAVEPERIOD=1.4290 S FLOW RATE=0.65470 L/S

10 JUN 88 15:42:12

FIGURE E.16

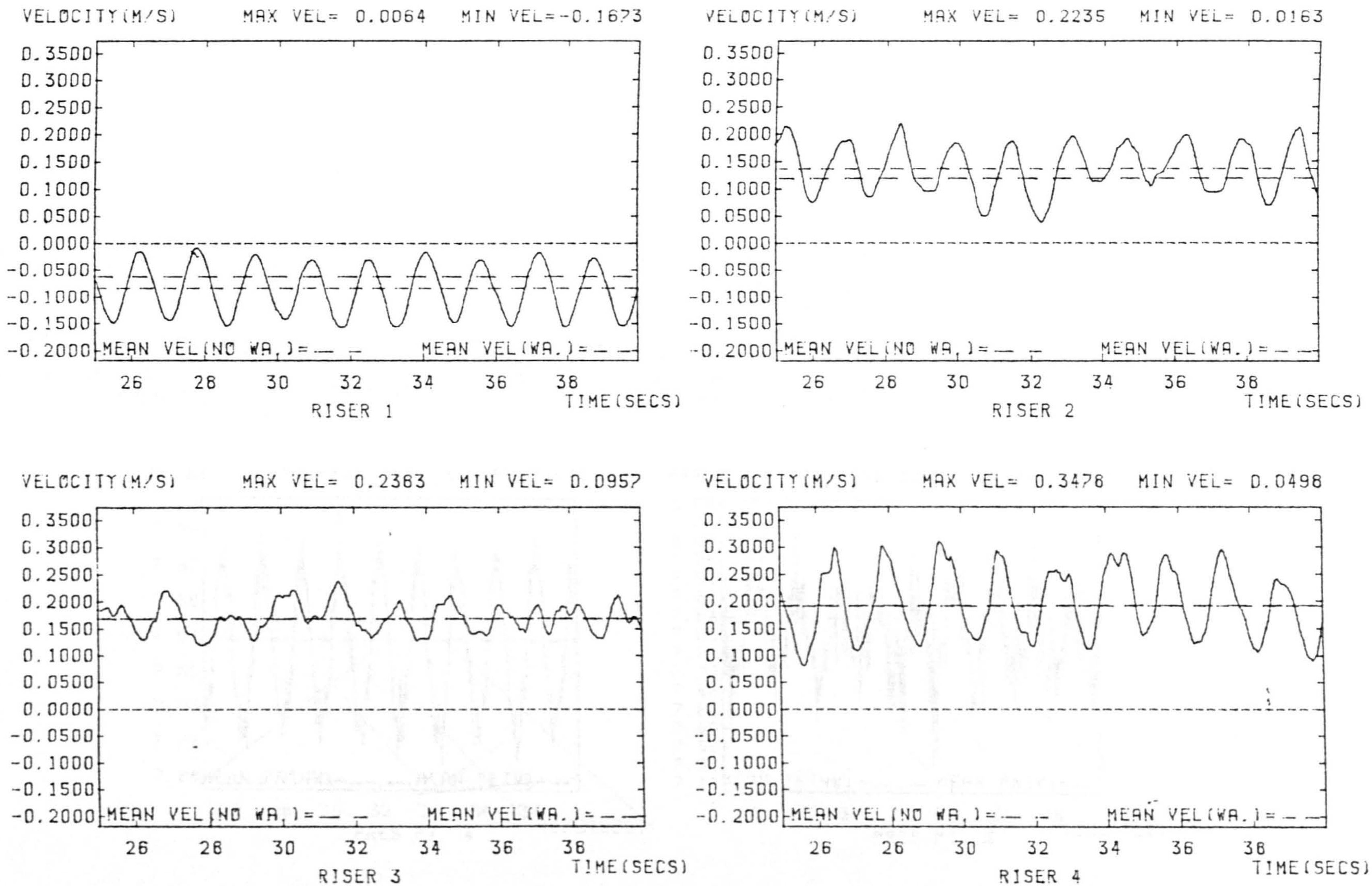

WAVEHEIGHT= 0.0660M WAVEPERIOD=1.4290 S FLOW RATE=0.94410 L/S

FIGURE E.17

11 JUN 88 8:56:05

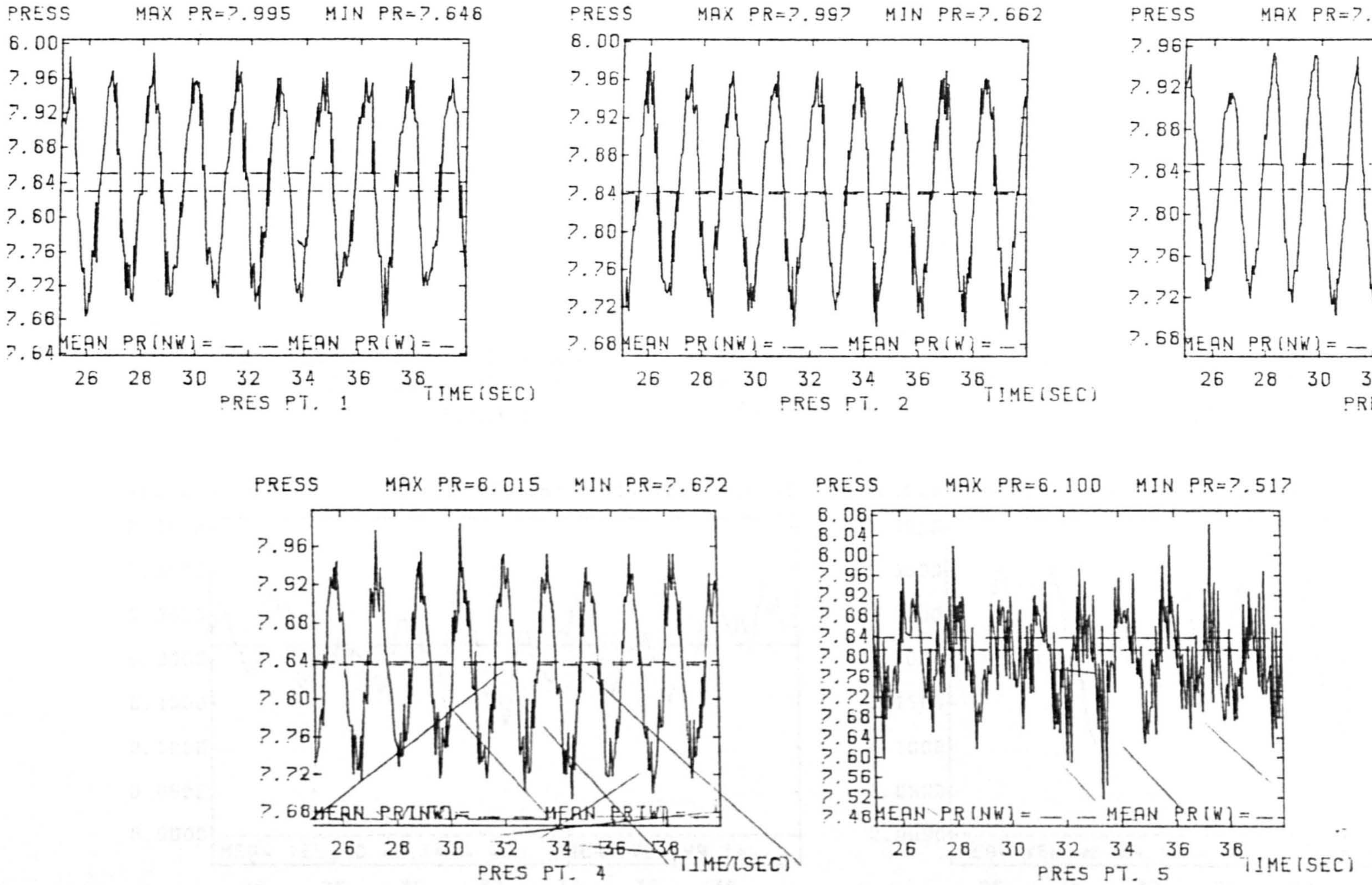

WAVEHEIGHT=0.0660 M WAVEPERIOD=1.4290 S FLOW RATE=0.94410 L/S

FIGURE E.18

11 JUN 88 9:16:41

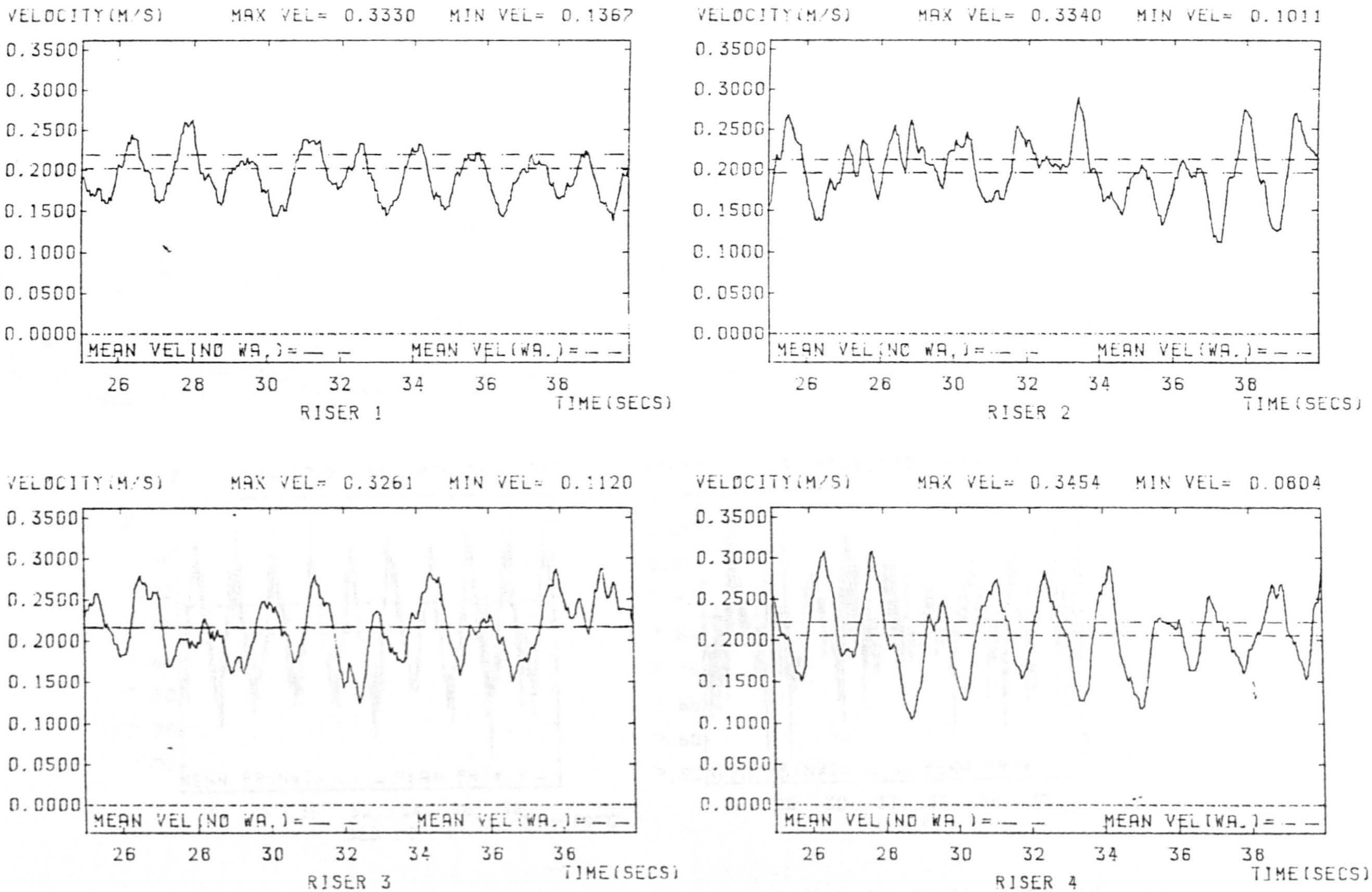

WAVEHEIGHT= 0.0660M WAVEPERIOD= 1.4290 S FLOW RATE=2.00000 L/S

FIGURE E.19

11 JUN 88 10:09:00

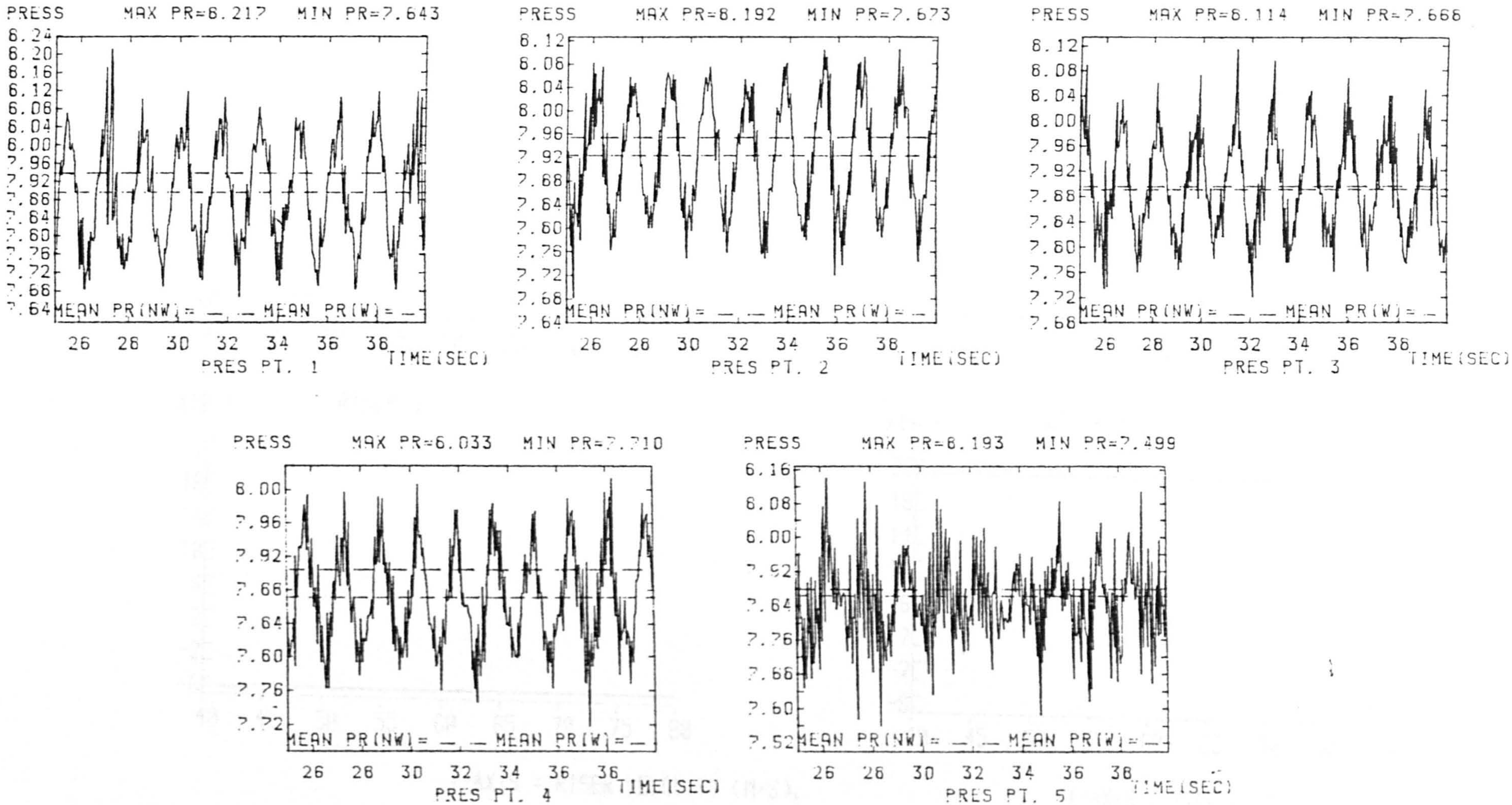

WAVEHEIGHT=0.0660 M WAVEPERIOD=1.4290 S FLOW RATE=2.00000 L/S

FIGURE E.20

11 JUN 88 9:48:39

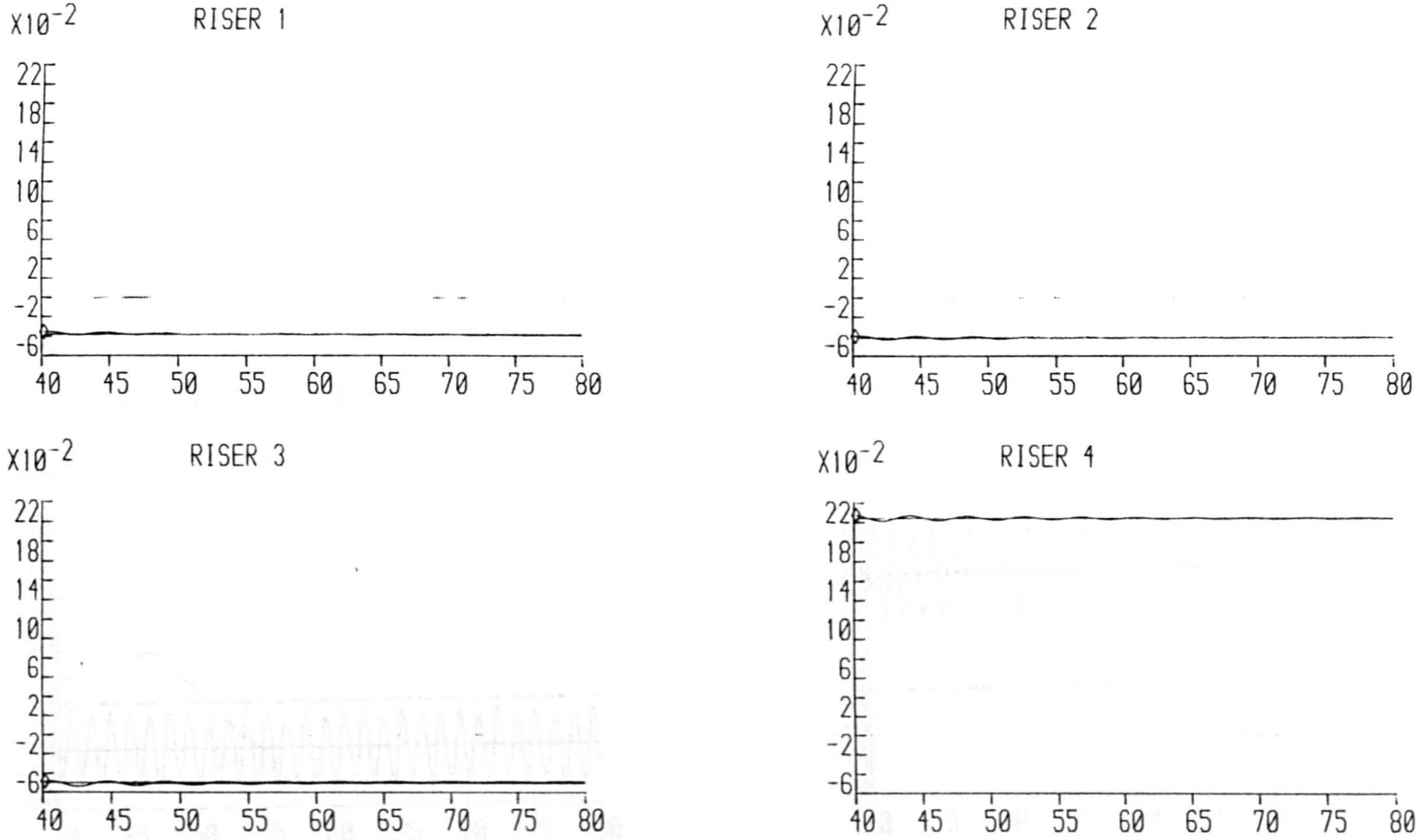

Y-AXIS = RISER VELOCITY (M/S), X-AXIS = TIME (SECS)

WAVEHEIGHT= 0.00000 WAVEPERIOD= 1.42900 FLOW RATE= 0.00019

FIGURE E.21

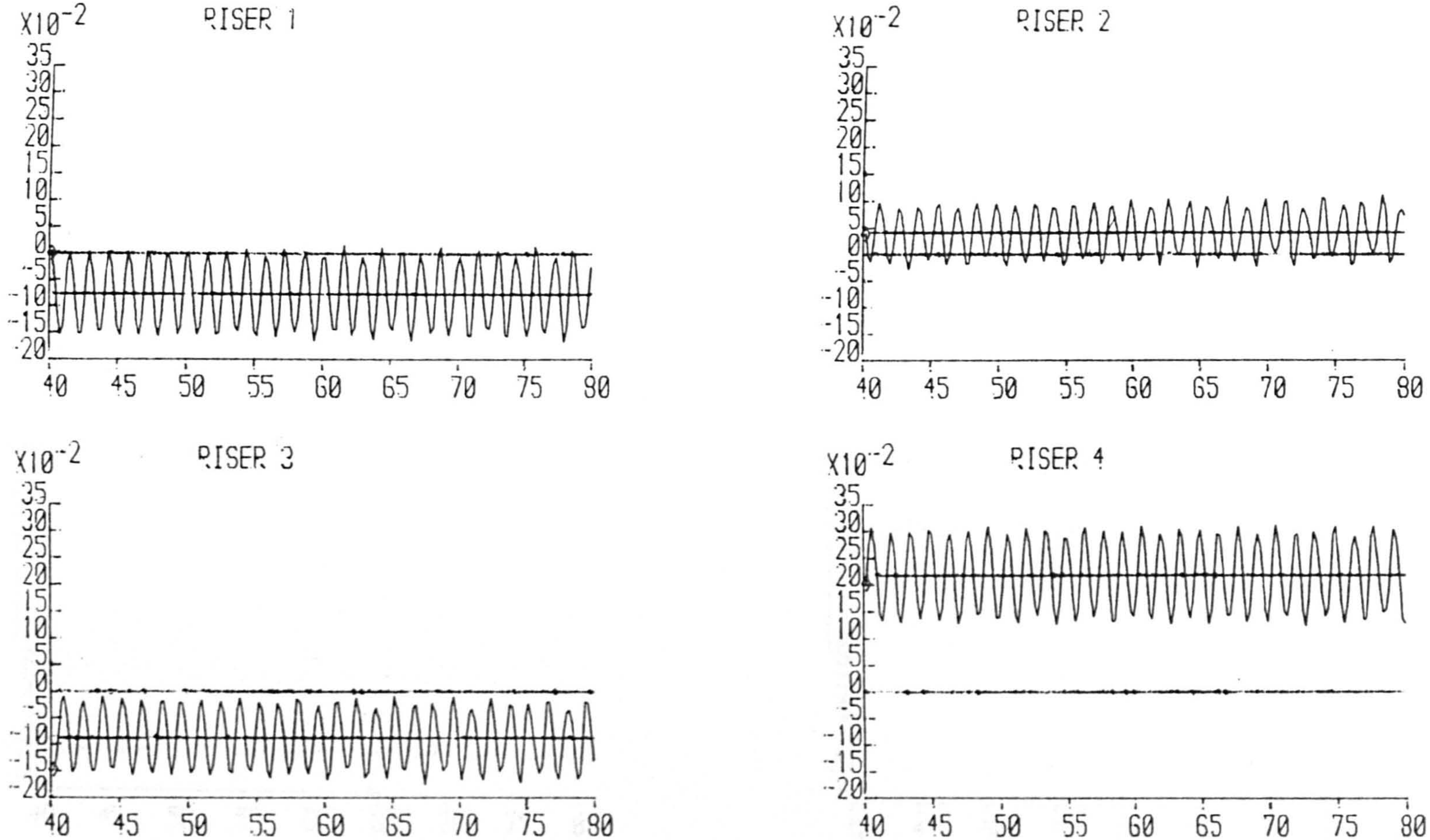

Y-AXIS = RISER VELOCITY (M/S), X-AXIS = TIME (SECS)

WAVEHEIGHT= 0.06600 WAVEPERIOD= 1.42900 FLOW RATE= 0.00019

FIGURE E.22

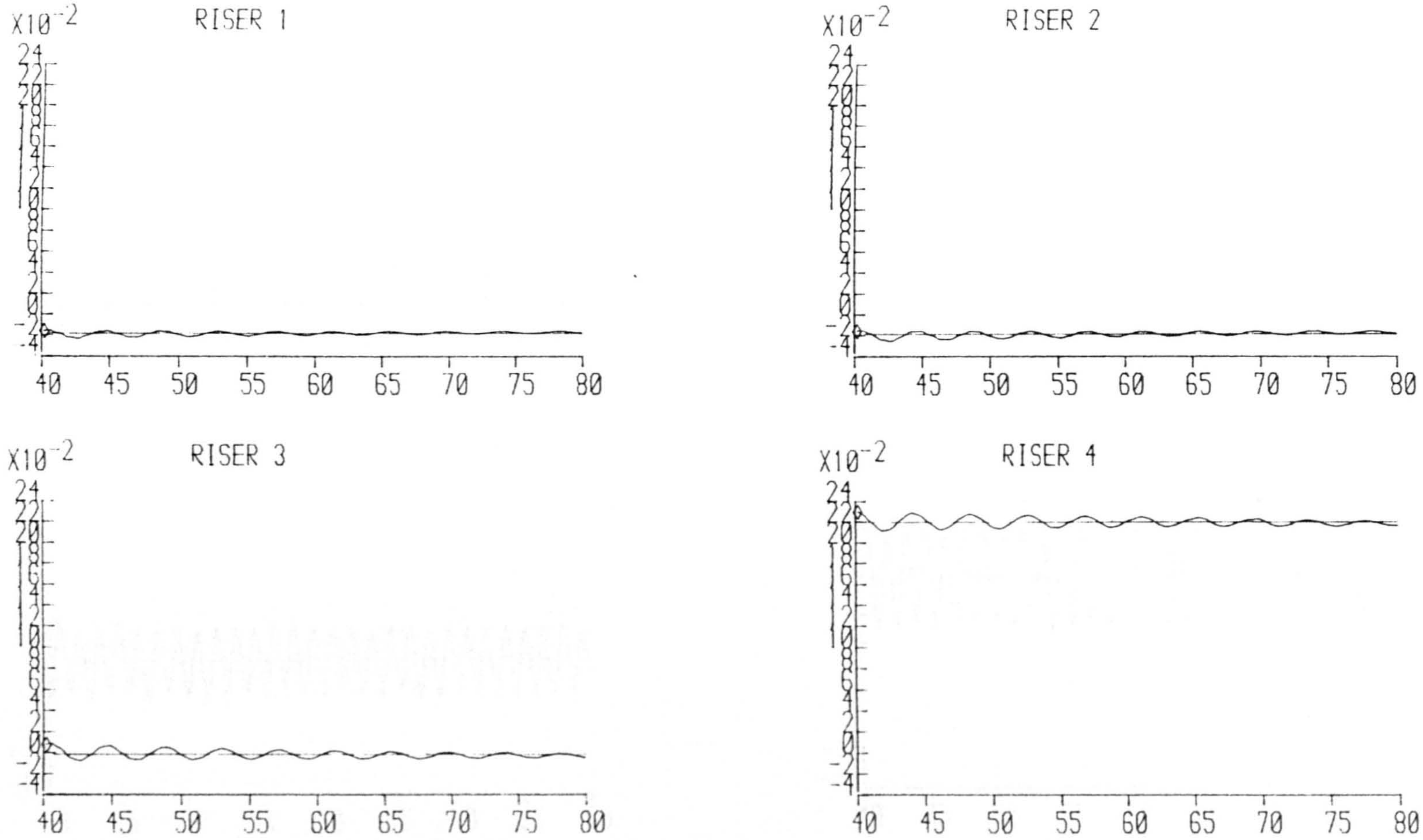

Y-AXIS = RISER VELOCITY (M/S), X-AXIS = TIME (SECS)

WAVEHEIGHT= 0.00000 WAVEPERIOD= 1.42900 FLOW RATE= 0.00035

FIGURE E.23

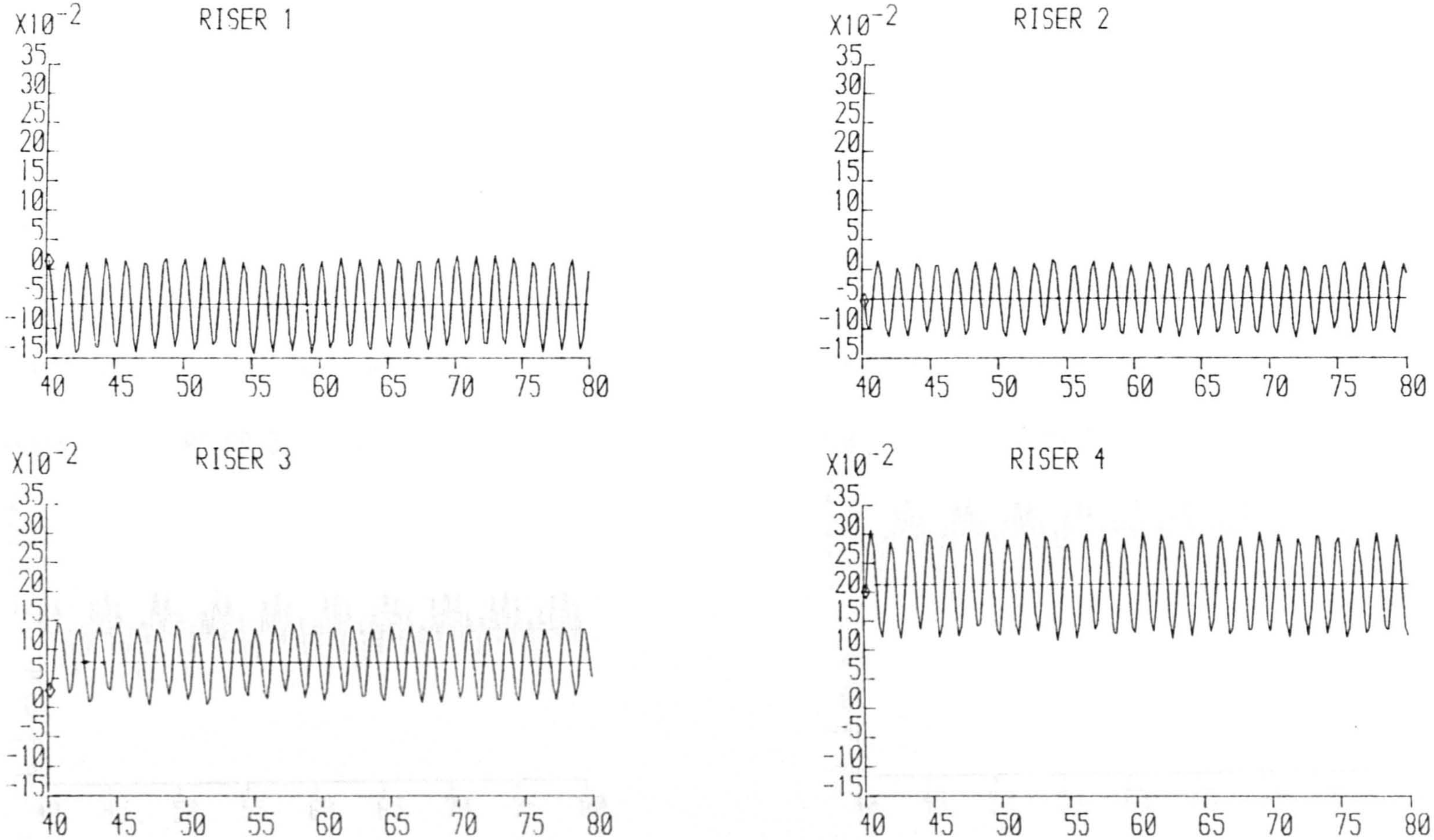

Y-AXIS = RISER VELOCITY (M/S), X-AXIS = TIME (SECS)

WAVEHEIGHT= 0.06600 WAVEPERIOD= 1.42900 FLOW RATE= 0.00035

FIGURE E.24

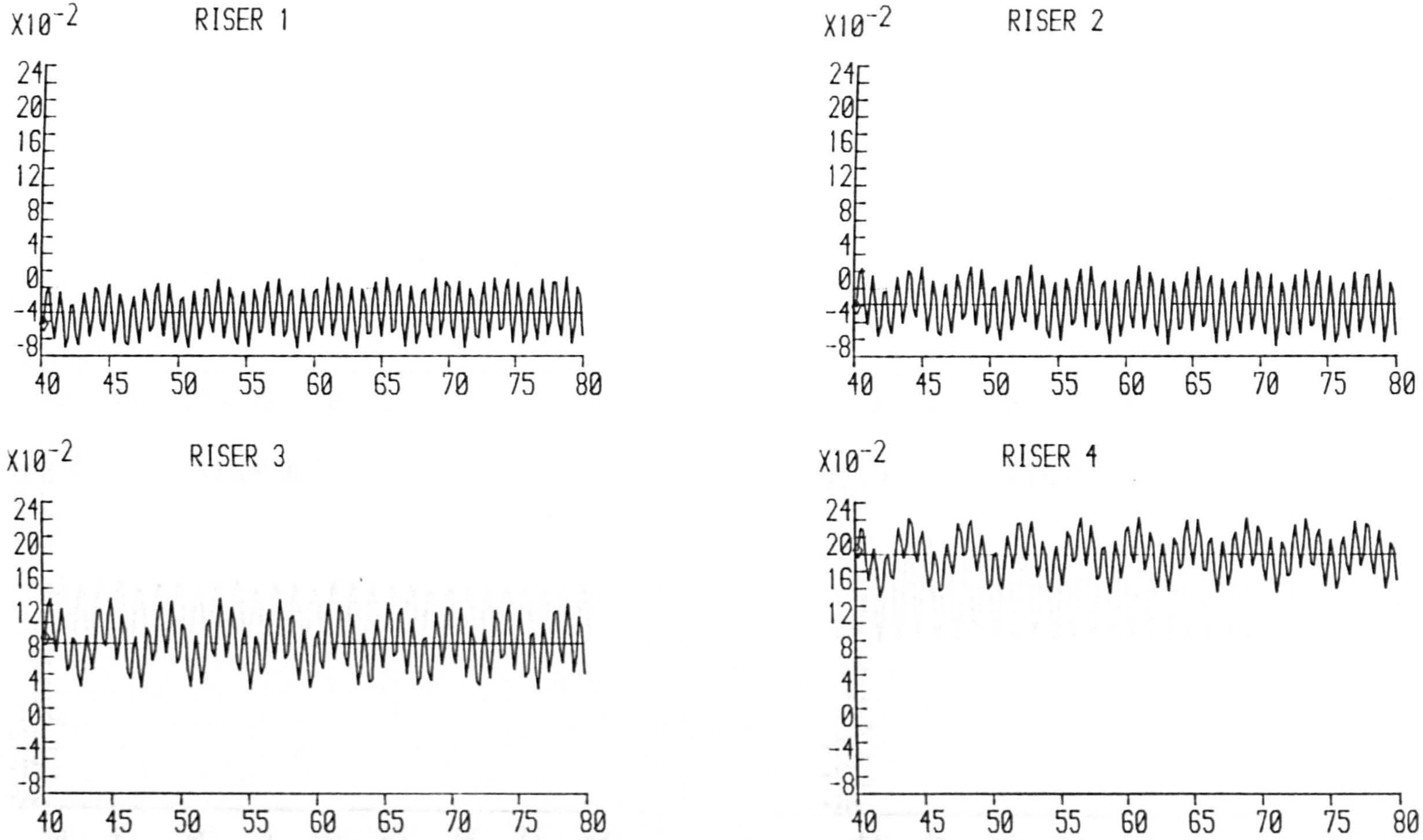

Y-AXIS = RISER VELOCITY (M/S), X-AXIS = TIME (SECS)

WAVEHEIGHT= 0.00000 WAVEPERIOD= 1.42900 FLOW RATE= 0.00048

FIGURE E.25

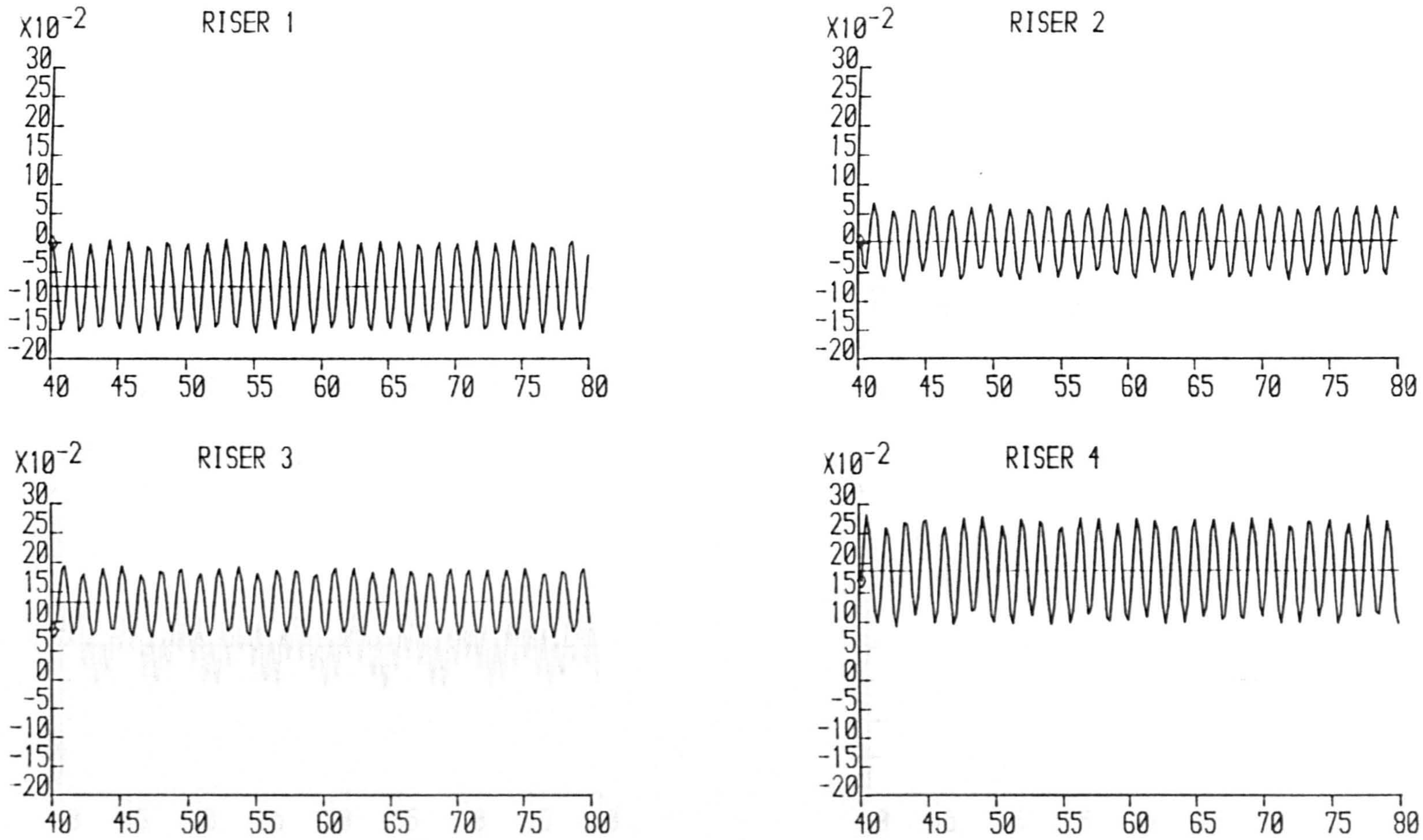

Y-AXIS = RISER VELOCITY (M/S), X-AXIS = TIME (SECS)

WAVEHEIGHT= 0.06600 WAVEPERIOD= 1.42900 FLOW RATE= 0.00048

FIGURE E.26

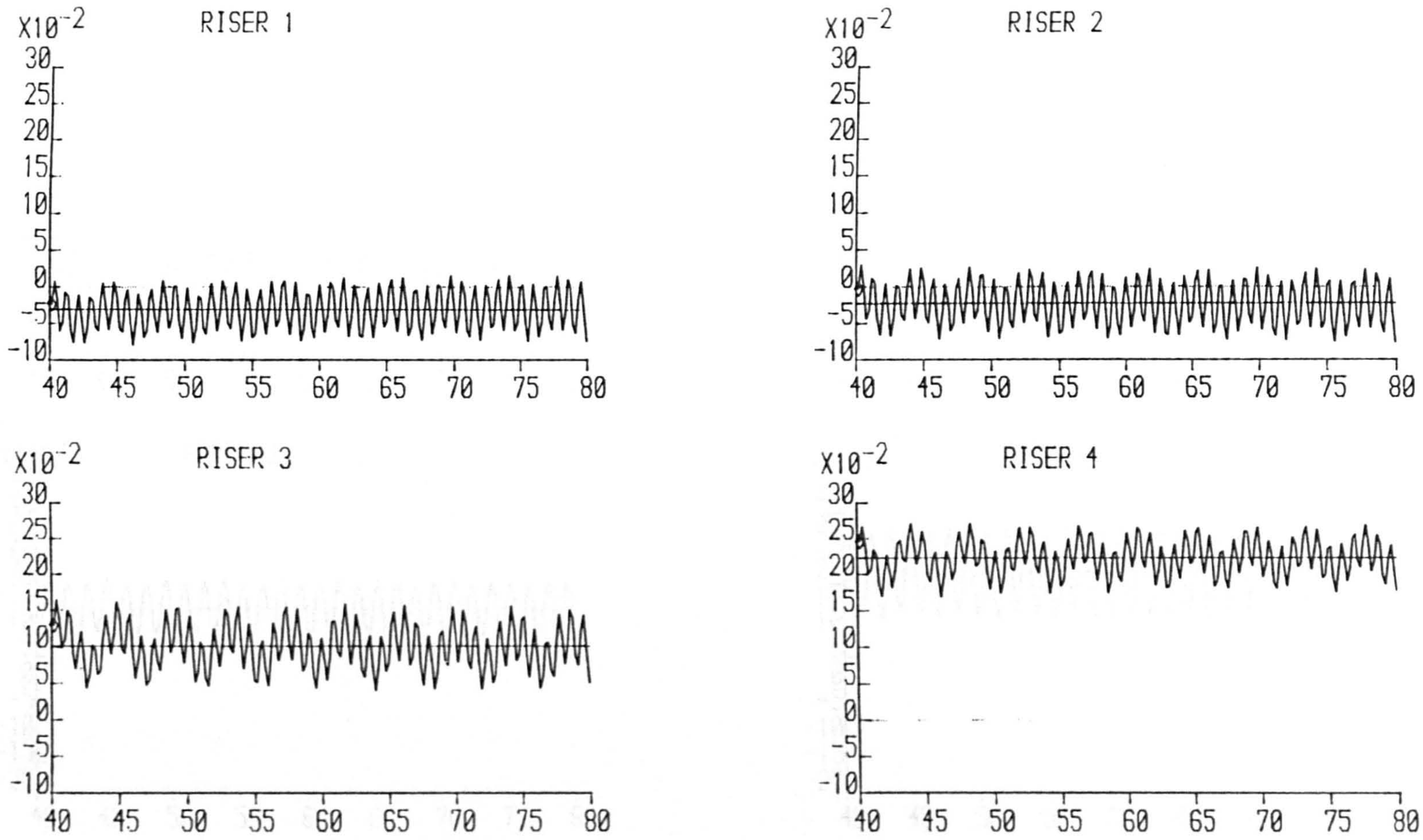

Y-AXIS = RISER VELOCITY (M/S), X-AXIS = TIME (SECS)

WAVEHEIGHT= 0.00000 WAVEPERIOD= 1.42900 FLOW RATE= 0.00053

FIGURE E.27

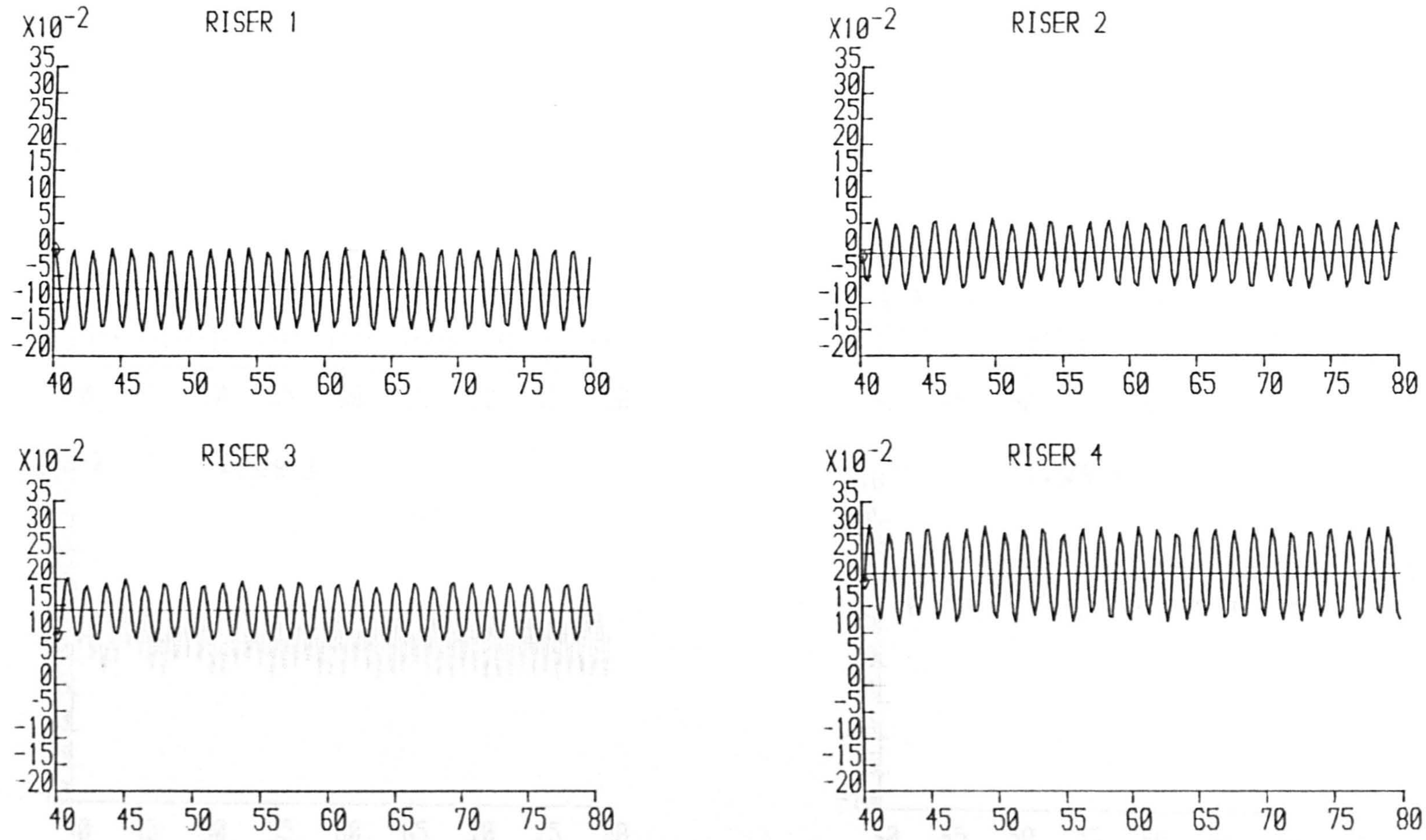

Y-AXIS = RISER VELOCITY (M/S), X-AXIS = TIME (SECS)

WAVEHEIGHT= 0.06600 WAVEPERIOD= 1.42900 FLOW RATE= 0.00053

FIGURE E.28

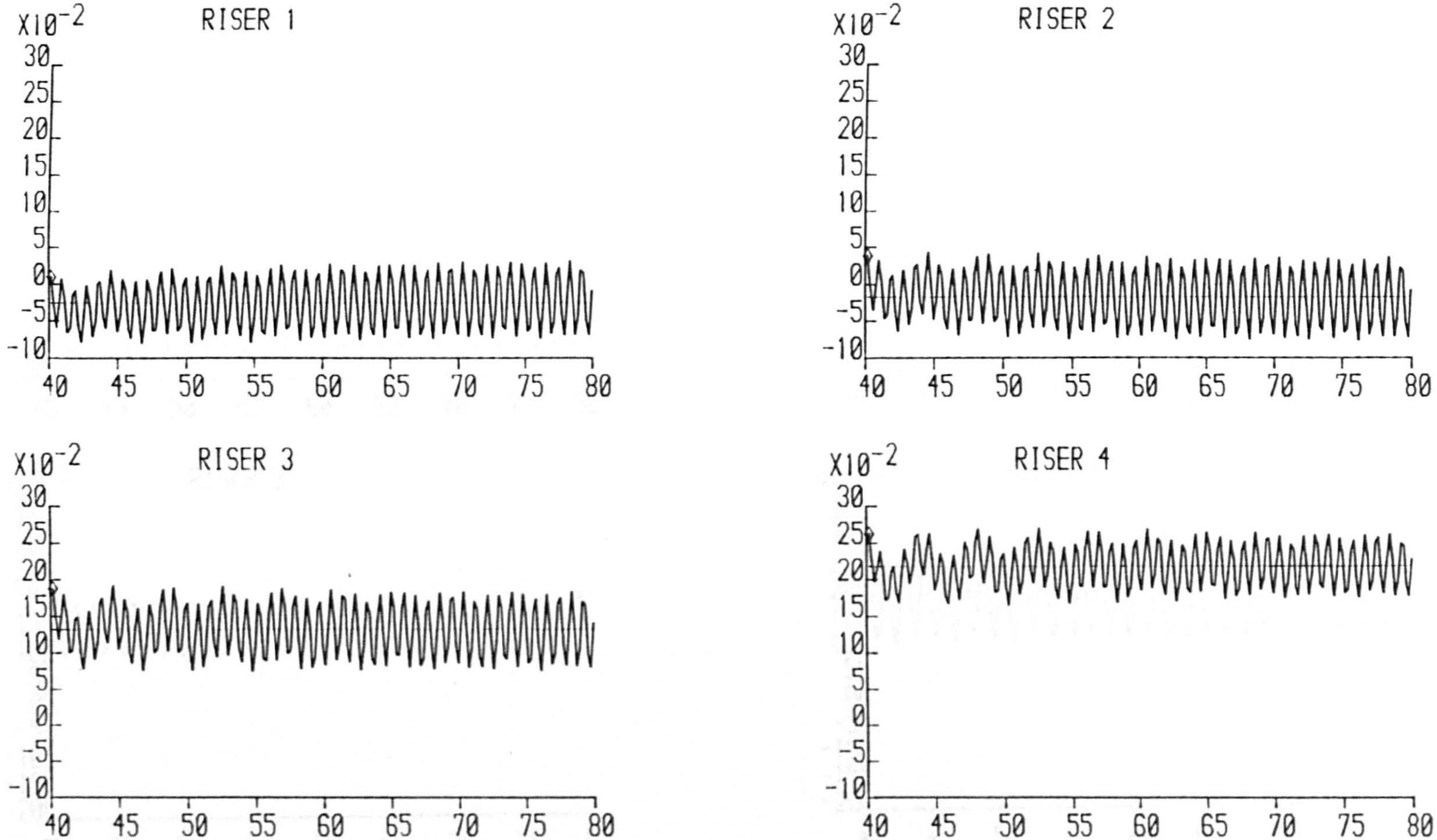

Y-AXIS = RISER VELOCITY (M/S), X-AXIS = TIME (SECS)

WAVEHEIGHT= 0.00000 WAVEPERIOD= 1.42900 FLOW RATE= 0.00060

FIGURE E.29

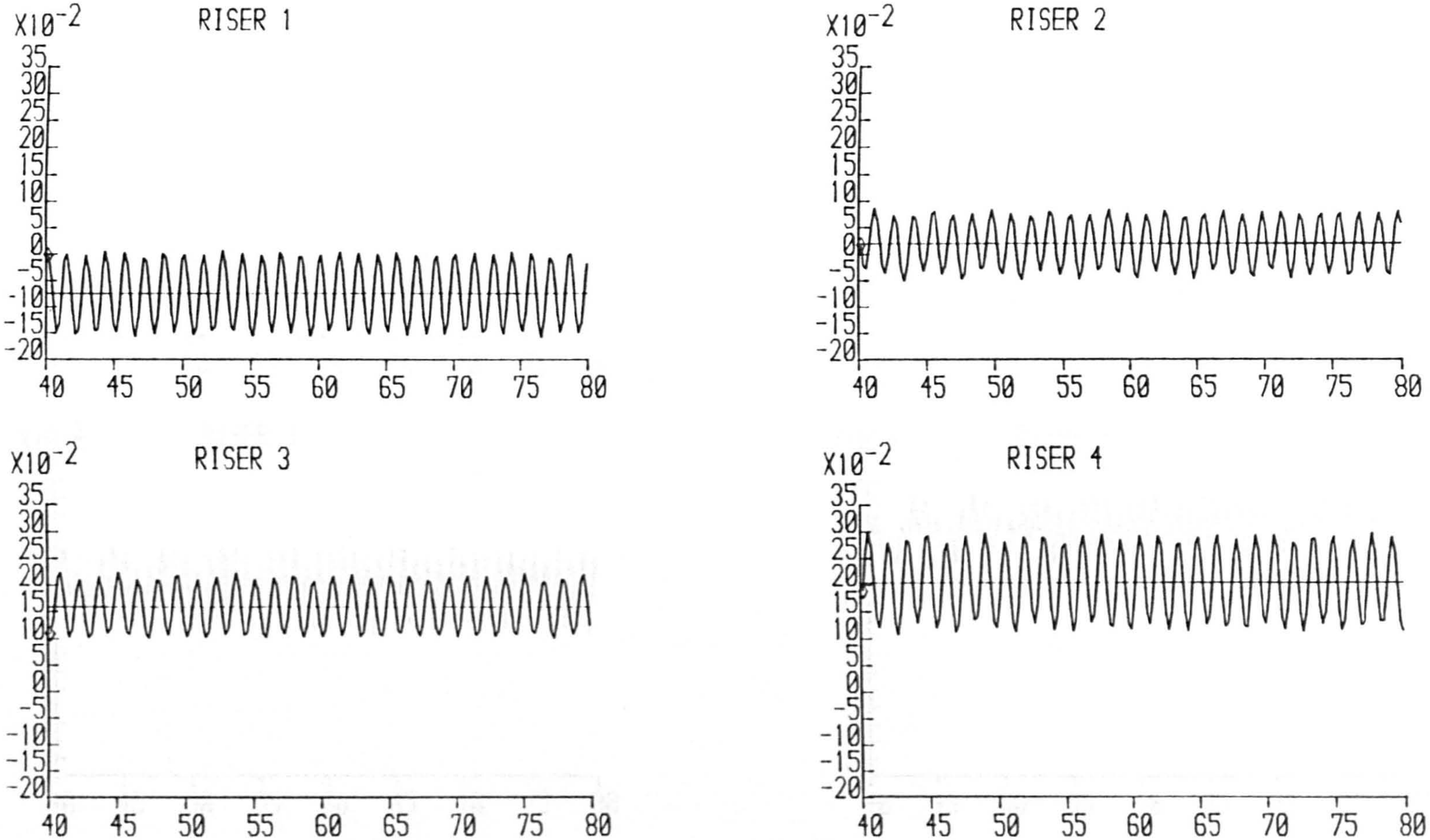

Y-AXIS = RISER VELOCITY (M/S), X-AXIS = TIME (SECS)

WAVEHEIGHT= 0.06600 WAVEPERIOD= 1.42900 FLOW RATE= 0.00060

FIGURE E.30

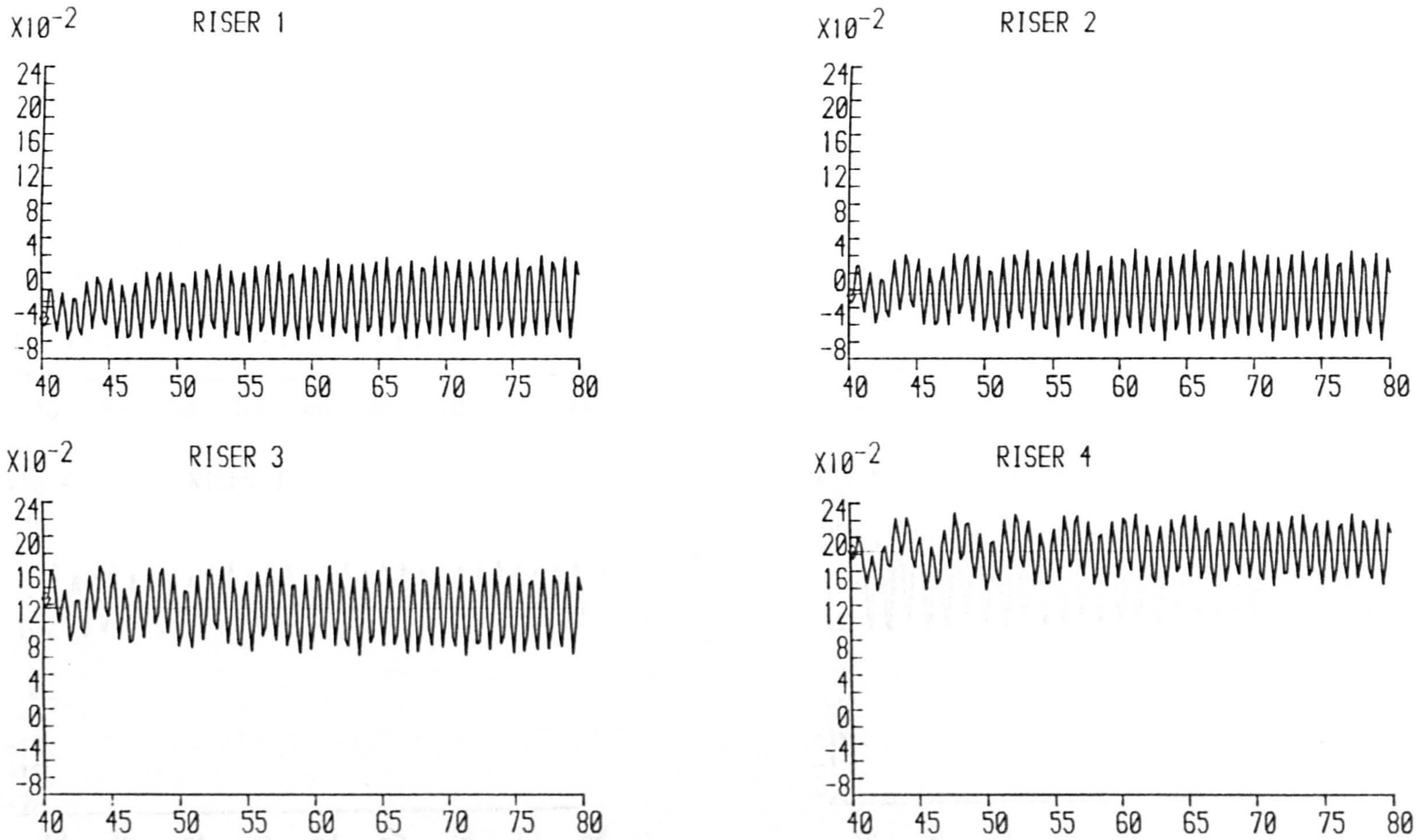

Y-AXIS = RISER VELOCITY (M/S), X-AXIS = TIME (SECS)

WAVEHEIGHT= 0.00000 WAVEPERIOD= 1.42900 FLOW RATE= 0.00063

FIGURE. E.31

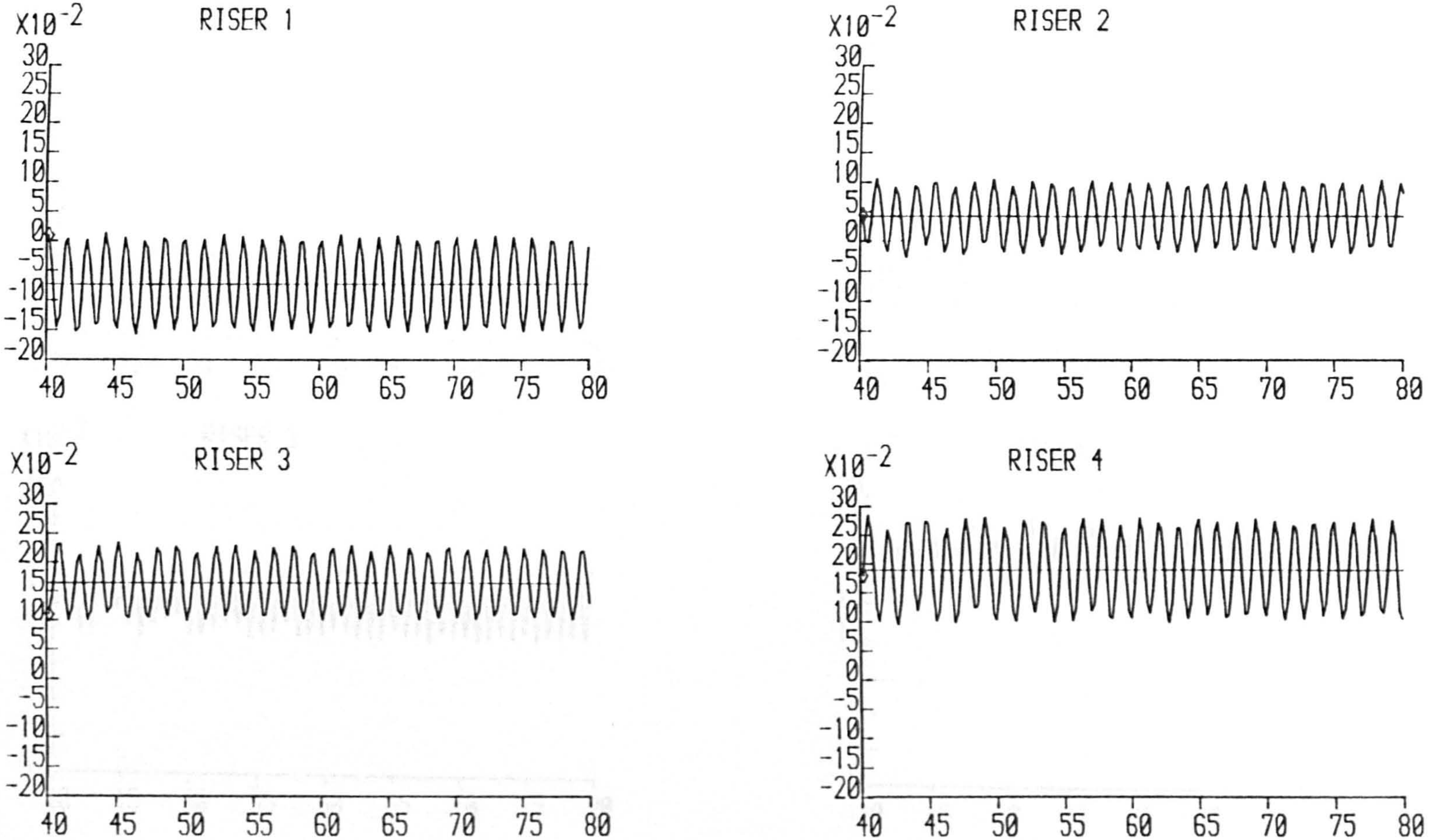

Y-AXIS = RISER VELOCITY (M/S), X-AXIS = TIME (SECS)

WAVEHEIGHT= 0.06600 WAVEPERIOD= 1.42900 FLOW RATE= 0.00063

FIGURE E.32

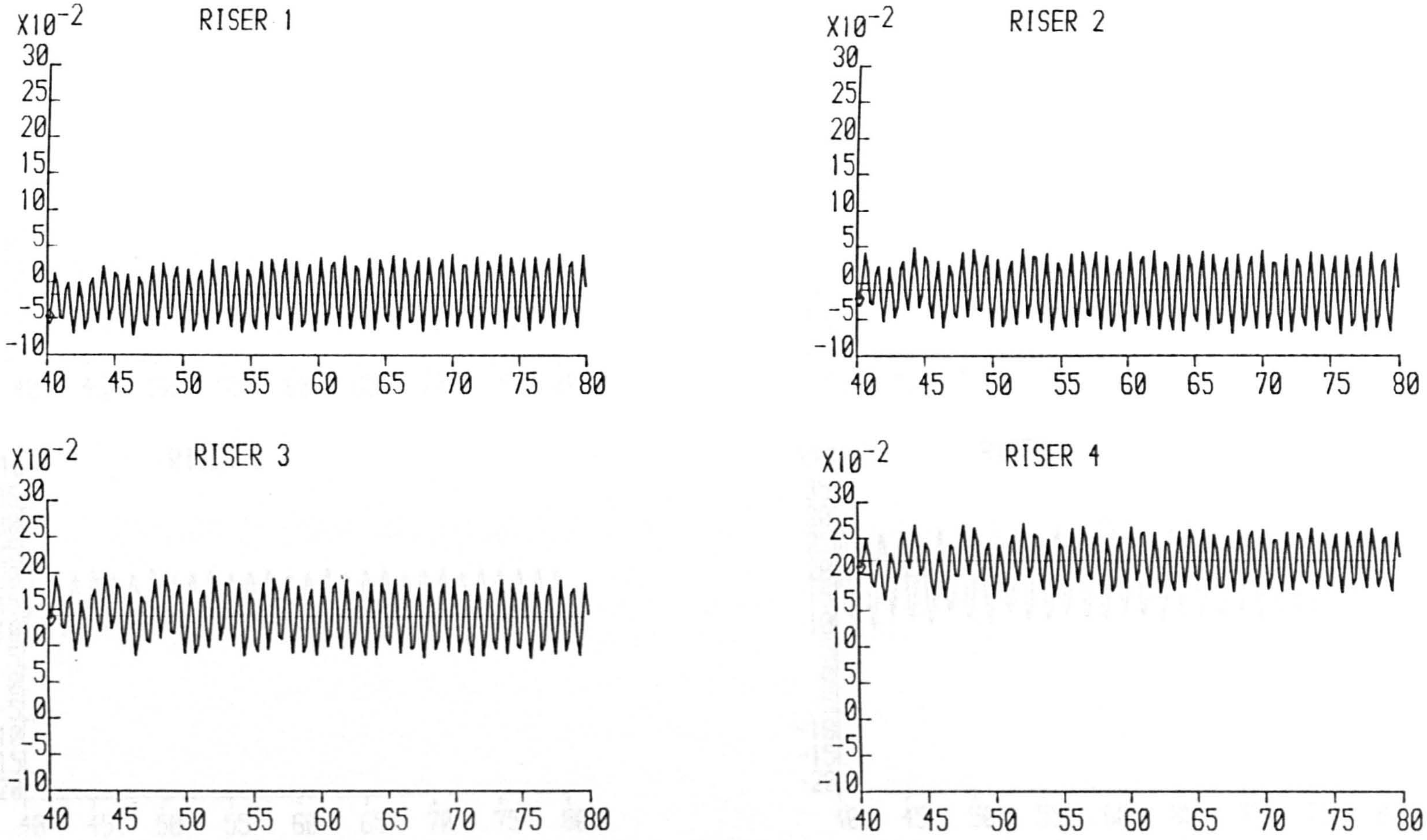

Y-AXIS = RISER VELOCITY (M/S), X-AXIS = TIME (SECS)

WAVEHEIGHT= 0.00000 WAVEPERIOD= 1.42900 FLOW RATE= 0.00065

FIGURE E.33

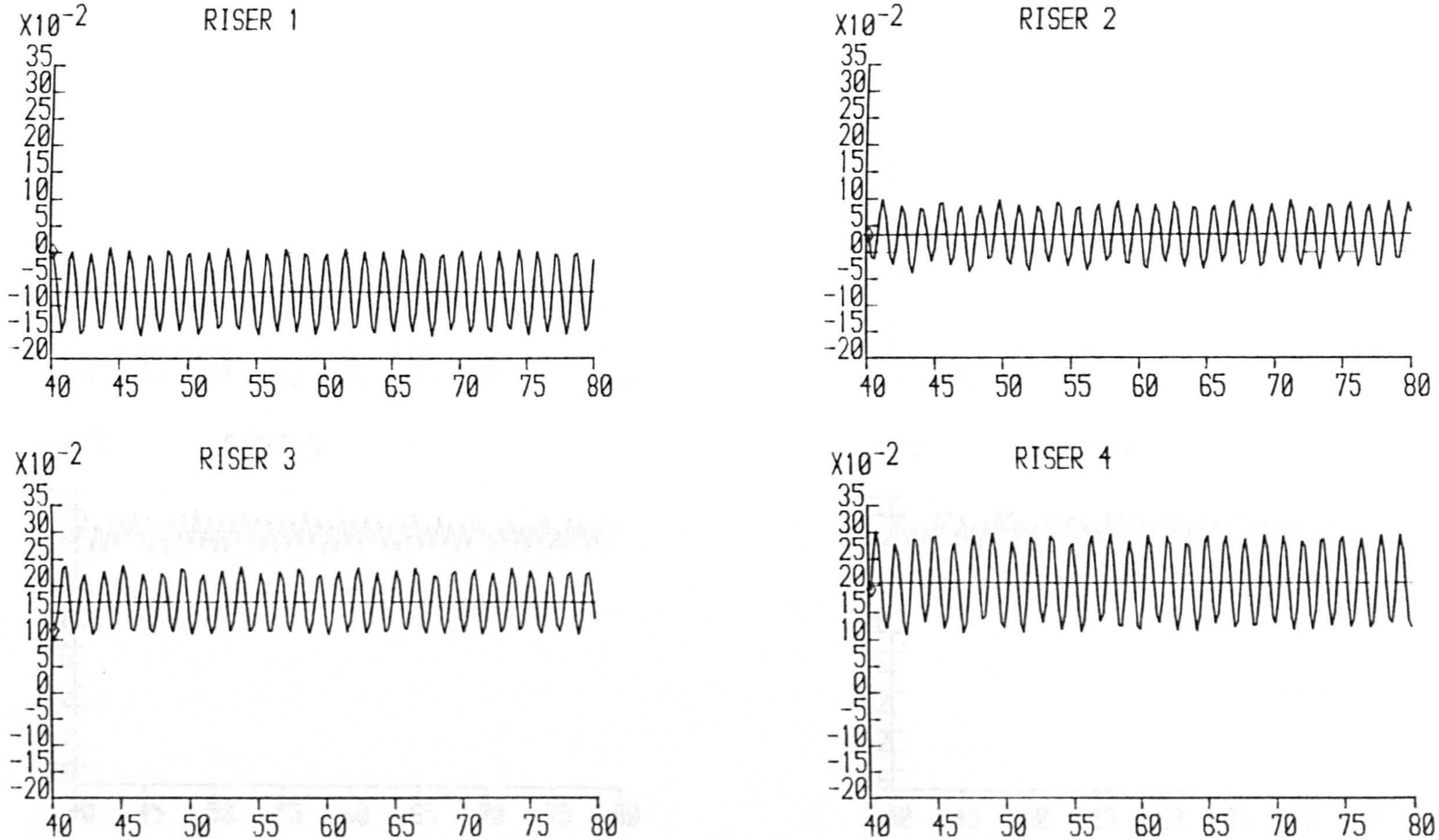

Y-AXIS = RISER VELOCITY (M/S), X-AXIS = TIME (SECS)

WAVEHEIGHT= 0.06600 WAVEPERIOD= 1.42900 FLOW RATE= 0.00065

FIGURE E.34

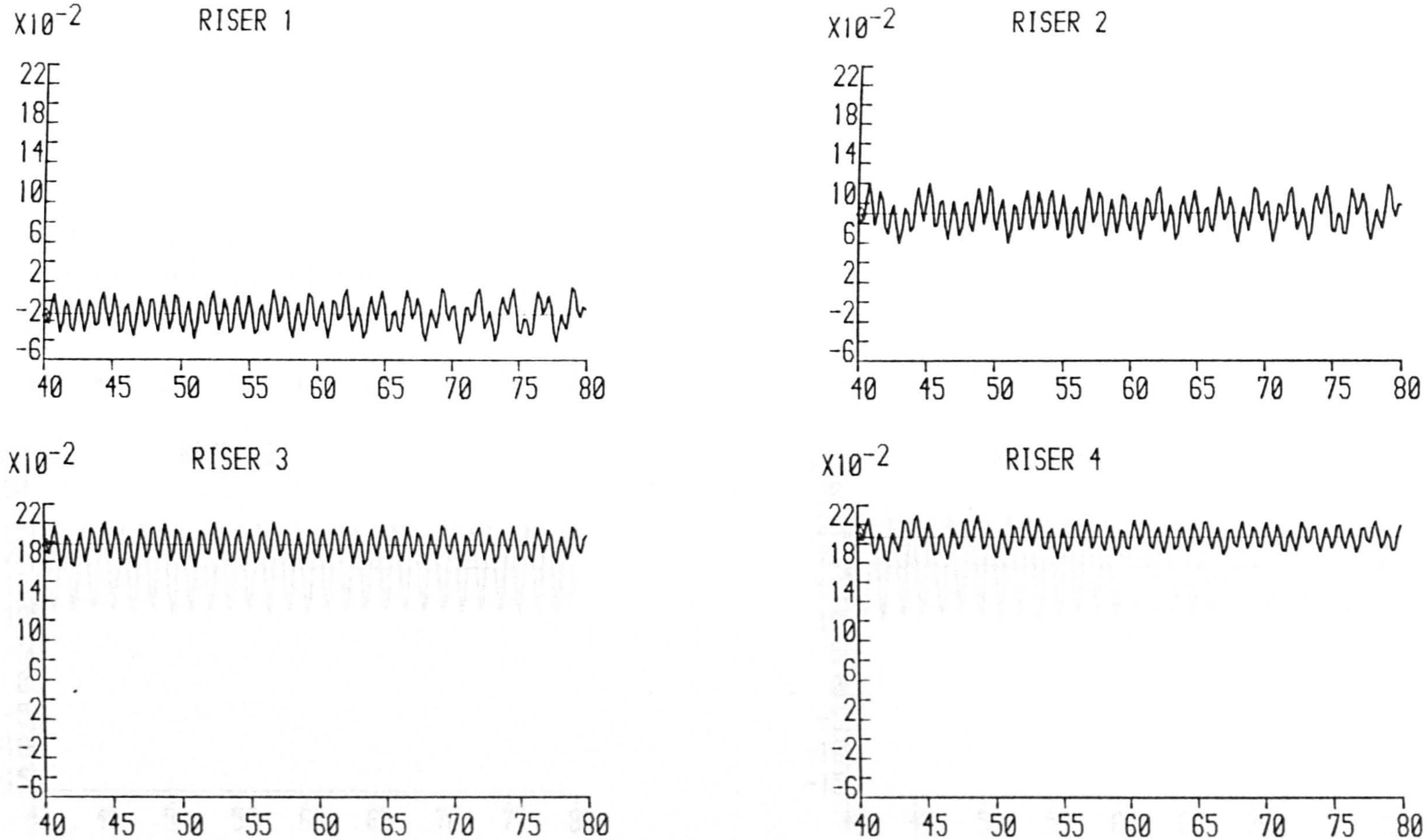

Y-AXIS = RISER VELOCITY (M/S), X-AXIS = TIME (SECS)

WAVEHEIGHT= 0.00000 WAVEPERIOD= 1.42900 FLOW RATE= 0.00094

FIGURE E.35

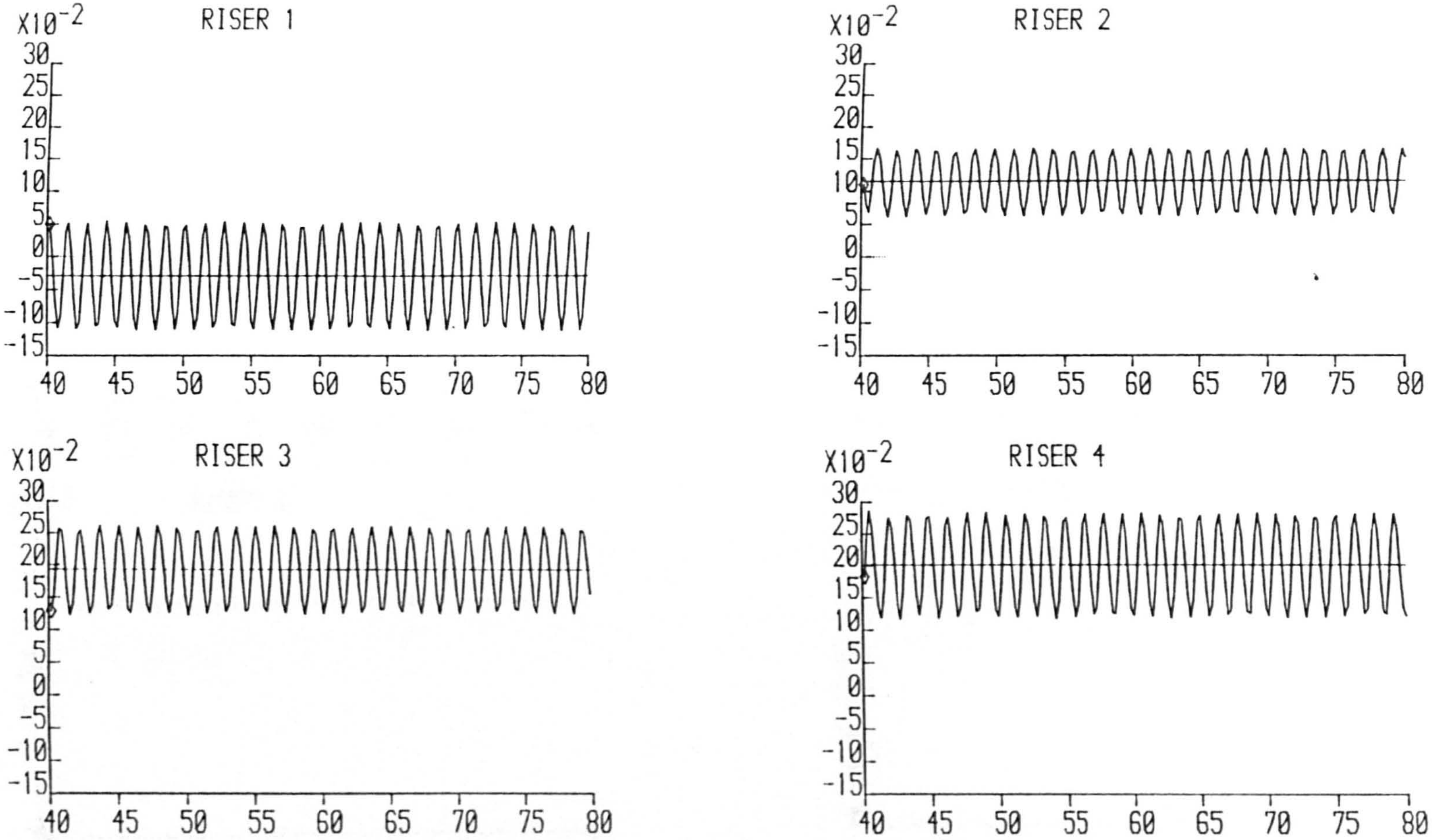

Y-AXIS = RISER VELOCITY (M/S), X-AXIS = TIME (SECS)

WAVEHEIGHT= 0.06600 WAVEPERIOD= 1.42900 FLOW RATE= 0.00094

FIGURE E.36

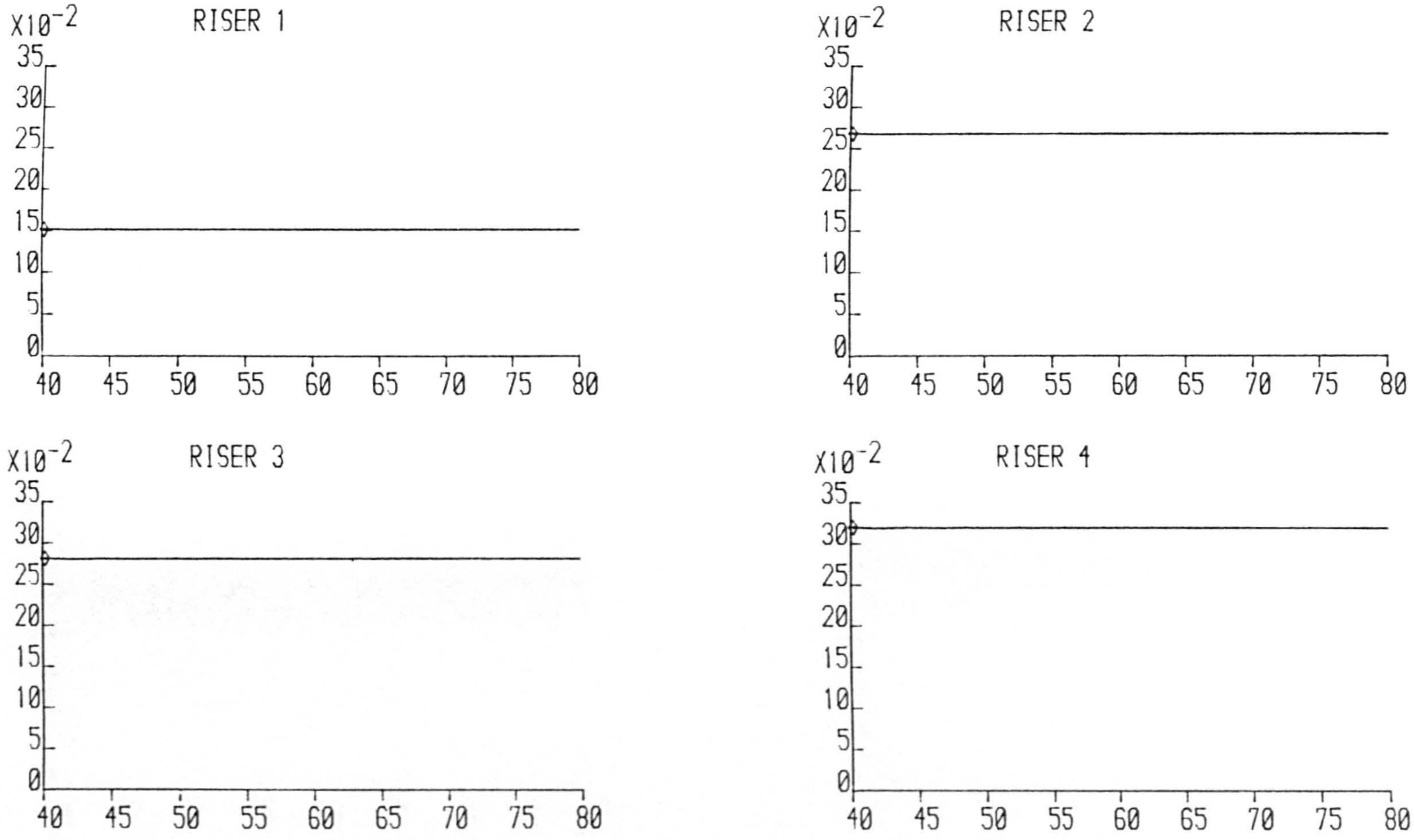

Y-AXIS = RISER VELOCITY (M/S), X-AXIS = TIME (SECS)

WAVEHEIGHT= 0.00000 WAVEPERIOD= 1.42900 FLOW RATE= 0.00200

FIGURE E.37

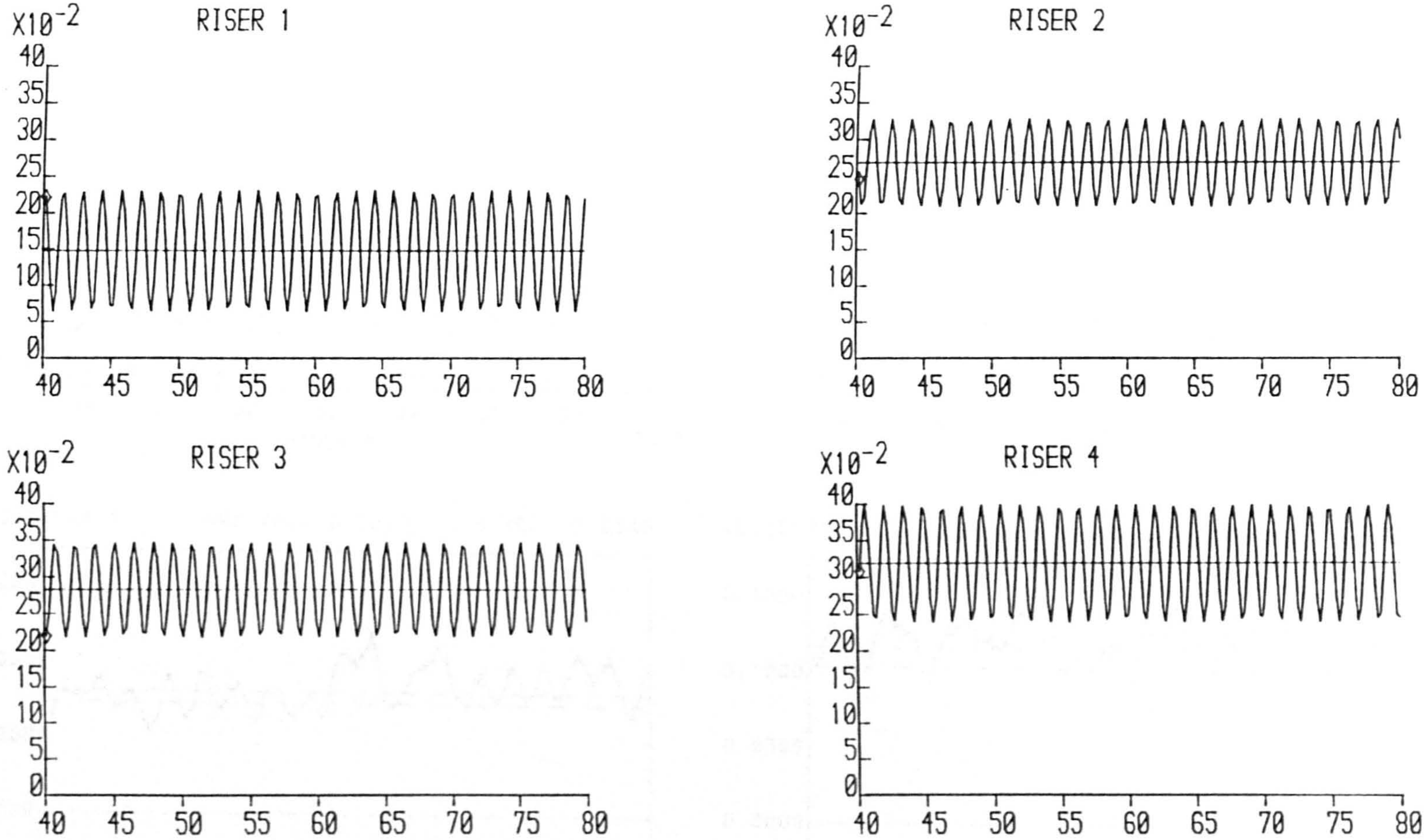

Y-AXIS = RISER VELOCITY (M/S), X-AXIS = TIME (SECS)

WAVEHEIGHT= 0.06600 WAVEPERIOD= 1.42900 FLOW RATE= 0.00200

FIGURE E.38

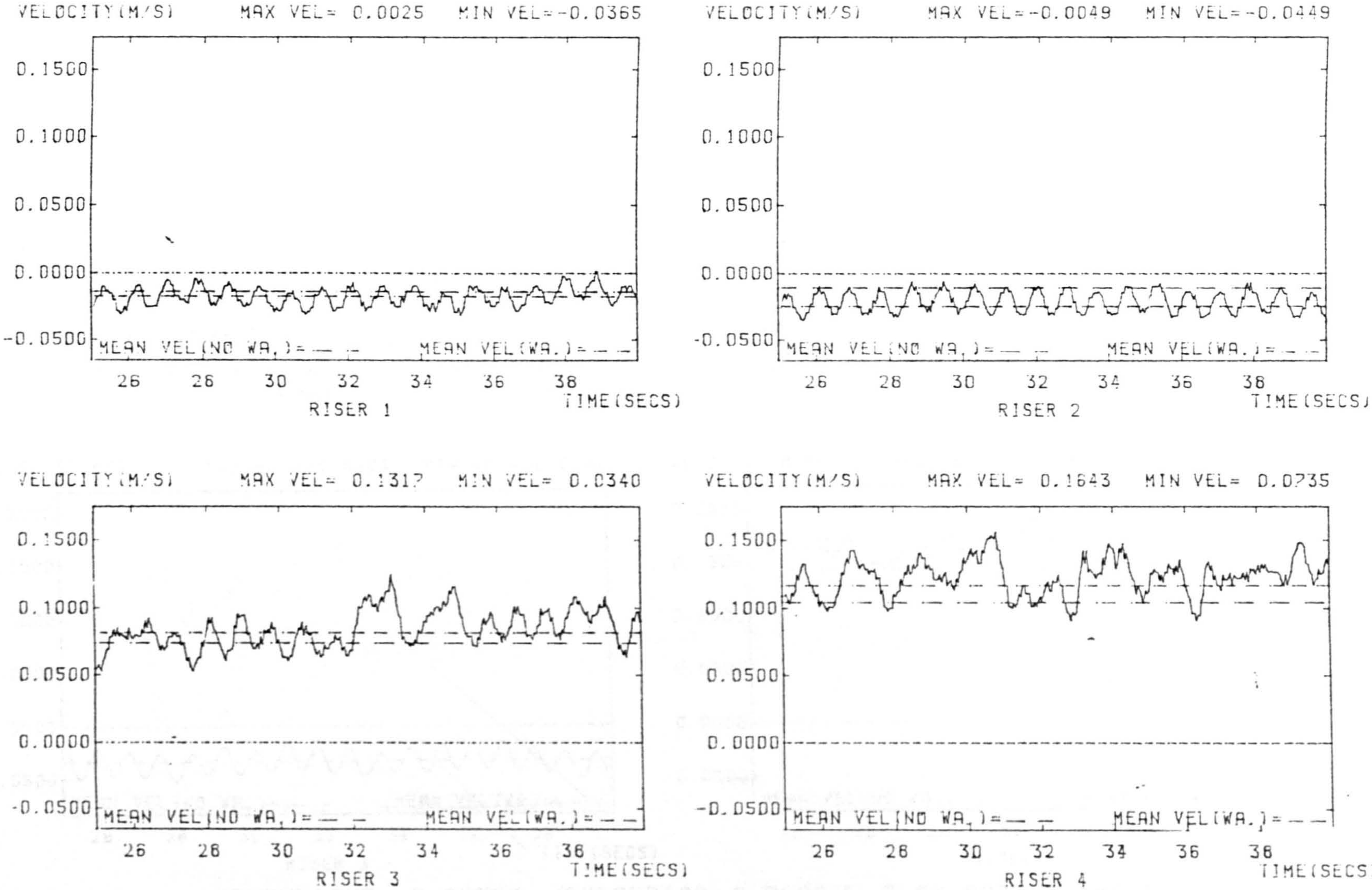

WAVEHEIGHT= 0.0550M WAVEPERIOD=0.7690 S FLOW RATE=0.18620 L/S

DIFFUSER CAPS FITTED

11 JUN 88 11:00:02

FIGURE E.39

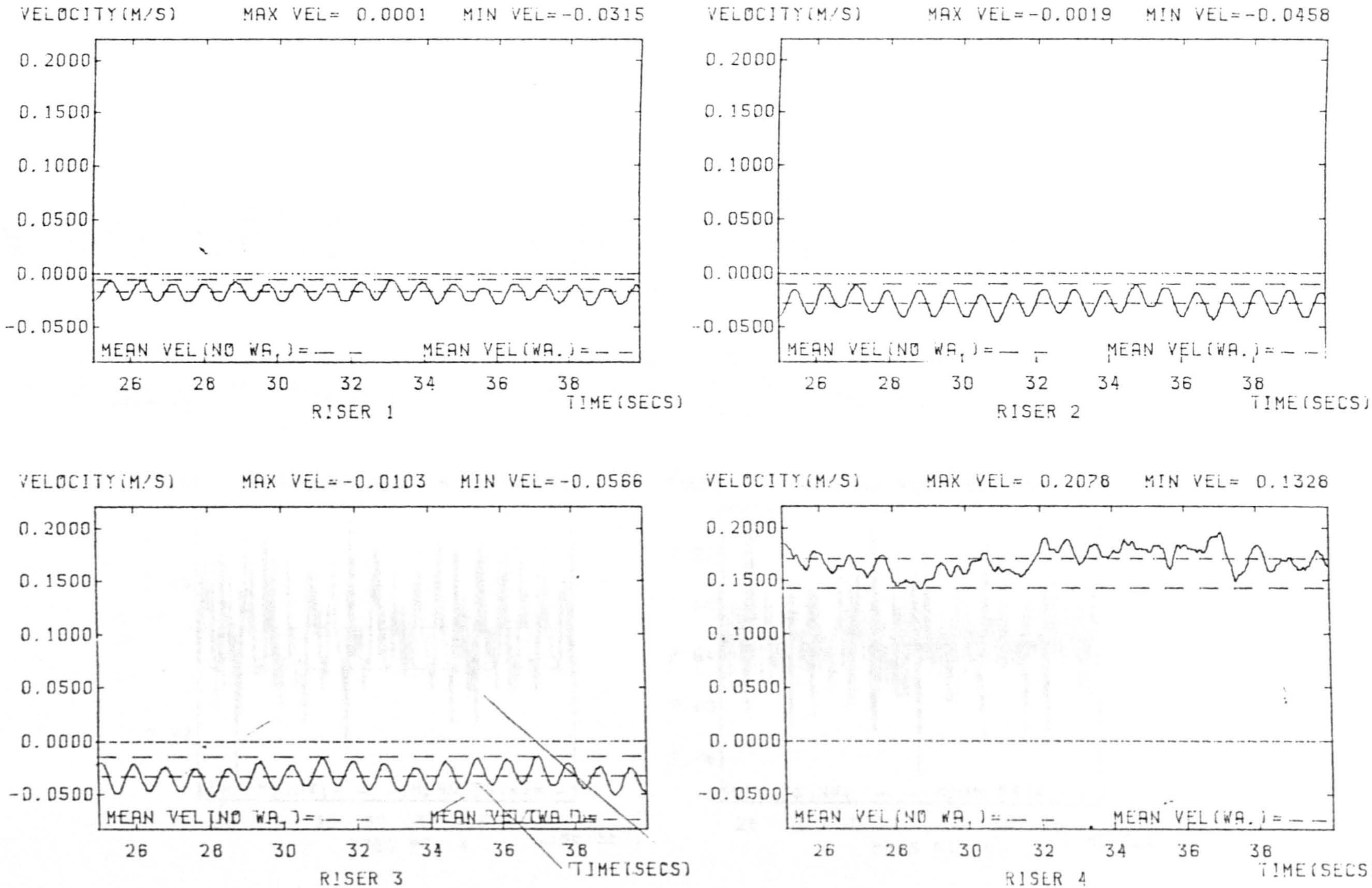

WAVEHEIGHT= 0.0550M WAVEPERIOD=0.7690 S FLOW RATE=0.18620 L/S

NO DIFFUSER CAPS

20 JUN 88 9:50:55

FIGURE E.40

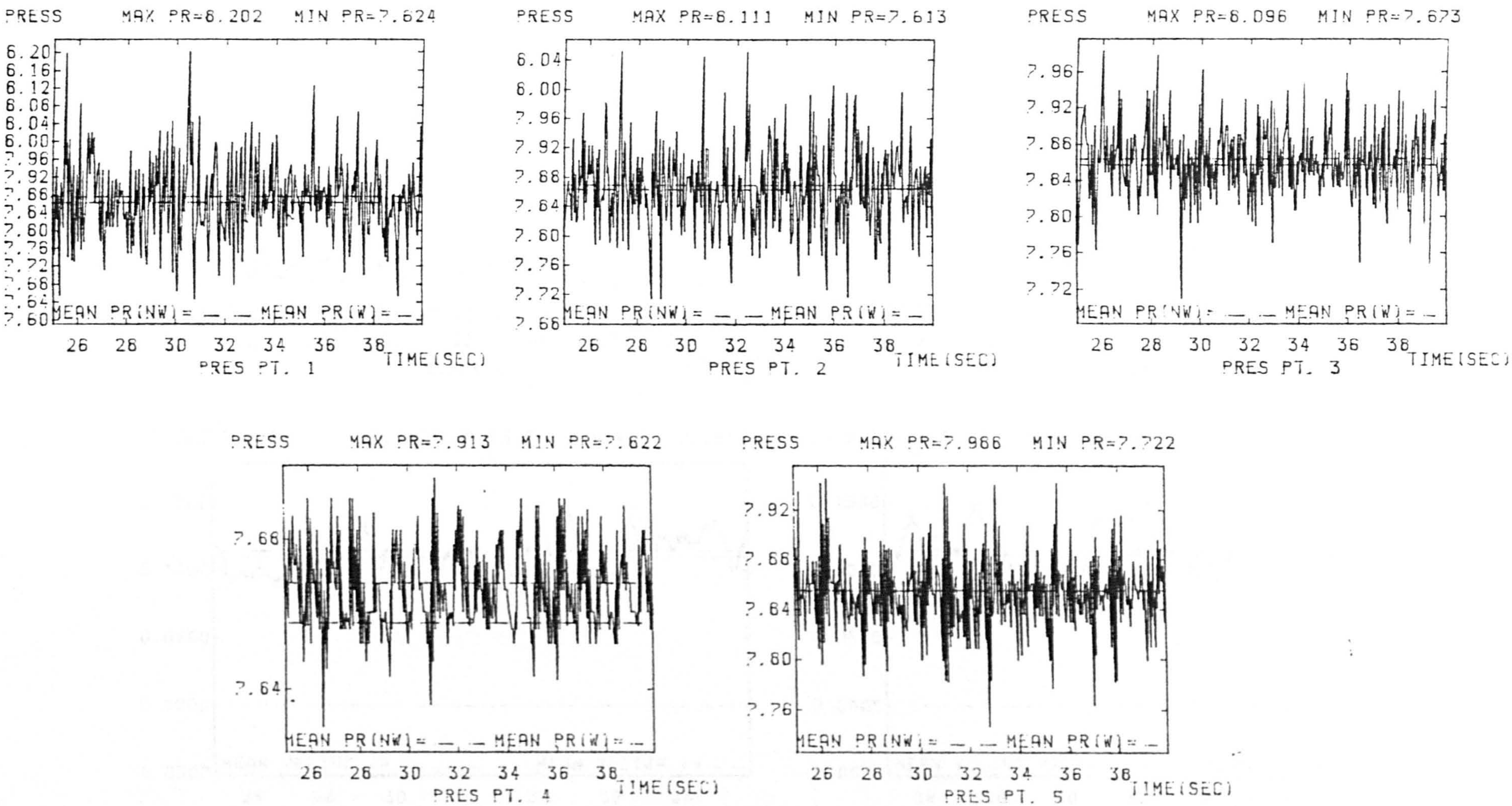

WAVEHEIGHT=0.0550 M WAVEPERIOD=0.7690 S FLOW RATE=0.16620 L/S

FIGURE E41

11 JUN 88 10:40:13

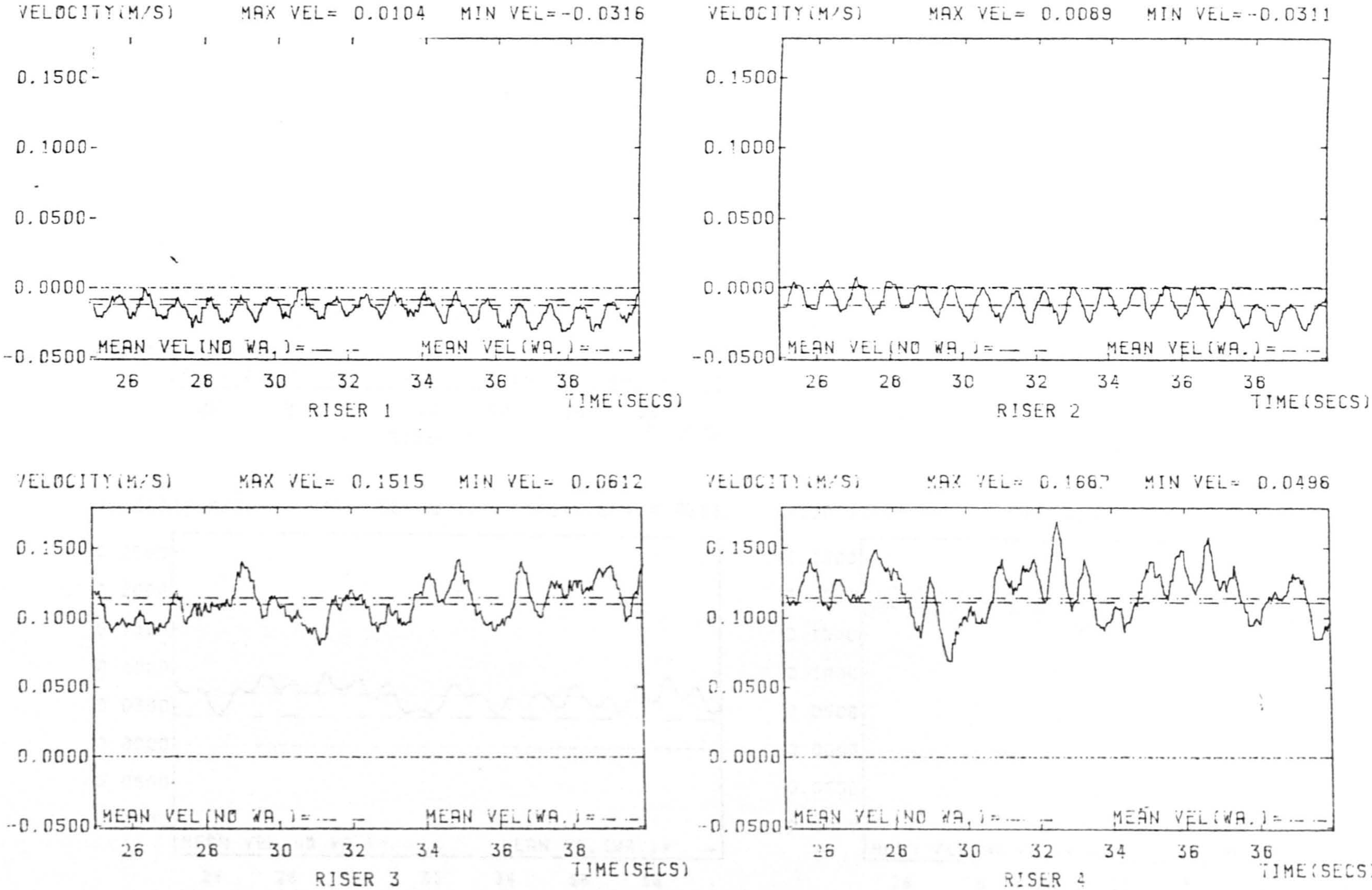

WAVEHEIGHT= 0.0660M WAVEPERIOD=0.7690 S FLOW RATE=0.35500 L/S

DIFFUSER CAPS FITTED

FIGURE E42

13 JUN 88 10:07:04

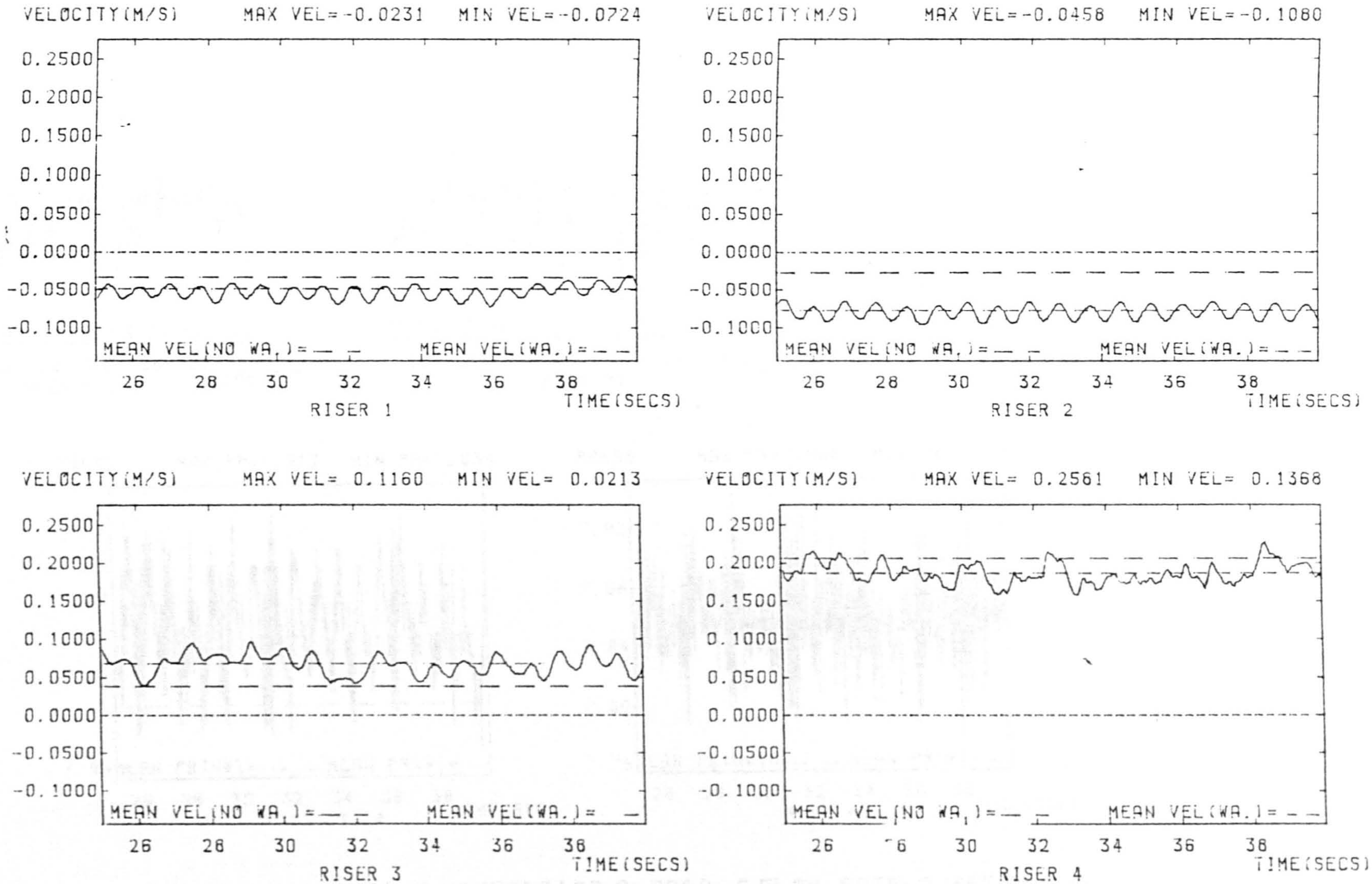

WAVEHEIGHT= 0.0550M WAVEPERIOD=0.7690 S FLOW RATE=0.35500 L/S

NO DIFFUSER CAPS

20 JUN 88 10:25:59

FIGURE E43

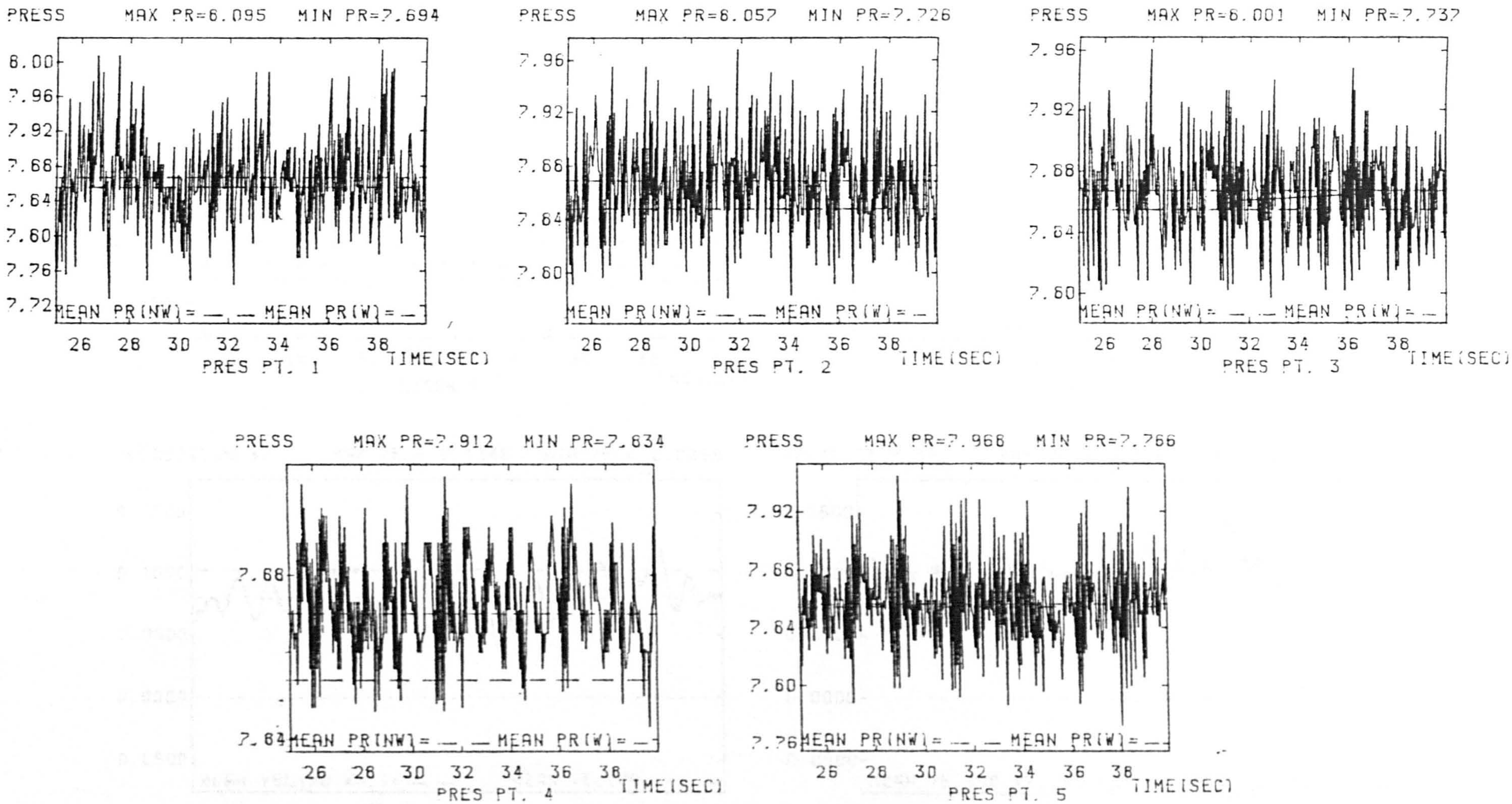

WAVEHEIGHT=0.0550 M WAVEPERIOD=0.7690 S FLOW RATE=0.35500 L/S

13 JUN 88 10:33:10

FIGURE E44

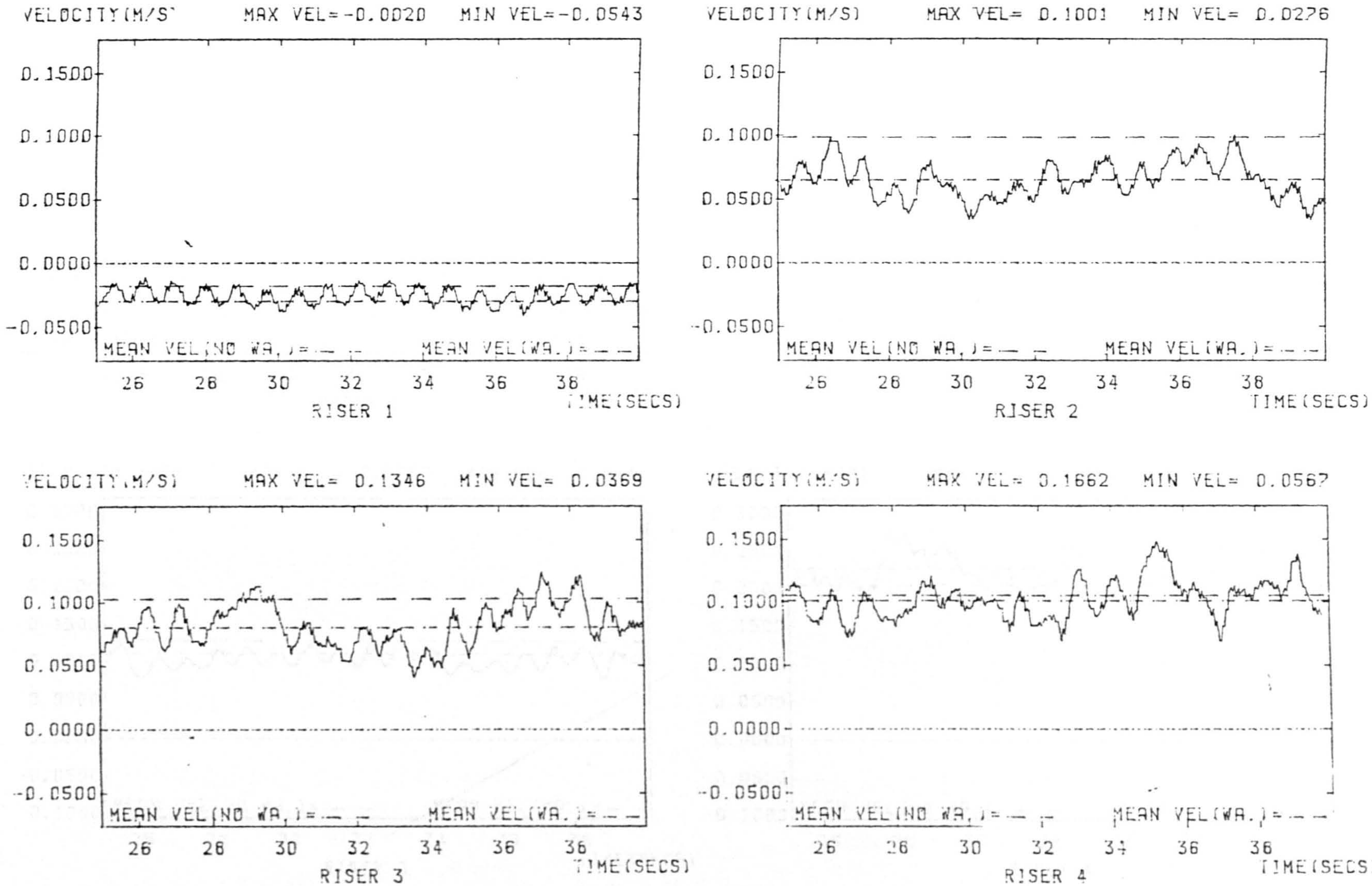

WAVEHEIGHT= 0.0550M WAVEPERIOD=0.7690 S FLOW RATE=0.48420 L/S

DIFFUSER CAPS FITTED

FIGURE E45

13 JUN 88 11:15:24

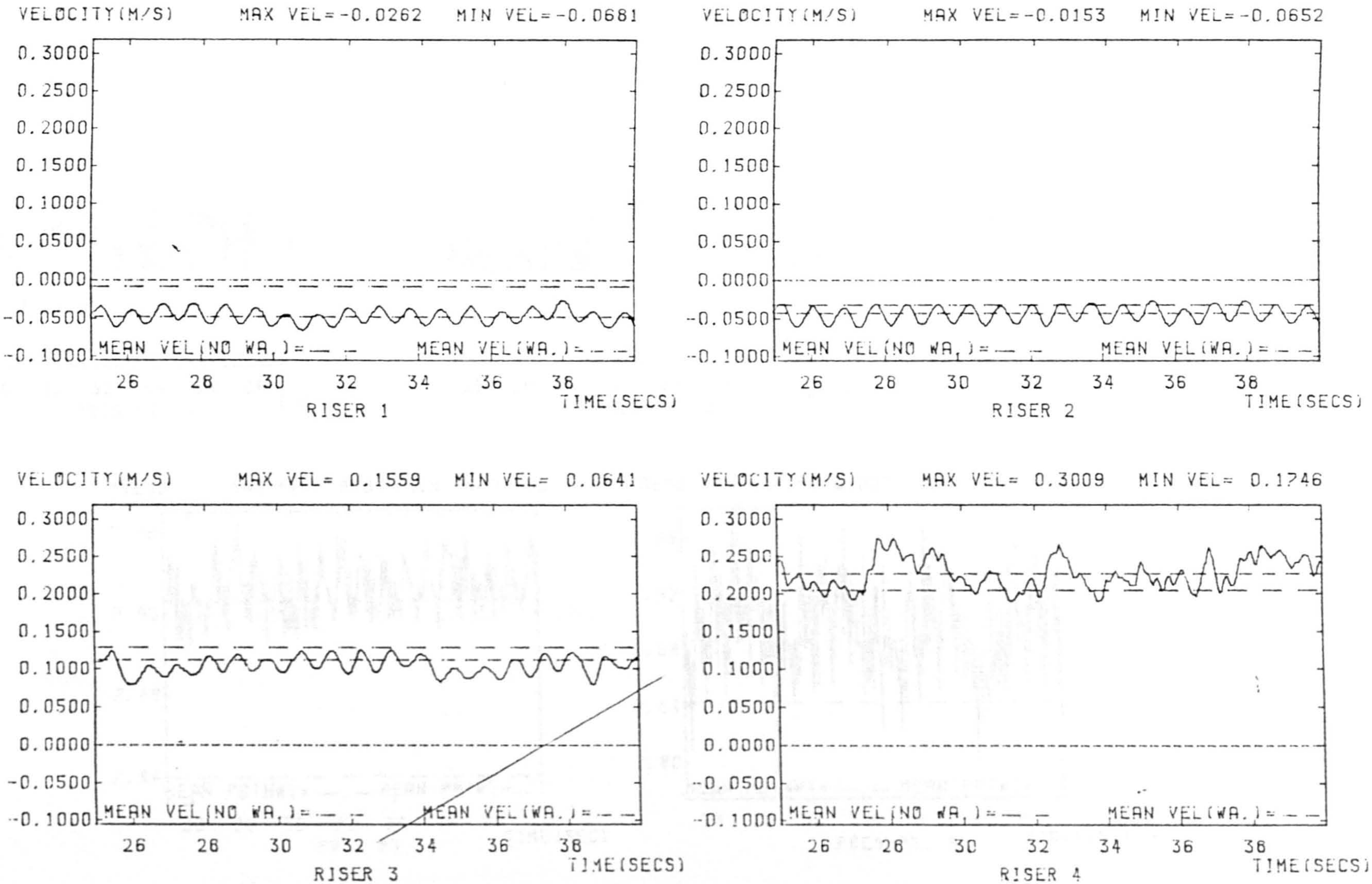

WAVEHEIGHT= 0.0550M WAVEPERIOD=0.7690 S FLOW RATE=0.48420 L/S

NO DIFFUSER CAPS

20 JUN 88 10:44:09

FIGURE E46

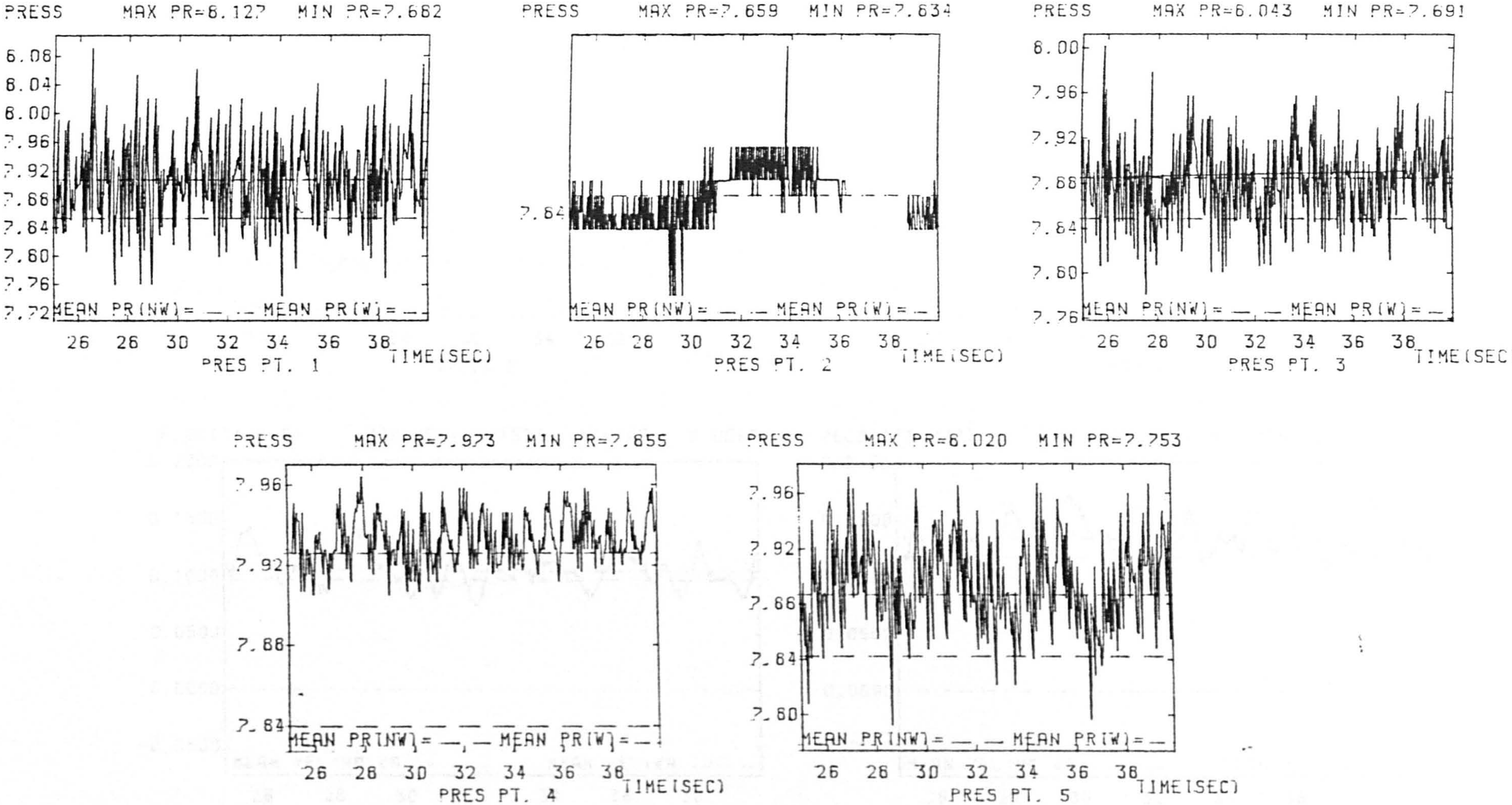

WAVEHEIGHT=0.0550 M WAVEPERIOD=0.7690 S FLOW RATE=0.48420 L/S

13 JUN 88 10:53:10

FIGURE E47

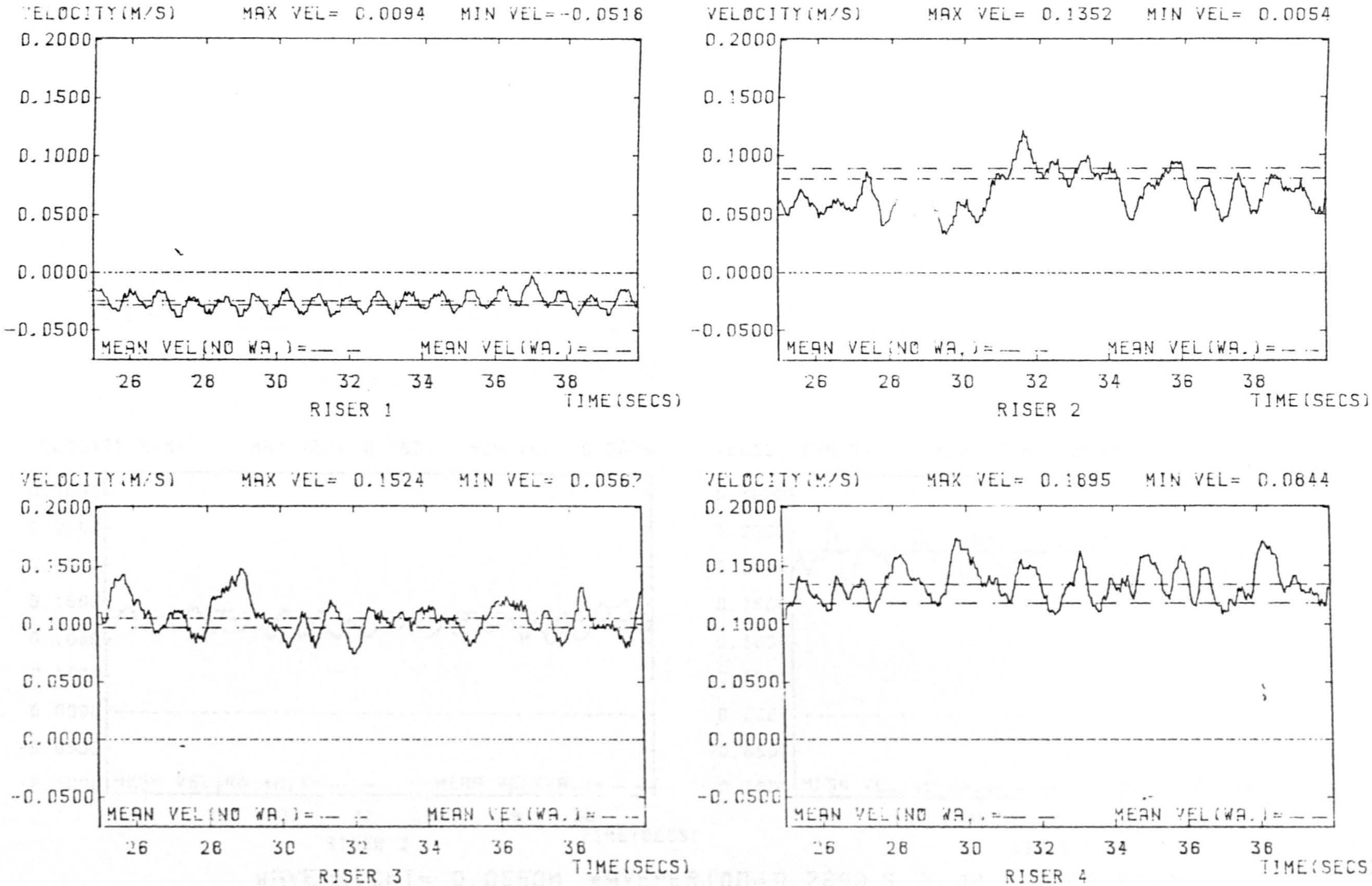

WAVEHEIGHT= 0.0550M WAVEPERIOD=0.7690 S FLOW RATE=0.53100 L/S

DIFFUSER CAPS FITTED

13 JUN 88 16:03:47

FIGURE E48

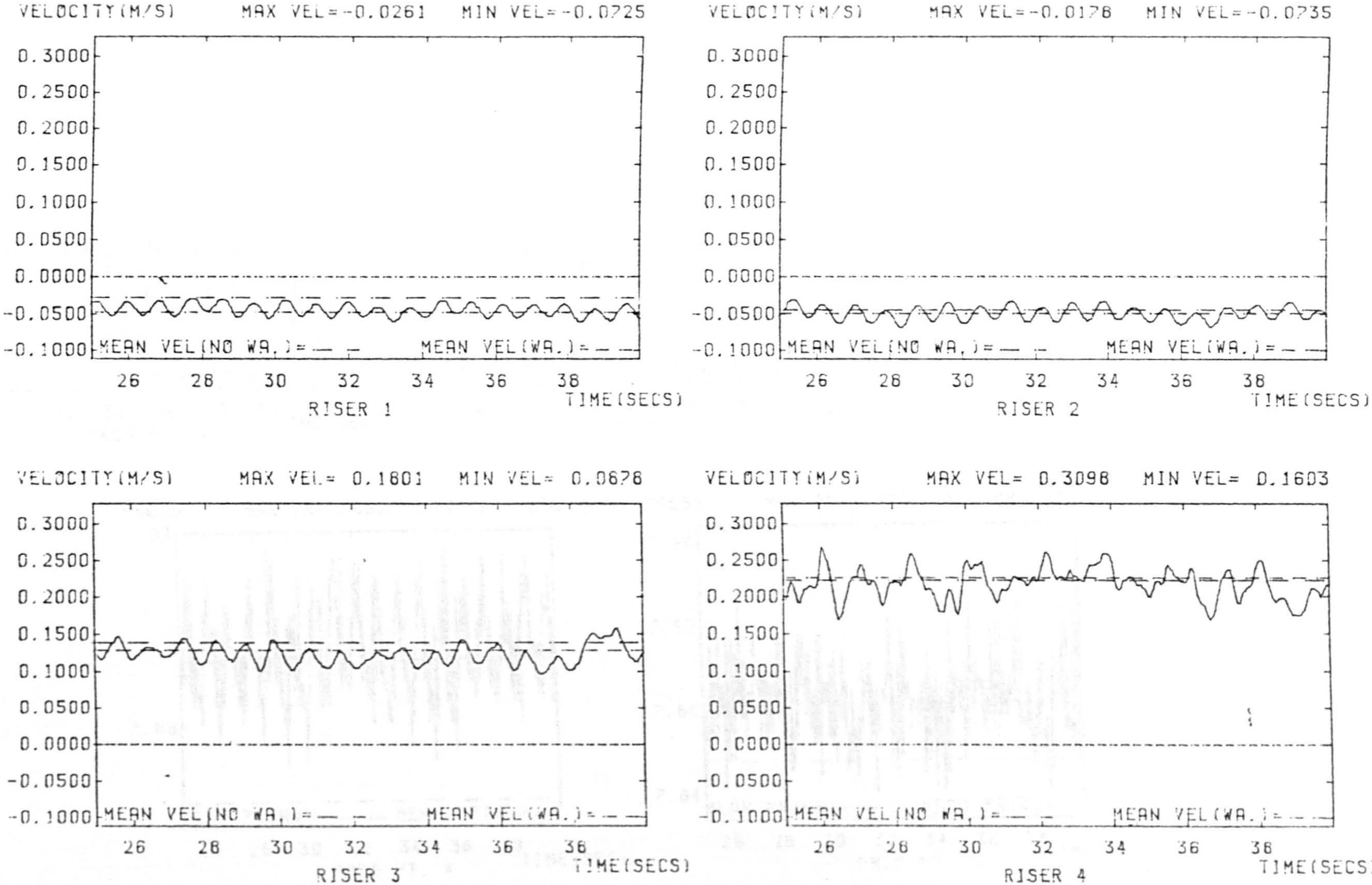

WAVEHEIGHT= 0.0550M WAVEPERIOD=0.7690 S FLOW RATE=0.53100 L/S

NO DIFFUSER CAPS

20 JUN 88 13:56:59

FIGURE E49

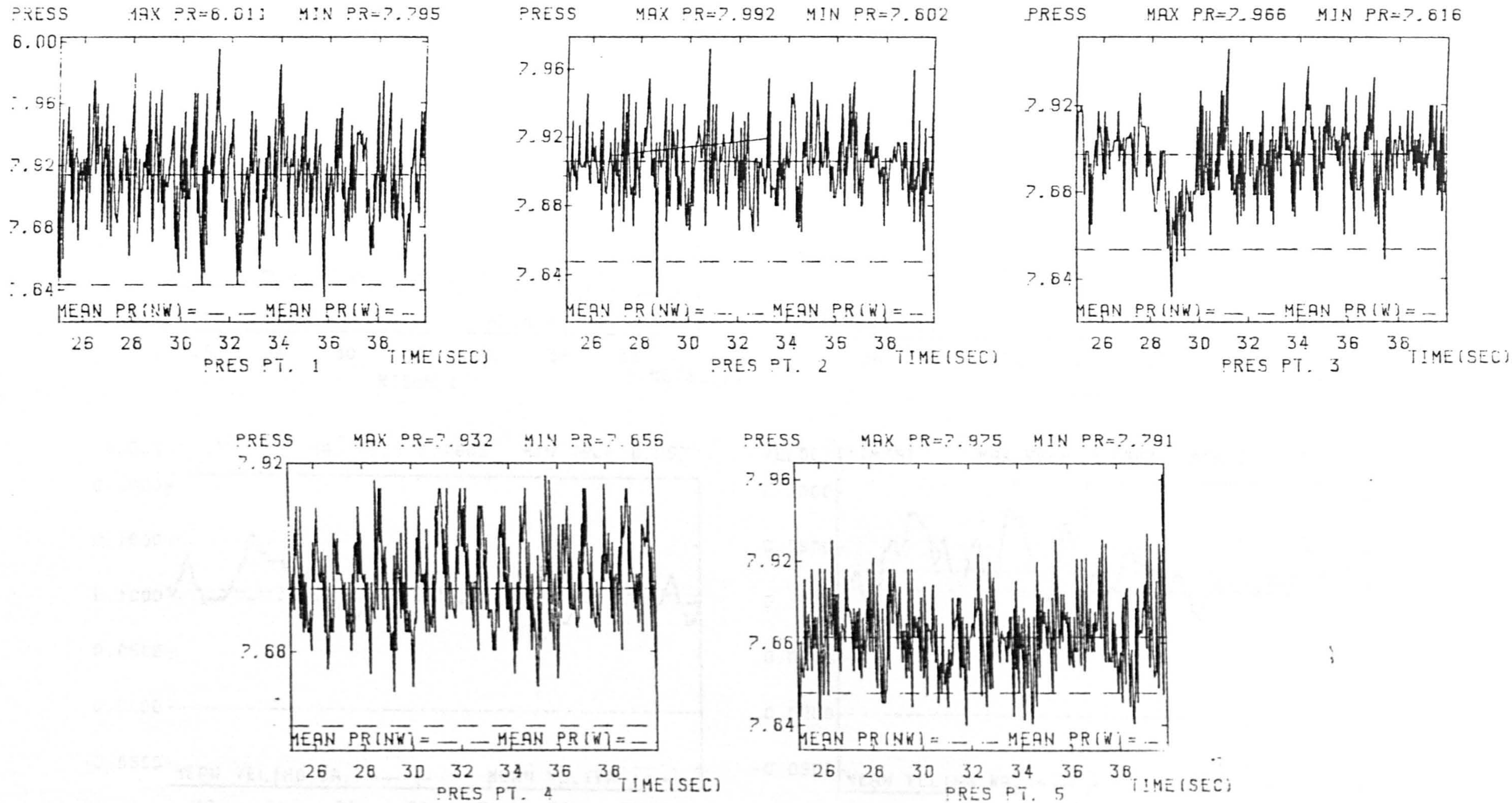

WAVEHEIGHT=0.0550 M WAVEPERIOD=0.7690 S FLOW RATE=0.53100 L/S

13 JUN 88 15:46:21

FIGURE E50

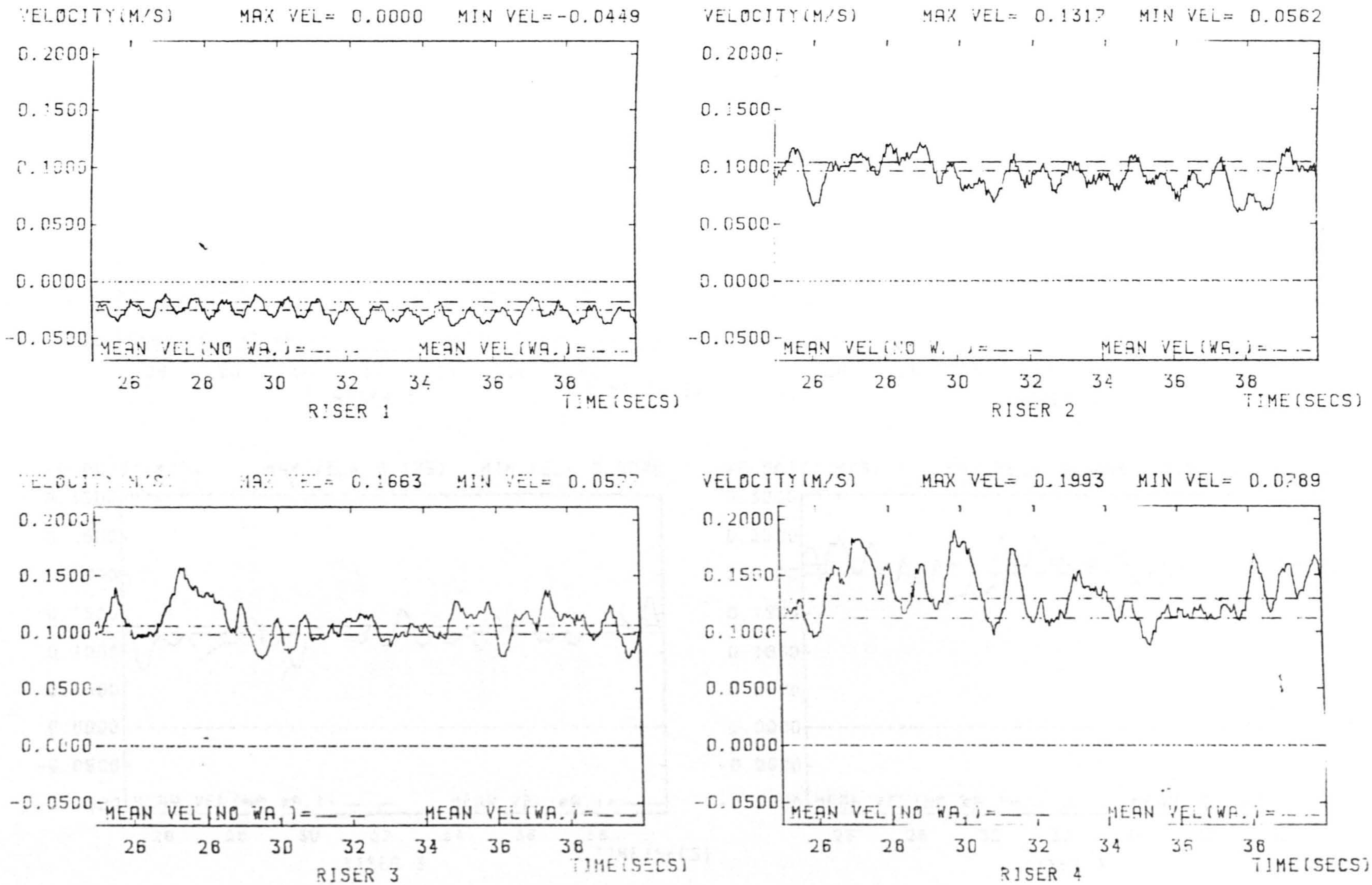

WAVEHEIGHT= 0.0550M WAVEPERIOD=0.7690 S FLOW RATE=0.60260 L/S

DIFFUSER CAPS FITTED

FIGURE E51

15 JUN 88 12:44:21

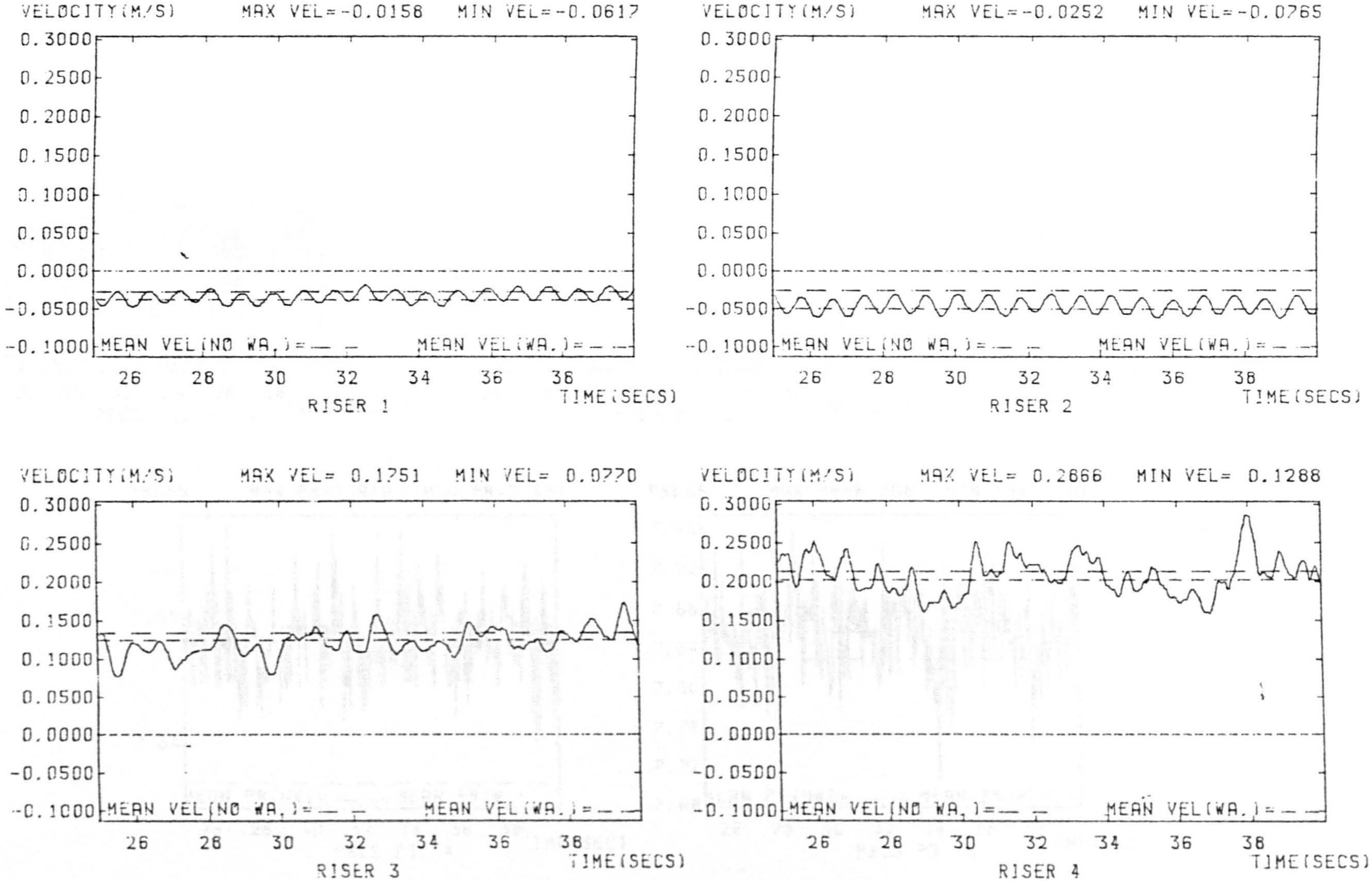

WAVEHEIGHT= 0.0550M WAVEPERIOD=0.7690 S FLOW RATE=0.60260 L/S

NO DIFFUSER CAPS

20 JUN 88 11:22:25

FIGURE E52

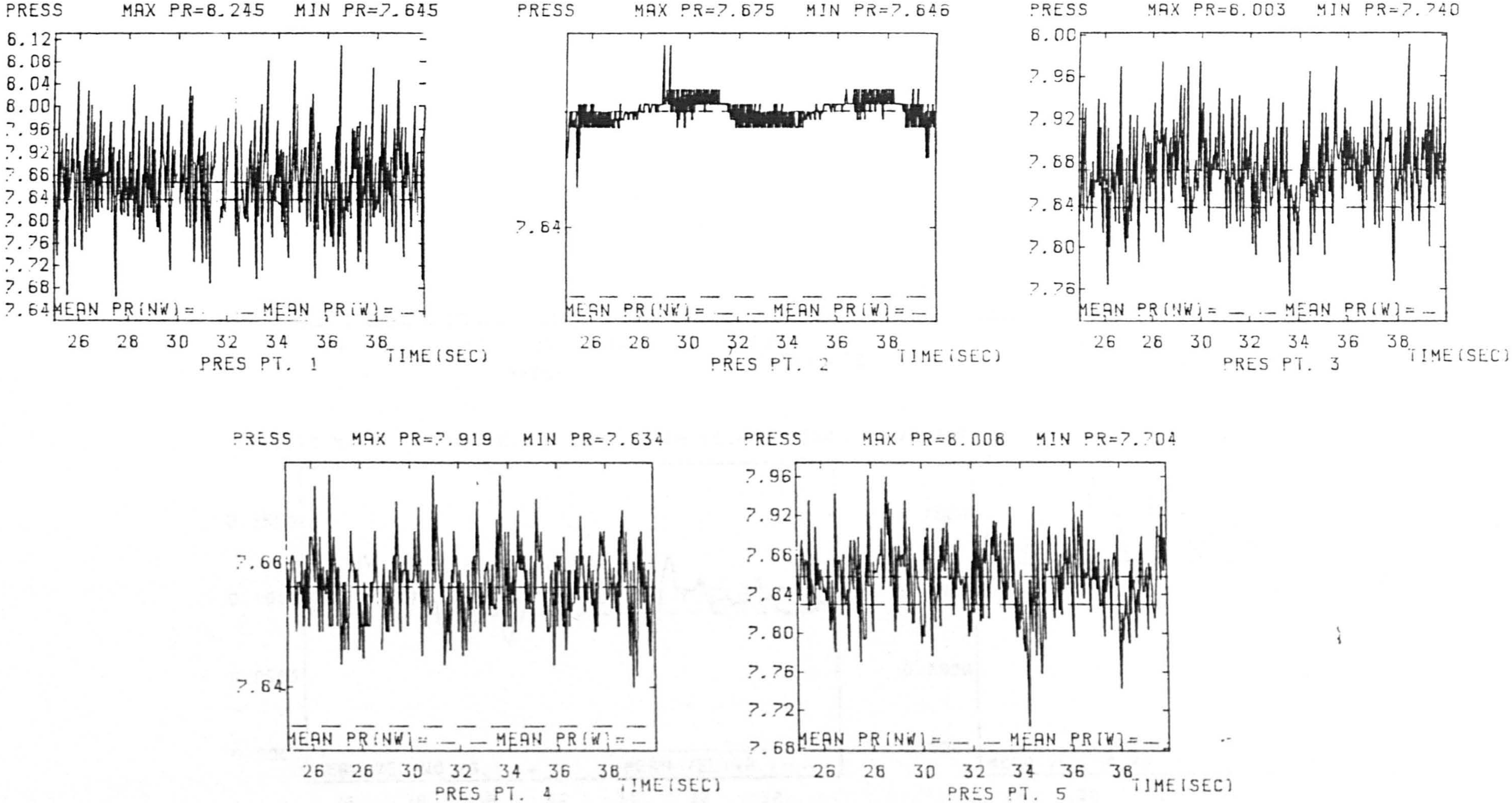

WAVEHEIGHT=0.0550 M WAVEPERIOD=0.7690 S FLOW RATE=0.60260 L/S

15 JUN 88 13:13:26

FIGURE E53

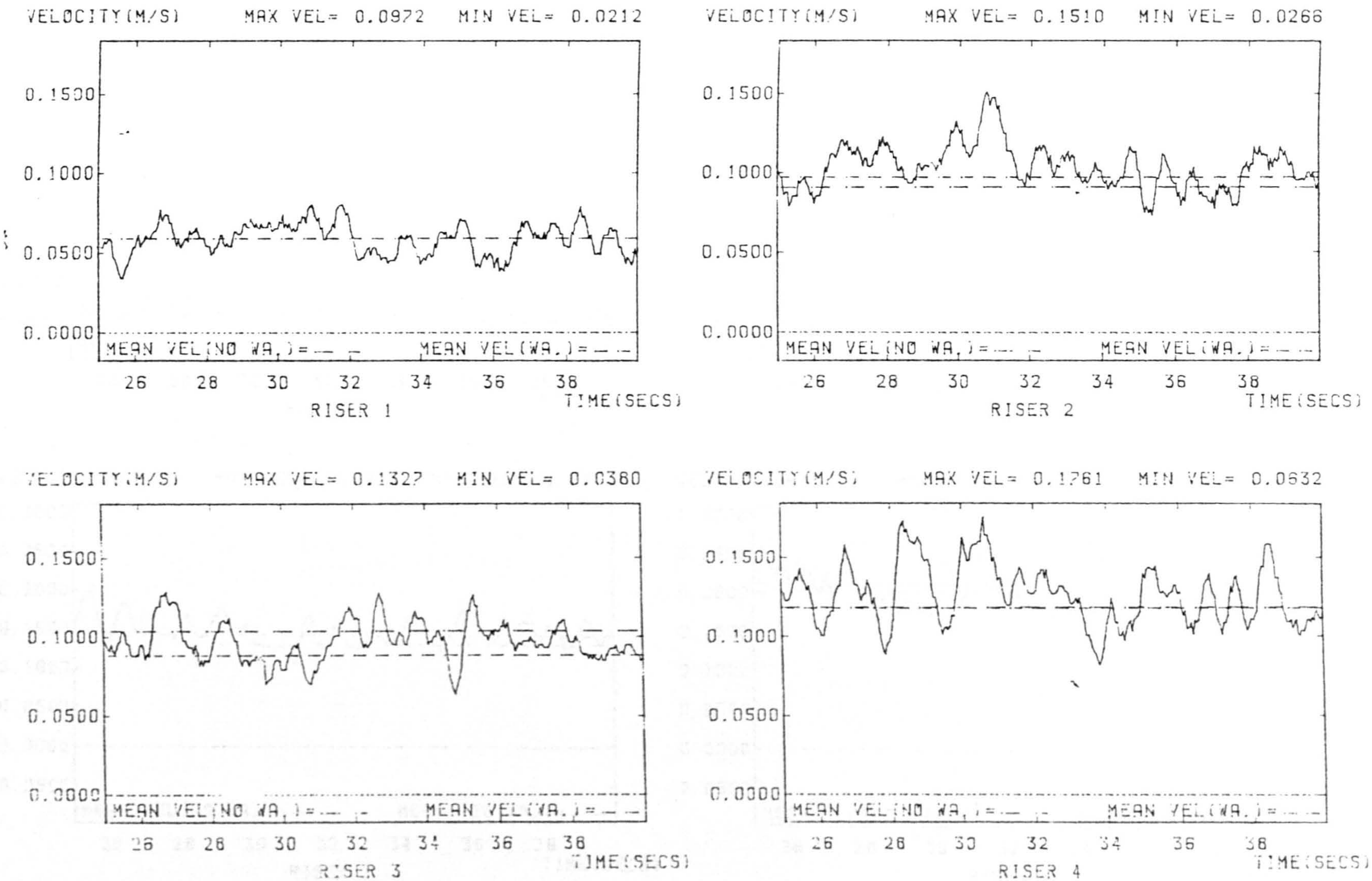

WAVEHEIGHT= 0.0550M WAVEPERIOD= 0.7690 S FLOW RATE=0.63100 L/S

DIFFUSER CAPS FITTED

FIGURE E54

15 JUN 88 13:57:12

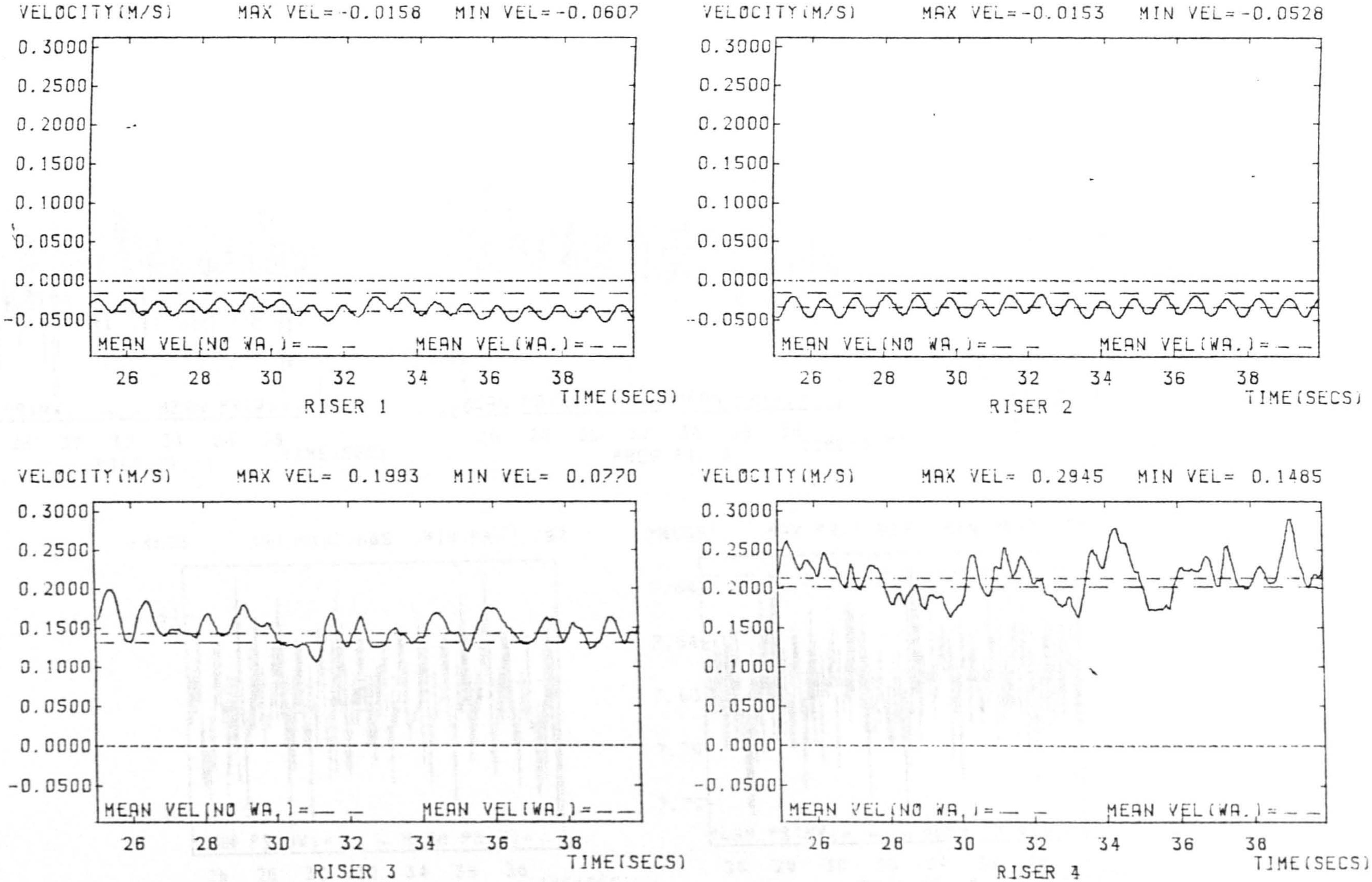

WAVEHEIGHT= 0.0550M WAVEPERIOD=0.7690 S FLOW RATE=0.63100 L/S

NO DIFFUSER CAPS

0 JUN 88 12:33:53

FIGURE E55

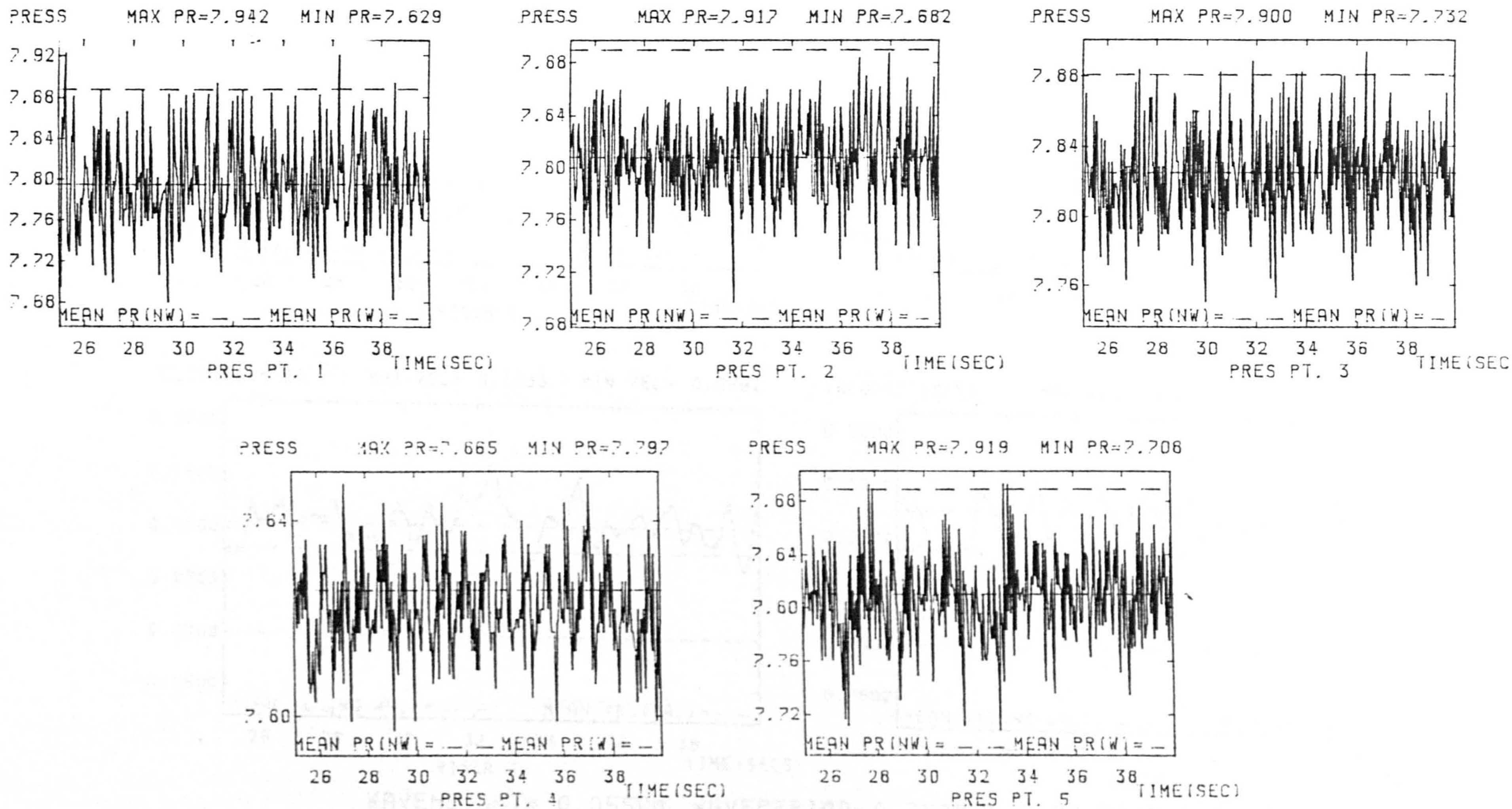

WAVEHEIGHT=0.0550 M WAVEPERIOD=0.7690 S FLOW RATE=0.63100 L/S

FIGURE E56

15 JUN 88 14:29:23

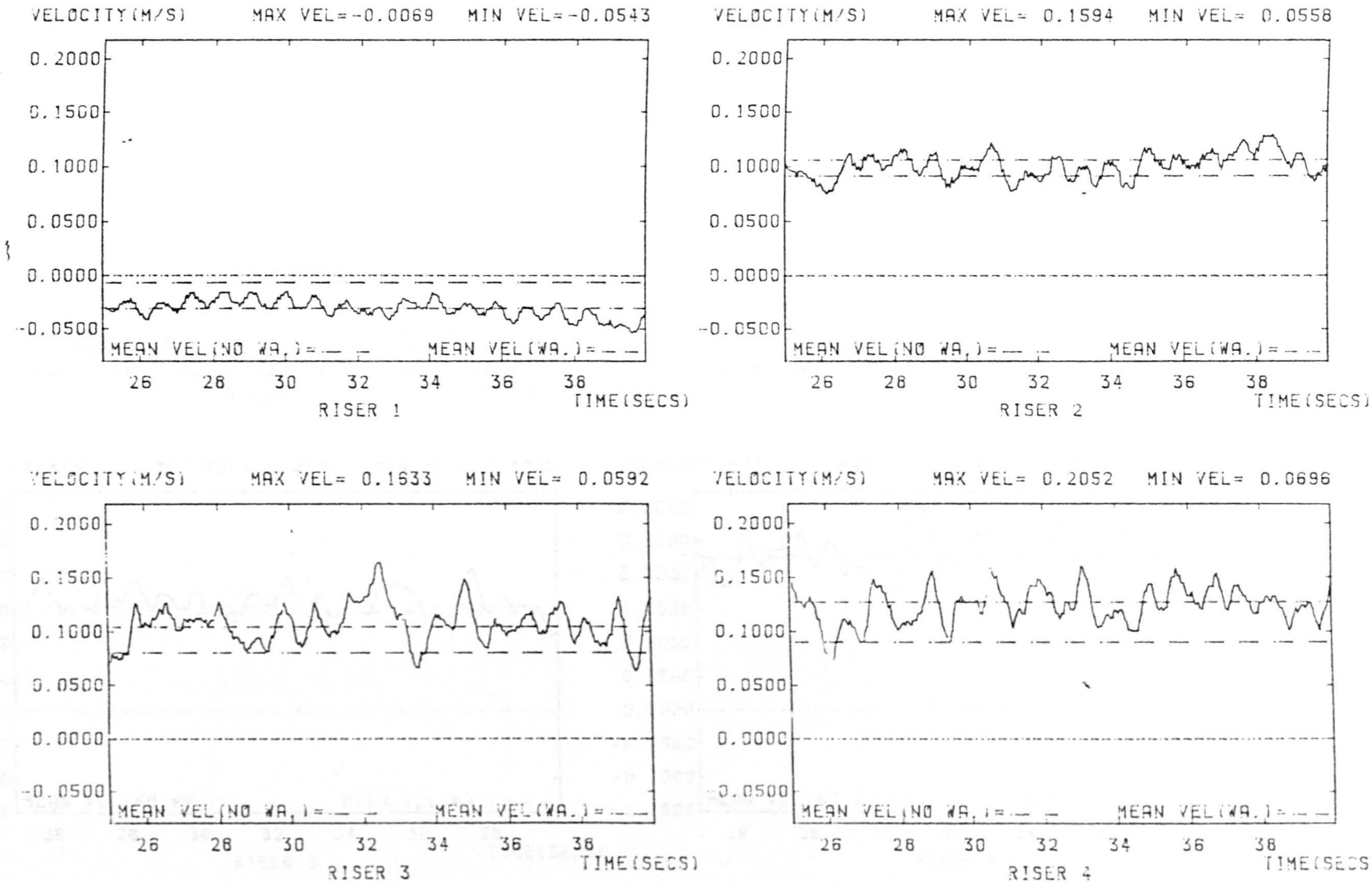

WAVEHEIGHT= 0.0550M WAVEPERIOD=0.7690 S FLOW RATE=0.65470 L/S

DIFFUSER CAPS FITTED

15 JUN 88 14:48:07

FIGURE E57

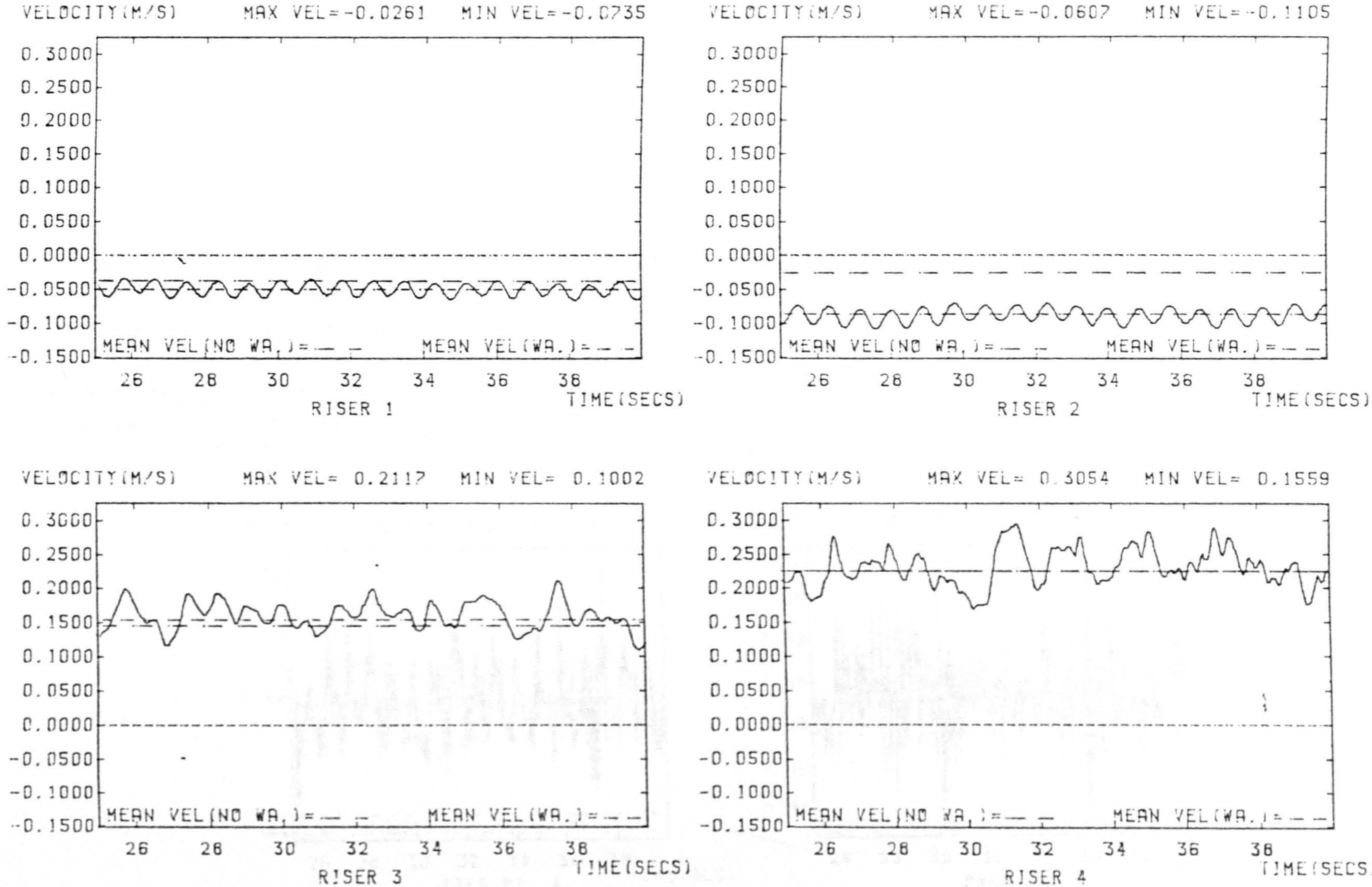

WAVEHEIGHT= 0.0550M WAVEPERIOD=0.7690 S FLOW RATE=0.65470 L/S

NO DIFFUSER CAPS

20 JUN 68 13:00:46

FIGURE E58

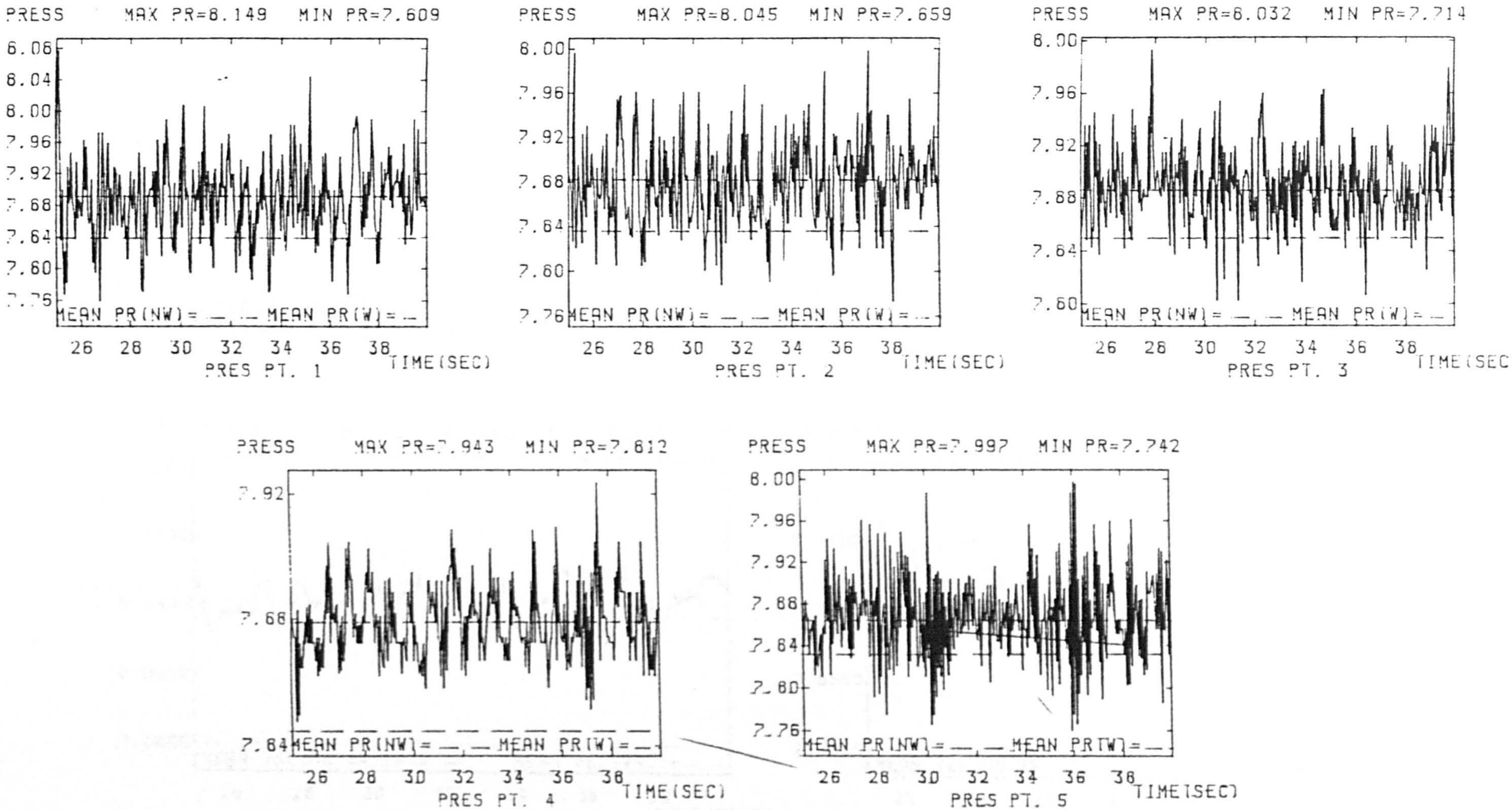

WAVEHEIGHT=0.0550 M WAVEPERIOD=0.7690 S FLOW RATE=0.65470 L/S

15 JUN 88 15:19:47

FIGURE E59

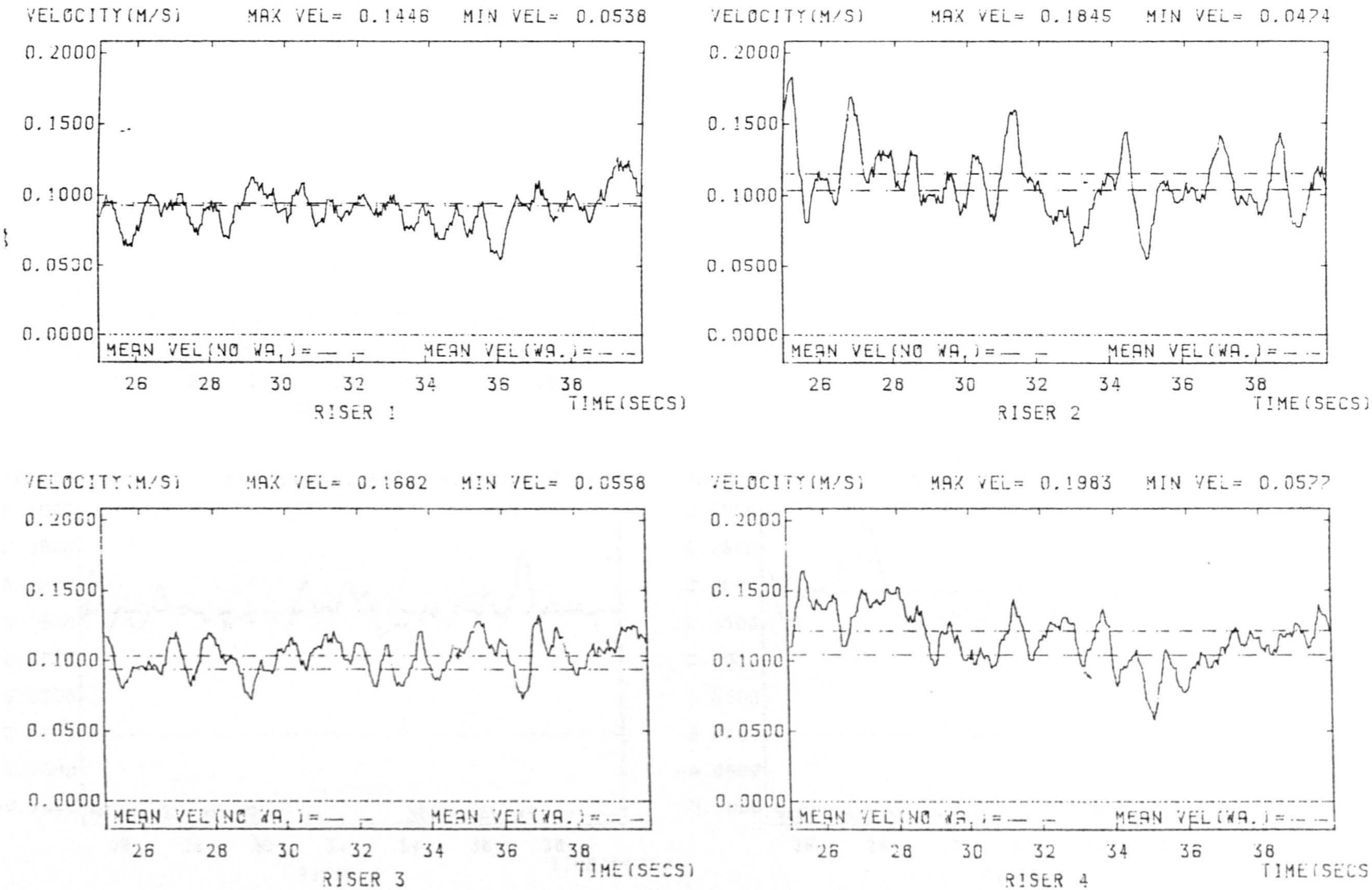

WAVEHEIGHT= 0.0550M WAVEPERIOD=0.7690 S FLOW RATE=0.94410 L/S

DIFFUSER CAPS FITTED

15 JUN 88 16:10:50

FIGURE E60

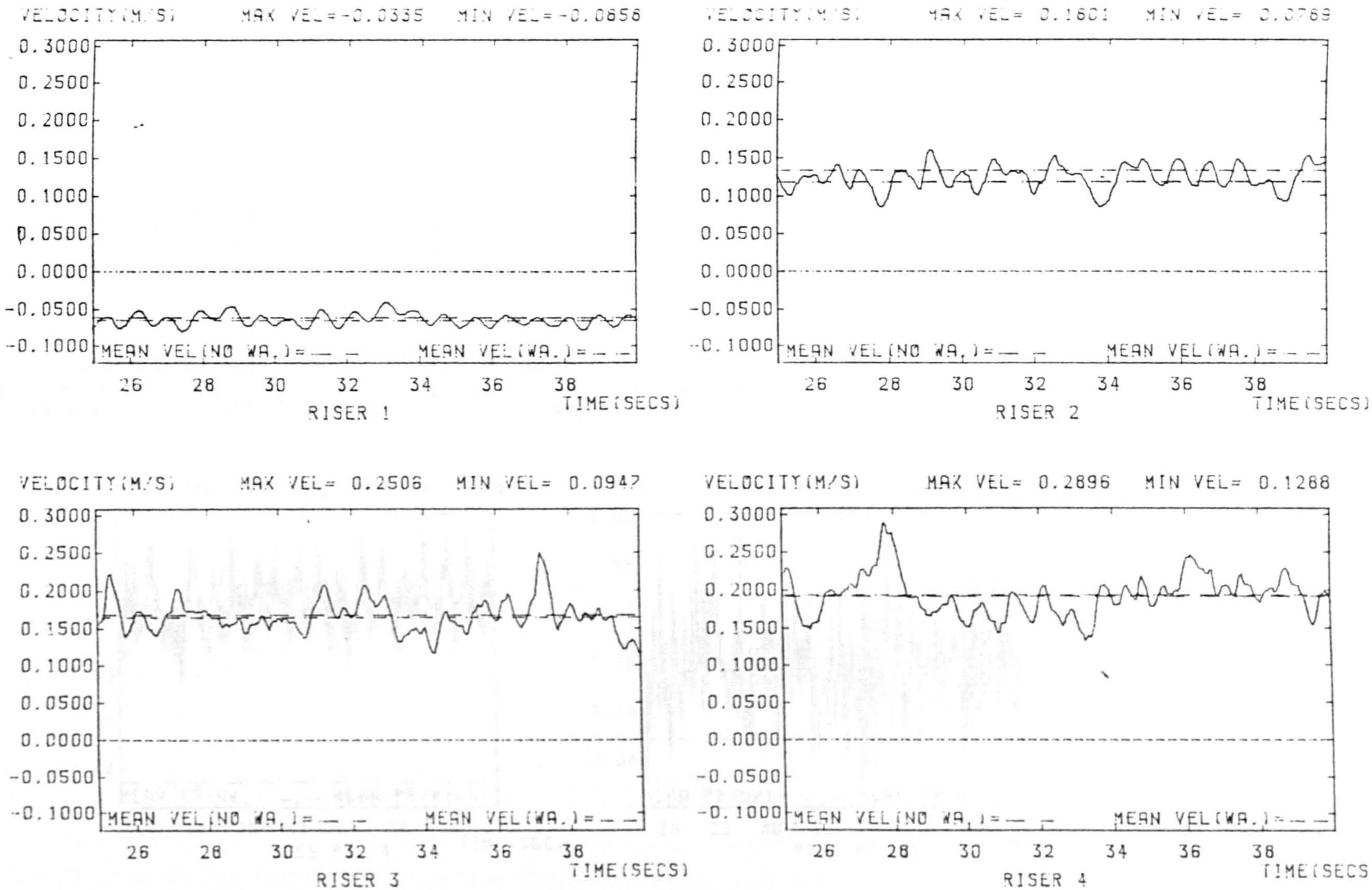

WAVEHEIGHT= 0.0550M WAVEPERIOD=0.7690 S FLOW RATE=0.94410 L/S

NO DIFFUSER CAPS

20 JUN 88 13:19:29

FIGURE E61

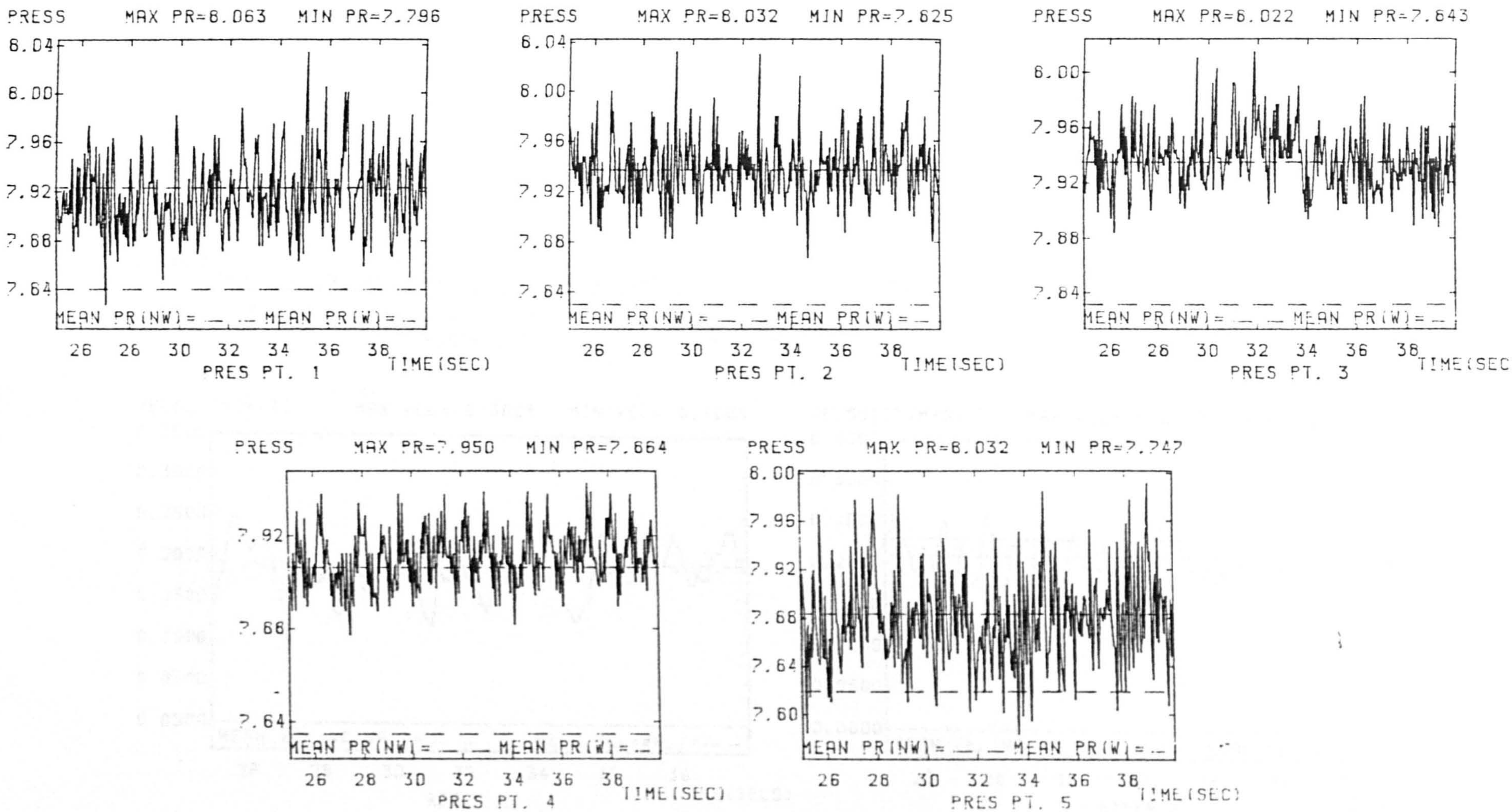

WAVEHEIGHT=0.0550 M WAVEPERIOD=0.7690 S FLOW RATE=0.94410 L/S

15 JUN 88 15:52:30

FIGURE E62

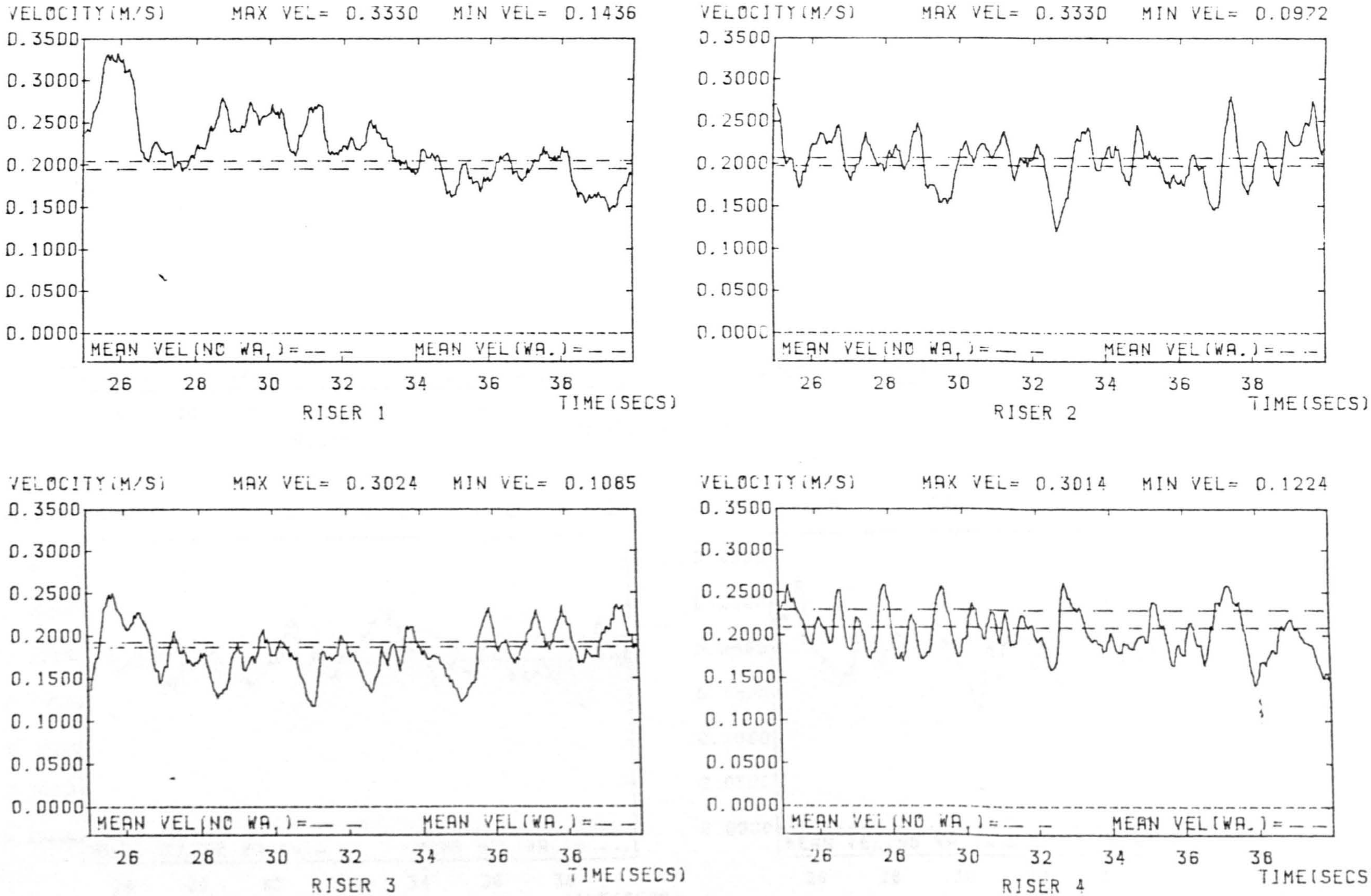

WAVEHEIGHT= 0.0550M WAVEPERIOD=0.7690 S FLOW RATE=2.00000 L/S

DIFFUSER CAPS FITTED

17 JUN 88 9:20:20

FIGURE E63

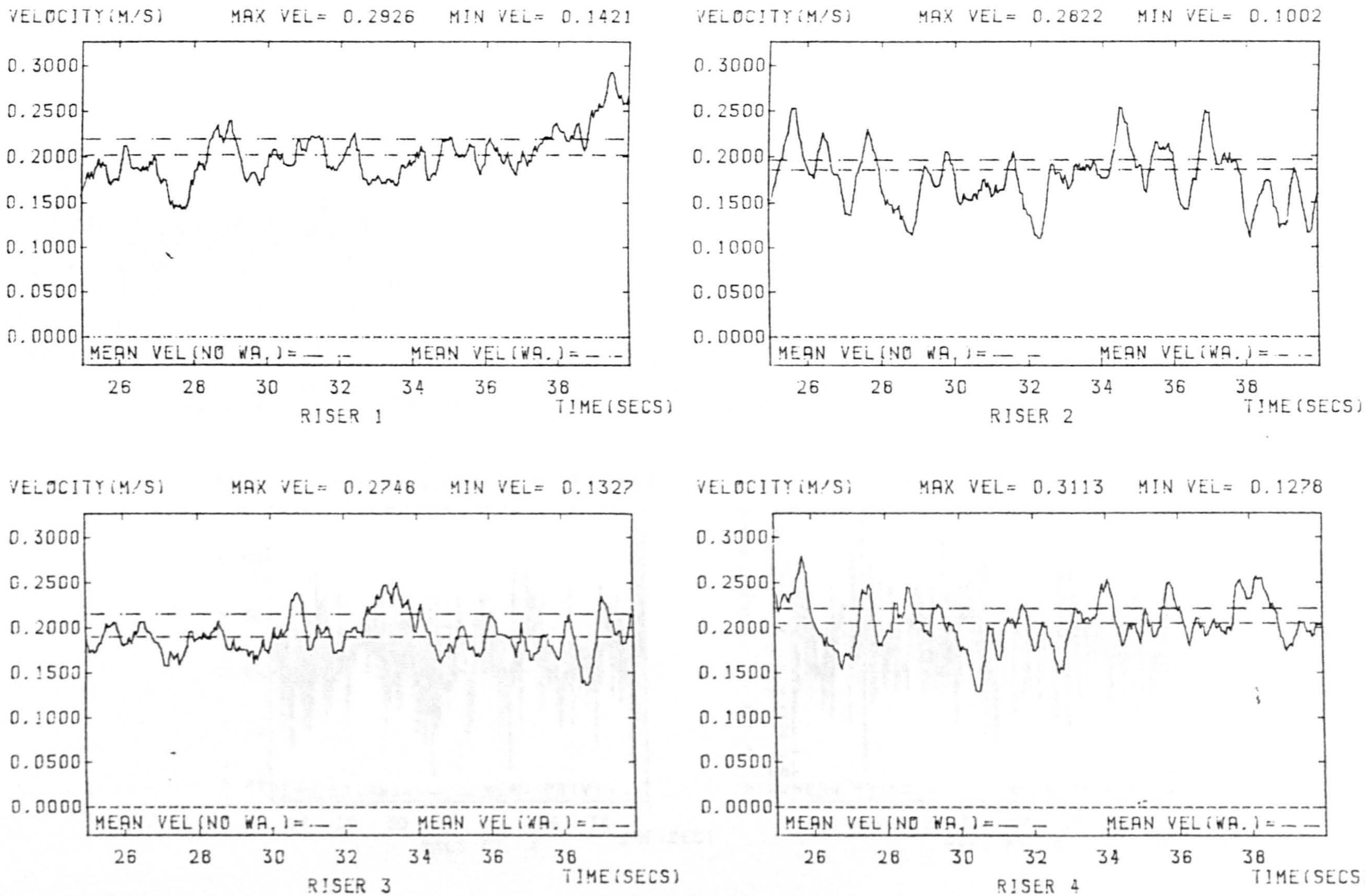

WAVEHEIGHT= 0.0550M WAVEPERIOD= 0.7690 S FLOW RATE=2.00000 L/S

NO DIFFUSER CAPS

20 JUN 88 13:38:41

FIGURE E64

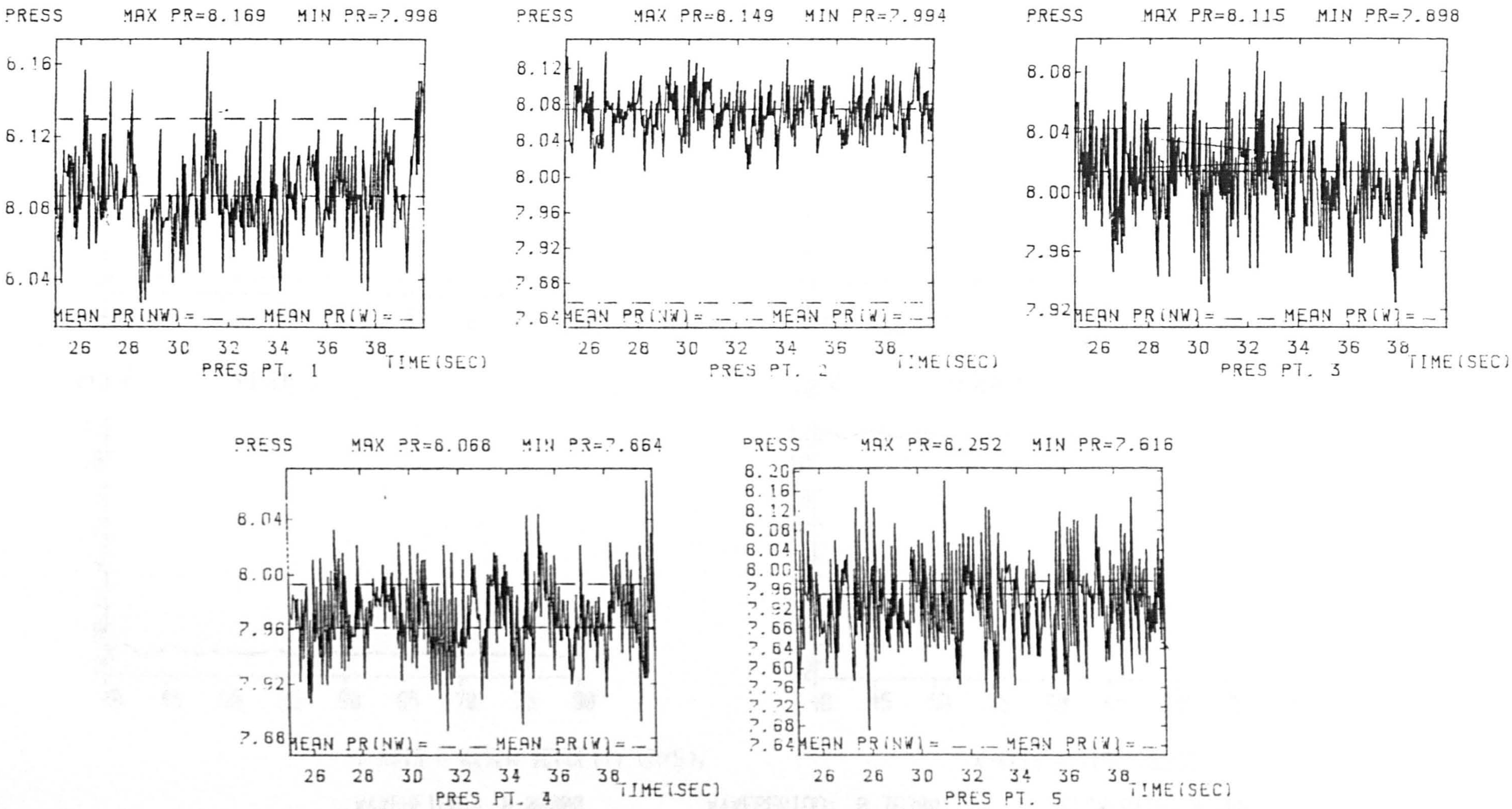

WAVEHEIGHT=0.0550 M WAVEPERIOD=0.7690 S FLOW RATE=2.00000 L/S

17 JUN 88 10:21:02

FIGURE E65

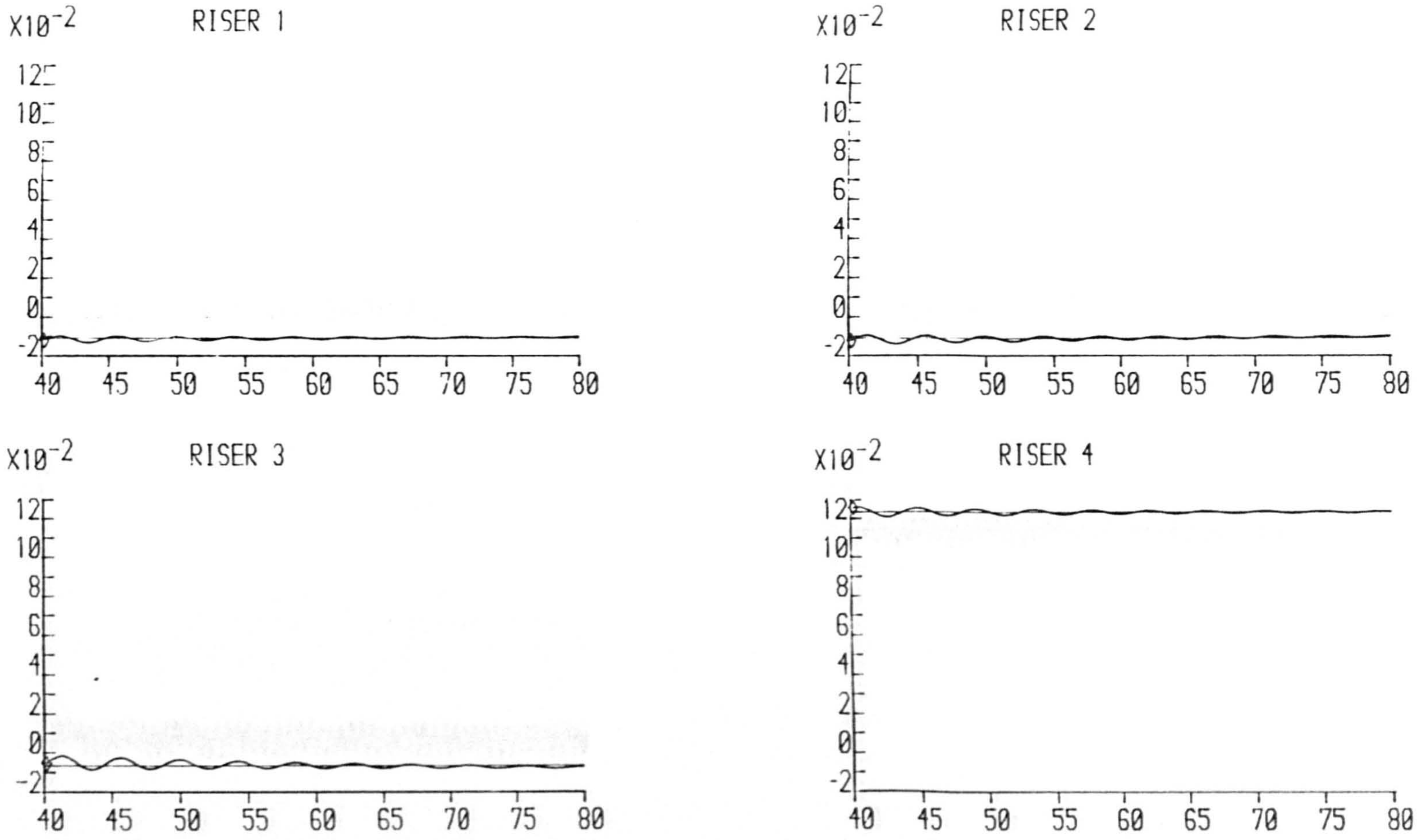

Y-AXIS = RISER VELOCITY (M/S), X-AXIS = TIME (SECS)

WAVEHEIGHT= 0.00000 WAVEPERIOD= 0.76900 FLOW RATE= 0.00019

FIGURE E66

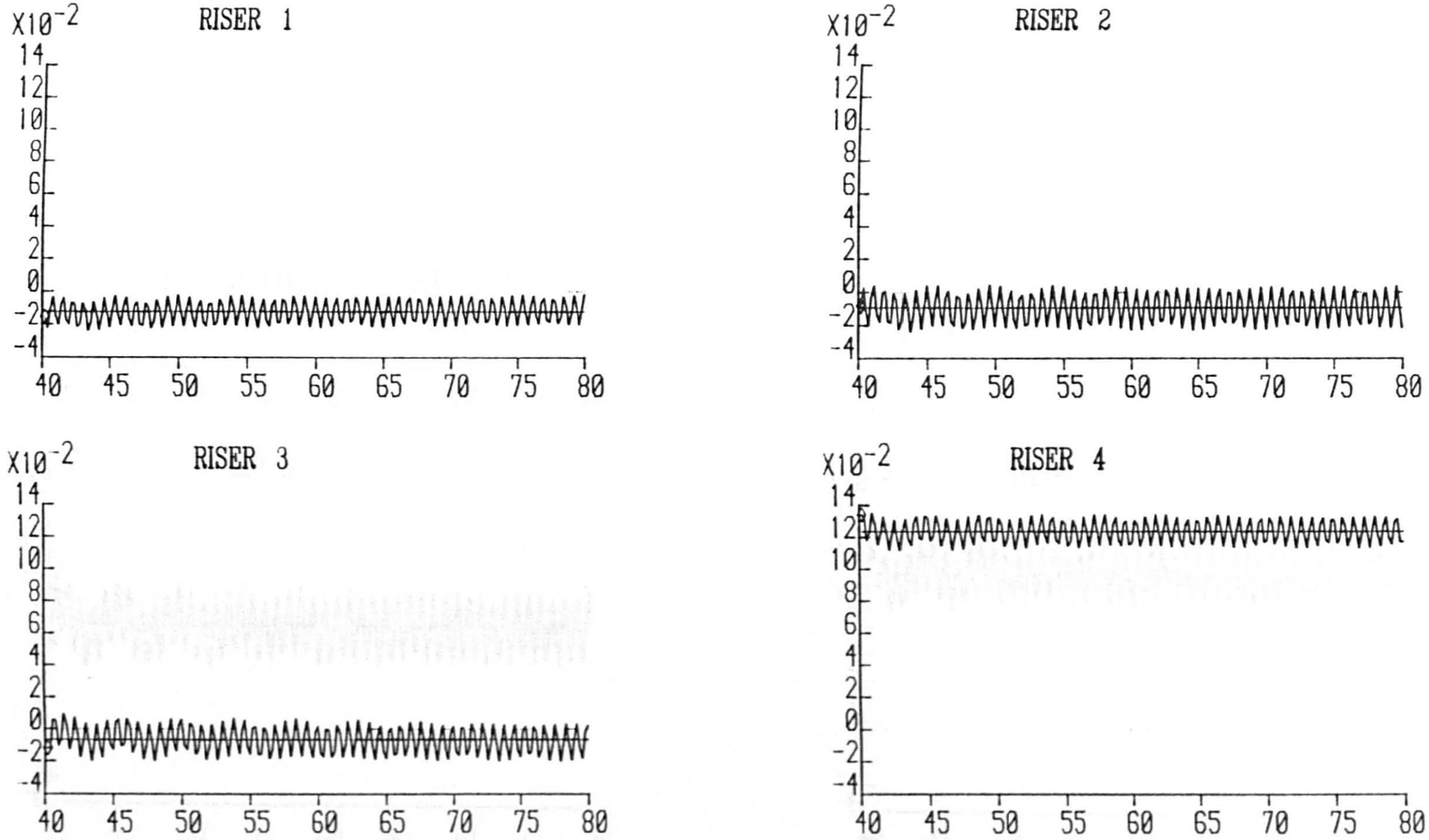

Y-AXIS = RISER VELOCITY (M/S), X-AXIS = TIME (SECS)

WAVEHEIGHT= 0.05500 WAVEPERIOD= 0.76900 FLOW RATE= 0.00019

FIGURE E.67

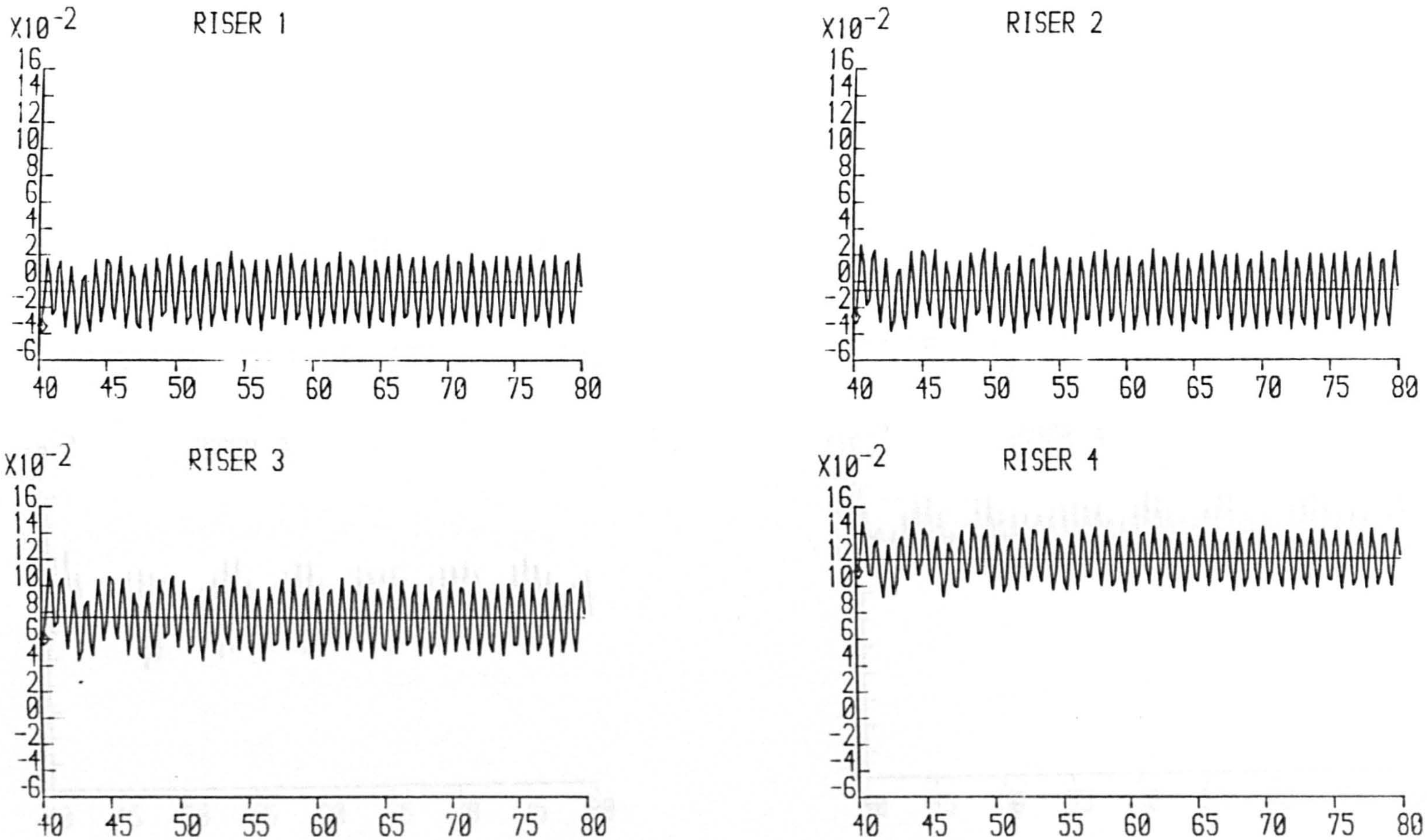

Y-AXIS = RISER VELOCITY (M/S), X-AXIS = TIME (SECS)

WAVEHEIGHT= 0.00000 WAVEPERIOD= 0.76900 FLOW RATE= 0.00035

FIGURE E68

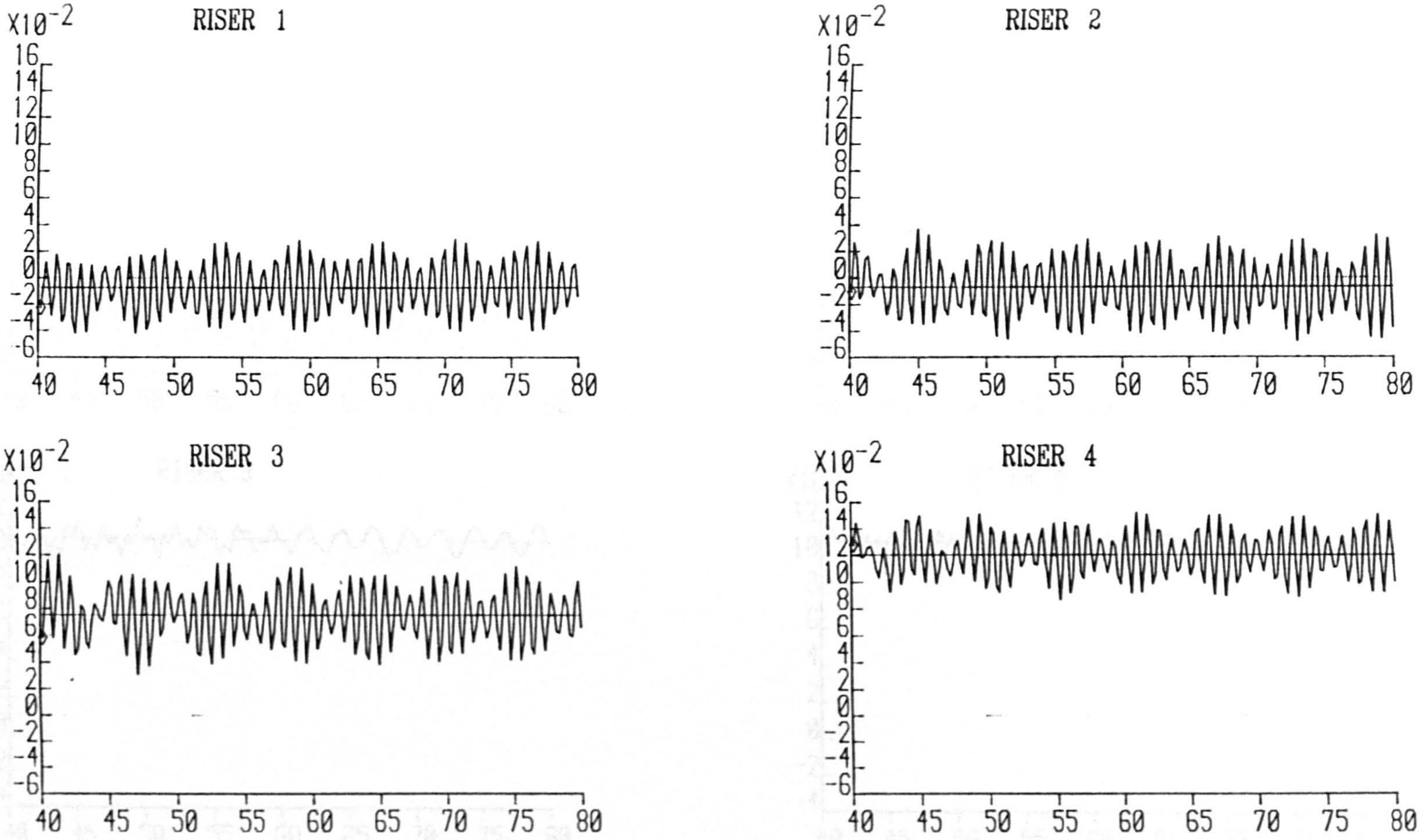

Y-AXIS = RISER VELOCITY (M/S), X-AXIS = TIME (SECS)

WAVEHEIGHT= 0.05500 WAVEPERIOD= 0.76900 FLOW RATE= 0.00035

FIGURE E69

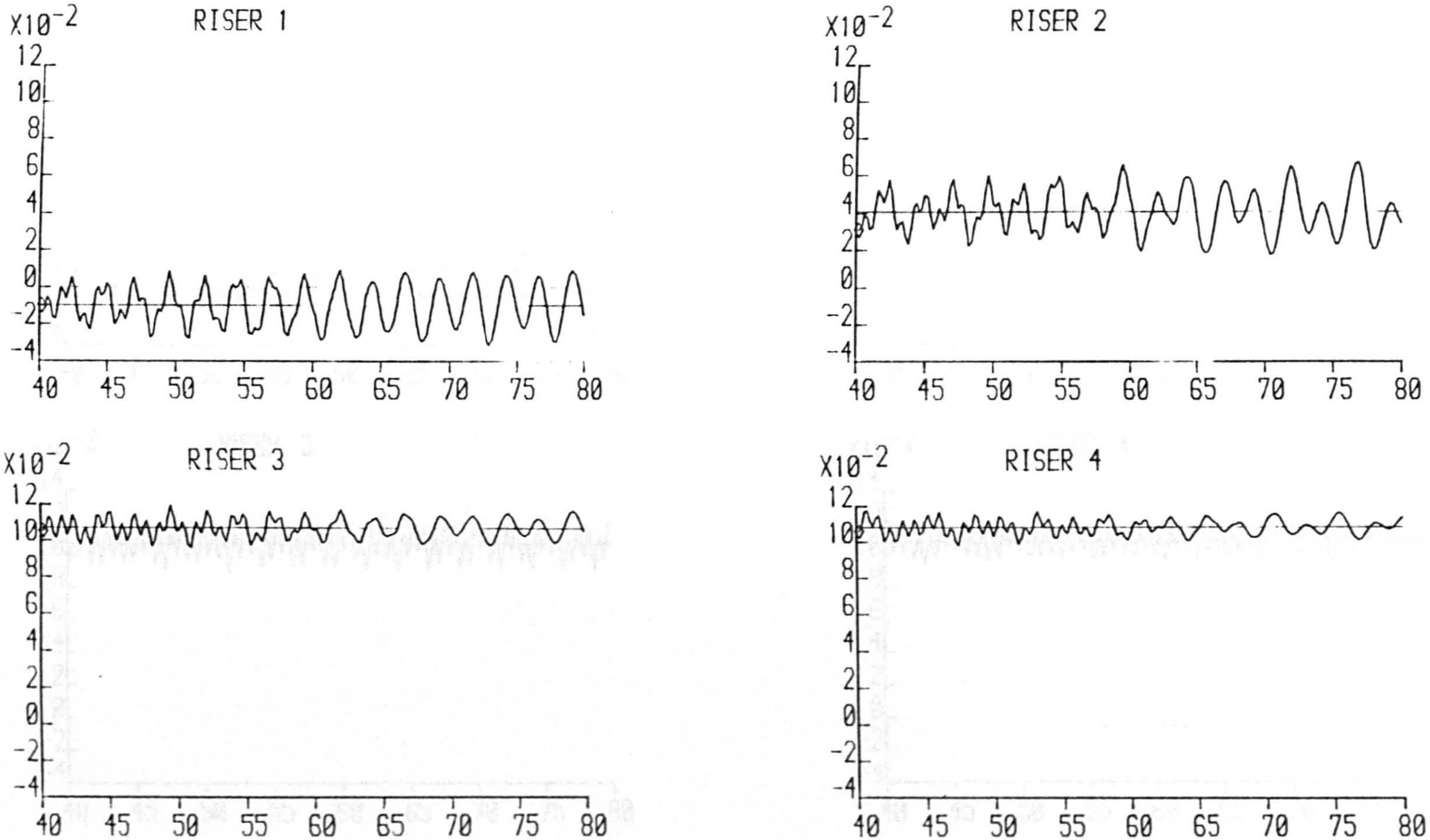

Y-AXIS = RISER VELOCITY (M/S), X-AXIS = TIME (SECS)

WAVEHEIGHT= 0.00000 WAVEPERIOD= 0.76900 FLOW RATE= 0.00048

FIGURE E70

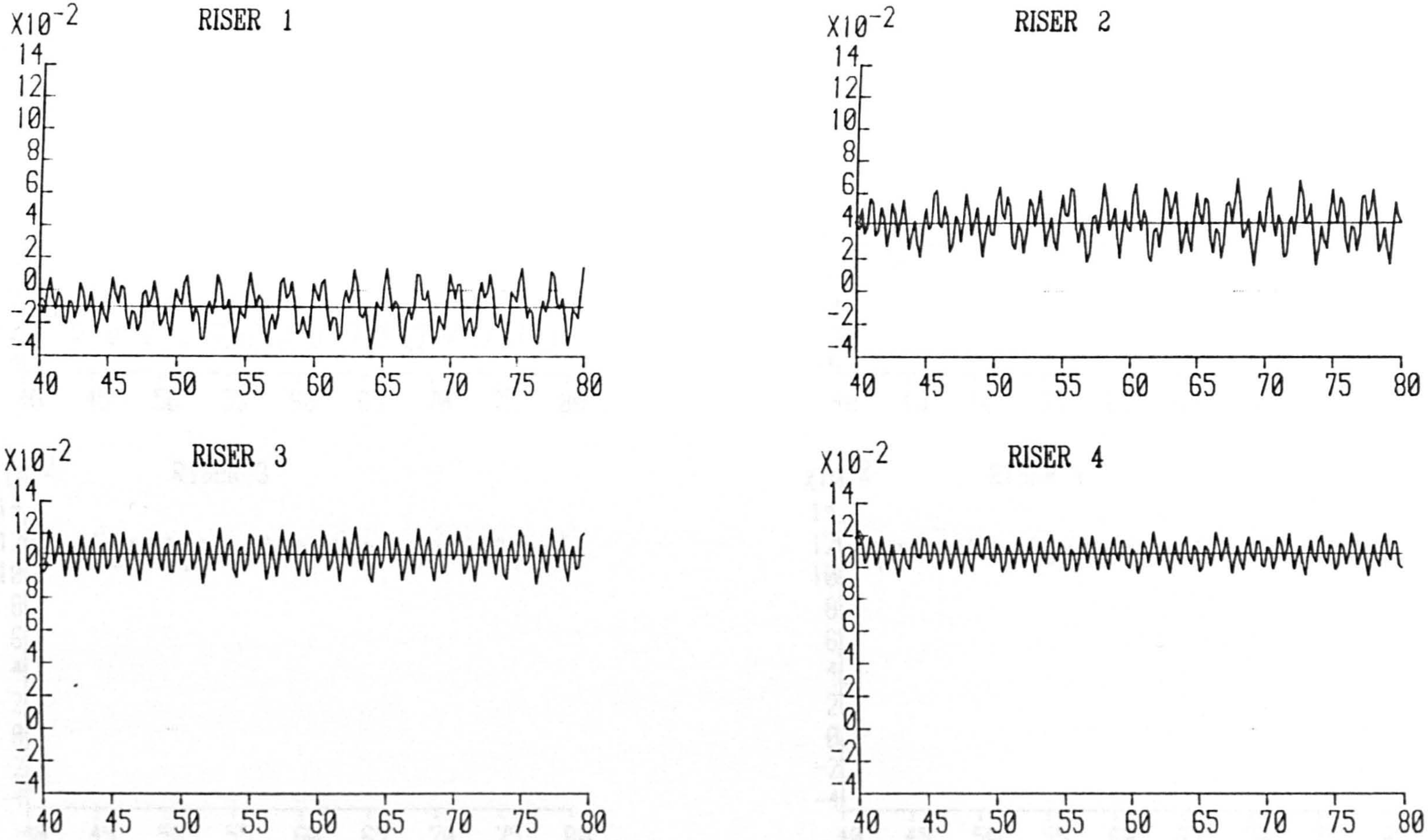

Y-AXIS = RISER VELOCITY (M/S), X-AXIS = TIME (SECS)

WAVEHEIGHT= 0.05500 WAVEPERIOD= 0.76900 FLOW RATE= 0.00048

FIGURE E71

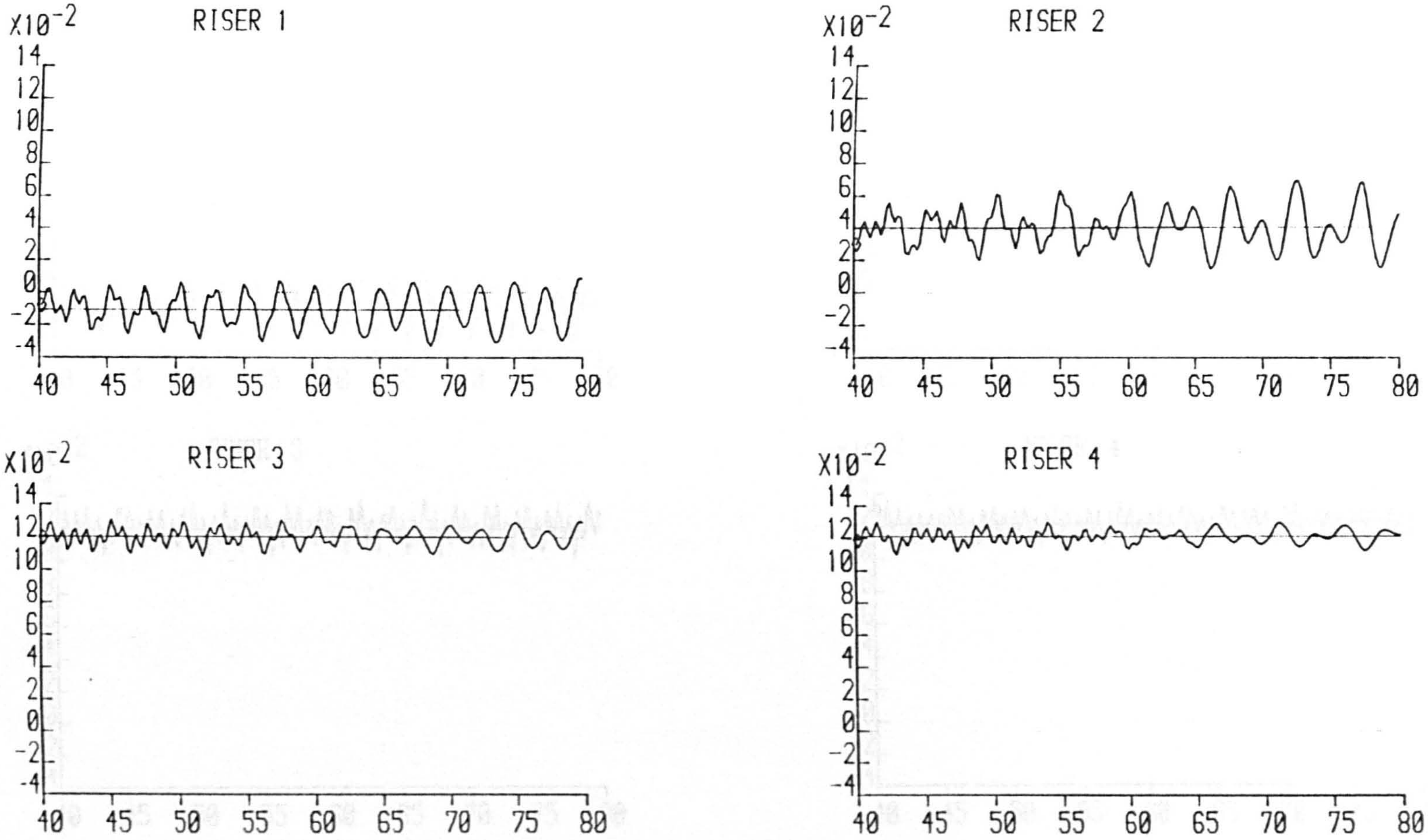

Y-AXIS = RISER VELOCITY (M/S), X-AXIS = TIME (SECS)

WAVEHEIGHT= 0.00000 WAVEPERIOD= 0.76900 FLOW RATE= 0.00053

FIGURE E72

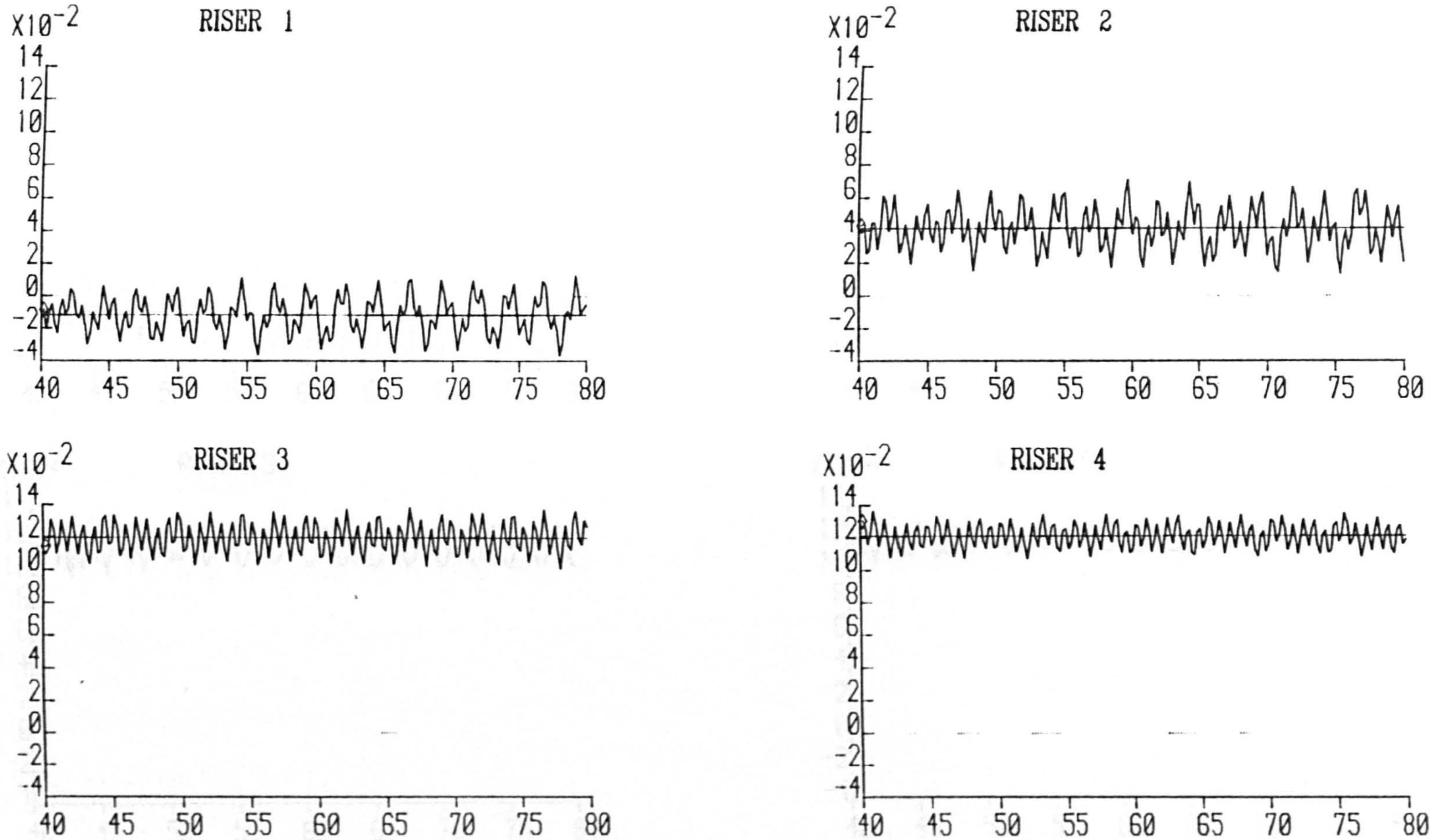

Y-AXIS = RISER VELOCITY (M/S). X-AXIS = TIME (SECS)

WAVEHEIGHT= 0.05500 WAVEPERIOD= 0.76900 FLOW RATE= 0.00053

FIGURE E73

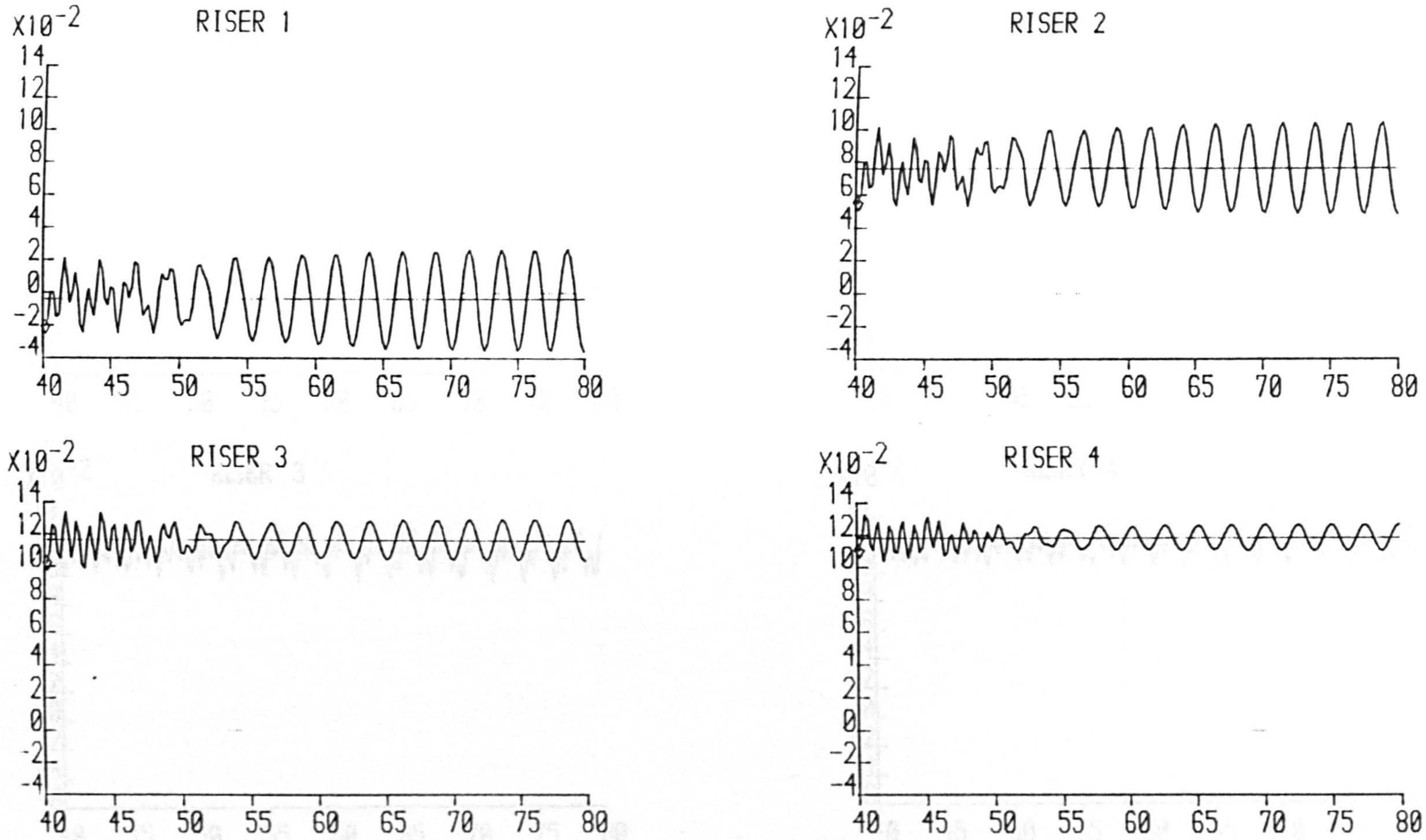

Y-AXIS = RISER VELOCITY (M/S), X-AXIS = TIME (SECS)

WAVEHEIGHT= 0.00000 WAVEPERIOD= 0.76900 FLOW RATE= 0.00060

FIGURE E74

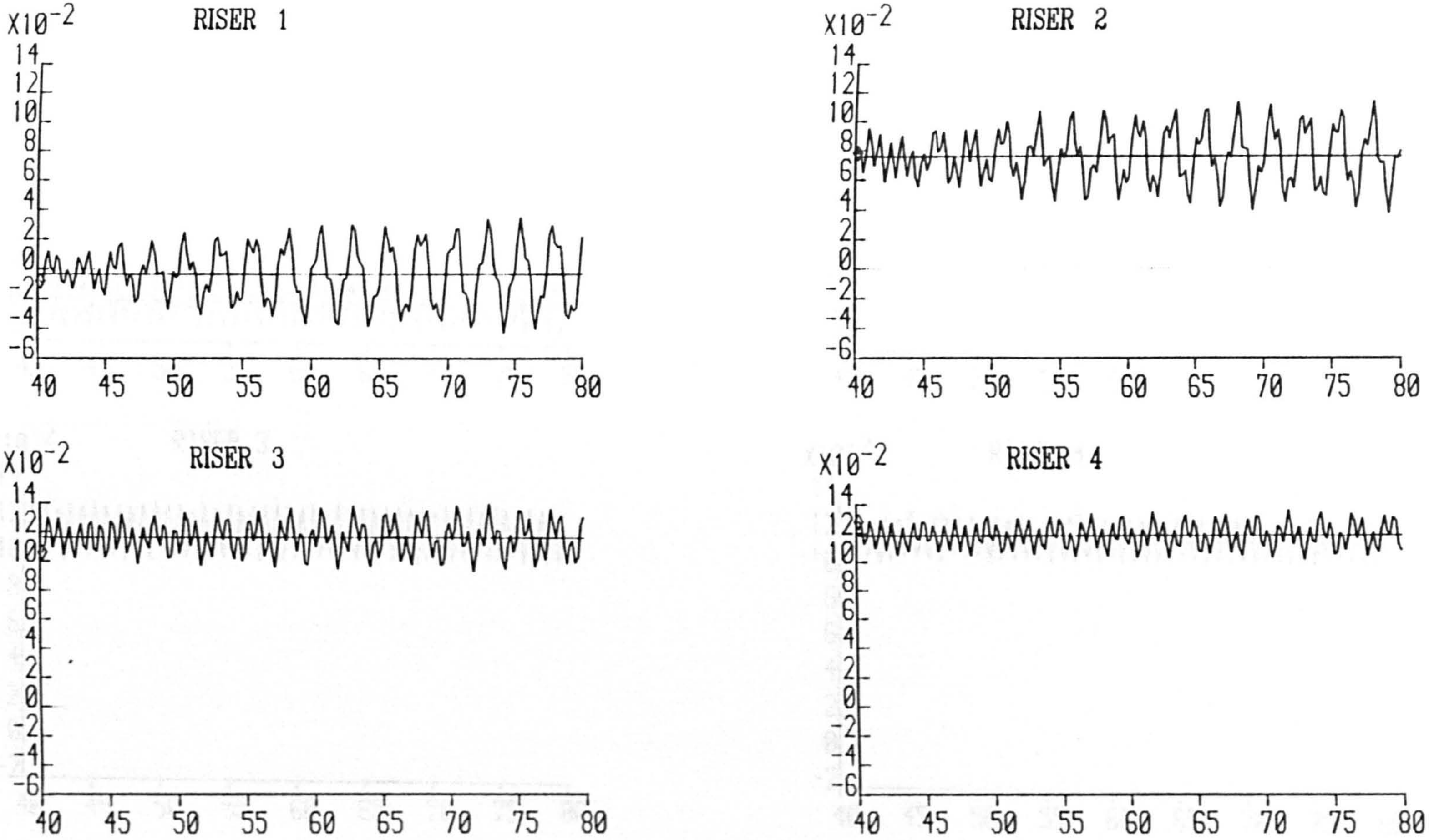

Y-AXIS = RISER VELOCITY (M/S), X-AXIS = TIME (SECS)

WAVEHEIGHT= 0.05500 WAVEPERIOD= 0.76900 FLOW RATE= 0.00060

FIGURE E75

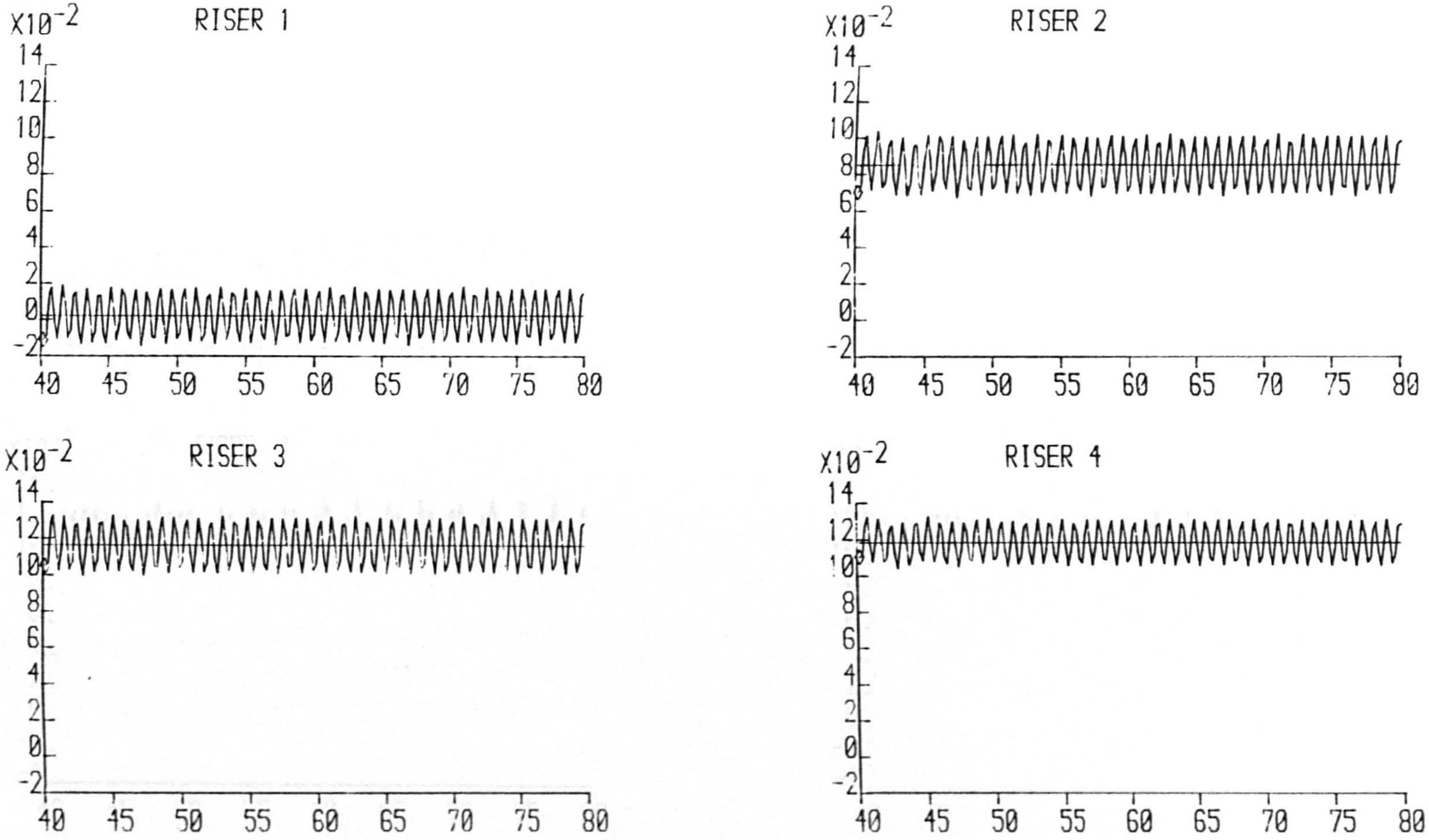

Y-AXIS = RISER VELOCITY (M/S), X-AXIS = TIME (SECS)

WAVEHEIGHT= 0.00000 WAVEPERIOD= 0.76900 FLOW RATE= 0.00063

FIGURE E76

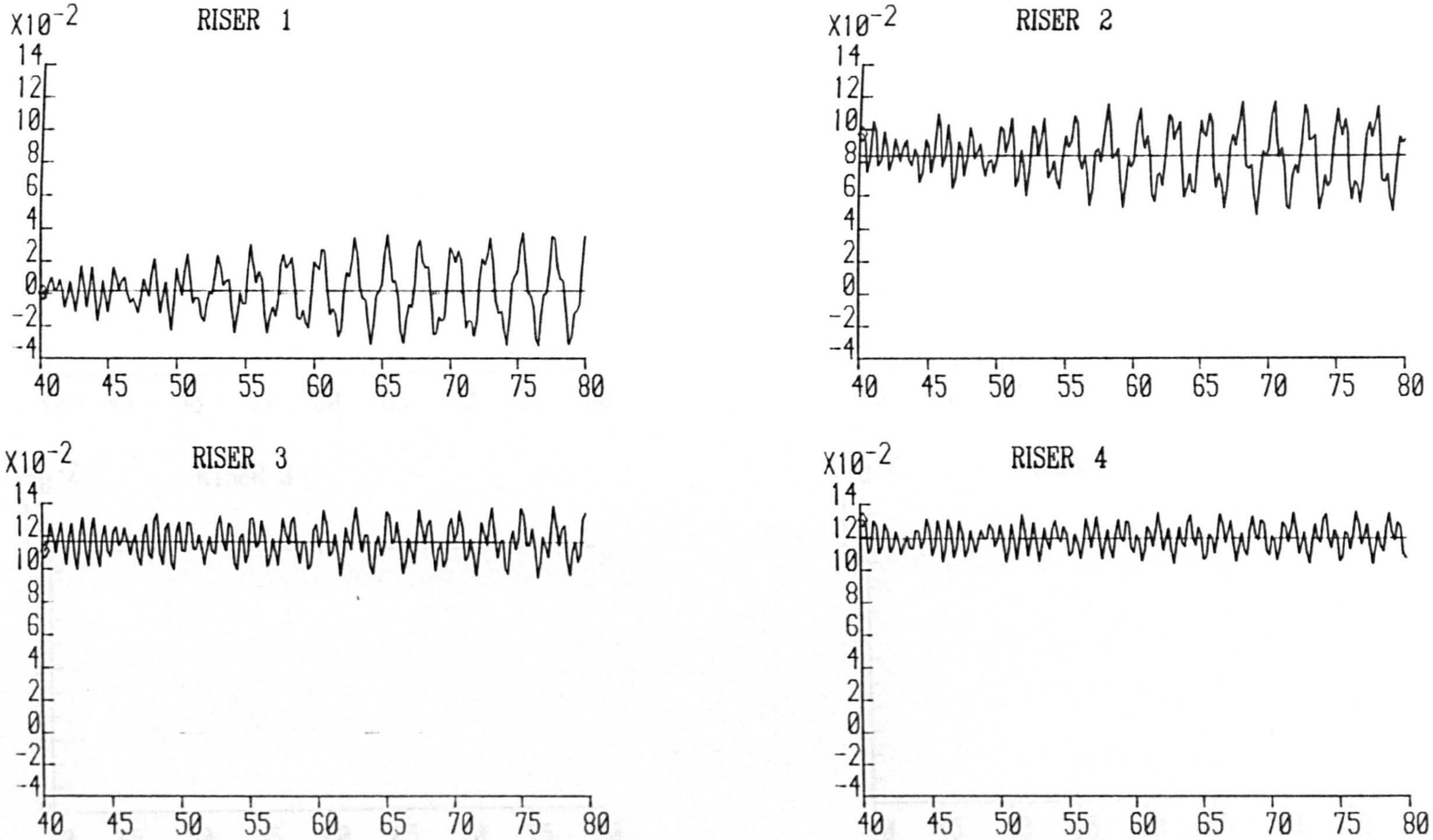

Y-AXIS = RISER VELOCITY (M/S), X-AXIS = TIME (SECS)

WAVEHEIGHT= 0.05500 WAVEPERIOD= 0.76900 FLOW RATE= 0.00063

FIGURE E77

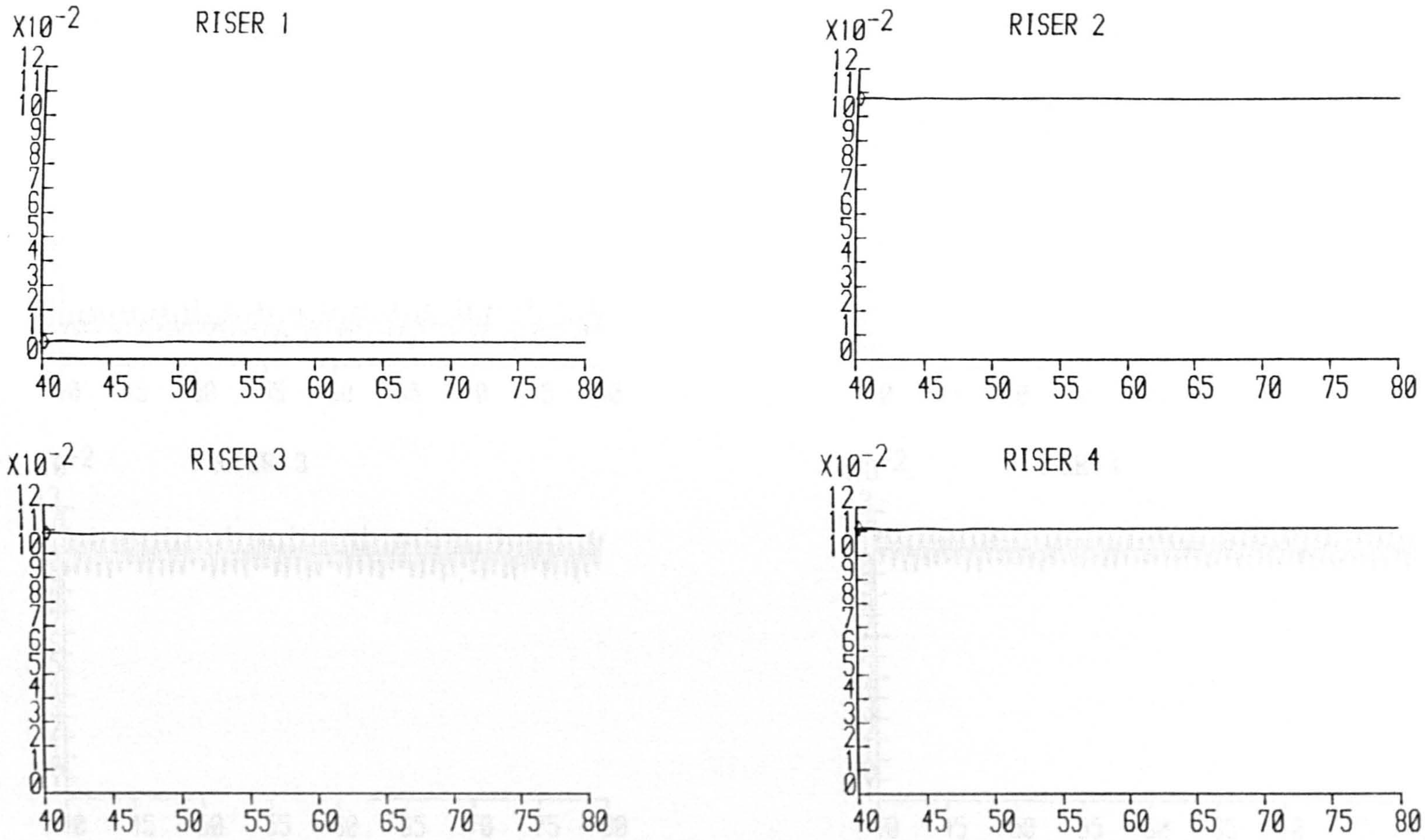

Y-AXIS = RISER VELOCITY (M/S), X-AXIS = TIME (SECS)

WAVEHEIGHT= 0.00000 WAVEPERIOD= 0.76900 FLOW RATE= 0.00065

FIGURE E78

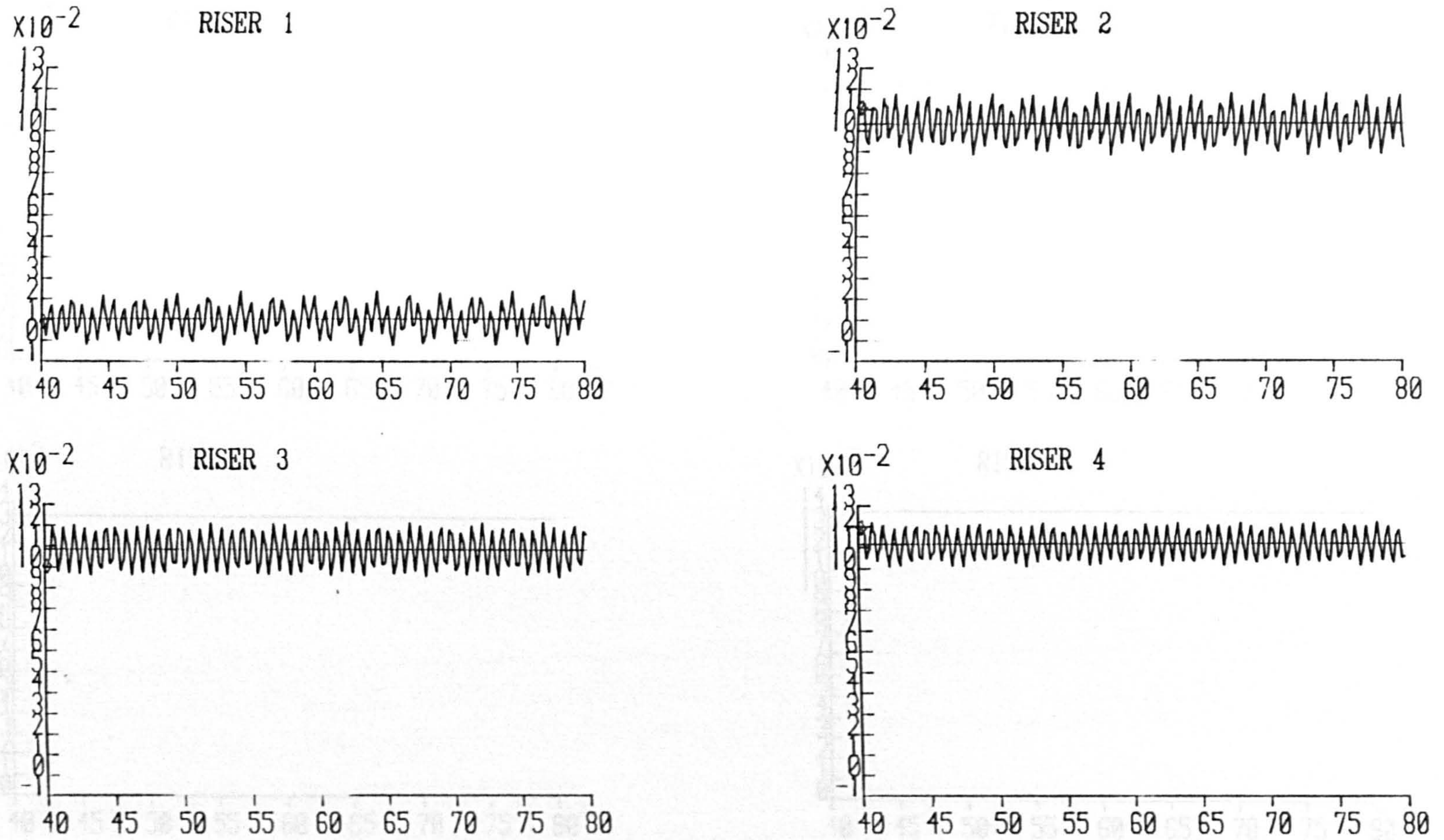

Y-AXIS = RISER VELOCITY (M/S), X-AXIS = TIME (SECS)

WAVEHEIGHT= 0.05500 WAVEPERIOD= 0.76900 FLOW RATE= 0.00065

FIGURE E79

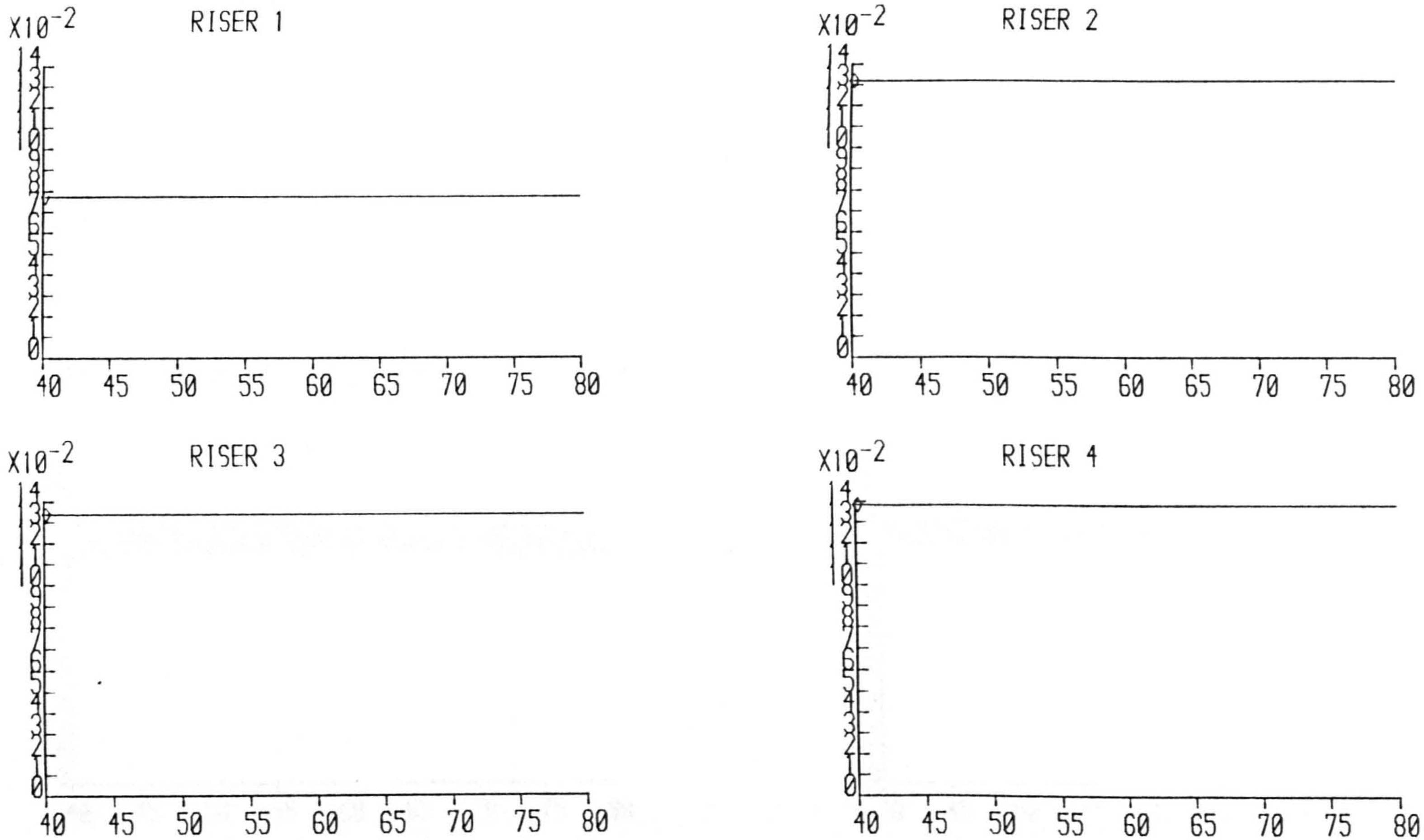

Y-AXIS = RISER VELOCITY (M/S), X-AXIS = TIME (SECS)

WAVEHEIGHT= 0.00000 WAVEPERIOD= 0.76900 FLOW RATE= 0.00094

FIGURE E80

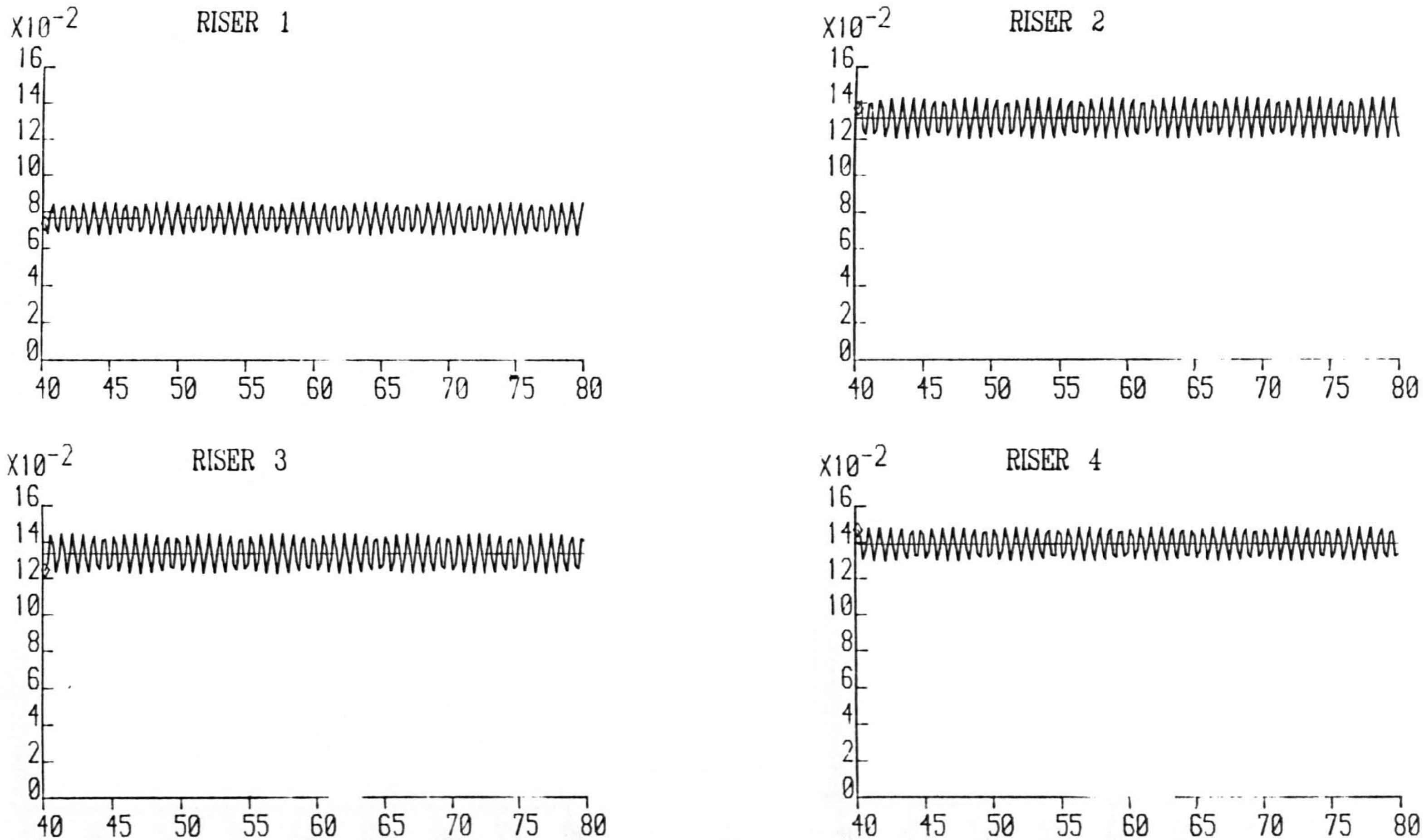

Y-AXIS = RISER VELOCITY (M/S), X-AXIS = TIME (SECS)

WAVEHEIGHT= 0.05500 WAVEPERIOD= 0.76900 FLOW RATE= 0.00094

FIGURE E81

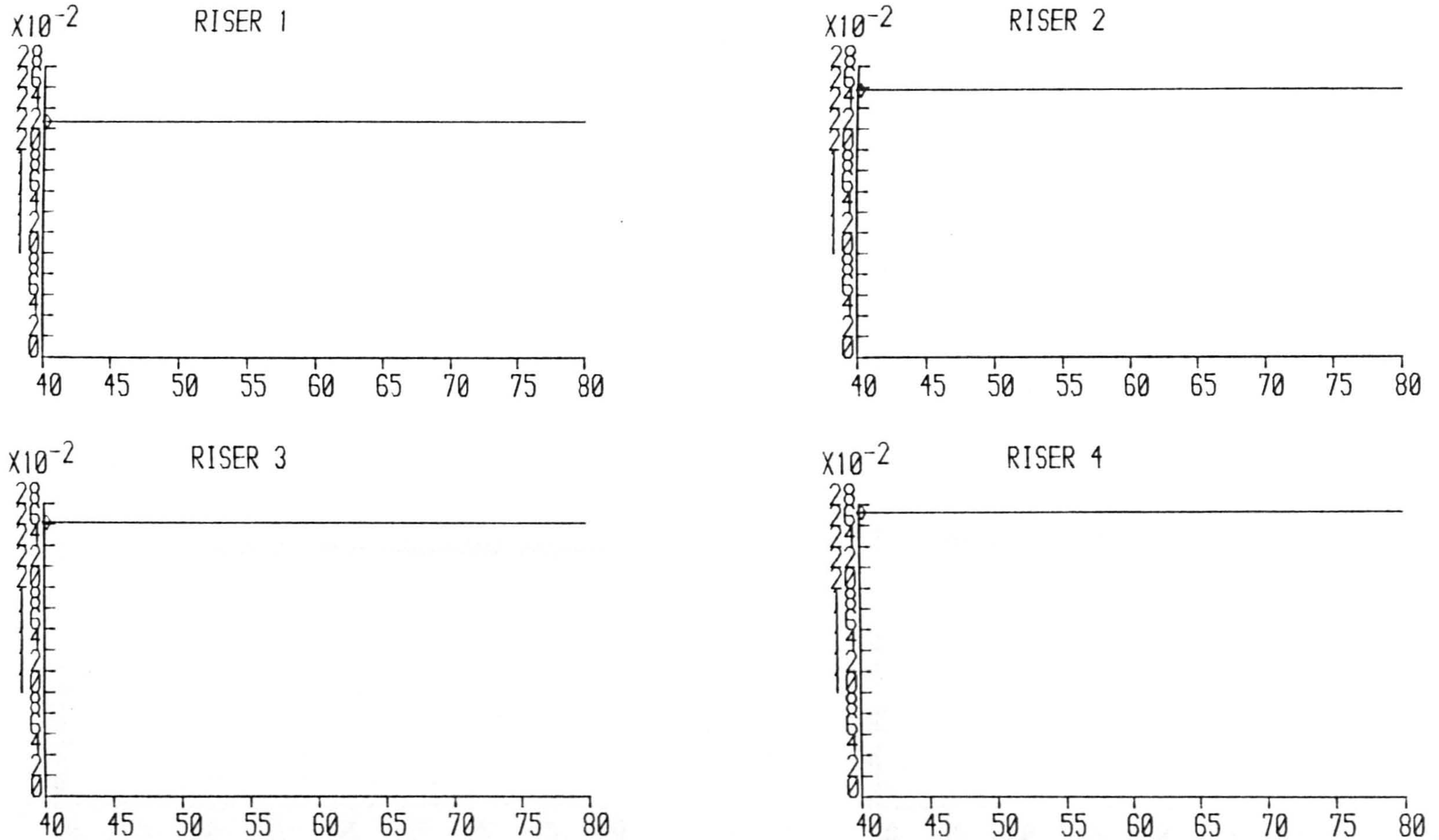

Y-AXIS = RISER VELOCITY (M/S), X-AXIS = TIME (SECS)

WAVEHEIGHT= 0.00000 WAVEPERIOD= 0.76900 FLOW RATE= 0.00200

FIGURE E82

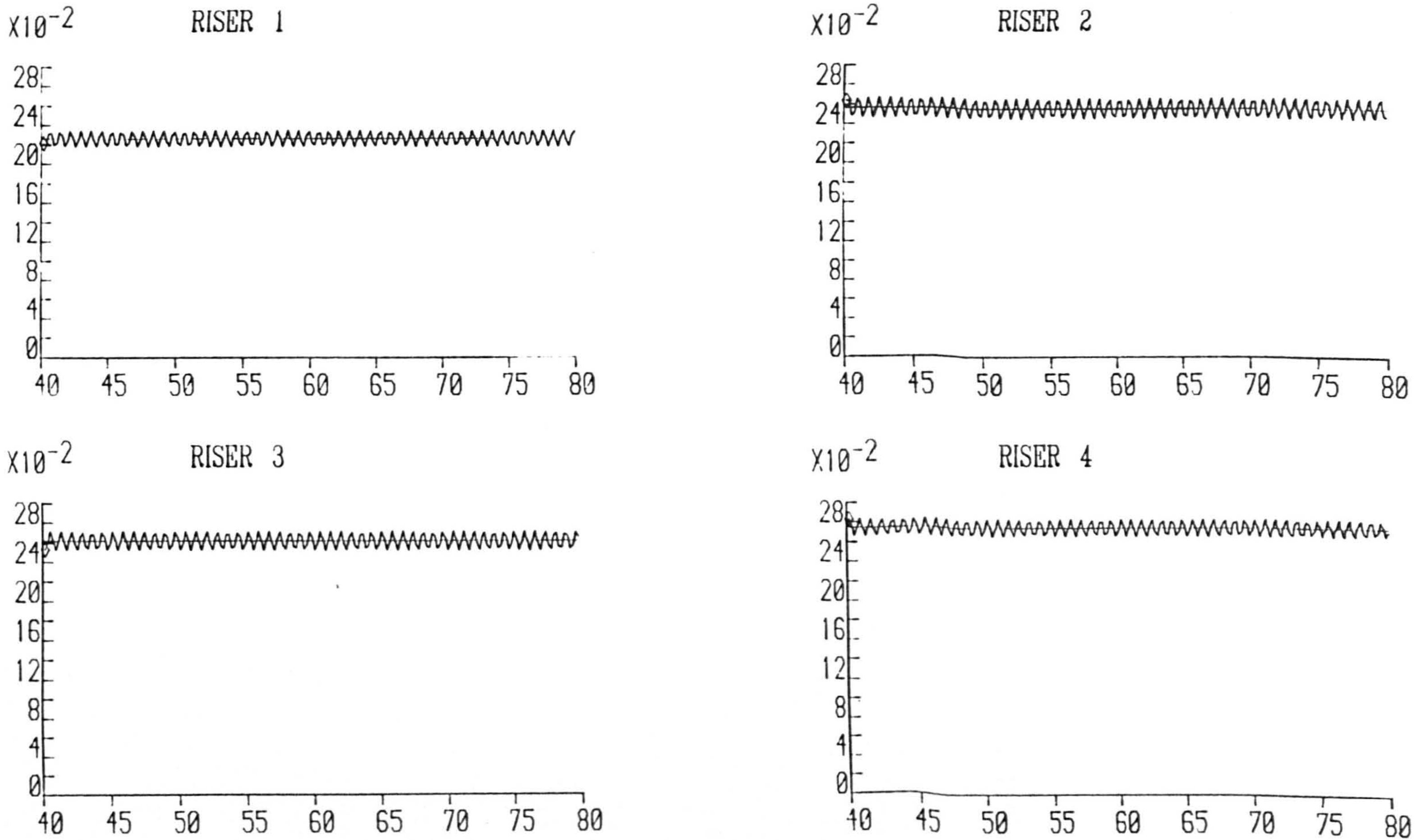

Y-AXIS = RISER VELOCITY (M/S), X-AXIS = TIME (SECS)

WAVEHEIGHT= 0.05500 WAVEPERIOD= 0.76900 FLOW RATE= 0.00200

FIGURE E83.

Appendix F

This appendix consists of two papers which have been written and presented during the course of this research. They are:-

1) "Investigation of Wave-Induced Oscillation in Sewage Outfalls" by Ali, K.H.M., Burrows, R. and Mort, R.B. and

2) "Wave Action on Multi-Riser Marine Outfalls" by Burrows, R. and Mort, R.B.

Investigation of Wave-Induced Oscillations in Sewage Outfalls

Kamil H. M. Ali*, Richard Burrows** and Richard Mort***

Abstract

The work described in this paper deals with the effect of wave action on the hydraulic performance of a sewage effluent outfall. The outfall under consideration is an inverted siphon, closely resembling a proposed outfall design to be undertaken by the North West Water Authority for the new Liverpool (U.K.) Waterfront sewage treatment works.

Experimental work was carried out to determine the effect on oscillations at the upstream end of the siphon of, (i) wave period and height, (ii) varying rates of discharge through the outfall, and (iii) the placing of a cover over the bellmouth spillway in order to prevent waves acting upon the outlet.

Numerical solutions were obtained using Henderson's[1] equations. This investigation concludes with the following observations:-

(1) that wave induced oscillations transmitted to the upstream end of the outfall are affected by three main factors, (a) wave energy (b) length of pipeline in the outfall system and (c) quantity of discharge in the system.

(2) that the placing of a cover over the outlet dramatically reduces oscillations within and upstream of the siphon structure.

Introduction

The discharge of domestic sewage, industrial wastes and surface water through outfalls to the sea has been practiced, for a long time, as an economical method of disposal. Many early outfalls, in the U.K., discharged their contents just below the low water mark with consequent pollution of the adjacent beaches and coastline. However, the increasing awareness of the need to reduce pollution along the shores, and in particular to improve the quality of bathing waters has led to the construction of longer outfalls.

The art and science of disposal of liquid wastes to sea has made very rapid advances in the past three decades; in part due to the technical developments which have made the construction of long outfalls into deep water economically practicable; and in part, under

*Senior Lecturer/**Lecturer/***Research Student, Department of Civil Engineering, University of Liverpool, P.O. Box 147, Liverpool L69 3BX, U.K.

pressure from stricter environmental controls and a change in emphasis from amenity to health considerations.

The behaviour of marine discharges is governed by a variety of physical factors which may vary widely and which cannot be controlled, such as sea temperature and salinity, tidal and ocean currents, winds and waves. In consequence, direct observation of trial discharges is not normally sufficient, since the full range of possible conditions, and the most adverse condition, would rarely be met in an experimental period of field investigation. Moreover there are apparent difficulties of scale which make interpretation difficult. Consequently, the hydrographic aspects of investigations are usually directed towards the construction of some form of model, simple or complex, which may be physical or mathematical, and which is intended to interpret and extend experimental data so as to enable predictions to be made of discharge behaviour under any postulated condition. Almost always this will necessitate extrapolation beyond the range of observations, with obvious danger of error unless there is reasonable understanding of the mechanisms which determine behaviour.

Almost all coastal towns in Britain discharge sewage to the sea either without treatment, or with just screening and maceration or (sometimes) after primary treatment. usually, especially when minimum pre-treatment is given, effluent is discharged to deep waters to achieve dilution and dispersion and where the action of waves on a submerged diffuser has little or no effect on the outfall's performance.

The outfall arrangement under consideration herein, however, is what may be termed a 'seawall discharge' exposed at low tide and greatly affected by wind-induced wave action, giving rise to pressure variations during falling and rising tides.

Henderson[1] undertook an analytical study of the effects of surface waves on the performance of diffusers constructed for a sea outfall in New Zealand; his analysis was based on a number of simplifying assumptions as follows: (i) the densities of effluent and ambient liquid are the same, (ii) the wave-induced (ambient) pressure variation is sinusoidal, (iii) the head in a storage tank on shore at the head of an outfall is constant, (iv) the change with time in the sum of the exit velocity head and head loss through the pipe is negligible, and (vi) the total head loss is constant.

When taking all the above into consideration, Henderson found that the storage was dependent upon the cross-sectional area of the pipe, acceleration due to gravity, the wave period and the length of the pipe.

Theoretical Considerations

Calculations of Minor Losses in the Inverted Siphon

The driving head, H_L, through this siphon can be given by the following relationship.

$$H_L = \left[k_1 + k_2 + k_3 + k_4 + k_5 + \frac{fL}{D} \right] \frac{V^2}{2g} = \frac{kV^2}{2g} \qquad (1)$$

where k_1 = energy-loss coefficient due to entry
k_2 = loss coefficient due to change of direction at B (Fig. 1)
k_3 = energy-loss coefficient due to vertical bend at C
k_4 = energy-loss coefficient due to vertical bend at D
k_5 = energy-loss coefficient due to expansion near exit
f = friction factor for siphon
V = mean velocity in the siphon
L = Length of siphon
g = acceleration due to gravity

For steady flow, the continuity equation gives:

$$Q = V A \qquad (2)$$

where A = cross sectional area of siphon.

Energy-loss coefficients, due to bends, depend markedly on the ratio centreline radius/diameter of pipe and on whether the bend is smooth or of the "Mitre" type (see Ref. 4, p 422). Substituting for the various loss coefficients, we obtain

$$H_L = \frac{Q^2}{2gA^2} (Z + \frac{fL}{D}) \qquad (3)$$

where $Z = k_1 + k_2 + k_3 + k_4 + k_5$

For Mitre bends Z = 4.45 and for smooth bends we obtain Z = 2.05.

We have ignored kinetic energy heads at the upstream and downstream sections. We have also assumed that the outfall spillway was operating free.

Dimensional Analysis of Wave Action on a Siphon

Using dimensional analysis, the wave height and period of the upstream oscillations H_2 and T_2 are given by

$$\frac{H_2}{H_1} = F_1 \left[\frac{d}{H_1}, \frac{D}{H_1}, \frac{L}{H_1}, \frac{gT_1^2}{H_1}, \frac{QT_1}{H_1^3}, \frac{A_1}{H_1^2}, \frac{A_2}{H_1^2} \right] \qquad (5)$$

and

$$\frac{T_2}{T_1} = F_2 \left[\frac{d}{H_1}, \frac{D}{H_1}, \frac{L}{H_1}, \frac{gT_1^2}{H_1}, \frac{QT_1}{H_1^3}, \frac{A_1}{H_1^2}, \frac{A_2}{H_1^2} \right] \qquad (6)$$

where d = mean depth, A_1 = area of upstream screen structure and A_2 = area of outlet ports.

The Effect of Wave Action on the Flow in the Outfall

Henderson[1] studied this problem and presented the following relationships for an ocean outfall:

$$h = \frac{H_1}{2} \sin\left[\frac{2\pi t}{T_1}\right] = \left[\frac{fL}{D} + \frac{A^2}{A_2{}^2}\right]\frac{V^2}{2g} + \frac{L}{g}\frac{dV}{dt} \qquad (7)$$

and

$$Q = A_1 \frac{dh}{dt} + AV \qquad (8)$$

The various symbols are defined in Fig. 3.

Henderson obtained an approximate solution to Eqs. (7) and (8) by assuming that

$$h = \left[\frac{fL}{D} + \frac{A^2}{A_2{}^2}\right]\frac{V^2}{2g} \qquad (9)$$

and obtained an expression for storage.

The present writers solved Eqs. (7) and (8) numerically using the Runge-Kutta forward integration[3] method. These results were checked using Escandes' finite difference method[2].

Experimental Arrangements and Procedures

An inverted siphon in the shape of a 'U' tube was placed in a wave tank; at the discharge end was placed a bellmouth outlet and at the inlet end was placed a reservoir tank. Details of the experimental arrangements are given in Fig. 2. The reservoir tank was designed to act independently of the wave tank. Wave paddles in the first tank were capable of being adjusted to provide various combinations of wave periods and amplitudes.

Resistance wave gauges were placed at three positions: (1) upstream of the siphon, (2) above the bellmouth discharge, and (3) above the inflow of the inlet shaft.

The wave gauges were calibrated before and after each experimental run.

Steady flow experiments were conducted to study minor losses in the inverted siphon. Head-discharge measurements were obtained for various flows. Minor losses were calculated using these results.

For the first part of the wave experiments, a shaft was added to the upstream end of the siphon. This was made from a length of pipe of the same diameter as the outfall. The shaft was used to amplify the wave induced oscillations which occur in the siphon; without the shaft, oscillation would have been transmitted to the reservoir which had a plan area 10 times that of the pipe. Waves of various heights and periods were passed over the outfall bellmouth and the consequential oscillations induced at the upstream end of the system were recorded. This process was then repeated using a range of discharges through the siphon.

In the second part of the wave-experiments, the circular inlet shaft was removed in order that oscillations in the reservoir tanks could be evaluated. The procedure used for the deep shaft was then repeated.

The final part of the experiments involved an investigation into the effects of placing a cover over the outfall spillway as shown in Fig. 3.

Waves of various heights and periods were passed down the flume and oscillations occurring at the upstream end of the siphon were recorded.

RESULTS

(1) Minor Loss Results

Steady flow experiments were conducted for various discharges in order to obtain the parameter Z in Eq. (3). Figure 4 shows the variation of Z with the Reynolds Number $R(= VD/\nu)$. This figure shows that Z decreases with the increase in R. The experimental values of Z cover the range $Z = 1.74 - 5.84$. Calculations give $Z = 2.05$ for a smooth bend and $Z = 4.45$ for a Mitre bend.

(2) Effect of Placing a Cover Over the Outfall (Fig. 3)

A series of experiments was conducted, using various wave heights, wave periods and discharges, to study the effect of the cover shown in Fig. 3 on the upstream oscillations. This cover was found to be extremely efficient in suppressing the oscillations in the upstream shaft.

(3) Wave Oscillation Results

(a) Experimental Results

Figures 5 - 8 show the upstream and downstream water level oscillations for the deep circular shaft ($A_1 = A$). These results are given for various discharges.

Figures 9 - 12 show similar plots for the case of an upstream approach channel ($A_1 = 10A$).

In the above experiments, the introduction of flow at the upstream end of the outfall resulted in considerable air-entrainment and marked agitation of the water surface.

Figure 13 shows a summary of some of the experimental results and it gives the variation of H_2/H_1 with $QT_1/H_1{}^3$. This figure shows that the values of H_2/H_1, for the deep shaft ($A_1/A = 1$), are much bigger than those for the shallow shaft ($A_1/A = 10$). Also, the values of H_2/H_1 in crease with the increase in T_1 (for a given Q).

For the deep shaft, the values of T_2/T_1 covered the range 5.1 - 10.2

whilst for the shallow shaft the range was 9.3 - 24.3.

(b) Numerical Results for the Model

Figure 13 also shows the variation of the theoretical values of H_2/H_1 with QT_1/H_1^3 for $T_1 = 1.13$ secs., $H_1 = 0.1$ m and $L = 7.8$ m. These results were obtained by numerically integrating Esq. (7) and (8) [Eq. (7) was modified to include minor losses (see Eq. (3))].

Figure 13 shows that:

(i) H_2/H_1 decreases slightly with the increase in Q

(ii) For a fixed Q, H_2/H_1 increases with the decrease in A_1/A.

(iii) The theoretical values of H_2/H_1 are much smaller than the experimental ones especially in the case of the deep shaft. Air entrainment, which was always present, might have caused a considerable increase in the experimental values of H_2 because of the bulking of the flow.

The experimental values of T_2/T_1, for the deep shaft, cover the range 5.1 - 10.2. The numerical solution yielded an almost constant value of about 4.60.

It is interesting to note that for mass oscillations in a surge tank, ignoring friction, T_2 is given

$$T_2 = 2\pi \sqrt{\frac{LA_1}{gA}} \tag{10}$$

For $L = 7.8$ m and $A_1 = A$, we obtain $T_2 = 5.60$ secs and $T_2/T_1 = 4.96$.

The range of T_2/T_1, for the shallow shaft ($A_1/A = 10$), was 9.3 - 24.3. Equation (10) gives $T_2/T_1 = 15.68$.

(c) Numerical Results for the Prototype

Figures 14 - 17 show the theoretical upstream oscillations for the prototype outfall ($L = 282$ m, $D = 2.7$ m, $A = A_1 = A_2$, roughness height $= 1.5$ mm). These figures, together with Table 1 show that:

(i) For $H_1 = 5$ m, $T_1 = 5$ secs and $Q = 1.5$ m^3/s, the increase in outfall length results in a decrease in H_2/H_1. Changing Q to 13 m^3/s results in a slight decrease in H_2/H_1 (for the same value of L).

(ii) For $Q = 13$ m^3/s, $T_1 = 5$ secs and $L = 282$ m, H_2/H_1 is almost independent of H_1.

(iii) For constant values of Q, L and H_1, the increase in T_1 results in a considerable increase in H_2/H_1 (from 0.02 for $T_1 = 1$ sec to 0.28 for $T_1 = 9$ secs).

(iv) The theoretical values of T_2 obtained from the numerical integration of Eqs. (7) and (8) are very close to the values calculated from Eq. (10).

Ongoing Research Program

A new hydraulic model of a conventional sea outfall has been constructed and it incorporates a system of (4-9) risers. This model is positioned in a versatile wave tank (50 m long x 1 m x 1 m). This model is being used to study the following phenomena:

(i) The effect of wave action and discharge on the circulation in the outfall system
(ii) Characteristics of saline wedges and sediment transport within the pipe. A detailed study will also be made of the flow rates required to purge the saline wedges.
(iii) This physical model will be used to verify mathematical models being developed for this outfall.

CONCLUSIONS

1. Minor losses in the model outfall are a function of the Reynolds number of the pipe.
2. The placing of a cover over the present outfall greatly reduced the upstream oscillations.
3. The theoretical results, obtained from the numerical integration of Henderson's equations, generally confirm the trends of the experimental results. The predicted values of H_2/H_1 were, however, much smaller than those of the experiments.
4. Dimensionless upstream oscillations, in this type of outfall, increase with the decrease in L, decrease in A_1/A and increase in T_1. The effects of Q and H_1 are very small.
5. The expression for T_2, obtained from simple frictionless surge-tank analysis, gives periods of upstream oscillation in very good agreement with the results obtained from the numerical analysis.
6. Wave-induced oscillations can be a major problem in this type of outfall.
7. Environmental factors rather than hydraulic ones might well decide the adequacy or otherwise of this type of outfall.

Acknowledgements

Part of this work was sponsored by the North West Water Authority, Liverpool, U.K., whose help and co-operation are appreciated.

References

1. HENDERSON, F. M. (1967), "The effect of wave action on the flow in the proposed ocean outfall of a sewage line, Napier", Report to Steven and Fitzmaurice Consulting Engineers, Christchurch, New Zealand.
2. JAEGER, C. (1961), "Engineering fluid mechanics", Blackie and Sons Ltd., London.
3. JEFFREY, A. (1982), "Mathematics for engineers and scientists, 2nd Ed. Von Nostrand Reinhold, U.K.
4. VENNARD, J. K. and STREET, R. L. (1976), "Elementary fluid mechanics", 5th Ed., John Wiley and Sons.

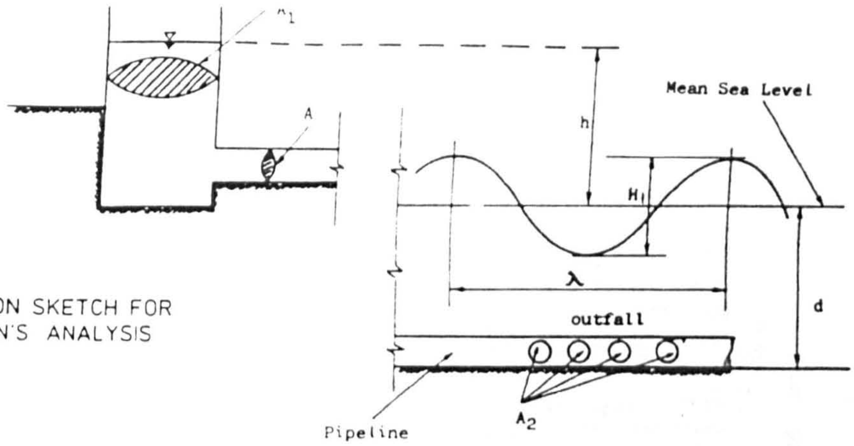

FIG 1
DEFINITION SKETCH FOR
HEDERSON'S ANALYSIS

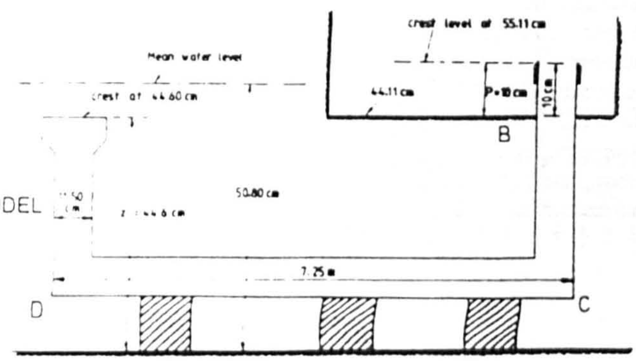

FIG 2
DETAILS OF MODEL
OUTFALL

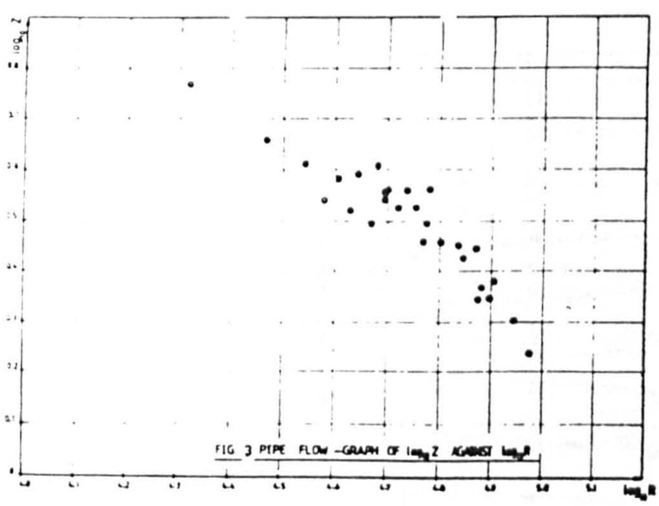

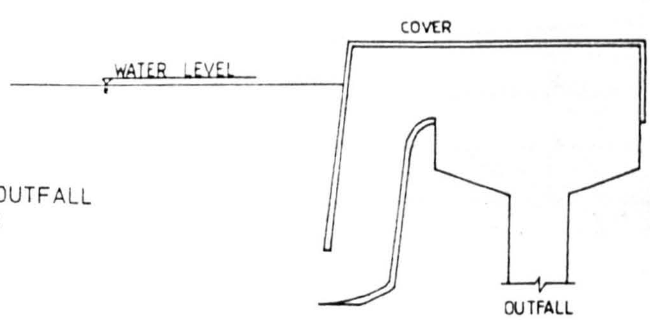

FIG 4
POSITION OF OUTFALL
COVER

8 Ali

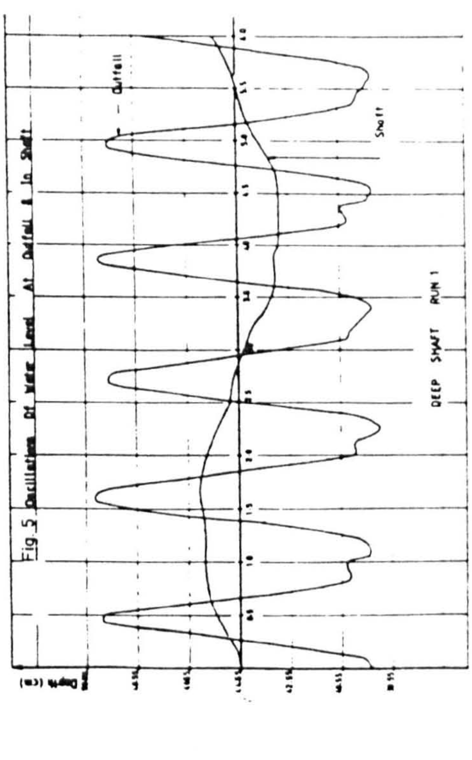
Fig 5 Oscillations Of Water Level At Outfall & In Shaft
Outfall
Shaft
DEEP SHAFT RUN 1
Depth (cm)

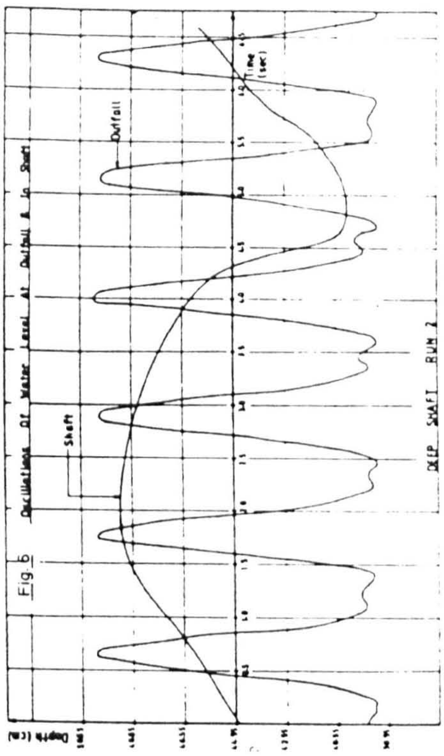
Fig 6 Oscillations Of Water Level At Outfall & In Shaft
Shaft
Outfall
Time (sec)
DEEP SHAFT RUN 2
Depth (cm)

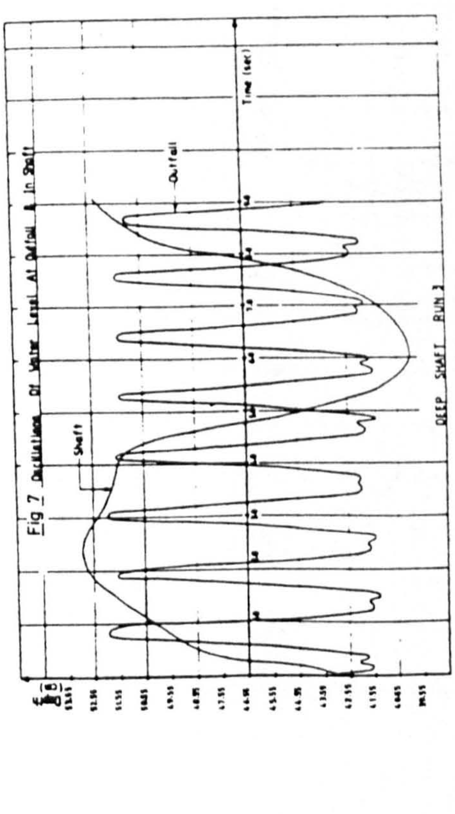
Fig 7 Oscillations Of Water Level At Outfall & In Shaft
Shaft
Outfall
Time (sec)
DEEP SHAFT RUN 3

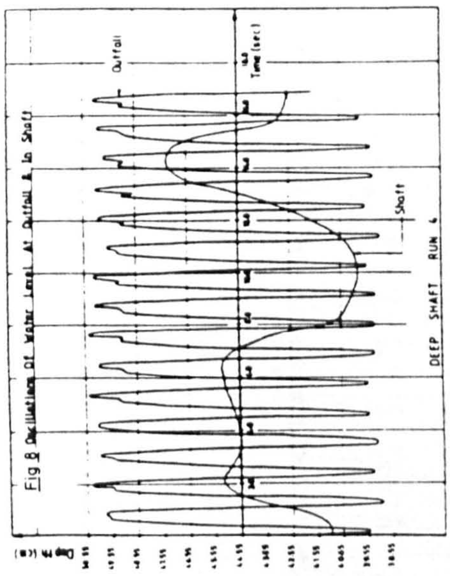
Fig 8 Oscillations Of Water Level At Outfall & In Shaft
Outfall
Shaft
Time (sec)
DEEP SHAFT RUN 4

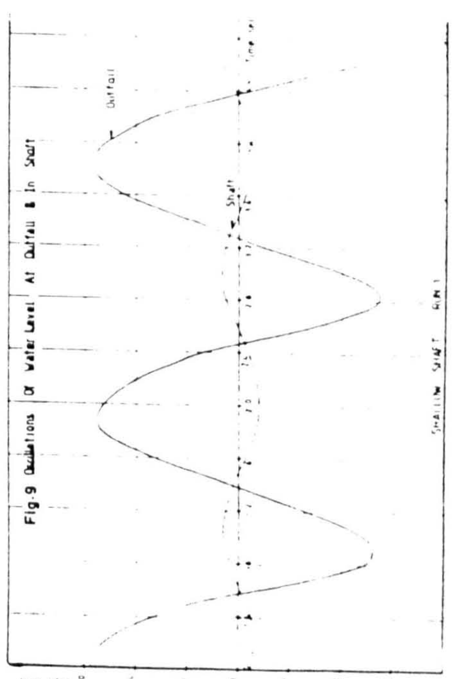

Fig.9 Oscillations Of Water Level At Outfall & In Shaft

SHALLOW SHAFT RUN 1

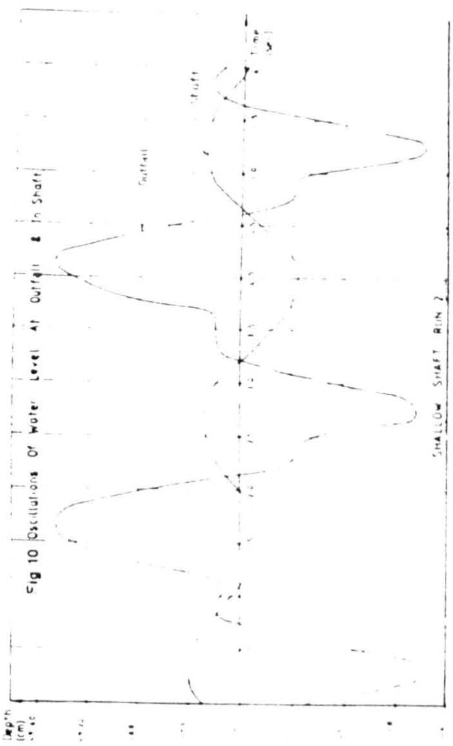

Fig 10 Oscillations Of Water Level At Outfall & In Shaft

SHALLOW SHAFT RUN 2

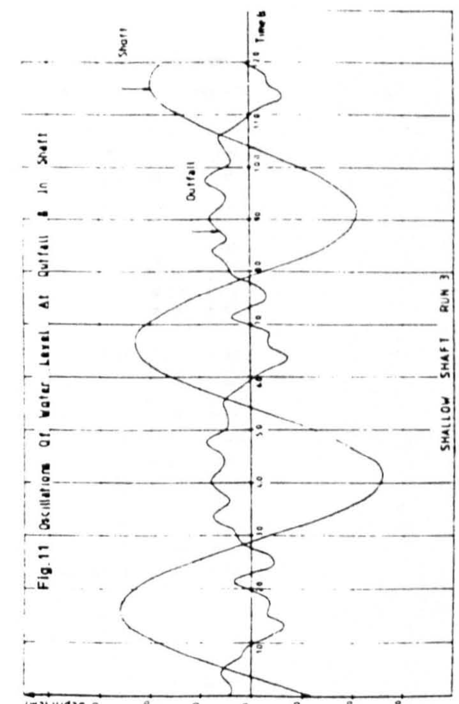

Fig.11 Oscillations Of Water Level At Outfall & In Shaft

SHALLOW SHAFT RUN 3

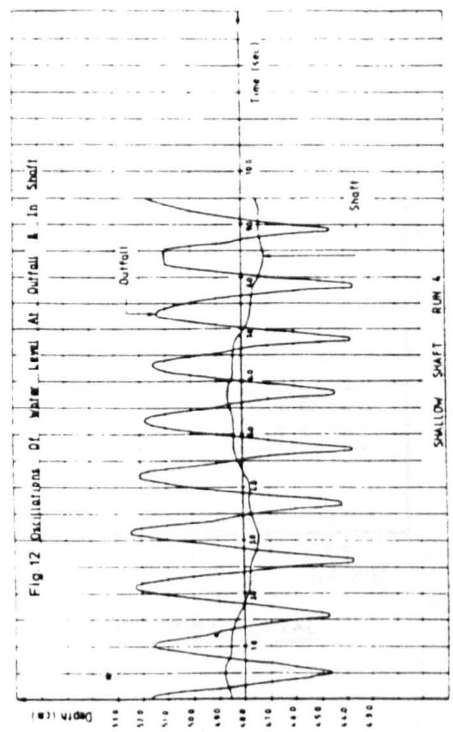

Fig 12 Oscillations Of Water Level At Outfall & In Shaft

SHALLOW SHAFT RUN 4

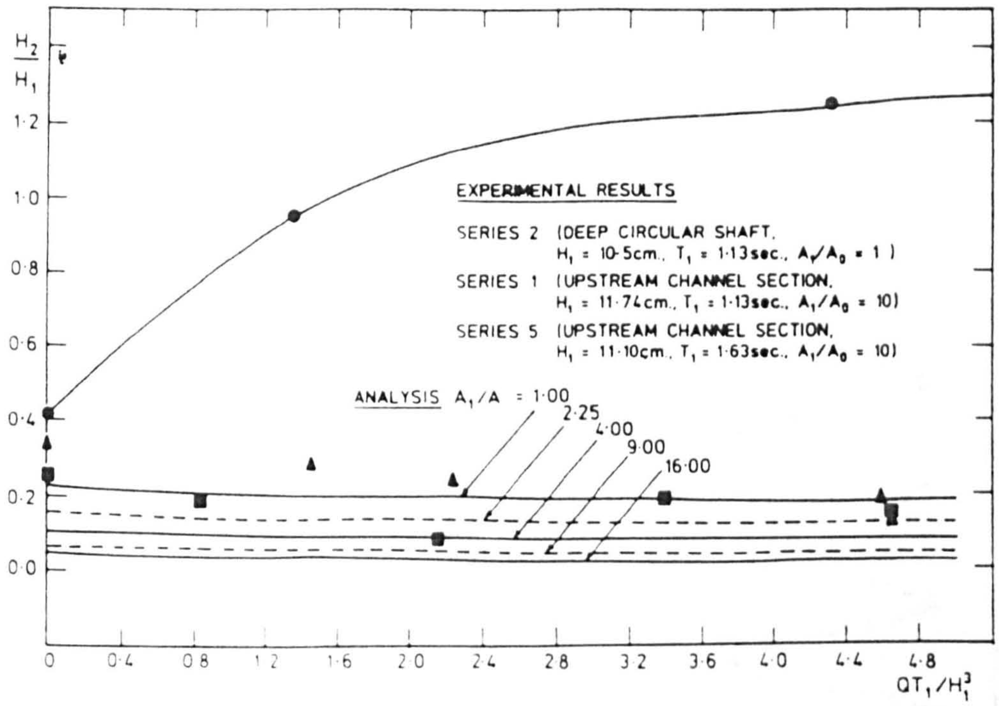

FIG. 13 COMPARISON BETWEEN THEORETICAL AND EXPERIMENTAL VALUES OF H_2/H_1

TABLE 1 COMPUTER RESULTS FOR UPSTREAM OSCILLATIONS IN THE OUTFALL

(Roughness height - 1.5 mm, D - 2.7 m, $A_0 - A_1 - A_2$ - 5.726 m^2)

Q (m^3/s)	H_1 (m)	T_1 (secs)	L (m)	L/H_1	H_2/H_1	T_2/T_1	QT_1/H_1^3	T_2 (EQ.10)	T_2(EQ.10)/T_1
1.5	5	5	100	20	0.32	4.62	0.06	20.06	4.01
•	•	•	200	40	0.20	5.54	•	28.37	5.67
•	•	•	300	60	0.16	6.77	•	34.75	6.95
•	•	•	400	80	0.14	8.13	•	40.12	8.02
•	•	•	500	100	0.12	8.92	•	44.86	8.97
13.0	5	5	100	20	0.28	4.31	0.52	20.06	4.01
•	•	•	200	40	0.18	5.54	•	28.37	5.67
•	•	•	300	60	0.15	6.92	•	34.75	6.95
•	•	•	400	80	0.12	8.31	•	40.12	8.02
•	•	•	500	100	0.10	8.92	•	44.86	8.97
1.5	5	5	285	57.0	0.17	6.62	0.06	33.87	6.77
2.0	•	•	•	•	0.17	•	0.08	•	•
5.0	•	•	•	•	0.16	•	0.20	•	•
8.0	•	•	•	•	0.16	•	0.32	•	•
13.0	•	•	•	•	0.15	•	0.52	•	•
13.0	1.0	5	282	282.0	0.15	6.62	65.00	33.69	6.74
•	3.0	•	•	94.0	0.15	•	2.41	•	•
•	5.0	•	•	56.4	0.14	•	0.52	•	•
•	7.0	•	•	40.3	0.14	•	0.19	•	•
•	9.0	•	•	31.3	0.14	•	0.09	•	•
13.0	5	1.0	285	57.0	0.02	34.0	0.10	33.87	33.87
•	•	3.0	•	•	0.08	11.3	0.31	•	11.29
•	•	5.0	•	•	0.15	6.8	0.52	•	6.77
•	•	7.0	•	•	0.21	4.9	0.73	•	4.84
•	•	9.0	•	•	0.28	3.8	0.94	•	3.76

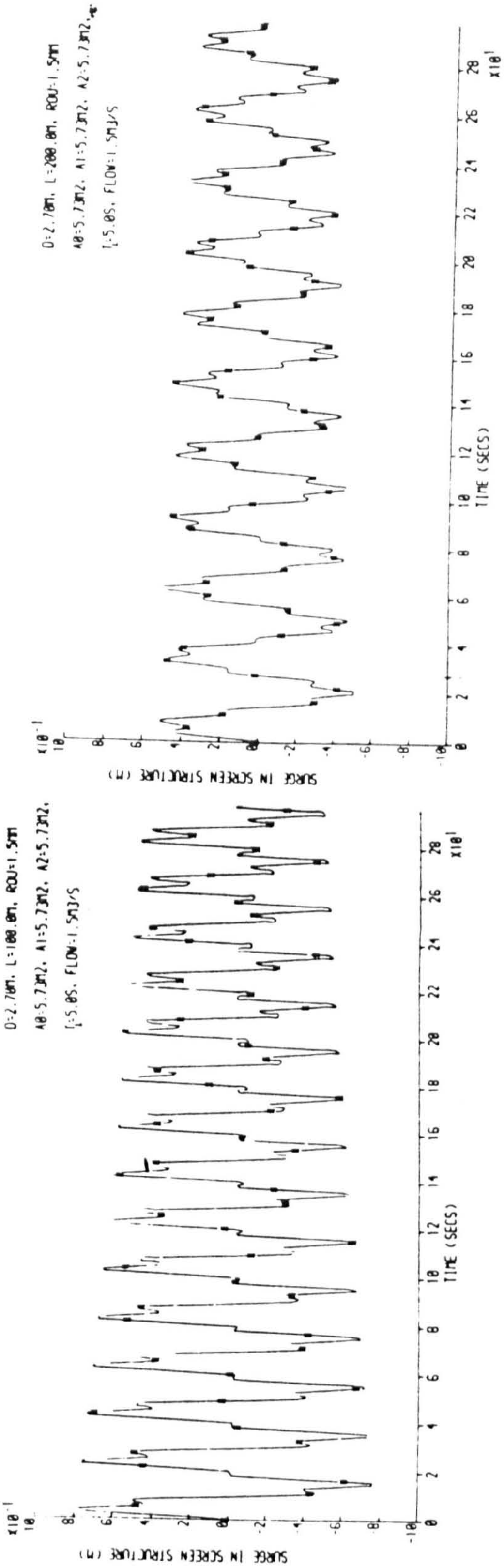

FIG. 14 EFFECT OF L ON THE UPSTREAM OSCILLATIONS OF A PROTOTYPE OUTFALL (H_1 = 5 m)

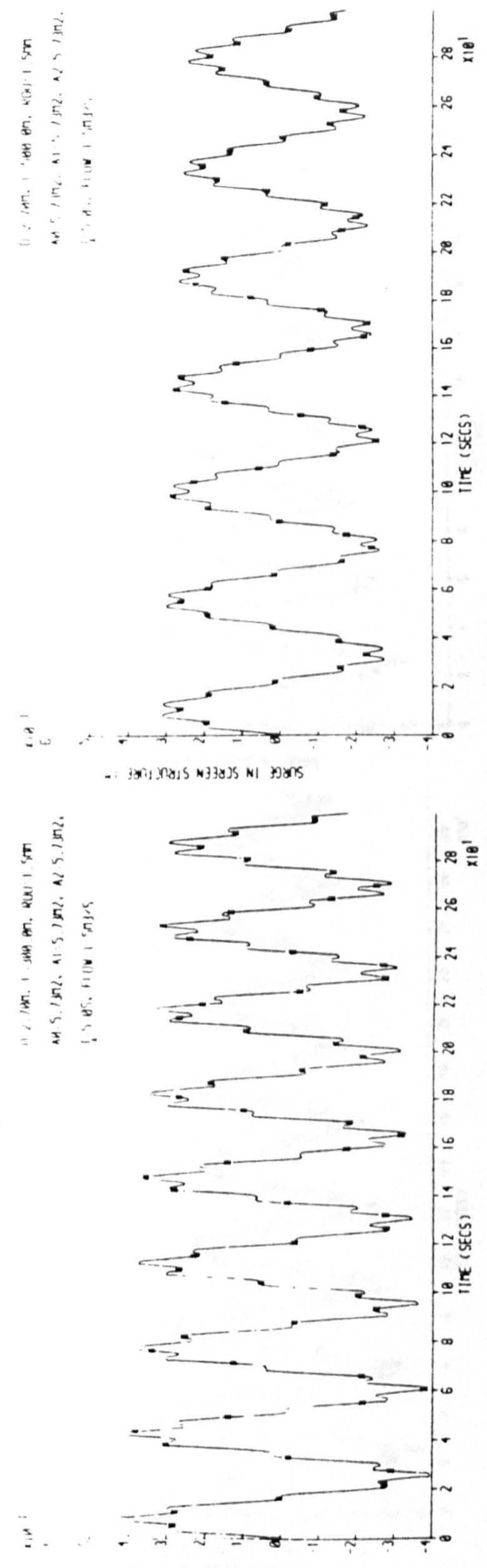

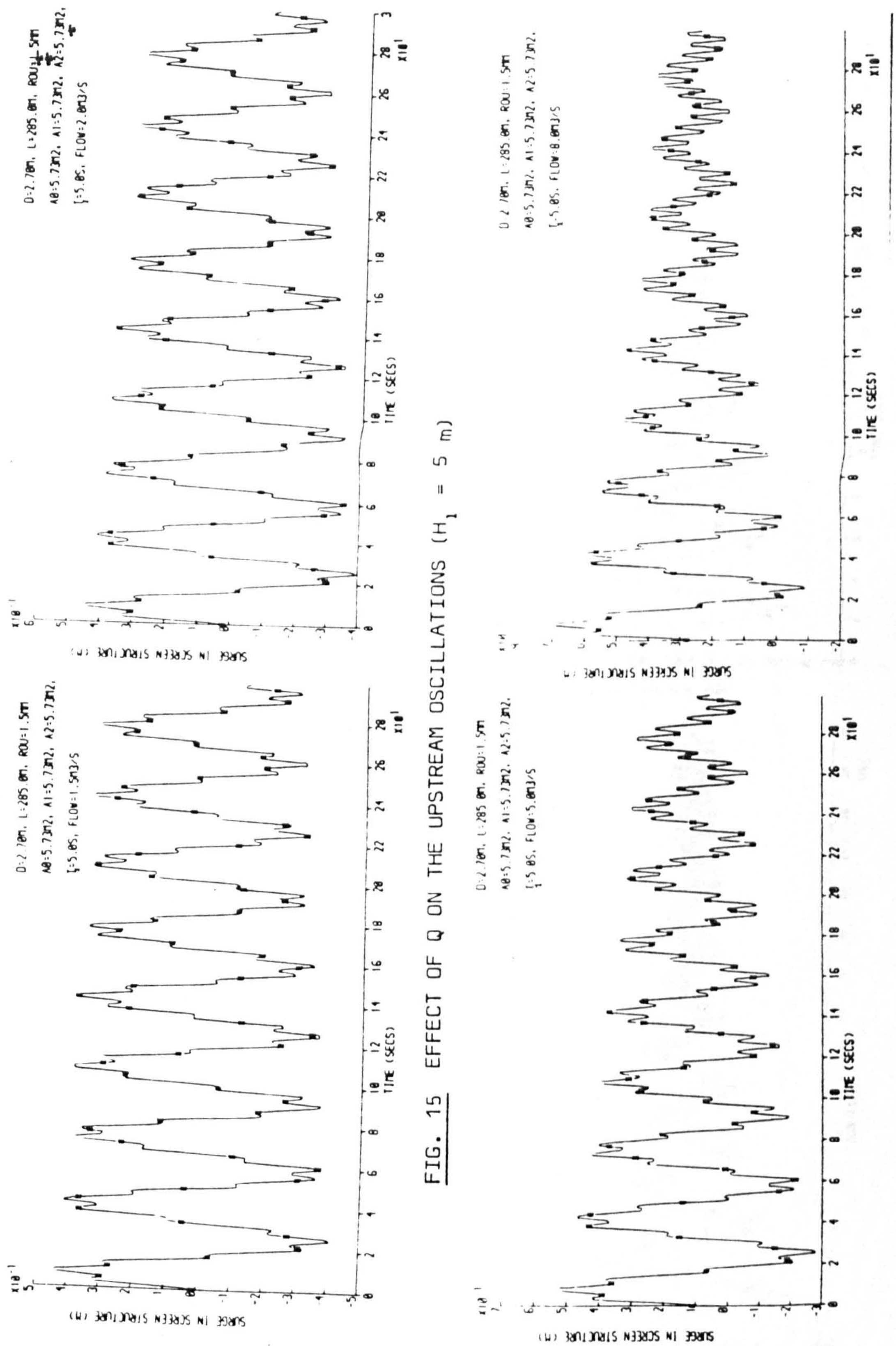

FIG. 15 EFFECT OF Q ON THE UPSTREAM OSCILLATIONS (H_1 = 5 m)

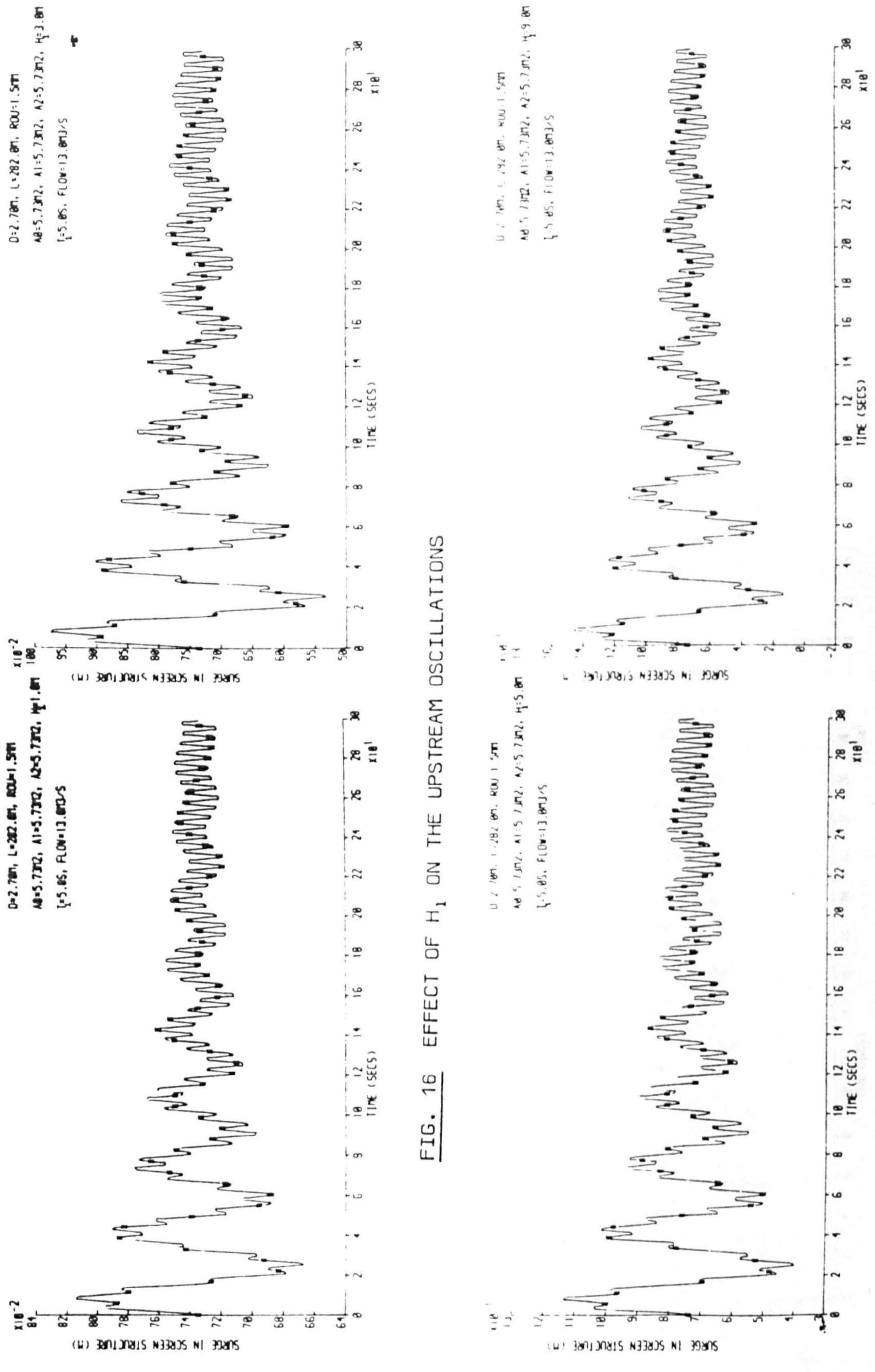

FIG. 16 EFFECT OF H_1 ON THE UPSTREAM OSCILLATIONS

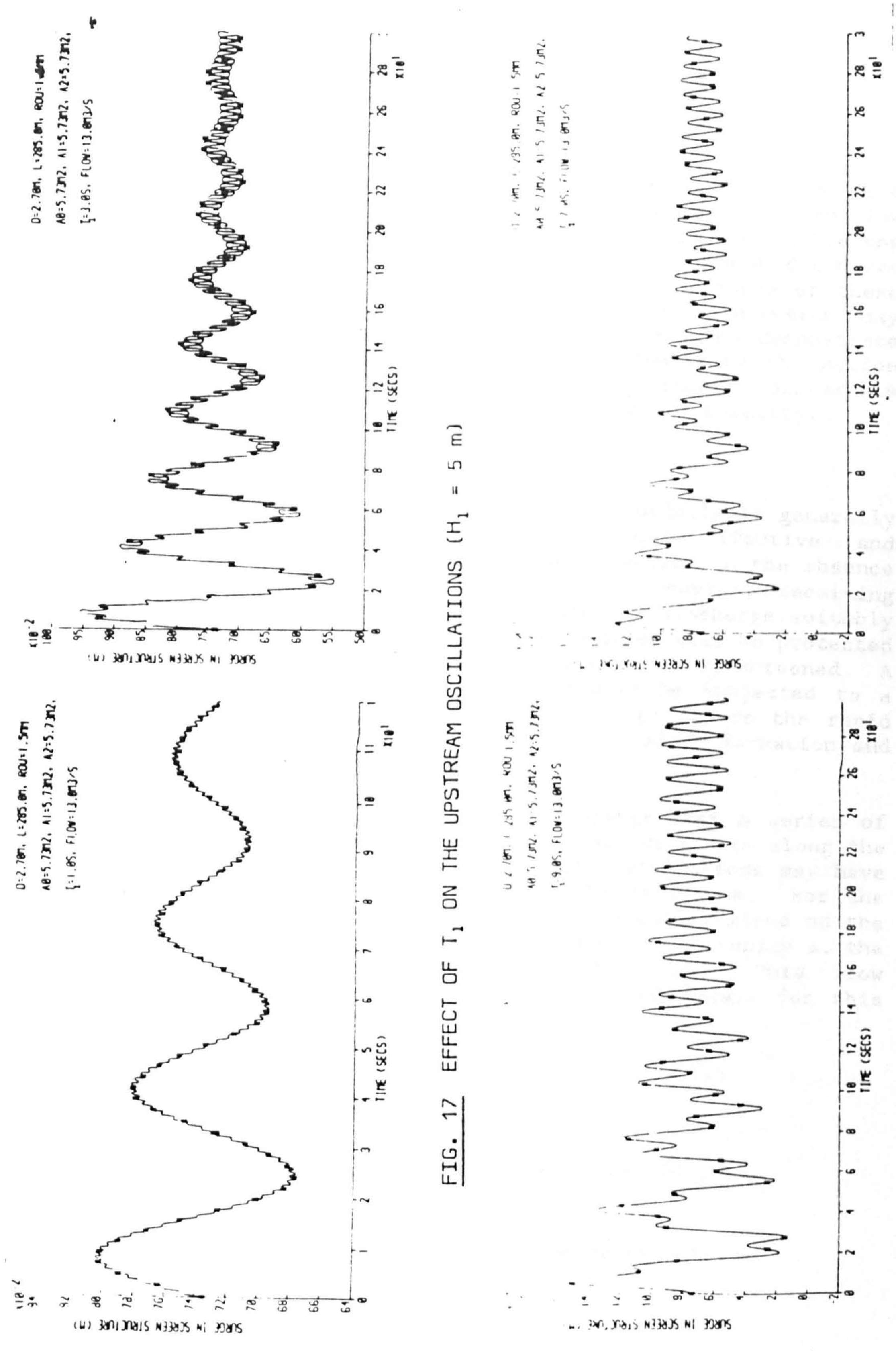

FIG. 17 EFFECT OF T_1 ON THE UPSTREAM OSCILLATIONS (H_1 = 5 m)

WAVE ACTION ON MULTI-RISER MARINE OUTFALLS

R. Burrows & R.B. Mort
Department of Civil Engineering, University of Liverpool, U.K.

Summary

Both experimental and numerical studies into the effects of wave action on the operation of sewage outfalls discharging into shallow water are reported. The inducement of internal circulation within the multi-riser diffuser systems associated with the seaward discharge manifold is of major concern to the operational performance of these systems, evidence suggesting that resulting saline intrusion may ultimately lead to partial blockage. Results presented demonstrate that the pressure differentials between risers created by the motion of waves in shallow receiving waters can significantly exacerbate these problems when discharges fall below the 'design' capacity.

1. Introduction

The disposal of sewage to the sea via long-sea outfalls is generally considered, within the U.K., to be a cost effective and environmentally acceptable practice. Its introduction in the absence of primary, or indeed secondary treatment, is, however, receiving criticism internationally (1). With the point of discharge suitably located perhaps several kilometres offshore, beaches will be protected from pollution provided that the sewage has been suitably screened. A further prerequisite is that the effluent should be subjected to a high degree of dilution in the receiving water to ensure the rapid depletion of pathogen concentrations and to avoid slick formation and consequential environmental stress.

The dilution is achieved by staging the discharge from a series of diffuser ports from risers spaced out at suitable distances along the seaward end of the sub-sea pipeline. Typical installations may have manifolds incorporating between, perhaps, 3 and 25 risers. For the purposes of initial dilution the efflux jet is normally sized on the basis of provision of a densimetric Froude number, F_D, of unity at the diffuser exit port under maximum design flow, Q_D. This flow characteristic is defined as follows, with input parameters for this application given in square brackets,

$$F_D = V/(\epsilon g L)^{1/2} \qquad (1)$$

where V = velocity of flow [$\equiv Q_D/(\pi D^2/4)$]
g = gravitational acceleration
L = relevant length dimension [$\equiv$ D, port diameter]
$\epsilon = (\rho_2 - \rho_1)/\rho_2$
ρ_2 = density of heavy fluid [saltwater]
ρ_1 = density of light fluid [freshwater/sewage]

An approximate flow balance from the risers can be achieved under the required design flow rate Q_D using standard methods of pipe flow hydraulics, to ensure that the appropriate dilution is achieved for each diffusing plume of effluent. Unfortunately, as flows Q drop below Q_D there is an increasing tendency for the discharge from the seaward risers to reduce and eventually reverse, setting up internal circulations within sections of the manifold system. This behaviour has been demonstrated visually by Charlton (2,3) and Wilkinson (4) from small scale experimental studies, and also numerically by Larsen (5) from a computer model of the system. As a result of the density excess of the saline influx a stratification wedge may form in the outfall and suspended sediments will tend to settle in the pipe invert. These particulate may either be drawn in with the saline water or fall out of the sewage flow above the wedge. If not purged out at times of diurnal maximum flow these deposits may accumulate and eventually lead to partial blockage or modify the hydraulic characteristics of the system so as to affect flow balances.

Purging velocities required to expel intruded seawater can be computed in the manner put forward by Wilkinson (6). Unfortunately, it may often be the case when outfalls are designed on future flow forecasts, that daily peak flows are inadequate to accomplish this flushing action in the early years of operation unless substantial storage is provided in the headworks. In these circumstances, it may be advisable to seal off the most landward risers initially and to bring them into operation only when flows build up to a point where daily purging of intruded seawater can be achieved. Sadly, this is not a common practice and apparent malfunctions observed in numerous outfalls (7) may well be partly attributable to these effects.

Charlton (3,8) has suggested several means for restricting saline intrusion including the introduction of venturi-type constrictions within the diffuser ports or the main outfall itself. These do, however, carry with them additional head losses and consequential pumping requirements, since to be effective they should be sized to provide adequate flow velocities under the conditions of low flow. For purposes of preventing or arresting saline intrusion a densimetric Froude number exceeding unity is again sought using equation (1). Unfortunately, although this requirement ($F_D > 1.0$) can be demonstrated for stratified flows in open channels, its justification is less clear for enclosed flow in pipes of circular section, where the selection of the appropriate length dimension, L, appears to be open to intuitive judgement (9). Diffuser ports sized in this manner may produce velocities under peak flows in excess of those optimal for plume dilution and the small size may lead to increased risk of blockage. Incorporation of valves on the diffuser ports could eliminate the intrusion problems. Simple flaps have been suggested (10) and flexible rubber 'duck-bill' arrangements have been employed (11) in several cases but no system has found extensive application to date.

From the above discussion it has been established that internal circulations are likely to exist in the normal operation of multi-riser outfalls as presently designed, and that these potentially lead to operational problems. A logical extension is, therefore, to investigate whether the situation is exacerbated by wave action. This is only likely to be a factor in shallow receiving waters where pressure fluctuations resulting from surface wave activity extend down to bed level. However, in these circumstances it is possible that the wave induced agitation of the sea bed may also give rise to significant influx of sea bed sediments if intrusive conditions result. The potential influence of waves has been suggested previously by Charlton (12) but no systematic experimental study of these effects has been reported and this deficiency inspired the research programme reported here.

2. Experimentation

The experimental installation used for the study is illustrated schematically in figure 1. The seaward end of an outfall was represented by a 5m length of acrylic pipe of 105mm internal diameter on to which were attached four 50mm internal diameter vertical acrylic riser pipes 400mm long, set at 500mm spacings to form the discharge manifold. Small diameter diffuser ports normally installed on the top of the risers were not included in the tests reported here. Flows were supplied from a header tank and measured either by V-notch in an intermediate stilling tank or (for high flows) by venturi-meter installed at the head of the model outfall section.

The complete pipe system was located within a wave flume 12m long, 750mm wide, with operational water depths up to 900mm. A 'Keelavite' wave generator at one end of the flume was capable of producing regular or random waves, the latter being defined by a target energy spectrum. Wave motion was recorded in the vicinity of the manifold section by surface piercing capacitance gauges and reflective interference of the wave trains was suppressed by a slatted wooden spending beach at the 'landward' end of the flume.

The oscillatory flow velocities in the risers, which occur as a result of the wave action were measured with a 'sensordata' ultrasonic velocity probe. This had to be inserted at a central section in each riser sequentially during each test run and dummy transducer arms were retained in the other risers to eliminate any differential effects on head losses within the risers. Whilst this procedure had some drawbacks, not least the experimental inconvenience, no alternative system could be found, hot-wire anemometry being unsuited to the reversing flows, and financial constraints prevented the acquisition of multiple ultrasonic probes. Visualisation of the oscillations and internal circulations under steady flow could be achieved either by release of dye films in the risers or by the complete colouration of the freshwater flows. The latter technique was also used extensively in a parallel study into the intrusive saline wedges which form in the pipe invert. This will be reported later by Mort (13). Pressures have also been recorded at five sections along the outfall, as shown (PT/-) in figure 1, using Druck PDCR42 miniature transducers set in housings attached to the pipe section. This data has yet to be fully utilized in the final calibration of the numerical model but should also provide empirical measures of the head losses across the pipe riser junctions, an aspect for which guidance is deficient.

Data collection and analysis was conducted using an Eclipse Computer system capable of receiving instantaneously up to 32 channels of information at a sampling frequency of 100Hz. In the present experiment a maximum of 11 channels were used (1 - velocity probe; 6 - pressure transducers; 3 - wave gauges and 1 - wave generator) with sampling of oscillatory signals selected at 20Hz. Computer software was developed specifically for the graphical presentation of the results (sample time series and statistics) from runs of 100 second duration.

In the planning of the study no attempt was made to replicate a typical outfall configuration. The aim was simply to demonstrate characteristic flow phenomena in such systems. Relative to existing outfalls, from geometric scaling, the spacing between risers is rather short in the model but this was constrained by the limited extent of the working section in the wave flume and the need to include at least four risers to provide scope for various alternative internal circulation loops. It was, nevertheless, necessary to select a flow rate at which the riser system should be hydraulically balanced and this was set at 2 litres/sec. Based on scale modelling to the densimetric Froude number, and using a model saline density of approximately 1.015, it was found that this flow would represent about 60% of the design capacity of a specific prototype, in which minimum flows would fall to about 10% of this capacity. A range of model flows spanning 0.3 - 2.0 litres/sec would, therefore, be representative of practical situations. Since the flow balance was set below the equivalent ultimate capacity it was recognised that the inter-riser flow variations experienced in the model would consequentially be less than those in a corresponding prototype. Flow balance itself was achieved by the *trial insertion of orifice rings* of differing size into the lower sections of the riser pipes.

The full programme of tests conducted covered 8 flow rates in the range 0.19 to 0.94 litres/sec to represent situations where major flow imbalances might be expected and at 2.0 litres/sec, the balanced flow Q_D. At each flow rate, tests were run with quiescent receiving water and with five different wave conditions, ranging in height between 3.2 and 6.5cm and in period between 0.67 and 2.0 secs.

3. Theoretical Modelling

The basis of the mathematical model developed for the outfall system operating under the influence of wave action follows from the earlier work of Larsen (5). It results from the application of the continuity and momentum equations to elements of flow within the pipe system and employs finite difference methods for solution.

3.1 Basic equations

Following directly from derivations in Steeter and Wylie (14), the continuity and momentum equations may be written respectively and for pipes of circular section, as

$$\frac{a^2}{g}\frac{\partial V}{\partial x} + \frac{V\partial H}{\partial x} + \frac{\partial H}{\partial t} + V\sin\theta = 0 \qquad (2)$$

$$\frac{g\partial H}{\partial x} + V\frac{\partial V}{\partial x} + \frac{\partial V}{\partial t} + \frac{fV|V|}{2D} = 0 \qquad (3)$$

where $a = (k/\rho)/[1+(k/E)(D/t')]$; k and ρ are bulk modulus and density of water respectively; E is Youngs modulus of the pipe material; D and t' are the pipe diameter and thickness respectively; and these terms account for potential expansion of the pipe and fluid compressibility brought about changes in pressure. With reference to figure 2, x is a distance along the outfall, V represents mean pipe flow velocity, H measures the elevation of the hydraulic grade line above the datum and can be expressed as $H = \{(p/\rho g) + z\}$ where p is the hydrostatic pressure and z the position head at that section of the pipe. The inclination of the outfall is given by θ, f is a friction factor taken from the Colebrook-White equation and t is time.

The equations can be expressed in finite difference form to represent flow in sub-elements of the pipe system of length Δx. This sub-division applied to the experimental configuration is indicated in figure 2. Solution to the problem can then be achieved, following specification of the relevant boundary conditions given below.

3.2 Boundary Conditions

- Upstream: this can be taken as a directly connected pump supply for which, at station $i = 0$, instantaneous velocity V_0 and head H_0 remain constant. Alternatively, supply to the outfall may be received from a dropshaft as shown in figure 2 which would act as a surge chamber and where the boundary conditions becomes the continuity requirement,

$$\frac{dH_D}{dt} = \frac{1}{A_D}(Q_p - AV_0) \qquad (4)$$

- Downstream: at the point of discharge from the riser port the pressure in the discharging fluid must be equal to that within the denser receiving water, which is subjected to attenuated oscillations as a result of the surface wave action. For regular waves at riser J in figure 2, the pressure can be expressed, from Ippen (15), as

$$P_J = \rho_2 g\, [y_J - \frac{H_W}{2}\frac{\cosh\{2\pi(d - y_J)/L\}}{\cosh\{2\pi d/L\}} \sin\{(2\pi x_J/L) - (2\pi t/T)\}] \qquad (5)$$

where H_W, t and L are the wave height, period and length respectively, the latter being obtained from $L = (gT^2/2\pi)\tanh(2\pi d/L)$; d is the water depth; and y_J is the depth of submergence of the riser ports.

3.3 Solution Method

Equations (2) and (3) written in finite difference form and applied to the discretised system of elements (of length Δx), with the above boundary conditions introduced, can be solved for V and H by various methods. Herein the method of characteristics has been used, with time steps Δt set at $(\Delta x/a)$ secs following from the recommendations of Streeter and Wylie (14).

Flow conditions in the risers have not been solved by an extension of the finite difference scheme, but instead, are dealt with by a lumped inertia method. This is appropriate since flow changes in these short narrow pipes will follow almost instantaneously as a result of wave induced pressure changes. Here, the net upward force exerted on the fluid contained in the riser must balance the rate of change of its momentum. Using the dimensions in figure 2 for riser J, this requirement becomes

$$(P_I{*} - P_J)\, A_J - \frac{f\, L_J\, V_J |V_J|}{2g\, D_J} = \rho_1 L_J A_J \left[\frac{dV_J}{dt} + g\right] \qquad (6)$$

where A_J, D_J and L_J are the riser area, diameter and length respectively. The second term on the left hand side represents frictional resistance forces. Pressure $P_I{*}$ at the base of the riser must be established from the total head at station i = I in the outfall but accounting for the head losses through the pipe junction. This also creates a head loss for flows continuing down the outfall as indicated as ΔH_I in figure 2. Presently, these losses are accounted for using the empirical results of Miller (16) but pressure measurements from the experimental studies will later enable an improved calibration of the numerical model to the experimental configuration tested. As an alternative to the use of $P_I{*}$ the value of P_I computed from the upstream outfall pipe element can be substituted with an additional term of $(-\Delta H_J \rho_1 g A_J)$ introduced to the left hand side of equation (6). ΔH_J then represents the required head loss associated with the outfall/riser junction. In this form, numerical calibration can be used to effect hydraulic balances in the mathematical model by the trial choice of ΔH_J at each junction, thereby modelling the effect of the orifice plates introduced for the same purpose in the physical model.

The main limitation of the model in its present form is that it is not able to account for stratification in the outfall and the density changes in the discharging fluid that result from intrusive flow conditions. Empirical means for specification of both the saline wedge profiles in the outfall pipe and the scale of mixing are required to improve the performance of the model.

4. Results and Discussion

Sample output from the experimental model discharging a low flow of 0.355 litres/sec ($Q/Q_D = 0.18$) under regular waves of height 6.4cm and period 1.43 seconds is illustrated in figure 3. This shows velocity oscillations in each riser over a duration between 25 and 40 seconds of a 100 second test run. Inserted on the plots are also the mean of the oscillating velocities (computed from the complete 100 second sample and indicated by a broken line) and the steady state condition in the absence of waves (shown chain dotted). Under these conditions it is clear that intrusion through seaward risers 1 and 2 occurs under steady flow conditions and that this is enhanced by wave action. Compensating increases in discharge from risers 3 and 4 leads to an overall continuity flow balance.

It must be appreciated that the time series for each riser were obtained from a sequence of repeated runs of the same conditions, since the velocity meter had to be transferred from riser to riser. A consequence of this is that slight variation in the repetition of conditions may give rise to apparent imbalance between inflows and outflows from the system. A further restriction is that since the time origin in the plots is not unique, instantaneous comparison of relative flows in each riser has no physical justification.

It was found from observation of the complete data series collected that the landward riser, number 4, consistently shows the greatest range of oscillation in both the experimental and numerical models. Note that the maximum and minimum values of velocity quoted on figure 3 also represent the statistics for the entire sample. They therefore indicate, by interpolation against the time series plotted, the presence or otherwise of long period oscillations possibly caused by reflective resonance in the wave flume. This feature was most apparent for the shorter wave periods when the resulting velocity variations, in risers 3 and 4 in particular, lose the characteristic sinusoidal form and show oscillations of apparently random amplitude over a range of frequencies.

Under a flow of 0.944 litres/sec for the same wave conditions as those in figure 3 the net effect of wave action appeared to be concentrated in the two most seaward risers as seen in figure 4.. Here increased wave induced intrusion in riser 1 is compensated for by an increased discharge from riser 2. This condition, representing $Q/Q_D = 0.47$ together with a range of intermediate flows down to $Q/Q_D = 0.18$, are represented in figure 5. This plots the mean flow rates through each riser (+ve discharging; -ve intrusive) for the different wave conditions tested. The gross disparity in flow distribution even at a flow of $Q/Q_D = 0.47$ is worth emphasis bearing in mind that the riser system was set to an approximate balance for $Q/Q_D = 1.0$. Furthermore, for flows of $Q/Q_D \cong 0.25$, which may loosely represent typical minimum conditions of discharge in prototype systems, only the two landward risers may be expected to be in a discharging condition.

The effect of waves on the behaviour shown in figure 5 is not consistent in terms of changes from riser to riser and this may be in large part explained by the above-mentioned inadequacy of the velocity measuring system. Nevertheless, it is clear that the effects are greatest for conditions of low flow in the outfall and that flows in all risers are generally affected. The general trend is for waves to increase intrusion within the seaward risers with the landward risers being forced to increase discharging flows to satisfy the continuity requirement.

The scale of the wave induced changes can be better appreciated in percentage terms as shown in figure 6. Whilst too much credibility should not be placed on these values because of the potential experimental errors, it is quite clear that for this model at least, the degree of intrusion of saline water into the outfall has been greatly increased by the wave action. It would appear from the results that the larger wave heights with associated longer periods generally prove to be most detrimental in this respect. However, no simple rule for practical application could be contemplated from such a limited data base since, in addition to scaled equivalents of H_W and T, the water depth and riser spacing will also be primary factors in governing the behaviour. These latter parameters were not varied in this programme of tests.

Although not covered in figures 5 and 6, tests have also been conducted with the outfall in a shut-down condition (Q = 0) when subjected to wave action. Internal circulations are again induced but these are weak and were found to be highly unstable. The systematic velocity measurements taken successively in each riser in general failed to demonstrate the required continuity balance. This arose partly because of this instability and partly because the scale of the velocities often approached the 2mm/sec resolution of the ultrasonic velocity probe, thus yielding inadequate time series. More reliable, but inherently qualitative evidence of the internal circulations was obtained by dye injection into each of the risers. A log of the motion of the dye films then illustrated the modes of flow and a sample of these results is presented in Table 1, where D denotes a discharging riser and I an intrusive situation.

It is either under shutdown or near design flow conditions that the numerical model in its present form is best able to represent the physical situation as no density stratification will take place within the pipe system. Figure 7 shows a sample output of the model under shutdown conditions which demonstrates features of the observed behaviour, the landward riser again being subjected to the greatest oscillations. These traces also demonstrate a weak longer period oscillation of about 4.4 second period, which matches the oscillations computed in the dropshaft modelled as part of the headworks. Although a larger period oscillation was noticed in the experimental data, this was not nearly so strong and was possibly induced from the wave field itself. The most likely explanation for the absence of this effect in the experimental model is the suppression of landward motion in the outfall caused by the venturi and the reduced pipe diameter upstream, which was not built into the mathematical description. Earlier steady flow testing of the computer model had demonstrated a rapid transient decay of numerical instabilities arising from assumed initial conditions in the time simulation and similar behaviour would therefore be expected when the model is run with wave action present. Another unknown factor which might influence the performance of the numerical model under these circumstances is the precise form of minor losses created at the pipe/riser junctions at such low flow velocities (low Reynolds Number). Future analysis of the pressure transducer records should potentially shed some new light in this area.

Notwithstanding the limitations of the numerical model when intrusion leads to density differentials and stratification, figure 8 is included for conditions closely matching those of figure 3. Whilst similar intrusive behaviour is observed between the two sets of results, the numerical disparities place into perspective the further advances necessary in the theoretical description before it could be considered for reliable synthesis of prototype systems.

5. Conclusions

1. At flows significantly below the ultimate capacity of an outfall system, it has been demonstrated that intrusive conditions are likely to occur in certain risers forming the seaward discharge manifold. There is evidence to suggest that this saline influx may lead to operational problems and possible malfunction in the long-term under conditions where this is not purged during regular outfall operation..

2. Wave action over the discharge manifold, in conditions where water depths are relatively shallow, has been shown to increase the scale of this intrusion and also to initiate intrusive internal circulations when the outfall is in a shut-down condition.

3. The data acquired and the range of conditions investigated in the work reported are inadequate to enable any quantitative assessment of the likely effects in practical outfall systems. Improved experimental techniques enabling instantaneous velocity measurement in each model riser are essential to improve the quality of results.

4. No attempt has been made to account for the presence of diffuser heads, with multiple ports, as incorporated on most riser systems. This will be investigated in later physical model tests. The presence of a significant flow constriction in such diffuser systems would be expected to suppress to some degree the scale of wave induced variations.

5. A complementary computer model developed as part of the study demonstrates similar behaviour to that observed in the experiment but with deficiencies in calibration in its present form. However, substantial empirical developments are necessary if saline wedge formation in the outfall pipe and density mixing of discharging fluid is to be realistically represented.

6. References

1. Mandl, V., "European community activities towards the protection of the marine environment". Proc. ICE Conference on Marine treatment of sewage and sludge, Brighton, 1987, 1-10.

2. Charlton, J.A., "Salinity intrusion into multiport sea outfalls", Proc. 18th A.S.C.E. International Conference on Coastal Engineering, Capetown, 1982.

3. Charlton, J.A., "Sea Outfalls". Developments in Hydraulic Engineering" edited by P. Novak, Elsevier, Amsterdam, 1985.

4. Williamson, D.L., "Seawater circulation in sewage outfall tunnels". Journal of Hydraulic Engineering, A.S.C.E., Vol. 111 No. 5, May 1985.

5. Larsen, T., "The influence of waves on the hydraulics of sea outfalls". Proc. 20th A.S.C.E. International Conference on Coastal Engineering, Taiwan, November, 1986

6. Williamson, D.L., "Purging of saline wedges from ocean outfalls". Journal of Hydraulic Engineering, A.S.C.E., Vol. 110, No. 12, December, 1984.

7. Grace, R.A., "Sea outfalls - a review of failure, damage and impairment mechanisms". Proc. I.C.E. Part 1, Paper No. 8766, February, 1985.

8. Charlton, J.A., "The venturi as a saline intrusion control for sea outfalls". Proc. I.C.E. Part 2, Paper No. 8980, December 1985.

9. Davies et al, "A laboratory study of primary saline intrusion in a circular pipe". I.A.H.R. Journal of Hydraulic Research, Vol. 26, No. 1, 1988

10. Hansen et al, "San Francisco ocean outfall port valve development". Proc. A.S.C.E. Hydraulics Speciality Conference, Chicago, 1980

11. Roberts, D.G.M. et al, "Weymouth and Portland marine treatment scheme: tunnel outfall and marine treatment works". Proc. I.C.E. Part 1, Paper No. 8749, February, 1984.

12. Charlton, J.A., "Outfall design guide for environmental protection: Section 6", edited by Neville-Jones & Dorling, W.R.C. publication, November, 1986.

13. Mort, R.B., "Investigation into the effects of wave action on long sea outfalls", Ph.D. thesis, University of Liverpool, 1988 (in preparation)

14. Streeter, V.L., and Wylie, E.B., "Fluid Mechanics", pub. McGraw-Hill, New York, 1975

15. Ippen, A.T., "Estuary and Coast-line Hydrodynamics", pub. McGraw-Hill, New York, 1966

16. Miller, D.S., "Internal flow systems", B.H.R.A. Fluid Engineering, 1978.

Table 1 Motion in risers under shutdown conditions (Q = 0) from observation of dye movements.

WAVE CONDITIONS		OBSERVED FLOWS*			
H_W (cm)	T (secs)	Riser 1	Riser 2	Riser 3	Riser 4
6.1	1.0	0	I	I	D
6.1	0.8	I	I	0	D
6.1	0.67	0	I	I	D
5.49	2.5	0	D	I	I
7.16	2.5	D	D	I	I
9.35	2.50	D	D	I	I
9.97	3.33	D	D	D	I
5.01	5.00	0	I	D	D

* D - discharging; I - intrusive
0 - zero.

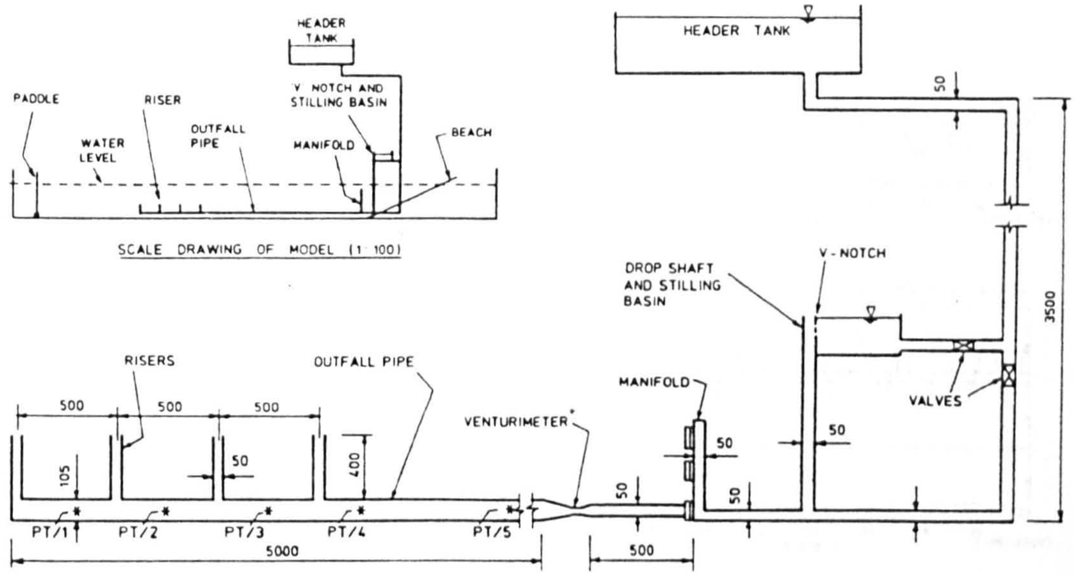

FIGURE 1: General arrangement of experimental apparatus

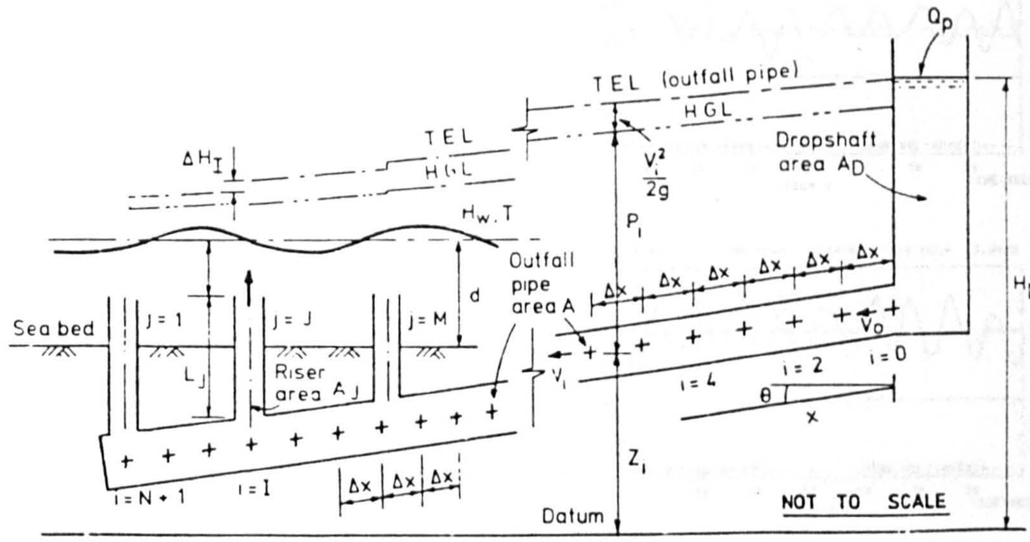

FIGURE 2: Definition sketch for numerical model

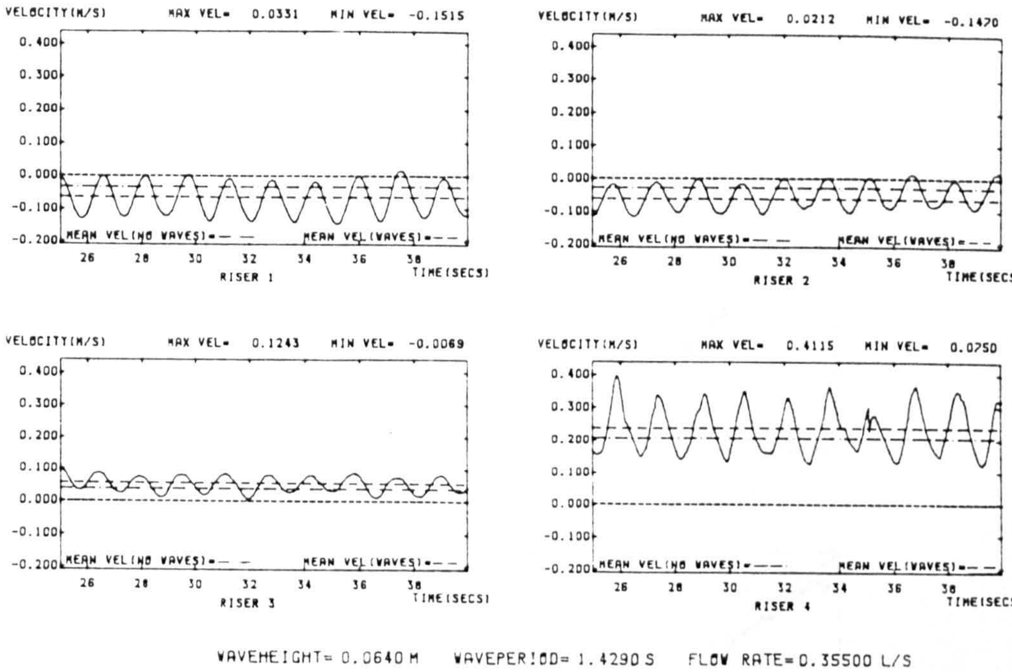

FIGURE 3: Experimental velocity fluctuations in risers for Q/Q_D = 0.18

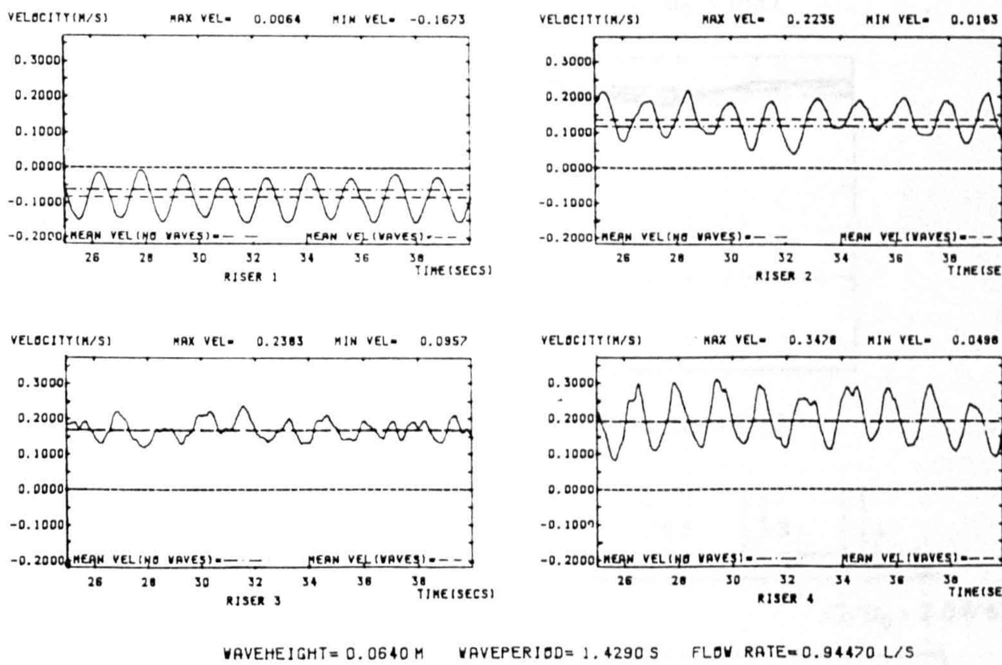

FIGURE 4: Experimental velocity fluctuations in risers for Q/Q_D = 0.47

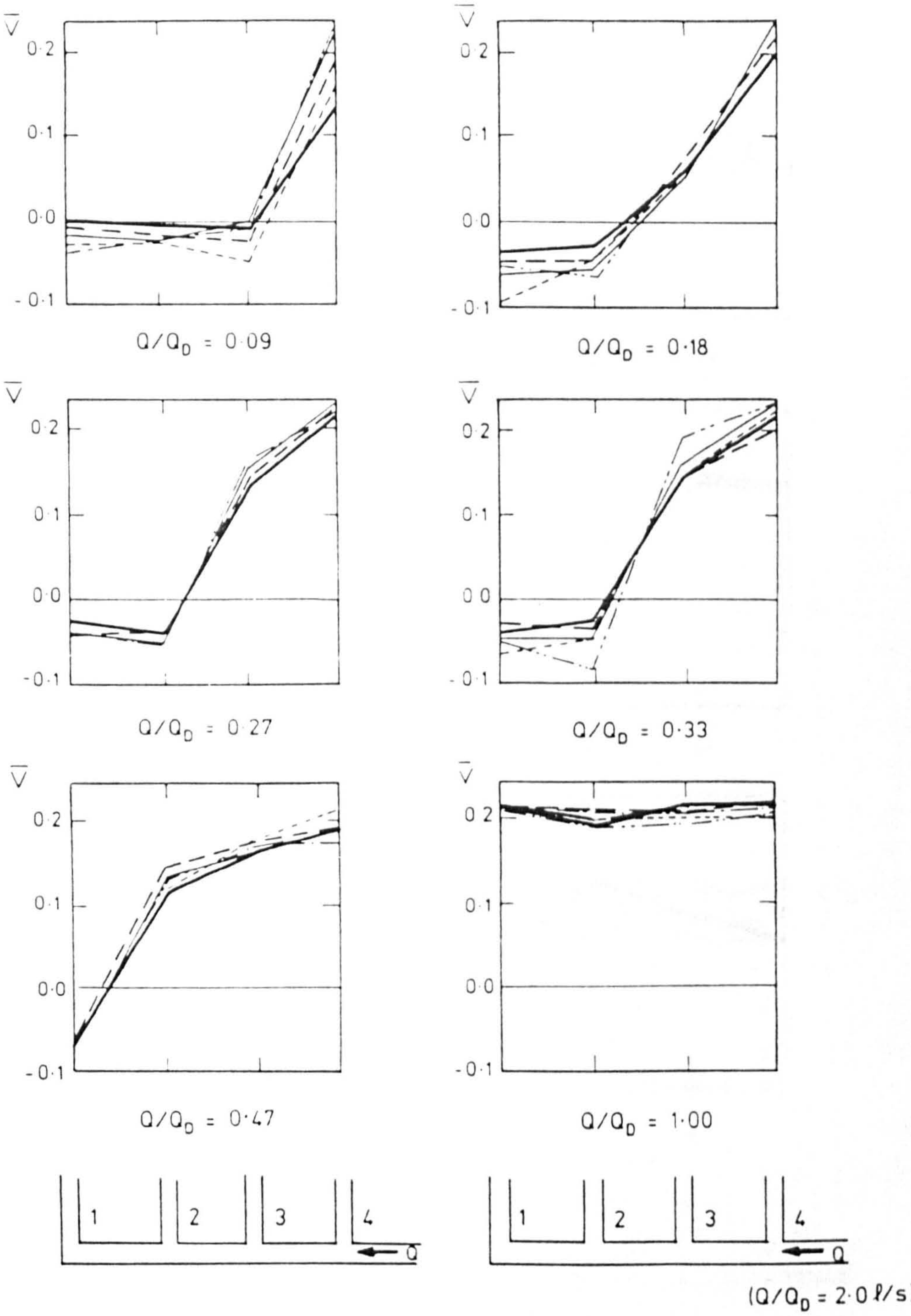

LEGEND

Wave Height (cm)	0	3·3	4·8	5·5	5·8	6·6
Wave Period (secs)	0	2·0	0·67	1·0	0·77	1·43
Symbol	———	— —	- - - -	—·—	—··—	———

FIGURE 5: **Experimental mean of riser velocities ($\overline{V}$) over full range of test conditions**

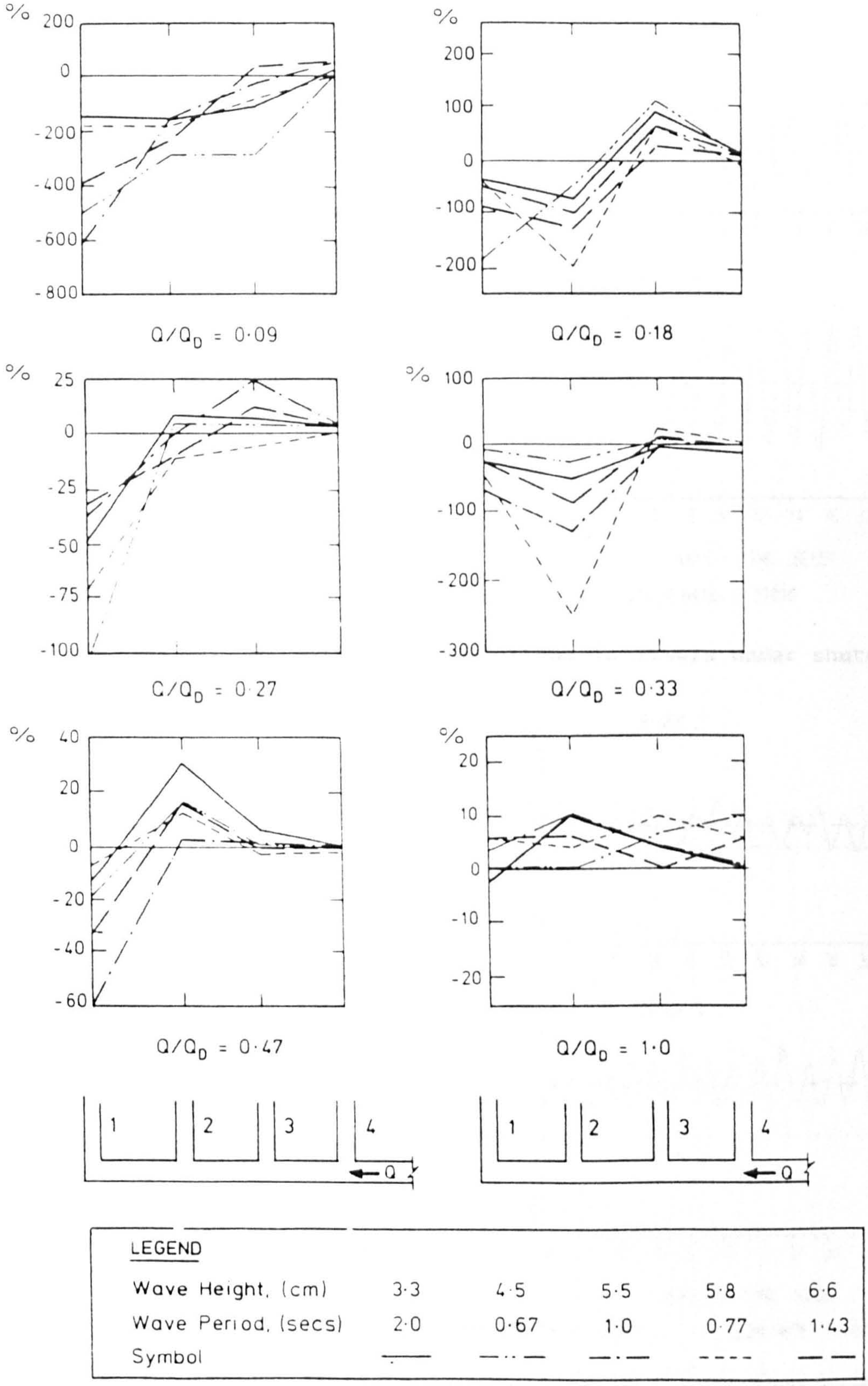

FIGURE 6: Percentage change in riser velocities from steady flow (quiescent receiving water) over full range of test conditions

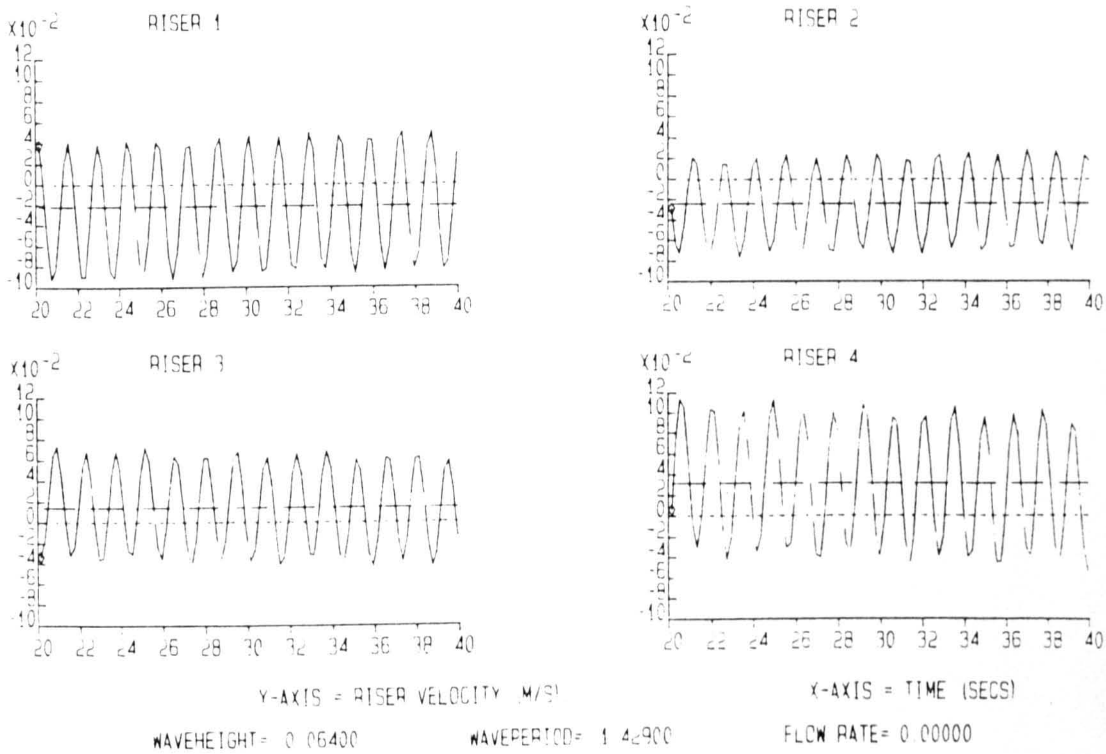

FIGURE 7: **Theoretical velocity fluctuations in risers under shutdown conditions (Q = 0)**

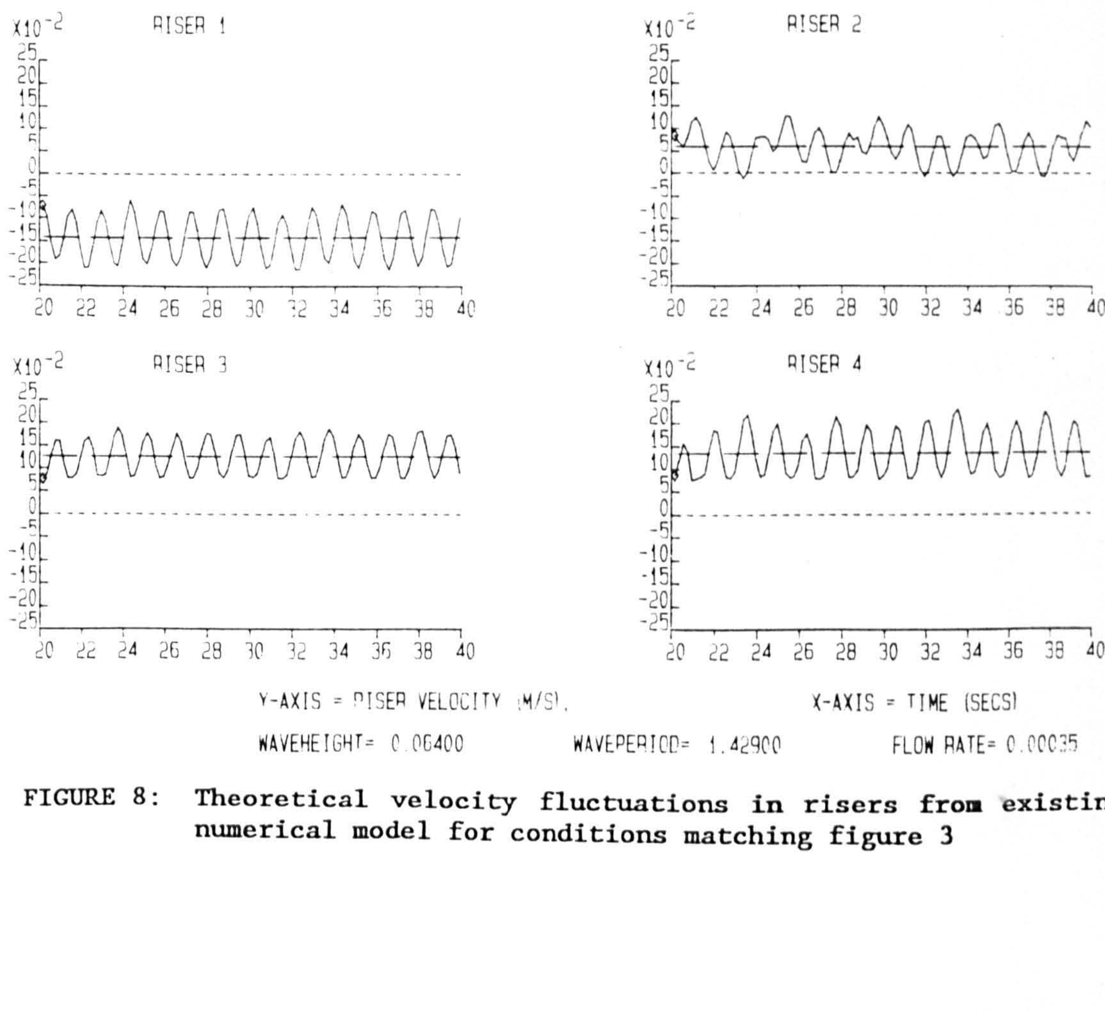

FIGURE 8: Theoretical velocity fluctuations in risers from existing numerical model for conditions matching figure 3